HUMAN-INDUCED EARTHQUAKES

Gillian R. Foulger[1], Miles Wilson[1], Jon Gluyas[1] & Richard Davies[2]

[1]Department of Earth Sciences, Durham University, Durham, U.K.

[2]Executive Office, Newcastle University, Newcastle upon Tyne, U.K.

Project funded by the Nederlandse Aardolie Maatschappij BV (NAM), Schepersmaat 2, 9405 TA Assen, The Netherlands

Report submitted to Jan van Elk and Dirk Doornhof (NAM)

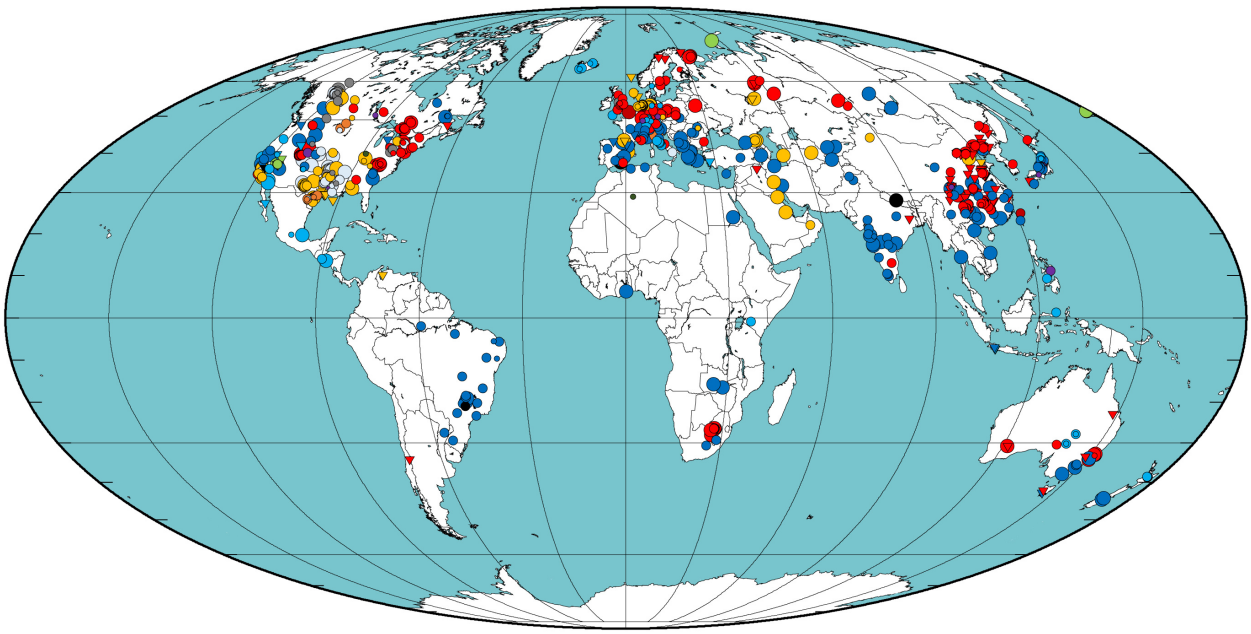

Cover picture: Map of the world in Mollweide projection, centered on the Greenwich meridian, showing all earthquakes postulated to be induced by humans.

It is difficult to predict, especially about the future.

Niels Bohr

TABLE OF CONTENTS

SECTION A: INTRODUCTION

1 Introduction 1

1.1 Intraplate earthquakes 2

1.2 Induced vs. triggered earthquakes 2

1.3 Factors involved in the nucleation of earthquakes 4

1.4 Earthquake locations 5

1.5 Earthquake magnitudes 6

1.6 Earthquake counts 6

1.7 The database 7

SECTION B: EXAMPLES OF CASE HISTORIES

2 Surface operations 9

2.1 Adding mass 9

2.1.1 Water impoundment behind dams 9

2.1.2 Erecting tall buildings 11

2.1.3 Coastal land gain 12

2.2 Removing mass 12

2.2.1 Quarrying 12

2.3 Surface operations: Summary 12

3 Extraction from the subsurface 13

3.1 Groundwater extraction 13

3.2 Mining 14

3.2.1 Traditional mining 14

3.2.1.1 UK mining-induced earthquakes 15

3.2.1.2 South African mining-induced earthquakes....16
3.2.2 Solution mining....17
3.2.3 Tunnel excavation....18
3.3 Hydrocarbons....19
3.3.1 Gas....19
3.3.2 Oil....21
3.4 Geothermal production (heat/fluids)....23
3.5 Extraction: Summary....24
4 Injection into the subsurface....25
4.1 Liquid....26
4.1.1 Military waste....26
4.1.2 Wastewater disposal....27
4.1.2.1 Oklahoma....29
4.1.3 Water injected for enhanced oil recovery....31
4.1.4 Enhanced Geothermal Systems (EGS)....32
4.1.5 Geothermal reinjection....35
4.1.6 Shale-gas hydrofracturing....38
4.1.7 Allowing mines to flood....40
4.1.8 Research projects....41
4.2 Gas....43
4.2.1 Natural gas storage....43
4.2.2 CO_2 for oil recovery....45
4.2.3 Carbon Capture and Storage (CCS)....45
4.3 Injection: Summary....47
5 Explosions....47
5.1 Nuclear....47
5.2 Chemical....48

5.3 Explosions: Summary 49

SECTION C: DISCUSSION & CONCLUSIONS

6 Earthquakes and belief systems 50

7 Correlations between parameters 50

7.1 Cases where a relationship is observed 51

7.2 Cases where a relationship is not observed 52

7.3 Other factors 52

8 Discussion and Summary 53

8.1 How common are induced earthquakes? 53

8.2 Hydraulics 55

8.3 How much stress loading is required to induce earthquakes? 56

8.4 Natural or induced? 60

8.5 Why are earthquakes induced by some industrial projects and not others? 62

8.6 Future trends 63

8.6.1 Earthquake prediction 63

8.6.2 Earthquake management 63

8.7 Possible future avenues of work 64

SECTION A: INTRODUCTION

1 Introduction

Many natural processes modulate the spatial and temporal occurrence of earthquakes. These include tectonic stress changes, the migration of fluids in the crust, Earth tides, surface ice and snow loading, heavy precipitation, atmospheric pressure, sediment unloading and groundwater loss [*e.g.*, Kundu *et al.*, 2015]. Such processes perturb stress on faults by only small amounts, but since rock failure in earthquakes is a critical process, nucleation of each event is ultimately brought about by a final, small change in stress. Thus, it is unsurprising that anthropogenic activity that perturbs stress in the crust, even if by just a small amount, from time to time modulates seismicity. In most cases such effects probably go unnoticed (Section 8.1), but as industrial projects become larger in scale and more numerous, the number of cases where a link is obvious is increasing.

The issues of mining- and dam-induced earthquakes have been known for several decades. Now, concern is growing amongst the general public about earthquakes induced, for example, by hydraulic fracturing for shale-gas extraction and waste-water disposal by injection into boreholes. As hydrocarbon reservoirs enter their tertiary phases of production, seismicity may also increase there.

The full extent of human activities that may induce earthquakes is, however, wider than generally appreciated. The present project aims to provide as near complete a catalog as possible of cases of induced seismicity that have been reported to date. Our work builds on reviews of the subject published in the past. McGarr [2002] provides a general overview. Nicol *et al.* [2011] assembled a list of 75 cases. Suckale [2009] listed 70 cases related to hydrocarbon fields alone, and most recently Davies *et al.* [2013] listed 198 cases.

In this project we built a database of 705 cases of anthropogenic projects postulated to induce earthquake activity. This is probably the largest compilation made to date. We constructed the database by searching published papers, conference abstracts, books, reports, and web-based material and personal communications we judge to be reliable.

Caveat emptor: It is not within the remit of this work to review or develop theories for anthropogenic earthquake induction, nor to judge whether reasonable claims of anthropogenesis are correct or not. Indeed, our database contains some cases where proposals of anthropogenic induction are tentative or have been challenged in later publications, *e.g.*, the 1983 M_W 6.2 Coalinga, California, event (Section 3.3.2). We leave judgment about individual cases to the user.

This new database is accompanied by this report which is structured as follows. Part A (Section 1) provides an introduction and the basics of some relevant background issues. Part B (Sections 2-5) gives examples of seismicity postulated to be related to:

a) Surface operations,
b) Extraction of mass from the subsurface,
c) Introduction of mass into the subsurface, and
d) Explosions.

Each of these categories is divided into sub-categories. In some cases, categorization of a particular case is tentative because more than one anthropogenic process may have preceded

or been ongoing at the time of the relevant earthquakes. For example, fluid extraction and injection are often conducted simultaneously in hydrocarbon reservoirs.

In Part C (Sections 6-8) we summarize features of the database. We also comment on some related issues with which scientists are currently grappling.

1.1 Intraplate earthquakes

Plate tectonic theory in its simplest form considers plates to be rigid and expects essentially all large earthquakes to occur in plate boundary zones. The fact that intraplate earthquakes occur, and may be large, is *prima facie* evidence that the plates are not rigid but simply deforming (usually, but not always) more slowly than the plate boundaries. Plate interiors deform for the same reasons as plate boundaries. They are structurally heterogeneous and stress within them changes cyclically as elastic- and viscoelastic stress diffuses through them following the great earthquakes and volcanic events that sum to bring about what geologists model as plate movements [Foulger *et al.*, 1992; Heki *et al.*, 1993]. The plate-boundary configuration is furthermore geometrically unstable and evolving. For example, in Europe the formation of graben such as the Rhine Graben (Germany) and the Bresse Graben (France and Switzerland), and the emplacement of volcanics such as the Vogelsberg and the Eifel volcanic fields (both in Germany) are likely ultimately related to southerly migration ("slab roll-back") of the Mediterranean collision zone between Africa and Europe. Intraplate European seismicity is probably ultimately related to the same process (Figure 1) [Nielsen *et al.*, 2007].

Intraplate seismicity is commonly expected to be relatively stable spatially, so that future earthquakes will occur in places where they have occurred in the past. This assumption has been re-visited in recent years, in particular as a result of geodetic work done in the New Madrid Seismic Zone, USA [e.g., Newman *et al.*, 1999; Stein *et al.*, 2009]. There, it is widely expected that future large earthquakes will follow the damaging 1811-1812 sequence of four $M \geq 7$ earthquakes [*e.g.*, Johnston & Schweig, 1996]. As a result, significant resources have been invested in earthquake hazard mitigation. Recent GPS surveying has, however, failed to detect any ongoing strain build-up. This observation has led to the proposal that the spatial distribution of intraplate earthquakes in general is not stationary and that the locations of past, large earthquakes are not a good predictors of future earthquakes (the "whack-a-mole" theory). Wrong forecasts of the likely location of future damaging earthquakes may lead to inefficient deployment of hazard-reduction resources. This theory thus has significant implications for public safety.

A non-stationary spatial pattern of seismicity accords with observations that the crust is critically stressed in most intraplate regions. Stress measurements made in boreholes commonly show that stress is close to the depth-dependent strength of the crust as estimated by laboratory experiments [*e.g.*, Brudy *et al.*, 1997; Zoback & Healy, 1984]. Furthermore, the ambient pore pressure is generally close to hydrostatic. The crust is, in general, pervasively faulted and these faults are, in general, close to failure. This conclusion is consistent with observations that anthropogenically induced seismicity may occur, and even be seemingly disproportionately large, in regions that have been historically aseismic.

1.2 Induced vs. triggered earthquakes

The fact that many if not all earthquakes related to human activity release more stress than artificially added to the crust was highlighted by McGarr [2002]. He suggested using the

terms “induced” for earthquakes resulting from an activity that causes a stress change comparable in magnitude to the ambient shear stress acting on a fault to cause slip. He further proposed using the term “triggered” where the anthropogenic stress change is much smaller, and “stimulated” where there are insufficient data to make the distinction.

It is beyond dispute that in many cases seismic strain energy released in earthquakes is many orders of magnitude larger than that introduced into the crust by the industrial activity. In this report, however, we use the term “induced” for all earthquakes postulated to be related to human activity. The reasons for this are:

a) All earthquakes probably release some pre-existing strain energy and are thus likely to be technically “triggered”. Indeed, only in cases where rock is entirely unstressed in its initial state could this not be the case. This is not possible in a heterogeneous, gravitating half-space. Even nuclear tests, which are purely explosive sources, trigger the release of some regional tectonic stress as is shown by the significant shear components in their focal mechanisms [*e.g.*, Toksöz & Kehrer, 1972].

b) The amount of tectonic strain energy loaded into the crust that is relieved seismically, on what time-scale, and the amount released aseismically are poorly understood. In deforming regions, *e.g.*, plate boundary zones, aseismic deformation can be measured geodetically [*e.g.*, Heki *et al.*, 1997] and surface subsidence is commonly observed above producing reservoirs [*e.g.*, the Wilmington Oilfield, California; Kovach, 1974; Nagel, 2001]. Observations suggest that only a fraction of the total strain energy is relieved seismically but it is difficult to determine what this fraction is. Surface geodetic data have low sensitivity to fault coupling at depth. Estimates of the percentage of strain energy that is dissipated aseismically varies from ~20% to 1000% [Villegas-Lanza *et al.*, 2016]. The recent under-prediction of the magnitude of the 2011 M_W 9 Tohoku-oki, Japan, earthquake which killed > 18,000 people and did as-yet-unassessable economic damage, brought into sharp focus the fact that our assumptions regarding the length of the “seismic cycle” may be incorrect. Even moderate and large earthquakes may not relieve all the stress on a particular fault so our ability to estimate long-term stress buildup in the crust is incomplete.

   The same considerations hold true for industrial projects. If the timescale of energy release is underestimated, and with it the size of the largest expected earthquake (which dominates the energy budget because of the fractal nature of earthquake magnitudes), the maximum expected future earthquake magnitude (M_{MAX}) may be underestimated.

c) It is at best impractical and at worst fundamentally impossible to determine whether some of the strain energy released in a seismic event pre-existed. Even in cases where the energy released is comparable to the amount anthropogenically added [*e.g.*, McGarr, 1991], much of the latter may have been relieved by aseismic deformation such as ground subsidence, or inflow of water at depth. These processes may in turn trigger earthquakes or load adjacent regions to seismic failure [*e.g.*, Guglielmi *et al.*, 2015].

Our use of the term “induced” as neutral and without implications for the origin of the causative stress change is in accord with the usage of the Committee on Induced Seismicity

Potential [Hitzman, 2013]. That committee uses the term "induced" to mean "earthquakes related to human activities".[1]

1.3 Factors involved in the nucleation of earthquakes

Shear slip on fault planes, with or without crack-opening or closing components, is the most common earthquake source process. Factors involved in nucleation, i.e. the onset of motion, include:

- the coefficient of friction on the fault plane;
- compressive normal stress on the fault plane;
- pore pressure in the fault zone; and
- shear stress on the fault.

According to the widely used "Coulomb Theory", the shear stress required for failure is

$$\tau = \tau_0 + \mu(\sigma_n - p) \qquad \text{Eq. 1}$$

where τ is the shear stress required for failure, τ_o is the cohesion, μ is the coefficient of friction, σ_n is the normal stress across the fault, and p is the pore pressure in the fault zone [*e.g.*, McGarr *et al.*, 2002]. The onset of an earthquake may thus result from reduction of the cohesion or normal stress on the fault plane, or increase in the shear stress or pore pressure.

The loss or gain of overlying weight, introduction of fluid into a fault zone, or the imposition of vertical and/or horizontal stress by other means *e.g.*, stress transfer from nearby earthquakes, can bring a fault closer to failure. Where there are rapid temperature changes, *e.g.*, where cold water is injected into geothermal areas, thermal effects may also be a significant.

Interestingly, both the anthropological addition and removal of material is associated with earthquake occurrence. The removal of water from aquifers (Section 3.1) and rock from mines (Section 3.2) may reduce the confining stress on fault planes. The introduction of water via reservoir impoundment (Section 2.1.1) or injection (Section 4.1) may alter the fluid pressure in fault zones. The cessation of groundwater pumping, *e.g.*, in mines, may result in the influx of groundwater and increase in pore pressure (Section 4.1.7). The addition of solid mass to the surface may also alter hydrogeological conditions (Section 2.1.2).

Theories for the mechanism of induced earthquakes include the asperity model of Pennington *et al.* [1986] which suggests that fluid extraction results in differential compaction or aseismic fault motion, which in turn increases stress on locked portions of faults. This stress is eventually relieved when asperities break. The poroelastic model of Segall [1985; 1992] suggests that declining pore pressures resulting from fluid extraction cause contraction of the reservoir rocks and stress build-up. *Ad hoc* theories for induced earthquakes at individual

[1] "*Some researchers (e.g., McGarr et al., 2002) draw a distinction between "induced" seismicity and "triggered" seismicity. Under this distinction, induced seismicity results from human-caused stress changes in the Earth's crust that are on the same order as the ambient stress on a fault that causes slip. Triggered seismicity results from stress changes that are a small fraction of the ambient stress on a fault that causes slip. Anthropogenic processes cannot "induce" large and potentially damaging earthquakes, but anthropogenic processes could potentially "trigger" such events. In this report we do not distinguish between the two and use the term "induced seismicity" to cover both categories."* Hitzman, M. W. (Ed.) (2013), Induced Seismicity Potential in Energy Technologies x+248 pp., National Academies Press, Washington, D.C..

localities may provide plausible explanations *a posteriori*. However, developing a method that can reliably predict *a priori* which industrial projects will induce earthquakes and which not is still a work in progress.

1.4 Earthquake locations

Earthquakes in our database date from 1868 to 2016. Seismological technology has improved vastly during this period, but even today the standard of monitoring is non-uniform. Many projects may not be monitored at all until nuisance seismicity has already begun, whereas others may be monitored by dense networks installed well before the onset of operations, in order to obtain a pre-operational baseline [*e.g.*, Cladouhos *et al.*, 2013]. As a result, the event locations, magnitudes and other information such as focal mechanisms in our database vary in quality.

Inaccurate hypocentral locations lower our ability to associate earthquakes with operations on the basis of spatial correlations, especially if the errors are larger than the separation between boreholes or producing horizons. An example is the case of the Crooked Lake, Alberta, earthquake sequences, thought to have been induced by shale-gas hydrofracturing (Section 4.1.6) [Schultz *et al.*, 2015]. A pre-operational seismic baseline was not available for small- and medium-magnitude earthquakes, there was little information on the local crustal structure, and most of the seismic data were from stations at distances of > 100 km. As a result, it is unclear whether lack of spatial correlation of some events with operations is real or merely a consequence of inaccurate locations.

By far the largest source of hypocentral uncertainty is imperfect knowledge of crustal structure. This factor is not usually included in the error estimates computed by popular hypocenter-location computer programs, which base uncertainty estimates on root-mean-square arrival-time residuals, assuming that the crustal model is perfect. These residuals may be reduced to quite small values by systematically mislocating hypocenters, giving a highly misleading idea of the quality of the result. Advanced earthquake location methods such as master-event techniques, relative location ["double-differencing"; Waldhauser & Ellsworth, 2000] or using waveform cross-correlation [Got *et al.*, 1994] can improve the accuracy of locations *relative to one another* but do not reduce systematic errors in the absolute accuracy of entire clusters of events. Accurate depths in particular are out of reach if geometrically strong data are not available because errors in hypocentral depth are typically 2-3 times the error in horizontal (epicentral) location. Too few and too distant seismic stations are also hindrances to obtaining accurate locations (Section 4.2.1).

For the purpose of locating earthquakes associated with relatively small-scale industrial projects, obtaining accurate local velocity models may be challenging. Available information may be limited to well-logs, global or national crustal models, or models from analogous geological areas [*e.g.*, Schultz *et al.*, 2015]. Such models are not adequate for reducing location uncertainties to sub-hectometer (100 m) levels. Ideally, high-quality crustal models based on active-source seismic surveying and/or one- and three-dimensional inversions of local earthquake data will be available. Projects will be monitored by dense networks of seismic stations with at least one station every 1-2 km^2. Experimental designs of this kind can return locations accurate to about a hectometer. Reducing errors still further requires calibration shots. This subject was recently discussed in detail by Foulger and Julian [2014] for the case of earthquakes induced by Enhanced Geothermal Systems (EGS) operations (Section 4.1.4).

In order to inform discussions regarding whether earthquakes are induced or natural, a pre-operation baseline is required. For this purpose, seismic networks must be deployed prior to commencement of operations. An effort to establish such a baseline for the entire UK prior to possible expansion of shale-gas hydrofracturing was recently made by Wilson *et al.* [2015].

1.5 Earthquake magnitudes

Because of the definitions of earthquake magnitudes, values quoted for a single event often differ by up to a whole magnitude unit, even if calculated correctly. This is because:

- Traditional scales such as local magnitude (M_L) use measurements of the amplitudes of certain seismic phases recorded on seismic stations. Amplitudes are a poor measure of the size of an earthquake because they are influenced by factors such as the orientation of the fault that slipped and source-to-station crustal structure. Because of these and other factors, different recordings of the same earthquake at different stations may yield different magnitudes even using the same scale.

- Different magnitude scales such as M_L and surface-wave magnitude (M_s) use different types of seismic waves. There are both systematic and random differences in the magnitudes calculated using them. For example, shallow earthquakes excite stronger surface waves than deep earthquakes, so M_S, which relies on measurements of the amplitudes of surface waves, underestimates the sizes of deeper earthquakes.

- Seismological practice is notoriously non-standard in respect of magnitudes, and local magnitude scales and practices often depart considerably from those originally defined. For example, many local seismic stations and networks use their own customized magnitude scales, often constructed by calibrating them against a few earthquakes measured in common with the nearest permanent or calibrated station. That station may in turn have been calibrated in the same way. Local magnitude M_L technically refers to recordings made on Wood-Anderson seismographs, but such instruments are now rare. As a result, magnitudes reported from one seismic network may not be comparable to those reported from another, even if the same magnitude scale has, in theory, been used.

In view of these factors, and because the information published is often limited, especially for older cases, it is beyond the scope of the present report to attempt to render all magnitudes to a single scale. In this report and the figures herein we thus do not discriminate between magnitude types reported. We record the information where available in both this report and the database, *e.g.*, M_L (local magnitude), m_b (body-wave magnitude), M_S (surface-wave magnitude), M_d (duration magnitude) and M_W (moment magnitude). Where magnitude type is not specified we use the notation M. Where several different estimates are published, we preferentially cite M_W. If M_W is not available, and more than one other magnitude has been published, we cite the largest. The inhomogeneous nature of the magnitude data needs to be borne in mind when considering the graphs and data.

1.6 Earthquake counts

The total number of earthquakes reported in a sequence depends strongly on the density of seismic monitoring. This may change with time, for example if additional seismic stations are installed after nuisance seismicity has begun. Earthquakes are a fractal phenomenon, and their numbers increase by about an order of magnitude for each reduction in magnitude unit.

Where numbers are required to be compared, they must thus be related to a common low-magnitude cut-off threshold.

The numbers of earthquakes induced may be of interest where monitoring networks are stable since this parameter may serve as a sensitive strainmeter. As a result, earthquake counts have been particularly useful for monitoring active volcanoes. The availability of many earthquakes is also an advantage for research purposes such as tracking injected fluids. In such cases, hypocentral distributions can be defined better if data are plentiful. From the point of view of potential damage from large earthquakes, however, the ones of most relevance are the relatively few large-magnitude events and possibly only the largest one.

1.7 The database

The approach we used to construct the database is described in Appendix 1. Challenges intrinsic to the task included:

- Incomplete reporting. This is without doubt severe and is quantified and discussed in Section 8.1;
- Ambiguous reporting, *e.g.*, "Seismicity is not reported";
- Lack of reported data, *e.g.*, operational parameters not given;
- Uncertainty regarding whether earthquakes were induced, *e.g.*, some postulated associations are based simply on short-term temporal correlations or weak spatial correlations that cannot be supported statistically and may be coincidences. Our approach was to include all reasonable proposals in the database. Responsibility for deciding how to treat particular cases is delegated to the user;
- Multiple possible induction processes ongoing simultaneously, *e.g.*, hydrocarbon extraction and wastewater injection;
- Non-uniformity of magnitude reporting. Many magnitude scales are used, instruments are often locally calibrated, magnitude type may not be reported, or several different magnitudes may be reported for the same earthquake in different publications (Section 1.5). Our approach was to report M_W if available, and if not the largest other magnitude;
- Lack of suitable networks to detect earthquakes. This hampers studies where earthquakes were not expected and suitable instruments were installed only after seismicity onset (Section 1.4);
- Poor accuracy of some earthquake locations (Section 1.4).

A list of the column headings in the database is given in

Table 1 and more detailed descriptions are provided in Appendix 2. An abbreviated version of the database is given in Appendix 3. The full database electronically in the form of an Excel spreadsheet is Appendix 4. Appendix 5 is an electronic collection of related published references as an EndNote library.

Appendix 6 comprises a bibliography of publications on induced earthquakes.

A suite of maps of the world and smaller regions plotting all cases is provided in Appendix 7.

Table 1: Data recorded in the database

Column contents	Column contents
Country	Project name
Project type (subclass)	Longitude
Latitude	Project end date
Project start date	End date of seismicity or monitoring
Start date of seismicity or monitoring	Magnitude type
Delay time	Date of largest earthquake
Depth of largest earthquake	Distance of largest earthquake from induction activity
Year of largest earthquake	Lithology/resource
Distance of furthest earthquake from induction activity	Depth of induction activity
Typical depth of earthquakes	Previous seismicity
Tectonic setting	Injection/extraction rate
Dam height	Total volume or mass injected/extracted
Units of injection/extraction rate	Maximum wellhead pressure during injection
Units of total volume or mass injected/extracted	Stress change postulated to have induced earthquake
Change in reservoir pressure	Bottom-hole temperature
Area of project	References
Notes	References used by Davies *et al.* [2013]
Project type	

SECTION B: EXAMPLES OF CASE HISTORIES

2 Surface operations

2.1 Adding mass

Earthquakes have been postulated to have been induced in association with three styles of surface mass addition–water impoundment behind dams (168 cases), erecting heavy buildings (1 case), and engineering accumulation of coastal sediments (1 case).

Seismic events in mines were known even before scientists understood what causes earthquakes. The earliest report of earthquakes induced by water reservoir impoundment is from Lake Mead, Nevada and Arizona, USA (Figure 2) [Carder, 1945]. It was followed by numerous additional reports in the 1960s and later. Now, several water-reservoir-induced earthquakes have resulted in fatalities and extensive property damage. The largest earthquake claimed to have been induced in this way is the 2008 M ~8 Wenchuan, China, earthquake, which has been associated with impoundment of the reservoir behind the Zipingpu dam.

In contrast, reports of earthquakes induced by erecting heavy buildings and engineering coastal land gain are, to date, rare and speculative. More case histories are needed before we can be confident that these activities are indeed seismogenic.

2.1.1 Water impoundment behind dams

A well-studied example is that of the Koyna Dam, India (Figure 3). A detailed overview of this case, along with a review of dam-induced earthquakes, is given by Gupta [2002]. The 103-m-high Koyna Dam was raised in 1962 and contains a reservoir up to 75 m deep and 52 km long. Five years after it was completed, a sequence of earthquakes with magnitudes up to M_S 6.3 occurred causing ~200 deaths and slightly damaging the dam. The largest earthquake nucleated at shallow depth, probably < 5 km, and its epicenter was ~10 km from the dam. Earthquake activity has continued subsequently, correlating to some extent with water level in the reservoir (Figure 4) [Talwani, 1995]. A M > 5 event occurs there about every four years.

A second notable example is the Nurek dam, Tadjikistan (Figure 5) [Keith *et al.*, 1982; Leith *et al.*, 1981; Simpson & Soboleva, 1977; Simpson & Negmatullaev, 1981]. Building of this dam began in 1961 and, at 317 m, it is the highest in the world. It contains a reservoir ~10 km^3 in volume (Figure 6). The largest earthquake to have occurred there to date is the 1972 M_S 4.6 event (Figure 7) [Simpson & Negmatullaev, 1981]. Seismicity is ongoing and there is evidence for correlation with periods of increase in water depth (Figure 8).

The largest volume reservoir in the world is 1.64×10^{11} m^3 and is contained by the 111-m-high Aswan dam, Egypt. Earthquakes induced there are thought to occur in two depth intervals at ~0-10 km and ~15-25 km (Figure 9 and Figure 10). This vertical separation is postulated to indicate two different processes/environments of induction [Awad & Mizoue, 1995]. The largest earthquake observed so far, a M 5.7 earthquake that occurred in 1981, is thought to have nucleated in the deeper zone.

A rare case where induced seismicity damaged the dam itself is that of the 105-m-high Xinfengjian Reservoir, China. Impoundment of the 1.39×10^{10} m^3 volume reservoir began in

1959 and was followed by the onset of seismic activity just one month later. A M_S 6.1 earthquake occurred in 1962 which caused minor cracking of the dam.

A case of particular interest is that of the May 2008 M_W ~8 Wenchuan, China, earthquake (Figure 11). This earthquake was so large relative to the height of the nearby Zipingpu dam (156 m) and the volume of the reservoir (~10^9 m^3) that it is controversial whether it was induced or not. It nevertheless occurred ~20 km from the dam within months of full impoundment of the reservoir. It was responsible for ~90,000 deaths and serious damage to more than 100 towns, including collapsing houses, roads and bridges.

The area lies at the transition between the low-strain-rate (< 10^{-10} per year), stable Sichuan Basin continental region and the tectonically active Tibet plateau where strain rates are > 10^{-8}/year. This transition is marked by the multi-stranded Longmenshan fault zone which accommodates both thrust and strike-slip motion. Paleoseismic work suggests an earthquake recurrence time for M 7-8 earthquakes of ~7,000 years [Klose, 2012].

Prior to impoundment of the reservoir, earthquake activity had been ongoing at a low level in the vicinity of the dam at a rate of ~40 recorded events per month. This rate increased at the beginning of the impoundment period, in October 2005, when the water level rose rapidly by ~80 m. The level peaked in October 2006 at ~120 m above pre-impoundment levels. At this point, earthquake activity surged to ~90 events per month but reduced thereafter (Figure 12).

The 2008 M_W ~8 mainshock nucleated at ~16 km depth and thrust motion propagated up toward the surface beneath the reservoir. Rupture then transitioned to strike-slip motion and propagated laterally along the fault in both directions, rupturing a > 300 km length of the Longmenshan thrust belt with an average slip of 2.4 m, peaking at 7.3 m. The source time function, which lasted 90 s, indicated that failure occurred in five sub-events that sequentially released 14%, 60%, 8%, 17% and 6% of the total moment (Figure 13) [Zhang *et al.*, 2008]. The average stress drop during the earthquake was 18 MPa, peaking at 53 MPa. Similar to other great earthquakes, this event thus owes its large size to the progressive activation of a chain of fault segments as each sub-event occurred.

The increase in shear and normal stresses caused by impoundment of the water reservoir that were orientated to encourage slip on the fault were calculated to be no more than a few kPa [Klose, 2012]. This is small, even compared with the stress changes associated with Earth tides (Section 8.3). Klose [2012] suggests that this stress modulated the timescale on which this great earthquake occurred, advancing it in time by ~60 years.

It has been much disputed whether or not the very small stress perturbation caused by this water-reservoir impoundment was sufficient to trigger such a large earthquake. It is, however, of the same order as stress loading suggested to encourage failure in other cases (*e.g.*, Section 3.1). A more relevant question is perhaps whether impoundment of the reservoir could have induced the initial M_W ~7.5 sub-event, since it is that sub-event that triggered the subsequent cascade of segment failures that resulted in the earthquake growing to a magnitude of M_W ~8.

In 2007 an unusual dam-related seismic sequence occurred in association with the Beni Haroun hydraulic complex in the Mila region, 30 km west of the city of Constantine, Algeria [Semmane *et al.*, 2012]. In that year, a sequence of earthquakes with magnitudes up to M_d 3.9 occurred. It is thought to have been induced by the leakage into the ground of ~400,000 m^3 of pressurized water as it was being pumped between two reservoirs. More than 7200 earthquakes were recorded over a ~2-month period.

The Beni Haroun hydraulic complex comprises a main dam 120 m high and a reservoir with a capacity of ~10^9 m^3 of water. This is connected by pipelines to a secondary reservoir, the Oued Athmania reservoir, about 15 km south of the main dam (Figure 14). A 6-km stretch of this pipeline system passes through a mountain at a depth of up to ~400 m below surface as a lined tunnel 1.4-3.6 m in diameter. The pumping system, which raises the water by ~600 m, has a capacity of 600,000 m^3/day.

In 2007 a large amount of water leaked from this tunnel via defective joints and penetrated deep into the ground via fractures, faults and karst cavities. Earthquakes onset within days of the leakage (Figure 15). The area had no prior record of swarm activity on a similar scale, and the installation of the project in 2000 had not been associated with an increase in seismicity. The events did not cause damage but they alarmed local people unaccustomed to earthquakes. It is reported that the earthquakes were heard loudly [Semmane *et al.*, 2012].

The Colorado River, USA, is dammed with numerous dams. The two largest are the 220-m-high Glen Canyon dam, a concrete arch that impounds Lake Powell on the Colorado River in Arizona, and the Hoover dam, some 600 km further downstream to the southwest. This has a similar height and impounds Lake Mead which is mostly in Nevada. Glen Canyon dam is built in Mesozoic sedimentary rocks whereas the Hoover dam is built in Tertiary volcanics, part of the tectonically active basin-range province. Somewhat unusually the intuitive expectation, that the latter might be seismogenic and the former not, is in this case borne out (Figure 16).

Currently, attention is focused on the 181-m-high Three Gorges dam, China (Figure 17). The 40 km^3 water reservoir was fully impounded in 2010 and power generated came online in 2012. The total generation capacity is 22,500 MW. The area lies within a seismogenic region that includes two major fault lines. The reservoir is not the largest in the world, but earthquakes are already being reported with a M_L 4.6 event occurring in 2014.[2]

2.1.2 Erecting tall buildings

Lin [2005] suggested that erection of the ~500-m high Taipei 101 building, Taiwan, influenced the pattern of seismicity in the immediate neighborhood of the building. This 700,000-tonne building increased stress on the ground at its base by ~0.47 MPa. In the eight-year period prior to building, nine earthquakes with $M_L \leq 2.0$ occurred whereas during the eight-year period that spanned construction and followed it, 20 earthquakes up to M 3.8 occurred. Earthquakes were unusually frequent during the construction period (Figure 18).

This unusual case is the only published report to date of earthquakes being induced by raising a heavy building. Taiwan lies in the convergent plate boundary zone where the Philippine Sea plate is subducting beneath the Eurasian plate at the Manila trench. As a consequence it is seismically active.

This case raises the question of whether other such examples exist, *e.g.*, in Japan. The building that is currently the tallest in the world, the 825-m-high Burj Khalifa, Dubai, weighs less than the Taipei 101 building, at only 450,000 tonnes. There are no known reports of altered earthquake activity from the New York or Tokyo regions where large buildings are common, though it may be that the issue has not been looked into in detail.

[2] https://journal.probeinternational.org/2014/04/07/three-gorges-dam-triggers-frequent-seismic-activities/

2.1.3 Coastal land gain

It has been suggested that the 2007 M_L 4.2 Folkestone, Kent, UK, earthquake was triggered by geoengineering of shingle accumulation in the harbor since 1806. There is substantial coastal land loss as a result of erosion to the southwest and northeast of Folkestone, but land gain by anthropogenic shingle accumulation in Folkestone harbor has been ongoing for ~200 years. An estimated total of ~2.8 x 10^9 kg had accumulated by 2007, altering the stress by an estimated 0.001-0.03 MPa at 2 km depth [Klose, 2007a]. The earthquake epicenter was located ~1 km (epicentral error ~5 km) from the shingle, and nucleated at shallow depth.

2.2 Removing mass

Surface operations that remove mass from the near-surface that are reported to induce earthquakes are limited to quarrying. Our database contains 16 such cases.

2.2.1 Quarrying

The largest earthquake that has been associated with quarrying is the 2013 M 6.1 Kuzbass, Siberia, event [Emanov *et al.*, 2014; Yakovlev *et al.*, 2013]. It occurred in the Bachatsky open-cast coal mine. This mine is 10 x 2.2 km in area, excavated to a depth of up to 320 m, and produces > 9 x 10^6 tonnes of coal per year. The event was strong enough to collapse buildings in local communities and to be felt in neighboring provinces.

Moderate earthquake activity had been detected in the mine in early 2012 when a M_L 4.3 event and associated aftershocks occurred. A dense local seismic network was installed, and a low level of small earthquakes with magnitudes up to ~ M_L 2 was found to be occurring. The magnitude of events increased with time, and 15 months later a M_L 3.9 event occurred followed a month later by the M 6.1 mainshock.

2.3 Surface operations: Summary

The impoundment of water in reservoirs behind dams is perhaps one of the best-known anthropological activities that induces earthquakes. It does so in abundance and accounts for 168 (24%) of all the cases in our database. Ignoring natural lakes where dams have made minor changes to the water level, reservoirs can be up to 8,502 km^2 in area (Lake Volta, behind the Akosombo Dam, Ghana). Earthquakes may thus be induced throughout relatively large regions.

In eight cases, earthquakes with M > 6 have been induced, associated with the dams at Zipingpu (China), Lake Hebgen (USA), Polyphyto (Greece), Koyna (India), Kariba (Zambia/Zimbabwe), Kremasta (Greece), Hsingfengkiang (China) and Killari (India). In China there are 348 reservoirs with volumes exceeding 0.1 km^3. Of these, 22 (6.3%) are reported to be seismogenic.

Much has been published on the mechanism of triggering [see Gupta, 2002 for a summary]. Stresses induced by reservoirs at the depths at which earthquakes occur are small, perhaps of the order of 0.1 MPa, and much smaller than typical stress drops in earthquakes which are commonly in the range 1-10 MPa. They are, nevertheless, larger than Earth tidal stresses. Despite this, it is speculated that the mechanism of induction may be that the surface load alters hydraulic conditions at depth, causing fluid to migrate into fault zones and increase pore pressure. This process may also explain the case of seismicity postulated to be induced

by erecting the Taipei 101 building, Taiwan (Section 2.1.2), and shingle accumulation at Folkstone, UK (Section 2.1.3).

3 Extraction from the subsurface

3.1 Groundwater extraction

We have identified five reported cases of earthquakes associated with the anthropogenic removal of groundwater. A particularly remarkable case is that of the 2011 M_W 5.1 Lorca, Spain, event that is postulated to have been induced by groundwater extraction (Figure 19) [Gonzalez *et al.*, 2012]. This earthquake caused extensive damage to the town of Lorca, seriously damaging both modern and historic buildings, killing nine people and injuring several hundred others (Figure 20).

The region lies in a transpressive shear zone, comprising thrust- and strike-slip faults, that forms part of the Nubia-Eurasia plate boundary. The M_W 5.1 mainshock nucleated on the Alhama de Murcia fault at unusually shallow depth (~3 km). This fault has generated several large earthquakes over the past few centuries. Considerable geodetic data were available, from radar interferometry and GPS surveying, constraining co-seismic deformation. Numerical modeling of this deformation was consistent with slip of up to ~15 cm on a ~10 x 10 km section of the fault in the depth interval ~1-4 km (Figure 21).

Geodetic data also constrained regional surface deformation over the several decades preceding the earthquake. To the southeast of the Alhama de Murcia fault, long-term groundwater pumping had resulted in the water table dropping by > 250 m in the period 1960-2010. This had been accompanied by surface subsidence at rates of > 10 cm/year, totaling > 2 m over the preceding 20 years. Significant environmental effects had occurred as a result (Figure 22).

González *et al.* [2012] calculated the subsurface stress change resulting from water-mass removal to investigate the effect of groundwater pumping on the Alhama de Murcia fault. The Coulomb stress changes would have encouraged faulting of the type that occurred. A slip deficit of up to ~12 cm had probably accumulated in the Alhama de Murcia fault since the last large earthquake on the fault segment ~200 years previously. Numerical modeling results were consistent with a groundwater crustal unloading process that enabled the tectonically accumulated stress to have been released in the 2011 M 5.1 earthquake. González *et al.* [2012] concluded that the cumulative long-term hydraulic unloading, coupled with the relative position and type of the fault with respect to the depleting aquifer, contributed to the stress conditions that resulted in the earthquake.

Several other cases of induced seismicity of this kind have been proposed. The 2015 M_W 7.8 Gorkha, Nepal, earthquake has been linked to removal of groundwater from the Gangetic plains to the south [Kundu *et al.*, 2015]. This thrust earthquake caused ~8000 deaths and ~$10 billion of economic loss, ~50% of the Gross Domestic Product of Nepal.

The Gangetic plains, which cover ~2.5 x 10^6 km^2, are home to ~0.5 billion people. Extraction of groundwater amounts to the removal of ~23 x 10^{12} m^3/year, equivalent to a drop in the water table of ~1 m/year (Figure 23). This load is being removed from the footwall of the Main Himalayan Thrust, thus encouraging slip on the fault zone in the same way as groundwater removal near Lorca, Spain (Figure 24). The plains comprise the most intensely irrigated region in southeast Asia and has the highest population density. Kundu *et al.* [2015]

suggest that anthropogenic crustal unloading causes a significant component of horizontal compression that adds to the secular compressional stress buildup along the Main Himalayan Thrust.

Kundu *et al.* [2015] calculated the Coulomb failure stress change to have been ~0.003-0.008 MPa since 1960. Such a stress change is at the lower limit of those induced by Earth tides (Section 8.3). It is comparable, however, to the calculated natural rate of stress accumulation on the Main Himalayan Thrust, which is ~0.001-0.002 MPa/year. The dewatering of the Gangetic plains is thus accelerating stress accumulation on the Main Himalayan Thrust by 4.5-20%.

In the San Joaquin Valley, California, the groundwater has been depleted by some 1.6×10^{11} m^3 over the past ~150 years [Amos *et al.*, 2014; McGarr, 1991]. Depletion and recharge from precipitation is seasonal, with most rapid depletion during the summer agricultural growing months and the most rapid recharge during the winter and spring. Annual fault-normal seasonal stress variations on the San Andreas fault zone from this source are calculated to be ~0.001 MPa, encouraging earthquakes during the summer and autumn months. The expected seasonality in seismicity is seen in earthquakes with $M > 1.25$. The stress rate calculated is similar to that calculated for the Main Himalayan Thrust from dewatering the adjacent agricultural area [Kundu *et al.*, 2015].

A similar process was suggested to modulate seismicity in the Gran Sasso chain in the central Apennines, Italy [Bella *et al.*, 1998]. There, tunneling for construction of a highway in the period 1970-1986 was observed to significantly change the hydrology of natural springs. Changes in the spatial pattern of local seismicity, an increase in seismic rate, and the occurrence of three $M > 3$ events were postulated to be linked to the hydraulic changes. In addition, Klose [2007b] attributes the 1989 M_L 5.6 Newcastle, New South Wales, Australia, event to the dewatering of deep coal mines bringing a local fault closer to failure.

3.2 Mining

Deep mine excavations strongly perturb the stresses in surrounding rocks and may reduce some components from values initially of the order of 100 MPa to atmospheric. The resulting stress differences can exceed the strength of competent rocks and cause earthquakes. These are traditionally known as “rock bursts” or “coal bumps”.

In modern times excellent seismic data have been recorded on dense, multicomponent arrays installed for hazard mitigation purposes. Propagation paths are short, through homogeneous rock, and free from the effects of weathering that degrade surface observations. Significant advances in understanding the source physics of earthquakes have been achieved using these data. In particular, it has been shown that many mining-induced earthquakes have net implosive source mechanisms, consistent with partial closure of the artificial voids created by the removal of mass [*e.g.*, Feignier & Young, 1992; Kusznir *et al.*, 1982; Rudajev & Sileny, 1985; Wong & McGarr, 1990; Wong *et al.*, 1989]. A detailed review of this aspect of mining seismicity is given by Miller *et al.* [1998b, Section 3.4].

3.2.1 Traditional mining

In recent years mining has delved progressively deeper and removed progressively larger masses. The increasing demand for coal and other minerals requires, in the absence of other

solutions, that this trend continues. The problem of mining-induced earthquakes is thus likely to grow with it unless management solutions are found.

Seismicity of this sort may be disproportionately serious because of the large loss of life and economic resources caused. This includes environmental damage such as surface subsidence which may render buildings beyond repair. Dealing with, and mitigating, mining-induced seismicity is likely to be a major technical challenge, and even a limiting factor, to the industry in future [*e.g.*, Tang *et al.*, 2010].

During the ~50-year period 1949-1997, over 2000 coal bursts occurred in 33 mines in China, killing several hundred people and costing > 1300 days in lost production [Tang *et al.*, 2010]. Figure 25 shows the distribution of state-owned coal mines and mining-induced seismicity in China. In 2007 some 102 coal mines and 20 other mines reported seismicity.

Li *et al.* [2007] report that seven of these were associated with events of $M > 4.0$ and 27 with events of $M \geq 3.0$. Earthquakes are shallow, occurring in the depth range 0-7 km. The largest coal mining event that has occurred in China is the 1977 M_L 4.3 event at Taiji mine, Beipiao, Liaoning [Li *et al.*, 2007]. Coal mining in China is increasing in depth of extraction and volume removed, and the problem of mining-induced seismicity is increasing also (Figure 26 and Figure 27).

One of the most spectacular cases of mining-induced seismicity occurred in 1989 in the Volkershausen Ernst Thaelmann/Merkers potash mine, Germany. An event with M_L 5.6 [Bennett *et al.*, 1994; Knoll, 1990] was associated with the collapse of ~3,200 pillars throughout an area of ~6 km^2 in the depth range 850-900 m. A large part of the local town of Düren was devastated, including several hundred buildings damaged and 19 totally destroyed. Three people are reported to have been killed and several injured. Seismic records suggest a multiple event involving three main sub-events with magnitudes of M_L 4.4, 5.1 and 5.5. The M_L 5.5 event was attributed in part to the injection of fluid waste which had increased pore pressure by ~0.3-1.1 MPa. The event was classified as a fluid-induced rockburst involving an earthquake in the overlying rock which induced collapse of the pillars [Knoll, 1990].

An unusual case that involved litigation over the cause of a fatal mine-related earthquake is that of the 2007 M_W 4.1 Crandall Coal Mine, Utah, event. Nine miners and rescuers were killed as a result of a gallery collapse. The cause of the collapse was variously attributed to triggering by a natural earthquake or unsafe back-stripping mining practices. The controversy was resolved by calculating the seismic moment tensor using recordings from regional seismic stations. The study showed that the focal mechanism was not consistent with shear slip on a fault, as would be expected for a natural earthquake, but with a rapidly closing crack, as would be expected for a gallery collapse (Figure 28) [Dreger et al., 2008]. The following year, the US Mine Safety and Health Administration levied fines totaling $1.85 million for unsafe mining practices at Crandall Coal Mine.

3.2.1.1 UK mining-induced earthquakes

The UK has a long history of mining dating from the Neolithic period that includes flint, lead, copper, coal, tin mining in Cornwall and gold mining in Wales (Figure 29). Over the last couple of centuries coal mining became a major industry. At the height of this industry, in 1913, 292 million tonnes of coal were extracted from 3024 mines, some of which were excavated to a depth of ~1200 m and even extended several kilometers offshore beneath the

North Sea[3,4]. In our database we have included the largest-magnitude earthquake recorded in each major UK coalfield.

Wilson *et al.* [2015] review earthquakes in the UK with the objective of determining a national baseline of seismic activity in advance of possible future shale-gas hydrofracturing. They use the earthquake database of the British Geological Survey. Of the ~8000 onshore British earthquakes in that catalogue for the period 1970-2012 they estimated ~21% to have been anthropogenic, the majority caused by coal mining (Figure 30). The correlation between coal production and earthquakes is shown in Figure 31 [Wilson *et al.*, 2015]. This is an interesting case history because it shows the effect on seismicity of a major reduction in coal production during the 1984-85 miners' strike. The economic cost of that strike is estimated to have been several billion pounds. The earthquake rate returned to a level corresponding to coal production following the end of the strike in the spring of 1985.

3.2.1.2 South African mining-induced earthquakes

The region that is perhaps the most renowned for large mining-induced earthquakes is South Africa. There, two of the world's richest ore bodies are mined–the gold-bearing conglomerates of the Witwatersrand Basin and the platinum-bearing pyroxenites of the Bushveld Complex. Both bodies extend to depths of several kilometers, and mining depths exceed 3.5 kilometers [Durrheim, 2010]. The current regional stress field is extensional but tectonically inactive. Mining-induced earthquakes are thought to result from collapses of up to ~1 m in the vertical. These collapses contract galleries in the form of horizontal tabular voids for up to several kilometers of their lengths. Earthquakes with magnitudes up to m_b 5.6 have occurred (the President Brand mine, Welkom, in 1994).

The problem of induced seismicity in South Africa became apparent early in the 20th century when large-scale mining penetrated to depths of several hundred meters. It is now a major issue and in recent decades great efforts have been made to mitigate the risk. These include development of the safest possible mining techniques, optimal design of equipment, and seismological monitoring. As a result, fatality rates have been reduced though they still run to several tens of deaths per year. A large body of literature has been published on the subject [*e.g.*, Amidzic *et al.*, 1999; Boettcher *et al.*, 2015; deBruyn & Bell, 1997; Durrheim, 2010; Durrheim *et al.*, 2013; Durrheim *et al.*, 2006; Heesakkers *et al.*, 2005; Jaku *et al.*, 2001; Julià *et al.*, 2009; Kozlowska *et al.*, 2015; Lippmann-Pipke *et al.*, 2011; Milev & Spottiswoode, 2002; Richardson & Jordan, 2002; Wright *et al.*, 2003; Yabe *et al.*, 2015; Ziegler *et al.*, 2015].

An example of a serious earthquake is a M_L 4.0 event that occurred in Western Deep Levels East gold mine in 1996. It nucleated in complex geology ahead of actual mining, and extensively damaged the area. Work at the time involved removing a large pillar formed by earlier, smaller-scale mining. This damaging earthquake had a significant impact on mining techniques and adherence to safe practice, and resulted in improved seismicity management strategies [Amidzic *et al.*, 1999].

---

[3] https://www.gov.uk/government/statistical-data-sets/historical-coal-data-coal-production-availability-and-consumption-1853-to-2011

[4] http://www.dmm.org.uk/mindex.htm

An even larger event, with M_L 5.3, occurred in the Klerksdorp district of South Africa in 2005. This earthquake caused serious damage to the nearby town of Stilfontein, injuring 58 people. Two mineworkers in a nearby gold mine were killed and thousands of others were evacuated. This large earthquake was attributed to stress loading by past mining, rather than the mining then ongoing [Durrheim *et al.*, 2006]. The case highlighted the issue of insufficiently well-documented past mining activities, a problem for all nations with long traditions of mining. It also raised the question of whether earthquakes induced by one industrial project could present hazard to others nearby. Furthermore, its delayed occurrence suggested that seismic hazard may remain a problem not only during deep mining but beyond mine closure.

Because of the problem that induced seismicity poses in deep South African gold mines, state-of-the-art monitoring networks have been installed. These networks have gathered unusually high-quality data which have enabled some remarkable advances in seismological techniques and knowledge. McGarr [1992b] derived full moment tensors for 10 Witwatersrand mining-induced earthquakes with magnitudes M 1.9-3.3. The earthquakes formed two distinct types. Seven involved substantial coseismic volumetric reduction combined with normal faulting and three had no significant volumetric component. McGarr [1992b] concluded that those with volumetric components involved interaction between a mine stope and a shear fault.

These conclusions were confirmed by later workers. Julià *et al.* [2009] obtained focal mechanisms for 76 mine tremors with M 0.5-2.6 that occurred at the deep AngloGold Ashanti Savuka gold mine. These events were recorded on 20 high-frequency geophones in the mine. The largest principal stress was vertical and was relieved by a combination of volumetric closure and normal faulting, consistent with the vertical closure of galleries. Richardson and Jordan [2002] studied seismicity associated with five deep mines in the Far West Rand district using data recorded in the period 1994-2000 by in-mine arrays of three-component sensors. Seismic rates exceeded 1,000 events per day. Some earthquakes occurred within 100 m of active mining faces or development tunnels, and were generally $M < 1$. They attributed those events to the response to blasting, stress perturbations from the excavation, and closure of individual stopes. Other events were distributed throughout the active mining region. Some had magnitudes of $M > 3$, and appeared to be similar to regional tectonic earthquakes.

3.2.2 Solution mining

Solution mining, or "in-situ leaching" recovers minerals via boreholes drilled into the deposit. A lixiviant–a liquid used to dissolve the target mineral–is pumped into the resource via an injection borehole. It circulates through the rock dissolving the mineral and is extracted via a production well. The lixiviant may be water (*e.g.*, to extract salt), or acid or sodium bicarbonate to extract metals, *e.g.*, uranium, copper, gold or lithium. Roughly half the world's uranium is produced by solution mining.

Our database contains eight cases of seismicity postulated to be associated with solution mining. The best-documented is from the Vauvert Field, France. There, brine is produced from a layer comprising ~50% salt at 1900-3000 m depth (Figure 32). Water is circulated through fractured zones via a well doublet. Some, but not all, of the cavities created dissipate by salt creep. Earthquakes occur where this process cannot keep up with mass removal. Additional seismicity results from hydraulic fracturing used to create porosity. Over 125,000

earthquakes with M -3 to -0.5 that occurred in the period 1992-2007 have been located [Godano *et al.*, 2010].

Larger earthquakes are reported for solution mines in the USA. There, three cases are documented from Attica (New York), Cleveland (Ohio), and Dale (New York). Of three M_L ~5 events that occurred near Attica, in 1929, 1966 and 1967, two had estimated hypocentral depths as shallow as 2-3 km [Herrmann, 1978]. They are postulated to have been induced by local salt solution mining, though this was not recognized at the time [Nicholson & Wesson, 1992].

In China, a M_L 4.6 earthquake is reported to have occurred in 1985 in association with solution mining of salt from depths of 800–1800 m at the Zigong salt mine, Sichuan Province [Li *et al.*, 2007]. This earthquake is reported to have induced the highest intensity of ground shaking observed for any mining-induced earthquake in China. It is the largest-magnitude mining-related event in any kind that is known from China.

At Mishraq, Iraq, earthquakes occurred in association with the mining of sulfur by injecting hot (~150˚C) water at pressures of 0.6-0.8 MPa into layers up to 190 m deep [Terashima, 1981]. Rapid surface subsidence occurred–up to several mm/day–and resulted in surface cracking. Felt earthquakes occurred 1973-1975 and were most numerous at times of high injection rate.

3.2.3 Tunnel excavation

We have identified 20 case histories of earthquakes accompanying the excavation of tunnels and cavities built for purposes that include power-station housing (*e.g.*, the underground powerhouse of the Pubugou, China hydroelectric station), water transport at hydro-electric and nuclear power stations (*e.g.*, the Yuzixi hydro-electric station, China, and the Forsmark nuclear plant, Sweden), road and railway transport (*e.g.*, the Ritsem tunnel, Sweden, and the Qinling railway tunnel, China) [Tang *et al.*, 2010].

A particularly well-documented illustrative example is the case of the Gotthard Base Tunnel, Switzerland, part of the New Alpine Traverse through the Swiss Alps [Husen *et al.*, 2012]. This 57-km-long tunnel was excavated for freight and passenger rail transport in the period 2002-2006 using drilling and blasting. It includes three Multi-Function Stations (MFSs) which divide the tunnel into five sections.

A series of 112 earthquakes with M_L -1.0 to 2.4 occurred 2005-2007 in association with excavation of the southernmost station, MFS Faido. The largest event was shallow (0.5-1.0 km below the surface) and felt strongly at the surface. No surface damage was reported. The station cavity was, however, damaged significantly including flaking of the reinforced walls and upwarping of the floor by ~0.5 m. The seismicity correlated spatially and temporally with excavation of the station (Figure 33 and Figure 34). Highly accurate locations obtained using a dense, temporary seismic network showed that, on average, the earthquakes occurred at the same depth as the tunnel. Some correlated with large rockbursts observed in the tunnel shortly after blasting.

The focal mechanism of the largest earthquake indicated normal faulting on a steep fault plane belonging to the fault system mapped locally. An estimate of the source dimensions suggested a failure region 50-170 m long. The tunnel traverses mostly igneous and metamorphic rocks, but it also crosses a complex of structures with different rheological

properties, including faulted and heavily fractured sections. Two-dimensional discontinuum modeling suggested that the earthquake activity resulted from an unfavorable juxtaposition of rocks with different rheologies combined with a fault zone. The horizontal stresses imposed by the excavations were relieved by shrinking of the tunnel which reactivated the fault zone.

3.3 Hydrocarbons

Reviews of induced seismicity associated with hydrocarbon production are provided by Suckale [2009; 2010]. There are ~ 67,000 hydrocarbon fields worldwide [Li, 2011] including ~ 1500 giant and major fields, and of the order of a million producing oil and gas wells. The seismic response to hydrocarbon production varies from field to field and no seismicity is reported for the vast majority. It is, however, unclear how complete reporting is. Many fields are not instrumented and it is thus inevitable that cases of seismogenesis go unpublished and even unnoticed (Section 8.1). Earthquakes account for only a small percentage of the deformation associated with reservoir compaction with the majority being taken up by ground subsidence or counteracted by fluid recharge from the sides. In many cases the earthquakes reported occurred on faults that were either not known before or considered to be tectonically inactive.

3.3.1 Gas

We have identified 36 cases of seismicity postulated to have been induced by extraction of natural gas from reservoirs. These cases are from Canada (1 case), China (1 case), France (2 cases) Germany (7 cases), Italy (1 case), the Netherlands (18 cases), Oman (1 case), the USA (4 cases) and Uzbekistan (1 case). By far the most numerous are from The Netherlands, which accounts for 50% of all cases we found.

Worldwide, the most extreme case of earthquakes induced by gas production is that of the Gazli reservoir, Uzbekistan. In 1976 and 1984, three M_S ~7 earthquakes occurred, seriously damaging the local town of Gazli and causing one death and ~100 injuries [Simpson & Leith, 1985]. An additional M_S 5.7 event occurred in 1978. A timeline of events is as follows:

- 1956 the field was discovered;
- 1963 pipelines to the Urals industrial region were completed;
- 1966 production of ~20 billion m^3/year of gas began. Reservoir pressure was initially ~7 MPa;
- 1968-71 production peaked;
- 1976 pressure had declined to 3-3.5 MPa; two M_S ~7 earthquakes occurred;
- 1978 a M_S 5.7 earthquake occurred;
- 1984 a third M_S ~7 earthquake occurred;
- 1985 pressure had declined to 1.5 MPa.

During the period when gas was produced it was drawn from a reservoir at a depth of ~2 km, hosted in an open anticline of tight Paleogene sandstones. This structure is cut by several blind faults and the M_S ~7 earthquakes are thought to have occurred on one of these (top panel, Figure 35). The epicenters of the events formed an arcuate array north of the field. Fault-plane solutions suggest that they occurred on a north-dipping, approximately east-west striking thrust fault, consistent with the tectonics of the region. Extrapolation of this fault to shallow depth suggests that it intersects with the gas reservoir (bottom panel, Figure 35).

In addition to this geometric correspondence, Simpson and Leith [1985] cite four indications that these events, although exceptionally large, were induced:

- previous seismic quiescence;
- the anomalous magnitude distribution of events which involved three M_S ~7 events rather than a clear mainshock-aftershock sequence;
- the large decrease in pressure in the gas reservoir; and
- source modeling that indicated that, unusually, rupture propagated downwards on the fault plane.

The proposal that these earthquakes were induced has nevertheless been challenged, *e.g.*, by Bossu *et al.* [1996], on the grounds that the stress perturbation on the fault was too small to have triggered such large earthquakes.

Possible analyses of this case are limited because details available about the recovery procedure are sparse. However, the case of Gazli is important because of its serious implications for the possible maximum magnitude of earthquakes that could conceivably be induced by gas extraction.

The largest earthquake postulated to have been induced by gas extraction in Europe is the 1951 M 5.5 event that occurred in the Caviaga Gasfield, Po Valley, Italy. There, large-scale extraction of methane at pressures > 10 MPa had been underway. The earthquake cannot be well studied because of the limited instrumentation in place at the time. Crude analysis of paper recordings of the largest, M_L 5.5, event suggested that it nucleated at ~5 km depth and had a thrust mechanism. The region where it occurred had previously been aseismic [Caloi *et al.*, 1956].

The case of Caviaga is the only $M \geq 5$ gas-extraction-induced earthquake reported for Europe. Several other European gas-extraction projects are associated with $M \geq 4$ seismicity. A case of abundant seismicity is the Lacq Gasfield, France, which has generated earthquakes with magnitudes up to M_L 4.2 (Figure 36). A full review of > 2000 earthquakes located there in the period 1974-1997 is given by Bardainne *et al.* [2008].

Production at Lacq started in 1957 with extraction of gas from a reservoir at a depth of 3.2-5 km, beneath a 600-m-deep oilfield. The reservoir occupies a 20-km-long, densely fractured anticline in Mesozoic limestones sealed by a Cretaceous marl (Figure 37) . Reservoir pressure decreased from 66 MPa to 2.3 MPa in the period 1957-2008 and surface subsidence of ~6 cm occurred.

The first earthquake noticed, which had an estimated magnitude of M 3-4, was felt in 1969 after the gas pressure had declined to 36 MPa. This, and the seismicity that followed, is unlikely to be natural because of its concentration in the gasfield and because Lacq is 30 km north of the nearest major seismically active structure, the Pyrenean Frontal Thrust (Figure 36). About 70% of the earthquakes located above the gas reservoir. They nucleated preferentially on faults optimally-oriented with respect to the poroelastic stress perturbation caused by gas removal. Poorly oriented faults tended to be aseismic. There is poor correlation between the surface subsidence and the seismicity with both seismic and aseismic regions subsiding. During the observation period, seismicity migrated from the centre to the periphery of the reservoir (Figure 38). Comparison of the spatial distribution of hypocenters

with theoretical deformation models favored the model of Odonne et al. [1999] rather than that of Segall [1989] (Figure 39).

Seismicity induced by gas extraction is particularly abundant in The Netherlands. There, ~300 gasfields are produced. Of these, just a few percent are reported to be seismically active but on a global scale this is an exceptionally high rate of reported seismogenesis. The induction mechanism is thought to be differential compaction [Gee *et al.*, 2016].

One of the largest earthquakes to be attributed to induction in The Netherlands to date is the 2012 Groningen M_L 3.4 event. In addition to this a further 8 events with M > 3.0 have occurred in that field (Figure 40). Seismicity was first recorded in December 1991 when the reservoir reached ~28% depletion, some 28 years after the start of gas extraction in 1962 (Figure 41).

Historically, The Netherlands had a low rate of natural seismicity compared with neighboring countries where much higher rates are associated with the Upper Rhine Graben (Figure 42 and Figure 43) [van Eck *et al.*, 2006]. Today, the vast majority of seismicity in the northern Netherlands is associated with gas extraction. Several hundred earthquakes have been recorded in the Groningen Field alone. This reservoir, the largest natural gasfield in Europe and the tenth-largest in the world, originally contained some 3 x 10^9 m^3 of gas in a porous sandstone formation up to 300 m thick and 45 x 25 km in area. Both the seismic rate and the magnitudes of the largest earthquakes have increased on a time scale of a few years (Figure 41 and Figure 44). An apparent increase in the slope of the Gutenberg-Richter distribution (the "*b*-value") with time is consistent, however, with a progressive reduction in the proportion of large to small earthquakes (Figure 45 and Figure 46) [van Eck *et al.*, 2006; Van Wees *et al.*, 2014]. Reservoir compaction is greatest in two northwesterly trending zones of the reservoir and the earthquakes correlate well with the southernmost of these (Figure 47).

A renowned case of seismicity induced by gas extraction in the USA is that of the Fashing Gasfield, Texas (Figure 48). Production there started in 1958 from a depth of 3.2 km. By 1983 the pressure had decreased by ~7 MPa and a M 3.4 earthquake occurred (Figure 49). The reservoir was replenished by water recharge as it became depleted and injection was undertaken for disposal of produced water. In 1992 a M 4.3 earthquake occurred and in 2011 the largest event, with M_W 4.8. This case is usually discussed jointly with the nearby Imogene Oilfield (Section 3.3.2).

3.3.2 Oil

In many oilfields multiple processes are underway including both oil and gas extraction, waste-water disposal, water injection to aid oil recovery and hydrofracturing or thermal fracturing. It is thus often difficult to unambiguously attribute associated seismicity to oil extraction alone (Section 1.7). Nevertheless, we have identified eight cases where earthquakes have been postulated to be associated with oil extraction. These are from the USA, Iran, Russia and Norway. The total is extraordinarily few compared with the large number of producing oilfields worldwide (Section 3.3).

One of the earliest reports of earthquakes accompanying oil production is from Goose Creek, Texas, where a series of slight earthquakes was reported in the 1920s (Figure 50). This field is remarkable for the major surface subsidence that occurred there. Following the extraction of several million barrels of oil an area ~10 km^2 in size subsided by up to 1 m over an ~8-year period [Nicholson & Wesson, 1992; Pratt & Johnson, 1926]. A substantial part of this

coastal area sank below sea level and industrial infrastructure had to be adapted to the flooded conditions.

The largest earthquake in our database attributed to oil extraction is the M_W 6.2 1983 Coalinga, California, event. This event, along with the 1985 M_W 6.1 Kettleman North Dome earthquake and the 1987 M_L 5.9 Montebello Fields (Whittier Narrows) earthquake, both also in California, were attributed by McGarr [1991] to the removal of oil from fields in uplifting anticlines. The Coalinga and Whittier Narrows events were felt throughout much of California and caused multiple deaths and injuries (Figure 51).

All three events nucleated at ~10 km depth. McGarr [1991] suggested that net extraction of oil and water reduced the average density of the upper crust, and that the seismic deformation was approximately equal to that required to restore isostatic equilibrium (Figure 52). This suggestion was challenged by other workers. Segall [1989] calculated stress loading and concluded that depletion of the reservoir would have only loaded the nucleation region by ~0.01-0.03 MPa. Nicholson and Wesson [1992] suggested an alternative explanation, that the earthquake might have occurred in response to larger stresses imposed by fluids migrating into the mid-to-lower crust. They suggested that changes in pressure resulting from withdrawal of oil might have induced such fluid migration and brought the fault closer to failure. It has also been suggested that the Coalinga earthquake was induced by extraction of groundwater for irrigation purposes from the nearby San Joaquin valley (Section 3.1) [Amos *et al.*, 2014]. A further suggestion is that the Coalinga earthquake contributed to stress buildup that was released six years later in the 1989 M_W 6.9 Loma Prieta earthquake. This event ruptured a section of the San Andreas fault system 96 km south of San Francisco and caused 63 deaths, 3,757 injuries and $5.6–6 billion of damage [Reasenberg & Simpson, 1992].

Another major damaging earthquake suspected to be associated with oil extraction in California is the 1933 M_L 6.3 Long Beach, California, earthquake which killed > 100 people and did $40 million of damage. This earthquake may have resulted from oil production in the nearby Wilmington and Huntington Beach Oilfields (Section 4.1.3) [Nicholson & Wesson, 1992].

An example where there is little dispute that earthquakes were primarily induced by oil extraction is from the Imogene Oilfield, Texas [Pennington *et al.*, 1986]. This field lies just ~25 km from the seismogenic Fashing Gasfield (Section 3.3.1; Figure 48). In 1984 a M_L 3.9 earthquake occurred in the Imogene Oilfield, followed by aftershocks located at 2-3 km depth at or near the reservoir bounding fault.

The Imogene Oilfield is contained in Cretaceous limestone and bounded by high-angle faults that splay at shallow depth. Production of oil began in 1944 from a 33-m-thick horizon at 2.4 km depth. By 1973 reservoir pressure had dropped from an initial 25 MPa to ~10 MPa. In the period 1972-1978 it was flooded with 55,000 m^3 of water via injection wells in an effort to mitigate this pressure reduction. This is, however, a much smaller volume than the ~ 1 million m^3 of oil and gas that had been produced, and flooding ceased several years before the 1984 earthquake. As a consequence, the seismicity has been attributed to depressurization of the field resulting from oil depletion.

The most spectacular example of subsidence and induced earthquakes associated with a producing oilfield is from the Wilmington Field, California, one of the largest oilfields in the USA (Figure 53 and Figure 50). Oil production began in 1936 and over the following 30

years up to 9 m of subsidence and 3.6 m of horizontal contraction occurred. Strain rates were > 1000 times greater than those along locked sections of the San Andreas fault [Kovach, 1974; Segall, 1989].

Seismicity onset above and below the reservoir when the reduction in pressure reached ~10 MPa. Eight earthquakes with magnitudes of M_L 2.4-5.1 occurred on shallow, low-angle bedding planes in the field. The largest, which occurred in 1949, sheared off hundreds of production wells causing > $9 million of damage. An area of ~ 5.7 km^2 was affected and ground deformation of up to 20 cm occurred. Because the event was so shallow, surface waves were generated [Nicholson & Wesson, 1992; Segall, 1989].

Seven of the eight earthquakes occurred during the oil production period and one occurred after significant water flooding began in 1958 to mitigate the subsidence. No further earthquakes occurred in the field after 1961 and subsidence had been arrested by 1966. This is a case where seismicity may have been stopped by the introduction of fluids rather than induced.

Despite the large quantities of oil produced from the Middle East, we have found only two accounts of earthquakes postulated to have been induced by oil extraction there. One reports hundreds of earthquakes with magnitudes up to M_L 4.24 in the Uthmaniyah-Hawaiyah and Haradh production divisions of the Ghawar oil/gas, Saudi Arabia. These earthquakes occurred below the production divisions and are attributed to hydrocarbon fluid extraction. Focal mechanism solutions and structural cross-sections suggest the active elements are crust-penetrative basement faults [Mogren & Mukhopadhyay, 2013].

The other example is from Kuwait, where 465 earthquakes are reported to have occurred in the period 1997-2007 with M 0.3-4.3. A large percentage locate in the oilfields, including the Sabiriyah, Raudhatain, Bahra, Minagish, Umm Gudair, Wafra, Abduliyah and Dharif Fields (Figure 54). It is considered likely that at least some of this seismic activity is associated with oil extraction [Al-Enezi *et al.*, 2008]. The largest event proposed to be related to Middle Eastern oilfields is the 1993 M 4.7 event in Kuwait. It was suggested that it was induced by the gushing and burning of oil wells by Iraqi armed forces leading to rapid pore pressure reduction and changes in subsurface stress [Bou-Rabee & Nur, 2002].

3.4 Geothermal production (heat/fluids)

Small, natural earthquakes are common in wet, high-temperature geothermal areas, and were known in Iceland as “hverakippur” long before they were studied scientifically. They are likely caused in part by active tectonics in plate-boundary zones and volcanoes, and in part by natural geothermal heat loss. This causes cooling and contraction of the geothermal heat source and stress is relieved by rock fracturing with a component of tensile failure. Both the opening and closing of voids have been identified seismically [Foulger, 1988a; b; Foulger & Long, 1984; Foulger *et al.*, 1989; Miller *et al.*, 1998a; Miller *et al.*, 1998b; Ross *et al.*, 1999]. It is to be expected that production from geothermal fields by the extraction of hot fluids will enhance the natural fluid- and heat-loss process and increase seismic rates.

It is, however, often difficult to attribute confidently earthquakes in an exploited geothermal areas to a particular process because they could result from production, re-injection or natural tectonic loading and heat loss. There is also the possibility that they are induced by natural recharge, either by shallow, cold groundwater or deep, hot water. Our database contains only six cases where earthquakes are postulated to have been associated with geothermal

production. These cases are the Cerro Prieto Field, Mexico [Glowacka & Nava, 1996], the Reykjanes and Svartsengi Fields, Iceland [Keiding *et al.*, 2010], Larderello, Italy [Batini *et al.*, 1985], The Geysers, USA [Eberhart-Phillips & Oppenheimer, 1984] and Olkaria, Kenya [Simiyu & Keller, 2000].

The largest earthquakes proposed to have been induced by geothermal production are the strike-slip events in the Imperial Valley (1979, M_L 6.6), Victoria (1980, M 6.1), and Cerro Prieto (1987, M 5.4) (Figure 55). Glowacka and Nava [1996] base this proposal on qualitative correlations between increases in sustained fluid extraction and periods of increased seismic moment release, with delays of ~1 year (Figure 56).

Electrical power production at Cerro Prieto began in 1973. A mixture of steam and water with temperatures of 250-350˚C is produced from depths of 1500-3000 m. In the period 1973-1996 > 1 km^3 of fluid was extracted. The region is part of the plate boundary between the Pacific and North American plates and the tectonics are dominated by the strike-slip Imperial fault which has a history of M > 6 earthquakes. Glowacka and Nava [1996] found that the numerical data are insufficient to support statistically a correlation between production and the large earthquakes but argue that pore pressure decreases in the geothermal field, which amounted to a few MPa, were sufficient to have triggered them. Earlier, Majer and McEvilly [1981; 1982] suggested, on the basis of data from local, temporary seismic network deployments, that earlier increases in production at Cerro Prieto correlated with increases in the rate of small earthquakes.

An example from Iceland where correlation between geothermal production and earthquakes has been proposed is from the Reykjanes and Svartsengi geothermal areas on the Reykjanes Peninsula [Keiding *et al.*, 2010]. These areas, which lie on the spreading plate boundary where it first comes on land in southwest Iceland, were studied intensively using Interferometric Synthetic Aperture Radar (InSAR) and GPS data from 1992-2009. Deformation detected was concluded to be associated with extension along the plate boundary and ~5 cm yr^{-1} of subsidence resulting from geothermal fluid extraction. Swarms of earthquakes with magnitudes up to M_L 4.1 occurred on the flanks of the rifts within which the geothermal areas lie. The events were postulated to have been induced by stress changes brought about by geothermal fluid extraction (Figure 57). This area is naturally seismically active since it comprises part of the spreading plate boundary, so it is not possible to rule out a tectonic origin for many of these earthquakes.

The case of The Geysers geothermal field, California, is complex. It is a vapor-dominated field and has been exploited for over 150 years, including generating electricity. It is intensely seismically active (Figure 58) and seismicity was recorded even before large-scale fluid injections began (Figure 59). Very likely the pre-injection seismicity, and some current seismicity, is production-related [Eberhart-Phillips & Oppenheimer, 1984]. It is problematic to distinguish production- from injection-related seismicity there currently, however, because both processes are going on simultaneously. In general over the last 50 years or so, the seismic rate as a whole appears to correlate grossly with injection. Seismicity at The Geysers is discussed in more detail in Section 4.1.5.

3.5 Extraction: Summary

Mining is by far the commonest cause of extraction-related induced earthquakes and contributes 267 cases to our database (Figure 60). The second most common postulated causative process is water reservoir impoundment, which contributes 168 entries. Five cases

relate to groundwater and six to geothermal resources. The largest earthquakes postulated to be induced by subsurface extraction are the M_W 7.8 Gorkha, Nepal, earthquake, the M_L 6.1 Bachatsky, Russia, earthquake, the M_S 7.3 Gazli, Uzbekistan earthquake and the M_L 6.6 Cerro Prieto, Imperial Valley, Mexico, earthquake.

In the case of groundwater-withdrawal cases, some extraordinarily small stress changes have been postulated to induce events–as small as 0.001 MPa [*e.g.*, for the 2015 M_W 7.8 Gorkha, Nepal, earthquake; Kundu *et al.*, 2015]. This small compared with Earth tides (Section 8.3). The ability of such small stresses to induce earthquakes is theoretically in keeping with the self-similar, critical earthquake nucleation process. However, such small effects may be comparable to many other natural and anthropogenic processes such as weather and the expansion of cities.

We summarize postulated gas-extraction induced earthquakes in Figure 61 which shows M_{MAX} for the 35 cases of where this parameter is reported. There is a continuous spectrum of sizes with the exception of the M_S 7.3 Gazli, Uzbekistan, event, which is 1.8 magnitude units larger than the second largest case.

Although oil extraction removes extremely large masses from the crust, we found surprisingly few cases of induced earthquakes. Possible reasons for this are:

- the process is only weakly seismogenic, perhaps because natural aquifer influx (peripheral or bottom water) partially replaces mass extracted;
- under-reporting; and
- ambiguity of process, since fluid injection is often done simultaneously with production.

For geothermal fields, Figure 62 shows a histogram of numbers of seismogenic power-producing fields ranked by size [data from Bertani, 2010]. It is clear that the larger the geothermal operation the more likely it is to induce earthquakes.

4 Injection into the subsurface

The burgeoning issue of injection-related earthquakes was recently highlighted by Ellsworth [2013] who pointed out the recent dramatic increase in earthquake rate for $M \geq 3$ events in the central and eastern USA. More than 100 such earthquakes occurred annually, on average, in the period 2010-2012 compared with just 21 events/year on average for the period 1967-2000. Despite the problem of incomplete reporting, our database shows that the trend toward increasing incidence of injection-related earthquakes is a broad international one and not confined to the USA.

Diverse fluids are injected into the ground for diverse reasons that include (Table 2):

- solution mining (Section 3.2.2);
- disposal of unwanted by products;
- enhancing oil recovery;
- fracturing rock (i.e. the very process that causes earthquakes);
- research into the earthquake nucleation process;
- underground heat storage by way of injection of hot water from waste heat processes;
- underground storage of natural gas, hydrogen and compressed air; and

- CO_2 geostorage to reduce emissions.

In addition, passive groundwater inflow may occur when reservoirs are produced or pumping to suppress groundwater levels is abandoned in mines.

Table 2: Classification categories of underground injection wells in The Code of Federal Regulations of the USA (40 CFR 144.6-Classification of wells)[5].

Class of well	Purpose
Class I	Industrial and Municipal Waste Disposal Wells
Class II	Oil and Gas Related Injection Wells
Class III	Injection Wells for Solution Mining
Class IV	Shallow Hazardous and Radioactive Injection Wells
Class V	Wells for Injection of Non-Hazardous Fluids into or Above Underground Sources of Drinking Water
Class VI	Wells Used for Geologic Sequestration of CO_2

Our database contains 180 projects where injections have been postulated to induce seismicity and includes examples of most of the above processes. Whereas in general, the removal of mass from the crust is expected to reduce the normal stress that prevents slip on faults, the introduction of fluids into faulted rock is expected to increase the pore pressure that encourages failure. Both these changes thus, capriciously, are predicted to induce earthquakes. In the case of injections, in addition to the hazard induced earthquakes pose to people and infrastructure there is the added risk that if the target formation or its caprock are ruptured by the direct or indirect effects of earthquakes, the injected fluid might escape. This could add to hazard, for example, where the injectate is polluted water, natural gas or CO_2.

4.1 Liquid

4.1.1 Military waste

Our database contains only one case where seismicity is postulated with a high degree of confidence to result from the injection of military waste. This is the legendary case of the so-called Denver earthquakes. Although not the first earthquakes to have been recognized as induced by human activity, they did result in widespread awareness both in the seismological community and the general public that human activity can induce earthquakes.

The incident began in 1961 when the Army Corps of Engineers drilled a 3.7-km deep well into highly fractured crystalline Precambrian basement at the Rocky Mountain Arsenal, northeast of Denver, Colorado [Evans, 1966; Hsieh & Bredehoeft, 1981]. The purpose of the well was disposal of contaminated wastewater which was done by injection into the bottom, unlined, 21 m. Disposal began in March 1962 at pressures ranging from atmospheric to ~ 7.2

[5] https://www.epa.gov/uic/general-information-about-injection-wells#regulates

MPa above formation pressure. In the four-year period up to 1966 a total of 625,000 m^3 of fluid were injected.

Minor earthquakes onset in the Denver area shortly after injection started and by 1967 over 1500 earthquakes, some of which had M 3-4, had been recorded (Figure 63). The correlation between volume injected and frequency of earthquakes, along with epicenters located within 8 km of the well, prompted Evans [1966] to suggest they had been induced.

Although waste disposal ceased in 1966, earthquake activity continued and in 1967 three earthquakes with $M_L > 5$ occurred, causing damage to infrastructure in Denver. Seismicity declined after 1967 and by the early 1980s had essentially ceased. It was interestingly pointed out that the large earthquakes that occurred after the end of injection weakened the temporal correlation between earthquakes and injection and thus the case argued for induction. It was immediately countered, however, that diffusion of the fluid would have continued after injection stopped and could account for the ongoing seismicity [Healy *et al.*, 1968]. This early case significantly increased understanding of the earthquake induction process.

4.1.2 Wastewater disposal

Large quantities of connate brine and/or connate brine mixed with injection water are typically co-produced with oil, especially as fields age. Water-to-oil ratios may exceed 20 [Gluyas & Peters, 2010]. Such produced water is commonly re-injected into depleted oilfields either for simple disposal or to maintain reservoir pressure and promote sweep thus aiding oil recovery. The cold water injected commonly leads to thermal fracturing, especially in low-permeability reservoirs. Indeed, thermal fracturing is a desirable outcome as it allows lower injection pressures (and thus lower pump power requirements and costs) to be used. In California alone there are currently ~2,300 wastewater injection wells.

We have identified 33 cases of induced seismicity specifically attributed to waste fluid injection. Of these, three are in Canada, two from China, one from Italy and 27 from the USA. A case of particular renown is that of wastewater disposal in Paradox Valley, Colorado, so-named because the Dolores River runs transversely across the valley. This case is noteworthy in particular because of the apparently large distances from the injecting well at which some of the postulated induced earthquakes nucleated [Ake *et al.*, 2005; Block *et al.*, 2015; King *et al.*, 2014; Yeck *et al.*, 2015].

At Paradox Valley, brine is injected into a sub-horizontal layer of Mississippian-age limestone at the bottom of a 4800-m-deep well. The objective is to reduce the salinity of Dolores River water and, as a consequence, the Colorado River into which it flows. Salt enters the Dolores River via groundwater inflow of brine ~ 8 times more saline than sea water. To reduce this, the shallow brine is extracted from the ground via nine production wells and re-injected at greater depth into a single disposal well at surface pressures up to 35 MPa [Yeck *et al.*, 2015]. Continuous injection has been underway since 1996. In the following two decades > 5,700 earthquakes surmised to have been induced were located, including a M 4.3 event in 2000 (Figure 64). Some epicenters lie > 10 km from the disposal well, and a few up to ~25 km distant.

A cautionary case where a large earthquake occurred close to critical infrastructure is that of the 1986 M_W 4.9 Painesville, Ohio, earthquake [Ahmad & Smith, 1988; McGarr, 2014; Nicholson *et al.*, 1988]. This event, which was felt in 11 states and parts of Canada, occurred

in Precambrian basement within 17 km of the Perry Nuclear Power Plant on the edge of Lake Erie. There, ground acceleration was as high as 0.23 g.

The injection of 1.2 x 10^6 m^3 of liquid agricultural waste into three wells ~12 km away was implicated. These injections began in 1976 and thus the mainshock and its associated M < 2.5 aftershocks did not onset until a decade after the suspected induction operations began. By then, a pressure increase of 11.8 MPa had been built up at the injection location.

Whether or not the earthquake sequence was induced is controversial. Similar earthquakes occurred in 1906, 1928, 1943 and 1958 (i.e. about every ~20 years) in a zone that includes the 1986 sequence, though most of those older locations are not instrumentally based. It is thus possible the 1986 earthquakes could have been natural. The long delay of seismicity after the start of injection also eroded confidence that the two processes were linked [Hitzman, 2013]. However, the many cases of postulated delayed earthquake induction that have occurred subsequently now render it more plausible that the 1986 Painesville earthquakes were induced.

A European case of earthquakes postulated to have been induced by wastewater disposal is that of the 2012 M_L 5.9 Emilia-Romagna, Italy, earthquake sequence which resulted in 27 fatalities [Cartlidge, 2014]. It was postulated that hydrocarbon exploitation at the Mirandola Field and geothermal exploitation at Casaglia both contributed to the stress changes that caused this earthquake sequence to occur. Because of the serious impact to people and infrastructure a Commission was established to investigate the possibility it was induced [Styles *et al.*, 2014].

The Commission found that there were statistical correlations between the increase of production parameters in the weeks before the earthquakes but that stress changes resulting from reservoir depletion would not have contributed. They concluded that, while it could not be ruled out that the anthropogenic extraction and injection of fluids contributed to activation of the pre-stressed fault system that failed, it was “highly unlikely” that the earthquake sequence had been induced.

A link between injection pressure and induced earthquakes is reported for the Huangjiachang Gasfield, Sichuan Basin, China [Lei *et al.*, 2013]. Few earthquakes occurred there until injection wellhead pressure rose above 2 MPa. After that, more than 5000 M > 1.0 earthquakes occurred close to reservoir depth, the largest with a magnitude of M_L 4.4.

The Sichuan Basin is relatively tectonically stable with only sparse historic seismicity. Gas is contained in shallow, high-porosity limestone/dolomite anticlines of Paleozoic and Mesozoic age. Local faults cross both reservoirs and basement. The Huangjiachang Gasfield itself is small and hosted in a fractured, jointed, karstified Permian limestone formation at a depth of 2500 m. Injection of wastewater began there in 2007 when a production well was converted to an injector. For the first two years, water was introduced under atmospheric pressure and seismic rates were low. In 2009 injection pressures were increased, ultimately reached 2.1 - 2.9 MPa, and seismicity onset.

Particularly vigorous induced seismicity is reported to have been induced by wastewater disposal in the Rongchang Field, also in the Sichuan Basin [Lei *et al.*, 2008]. Earthquakes onset there in 1989, only two months after water injection began. More than 32,000 earthquakes were observed, the largest with M_L 5.2. That event reactivated a thrust fault in

the basement. Earthquake locations suggested that seismic failure occurred in both the reservoir and the basement.

4.1.2.1 Oklahoma

In recent years the issue of induced earthquakes in Oklahoma has become particularly prominent because of an unprecedented surge in seismic rate there that onset in 2009 (Figure 65) [Ellsworth, 2013]. This has rendered Oklahoma the most seismically active state in the USA for earthquakes with M > 3 in the period 2008-2013. Rates exceeded even those of California which hosts the San Andreas fault zone and several seismogenic volcanic and geothermal areas [D. Oppenheimer, personal communication][6]. The seismic rate of Oklahoma also exceeds that of the New Madrid Seismic Zone in Missouri and neighboring states, formerly considered to be the most hazardous intraplate seismic zone in the USA. The largest event since 1950 in the New Madrid Seismic Zone has been M 4.9 whereas in Oklahoma it has been M_W 5.7.

Although faulting in Oklahoma is widespread, only one fault is known to have been active historically. This is the Meers fault, which is thought to have generated M 6.5-7 earthquakes over the last 3,500 years [McNamara *et al.*, 2015]. It was suspected early that Oklahoma might be experiencing earthquakes induced by hydrocarbon-related activities. The injection of water for enhanced oil recovery has been practiced since the 1930s and it has been suggested that the 1952 M ~5.6 event (the El Reno earthquake) was related to the extraction of oil and gas [Nicholson & Wesson, 1992]. Hough and Page [2015] studied the historic rate of earthquake occurrence in Oklahoma by looking at population statistics to see if the population had been sufficiently stable historically for comparable earthquake activity to have been noted in the past. Oklahoma has had a large and well-distributed population from early in the 20th century, suggesting that that knowledge of M ≥4 earthquakes is nearly complete (Figure 66). Industrially induced earthquakes in Oklahoma are thus now essentially beyond doubt.

As is the case elsewhere, multiple industrial processes are underway simultaneously in the hydrocarbon fields of Oklahoma so it is generally difficult to be certain which may have induced any particular earthquake. In addition to hydrocarbon production there are ~7,000 injection wells that are used for:

- the disposal of produced brine (the dominant use);
- enhanced oil recovery;
- hydrofracturing to increase permeability in shale; and
- the disposal of hydrofracture fluid.

Most of the fluid is injected into the Arbuckle Group, a sequence of carbonates and sandstones closely overlying Precambrian crystalline basement (Figure 67).

The largest and most damaging earthquake ever to have occurred in Oklahoma, the 2011 M_W 5.7 Prague earthquake, along with its associated sequence, is relatively unambiguously associated with wastewater disposal into a depleted oilfield [*e.g.*, Keranen *et al.*, 2013]. The Prague earthquake was felt in at least 17 states and in Chicago at a distance of 1,000 km. It

[6] *e.g.*, http://www.nytimes.com/2016/03/29/us/earthquake-risk-in-oklahoma-and-kansas-comparable-to-california.html?_r=0

caused considerable damage to local infrastructure, destroying 14 houses, and injuring two people. It is, to date, the largest earthquake in the world associated with waste-water disposal and led to a re-assessment of both the potential size of injection-induced earthquakes and the delay time following the onset of operations.

Earthquake activity in the Prague area began in February 2010 with a M_W 4.1 earthquake in the Wilzetta Oilfield. This lies within the ~200-km-long Pennsylvanian Wilzetta fault zone (Figure 68). In 2011 this activity culminated in the Prague sequence that included three earthquakes with M_W 5.0, 5.7, and 5.0 (Figure 69) on 5, 6, and 8 November, along with prolific aftershocks. Analysis of hypocentral locations and focal mechanisms using data from 1,183 aftershocks recorded on a dense temporary seismic network clarified the geometry of the hypocentral zone (Figure 70) [Keranen *et al.*, 2013]. Failure comprised strike-slip motion on planes that dip steeply and intersect both the sedimentary layers and the basement. The tip of the initial rupture plane lay within ~200 m of active injection wells at a depth of ~1 km.

In the Wilzetta zone, oil is contained in fault-bounded structural traps that are barriers to fluid migration through the porous limestone host formation. Where the Prague sequence occurred, production had been ongoing since the 1950s but is now at a low level. Three active waste-disposal injection wells which came online in 1993 are in the vicinity (Figure 70). They inject water into sealed rock compartments at ~1.3 - 2.1 km depth.

Over the 17-year period 1993-2011 injection pressure progressively increased from atmospheric to reach 3.6 MPa in 2006. Seismicity is thought to have onset when the injected volume exceeded that extracted from the fault-bounded compartment. Once the compartment had been refilled ongoing injection is thought to have reduced the confining stress on the reservoir-bounding faults which failed as a consequence. More stress was released than corresponds to the total volume injected, so tectonic stress was likely also released. Both injection and $M > 3$ earthquakes continue in the Wilzetta Field at the time of writing.

Figure 71 shows seismicity and oil production in Oklahoma for the last century. Between 2009 and 2014, 26 $M \geq 4$ events occurred in the state. Over 100 $M \geq 3.5$ events occurred in 2014 alone. Monthly statewide wastewater injectate volume has doubled since 1997 [Walsh & Zoback, 2015]. Correlations between earthquakes and injection or production are rare. Figure 69 and Figure 72 show earthquakes and fluid injections for the entire state and for individual study areas. Earthquakes do not correlate with faults and most earthquakes occur in the least faulted part of Oklahoma.

It is thought that faults that fail in general in Oklahoma are those favorably oriented relative to the regional stress direction. Most events occur at depths of 5-6 km in the crystalline basement, on faults of the order of kilometers or tens of kilometers in length. Such faults can maximally sustain M 5-6 earthquakes. Some earthquakes occur on well-known faults that have large seismic potentials and the length of fault activated can be determined from aftershock distributions.

The earthquake activity of Oklahoma exhibits both similarities and differences compared with other examples of induced seismicity. No short-term monthly correlation with injection is apparent and seismicity increased many years after the start of injections, 17 years in the case of the Prague sequence. In this it resembles the case of the Wilmington Oilfield, California, where induced seismicity onset years after water injection began for enhanced oil recovery (Section 4.1.3). However, it is unlike that associated with the Rocky Mountain Arsenal, Colorado (the “Denver earthquakes”; Section 4.1.1) where earthquakes onset almost

immediately after injections began. Induced earthquake sequences do not necessarily start with the largest event, and stress from one induced earthquake may trigger larger subsequent events.

In addition to earthquakes in Oklahoma being induced by hydrocarbon-related operations, they may also be triggered by natural regional earthquakes. Van der Elst *et al.* [2013] studied earthquakes there for time periods following several large, distant earthquakes. A surge in earthquake activity, including a M_W 4.1 event near Prague, occurred following the 27 February 2010 M_W 8.8 Maule, Chile, earthquake (Figure 73). Earthquakes in Oklahoma are thus induced both by anthropogenic and natural processes.

4.1.3 Water injected for enhanced oil recovery

Enhanced oil recovery includes low salinity water injection, water alternating gas injection, injection of water viscosifiers and thermal and chemical methods all of which aim to modify either the viscosity of one or more of the fluids or the surface properties of the host reservoir. Distinguishing earthquakes induced by these processes from events induced by oil extraction may not be straightforward if both processes are underway simultaneously. Temporal associations are persuasive, *e.g.*, cases where seismicity rates surge shortly after water injection commences in producing oilfields that were previously aseismic.

We have found 38 cases of seismicity proposed to have been induced by enhanced oil recovery. Of these, 24 are from the USA and the rest from Canada, China, Denmark, France, Kuwait, Norway, Romania, Russia and Turkmenistan.

The classic example is the case of the Rangely Oilfield, Colorado, where induced earthquakes could be controlled (see also Section 4.1.8) [Raleigh *et al.*, 1976]. There, water injection for oil recovery was conducted in wells up to 2 km deep where the formation pressure was ~17 MPa. Seismicity could be increased or decreased by varying the pore pressure around 26 MPa (Figure 74). This experimental case led to hopes that earthquakes might be controlled, including damaging events on the San Andreas fault system. However, it was quickly realized that the fractal nature of earthquakes is such that the stress released by a few moderate earthquakes cannot substitute for a single large earthquake. Thus, hopes that damaging earthquakes might be averted using engineering means were not realized.

The largest earthquakes postulated to have been induced by water flooding or reinjection for enhanced oil recovery are the M 6.2 1983 Coalinga event, the 1985 M_W 6.1 Kettleman North Dome event, and the 1987 M_L 5.9 Montebello Fields (Whittier Narrows) event, all in California. The primary cause for these earthquakes is, however, probably oil extraction (Section 3.3.2) [McGarr, 1991].

More clear-cut examples come from the Newport-Inglewood fault zone, Los Angeles Basin, California. Of the 3 billion barrels of original reserves in the giant Wilmington Oilfield, 2.7 billion (~440,000,000 m^3) have been removed. Early production from this field may have contributed to the damaging 1933 M_L 6.3 Long Beach, California, earthquake, and the events of 1947, 1949, 1951, 1954, 1955, and 1961 (Section 3.3.2) [Kovach, 1974].

Water flooding for enhanced oil recovery and to counteract massive subsidence started there in 1954. Despite significant ambiguity regarding causation, earthquakes with magnitudes up to M 3.0 that occurred during 1971 are thought to have correlated with injection volumes. Following these small events, injection was continued at approximately the same volumetric

rate as production and the suspected induced seismicity did not continue [Nicholson & Wesson, 1992].

A more persuasive case of water-flooding-induced seismicity which caused significant damage and loss of life is that of the Inglewood Field, some 20 km further north along the Newport-Inglewood fault zone. In December 1963 the earth dam containing the nearby Baldwin Hills Reservoir failed, releasing 11 x 10^6 m^3 of water into a residential area. This flood damaged over 1,000 homes, killed five people and caused $12 million of damage. Failure of the dam was attributed to cumulative fault displacements that resulted from water flooding of the Inglewood Oilfield for enhanced oil recovery [Castle & Yerkes, 1976; Hamilton & Meehan, 1971].

Discovered in 1924, the Inglewood Oilfield occupies an anticline within a zone of faults and folds. Reserves were initially 430 million barrels but the field is now ~93% depleted. For the first three decades production occurred under only exsolution-gas (pressure depletion) drive and peripheral-water drive. Some 83 x 10^6 m^3 of oil, water and sand were extracted. Pressures declined from 3.9 to 0.34 MPa from the start of production up to the 1950s. A well-defined subsidence bowl centered on the oilfield developed and surface deformation was monitored from 1939. Subsidence was up to 1.75 m in the period 1911-1963. Horizontal displacements were up to 0.68 m in the period 1934-1961 with radially oriented extension. The Baldwin Hills reservoir lay on the edge of this subsidence bowl.

In 1954 a water-flood program for enhanced oil recovery began which was expanded to a full-scale program in 1957. Acceleration of deformation in the form of surface cracks, creep and small jumps in fault displacement onset immediately on minor faults and joints concentric to the center of subsidence. There had been close correlation between subsidence and liquid production, and a sharp reduction in subsidence occurred in the eastern part of the field when major water-flooding began. The orientation of the horizontal displacements and strain were consistent with the operations and a cause for the deformation of tectonic origin could be rejected to a high degree of certainty.

Increased shallow seismicity onset in 1962 and the following year the Baldwin Hills dam ruptured. It was deduced that movement on one of the faults allowed water to flow into the soil under the dam, resulting in failure. This case, and that of the Wilmington Oilfield, highlight the risk of conducting major hydrocarbon operations near to dense populations, particularly where prior tectonic activity is known.

4.1.4 Enhanced Geothermal Systems (EGS)

The extraction of geothermal heat from bodies of rock that contain insufficient water naturally was pioneered in the 1970s by the "hot dry rock" projects of Fenton Hill, New Mexico, and Cornwall, UK. These projects did not lead directly to economic development and were abandoned. The technology was resurrected early in the 21st century as "Enhanced Geothermal Systems" (EGS). An important milestone in this process was the landmark report "*The Future of Geothermal Energy*", prepared by the Massachusetts Institute of Technology for the U.S. Department of Energy [Tester & al., 2006][7].

[7] http://geothermal.inel.gov and http://www1.eere.energy.gov/geothermal/egs_technology.html

The fundamental concept of EGS is to pump high-pressure fluid into a well to hydrofracture and thermofracture hot rock, enhancing permeability and creating an underground heat exchanger. If one or more production wells do not already exist, they are drilled into the fractured rock mass. Cold water is pumped down the injection well, circulates through the hot rock, and hot water and steam are produced via production wells.

The objective of injection is to produce a network of fractures in the otherwise low-permeability target formation. As is the case for shale-gas hydrofracturing, earthquakes are an inevitable consequence of a successful EGS project. Dense seismometer networks are installed prior to hydrofracturing in order to obtain the best possible earthquake hypocentral locations, magnitudes and source mechanisms since these results can assist in targeting the production well. Such projects are currently providing superb data and advancing basic seismology.

Notable EGS projects have been conducted at:

- Fenton Hill, New Mexico [e.g., Ferrazzini *et al*., 1990];
- Cornwall, UK [e.g., Turbitt *et al*., 1983];
- Soultz-sous-Forêts, France [e.g., Baisch *et al*., 2010; Calo *et al*., 2014];
- Basel, Switzerland [*e.g*., Zang *et al*., 2014a];
- Newberry volcano, Oregon [Cladouhos *et al*., 2013];
- the Coso geothermal area, California (see Section 4.1.5) [Julian *et al*., 2010];
- Desert Peak, Nevada [Chabora *et al*., 2012]; and
- Cooper Basin, Australia [e.g., Asanuma *et al*., 2005].

The Fenton Hill, New Mexico, hot dry rock project was the first of its kind. It was completed in 1977 in rock at a depth of ~2.6 km and temperatures of 185°C. Work at Fenton Hill continued into the 1990s, achieving a production of ~10 MW thermal, but was terminated because of lack of funding.

An early modern EGS project commenced at Soultz-sous-Forêts, in the central Upper Rhine Graben, France in 1987 (Figure 75) [Baisch *et al.*, 2010; Calo *et al.*, 2014]. The site lies in highly fractured granite overlain by ~1,400 m of sediments. It contains three ~5,000 m deep injection wells and several shallower wells. Massive hydraulic stimulations were performed in the injectors at depths > 4,000 m. In 2000, well GPK2 was stimulated with ~23,000 m^3 of water at flow rates of 30–50 l/s and overpressures of up to 13 MPa. Well GPK3 was stimulated in 2003 with ~37,000 m^3 of water at similar flow rates and overpressures. Well GPK4 was stimulated twice with a total of ~22,000 m^3 of fluid. In 2010 the project began to deliver 1.5 MW to the grid, a world first.

The hydraulic injections were monitored using a sparse local seismic network of multi-component, down-hole sensors at depths of 1500-3500 m. More than 114,000 seismic events were detected at rates of up to 8000 events per day (Figure 76). The activity migrated away from the injection well with time and, as has been observed elsewhere, the largest events occurred after injection had stopped. Such behavior causes problems for "traffic light" systems designed to adjust injection strategies to avoid large earthquakes on the basis of the ongoing seismicity. Earthquake magnitudes eventually reached M_L 2.9 and, although modest in size, caused public concern. After the largest event in 2003 the flow rates and volumes of stimulations were scaled back.

The larger events are thought to have occurred on a sub-vertical structure that might be a component of the Rhine Graben complex. The project demonstrated that a better understanding of the induced seismicity associated with such projects is needed if the problem is not to jeopardize commercial implementation of EGS technology.

Perhaps the most infamous case example of nuisance seismicity induced by EGS operations is that of the Basel, Switzerland project. The city of Basel is located where the Upper Rhine Graben intersects the Jura Mountains fold/thrust belt (Figure 1). Basel has a history of large-magnitude seismicity, including the largest historical event in NW Europe, the M ~6.5 earthquake of 1356, which destroyed the city. There may have been additional M ~7 events in the post-Pleistocene period.

Details of this disappointing project are published in many papers, including a concise summary by Häring *et al.* [2008] and a collection published as a Special Issue of Geothermics in 2014 [Zang *et al.*, 2014a]. In brief, the project was designed to provide power to the city of Basel. A seismic network was installed in 2006 and the Basel-1 well was drilled the same year to a depth of 5 km. The wellbore intersects 2.4 km of sedimentary rocks and 2.6 km of granitic basement.

The granite in the open hole below 4629 m was hydraulically stimulated with a total of 11,570 m^3 of fluid. The initial plan was to inject over a period of 21 days. However, seismicity became intense during the first 6 days, with events up to M_L 2.6 occurring in the depth range ~4.6-5.0 km (Figure 77). These events precipitated cessation of injection in response to a pre-approved procedure. Five hours after the well was shut in an earthquake with M_L 3.4 occurred and a further three M > 3 events followed over the next 56 days (Figure 78). There was considerable citizen anxiety and the project is now abandoned.

EGS has been extensively conducted in Cooper Basin, Australia, where the largest earthquake induced to date has a magnitude of M_W 3.7. Cooper Basin is ideal for development of EGS. It lies in the interior of Australia in southwest Queensland, remote from large population centres. It contains significant oil and gas resources which have been explored and exploited since the 1960s so industrial infrastructure was already in place in 2002 when geothermal exploration started. The target heat source is granitic rocks with temperatures up to 240˚C at 3.5 km depth. These are the hottest known granitic rocks in the world at economic drilling depths that are not in the vicinity of active volcanoes.

Six deep wells were drilled into the granite to depths of 3629-4852 m. Four of these are in the Habanero Field and the other two are 9 and 18 km away in the Jolokia and Savina Fields. EGS fluid injection experiments were conducted 2003-2012 and documented in detail in several published papers [*e.g.*, Asanuma *et al.*, 2005; Baisch *et al.*, 2009a; Baisch *et al.*, 2009b; Baisch *et al.*, 2006a; Baisch *et al.*, 2006b; Baisch *et al.*, 2015; Kaieda *et al.*, 2010]. Some of the injections induced over 20,000 earthquakes which were well-recorded by dense, modern seismic networks.

Despite the fact that all the stimulations were conducted in the same granite formation, they induced variable seismic responses (Figure 79). These are exemplified by two that were carried out in 2010 and 2012 [Baisch *et al.*, 2015]. The 2010 stimulation injected fluid into the Jolokia well at a depth of > 4000 m. It induced only minor seismic activity, even at extremely high fluid pressures (~120 MPa), and the injection rate achieved was only ~1.0 l/s, one to two orders of magnitude less than typical. Only 73 earthquakes with M_L −1.4 to 1.0 were recorded over an eight-day stimulation period and an additional 139 over the next six

months. The largest of these was M 1.6 which occurred 127 days after the end of the injection. This is another case where the largest induced earthquake occurred after injection had terminated. Hypocenters clustered around the injection well at distances of a few tens or hundreds of meters, suggesting that the events occurred on steeply dipping fractures poorly oriented for shearing in the regional stress field.

The 2012 stimulation was carried out in well Habanero 4. Approximately 34,000 m^3 of water were injected at depths of 4100-4400 m, flow rates of > 60 l/s, and wellhead pressures of ~50 MPa. This induced > 29,000 earthquakes with M_L -1.6 to 3.0 which were recorded on a local 24-station network. Of these, 21,720 could be located and focal mechanisms determined for 525. This is probably the most prolific EGS-induced earthquake dataset ever collected. In contrast to the well-hugging, sub-vertical fracture activated by stimulation of well Jolokia 1, the Habanero 4 stimulation activated a single, sub-horizontal fault zone thought to have a vertical thickness of only a few meters and extending to > 1.5 km from the well. Failure was consistent with the regional stress field.

These two very different styles of seismic response characterized injections in different wells penetrating the same granite formation. This case history exemplifies the challenge of predicting the behavior of formations under stimulation, even when excellent geological knowledge is available. Despite the major technological advances achieved in the Cooper Basin project, due to low oil prices and the withdrawal of support, the project was decommissioned in 2016.

Despite the challenges that currently face the development of EGS, much has been learned in recent years that will underpin the future of the industry. Because it is known beforehand that projects induce seismicity, exemplary seismic monitoring and public outreach practices have been developed. These include installing custom-designed networks of three-component borehole instruments well in advance of operations in order to obtain a pre-operational baseline for seismic activity. Data are streamed to public websites and outreach includes town-hall meetings, installing seismometers in public buildings in nearby communities, distributing information to the public orally, in printed form and on the internet, and involving local communities in the commercial activity.

4.1.5 Geothermal reinjection

Water is re-injected into exploited geothermal fields in order to maintain pressure. Although classified technically as renewable resources, geothermal fields are, in reality, not so. If large quantities of hot fluid are removed at high rates for many years, exceeding natural recharge, the resource will become depleted. This is typically manifest as a progressive reduction in reservoir pressure leading to reduced production. To maintain pressure, water is re-injected. The aim is to re-inject in a way that does not compromise production wells by reducing the temperature of produced fluids.

Perhaps the most remarkable case of seismicity that can be attributed with confidence to geothermal reinjection is that of The Geysers geothermal field, California (Figure 58). The Geysers is a steam-dominated geothermal reservoir that lies in the strike-slip stress regime of the San Andreas fault system in California. Exploitation there began in the 1860s. Steam was first used to generate electricity in 1922 when one kilowatt was produced. Production peaked in 1987 at about 3.5 x 10^3 kg s^{-1} of steam from which 1800 MW of electricity were generated (Figure 59).

Power production decreased thereafter because the modest amount of reinjection done could not maintain the falling steam pressure. At that time, condensate was the main re-injectate and less was available than the amount of water produced. Reservoir pressure is sub-hydrostatic and thus the water could be reintroduced "under vacuum", i.e. simply poured into boreholes to drain back into the formation under gravity.

The US Geological Survey routinely locates > 10,000 earthquakes in The Geysers reservoir each year. The annual seismic rate is currently 200-300 M 2 earthquakes and 1-2 M 4 earthquakes. The Geysers earthquake dataset is without doubt the richest set of induced earthquake data available in the world with > 250,000 located events in the catalog of the Northern California Earthquake Data Center[8].

For many years it was not acknowledged that the industrial activity induced the earthquakes. However, as data accumulated the link could not be denied. It was initially assumed that production caused the earthquakes as a result of the contracting reservoir collapsing in on itself. Surface deformation is indeed large, and subsidence rates of up to 5 cm/year have been reported [Lofgren, 1978; Mossop & Segall, 1999; Vasco *et al.*, 2013].

In recent years, however, it has become clear that seismicity correlates better with reinjection than with production [*e.g.*, Majer & Peterson, 2007; Stark, 1990]. It has been possible to make this link in particular since 1998 when the first of two major water-acquisition and reinjection projects began. The South East Geysers Effluent Project (SEGEP) began to re-inject water via a 46-km-long pipeline from Lake County that delivers up to 22 x 10^6 l/day. In 2003 the second project came online, the Santa Rosa Geysers Recharge Project (SGRP), which delivers up to 41 x 10^6 l/day via a 64-km-long pipeline from Santa Rosa (Figure 59) [Majer & Peterson, 2007]. Surges in earthquake rate correlate with the increases in water injection that accompanied the onset of those projects.

In addition to the correlation between the seismicity in general and injection, surges of earthquakes correlate with both individual injections and injection wells [Majer & Peterson, 2007; Stark, 1990]. In the high-temperature northwest Geysers, for example, a sharp increase in injection in late 2004 correlated with surges of earthquakes that cluster around the bottom of a well (Figure 80).

Ground shaking from earthquakes with Modified Mercalli intensities of II – VI are felt daily in settlements near The Geysers. The largest earthquake that has occurred there is the 2014 M_W 4.5 event. On the basis of historical seismicity, the absence of continuous, long faults in the reservoir, and the lack of alignment of epicenters, Majer *et al.* [2007] tentatively suggested that the largest earthquake that could occur was M ~5.0.

An extensive review of The Geysers seismicity is provided by Majer and Peterson [2007]. They conclude that the seismicity results from a diverse set of processes that may work independently or together and either enhance or possibly reduce seismicity. To the processes listed in Section 1.3, thermal contraction from cooling the rock matrix can be added.

A second example of particularly rich geothermal-induced seismicity is that of the Coso geothermal field. This field lies in the southwestern corner of the Basin and Range province in eastern California, at a right releasing step-over in the southern Owens Valley fault zone

[8] http://www.ncedc.org

[Monastero *et al.*, 2005]. It lies on a US Navy weapons test site, and is thus uninhabited and not generally accessible to the public. Electricity has been generated there since the 1980s, producing about 250 MW. Because there is a shortage of water locally, only about half the volume produced can be replaced by reinjection and a major lowering of the local water table has resulted.

There is a high level of tectonic seismicity in the region, but even in this context the geothermal field is anomalously seismogenic. Several thousand locatable earthquakes per year occur within the ~ 5 x 5 km production field, the majority of which must be induced by operations. These earthquakes have been subject to detailed research by numerous institutions for many years [*e.g.*, Julian *et al.*, 2004; Julian *et al.*, 2007; Kaven *et al.*, 2014; Monastero *et al.*, 2005]. Most production and reinjection data are proprietary, so published detailed correlations between operations and seismicity are rare.

One of these rare cases is described by Julian *et al.* [2007]. In 2005 an existing well at Coso was used in an experimental Enhanced Geothermal Systems operation. Fluid was injected at rates of up to 20 l/s into well 34-9RD2 on the east flank of the reservoir. The objective was to increase permeability and enhance production in a cluster of nearby producing wells. The well was re-worked in advance of the project including deepening it and replacing the existing slotted liner with an un-slotted one.

During the work, major unexpected circulation-loss zones were encountered resulting in a total loss of up to 20 l/s of drilling mud at a depth of about 2672 m. The planned EGS project thus instantly metamorphosed into an unplanned reinjection operation. A vigorous earthquake swarm onset immediately. High-resolution locations, relative locations, and full moment tensors were determined using data from the high-quality seismic network operated by the Geothermal Program Office of the US Navy, which had been densified with an array of temporary stations for the purpose of monitoring the EGS experiment. As a result, an exceptionally high-quality dataset was available from a total of 36 digital, three-component stations.

The results showed that the swarm activated several hundred meters of a preexisting fault immediately adjacent to the well that opened in tensile mode. The existence of the structure deduced from the seismic evidence was confirmed by surface geological mapping and by data from a borehole televiewer log. This experiment was an early demonstration of the potential of earthquake techniques to yield information on the detailed subsurface fracture network in a geothermal reservoir.

In Europe, three geothermal projects have been associated with M > 3 induced earthquakes, all of them in Italy:

- Larderello-Travale (M_{MAX} 3.2);
- the Monte Amiata geothermal field (M_{MAX} 3.5); and
- the Torre Alfina Field (M_{MAX} 3.0).

Of these, the most notable case is that of the Larderello-Travale, Tuscany, vapor-dominated system. Tuscany is an active tectonic region with a transcurrent/transtensional/strike-slip deformation style, high thermal gradients and temperatures up to 400˚C. Within it there are several geothermal fields of economic interest. The shallower Larderello-Travale reservoirs are contained in Triassic carbonate and evaporite rocks. The deeper reservoirs are in fractured, metamorphic basement.

Larderello-Travale has generated electricity almost continuously since 1904, and the reservoir is thought to have a long history of seismicity. In the early 1970s, injection of cold condensate from the power plants was initiated in order to recharge the upper reservoir. A seismic monitoring network was installed, in part to monitor the impact of the injection. It is only since this network was installed that the seismicity could be studied in detail [Batini *et al.*, 1985; Batini *et al.*, 1980].

The activity is variable regarding both event rate and *b*-values. The events are mostly shallower than 8 km, with 75% located in the depth range 3.0-5.5 km. The largest event reported is a M 3.2 event that occurred in 1977. Events studied in detail were found to have significant non-shear components in their focal mechanisms, indicating a tensile component [Kravania *et al.*, 2000]. As would be expected, seismicity is reported to have enhanced the permeability.

Because of the long history of seismic activity many of the events are thought to be natural. Nevertheless, a clear correlation between volume of injected water and number of events is reported for small-magnitude earthquakes. Events with $M \geq 2.0$ are not thought to occur in response to injection [Batini *et al.*, 1985; Evans *et al.*, 2012].

4.1.6 Shale-gas hydrofracturing

Gas-bearing shale formations are hydrofractured ("fracked") in order to increase permeability so the gas can be extracted. It is typically done by drilling horizontal wells at relatively shallow depths (up to ~2 km deep) into the target formation. Fluids are injected containing chemicals and solids designed to propagate fractures and prop them open. The method has been extensively applied in the USA where it has brought about a major reduction in the cost of natural gas (Figure 81). As a result of this success there is widespread interest in other countries in implementing the technology. However, in shale-gas regions where population density is high there may be public concern about potential environmental effects, including ground-water pollution, industrialization and induced earthquakes.

Although over 2.5 million shale-gas hydrofracturing jobs have been completed worldwide, to date maximum magnitudes of only 21 cases of induced seismicity have been reported (Figure 82). Of these cases, eight are from the USA, 12 are from Canada, and one is from the UK [Baisch & Vörös, 2011; de Pater & Baisch, 2011]. This amounts to only 0.001% of all shale-gas hydrofracturing jobs (Section 8.1). Of those cases, notably large earthquakes are reported from British Columbia (M 4.4, 4.4 and 3.8 events) and Alberta (M_L 4.4), both in Canada [Kao *et al.*, 2015; Schultz *et al.*, 2015]. In the USA the largest shale-gas hydrofracturing-related earthquakes reported have been four $M > 3$ events in Oklahoma and Ohio [Darold *et al.*, 2014; Skoumal *et al.*, 2015].

These statistics are misleading because the fundamental purpose of hydrofracturing in gas-bearing shale is to crack the rock, i.e. to induce the very process that causes earthquakes. Thus, all successful hydrofracturing jobs induce earthquakes. The desire is, of course, that the earthquakes are small and do not cause nuisance by endangering health and safety, damaging infrastructure or the environment, or annoying citizens. Meeting this objective is helped in the USA and Canada by operating in regions of low population density. Seismic monitoring is commonly done because the earthquake locations can provide information of use to operations, *e.g.*, the location and volume of the fractured network created. However, if nuisance seismicity is not induced there is little reason to report it. Seismic analyses focus on

investigating the spatial distribution and mode of fracture achieved, the results are not of public interest, and they are likely to remain proprietary.

One of the most remarkable of these cases is a sequence associated with injection operations in 2013 near Crooked Lake, Alberta. This sequence induced the highest-magnitude shale-gas hydrofracturing-related earthquakes on record to date. The target formation is the Devonian Duvemay organic-rich shale. Hydraulic fracturing operations there involve multi-stage, high-pressure operations using proppant-weight-in-well of typically 60 MPa and volumes typically of a few thousand m^3. Of ~3000 hydrofracturing operations in Alberta in 2013, only three (0.1%) are reported to have been accompanied by noteworthy seismicity, with 160 events up to M_L 4.4 being observed over a ~2-year period [Schultz *et al.*, 2015].

The quality of information about the sequences is limited because local seismic stations were not available and detailed information on local crustal structure was absent. Data from distant stations therefore had to be processed creatively. A close spatial and temporal correlation was reported between the earthquakes and the shale-gas hydrofracturing (Figure 83 and Figure 84). Correlation was also observed between injection stages, a "screen-out" (i.e. an interruption in the flow of slurry that caused shutdown of injection) and seismicity. Associations between screen-outs and seismicity have been reported from elsewhere [Clarke *et al.*, 2014a; Skoumal *et al.*, 2015]. The seismicity may have interfered with operations at Crooked Lake.

A classic case history is that of the Horn River Basin, a major shale gas production area in British Columbia. Fracking commenced there in 2006 and shale gas production peaked in 2010 and 2011 [Farahbod *et al.*, 2015]. Prior to shale-gas hydrofracturing, seismicity rates were low and only 24 earthquakes with M 1.8-2.9 were located in a ~2-year period in the area. When shale-gas hydrofracturing started, the seismic rate increased to over 100 earthquakes per year and correlated with days when hydrofracturing was conducted (Figure 85). A logarithmic correlation between seismic moment, maximum magnitude and volume injected was observed (Figure 86).

For the entire Horn River Basin, injected volume was more closely related to induced seismicity than injection pressure. Increases in injected volume are reported to increase earthquake frequency but not magnitude, and large earthquakes (seismic moment release $>10^{14}$ N m, i.e., M ~3.5) occurred only when ~150,000 m^3 of fluid were injected per month. Time lags between injections and seismicity ranged from days to several months.

The embryonic UK shale-gas industry began with the unfortunate case of the 2011 Preese Hall, Lancashire, earthquake sequence. There, the first UK dedicated multi-stage shale-gas hydrofracturing operation was conducted in a 1000-m section of the Carboniferous gas-bearing Bowland Shale. Following the injection of 2245 m^3 of fluid and 117 tonnes of proppant, a nearby M_L 2.3 earthquake was reported by the British Geological Survey. The earthquake was felt, and was unusual in this location. The nearest monitoring station was 80 km away. Additional seismic stations were deployed rapidly but no aftershocks were recorded. UK shale-gas hydrofracturing thus started life with a very rare phenomenon–the induction of a nuisance earthquake.

Operations continued, but about six weeks later a second felt event with M_L 1.5 occurred ~1.0 km from the well. Citizen disquiet followed and operations were suspended. A total of 52 earthquakes in the magnitude range M_L -2.0 to 2.3 were detected with similar waveforms to the two largest events. A government enquiry and 18-month suspension of operations

ensued while the problem was investigated. The close relationship between operational parameters and seismicity left little doubt that the earthquakes had been induced by the hydrofracturing (Figure 87).

The UK Department of Energy and Climate Change (DECC) commissioned a review and recommendations for the mitigation of seismic risk associated with future shale-gas hydrofracturing operations in the UK. Recommendations included the monitoring of test injections prior to the main injections, monitoring fracture growth during injections, near-real-time seismic monitoring of injections, and halting or changing injection strategy at the occurrence of seismicity with a threshold magnitude of M_L 0.5 [Green *et al.*, 2012].

Detailed studies of the locations and fault mechanisms of the poorly recorded seismicity in the years that followed, combined with seismic reflection data, showed that the earthquakes likely occurred a few hundred meters below the well perforations on a fault that was not known to exist at the time [Clarke *et al.*, 2014b; Green *et al.*, 2012]. The fault does not intersect the borehole but was close enough that hydrofracture fluid may have leaked into it, reducing the normal stress and permitting strike-slip motion to occur. The fault that slipped is an ancient transpressional fault that formed at the end of a Carboniferous basin inversion and which had been inactive for the last 260 Ma. This case history showed that even long-inactive faults, which are common in most continental crust, are close to failure and may be induced to slip if injections occur nearby.

4.1.7 Allowing mines to flood

Removal of mining material reduces confining stress on nearby faults and brings them closer to failure. The simultaneous pumping out of water during mining lowers the pore pressure and thus increases the strength of faults, counteracting the effect of rock removal. These two process may roughly balance until a mine is abandoned and pumping stopped. After this, natural groundwater recharge may encourage seismicity.

A classic case where this is thought to have occurred is that of the 1994 Cacoosing Valley, Pennsylvania, earthquake sequence (Figure 88) [Seeber *et al.*, 1998]. Groundwater recharge is thought to be responsible for a M_L 4.4 earthquake that occurred beneath an 800-m-wide carbonate quarry from which ~4 x 10^6 m^3 had been removed. The earthquake caused ~$2 million of damage to nearby homes. The quarry had been excavated to an average depth of 50 m over the 58-year time period 1934-1992. Groundwater pumping had been done during the mining period to prevent the quarry from flooding. After mining stopped this pumping ceased and the water table rose by ~10 m over a period of a few months. The rock is highly permeable karstic carbonate, and depletion of groundwater, along with subsequent recharge, likely extended over a wider area than the footprint of the quarry.

Earthquake activity commenced approximately five months after cessation of pumping. A sequence of 67 aftershocks was recorded on a rapidly deployed temporary seismometer network. The aftershock sequence occurred in the upper 2.5 km and formed a planar pattern that was interpreted as the fault plane that slipped. Focal mechanism studies suggested that the mainshock had a thrust mechanism and that the earthquakes were situated in the hanging wall block such that unloading by rock removal would have encouraged slip (Figure 89). Surprisingly, the seismic sequence did not activate any of the plentiful, known, large-displacement faults in the region. Instead, stress was released on a fracture set of small, unmapped faults which probably had a more suitable orientation. The mining had reduced

confining stress by ~0.13 MPa, which may be compared with a calculated stress drop of 1-4 MPa for the M_L 4.4 mainshock.

The Cacoosing Valley event is thought to be similar to one that occurred two decades earlier beneath a large quarry at Wappinger Falls, New York [Pomeroy *et al.*, 1976]. There, a m_b 3.3 earthquake occurred in 1974. Again, the mainshock and associated aftershocks nucleated at exceptionally shallow depth with some aftershocks as shallow as 0.5 km. Slip occurred on a reverse fault immediately below a large quarry and had source mechanisms consistent with the regional stress field. Over the preceding ~75 years ~30 x 10^6 m^3 of rock had been removed by open-casting down to a depth of ~50 m. This changed the stress by ~1.5 MPa at the surface and reduced the normal stress on faults below.

4.1.8 Research projects

In the wake of the Denver, Colorado earthquakes (Section 4.1.1) there was speculation that earthquakes might be controllable. If they could be induced, perhaps they could also be prevented. Partly as a result of these ideas, a series of earthquake-induction experiments have been conducted for research purposes. These have investigated the physical properties of natural fault zones and the processes that accompany earthquake occurrence. We have identified 13 cases of earthquakes induced by research projects.

The first such project was conducted in 1969 at the Rangely Oilfield, Colorado [Raleigh *et al.*, 1976]. This oilfield occupies Mesozoic and Paleozoic sedimentary rocks at a depth of ~1700 m and is underlain by crystalline basement at ~3000 m. There is little significant local faulting, but earthquake activity was known to occur associated with water flooding for enhanced recovery (Section 4.1.3). As a result, a seismograph array and prior earthquake record were already available. The fluid pressure in wells in the vicinity of the earthquakes was experimentally cycled to investigate the effect on the seismicity. A close correlation between seismicity and high pore pressure was observed, and events up to M_L 3.1 were induced (Figure 90).

In 1970, shortly after the Rangely experiment, another experiment was conducted at Matsushiro, Japan. A volume of 2883 m^3 of water at wellhead pressures of 1.4-5.0 MPa was pumped into an 1800-m-deep well to test whether earthquakes were induced by increasing pore pressure in a fault zone. After several days of injection earthquake activity onset within a few kilometers of the well [Ohtake, 1974].

After a hiatus in experimenting of 16 years, in 1990, perhaps the best known research experiment to study fluid-induced seismicity was begun–the Kontinentales Tiefbohrprogramm der Bundesrepublik Deutschland (KTB), the German Continental Deep Drilling Program. The literature documenting this project is extensive and includes a 1997 special section of Journal of Geophysical Research (No. 102) [*e.g.*, Baisch & Harjes, 2003; Baisch *et al.*, 2002; Bohnhoff *et al.*, 2004; Erzinger & Stober, 2005; Fielitz & Wegler, 2015; Grasle *et al.*, 2006; Jahr *et al.*, 2005; Jahr *et al.*, 2007; Jahr *et al.*, 2008; Jost *et al.*, 1998; Shapiro *et al.*, 2006; Zoback & Harjes, 1997].

The main borehole was drilled 1990-1994 to a depth of 9.1 km. The first hydraulic stimulation was conducted in 1994 at depths and pressures close to the brittle-ductile transition. About 400 earthquakes up to M_L 1.2 were induced at about 8.8 km depth (Figure 91). Focal mechanisms were consistent with stress measured in the borehole. Seismicity onset within a few hours of pumping and a few tens of meters from the borehole. Modeling

suggested that the earthquakes occurred in response to pressure perturbations of < 1 MPa, i.e. less than 1% of the ambient, hydrostatic pore pressure at the nucleation depth.

An important conclusion of this experiment was that differential stress in the crust is limited by the frictional strength of well-oriented, pre-existing faults ("Byerlee's Law"), and that the crust is in brittle failure equilibrium even at great depth in relatively stable intraplate areas. Hydraulic experiments at the site have continued up to recent years [*e.g.*, Jahr *et al.*, 2008].

A later project conducted in the Phillipines in 1997 injected 36,000 m^3 of water into a well intersecting a creeping portion of the Philippine Fault at the Tongonan geothermal field. The water entered the formation at depths of 1308-2177 m below the surface [Prioul *et al.*, 2000]. Several hundred earthquakes were observed but all occurred away from the fault and within the geothermal reservoir. Prioul *et al.* [2000] concluded that tectonic stress on the fault is relieved aseismically and as a consequence there was no differential shear stress to release by the water injection.

In the same year, a water-injection experiment was conducted in the Nojima fault zone, Japan, shortly after it ruptured in the 1995 M 6.9 Kobe earthquake [Tadokoro *et al.*, 2000]. This experiment offered the opportunity to gather information on the physical properties of a fault plane in the immediate post-rupture period. Over periods of a few days, 258 m^3 of water were injected into an 1800-m-deep borehole at a pressure of ~4 MPa at the surface, entering the fault zone at 1480-1670 m depth. An increase in M -2 to 1 earthquakes occurred a few days after each injection. It was concluded that the fault zone was highly permeable and could slip with pore-fluid pressure increases of less than 10%.

Two additional experiments have been conducted in recent years, the first in 2013 as part of the Wenchuan Earthquake Fault Science Drilling (WFSD) project [Ma *et al.*, 2015]. This project studied the fault healing process. Over the four-month period November 2013 - March 2014, 47,520 m^3 of water at pressures of 10-15 MPa were injected at rates of up to 1.7 l/s into a 552-m-deep well that intersected a fault zone at 430 m depth. The fault was activated and over 20,000 earthquakes up to M ~1 were detected using downhole observations. The hypocentral zone suggested failure in the same sense as the regional stress.

A similar phenomenon was reported by Guglielmi *et al.* [2015] in an experiment that stimulated an inactive fault in a carbonate formation. The experiment injected 0.95 m^3 of water into a 518-m-deep underground experimental facility in southeastern France where a vertical well intersected a fault at a depth of 282 m. Aseismic shear slip started at a pressure of ~1.5 MPa, and ~80 earthquakes occurred a few meters from the injection point. These accounted for only a small fraction of the slip on the fault, however. The accumulated moment at the end of the experiment was $M_o = 65 \times 10^9$ Nm, (equivalent to an event with M_W 1.17). This was far larger than the moment released by the seismicity, which was $M_o < -2$ Nm. Aseismic slip dominated deformation in the fault zone and the earthquakes occurred in the rock mass outside the pressurized zone. Other experiments have been performed in a salt solution mine at Cerville-Buissoncourt in Lorraine, France [Kinscher *et al.*, 2015; Mercerat *et al.*, 2010] and the Wairakei geothermal field, New Zealand [Allis *et al.*, 1985; Davis & Frohlich, 1993].

This multi-decade, multi-nation research subject has yielded a vast amount of data and answered some critical questions, not always the ones originally posed and not always with the preferred answer. Relieving in a controlled way the stress naturally released in large

earthquakes is likely to be scientifically and politically difficult. The continental crust is near to failure, even to great depths and where large faults are not known. Earthquakes can be induced by relatively small stress perturbations, but in some cases stress on a targeted fault is relieved aseismically. In these cases, motion on that fault may induce secondary earthquakes in the surrounding rock mass. Fluid injection may thus induce primarily aseismic slip, and seismicity may be a secondary effect, with imperfect spatial correlation with the injection activities. In many cases of induced seismicity more stress is released than is loaded on faults by the anthropogenic process, since pre-existing tectonic stress is also released. However, the Wenchuan and southeastern France experiments illustrate that the reverse sometimes occurs– that some of the anthropogenically loaded stress may be released aseismically.

4.2 Gas

4.2.1 Natural gas storage

In order to stabilize supply, and for energy security, nations store natural gas reserves often underground. As of May 2015, 268 underground gas storage facilities existed or were planned in Europe (Figure 92), and there were over 400 in the USA.

Depleted hydrocarbon reservoirs, aquifers, and salt cavern formations are obvious repositories because they are usually well understood geologically. Furthermore, in the case of hydrocarbon reservoirs, engineering infrastructure including wells and pipelines may already be in place. In addition, they may be conveniently close to consumption centers.

We have identified seven cases of induced seismicity reported to have been associated with underground gas storage:

- Gazli, Uzbekistan [Simpson & Leith, 1985];
- the Castor project (in the old Amposta Field), Spain [Cesca *et al*., 2014; Gaite *et al*., 2016];
- Bergermeer, Norg and Grijpskerk, Netherlands [Anonymous, 2014];
- Háje, Czech Republic [Benetatos *et al*., 2013; Zedník *et al*., 2001]; and
- Hutubi, China [Tang *et al*., 2015].

A few small earthquakes up to M 0.7 were recorded in 2013 in association with the injection of cushion gas in the Bergermeer Gasfield. Up to 15 earthquakes per month up to M 1.5, several of which were felt, were reported for the Háje storage facility. Larger earthquakes were reported in association with gas storage at Hutubi, with over 700 earthquakes up to M 3.6 in the period 2009-2015.

The case of the Gazli Gasfield, Uzbekistan, is primarily renowned for the three damaging M_S ~7 earthquakes that caused death and destruction in the local town of Gazli in 1976 and 1984 (Section 3.3.1). When this field had been largely depleted, it was used for storage. Gas was cycled in and out as required. Plotnikova *et al.* [1996] report seismicity induced by this process that correlates with the amount of gas stored (Figure 93). Earthquakes with magnitudes up to M 5 for are reported.

By far the best-documented case is, however, that of the Castor project, Spain. This project aimed to use a depleted oilfield in the Gulf of Valencia, the old Amposta Field, ~20 km from the coast of northeast Spain (Figure 94). It was planned to store 1.3×10^9 m^3 of natural gas in

this reservoir, sufficient to meet 25% of Spain's storage requirements. Earthquake activity onset shortly after the commencement of gas injection, however. Ultimately, on 1 October, 2013, the largest earthquake, with M_W 4.3, occurred. Public reaction to the earthquakes was negative, perhaps not least because the population had been sensitized by the 2011 M_W 5.1 Lorca earthquake which occurred only two years before and 250 km further south along the coast (Section 3.1). As a result, we understand that the project has been discontinued.

The old Amposta oil reservoir occupies fractured and brecciated Lower Cretaceous dolomitic limestone and is one of several in the region (Figure 95). It produced 56 million barrels (~9 x 10^6 m^3) of estimated total in place volume of 140 million barrels of oil (22 x 10^6 m^3) in the period 1973-1989. Secondary injection for enhanced recovery was not needed because of strong natural water drive. After 1989 the field was largely depleted and lay dormant.

Installation of the necessary infrastructure for conversion of the reservoir into a gas storage facility commenced in March 2009 and included a platform and a gas pipeline. Injection of an initial ~10^8 m^3 (at 25˚C and 0.1 MPa pressure) of cushion gas (i.e. gas intended as permanent inventory in the reservoir) was conducted 2-16 September, 2013 at 1.75 km below sea level.

Three days after injection began, seismicity onset (Figure 96). Earthquakes with magnitudes up to M 2.6 occurred (Figure 97). Injection was stopped 16 September but earthquakes continued to occur. The largest, a M_W 4.3 event, occurred 1 October, two weeks after injection stopped. In total, over 1000 earthquakes were detected, more than 420 with $M \geq 2$ (Figure 97). Seismicity was still ongoing in 2016 [Gaite *et al.*, 2016].

Accurate hypocentral locations were difficult to determine because the project, being offshore, was monitored by a seismic network with limited coverage. The closest station was 26 km from the Castor platform and, since most of the stations were on land, there was restricted azimuthal coverage [Gaite *et al.*, 2016]. As a result, different studies of the hypocentral locations show different results and even the orientation of the hypocentral distribution as a whole (which might contribute to identifying the activated fault structure) and the hypocentral depths (which are important to determine whether or not the earthquakes were linked to the gas injection) vary significantly between studies. Both NW and NE orientations for the hypocentral zone are reported, along with depths that vary from close to the gas injection depth to several kilometers deeper (Figure 96) [*e.g.*, Cesca *et al.*, 2014; Gaite *et al.*, 2016].

Nevertheless, the epicentral area forms part of the dominantly ENE-WSW Catalan-Valencian normal-faulting extensional region [Perea *et al.*, 2012] and focal mechanism studies of the mainshock show motion compatible with slip in this sense [Cesca *et al.*, 2014]. The most significant potentially seismogenic feature near the old Amposta Field is the 51-km-long NE-SW oriented, Fosa de Amposta fault system [Gaite *et al.*, 2016]. Such a major fault zone, were it to rupture in its entirety, is potentially capable of generating a M 5-7 earthquake (Figure 98). Combined interpretation of the hypocentral locations and source mechanisms suggests that this fault was not activated, however.

The activity of September and October 2013 was unusual for the area regards both magnitude and seismic rate compared with the preceding two decades (Figure 94). Although earthquake activity occurs along the coast of Spain to the north and south, the Pyrenees mountain chain, Portugal, and the coast of North Africa, no significant historical seismicity was known to have involved the fault system local to the Castor project prior to the gas injection. For this

reason, and because of the very close spatial and temporal correlation with the gas injection, there is little doubt that the earthquakes were induced.

4.2.2 CO_2 for oil recovery

There are approximately 100 enhanced oil recovery injection sites where CO_2 is used, mostly in Texas. We have, however, found only two cases where seismicity is postulated to be unambiguously induced by this process. These are the cases of the Cogdell Field, Texas [Gan & Frohlich, 2013] and Weyburn Oilfield, Saskatchewan [Maxwell & Fabriol, 2004; Verdon *et al.*, 2013]. The latter is a hybrid project and also considered to be a case of Carbon Capture and Storage (CCS) so it is described in Section 4.2.3.

The case of the Cogdell Oilfield is described in detail by Gan and Frolich [2013]. Early on in its history, this field generated earthquakes surmised to have been induced by water injection. Lately, CO_2 has been injected for enhanced oil recovery and this is associated with earthquakes up to M_W 4.4 (Figure 99).

The Cogdell Oilfield is a large subsurface limestone reef mound, not a fault-bounded oil trap, and there are no geologically mapped faults nearby. Production began in 1949 and in the period 1957-1983 oil recovery was enhanced by brine injection. In the period 1975-1982 this was associated with earthquakes that were surmised to have been induced. They included a M_L 5.3 event in 1978. Despite its size, this earthquake was only poorly located, an indication of the rudimentary nature of seismic monitoring in Texas at this time. Davis and Pennington [1989] suggested that the seismicity correlated with injection volume at Cogdell and concluded that earthquakes occurred where reservoir pressure gradients were high.

Enhanced oil recovery using gas began in 2001 and injection built up to a constant, high level of ~ 40 x 10^6 m^3/mo from 2004 onwards. Injection was conducted at ~2.1 km depth, 20 MPa pressure and 75˚C, under which conditions CO_2 is supercritical. In 2006, after 23 years of seismic quiescence and following a significant increase in gas injection rate, earthquakes onset again. Over the following five years 18 earthquakes with M > 3 and occurred and in 2011 one with M_W 4.4.

The 21-month period March 2009 - December 2010 could be studied in detail because at this time USArray, a rolling program to cover the entire country with temporary seismic stations[9], swept across Texas. During this period the network recorded 93 locatable events, many within 2 km of wells actively injecting gas into the Cogdell Oilfield. Locations, coupled with focal mechanisms, suggested that the events occurred on previously unknown faults. Interestingly, although the neighboring Kelly-Snyder and Salt Creek Fields have similar operational histories, seismicity does not appear to be induced in them.

4.2.3 Carbon Capture and Storage (CCS)

The issue of induced earthquakes is particularly important in the case of Carbon Capture and Storage (CCS). In addition to causing a nuisance, earthquakes could also rupture the impermeable containment caprock that contains the CO_2 in the storage reservoir, and release it back into the environment. Carbon geostorage is in its infancy, but there are already 20-30

[9] http://www.usarray.org

tests underway globally, including eight operational commercial-scale CCS plants[10]. Of these, three are reported to be seismogenic. The Sleipner Field (Norwegian North Sea), the Weyburn Field (Saskatchewan, Canada) and In Salah (Algeria) provide an illustrative range of seismic responses [Verdon *et al.*, 2013].

In the Sleipner Field, since 1996 CO_2 has been removed from the natural gas produced and re-injected into a shallow saline aquifer (the Utsira Formation) at a rate of ~10^6 tonnes/year. The aquifer is large and comprises well-connected, little-faulted sandstone with high porosity and permeability at ~1 km depth beneath North Sea mean sea level. By 2011 the total volume of CO_2 injected amounted to only ~0.003% of the available pore space. No pore-pressure increase, mechanical deformation or seismicity has been detected for the entire >20 years of injection. The Sleipner Field is, however, not seismically monitored locally so small earthquakes would go undetected. The nearest earthquakes to the Sleipner Field listed in the British Geological Survey catalogue are a M_L 3.5 event at 1 km distance and a M 2.5 earthquake at 6 km distance. The uncertainties in these locations may be considerable.

The Weyburn Oilfield, Saskatchewan, Canada, has been exploited for 45 years and is somewhat seismogenic. CO_2 injections started in 2000 both for enhanced oil production and CO_2 sequestration and now ~3 x 10^6 tonnes/year are injected annually. This is accompanied by minor earthquake activity. Figure 100 shows the relationship between earthquake occurrence and CO_2 and water injection. Some of the earthquakes clustered near injection wells, but no clear temporal correlations are apparent. All the earthquakes were small.

Vigorous earthquake activity accompanied CO_2 sequestration at the producing In Salah Gasfield, Algeria. There, CO_2 was injected into a low-permeability, 13–20% porosity, ~ 20-m-thick fractured sandstone in a non-producing, water-dominated part of field at depth of 1,850–1,950 m. Hundreds of earthquakes occurred, accompanied by uplift detected using InSAR.

CO_2 injection at In Salah started in 2004 and over the following nine years a total of ~ 3.85 x 10^6 tonnes of CO_2 produced from several nearby gas wells were re-injected via horizontal boreholes. There was little apparent pressure communication with the producing part of the field. Calculations suggest that pore pressures increased from initial conditions of ~18 MPa at the injection points to ~30 MPa whilst at the same time they reduced in the production parts of the reservoir (Figure 101). Deformation measured using InSAR detected surface blistering-type uplift of up to ~1 cm/year locally around the injection wells.

A three-component borehole seismometer deployed nearby detected over 1000 events in 2010. The data were consistent with locations in the receiving formation beneath the injection well though there was no clear correlation with CO_2 injection (Figure 102). The project has since been terminated as a result of seal integrity concerns.

Verdon *et al.* [2013] conclude that at Sleipner, where the target aquifer is large and pressure increases during injection minimal, little deformation, either seismic or aseismic, results. At Weyburn, deformation and seismicity may be partly mitigated by ongoing oil extraction which serves to offset pressure increase resulting from the CO_2 injections. At In Salah, however, the formation into which CO_2 is injected had poor pressure communication with the producing parts of the reservoir and natural gas extraction did not compensate for the

[10] http://www.ccsassociation.org/faqs/ccs-globally/

injections. Pore pressures increased significantly as a consequence leading to both seismic and aseismic deformation.

A CCS demonstration site reported to be seismogenic is at Decatur, Illinois [Kaven *et al.*, 2015]. There, ~10^6 tonnes of supercritical CO_2 were injected over a period of three years at a depth of 2.1 km into a regionally extensive, 460-m-thick high porosity/permeability sandstone. The CO_2 used is a by-product of local ethanol production. Approximately 180 earthquakes up to M_W 1.26 were reported over a period of about two years within a few kilometers of the injection well and at the approximate depth of injection. Kaven *et al.* [2015] concluded that earthquakes nucleate on preexisting faults in the basement that are well oriented with respect to the regional stress field. They further conclude that little seismic hazard is posed to the host formation because the earthquakes are relatively distant and small.

All other CCS projects have, to date, been shorter in duration and typically with total volumes no more than 10s or 100s of thousands of tonnes. CCS projects have developed recently in China where eleven projects are reported including five as recent as 2014 [Huaman & Jun, 2014]. Limited information is available on these projects and none regarding seismicity induced by subsurface CO_2 injection.

4.3 Injection: Summary

Diverse fluids are injected into the ground for diverse reasons and related seismogenic behavior is diverse. For a large majority of projects no earthquakes are reported. For others, minor, small-magnitude earthquakes occur that are of insufficient public interest to result in publication of details. For a small minority seismicity induced is sufficiently troublesome to hinder operations or, in rare cases, result in project abandonment.

Spatial, temporal, and magnitude correlations with the postulated causative operations are variable. Earthquakes thought to be induced may be co-located with injections at a level of 10s or 100s of m or they may occur up to tens of kilometers distant. Earthquakes may onset as soon as operations begin or be delayed for decades. Small operations may induce large earthquakes and large operations may be aseismic.

An interesting question is why Oklahoma is highly seismogenic while large-scale injection projects are conducted in many states of the USA without nuisance earthquakes. We are not aware of any current theories regarding this.

5 Explosions

5.1 Nuclear

Since the first test of a nuclear device, the Trinity explosion of July 16, 1945, approximately 2000 such tests have been conducted by eight nations, 1,352 of them underground. We have found reports of seismicity associated with 22 of these, 21 in the USA and one in Russia [Boucher *et al.*, 1969; Engdahl, 1972; Hamilton *et al.*, 1972; McKeown, 1975; McKeown & Dickey, 1969].

American nuclear tests were conducted at the Nevada Test Site for the 48-year-period 1945-1992 (Figure 103). Boucher *et al.* [1969] investigated the possibility of induced seismicity associated with 16 nuclear tests by searching the University of Nevada database of earthquake locations. They reported that seismicity was induced after all of the 10 tests where the explosion itself registered $m_b \geq 5.0$. (We have not included the explosions themselves in

the database.) The largest earthquake induced was at least one magnitude unit smaller than the inducting explosion. This suggests that earthquakes may have been induced by many, if not all of the tests, but some were too small to be clearly recorded.

A test ironically named Faultless (19/01/1968) is infamous for having induced clearly visible surface slip on faults up to 40 km from ground zero, even though the test was only one megaton in yield. Ground deformation associated with this, and other nuclear tests, has been captured on film [McKeown & Dickey, 1969][11].

Carefully-documented studies of the seismicity induced by large nuclear tests were done for the Benham (19/12/1968), Purse (07/05/1969), Jorum (16/09/1969) and Handley (26/03/1970) tests (Figure 104) [Hamilton *et al.*, 1972; McKeown, 1975]. The earthquakes induced occurred immediately after the tests and clustered on Pahute Mesa, Nevada, where there is a four-kilometer-thick sequence of volcanic rocks containing both calderas and basin-range-type normal faults. Most of the induced earthquakes occurred over periods of 10-70 days following the tests, at depths of less than five kilometers and distances smaller than ~15 km from ground zero.

The spatial distribution of the earthquakes was found to be mostly controlled by local geological structure. The scales and fractal dimensions of the two sets of faults compared with those of the test-related earthquakes suggested that events occurred on faults in the buried caldera ring-fracture zones rather than on the regional basin-range faults (Figure 104). McKeown [1975] concluded that the subsidiary, not the dominant, fault and fracture system in the region had been activated.

Underground nuclear tests in Amchitka, Alaska, resulted in permanent displacement on geological faults of as much as 1 m in the vertical and 15 cm in the horizontal for fault lengths up to 8 km [McKeown & Dickey, 1969]. The seismic effects of tests Milrow (1969) and Cannikin (1971) there were monitored by local seismic stations. Both tests generated several hundred small earthquakes with $M < 4$. They were thought to be related to deterioration of the explosion cavity. The sequences concluded with large, complex events and simultaneous subsidence of the surface resulting from final collapse of the explosion cavity. In the case of the Cannikin test, small tectonic events continued up to 13 km from ground zero for several weeks. The events were shallow, had waveforms characteristic of normal tectonic earthquakes, and focal mechanisms consistent with existing faults. They are thought to have represented release of ambient tectonic stresses as a result of the explosions. The more modest post-test seismic response from tests in Amchitka compared with those conducted in Nevada is thought to result from the lower level of tectonic stress [Engdahl, 1972].

5.2 Chemical

Most large chemical explosions are associated with rocket launching, military research and operations, and military, space-program, and industrial accidents. Such explosions may be equivalent of several kilotonnes (kt) of TNT. They occur at the surface on land or on ships and are thus poorly coupled to the ground. Tsunamis, but not earthquakes, have been reported in association with some of these.

---

[11] See, for example, https://www.youtube.com/watch?v=6ETHnsKnKiA

It has been suggested that deep penetrating bombs may modulate earthquake activity. Balassanian [2005] examined earthquake activity over ~2-year periods spanning bombing incidents at Kosovo, Yugoslavia (1999), Baghdad, Iraq (1991), Tora Bora, Afghanistan (2001) and Kirkuk, Iraq (2003). It was suggested that the incidence of $M \geq 5$ earthquakes increased within 1000 km and one year of the bombings after the attacks on Kosovo and Tora Bora but not after those on Baghdad and Kirkuk. Arkhipova *et al.* [2012] suggested that the 23 October, 2011 M 7.8 Van earthquake, eastern Turkey, was encouraged by mass bombing associated with the Libyan conflict, 1300-1500 km away.

Deep penetrating bombs explode at depths of a few meters in the ground, improving the coupling by factors of several tens of percent compared with equivalent surface explosions. Nevertheless, deep penetrating bombs are generally not larger than the equivalent of ~1 kt of TNT, much smaller than the megatonne- or multi-megatonne scale typical of the nuclear devices reported to have induced earthquakes (Section 5.1). In the case of the nuclear tests, earthquakes have been induced out to a maximum of ~40 km away and activity has decayed away over periods of a few days or weeks [Boucher *et al.*, 1969].

Given the relatively small subsurface effects of chemical explosions and the great distances and relatively long time delays of the earthquakes postulated to have been induced by them, these suggestions must be considered speculative. Without them, there are no credible reports of earthquakes induced by chemical explosions. This ignores large landslides which may be considered to represent earthquakes at the free surface with focal mechanisms equivalent to a net force [Julian *et al.*, 1998].

5.3 Explosions: Summary

Only nuclear explosions are known to induce earthquakes. Not only do they induce aftershocks that may persist for some time after the blast, but tectonic stress is also released simultaneously with the explosions themselves. This is shown by the focal mechanisms of the blasts, which often involve both shear and explosive components (Figure 28) [Toksöz & Kehrer, 1972; Wallace *et al.*, 1983]. The largest earthquake we have found reported to have been induced by a nuclear test had a magnitude of m_b 4.9 and was associated with collapse of the cavity of the Cannikin, Amchitka test.

SECTION C: DISCUSSION & CONCLUSIONS

6 Earthquakes and belief systems

Public attitudes to induced earthquakes may have major implications for industrial projects. However, human reactions to earthquakes may not be based on a full understanding of seismology, or even on scientific evidence of any kind. Because of their apparently random and spontaneous nature, and lack of obvious causes, earthquakes have for millennia been explained in terms of folklore, religion, and other belief systems [e.g., Harris, 2012]. This includes Chinese, Russian and Japanese folklore and the religions of the ancient Greeks and Polynesians. All three mainstream Abrahamic religions–Christianity, Islam and Judaism–are based on ancient texts that attribute earthquakes to perceived shortfalls in human moral behavior.

Recent cases where explanations for earthquakes in terms of belief systems have had significant societal impacts include:

- In 2015, the Malaysian government attributed a M_W 6.0 earthquake that killed 18 people to tourists posing nude on Mt. Kinabalu, one of the country's sacred mountains.
- In 2014 local people in the Altai Mountains, Siberia, attributed earthquakes to the removal of the mummified remains of a 5th-century BC noblewoman for archaeological research.
- In 2010, the American evangelist Pat Robertson allegedly attributed the devastating M_W 7.0 Haiti earthquake to the successful 1791-1804 anti-slavery insurrection on the island.

These examples serve to emphasize that public information and outreach is a potentially important precursor to any industrial project that might cause earthquakes.

7 Correlations between parameters

The magnitudes of the largest earthquakes postulated to be associated with projects of different types varies greatly (Figure 60). The largest earthquakes have been reported for water reservoirs, conventional oil and gas exploitation, and geothermal operations. Median magnitudes also vary between project types but the most commonly reported are $3 \leq M < 4$ which apply to water reservoirs, construction, conventional oil and gas, hydrofracturing, mining, and research projects. In some cases, however, the total number of cases reported is small. For all project types it is virtually certain that large numbers of smaller induced M_{MAX} earthquakes have not been reported.

Relationships between various seismic and operational parameters have been suggested for a number of individual projects. For example, there is a clear relationship between the seismic moment released and the volume injected in shale gas hydrofracturing operations at the Etsho area, Horn River Basin, British Columbia (Figure 86) [Farahbod *et al*., 2015]. A question of interest for future projects is, however, what correlations might exist for all projects of the same kind.

From the point of view of nuisance, the magnitudes of the largest earthquakes induced are by

far the most important. Seismic rate and the total number of earthquakes are of secondary importance because the fractal nature of earthquakes means that most are small. Furthermore, because of incomplete reporting, many cases of induced earthquakes too small to be of significant consequence probably have not been made known. Because a large and systematic part of the true dataset is missing, correlations with operational parameters cannot convey any information on average M_{MAX}. Of interest is whether *the largest* M_{MAX} correlates with operational parameters.

This is illustrated, for example, by Figure 105, which shows a plot of M_{MAX} vs. water reservoir volume for 126 cases. Clearly the magnitude of *the largest* M_{MAX} increases with reservoir volume. However, there is no significant correlation between M_{MAX} and reservoir volume for the dataset as a whole. If reporting were complete, the region of the plot beneath the M_{MAX} upper bound would be populated with points down to small magnitudes. Because the reported data are biased in this way we have not calculated correlation coefficients between all values of M_{MAX} and other parameters.

7.1 Cases where a relationship is observed

- *Water reservoir volume* (Figure 105): Volumes plotted range from 0.004 km^3 to 164 km^3. There is a nearly linear boundary to the upper left of the cloud of points which suggests a relationship between reservoir volume and the largest possible M_{MAX}. Interestingly, the 2008 M_W ~8 Wenchuan, China, which is disputed because of its seemingly disproportionately large size, also plots on this alignment.
- *Water reservoir mass per unit area* (Figure 106): There is a weak tendency for the largest M_{MAX} (i.e. the upper bound of M_{MAX}) to increase with reservoir water mass per unit area.
- *Volume added or removed in surface operations* (Figure 107): We combined as many cases of surface operations as possible. There is a clear tendency for the largest M_{MAX} to increase with this parameter?
- *Volume of material removed from the subsurface*: We combined conventional oil and gas, geothermal, and mining-produced volumes (Figure 108). There is a weak tendency for the largest reported M_{MAX} to increase with volume produced. The relationship for M_{MAX} for injection volumes proposed by McGarr [2014] on the basis of theoretical considerations fits these data well (Figure 109).
- *Fracking – injection pressure, rate and volume* (Figure 110): We observe a tendency for the largest M_{MAX} to increase with all these parameters. This is in agreement with the relationship proposed by McGarr [2014].
- *Injected volume for all projects* (Figure 111): We found data for 69 cases to study this parameter. The largest earthquake reported is the 2011 M_W 5.7 Prague, Oklahoma, event. This and a small number of additional earthquakes, mostly postulated to be induced by waste fluid injection, exceed the upper-bound magnitude limit proposed by McGarr [2014].
- *Volume or proxy volume removed from or added to the subsurface* (Figure 112): We calculated volume or proxy volume (mass converted to volume using an appropriate density) for 218 cases. There is a clear, systematic upper bound for M_{MAX}. The relationship proposed by McGarr [2014] for injection volumes fits this wider dataset well.
- *Mass removed from or added to the subsurface* (Figure 113): As with volume, there is a clear linear observed upper bound to M_{MAX}.

- *Yield of nuclear devices* (Figure 114): The magnitudes of induced earthquakes correlate strongly with explosion size for the seven cases for which data are available. This finding is in agreement with the correlation between the activated-fault length and explosive yield at Pahute Mesa, Nevada Test Site (Figure 115) [McKeown & Dickey, 1969].
- *Project scale* (Figure 116): We updated the plot of McGarr *et al*. [2002] with 20 additional cases from our expanded database. Addition more data generally confirmed the earlier observations. Two cases exceed the empirical upper bound of McGarr *et al*. [2002]–the 1979 M_L 6.6 Imperial Valley, California, earthquake (linked to the Cerro Prieto geothermal field; Section 3.4) and the 2008 M_W ~ 8 Wenchuan, China, earthquake (Section 2.1.1).
- *Project type* (Figure 117): The largest earthquakes postulated to have been induced, in order of decreasing magnitude, are associated with water reservoirs, groundwater extraction and conventional oil and gas operations. These have all been linked to earthquakes with M >7. To date, only relatively small earthquakes have been postulated to be associated with CCS, research experiments, construction and hydrofracturing. The number of projects in each category varies.
- *Distance of epicenter from the inducing project* (Figure 118): There is a tendency for the largest reported M_{MAX} to decrease with distance from the project.

7.2 Cases where a relationship is not observed

- *Dam height* (Figure 119): The number of cases for which data are available is 159. Many are from Brazil, China, and the USA. There is no tendency for the largest reported M_{MAX} to correlate with dam height.
- *Water reservoir area* (Figure 120): Reservoir areas for seismogenic cases range from 1.6 km^2 to 53,600 km^2. No significant tendency is seen for the largest M_{MAX} to increase with reservoir area. This result is perhaps unsurprising because large parts of a reservoir may be shallow.
- *Pressure change in subsurface reservoirs* (Figure 121): There is no correlation between the largest reported M_{MAX} and reservoir pressure change for the 55 cases where data are available.
- *Injection pressure* (Figure 122): We were able to study this relationship for 79 cases. Pressures range from atmospheric to 89 MPa. No relationship is apparent.
- *Injection rate for all projects* (Figure 123): This is independent of the largest reported M_{MAX}. Although some individual projects report correlations between earthquakes and injection rates, there is no clear correlation for projects as a whole.

7.3 Other factors

The largest reported induced earthquake has increased with time from ~ M 6.3 in 1933 to ~ M 8 in 2008 (Figure 124). The number of reported cases of induced seismicity has also increased greatly, probably becasue of the increasing number of large-scale industrial projects. The lower magnitude threshold of reporting is reducing, probably partly because of improved monitoring.

Figure 125 shows the distribution of induced earthquakes by tectonic regime is shown in. By far the most numerous are from intraplate areas (79% of all cases) with the next largest category (13%) located in convergent plate-boundary zones. Most large industrial projects

are conducted on land and most land is in the interior of plates with plate boundaries usually comprising relatively (though not absolutely) narrow zones. Most spreading plate boundaries are in the oceans and currently beyond reach of industrial development. The predominance of induced earthquakes in intraplate regions highlights the likelihood that affected regions may not be traditionally associated with seismicity nor accustomed to it historically.

The seemingly surprising lack of a relationship between M_{MAX} and operational parameters such as injection pressure and rate, coupled with the difficulty of predicting which projects will be seismogenetic and which will not, suggests that non-operational parameters are important. The pre-existing stress state is the most obvious such parameter. However, several lines of research indicate that most faults in the crust are nearly critically stressed, though they may not be optimally oriented to do so under ambient conditions. The local geology, and in particular the nature of pre-existing faults and fractures, must be important for understanding the extreme variations in seismogenesis between apparently similar projects in different locations. Geological and tectonic factors may thus be more important than engineering parameters. In order for significant earthquakes to occur, faults that are suitably orientated and stressed must exist.

It is interesting to speculate what the empirical results of the present study might imply for particular projects. For example, at The Geysers geothermal field, California, net production (i.e. total production minus re-injection) since 1960 has been ~ 1.7 x 10^9 m^3. The relationship of McGarr [2014] which links fluid-injection volume to M_{MAX} (Figure 112) fits well data from all volumetric projects. This relationship predicts that the upper bound to induced earthquakes associated with The Geysers volume change is M 7.0. This geothermal field has a maximum NW-SE long dimension of ~ 21 km. The largest induced earthquake that has occurred at projects of this scale is ~ M 6.6 (Figure 116).

To date, the largest earthquake that has occurred at The Geysers is the 2014 M_W 4.5 event. There is no evidence that a fault long enough to sustain a M 6.6 or 7.0 earthquake exists in the reservoir. However, The Geysers lies between the regional Mercuryville fault to the southwest and the Collayomi fault zone to the northeast, within the active Pacific/North America transform plate boundary zone. There is no evidence that the Mercuryville fault zone is active, but the Collayomi fault zone contains at least one active fault [Lofgren, 1981].

8 Discussion and Summary

8.1 How common are induced earthquakes?

The total number of industrial projects in various categories, along with the number reported to be seismogenic are given in Table 3. Without doubt under-reporting is severe. Seismicity at projects far from human habitation is likely to escape notice. Known cases may not be made publically known unless they are of large-magnitude, a nuisance, or unusual interest. For example, ~2.5 million shale-gas hydrofracture jobs have now been completed world-wide. All successful hydrofracturing projects induce small earthquakes but we found only 21 cases where seismicity has been reported (Table 3, Section 4.1.6). The absence of reports of seismicity thus does not correspond to an absence of seismicity. Some earthquakes may also have been reported by national seismic networks without their induced nature being recognized.

Table 3: Induced seismicity statistics for the total numbers of projects of different types, the number that are seismogenic, and related data.

Project type	# projects	# cases in the database	% projects that are seismogenic	Observed maximum magnitude (M_{MAX})	# seismogenic projects reported by Hitzman et al., (2013)	Source for # projects
CCS	75	2	2.67	1.7	-	Huaman and Jun (2014)
Construction	*unknown*	2	-	4.2	-	
Conventional oil and gas	67,000 fields	116	0.17	7.3	65	Li (2011)
Fracking	2,500,000 wells	21	0.00	4.4	2	King (2012)
Geothermal	*unknown*	56	-	6.6	26	Bertani (2010)
Groundwater extraction	*unknown*	5	-	7.8	-	
Mining	13,262 currently active mines	267	2.01	6.1	8 ("other")	http://mrdata.usgs.gov/
Nuclear (Underground)	1,352 tests	22	1.63	4.9	-	Pavlovski (1998)
Research	*unknown*	13	-	3.1	-	
Waste fluid injection wells (Class II wells)	151,000 wells (USA only)	33	0.02	5.7	11	Hitzman *et al.*, (2013)
Water dam	6,862 reservoirs (>0.1 km^3)	168	2.45	7.9	44	Lehner *et al.* (2011)
Total		**705**			**156**	

A histogram showing M_{MAX} for the 562 seismogenic projects where this parameter is reported is shown in Figure 126. The same data are shown as a plot of cumulative number of cases vs. M_{MAX} in Figure 127. The linearity of the distribution at the high-magnitude end suggests that reporting is complete for M_{MAX} 5 and above, and that underreporting becomes progressively greater for projects smaller than M_{MAX} 4. Downward extrapolation of the linear, M_{MAX} 5 - 7 part of the plot suggests that approximately 30% of M ~ 4 induced earthquakes have gone unrecognized or unreported, as have 60% of M ~ 3 events and ~ 90% of those with M ~ 2 (Table 4).

Table 4: Number of reported M_{MAX} values and number predicted from downward extrapolation of the linear trend of earthquakes with M_{MAX} 5 - 7 shown in Figure 127.

M_{MAX}	# reported earthquakes	# predicted earthquakes
7	4	4
6	17	16
5	68	67
4	181	~250
3	371	~1000
2	497	~4000

The hydrocarbon fields around Britain provide a regional example of this problem. Comparison of the UK earthquake database of the British Geological Survey with maps of hydrocarbon fields in the North Sea suggests correlations between fields and earthquake locations (Figure 128). Expanded maps of several fields are shown in Figure 129. There is spatial correlation between seismicity and the Beatrice Oilfield (Moray Firth), the Britannia Gasfield, the Southern North Sea Gas Province and the Leman Gasfield.

Most of the recorded earthquakes in the southern North Sea occur in or near fields developed in Permian Rotliegend reservoirs. There, gas is produced using simple pressure depletion from fields, most of which were near hydrostatic pressure when first discovered. Water is not injected to support production. Many of the poorer-quality wells used to explore and appraise this gas province were prop-fracked to obtain initial gas flow and a few fields [*e.g.*, Clipper South, Gluyas & Swarbrick, in press, 2016; Purvis *et al.*, 2010] used hydrofracturing in development wells. The Viking Graben contains mostly oilfields that were developed by allowing natural pressure decline to deliver the first oil and then injecting water to support continued production. The water used is seawater at typical North Sea temperatures of ~ 4˚C, while the reservoirs are at 90-140˚C. The central North Sea and Moray Firth contain a heterogeneous mix of oil and gas fields produced by a combination of pressure depletion and water injection. When discovered, a few fields were naturally at very high pressure and close to the fracture gradient.

Many of these activities are potentially seismogenic. Nevertheless, there are no reports of induced seismicity from these fields. Comparison of seismicity with hydrocarbon production information available from the Department of Energy and Climate Change (DECC) for the period 1975-2008 fails to show temporal correlations, and because the North Sea was seismogenic before hydrocarbon production started, it cannot be ruled out that the seismicity is natural. Clearly detailed work on individual events and their possible connection to activity in individual oil and gas fields is required before the seismic events could be categorized as natural or induced [Wilson *et al.*, 2015].

8.2 Hydraulics

Groundwater has a major influence on earthquake occurrence. Overwhelming, observational data show that pore pressure in fault zones can strongly influence seismicity (Section 1.3). The 2011 M_W 5.1 Lorca, Spain, earthquake is a particularly compelling example (Section

3.1). These facts imply an unfortunate association between earthquakes and human need to manage water, both for utilization and for flood control.

The Lorca case and the four other cases we found of earthquakes possibly linked to groundwater extraction, raise the question of whether other recent earthquakes that were both shallow and located where major local anthropogenic water table changes have occurred might have been induced. An example is the 2011 M 7.1 Christchurch, New Zealand, earthquake (Figure 130). The city of Christchurch is built on what was once an extensive swamp fed by the rivers Avon and Heathcote and numerous smaller streams. Major engineering changes have been made there to control water over the last century.

The 1811-1812 M ~7 New Madrid earthquakes occurred in the central Mississippi river valley, and affected the states of Missouri, Illinois, Kentucky, Tennessee, and Arkansas. This renowned sequence included three M ~7 earthquakes and probably seven with M > ~6.5. These earthquakes are remarkable for having been felt at distances of up to 1700 km as a result of the efficient transmission in the lithosphere of the eastern USA. They are also remarkable in that they occurred in an intraplate area far from the nearest plate boundary. They thus serve as a curiosity in the context of the current paradigm that expects large earthquakes to occur in plate boundary zones.

The New Madrid earthquakes occurred at and just south of the confluence of the 6,000 m^3/s Middle Mississippi and the 8,000 m^3/s Ohio rivers which forms the Lower Mississippi River. The possibility that the earthquake activity is linked to local hydraulics has been suggested previously but not seriously entertained. In view of the growing evidence that hydraulic changes can modulate the seismic behavior of faults it may be timely to revisit this possibility with geological investigation into the pre-earthquake hydraulic activity and numerical modeling.

Hydraulic effects may explain the apparently paradoxical observations that both mass addition and mass removal can induce earthquakes. This is illustrated by the fact that the commonest anthropogenic earthquake-induction process is mining (i.e. mass removal–38% of cases; Figure 131) and the second most common is water reservoir impoundment (i.e. mass addition–24%). Hydraulic changes induced by mass redistribution may result in migration of fluid into fault zones, increasing pore pressure. This process may thus explain the possible induction of earthquakes in the single case reported of erecting a heavy building (the Taipei 101 building; Section 2.1.2). It may also help to understand some cases of earthquakes induction by hydrocarbon extraction in the absence of fluid injections, since natural groundwater recharge may occur.

Examination of global earthquake databases shows that it is not uncommon for moderate earthquakes to occur near large lakes and reservoirs, *e.g.*, in east Africa, even though induction has not been proposed. Intraplate earthquakes in the UK are not currently understood. At least 21% of UK earthquakes in the British Geological Survey catalog are thought to be related to mines, but the remaining majority are probably natural. The seismic rate in the UK is ~ one M_L 3.6 event per year [Wilson *et al.*, 2015] and a possible link with hydraulics would be interesting to investigate.

8.3 How much stress loading is required to induce earthquakes?

Earthquakes occur naturally, without any human intervention at all. The minimum amount of added anthropogenic stress needed for an earthquake to onset is thus zero.

Many natural processes contribute simultaneously to stress build-up on faults. These include tectonic deformation, volcanism, natural heat loss, isostatic uplift following deglaciation or oceanic unloading, Earth tides, intraplate deformation resulting from distant plate boundary events, remote large earthquakes, erosion, dissolution, the natural migration of groundwater and the weather. To these are added anthropogenic activities. It is fundamentally an ill-posed question to ask the origin of the final stress increment that "broke the camel's back" and precipitated an earthquake. In the cases of large earthquakes this question may be akin to that of whether a windmill could have been responsible for a hurricane.

It has been suggested that instead of viewing industrial activity as inducing earthquakes, it could instead be viewed as modulating the timescale on which inevitable earthquakes occur. Unfortunately it cannot be known how events would have occurred had the industrial activity not occurred because history cannot be re-run with a change of circumstance. Furthermore, had an equivalent earthquake occurred at a different time, it cannot be known if it would have affected people and infrastructure to the same extent. Nevertheless, in the cases of many industrial projects, the association between earthquakes and the project is undeniable. In those cases the above arguments may be of academic interest only.

A wide range of stress changes brought about by anthropogenic activities has been postulated to have induced earthquakes, from a fraction of a MPa [*e.g.*, Keranen *et al.*, 2014], the equivalent of about a meter of rock overburden, to several tens of MPa (Table 5) (Figure 132). For example, the 2007 M_L 4.2 Folkestone, UK, earthquake and the 2008 M_W ~8 Wenchuan, China, earthquake have been attributed to anthropogenic changes of only a few kPa.

Table 5: Conversions for commonly used units of pressure

1 bar = 0.1 MPa, equivalent to ~ 4 m of rock overburden
1 atmosphere = 0.1 MPa
1 kg/cm^2 = 0.1 MPa
1 pound/inch^2 (psi) = 6.9 x 10^{-3} MPa
1 acre-foot/football field = 29 x 10^{-6} MPa (see footnote[12])
Hydrostatic gradient = 10 MPa/km
Lithostatic gradient = ~ 25 MPa/km

The minimum amount of stress loading that might plausibly induce an earthquake is of interest. The question "How much stress change is needed to induce earthquakes?" may be unanswerable. However, it may be possible to address the question "What is the minimum stress change that can be demonstrated to have induced earthquakes?" This could be attempted by exploring the natural stress changes known to correlate with earthquakes, as follows (Table 6).

[12] American football, including end zones.

Table 6: Stress changes associated with some natural processes postulated to induce earthquakes.

Effect	Stress change (MPa)
Earth tides	0.05
Seismic static stress changes	0.03
Remote triggering	~0.5
Typhoons	0.003

Earth tides

The spatial non-uniformity of the gravitational fields of the Sun and Moon (and to a much smaller extent, other celestial bodies) produces stresses in the solid body of Earth approaching 0.005 MPa. Loading of the solid Earth by the ocean tides produces additional stresses that can be about an order of magnitude larger but depend strongly on geographic location. The stress drops of most earthquakes are in the range 1 - 10 MPa so tides might sometimes have a detectable effect on earthquake occurrence.

Most early studies of earthquakes and tides failed to find any significant correlation. The main cause of this failure was probably over-simplification of the problem. Both stresses and earthquake mechanisms are tensors, but many studies looked, for example, for correlations between seismicity and tidal amplitude ranges, effectively treating both stress and earthquake mechanism as scalars. Another difficulty with any such analysis was the difficulty of computing ocean tides from the complicated shapes of the ocean basins.

There were, however, two exceptions to this failure. First, deep moonquakes, detected by seismometers placed by Apollo astronauts, correlate strongly with tides [Latham *et al.*, 1973]. Second, earthquakes at volcanic and geothermal areas show a tidal effect that is fairly easily detected [*e.g.*, McNutt & Beavan, 1981]. This suggests that interactions between fluid pressure and the volumetric components of earthquake mechanisms are important. Most recently, studies that account for earthquake focal mechanisms and compute ocean loading accurately have found that the occurrence of shallow thrust-faulting earthquakes does correlate significantly with tidal stresses [Cochran *et al.*, 2004].

Static stress changes resulting from large earthquakes

The 1989 M_W 6.9 Loma Prieta, California, earthquake modulated seismicity in the region around the epicenter out to distances where the coseismic stress changes were no more than 0.01 MPa (equivalent to ~0.4 m of overburden) [Reasenberg & Simpson, 1992]. The 1992 M_W 7.3 Landers, California, earthquake also modulated the seismicity nearby. Aftershocks were abundant up to about two source dimensions from the mainshock (a few tens of km), where the Coulomb stress on optimally orientated faults was increased by > 0.05 MPa. They were sparse where stress was reduced by this amount (Figure 133). The 1992 M_W 6.5 Big Bear aftershock occurred in a region where stress was increased by 0.3 MPa [King *et al.*, 1994]. The effect of static stress changes on neighboring faults has also been expressed in terms of the number of years by which the next large earthquake has been advanced in time [*e.g.*, King *et al.*, 1994; Reasenberg & Simpson, 1992].

Remote triggering

The 1992 M_W 7.3 Landers, California, earthquake is particularly remarkable because it precipitated earthquake activity up to 17 source dimensions distant from the mainshock (1,250 km). Most of this activity occurred at volcanic or geothermal areas such as Yellowstone. Static stress changes are vanishingly small at such distances. These remote earthquakes are thought to have been triggered by dynamic stress changes of a few tenths of a MPa in the propagating shear and surface elastic waves interacting with fluids in the hydrothermal and magmatic systems [Hill *et al.*, 1993]. The phenomenon of remote triggering has subsequently been recognized elsewhere. When first unambiguously recognized following the Landers earthquake, it was thought that only volcanic and geothermal areas were affected and that the process might reveal the locations of geothermal areas previously unknown. However, remote triggering has now been reported in other environments, *e.g.*, the hydrocarbon region of Oklahoma (Figure 73) [van der Elst *et al.*, 2013].

Weather

A number of studies have postulated that earthquakes were induced by heavy rainfall [Ie.g., Husen *et al.*, 2007; Roth *et al.*, 1992]. In addition, a recent report suggests correlations between "slow earthquakes" (accelerated creep on faults) and atmospheric pressure changes accompanying typhoons in Taiwan. [Liu *et al.*, 2009]. Such pressure changes alter stress on land areas but not beneath the ocean because seawater flow can maintain pressure equilibrium offshore. The effect contributes a stress change of ~ 0.003 MPa that encourages slip on coast-parallel thrust faults. This phenomenon might also be useful for estimating minimum triggering stress thresholds.

How large are induced earthquakes?

The stress change that might induce an earthquake is not related to the total stress reduction brought about by the earthquake or to the final magnitude of the earthquake (Figure 131). The final size of an earthquake is determined by how much of a fault was in a sufficiently critical state to move, once activation began. If slip on a fault reduces to almost zero before the next event starts, a series of discrete events is recognized. If slip does not stop, the event may grow into a large or great earthquake and all the strain relief is considered to have occurred in a single event. Great earthquakes (events with $M \geq 8$) that rupture much of the lithosphere typically comprise a cascading chain of $M > 7$ sub-events, each triggered by the stress changes caused by the previous ones. Although likely very rare, it cannot be ruled out that industrial activity could contribute to the onset of the first sub-event.

In the case of recent seismicity in Oklahoma, in particular the 2011 Prague sequence (Section 4.1.2.1) Keranen *et al.* [2013] concluded that stress from fluid injections may build up for decades before the onset of induced earthquakes. They further concluded that the initial M_W 5 rupture triggered successive earthquakes, including the M_W 5.7 event that occurred the following day. In the case of the great 2008 M_W ~ 8 Wenchuan earthquake (Section 2.1.1), once the first sub-event began, slip on the fault did not stop until several large fault segments had failed.

This view is consistent with the findings of McGarr [2014]. He derived a relationship that related volume injected to the size of fluid-injection-induced earthquakes and showed that it fit well observations of 18 of the largest-magnitude earthquakes (Figure 109). However, he

also pointed out that this upper bound only applies to induced earthquakes whose source regions were confined to the volumes directly affected by the injection, and that if fault slip propagated outside of this volume then larger earthquakes could occur.

8.4 Natural or induced?

There is great variation between cases regarding the strength of the evidence for induction. In some cases the association with an industrial activity is beyond any reasonable doubt. For example, over 250,000 earthquakes have been located in a tight cluster in The Geysers geothermal area, California, by the U.S. Geological Survey during the last half century. At the other end of the spectrum, induction has been suggested for cases where only one earthquake occurred and the calculated stress changes were smaller than those induced by Earth tides, *e.g.*, for the 2007 M_L 4.2 Folkestone, UK, earthquake, for which an inductive stress change of 0.001-0.03 MPa was proposed [Klose, 2007a]. For those cases, simple coincidence cannot be ruled out (Section 2.1.3 and Section 8.3).

The number of cases postulated to be induced is increasing rapidly and with it the urgency for management strategies. It is desirable, not only to know *a posteriori* whether an earthquake was natural or induced, but also to forecast which projects may be seismogenic and how great the hazard is likely to be. In the past, schemes have been proposed to address the question whether earthquakes are natural or induced. For example, Davis and Frohlich [1993] list seven questions to profile a seismic sequence and judge whether it was induced or not (Table 7).

In the light of the large number of case histories now available, some parameters suggested earlier to be diagnostic can be re-visited. These include:

1. *Whether the region had a previous history of seismicity*. Induced earthquakes have now been postulated to occur in both historically seismic and aseismic areas. Evidence from research in boreholes suggests that faults everywhere, in both traditionally seismic and aseismic regions, are close to failure.
2. *Close temporal association with the induction activity*. Reported delays in the onset of postulated inducted seismicity vary from essentially zero to several decades.
3. *In the case of injection-related earthquakes, proximity of a few kilometers*. Distances of up to 25 km have now been reported (Figure 118; Section 4.1.2).
4. *Known geological structures that can channel flow*. Many earthquakes postulated to be induced have been attributed to previously unknown faults.
5. *Substantial stress changes*. Stress changes as small as a few kPa have now been postulated to induce earthquakes (Section 2.1.3).

Simple criteria for deciding whether an earthquake is induced or not are thus elusive. There is extreme diversity in the circumstances of cases. Postulated induction activities may take place over time periods from a few minutes to decades. The volumes of material added or removed vary over many orders of magnitude and the maximum magnitude of events postulated to be induced vary from $M < 0$ to $M \sim 8$.

Table 7: Seven questions proposed by Davis and Frohlich [1993] to be diagnostic of earthquakes induced by fluid injection [from Davis & Frohlich, 1993].

	Question	Earthquakes Clearly Not Induced	Earthquakes Clearly Induced	I Denver, Colorado	II Painesville, Ohio
	Background Seismicity				
1	Are these events the first known earthquakes of this character in the region?	NO	YES	YES	NO
	Temporal Correlation				
2	Is there a clear correlation between injection and seismicity	NO	YES	YES	NO
	Spatial Correlation				
3a	Are epicenters near wells (within 5 km)?	NO	YES	YES	YES?
3b	Do some earthquakes occur at or near injection depths?	NO	YES	YES	YES?
3c	If not, are there known geologic structures that may channel flow to sites of earthquakes?	NO	YES	NO?	NO?
	Injection Practices				
4a	Are changes in fluid pressure at well bottoms sufficient to encourage seismicity?	NO	YES	YES	YES
4b	Are changes in fluid pressure at hypocentral locations sufficient to encourage seismicity?	NO	YES	YES	NO?
	TOTAL "YES" ANSWERS	**0**	**7**	**6**	**3**

Several unusual characteristics are commonly, though not universally, reported for earthquakes suspected of having been induced. These include:

1. Unusually shallow nucleation depths (*e.g.*, the 2011 M_W 5.1 Lorca, Spain, earthquake, Section 3.1);
2. Occurrence on previously unknown faults ("blind faults"; *e.g.*, in the Cogdell oilfield, Texas, Section 4.2.2);
3. Release of stress in the same sense as the regional on suitably orientated structures (*e.g.*, in Oklahoma, Section 4.1.2.1);
4. The largest earthquake in a sequence occurring after the induction activity has ceased, suggesting that fluid diffusion is important (*e.g.*, the 1962-1968 Denver earthquakes, Section 4.1.1);

5. Faults in the basement beneath water and hydrocarbon reservoirs being reactivated, sometimes transecting the sedimentary formations above (*e.g.*, the Coalinga, California, earthquake; Section 3.3.2).

These observations raise a number of questions. For example, if induced seismicity commonly occurs on previously unknown faults, could hazard be reduced by extensive subsurface mapping prior to operations? Since the crust is thought to be pervasively faulted and near to failure essentially everywhere, it is not clear this would be the case–perhaps everywhere should be considered potentially seismogenic. Also, if large earthquakes occur after operations have stopped, for how long should seismic hazard mitigation measures be continued after the end of a project?

More reliable, but less universally applicable ways of discriminating include:

1. Simple spatial and temporal associations, *e.g.*, earthquakes onsetting as soon as injection starts and close to the injection point;
2. Visual observation, *e.g.*, gallery collapses in mines or ground rupture when a nuclear test is conducted;
3. Earthquake focal mechanisms, *e.g.*, discriminating between natural, shear-faulting earthquakes and volumetric mining collapses, as was done by McGarr [1992a; b] for well-recorded earthquakes in South African gold mines and Dreger *et al.* [2008] for a mining collapse in Utah.

Work is currently ongoing to develop additional ways of discriminating induced from natural earthquakes. These include using statistical features of background earthquakes and clustered sub-populations. For example, Zaliapin and Ben-Zion [2016] have suggested several statistical features that may distinguish induced seismicity from natural tectonic activity including a higher rate of background events and more rapid aftershock decay.

8.5 Why are earthquakes induced by some industrial projects and not others?

In addition to needing an explanation for why earthquakes occur at particular projects, any theory for induced earthquakes must be able to explain why they do not occur at most projects. This endeavor is hampered by under-reporting (Section 8.1; Table 3). A necessary pre-requisite to explaining the incidence of induced seismicity as a whole or in different categories is to know its true extent.

In the context of industrial activity as a whole, reports of induced earthquakes are extraordinarily rare (Table 3). Only ~ 2% of mines, water reservoirs, and CCS projects are reported to be seismogenic. All other categories of project for which we found data were < 2% seismogenic.

Individual cases of induced seismicity are diverse and site-specific and the lack of similarities is perhaps a stronger feature than common factors. With the exception of large geothermal projects and hydrofracturing (where almost all are probably seismogenic but only 0.001% are reported to be so) it is seemingly unpredictable which projects will report induced earthquakes. Many if not most induced earthquakes, except at hydrofracturing projects, were unexpected. On the other hand, a research experiment that specifically aimed to induce seismicity, by injecting water into an active fault zone, surprisingly failed to do so (Section 4.1.8) [Prioul *et al.*, 2000].

A large majority of induced earthquakes occur in intraplate areas (Figure 125). This does not come as a surprise in view of the fact that rocks seem to be close to failure everywhere so the potential for inducing earthquakes in intraplate and plate-boundary regions may be similar (Section 1.1). This, coupled with the observation that many earthquake sequences were unexpected and in areas previously aseismic, means that populations may be unprepared for earthquakes. To add to this, pre-industrial seismic risk assessments may be difficult if there is no history of seismicity or seismic monitoring. Wilson *et al.* [2015] recently tried to rectify this problem for the UK in advance of possible expansion of the shale-gas industry by estimating a baseline for UK seismicity.

For most non-research purposes the parameter of importance is not whether seismicity is induced but whether nuisance seismicity is induced. M_{MAX} is thus critical. In Section 7 we describe an initial examination of the database for correlations. The currently observed upper limit to M_{MAX} correlates with water reservoir volume, volume extracted/injected, yield of nuclear tests and scale of project. These are all basically measures of project size. Factors such as reservoir pressure change, injection/extraction rate, and injection pressure do not correlate with the largest M_{MAX}.

Suggestions have been made regarding what operational parameters might be adjusted in order to mitigate induced seismicity. These suggestions include injecting into formations that are sealed from the basement, and avoiding known faults. There has, however, yet to be a demonstration of an approach that works in general for projects of a particular type. It is also not clear how we would we recognize success since there can be no evidence for the earthquake that did not occur. More complete reporting would be beneficial.

8.6 Future trends

8.6.1 Earthquake prediction

There is presently no reliable method to predict earthquakes. Current approaches to reducing hazard comprise general long-term forecasting based on the history of past earthquakes including instrumental data, historical documents, and paleoseismology using methods such as trenching [*e.g.*, Obermeier, 1996]. This approach assumes that patterns of seismicity persist in local areas. It cannot make precise predictions, even in plate boundary zones [Lindh, 2005], and may work even more poorly in intraplate areas (Section 1.1) [Stein *et al.*, 2015]. In regions with little history of seismicity it may not be possible to implement.

Nicol *et al.* [2011] reviewed this issue from the point of view of CCS. They pointed out that the focus tends to be on reservoir-scale pressure increases and the effect of crustal loading on local faults is not routinely considered. Modeling crustal loading or unloading, and likely effects on the dynamics of groundwater, might be fruitful avenues of approach. Another useful approach could be to study jointly surface deformation and seismicity. In many of the cases in our database pre-seismic deformation ranging from large to small is reported. Although the two have been jointly interpreted in the case of several individual projects [*e.g.*, Goertz-Allmann *et al.*, 2014; Keiding *et al.*, 2010] we are not aware that systematic relationships have been explored for induced earthquakes as a whole.

8.6.2 Earthquake management

There is a weak tendency for the size of the largest induced earthquake to increase with time (Figure 124). There is also a strong tendency for the number of reports of induced seismicity

to increase with time and for the lower limit of magnitude reporting to reduce. The latter is likely partly a result of improved instrumentation. It is not clear if the former reflects improved reporting or simply larger induced earthquakes.

Coal mining in China is an illustrative case. The expanding Chinese economy is founded on coal as an energy source but at the same time shallow resources are being rapidly depleted (Figure 134). The future trend is thus to go deeper [Li *et al.*, 2007]. In the two decades from 1980-2000 the average mining depth increased from 288 m to 500 m. Now, over 75% of the coal has been removed from the top 1000 m and the recent increase in mine seismicity there results largely from increases in mining depth and the size of galleries. Super-deep mines (>1200 m in depth), as have induced seismicity in South Africa for decades, are planned in China for the future. Fluid injection for waste disposal, enhanced oil recovery, hydrofracturing and geothermal energy, are also expanding rapidly and have resulted in some of the most significant increases in induced seismicity in recent years [Ellsworth, 2013]. Other industries such as building dams and CCS may be expected to expand over the coming years.

Management of the problem is moving forward rapidly as additional stakeholders become involved [*e.g.*, Wang *et al.*, 2016]. For example, the issue of induced earthquakes is now of concern to the US Army Corps of Engineers because of the threat to critical federal infrastructure, *e.g.*, levees and dams. No societal benefit comes without price (there is no free lunch), but public policy, engineering, preparation, and outreach can enable societally beneficial projects to go ahead under circumstances that are understood and acceptable to stakeholders.

8.7 Possible future avenues of work

The following are recommended avenues of future work:

1. Publish a peer-reviewed paper on the work done to date;
2. Maintain the database up to date by adding new cases of induced seismicity on a monthly basis;
3. Investigate the effect of Earth tides to estimate the minimum stress change observed to modulate earthquake activity. This will provide one measure of the minimum anthropogenic stress change required before an earthquake can plausibly be attributed to human induction;
4. Investigate possible links between UK earthquakes and hydrology;
5. Establish a website to host the database and engage with stakeholders;
6. Improve the magnitude data in the database by determining M_W for as many cases as possible;
7. Investigate correlations between parameters in more detail;
8. Study the relationship between surface deformation and induced seismicity.

Acknowledgments

This work benefitted from discussions with Julian Bommer, Bruce Julian, Kosuke Heki, Tianhui Ma, Steve Spottiswoode, Michelle Grobbelaar and Deborah Weiser. Ang Li assisted with locating Chinese cases. Bruce Julian plotted the maps in Appendix 7. The project was funded by the Nederlandse Aardolie Maatschappij BV (NAM), Schepersmaat 2, 9405 TA Assen, The Netherlands and this report was submitted to Jan van Elk and Dirk Doornhof (NAM).

References

Ahmad, M. U., and J. A. Smith (1988), Earthquakes, injection wells, and the Perry Nuclear Power Plant, Cleveland, Ohio, Geology, 16, 739-742.

Ake, J., K. Mahrer, D. O'Connell, and L. Block (2005), Deep-injection and closely monitored induced seismicity at Paradox Valley, Colorado, Bull. seismol. Soc. Am., 95, 664-683.

Al-Enezi, A., L. Petrat, R. Abdel-Fattah, and G. D. M. Technologie (2008), Induced seismicity and surface deformation within Kuwait's oil fields, Proceedings of the Proc. Int. Conf. Geol. Seismol, pp. 177-183.

Allis, R. G., S. A. Currie, J. D. Leaver, and S. Sherburn (1985), Results of injection testing at Wairakei geothermal field, New Zealand, Transactions of the Geothermal Resources Council, 289-294.

Amidzic, D., S. K. Murphy, and G. Van Aswegen (1999), Case study of a large seismic event at a South African gold mine, Proceedings of the 9th ISRM Congress.

Amos, C. B., P. Audet, W. C. Hammond, R. Bürgmann, I. A. Johanson, and G. Blewitt (2014), Uplift and seismicity driven by groundwater depletion in central California, Nature, 509, 483-486.

Anonymous (2014), Literature review on injection-related induced seismicity and its relevance to nitrogen injection, pp 46, Earth, Environmental and Life Sciences, Utrecht, Netherlands Report TNO 2014 R11761.

Arkhipova, E. V., A. D. Zhigalin, L. I. Morozova, and A. V. Nikolaev (2012), The Van earthquake on October 23, 2011: Natural and technogenic causes, Proceedings of the Doklady Earth Sciences Conference, pp. 1176-1179.

Asanuma, H., N. Soma, H. Kaieda, Y. Kumano, T. Izumi, K. Tezuka, H. Niitsuma, and D. Wyborn (2005), Microseismic monitoring of hydraulic stimulation at the Australian HDR project in Cooper Basin, Proceedings of the Proceedings World Geothermal Congress, pp. 24-29.

Avouac, J.-P. (2012), Earthquakes: Human-induced shaking, Nature Geoscience, 5, 763–764.

Awad, M., and M. Mizoue (1995), Earthquake activity in the Aswan region, Egypt, Pure Appl. Geophys., 145, 69-86.

Baisch, S., and H. P. Harjes (2003), A model for fluid-injection-induced seismicity at the KTB, Germany, Geophys. J. Int., 152, 160-170.

Baisch, S., and R. Vörös (2011), Geomechanical study of Blackpool seismicity, pp 58, Report prepared for Cuadrilla Ltd. by Q-con GmbH.

Baisch, S., R. Voeroes, R. Weidler, and D. Wyborn (2009a), Investigation of Fault Mechanisms during Geothermal Reservoir Stimulation Experiments in the Cooper Basin, Australia, Bull. seismol. Soc. Am., 99, 148-158.

Baisch, S., R. Vörös, R. Weidler, and D. Wyborn (2009b), Investigation of fault mechanisms during geothermal reservoir stimulation experiments in the Cooper Basin, Australia, Bull. seismol. Soc. Am., 99, 148-158.

Baisch, S., M. Bohnhoff, L. Ceranna, Y. Tu, and H. P. Harjes (2002), Probing the crust to 9-km depth: Fluid-injection experiments and induced seismicity at the KTB superdeep drilling hole, Germany, Bull. seismol. Soc. Am., 92, 2369-2380.

Baisch, S., R. Weidler, R. Voros, D. Wyborn, and L. de Graaf (2006a), Induced seismicity during the stimulation of a geothermal HFR reservoir in the Cooper Basin, Australia, Bull. seismol. Soc. Am., 96, 2242-2256.

Baisch, S., R. Weidler, R. Vörös, D. Wyborn, and L. de Graaf (2006b), Induced seismicity during the stimulation of a geothermal HFR reservoir in the Cooper Basin, Australia, Bull. seismol. Soc. Am., 96, 2242-2256.

Baisch, S., R. Voeroes, E. Rothert, H. Stang, R. Jung, and R. Schellschmidt (2010), A numerical model for fluid injection induced seismicity at Soultz-sous-Forets, International Journal of Rock Mechanics and Mining Sciences, 47, 405-413.

Baisch, S., E. Rothert, H. Stang, R. Voeroes, C. Koch, and A. McMahon (2015), Continued geothermal reservoir stimulation experiments in the Cooper Basin (Australia), Bull. seismol. Soc. Am., 105, 198-209.

Balassanian, S. Y. (2005), Earthquakes induced by deep penetrating bombing?, Acta Seismologica Sinica, 18, 741-745.

Bardainne, T., N. Dubos-Sallee, G. Senechal, P. Gaillot, and H. Perroud (2008), Analysis of the induced seismicity of the Lacq gas field (southwestern France) and model of deformation, Geophys. J. Int., 172, 1151-1162.

Batini, F., R. Console, and G. Luongo (1985), Seismological study of Larderello-Travale geothermal area, Geothermics, 14, 255–272.

Batini, F., C. Bufe, G. M. Cameli, R. Console, and A. Fiordelisi (1980), Seismic monitoring in Italian geothermal areas I: seismic activity in the Larderello-Travale region, Proceedings of the Second DOE-ENEL Workshop on Cooperative Research in Geothermal Energy, Lawrence Berkeley Laboratory, Berkeley, CA, USA, October 20–22, pp. 20–47.

Bella, F., P. F. Biagi, M. Caputo, E. Cozzi, G. Della Monica, A. Ermini, W. Plastino, and V. Sgrigna (1998), Aquifer-induced seismicity in the Central Apennines (Italy), Pure Appl. Geophys., 153, 179-194.

Benetatos, C., J. Malek, and F. Verga (2013), Moment tensor inversion for two micro-earthquakes occurring inside the Haje gas storage facilities, Czech Republic, Journal of Seismology, 17, 557-577.

Bennett, T. J., M. E. Marshall, B. W. Barker, and J. R. Murphy (1994), Characteristics of rockbursts for use in seismic discrimination, Maxwell Labs Inc, San Diego, California SSS-FR-93-14382.

Bertani, R. (2010), Geothermal power generation in the world: 2005–2010 update report, Proceedings of the World Geothermal Congress 2010, Bali, Indonesia, 25-29 April 2010.

Block, L. V., C. K. Wood, W. L. Yeck, and V. M. King (2015), Induced seismicity constraints on subsurface geological structure, Paradox Valley, Colorado, Geophys. J. Int., 200, 1170-1193.

Boettcher, M. S., D. L. Kane, A. McGarr, M. J. S. Johnston, and Z. Reches (2015), Moment tensors and other source parameters of mining-induced earthquakes in TauTona Mine, South Africa, Bull. seismol. Soc. Am., 105, 1576-1593.

Bohnhoff, M., S. Baisch, and H. P. Harjes (2004), Fault mechanisms of induced seismicity at the superdeep German Continental Deep Drilling Program (KTB) borehole and their relation to fault structure and stress field, J. Geophys. Res., 109.

Bossu, R., J. R. Grasso, L. M. Plotnikova, B. Nurtaev, J. Frechet, and M. Moisy (1996), Complexity of intracontinental seismic faultings: The Gazli, Uzbekistan, sequence, Bull. seismol. Soc. Am., 86, 959–971.

Bou-Rabee, F., and A. Nur (2002), The 1993 M 4. 7 Kuwait earthquake: Induced by the burning of the oil fields, Kuwait J. Sci. Eng, 29, 155-163.

Boucher, G., A. Ryall, and A. E. Jones (1969), Earthquakes associated with underground nuclear explosions, J. Geophys. Res., 74, 3808-3820.

Bourne, S. J., S. J. Oates, J. J. Bommer, B. Dost, J. van Elk, and D. Doornhof (2015), Monte Carlo method for probabilistic hazard assessment of induced seismicity due to conventional natural gas production, Bull. seismol. Soc. Am., 105, 1721-1738.

Brudy, M., M. D. Zoback, K. Fuchs, F. Rummel, and J. Baumgartner (1997), Estimation of the complete stress tensor to 8 km depth in the KTB scientific drill holes: Implications for crustal strength, J. Geophys. Res., 102, 18453-18475.

Calo, M., C. Dorbath, and M. Frogneux (2014), Injection tests at the EGS reservoir of Soultz-sous-Forets. Seismic response of the GPK4 stimulations, Geothermics, 52, 50-58.

Caloi, P., M. De Panfilis, D. Di Filippo, L. Marcelli, and M. C. Spadea (1956), Terremoti della Val Padana del 15-16 maggio 1951, Annals of Geophysics, 9, 63-105.

Carder, D. S. (1945), Seismic investigations in the Boulder Dam area, 1940-1944, and the influence of reservoir loading on local earthquake activity, Bull. seismol. Soc. Am., 35, 175-192.

Cartlidge, E. (2014), Human activity may have triggered fatal Italian earthquakes, panel says, Science, 344, 141.

Castle, R. O., and R. F. Yerkes (1976), Recent surface movements in the Baldwin Hills, Los Angeles county, California, U.S. Geological Survey Professional Paper 882, pp viii+125, U.S. Geological Survey, Washington, D.C.

Cesca, S., F. Grigoli, S. Heimann, A. Gonzalez, E. Buforn, S. Maghsoudi, E. Blanch, and T. Dahm (2014), The 2013 September-October seismic sequence offshore Spain: a case of seismicity triggered by gas injection?, Geophys. J. Int., 198, 941-953.

Chabora, E., E. Zemach, P. Spielman, P. Drakos, S. Hickman, S. Lutz, K. Boyle, A. Falconer, A. Robertson-Tait, N. C. Davatzes, P. Rose, E. Majer, and S. Jarpe (2012), Hydraulic stimulation of Well 27-15, Desert Peak geothermal field, Nevada, U.S.A., Proceedings of the 37th Standford Geothermal Workshop, Stanford, CA.

Cladouhos, T., S. Petty, Y. Nordin, M. Moore, K. Grasso, M. Uddenberg, M. Swyer, B. Julian, and G. Foulger (2013), Microseismic monitoring of Newberry Volcano EGS Demonstration, Proceedings of the Thirty-Eighth Workshop on Geothermal Reservoir Engineering, Stanford University, Stanford, California, February 11-13, 2013.

Clarke, H., L. Eisner, P. Styles, and P. Turner (2014a), Felt seismicity associated with shale gas hydraulic fracturing: The first documented example in Europe, Geophys. Res. Lett., 41, 8308-8314.

Clarke, H., L. Eisner, P. Styles, and P. Turner (2014b), Felt seismicity associated with shale gas hydraulic fracturing: The first documented example in Europe, Geophys. Res. Lett., 41, 8308–8314.

Cochran, E. S., J. Vidale, and S. Tanaka (2004), Earth tides can trigger shallow thrust fault earthquakes, Science, 306, 1164-1166.

Darold, A., A. A. Holland, C. Chen, and A. Youngblood (2014), Preliminary analysis of seismicity near Eagleton 1-29, Carter County, July 2014, pp 17, Oklahoma Geological Survey Open-File Report OF2-2014.

Davies, R., G. Foulger, A. Bindley, and P. Styles (2013), Induced seismicity and hydraulic fracturing for the recovery of hydrocarbons, Marine and Petroleum Geology, 45, 171-185.

Davis, S. D., and W. D. Pennington (1989), Induced seismic deformation in the Cogdell oil field of west Texas, Bull. seismol. Soc. Am., 79, 1477-1495.

Davis, S. D., and C. Frohlich (1993), Did (or will) fluid injection cause earthquakes?-criteria for a rational assessment, Seismol. Res. Lett., 64, 207-224.

de Pater, C. J., and S. Baisch (2011), Geomechanical study of Bowland Shale seismicity. Synthesis report, pp 71.

deBruyn, I. A., and F. G. Bell (1997), Mining and induced seismicity in South Africa: A survey, Proceedings of the International Symposium on Engineering Geology and the Environment, Athens, Greece, 23-27 June, pp. 2321-2326.

Deichmann, N., and J. Ernst (2009), Earthquake focal mechanisms of the induced seismicity in 2006 and 2007 below Basel (Switzerland), Swiss Journal of Geosciences, 102, 457-466.

Deichmann, N., and D. Giardini (2009), Earthquakes induced by the stimulation of an Enhanced Geothermal System below Basel (Switzerland), Seismol. Res. Lett., 80, 784–798.

Dreger, D., S. R. Ford, and W. R. Walter (2008), Source analysis of the Crandall Canyon, Utah mine collapse, Science, 321, 217.

Durrheim, R. J. (2010), Mitigating the risk of rockbursts in the deep hard rock mines of South Africa: 100 years of research, *in* Extracting the Science: a century of mining research, edited by J. Brune, pp. 156-171, Society for Mining, Metallurgy, and Exploration, Inc.

Durrheim, R. J., D. Vogt, and M. Manzi (2013), Advances in geophysical technologies for the exploration and safe mining of deep gold ore bodies in the Witwatersrand basin, South Africa, *in* Mineral Deposit Research for a High-Tech World, edited by E. Jonsson, pp. 118-121.

Durrheim, R. J., R. L. Anderson, A. Cichowicz, R. Ebrahim-Trolloped, G. Hubert, A. Kijko, A. McGarr, W. Ortlepp, and N. van der Merwe (2006), The risks to miners, mines, and the public posed by large seismic events in the gold mining districts of South Africa, Proceedings of the Proceedings of the Third International Seminar on Deep and High Stress Mining, 2-4 October 2006, Quebec City, Canada.

Eberhart-Phillips, D., and D. H. Oppenheimer (1984), Induced seismicity in The Geysers geothermal area, California, J. Geophys. Res., 89, 1191-1207.

Ellsworth, W. L. (2013), Injection-induced earthquakes, Science, 341, 142-149.

Emanov, A. F., A. A. Emanov, A. V. Fateev, E. V. Leskova, E. V. Shevkunova, and V. G. Podkorytova (2014), Mining-induced seismicity at open pit mines in Kuzbass (Bachatsky earthquake on June 18, 2013), Journal of Mining Science, 50, 224-228.

Engdahl, E. R. (1972), Seismic effects of the MILROW and CANNIKIN nuclear explosions, Bull. seismol. Soc. Am., 62, 1411-1423.

Erzinger, J., and I. Stober (2005), Introduction to special issue: long-term fluid production in the KTB pilot hole, Germany, Geofluids, 5, 1-7.

Evans, D. M. (1966), The Denver area earthquakes and the Rocky Mountain Arsenal disposal well, The Mountain Geologist, 3, 23-36.

Evans, K. F., A. Zappone, T. Kraft, N. Deichmann, and F. Moia (2012), A survey of the induced seismic responses to fluid injection in geothermal and CO_2 reservoirs in Europe, Geothermics, 41, 30-54.

Farahbod, A. M., H. Kao, D. M. Walker, and J. F. Cassidy (2015), Investigation of regional seismicity before and after hydraulic fracturing in the Horn River Basin, northeast British Columbia, Canadian Journal of Earth Sciences, 52, 112-122.

Feignier, B., and R. P. Young (1992), Moment tensor inversion of induced microseismic events: Evidence of non-shear failures in the $-4 < M < -2$ moment magnitude range, Geophys. Res. Lett., 19, 1503-1506.

Ferrazzini, V., B. Chouet, M. Fehler, and K. Aki (1990), Quantitative analysis of long-period events recorded during hydrofracture experiments at Fenton Hill, New Mexico, J. Geophys. Res., 95, 21871-21884.

Fielitz, D., and U. Wegler (2015), Intrinsic and scattering attenuation as derived from fluid induced microseismicity at the German Continental Deep Drilling site, Geophys. J. Int., 201, 1346-1361.

Foulger, G. R. (1988a), Hengill triple junction, SW Iceland; 2. Anomalous earthquake focal mechanisms and implications for process within the geothermal reservoir and at accretionary plate boundaries, J. Geophys. Res., 93, 13,507-513,523.

Foulger, G. R. (1988b), Hengill triple junction, SW Iceland; 1. Tectonic structure and the spatial and temporal distribution of local earthquakes, J. Geophys. Res., 93, 13493-13506.

Foulger, G. R., and R. E. Long (1984), Anomalous focal mechanisms; tensile crack formation on an accreting plate boundary, Nature, 310, 43-45.
Foulger, G. R., and B. R. Julian (2014), Maximizing EGS earthquake location accuracies, Proceedings of the Thirty-Ninth Workshop on Geothermal Reservoir Engineering, Stanford, California, February 24-26, 2014, SGP-TR-202.
Foulger, G. R., R. E. Long, P. Einarsson, and A. Björnsson (1989), Implosive earthquakes at the active accretionary plate boundary in northern Iceland, Nature, 337, 640-642.
Foulger, G. R., C.-H. Jahn, G. Seeber, P. Einarsson, B. R. Julian, and K. Heki (1992), Post-rifting stress relaxation at the divergent plate boundary in Iceland, Nature, 358, 488-490.
Gaite, B., A. Ugalde, A. Villaseñor, and E. Blanch (2016), Improving the location of induced earthquakes associated with an underground gas storage in the Gulf of Valencia (Spain), Phys. Earth Planet. Int., 254, 46–59.
Gan, W., and C. Frohlich (2013), Gas injection may have triggered earthquakes in the Cogdell oil field, Texas, Proc. Nat. Acad. Sci., 110, 18786-18791.
Gee, D., A. Sowter, S. Marsh, and J. G. Gluyas (2016), Monitoring land subsidence due to natural gas extraction; validation of the Intermittent SBAS (ISBAS) DInSAR algorithm over reservoirs of North Holland, Netherlands, Marine and Petroleum Geology, submitted.
Glowacka, E., and F. A. Nava (1996), Major earthquakes in Mexicali Valley, Mexico, and fluid extraction at Cerro Prieto geothermal field, Bull. seismol. Soc. Am., 86, 93-105.
Gluyas, J., and R. Swarbrick (in press, 2016), Petroleum Geoscience, 2nd ed., Wiley-Blackwell.
Gluyas, J. G., and A. Peters (2010), Late field-life for oil reservoirs – a hydrogeological problem, paper presented at British Hydrological Society Third International Symposium, Managing Consequences of a Changing Global Environment.
Godano, M., E. Gaucher, T. Bardainne, M. Regnier, A. Deschamps, and M. Valette (2010), Assessment of focal mechanisms of microseismic events computed from two three-component receivers: application to the Arkema-Vauvert field (France), Geophysical Prospecting, 58, 772-787.
Goertz-Allmann, B. P., D. Kuhn, V. Oye, B. Bohloli, and E. Aker (2014), Combining microseismic and geomechanical observations to interpret storage integrity at the In Salah CCS site, Geophys. J. Int., 198, 447-461.
Gonzalez, P. J., K. F. Tiampo, M. Palano, F. Cannavo, and J. Fernandez (2012), The 2011 Lorca earthquake slip distribution controlled by groundwater crustal unloading, Nature Geoscience, 5, 821-825.
Got, J.-L., J. Frechet, and F. W. Klein (1994), Deep fault plane geometry inferred from multiplet relative relocation beneath the south flank of Kilauea, J. Geophys. Res., 99, 15375-15386.
Grasle, W., W. Kessels, H. J. Kumpel, and X. Li (2006), Hydraulic observations from a 1 year fluid production test in the 4000 m deep KTB pilot borehole, Geofluids, 6, 8-23.
Green, C. A., P. Styles, and B. J. Baptie (2012), Preese Hall shale gas fracturing review & recommendations for induced seismic mitigation: UK Deparment of Energy and Climate Change, Induced Seismicity Mitigation Report, pp iv+26 5055.
Guglielmi, Y., F. Cappa, J.-P. Avouac, P. Henry, and D. Elsworth (2015), Seismicity triggered by fluid injection-induced aseismic slip, Science, 348, 1224-1226.
Gupta, H. K. (2002), A review of recent studies of triggered earthquakes by artificial water reservoirs with special emphasis on earthquakes in Koyna, India, Earth-Science Reviews, 58, 279-310.
Hamilton, D. H., and R. L. Meehan (1971), Ground rupture in the Baldwin Hills, Science, 172, 333-344.

Hamilton, R. M., B. E. Smith, F. G. Fischer, and P. J. Papanek (1972), Earthquakes caused by underground nuclear explosions on Pahute Mesa, Nevada Test Site, Bull. seismol. Soc. Am., 62, 1319-1341.

Hanks, T. C. (1977), Earthquake stress drops, ambient tectonic stresses and stresses that drive plate motions, Pure Appl. Geophys., 115, 441-458.

Hanks, T. C., and H. Kanamori (1979), A moment magnitude scale, J. Geophys. Res., 84, 2348-2350.

Häring, M. O., U. Schanz, F. Ladner, and B. C. Dyer (2008), Characterisation of the Basel 1 enhanced geothermal system, Geothermics, 37, 469-495.

Harris, D. (2012), The impact of cultural and religious influences during natural disasters (volcano eruptions), Earthquake-Report.com, http://earthquake-report.com/2012/09/27/the-impact-of-cultural-and-religious-influences-during-natural-disasters-volcano-eruptions/, 3:05 pm September 27, 2012.

Hartline, C. (2014), Seismic Monitoring Advisory Committee Review, pp 44, Calpine Corporation.

Healy, J. H., W. W. Rubey, D. T. Griggs, and C. B. Raleigh (1968), The Denver earthquakes, Science, 61, 1301-1310.

Heesakkers, V., S. K. Murphy, G. van Aswegen, R. Domoney, S. Addams, T. Dewers, M. Zechmeister, and Z. Reches (2005), The rupture zone of the M=2.2 earthquake that reactivated the ancient Pretorius Fault in TauTona Mine, South Africa, Proceedings of the Fall Meeting of the American Geophysical Union abstract #S31B-04, San Francisco.

Heki, K., S. Miyazaki, and H. Tsuji (1997), Silent fault slip following an interplate thrust earthquake at the Japan Trench, Nature, 386, 595-598.

Heki, K., G. R. Foulger, B. R. Julian, and C.-H. Jahn (1993), Plate dynamics near divergent boundaries: Geophysical implications of postrifting crustal deformation in NE Iceland, J. Geophys. Res., 98, 14279-14297.

Herrmann, R. B. (1978), A seismological study of two Attica, New York earthquakes, Bull. seismol. Soc. Am., 68, 641-651.

Hill, D. P., P. A. Reasenberg, A. Michael, W. J. Arabasz, G. Beroza, D. Brumbaugh, J. N. Brune, R. Castro, S. Davis, D. dePolo, W. L. Ellsworth, J. Gomberg, S. Harmsen, L. House, S. M. Jackson, M. J. S. Johnston, L. Jones, R. Keller, S. Malone, L. Munguia, S. Nava, J. C. Pechmann, A. Sanford, R. W. Simpson, R. B. Smith, M. Stark, M. Stickney, A. Vidal, S. Walter, V. Wong, and J. Zollweg (1993), Seismicity remotely triggered by the magnitude 7.3 Landers, California, earthquake, Science, 260, 1617-1623.

Hitzman, M. W. (Ed.) (2013), Induced Seismicity Potential in Energy Technologies x+248 pp., National Academies Press, Washington, D.C.

Hough, S. E., and M. Page (2015), A Century of Induced Earthquakes in Oklahoma?, Bull. seismol. Soc. Am., 105, 2863-2870.

Hsieh, P. A., and J. D. Bredehoeft (1981), A reservoir analysis of the Denver earthquakes: A case of induced seismicity, J. Geophys. Res., 86, 903-920.

Huaman, R. N. E., and T. X. Jun (2014), Energy related CO_2 emissions and the progress on CCS projects: a review, Renewable and Sustainable Energy Reviews, 31, 368-385.

Husen, S., C. Bachmann, and D. Giardini (2007), Locally triggered seismicity in the central Swiss Alps following the large rainfall event of August 2005, Geophys. J. Int., 171, 1126-1134.

Husen, S., E. Kissling, and A. von Deschwanden (2012), Induced seismicity during the construction of the Gotthard Base Tunnel, Switzerland: hypocenter locations and source dimensions, Journal of Seismology, 16, 195-213.

Jahr, T., G. Jentzsch, H. Letz, and M. Sauter (2005), Fluid injection and surface deformation at the KTB location: Modelling of expected tilt effects, Geofluids, 5, 20-27.

Jahr, T., G. Jentzsch, H. Letz, and A. Gebauer (2007), Tilt observation around the KTB-site Germany: Monitoring and modelling of fluid induced deformation of the upper crust of the Earth, *in* Dynamic Planet: Monitoring and Understanding a Dynamic Planet with Geodetic and Oceanographic Tools, edited by P. Tregoning and C. Rizos, pp. 467-472.

Jahr, T., G. Jentzsch, A. Gebauer, and T. Lau (2008), Deformation, seismicity, and fluids: Results of the 2004/2005 water injection experiment at the KTB/Germany, J. Geophys. Res., 113.

Jaku, E. P., A. J. Jager, and M. K. C. Roberts (2001), A review of rock-related fatality trends in the South African gold mining industry, *in* Rock Mechanics in the National Interest, edited by D. Elsworth, J. P. Tinucci and K. A. Heasley, pp. 467-471.

Johnston, A. C., and E. S. Schweig (1996), The enigma of the New Madrid earthquakes of 1811-1812, Annual Review of Earth and Planetary Sciences,, 24, 339-384.

Jost, M. L., T. Busselberg, O. Jost, and H. P. Harjes (1998), Source parameters of injection-induced microearthquakes at 9 km depth at the KTB deep drilling site, Germany, Bull. seismol. Soc. Am., 88, 815-832.

Julià, J., A. A. Nyblade, R. Durrheim, L. Linzer, R. Gök, P. Dirks, and W. Walter (2009), Source mechanisms of mine-related seismicity, Savuka mine, South Africa, Bull. seismol. Soc. Am., 99, 2801-2814.

Julian, B. R., A. D. Miller, and G. R. Foulger (1998), Non-double-couple earthquakes I. Theory, Rev. Geophys., 36, 525-549.

Julian, B. R., G. R. Foulger, and K. Richards-Dinger (2004), The Coso Geothermal Area: A Laboratory for Advanced MEQ Studies for Geothermal Monitoring, Proceedings of the Geothermal Resources Council Annual Meeting, Palm Springs, August 2004.

Julian, B. R., G. R. Foulger, and F. Monastero (2007), Microearthquake moment tensors from the Coso Geothermal area, Proceedings of the Thirty-Second Workshop on Geothermal Reservoir Engineering, Stanford University, Stanford, California, January 22-24, pp. SGP-TR-183.

Julian, B. R., G. R. Foulger, F. C. Monastero, and S. Bjornstad (2010), Imaging hydraulic fractures in a geothermal reservoir, Geophys. Res. Lett., 37.

Kaieda, H., S. Sasaki, and D. Wyborn (2010), Comparison of characteristics of micro-earthquakes observed during hydraulic stimulation operations in Ogachi, Hijiori and Cooper Basin HDR projects, Proceedings of the World Geothermal Congress, Bali, Indonesia, April 25 - 30.

Kao, H., A. M. Farahbod, J. F. Cassidy, M. Lamontagne, D. Snyder, and D. Lavoie (2015), Natural resources canada's induced seismicity research, Proceedings of the Schatzalp Induced Seismicity Workshop, Davos, Switzerland, 10-13 March.

Kaven, J. O., S. H. Hickman, and N. C. Davatzes (2014), Micro-seismicity and seismic moment release within the Coso Geothermal Field, California, Proceedings of the Thirty-Ninth Workshop on Geothermal Reservoir Engineering, Stanford University, Stanford, California, February 24-26, 2014, pp. SGP-TR-202.

Kaven, J. O., S. H. Hickman, A. F. McGarr, and W. L. Ellsworth (2015), Surface monitoring of microseismicity at the Decatur, Illinois, CO_2 sequestration demonstration site, Seismol. Res. Lett., 86, 1096-1101.

Keiding, M., T. Arnadottir, S. Jonsson, J. Decriem, and A. Hooper (2010), Plate boundary deformation and man-made subsidence around geothermal fields on the Reykjanes Peninsula, Iceland, J. Volc. Geotherm. Res., 194, 139-149.

Keith, C. M., D. W. Simpson, and O. V. Soboleva (1982), Induced seismicity and style of deformation at Nurek reservoir, Tadjik ssr, J. Geophys. Res., 87, 4609-4624.

Keranen, K. M., H. M. Savage, G. A. Abers, and E. S. Cochran (2013), Potentially induced earthquakes in Oklahoma, USA: Links between wastewater injection and the 2011 Mw 5.7 earthquake sequence, Geology, 41, 699-702.

Keranen, K. M., M. Weingarten, G. A. Abers, B. A. Bekins, and S. Ge (2014), Sharp increase in central Oklahoma seismicity since 2008 induced by massive wastewater injection, Science, 345, 448-451.

King, G. C. P., R. S. Stein, and J. Lin (1994), Static stress changes and the triggering of earthquakes, Bull. seismol. Soc. Am., in press.

King, V. M., L. V. Block, W. L. Yeck, C. K. Wood, and S. A. Derouin (2014), Geological structure of the Paradox Valley Region, Colorado, and relationship to seismicity induced by deep well injection, J. Geophys. Res., 119, 4955-4978.

Kinscher, J., P. Bernard, I. Contrucci, A. Mangeney, J. P. Piguet, and P. Bigarre (2015), Location of microseismic swarms induced by salt solution mining, Geophys. J. Int., 200, 337-362.

Klein, F. W., P. Einarsson, and M. Wyss (1977), The Reykjanes Peninsula, Iceland, earthquake swarm of September 1972 and its tectonic significance, J. Geophys. Res., 82, 865-887.

Klose, C. D. (2007a), Coastal land loss and gain as potential earthquake trigger mechanism in SCRs, Proceedings of the Fall Meeting of the American Geophysical Union abstract #T51D-0759, San Francisco, 10–14 December.

Klose, C. D. (2007b), Geomechanical modeling of the nucleation process of Australia's 1989 M5.6 Newcastle earthquake, Earth planet. Sci. Lett., 256, 547-553.

Klose, C. D. (2012), Evidence for anthropogenic surface loading as trigger mechanism of the 2008 Wenchuan earthquake, Environmental Earth Sciences, 66, 1439-1447.

Knoll, P. (1990), The fluid-induced tectonic rock burst of March 13, 1989 in Werra potash mining district of the GDR (first results), Gerlands Beitrage zur Geophysik, 99, 239-245.

Kovach, R. L. (1974), Source mechanisms for Wilmington oil field, California, subsidence earthquakes, Bull. seismol. Soc. Am., 64, 699–711.

Kozlowska, M., B. Orlecka-Sikora, G. Kwiatek, M. S. Boettcher, and G. Dresen (2015), Nanoseismicity and picoseismicity rate changes from static stress triggering caused by a Mw 2.2 earthquake in Mponeng gold mine, South Africa, J. Geophys. Res., 120, 290-307.

Kravania, S., F. Batini, A. Fiordelise, and G. F. Panza (2000), Full moment tensor retrieval from waveform inversion in the Larderello geothermal area, Pure Appl. Geophys., 157, 1379-1392.

Kundu, B., N. K. Vissa, and V. K. Gahalaut (2015), Influence of anthropogenic groundwater unloading in Indo-Gangetic plains on the 25 April 2015 Mw 7.8 Gorkha, Nepal earthquake, Geophys. Res. Lett., 42, 10,607–610,613.

Kusznir, N. J., N. H. Al-Saigh, and D. P. Ashwin (1982), Induced seismicity generated by longwall coal mining in the North Staffordshire coal-field, U. K., Proceedings of the Procedings of the First International Congress on Rockbursts and Seismicity in Mines, Johannesburg, South Africa, pp. 153-160.

Latham, G., J. Dorman, F. Duennebier, M. Ewing, D. Lammlein, and Y. Nakamura (1973), Moonquakes, meteoroids, and the state of the lunar interior, Proceedings of the Third Lunar and Planetary Science Conference abstract, Houston, Texas, January 10-13.

Lei, X., G. Yu, S. Ma, X. Wen, and Q. Wang (2008), Earthquakes induced by water injection at~ 3 km depth within the Rongchang gas field, Chongqing, China, J. Geophys. Res., 113.

Lei, X., S. Ma, W. Chen, C. Pang, J. Zeng, and B. Jiang (2013), A detailed view of the injection-induced seismicity in a natural gas reservoir in Zigong, southwestern Sichuan Basin, China, J. Geophys. Res., 118, 4296-4311.

Leith, W., D. W. Simpson, and W. Alvarez (1981), Structure and permeability - geologic controls on induced seismicity at Nurek reservoir, Tadjikistan, USSR, Geology, 9, 440-444.

Li, G. (2011), World atlas of oil and gas basins, Wiley-Blackwell, 496 pp.

Li, T., M. F. Cai, and M. Cai (2007), A review of mining-induced seismicity in China, International Journal of Rock Mechanics and Mining Sciences, 44, 1149-1171.

Lin, C. H. (2005), Seismicity increase after the construction of the world's tallest building: An active blind fault beneath the Taipei 101, Geophys. Res. Lett., 32.

Lindh, A. G. (2005), Success and failure at Parkfield, Seismol. Res. Lett., 76, 3-6.

Lippmann-Pipke, J., J. Erzinger, M. Zimmer, C. Kujawa, M. Boettcher, E. Van Heerden, A. Bester, H. Moller, N. A. Stroncik, and Z. Reches (2011), Geogas transport in fractured hard rock - Correlations with mining seismicity at 3.54 km depth, TauTona gold mine, South Africa, Applied Geochemistry, 26, 2134-2146.

Liu, C., A. T. Linde, and I. S. Sacks (2009), Slow earthquakes triggered by typhoons, Nature, 459, 833-836.

Lofgren, B. E. (1978), Monitoring crustal deformation in The Geysers-Clear Lake geothermal area, California, Open-File Report 78-597, pp iv+26, 28 maps, U.S. Geological Survey, Washington, D.C.

Lofgren, B. E. (1981), Monitoring crustal deformation in the Geyser-Clear Lake region, *in* Research in the Geysers-Clear Lake geothermal area, Northern California, edited by R. J. McLaughlin and J. M. Donnelly-Nolan, p. viii+259, U.S. Geological Survey Professional Paper 1141, Washington, D.C.

Ma, X., Z. Li, P. Hua, J. Jiang, F. Zhao, C. Han, P. Yuan, S. Lu, and L. Peng (2015), Fluid-injection-induced seismicity experiment of the WFSD-3P borehole, Acta Geologica Sinica (English Edition), 89, 1057-1058.

Majer, E. L., and T. V. McEvilly (1981), Detailed microearthquake studies at the Cerro Prieto Geothermal Field, Proceedings of the Third Symposium on the Cerro Prieto Geothermal Field, Baja California, Mexico, Lawrence Berkeley Laboratory, Berkeley, California, March 24-26, pp. 347-352.

Majer, E. L., and T. V. McEvilly (1982), Seismological studies at the Cerro Prieto Field: 1978-1982, Proceedings of the Fourth Symposium on the Cerro Prieto Geothermal Field, Baja California, Mexico, Lawrence Berkeley Laboratory, Berkeley, California, 10–12 August, pp. 145-151.

Majer, E. L., and J. E. Peterson (2007), The impact of injection on seismicity at The Geysers, California Geothermal Field, International Journal of Rock Mechanics and Mining Sciences, 44, 1079-1090.

Majer, E. L., R. Baria, M. Stark, S. Oates, J. Bommer, B. Smith, and H. Asanuma (2007), Induced seismicity associated with enhanced geothermal systems, Geothermics, 36, 185-222.

Maxwell, S. C., and H. Fabriol (2004), Passive Seismic Imaging of CO_2 Sequestration at Weyburn, Proceedings of the Society of Engineering Geophysicists International Exposition and 74th Annual Meeting, Denver, Colorado, 10-15 October.

McGarr, A. (1991), On a possible connection between three major earthquakes in California and oil production, Bull. seismol. Soc. Am., 81, 948-970.

McGarr, A. (1992a), An implosive component in the seismic moment tensor of a mining-induced tremor, Geophys. Res. Lett., 19, 1579-1582.

McGarr, A. (1992b), Moment tensors of ten Witwatersrand mine tremors, Pure Appl. Geophys., 139, 781-800.

McGarr, A. (2014), Maximum magnitude earthquakes induced by fluid injection, Journal of Geophysical Research-Solid Earth, 119, 1008-1019.
McGarr, A., D. Simpson, and L. Seeber (2002), Case histories of induced and triggered seismicity, *in* International Geophysics Series, International Handbook of Earthquake and Engineering Seismology, edited by W. H. Lee, P. Jennings, C. Kisslinger and H. Kanamori, pp. 647-664.
McKeown, F. A. (1975), Relation of geological structure to seismicity at Pahute Mesa, Nevada Test Site, Bull. seismol. Soc. Am., 65, 747-764.
McKeown, F. A., and D. D. Dickey (1969), Fault displacements and motion related to nuclear explosions, Bull. seismol. Soc. Am., 59, 2253-2269.
McNamara, D. E., H. M. Benz, R. B. Herrmann, E. A. Bergman, P. Earle, A. Holland, R. Baldwin, and A. Gassner (2015), Earthquake hypocenters and focal mechanisms in central Oklahoma reveal a complex system of reactivated subsurface strike-slip faulting, Geophys. Res. Lett., 42, 2742-2749.
McNutt, S. R., and R. J. Beavan (1981), Volcanic earthquakes at Pavlof volcano correlated with the solid earth tide, Nature, 194, 615-618.
Mercerat, E. D., L. Driad-Lebeau, and P. Bernard (2010), Induced seismicity monitoring of an underground salt cavern prone to collapse, Pure Appl. Geophys., 167, 5-25.
Milev, A. M., and S. M. Spottiswoode (2002), Effect of the rock properties on mining-induced seismicity around the Ventersdorp Contact Reef, Witwatersrand basin, south Africa, Pure Appl. Geophys., 159, 165-177.
Miller, A. D., B. R. Julian, and G. R. Foulger (1998a), Three-dimensional seismic structure and moment tensors of non-double-couple earthquakes at the Hengill-Grensdalur volcanic complex, Iceland, Geophys. J. Int., 133, 309-325.
Miller, A. D., G. R. Foulger, and B. R. Julian (1998b), Non-double-couple earthquakes II. Observations, Rev. Geophys., 36, 551-568.
Mogren, S. M., and M. Mukhopadhyay (2013), Study of seismogenic crust in the eastern province of saudi arabia and its relation to the seismicity of the ghawar fields, paper presented at American Geophysical Union Fall Meeting, 9-13 December.
Monastero, F. C., A. M. Katzenstein, J. S. Miller, J. R. Unruh, M. C. Adams, and K. Richards-Dinger (2005), The Coso geothermal field: A nascent metamorphic core complex, Bull. Geol. Soc. Am., 117, 1534-1553.
Mossop, A., and P. Segall (1999), Volume strain within The Geysers geothermal field, J. Geophys. Res., 104, 29113-29131.
Nagel, N. B. (2001), Compaction and subsidence issues within the petroleum industry: From Wilmington to Ekofisk and beyond, Physics and Chemistry of the Earth, Part A: Solid Earth and Geodesy, 26, 3-14.
Newman, A., S. Stein, J. Weber, J. Engeln, A. Mao, and T. Dixon (1999), Slow deformation and low seismic hazard at the New Madrid seismic zone, Science, 284, 619-621.
Nicholson, C., and R. L. Wesson (1992), Triggered earthquakes and deep well activities, Pure Appl. Geophys., 139, 561-578.
Nicholson, C., E. Roeloffs, and R. L. Wesson (1988), The northeastern Ohio earthquake of 31 January 1986: Was it induced?, Bull. seismol. Soc. Am., 78, 188-217.
Nicol, A., R. Carne, M. Gerstenberger, and A. Christophersen (2011), Induced seismicity and its implications for CO_2 storage risk, *in* 10th International Conference on Greenhouse Gas Control Technologies, edited by J. Gale, C. Hendriks and W. Turkenberg, pp. 3699-3706.
Nielsen, S. B., R. Stephenson, and E. Thomsen (2007), Dynamics of Mid-Palaeocene North Atlantic rifting linked with European intra-plate deformations, Nature, 450, 1071-1074.
Obermeier, S. F. (1996), Use of liquefaction-induced features for paleoseismic analysis, Engineering Geology, 44, 1-76.

Odonne, F., I. Ménard, G. Massonat, and J.-P. Rolando (1999), Abnormal reverse faulting above a depleting reservoir, Geology, 27, 111–114.

Ohtake, M. (1974), Seismic activity induced by water injection at Matsushiro, Japan, Journal of Physics of the Earth, 22, 163-176.

Pavlovski, O. A. (1998), Radiological consequences of nuclear testing for the population of the former USSR (Input information, models, dose and risk estimates), *in* Atmopspheric Nuclear Tests (Environmental and human consequences), Proceedings of the NATO Advanced Research Workshop, edited by C. S. Shapiro, pp. 219-260, Springer, Berlin.

Pennington, W. D., S. D. Davis, S. M. Carlson, J. DuPree, and T. E. Ewing (1986), The evolution of seismic barriers and asperities caused by the depressuring of fault planes in oil and gas fields of South Texas, Bull. seismol. Soc. Am., 76, 939-948.

Perea, H., E. Masana, and P. Santanach (2012), An active zone characterized by slow normal faults, the northwestern margin of the Valencia trough (NE Iberia): a review, Journal of Iberian Geology, 38, 31-52.

Plotnikova, I. M., B. S. Nurtaev, J. R. Grasso, L. M. Matasova, and R. Bossu (1996), The character and extent of seismic deformation in the focal zone of Gazli earthquakes of 1976 and 1984, M>7.0, Pure Appl. Geophys., 147, 377-387.

Pomeroy, P. W., D. W. Simpson, and M. L. Sbar (1976), Earthquakes triggered by surface quarrying-the Wappingers Falls, New York sequence of June, 1974, Bull. seismol. Soc. Am., 66, 685-700.

Pratt, W. E., and D. W. Johnson (1926), Local subsidence of the Goose Creek oil field, J. Geol., 34, 577-590.

Prioul, R., F. H. Cornet, C. Dorbath, L. Dorbath, M. Ogena, and E. Ramos (2000), An induced seismicity experiment across a creeping segment of the Philippine Fault, J. Geophys. Res., 105, 13595-13612.

Purvis, K., K. E. Overshott, J. C. Madgett, and T. Niven (2010), The Ensign enigma: improving well deliverability in a tight gas reservoir, Proceedings of the Petroleum Geology: From Mature Basins to New Frontiers – Proceedings of the 7th Petroleum Geology Conference, London, pp. 325-336.

Raleigh, C. B., J. H. Healy, and J. D. Bredehoeft (1976), An experiment in earthquake control at Rangely, Colorado, Science, 191, 1230-1237.

Reasenberg, P. A., and R. W. Simpson (1992), Response of regional seismicity to the static stress change produced by the Loma Prieta earthquake, Science, 255, 1687-1690.

Richardson, E., and T. H. Jordan (2002), Seismicity in deep gold mines of South Africa: Implications for tectonic earthquakes, Bull. seismol. Soc. Am., 92, 1766-1782.

Ross, A., G. R. Foulger, and B. R. Julian (1999), Source processes of industrially-induced earthquakes at The Geysers geothermal area, California, Geophysics, 64, 1877-1889.

Roth, P., N. Pavoni, and N. Deichmann (1992), Seismotectonics of the eastern Swiss Alps and evidence for precipitation-induced variations of seismic activity, Tectonophysics, 207, 183-197.

Rudajev, V., and J. Sileny (1985), Seismic events with non-shear components: II Rockbursts with implosive source component, Pure Appl. Geophys., 123, 17-25.

Schultz, R., V. Stern, M. Novakovic, G. Atkinson, and Y. J. Gu (2015), Hydraulic fracturing and the Crooked Lake Sequences: Insights gleaned from regional seismic networks, Geophys. Res. Lett., 42, 2750-2758.

Seeber, L., J. G. Armbruster, W.-Y. Kim, and N. Barstow (1998), The 1994 Cacoosing Valley earthquakes near Reading, Pennsylvania: A shallow rupture triggered by quarry unloading, J. Geophys. Res., 103, 24505-24521.

Segall, P. (1985), Stress and subsidence resulting from subsurface fluid withdrawal in the epicentral region of the 1983 Coalinga earthquake, J. Geophys. Res., 90, 6801-6816.

Segall, P. (1989), Earthquakes triggered by fluid extraction, Geology, 17, 942-946.
Segall, P. (1992), Induced stresses due to fluid extraction from axisymmetrical reservoirs, Pure Appl. Geophys., 139, 535-560.
Semmane, F., I. Abacha, A. K. Yelles-Chaouche, A. Haned, H. Beldjoudi, and A. Amrani (2012), The earthquake swarm of December 2007 in the Mila region of northeastern Algeria, Natural Hazards, 64, 1855-1871.
Shapiro, S. A., J. Kummerow, C. Dinske, G. Asch, E. Rothert, J. Erzinger, H. J. Kumpel, and R. Kind (2006), Fluid induced seismicity guided by a continental fault: Injection experiment of 2004/2005 at the German Deep Drilling Site (KTB), Geophys. Res. Lett., 33.
Simiyu, S. M., and G. R. Keller (2000), Seismic monitoring of the Olkaria Geothermal area, Kenya Rift valley, J. Volc. Geotherm. Res., 95, 197-208.
Simpson, D. W., and O. V. Soboleva (1977), Water level variations and reservoir-induced seismicity at Nurek, USSR, Transactions-American Geophysical Union, 58, 1196-1196.
Simpson, D. W., and S. K. Negmatullaev (1981), Induced seismicity at Nurek reservoir, Tadjikistan, USSR, Bull. seismol. Soc. Am., 71, 1561-1586.
Simpson, D. W., and W. Leith (1985), The 1976 and 1984 Gazli, USSR, earthquakes—were they induced?, Bull. seismol. Soc. Am., 75, 1465-1468.
Skoumal, R. J., M. R. Brudzinski, and B. S. Currie (2015), Earthquakes induced by hydraulic fracturing in Poland Township, Ohio, Bull. seismol. Soc. Am., 105, 189-197.
Stark, M. A. (1990), Imaging injected water in The Geysers reservoir using microearthquake data, GRC Transactions, 17, 1697-1704.
Stein, S., M. Liu, E. Calais, and Q. Li (2009), Midcontinent earthquakes as a complex system, Seismol. Res. Lett., 80, 551-553.
Stein, S., M. Liu, T. Camelbeeck, M. Merino, A. Landgraf, E. Hintersberger, and S. Kuebler (2015), Challenges in assessing seismic hazard in intraplate Europe, *in* Seismicity, Fault Rupture and Earthquake Hazards in Slowly Deforming Regions, edited by A. Landgraf, S. Kuebler, E. Hintersberger and S. Stein, Geological Society, London, Special Publications, London.
Styles, P., P. Gasparini, E. Huenges, P. Scandone, S. Lasocki, and F. Terlizzese (2014), Report on the hydrocarbon exploration and seismicity in Emilia region, pp 213, International Commission on Hydrocarbon Exploration and Seismicity in the Emilia Region.
Suckale, J. (2009), Induced seismicity in hydrocarbon fields, Advances in Geophysics, 51, 55-106.
Suckale, J. (2010), Moderate-to-large seismicity induced by hydrocarbon production, The Leading Edge, 29, 310-319.
Tadokoro, K., M. Ando, and K. Nishigami (2000), Induced earthquakes accompanying the water injection experiment at the Nojima fault zone, Japan: Seismicity and its migration, J. Geophys. Res., 105, 6089-6104.
Talwani, P. (1995), Speculation on the causes of continuing seismicity near Koyna reservoir, India, Pure Appl. Geophys., 145, 167-174.
Tang, C., J. W. Wang, and J. Zhang (2010), Preliminary engineering application of microseismic monitoring technique to rockburst prediction in tunneling of Jinping II project, Journal of Rock Mechanics and Geotechnical Engineering, 3.
Tang, L., M. Zhang, L. Sun, and L. Wen (2015), Injection-induced seismicity in a natural gas reservoir in Hutubi, southern Junggar Basin, northwest China, paper presented at AGU Fall Meeting.
Terashima, T. (1981), Survey on induced seismicity at Mishraq area in Iraq, Journal of Physics of the Earth, 29, 371-375.

Tester, J. W., and e. al. (2006), The future of geothermal energy, pp 372, Massachusetts Institute of Technology, Cambridge, Massachusetts.

Toksöz, M. N., and H. K. Kehrer (1972), Tectonic strain release by underground nuclear explosions and its effect on seismic discrimination, Geophys. J. R. astron. Soc., 31, 141-161.

Turbitt, T., A. B. Walker, and C. W. A. Browitt (1983), Monitoring of the background and induced seismicity at the Cornwall geothermal energy site, Geophys. J. R. astron. Soc., 73, 299-299.

van der Elst, N. J., H. M. Savage, K. M. Keranen, and G. A. Abers (2013), Enhanced remote earthquake triggering at fluid-injection sites in the midwestern United States, Science, 341, 164-167.

van Eck, T., F. Goutbeek, H. Haak, and B. Dost (2006), Seismic hazard due to small-magnitude, shallow-source, induced earthquakes in The Netherlands, Engineering Geology, 87, 105-121.

Van Wees, J. D., L. Buijze, K. Van Thienen-Visser, M. Nepveu, B. B. T. Wassing, B. Orlic, and P. A. Fokker (2014), Geomechanics response and induced seismicity during gas field depletion in the Netherlands, Geothermics, 52, 206-219.

Vasco, D. W., J. Rutqvist, A. Ferretti, A. Rucci, F. Bellotti, P. Dobson, C. Oldenburg, J. Garcia, M. Walters, and C. Hartline (2013), Monitoring deformation at The Geysers Geothermal Field, California using C-band and X-band interferometric synthetic aperture radar, Geophys. Res. Lett., 40, 2567–2572.

Verdon, J. P., J.-M. Kendall, A. L. Stork, R. A. Chadwick, D. J. White, and R. C. Bissell (2013), Comparison of geomechanical deformation induced by megatonne-scale CO2 storage at Sleipner, Weyburn, and In Salah, Proceedings of the National Academy of Sciences, 110, E2762-E2771.

Villegas-Lanza, J. C., J.-M. Nocquet, F. Rolandone, M. Vallée, H. Tavera, F. Bondoux, T. Tran, X. Martin, and M. Chlieh (2016), A mixed seismic–aseismic stress release episode in the Andean subduction zone, Nature Geoscience, 9, 150–154.

Waldhauser, F., and W. L. Ellsworth (2000), A double-difference earthquake location algorithm: Method and application to the northern Hayward Fault, California, Bull. seismol. Soc. Am., 90, 1353-1368.

Wallace, T., D. V. Helmberger, and G. R. Engen (1983), Evidence of tectonic release from underground nuclear explosions in long-period *P* waves, Bull. seismol. Soc. Am., 73, 593-613.

Walsh, F. R., and M. D. Zoback (2015), Oklahoma's recent earthquakes and saltwater disposal, Science Advances, 1, no. e1500195.

Wang, P., M. J. Small, W. Harbert, and M. Pozzi (2016), A bayesian approach for assessing seismic transitions associated with wastewater injections, Bull. seismol. Soc. Am., 106, 832-845.

Wilson, M. P., R. J. Davies, G. R. Foulger, B. R. Julian, P. Styles, J. G. Gluyas, and S. Almond (2015), Anthropogenic earthquakes in the UK: A national baseline prior to shale exploitation, Marine and Petroleum Geology, 68, 1-17.

Wong, I. G., and A. McGarr (1990), Implosional failure in mining-induced seismicity: A critical review, *in* Rockbursts and Seismicity in Mines, edited by C. Fairhurst, pp. 45-51, Bakema, Rotterdam.

Wong, I. G., J. R. Humphrey, J. A. Adams, and W. J. Silva (1989), Observations of mine seismicity in the eastern Wasatch Plateau, Utah, U. S. A.: A possible case of implosional failure, Pure Appl. Geophys., 129, 369-405.

Wright, C., E. M. Kgaswane, M. T. O. Kwadiba, R. E. Simon, T. K. Nguuri, and R. McRae-Samuel (2003), South African seismicity, April 1997 to April 1999, and regional variations in the crust and uppermost mantle of the Kaapvaal craton, Lithos, 71, 369-392.

Yabe, Y., M. Nakatani, M. Naoi, J. Philipp, C. Janssen, T. Watanabe, T. Katsura, H. Kawakata, D. Georg, and H. Ogasawara (2015), Nucleation process of an M2 earthquake in a deep gold mine in South Africa inferred from on-fault foreshock activity, J. Geophys. Res., 120, 5574-5594.

Yakovlev, D. V., T. I. Lazarevich, and S. V. Tsirel (2013), Natural and induced seismic activity in Kuzbass, Journal of Mining Science, 49, 862-872.

Yeck, W. L., L. V. Block, C. K. Wood, and V. M. King (2015), Maximum magnitude estimations of induced earthquakes at Paradox Valley, Colorado, from cumulative injection volume and geometry of seismicity clusters, Geophys. J. Int., 200, 322-336.

Zaliapin, I., and Y. Ben-Zion (2016), Discriminating characteristics of tectonic and human-induced seismicity, Bull. seismol. Soc. Am., 106, 846-859.

Zang, A., E. Majer, and D. Bruhn (2014a), Preface to special issue: Analysis of induced seismicity in geothermal operations, Geothermics, 52, 1-5.

Zang, A., V. Oye, P. Jousset, N. Deichmann, R. Gritto, A. McGarr, E. Majer, and D. Bruhn (2014b), Analysis of induced seismicity in geothermal reservoirs - An overview, Geothermics, 52, 6-21.

Zedník, J., J. Pospíšil, B. Růžek, J. Horálek, A. Boušková, P. Jedlička, Z. Skácelová, V. Nehybka, K. Holub, and J. Rušajová (2001), Earthquakes in the Czech Republic and surrounding regions in 1995–1999, Studia Geophysica et Geodaetica, 45, 267-282.

Zhang, Y., W. Feng, L. Xu, C. Zhou, and Y. Chen (2008), Spatio-temporal rupture process of the 2008 great Wenchuan earthquake, Science in China Series D: Earth Sciences, 52, 145-154.

Ziegler, M., K. Reiter, O. Heidbach, A. Zang, G. Kwiatek, D. Stromeyer, T. Dahm, G. Dresen, and G. Hofmann (2015), Mining-Induced Stress Transfer and Its Relation to a 1.9 Seismic Event in an Ultra-deep South African Gold Mine, Pure Appl. Geophys., 172, 2557-2570.

Zoback, M. D., and J. H. Healy (1984), Friction, faulting, and insitu stress, Annales Geophysicae, 2, 689-698.

Zoback, M. D., and H. P. Harjes (1997), Injection-induced earthquakes and crustal stress at 9 km depth at the KTB deep drilling site, Germany, Journal of Geophysical Research-Solid Earth, 102, 18477-18491.

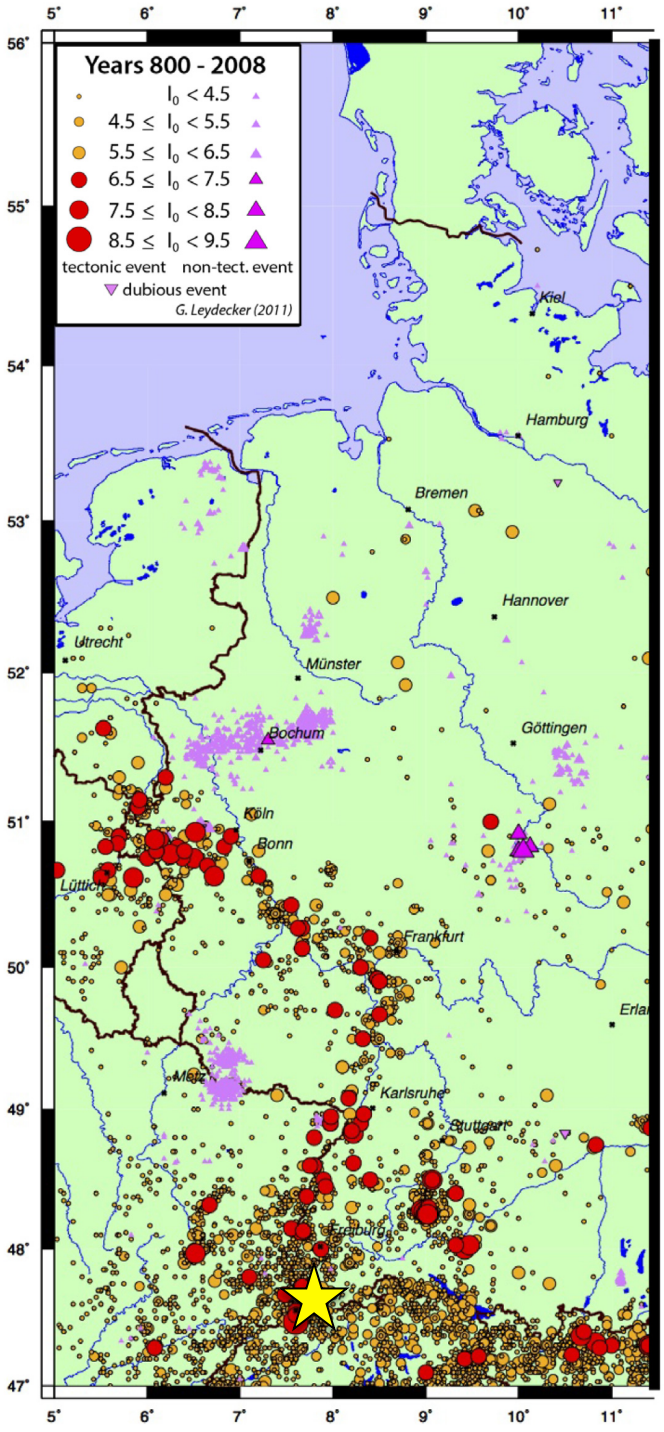

Figure 1: Map of central Europe showing historical earthquakes with different epicentral intensities from 800 AD [from Stein *et al.*, 2015]. Yellow star: the city of Basel, Switzerland.

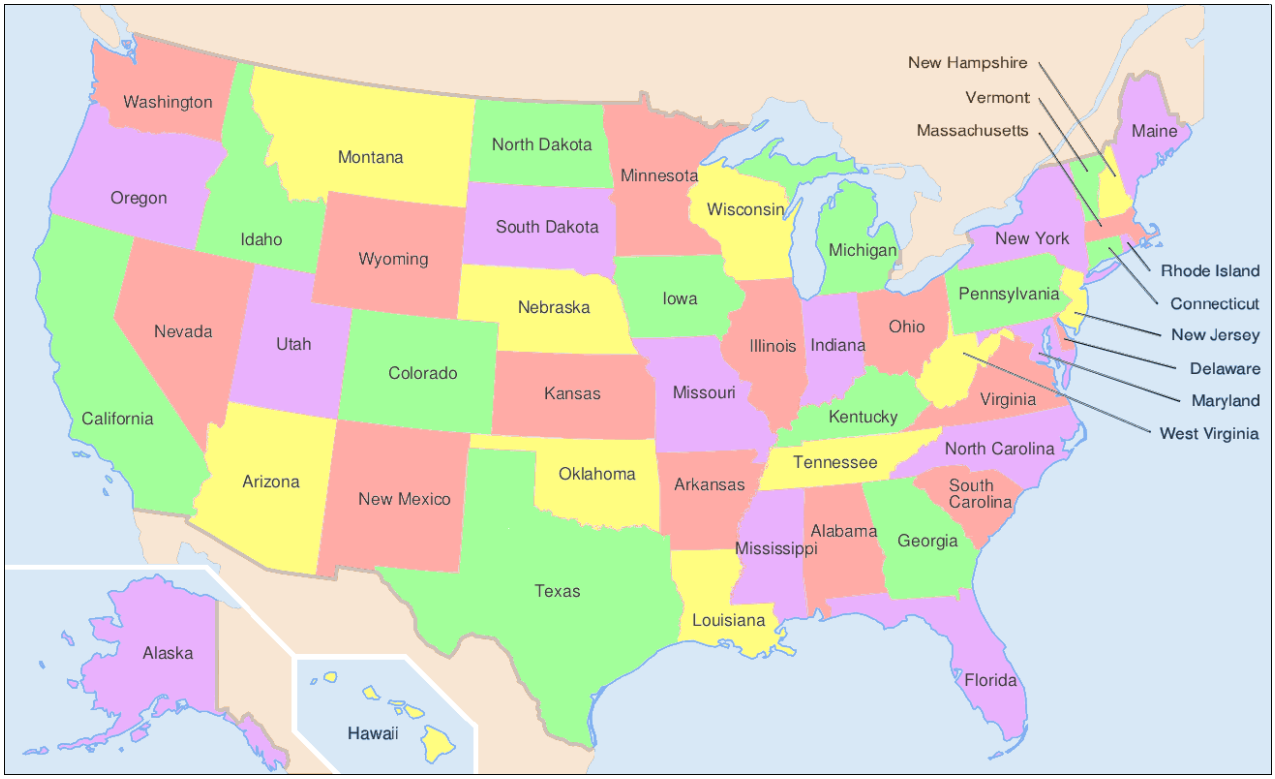

Figure 2: Map of USA showing state names[13].

[13] From https://commons.wikimedia.org/wiki/File:Map_of_USA_showing_state_names.png

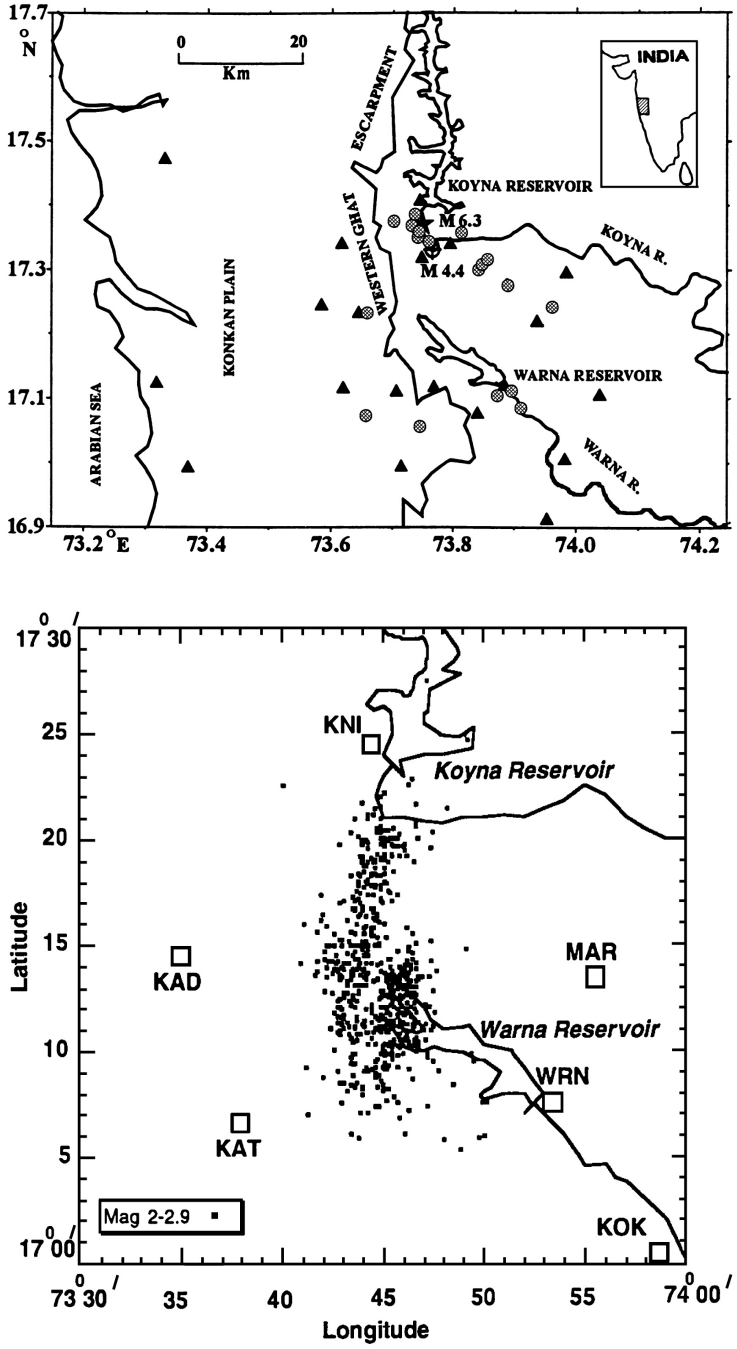

Figure 3: Top: Map of the Koyna, India, area showing the dam, reservoir, seismic stations and boreholes. Bottom: Same area showing earthquakes with M 2-2.9 for the period October 1993 to December 1994 [from Gupta, 2002].

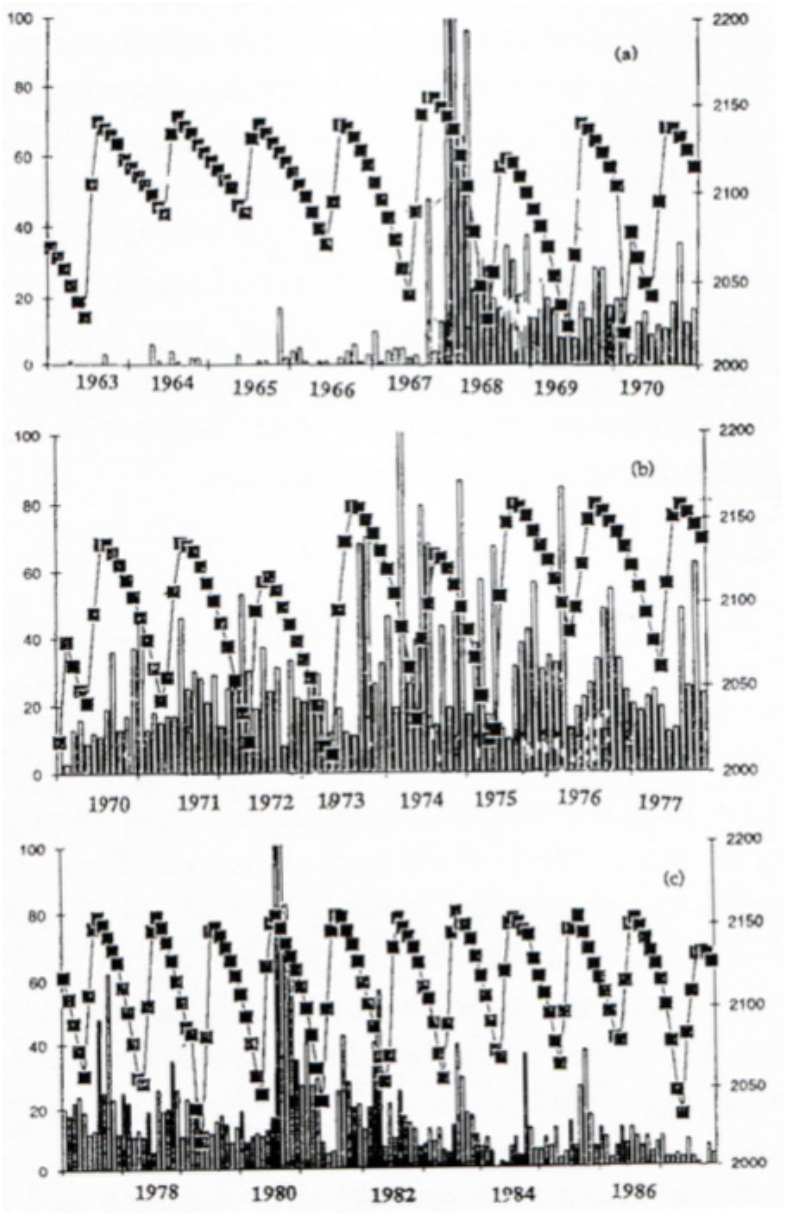

Figure 4: Number of earthquakes in the region of the Koyna dam, India, for the period 1963-1986 (left axis), along with reservoir water level (right axis, in m) [from Talwani, 1995].

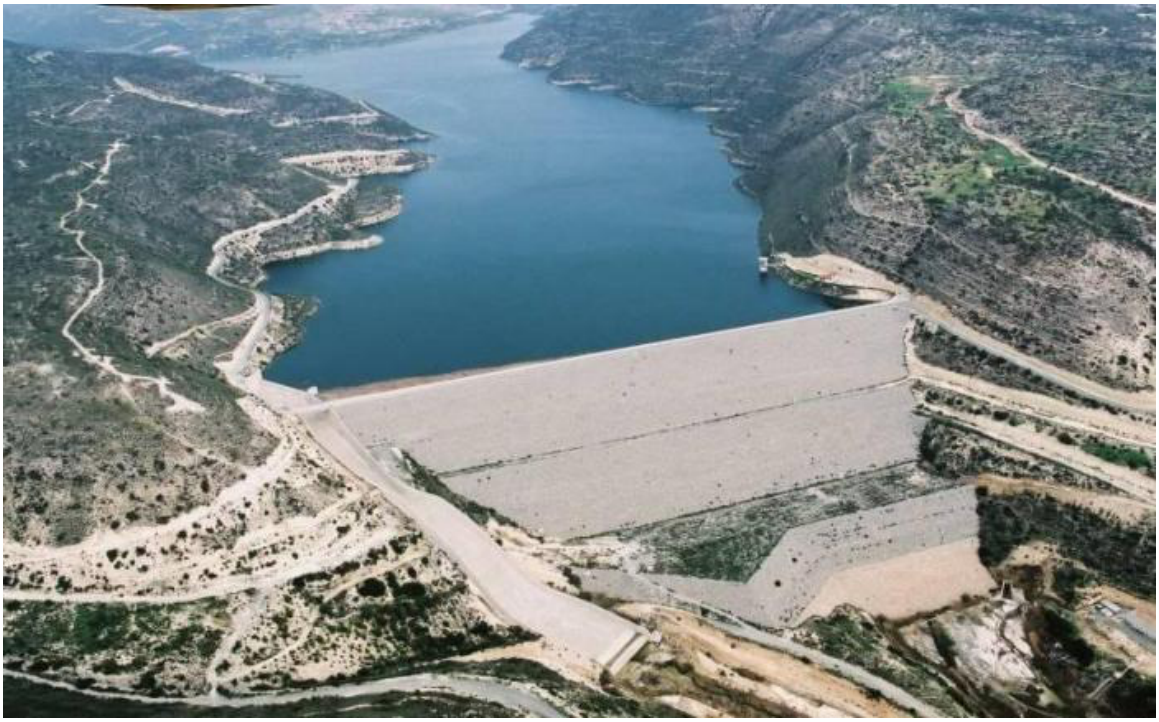

Figure 5: Aerial photograph of Nurek dam, Tadjikistan[14].

[14] http://www.slideshare.net/wahedullahsabawoon/the-purposes-of-building-a-dam

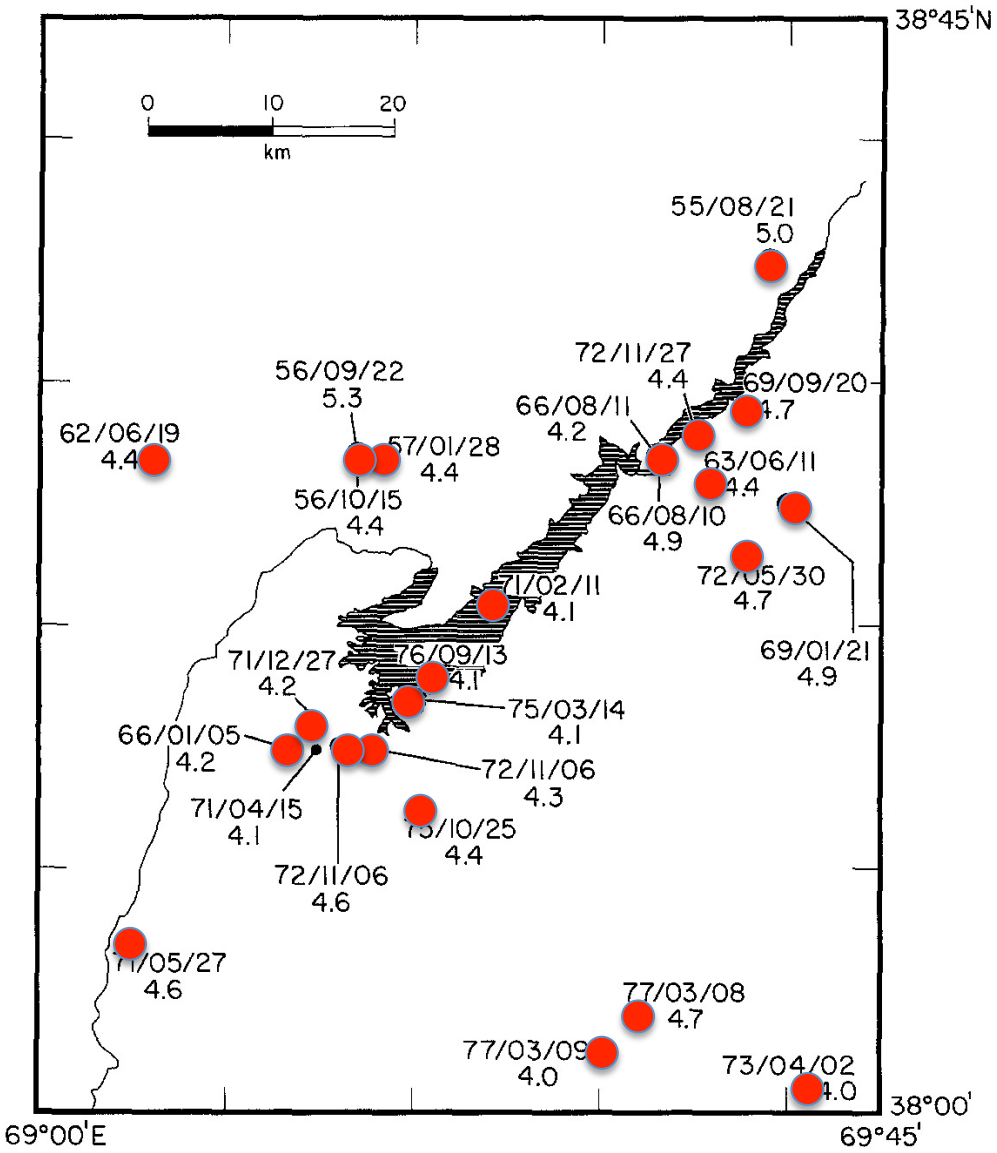

Figure 6: Map of Nurek dam and reservoir, Tadjikistan, showing earthquakes with M $\geq$ 4.0 for the period 1955-1979 [from Simpson & Negmatullaev, 1981].

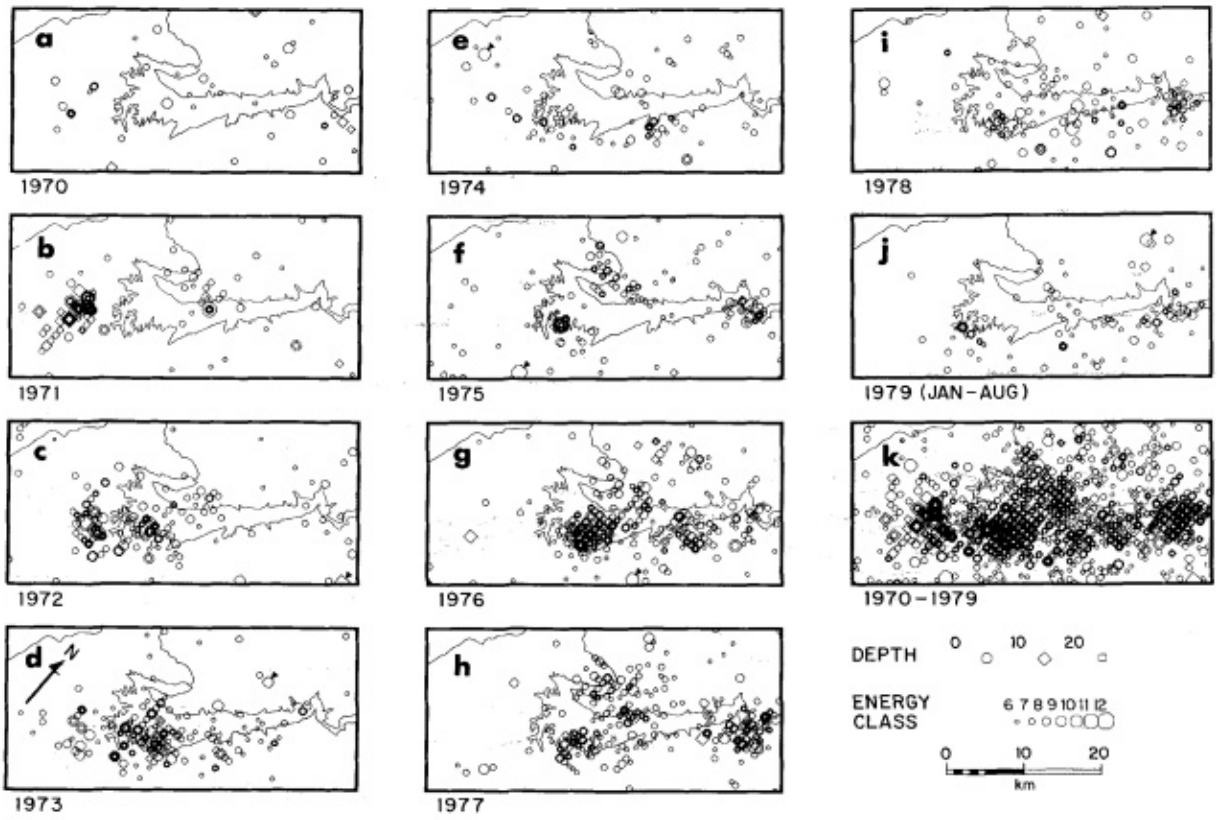

Figure 7: Yearly earthquakes in the vicinity of Nurek dam, Tadjikistan, for the period 1970-1979 [from Simpson & Negmatullaev, 1981].

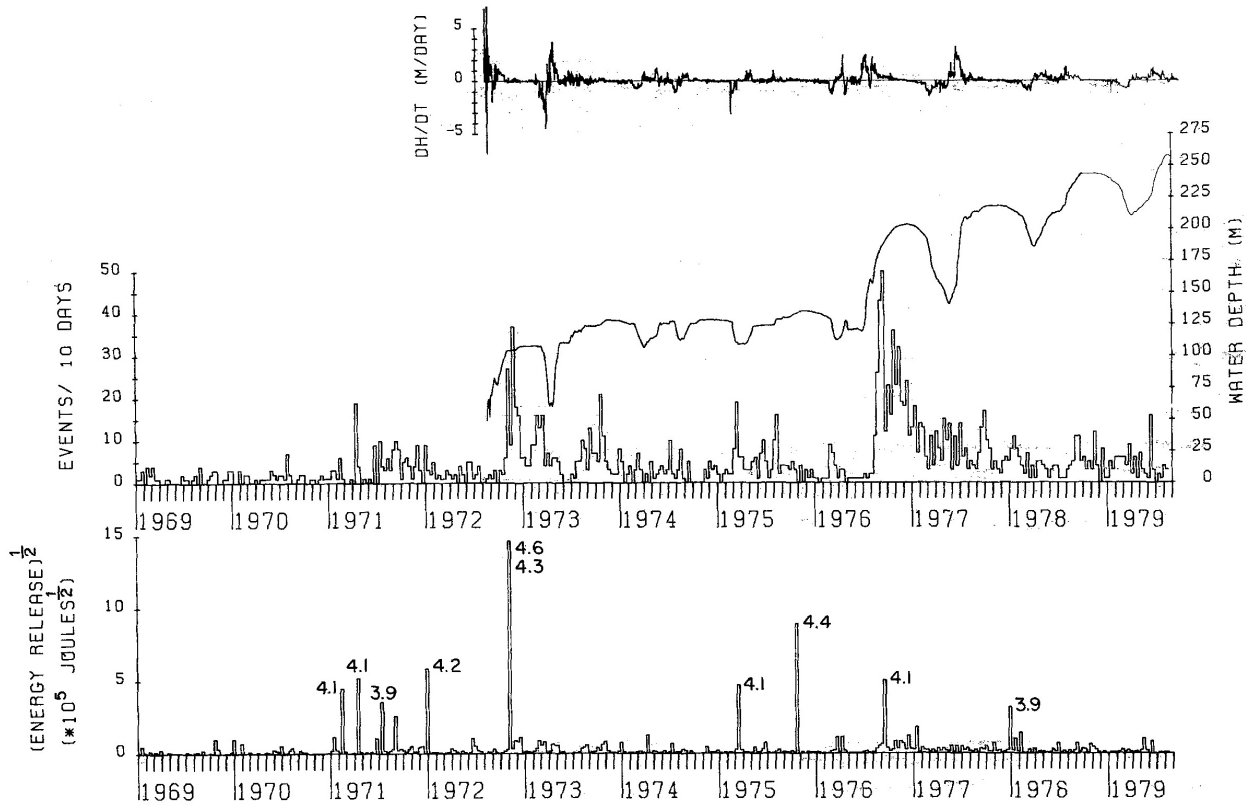

Figure 8: Water depth and seismicity for the period 1969-1979 in the vicinity of Nurek dam, Tadjikistan [from Simpson & Negmatullaev, 1981].

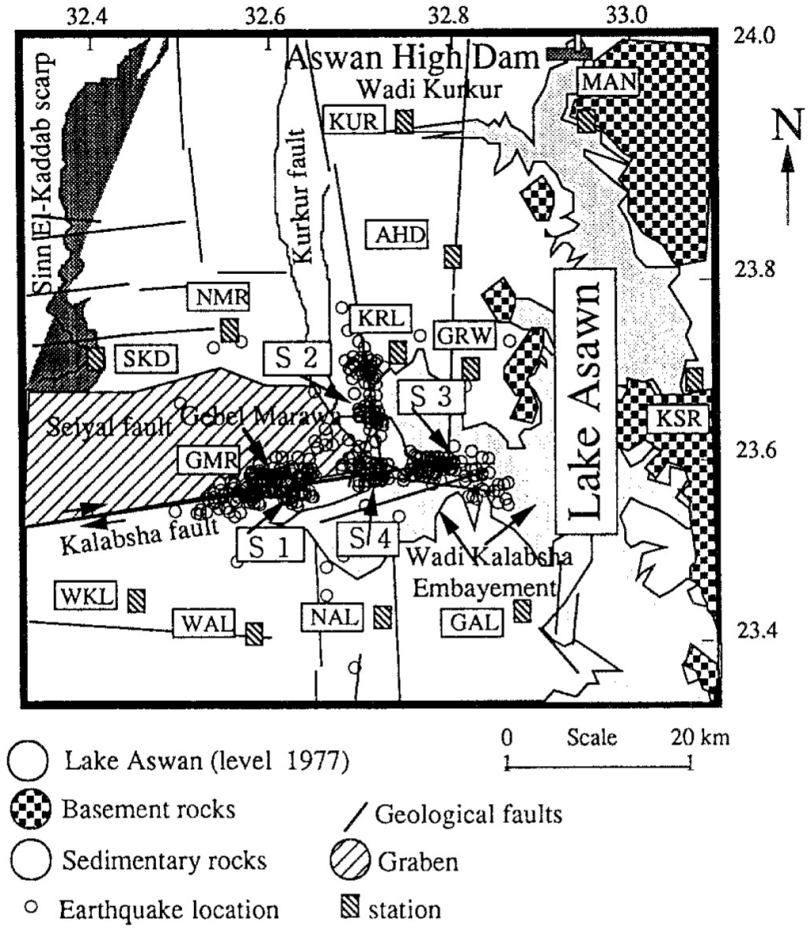

Figure 9: Map showing Lake Aswan, Egypt, and epicenters of induced earthquakes [from Awad & Mizoue, 1995].

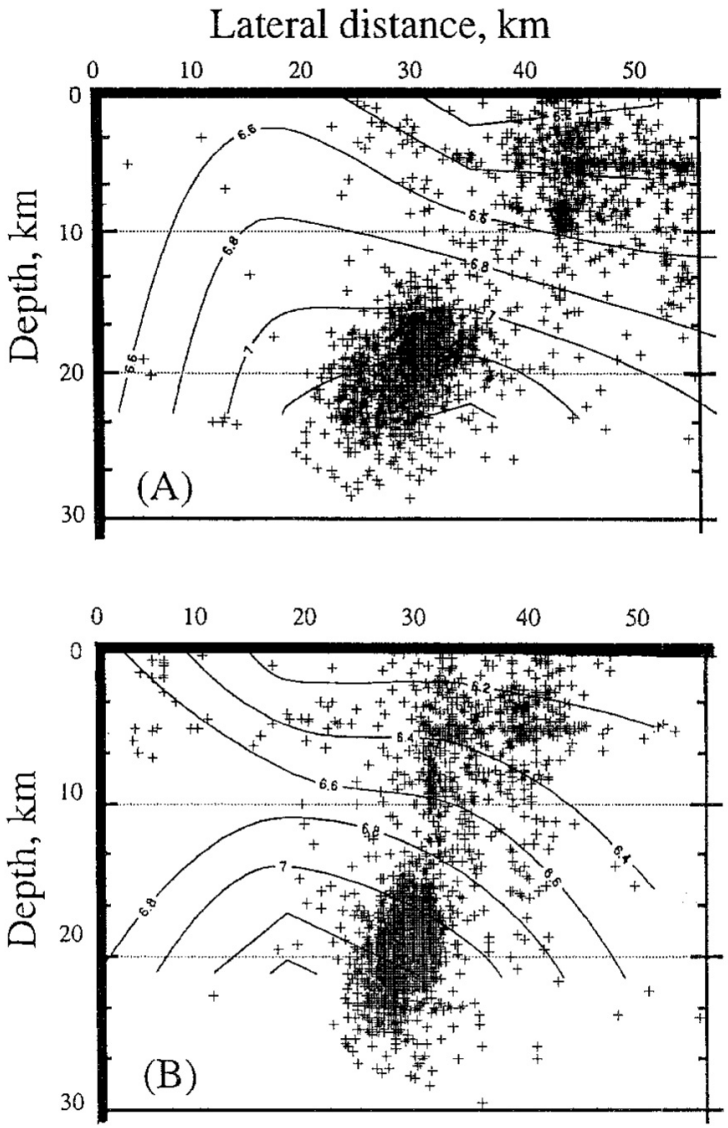

Figure 10: Cross sections showing hypocentral distribution of earthquakes postulated to have been induced by impoundment of Lake Aswan [from Awad & Mizoue, 1995].

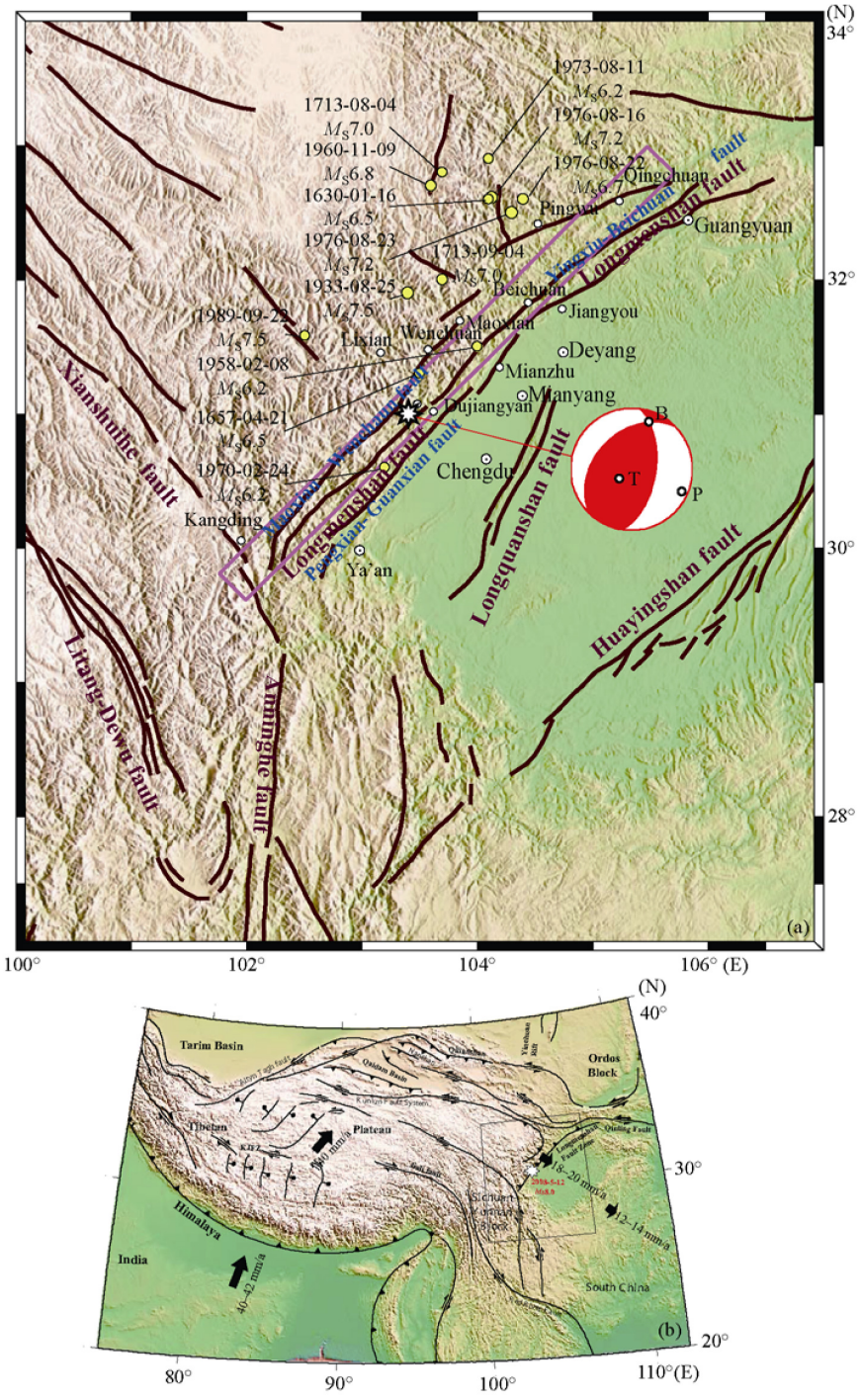

Figure 11: Top: Star: location of the 2008 M_W ~ 8 Wenchuan, China, earthquake; lines: main faults of the Longmenshan fault zone; yellow circles: historical earthquakes; white circles: main cities; lilac rectangle: projection of the fault plane that slipped; beach ball: lower hemisphere projection of the focal mechanism of the mainshock. Bottom: regional tectonic setting [from Zhang *et al.*, 2008].

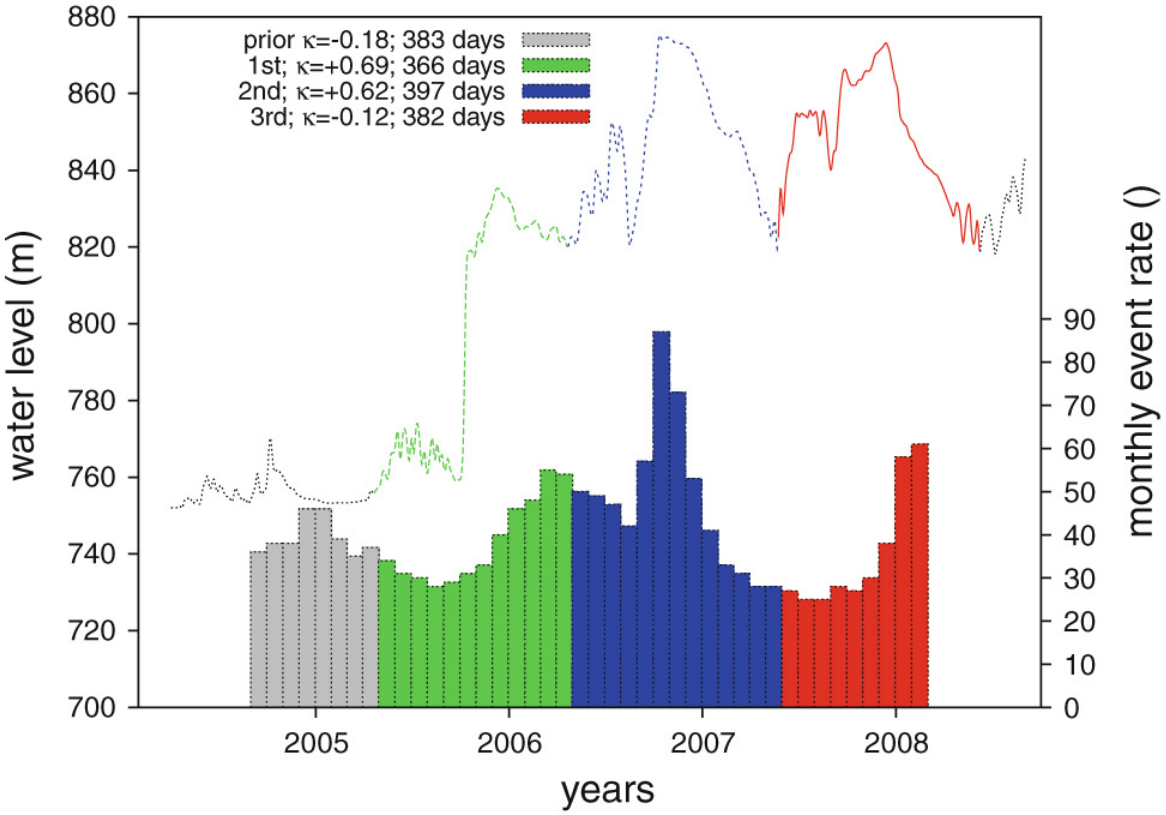

Figure 12: Water level change in the Zipingpu, China, water reservoir and earthquake event rate in the vicinity for the years prior to the May 2008 $M_W \sim 8$ Wenchuan earthquake [from Klose, 2012].

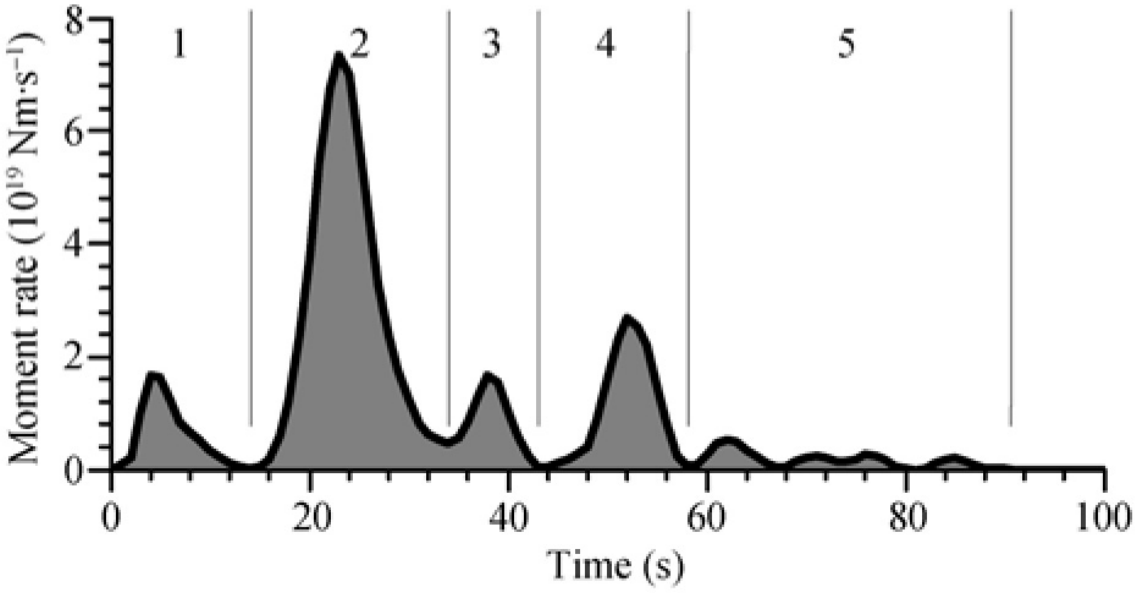

Figure 13: Source time function of the 2008 great Wenchuan, China earthquake [from Zhang *et al.*, 2008].

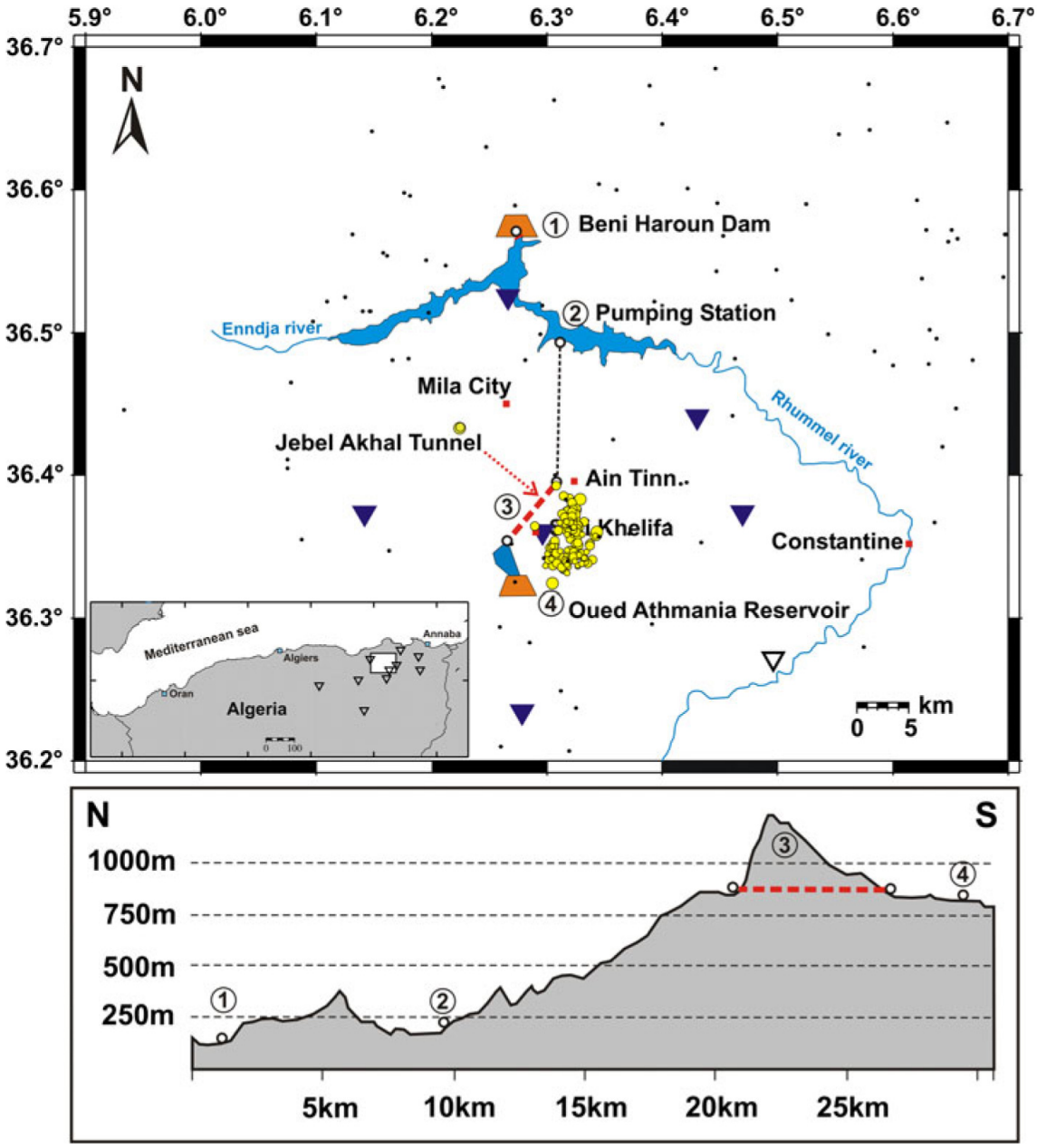

Figure 14: Map of the hydraulic system in the Mila region, Algeria. Top: Water transport system (dashed lines) from Beni Haroun dam to Oued Athmania reservoir. Red dashed line: tunnel passing through Mt. Jebel Akhal; black dots: seismicity for the two-year period 2006–2007; triangles: seismic stations; yellow dots: epicenters of earthquake deduced to be triggered by water leakage. Bottom: topographic profile of the hydraulic system [from Semmane *et al.*, 2012].

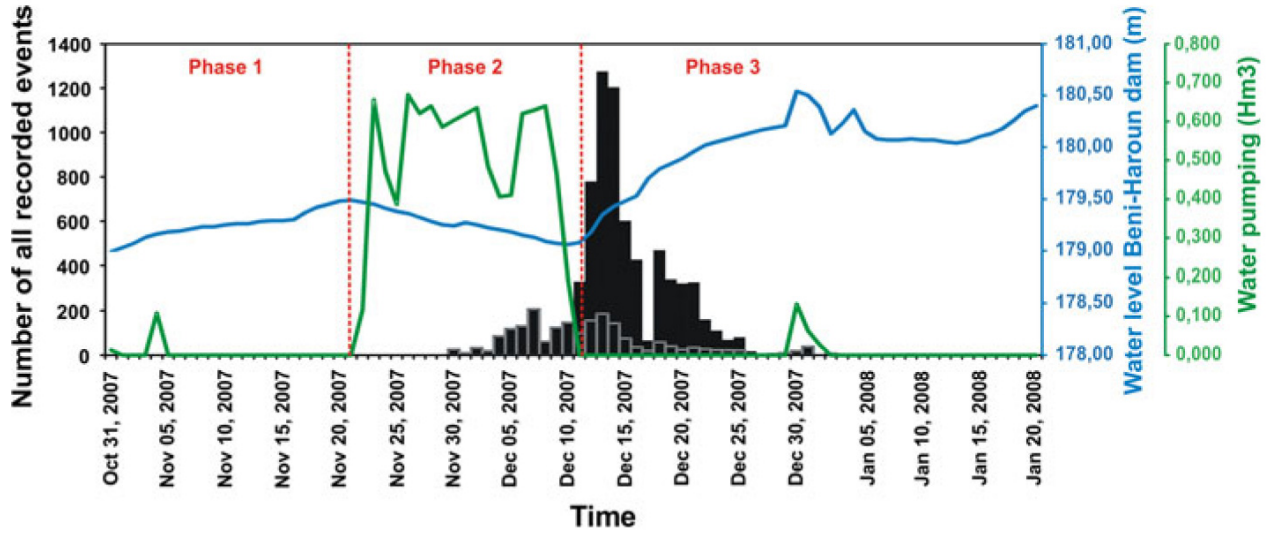

Figure 15: Number of earthquakes recorded, water level in the Beni Haroun dam, and volumes of water pumped vs. time around the seismogenic period. Black histogram: events recorded; gray histogram: events recorded by the network, discarding a temporary station deployed in the epicentral area for 17 days during the swarm [from Semmane *et al.*, 2012]. This shows an example of the effect of varying the number of seismic stations deployed.

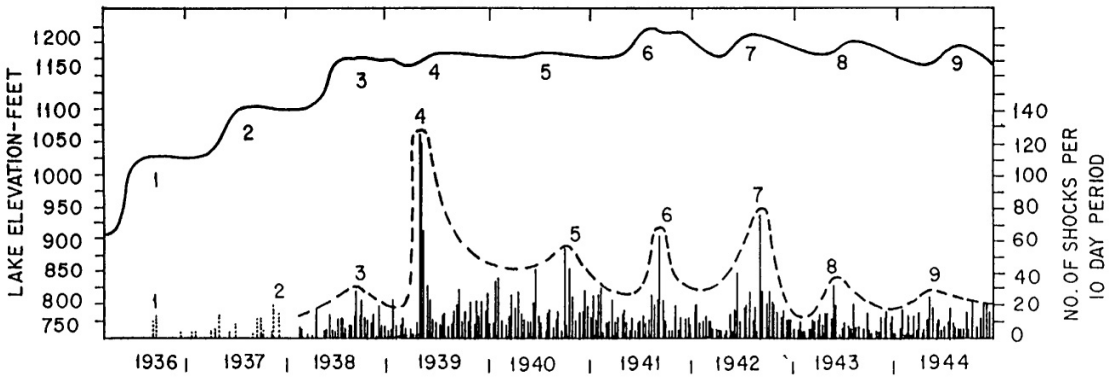

Figure 16: Earthquakes and water level at Lake Mead, Arizona, which is impounded behind Hoover dam [from Gupta, 2002].

Figure 17: Aerial photograph of the Three Gorges dam, China[15].

[15] http://vizts.com/three-gorges-dam/three-gorges-dam-3/

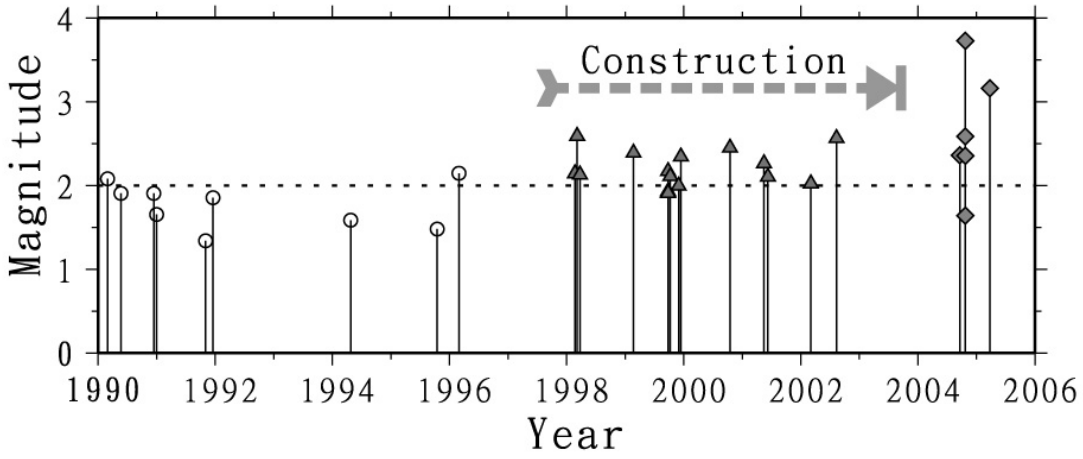

Figure 18: Earthquake history for a 16-year period spanning the construction of the Taipei 101 building, Taiwan [from Lin, 2005].

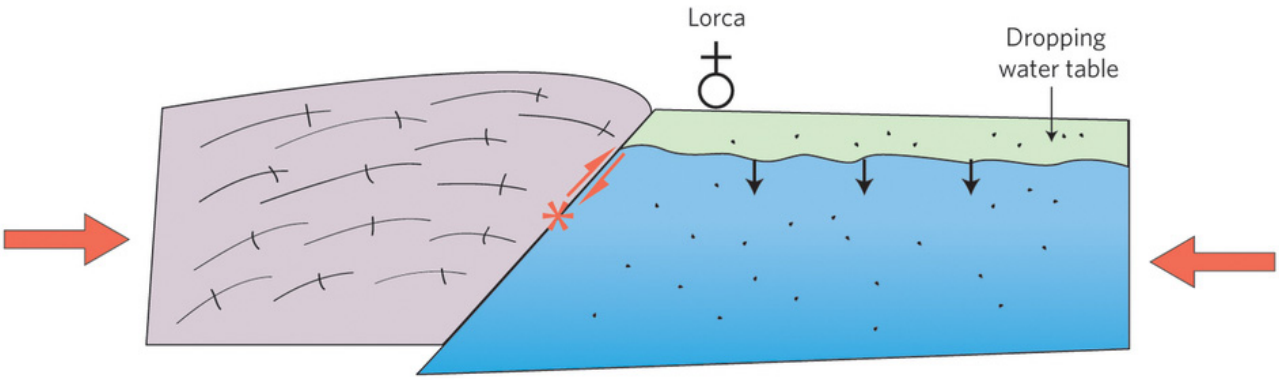

Figure 19: Schematic figure showing the mechanism proposed by Gonzalez *et al.* [2012] for inducing the 2011 M_W 5.1 Lorca, Spain, earthquake [from Avouac, 2012].

Figure 20: Destruction in the church of Santiago resulting from the 2011 M_W 5.1 Lorca, Spain, earthquake [16].

[16] https://en.wikipedia.org/wiki/2011_Lorca_earthquake

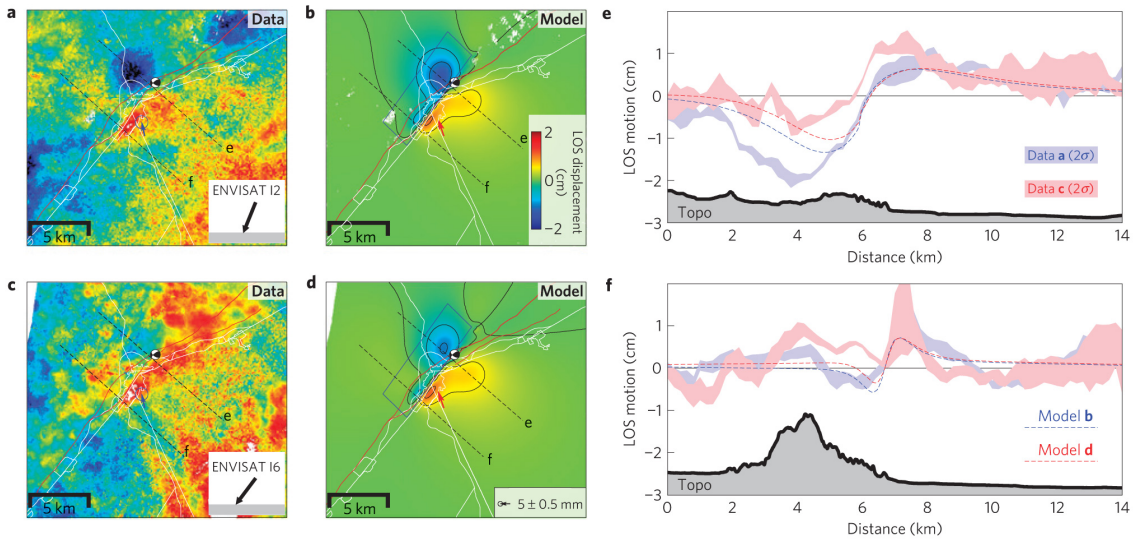

Figure 21: (a–d): ground deformation data and model for the 2011 M_W 5.1 Lorca, Spain, earthquake. (a and c): descending line-of-sight (LOS) displacement map and horizontal GPS vector; (b and d): distributed slip model predictions. Insets in a and c indicate LOS angle, positive values away from the satellite. Blue rectangle: fault surface projection; dashed lines: profile locations; (e and f): observed and simulated data along two profiles, and local topography [from Gonzalez *et al.*, 2012].

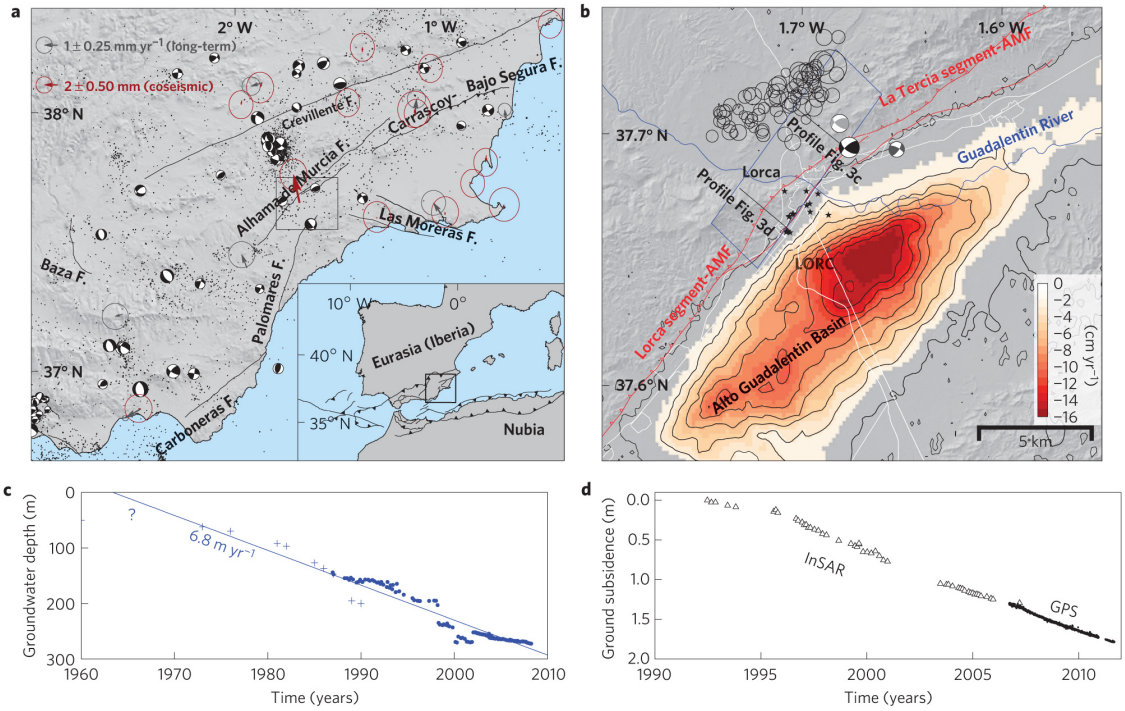

Figure 22: Location and kinematics of the Lorca earthquake. a: southwest Spain seismicity (2000–2010), focal mechanisms (1970–2010), long-term GPS velocity (2006–2011, gray) and coseismic vectors (red). Major mapped faults are labeled. b: Lorca city and Alto Guadalentin Basin. Mainshock focal mechanisms (black), pre-shock (light gray), largest aftershock (dark gray), and relocated seismic sequence. Black stars are damage locations, red lines are faults. Contour lines indicate 2 cm yr^{-1} InSAR subsidence due to groundwater pumping. Blue rectangle: fault surface projection. AMF, Alhama de Murcia Fault. c, Groundwater depth. d, InSAR (triangles) and line-of-sight (LOS)-projected GPS ground-surface subsidence at station LORC [from Gonzalez *et al.*, 2012].

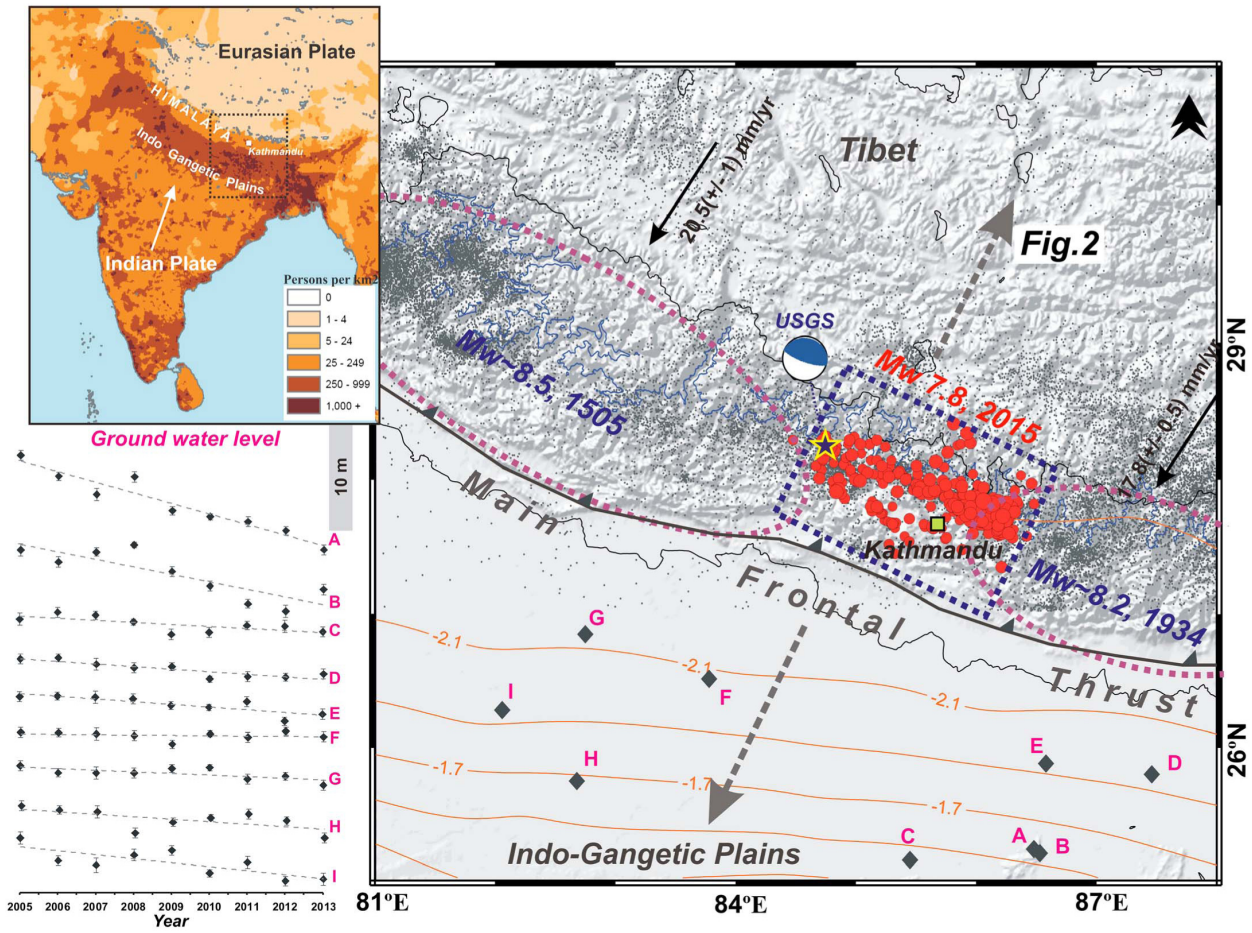

Figure 23: Seismotectonic context of the 2015 M_W 7.8 Gorkha, Nepal earthquake. Black star: epicenter of the mainshock; red circles: aftershocks; black arrows: convergence rate; gray dots: mid-crustal seismicity 1995-2008; blue contour: 3500-m elevation; ellipses: approximate rupture locations of historic events since 1505; orange contours: anthropogenic groundwater loss in cm yr^{-1} water thickness for the period 2002-2008 (multiply by 5 to get drop in water table); black diamonds: sampling sites; inset at left: site depletion trends; inset top left: population density (people/km^2) [from Kundu *et al.*, 2015].

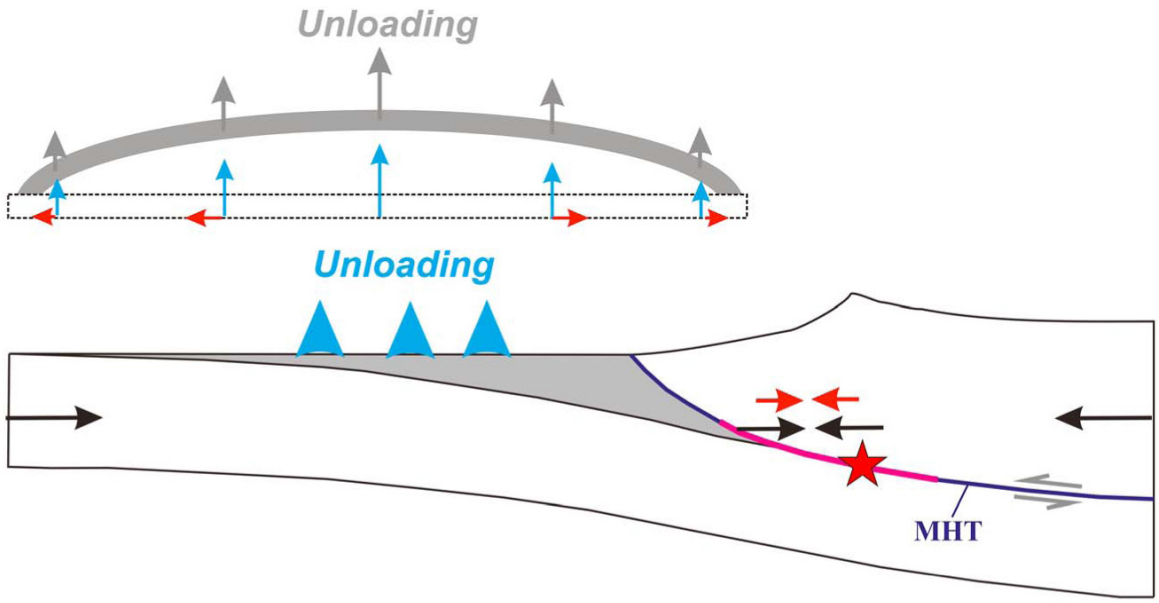

Figure 24: Schematic diagram showing the effect of unloading by anthropogenic groundwater loss on the Main Himalayan Thrust. Dewatering induces a component of horizontal compression (red arrows) that adds to the secular interseismic contraction (black arrows) at seismogenic depths. Red star: the 2015 Gorkha, Nepal earthquake; pink line: the associated rupture [from Kundu *et al.*, 2015, after].

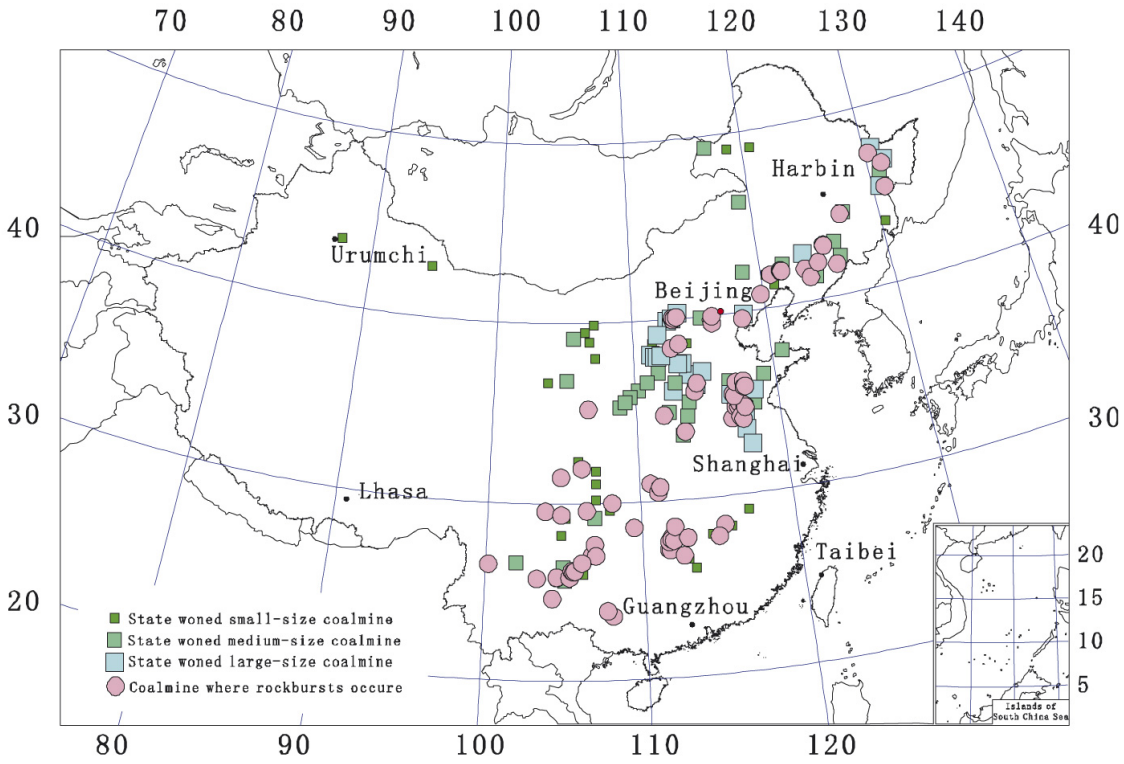

Figure 25: State-owned coal mines and mining-induced seismicity in China [from Li *et al.*, 2007].

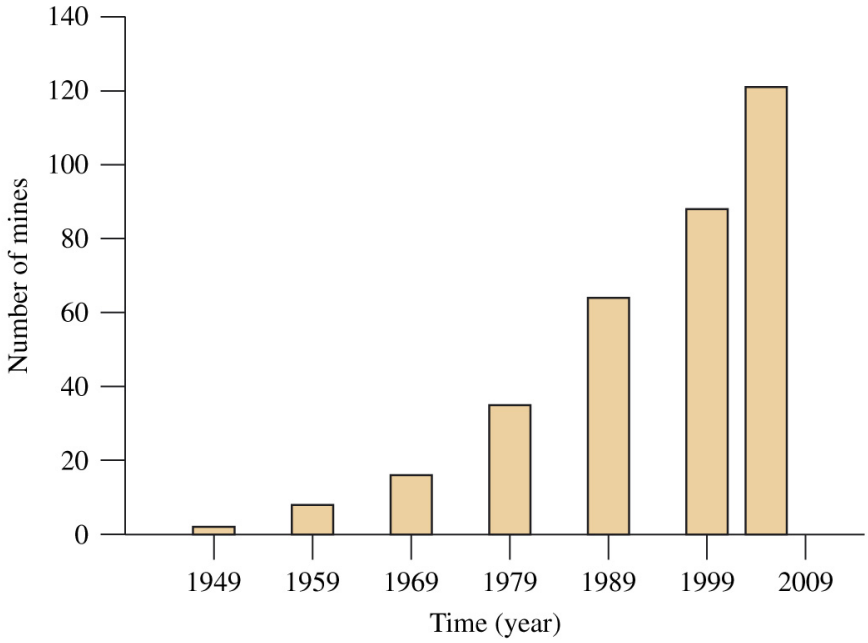

Figure 26: Number of mines in China with rockburst hazard vs. time [from Li *et al.*, 2007].

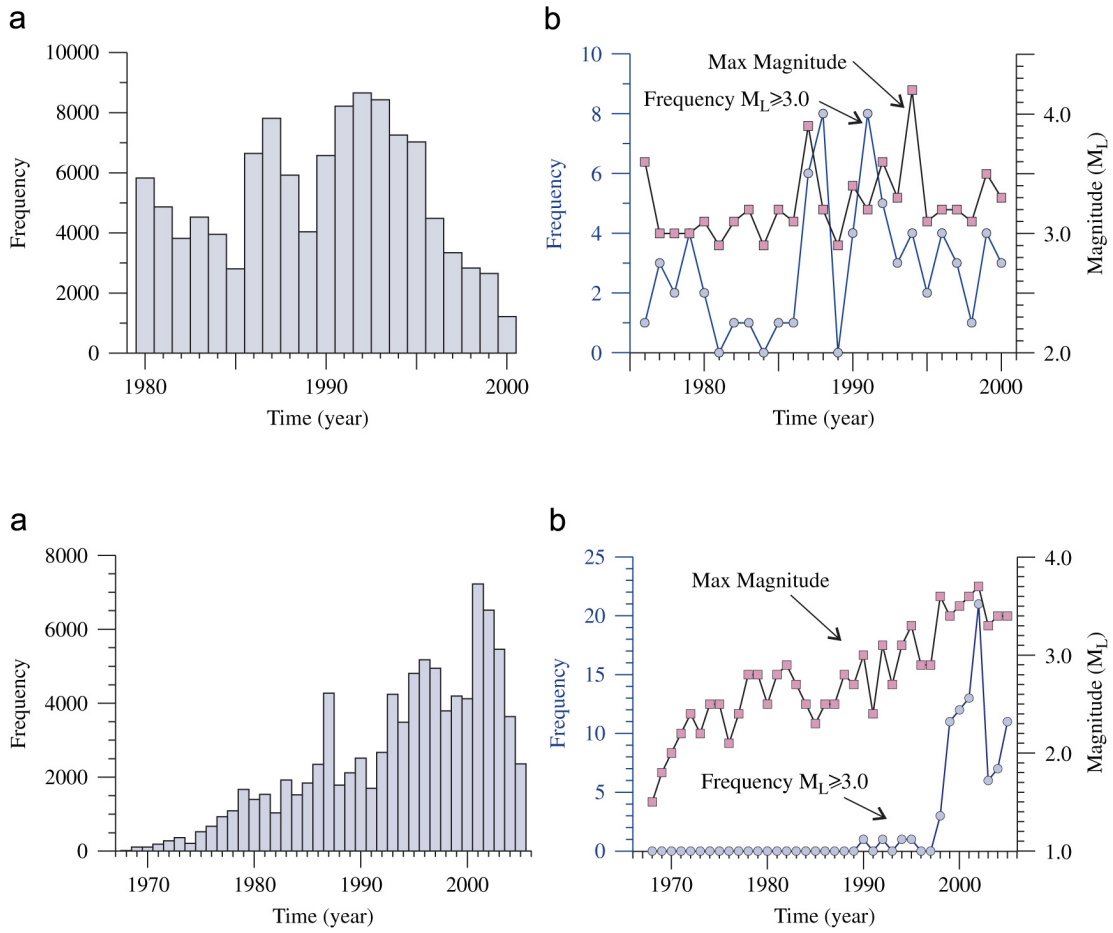

Figure 27: Top panels: Mining-induced earthquakes at Mentougou coal mine, Beijing, (a) events M > 1.0, (b) events M > 3.0 and the maximum event magnitudes. Bottom panels: same as top panels except for the Fushun coal mine field in Liaoning Province [from Li *et al.*, 2007].

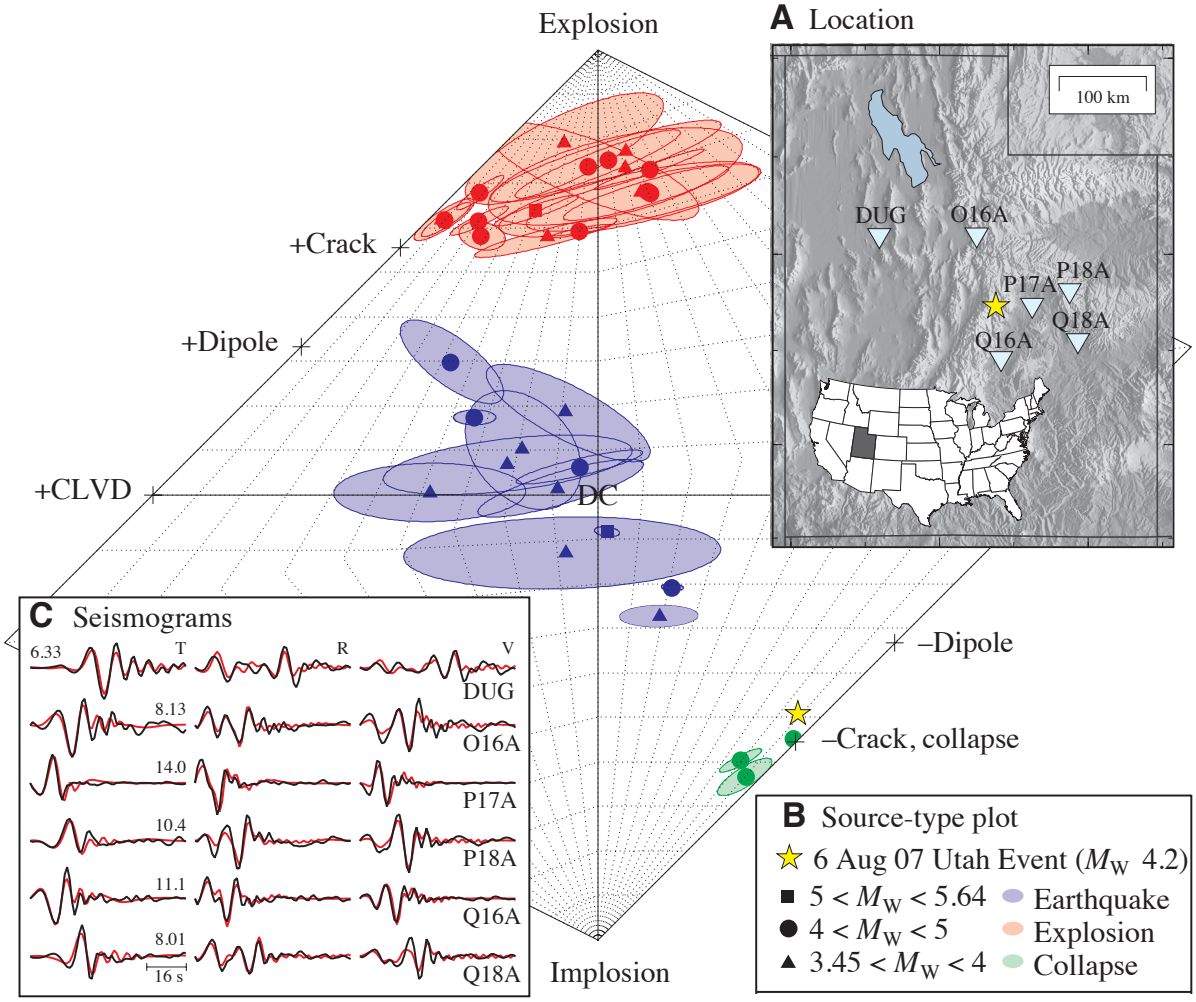

Figure 28: (A) Locations of the 6 August 2007 Crandall mine, Utah, earthquake and six of the closest USArray and Advanced National Seismic System (ANSS) seismic stations. (B) Source-type plot showing separation of populations of earthquakes, explosions, and collapses. Yellow star shows the focal mechanisms solution. (C) Observed seismograms (black) compared to synthetics (red) for the solution, which is similar to a horizontal closing crack (B). The maximum displacement (10-7 m) of each set of tangential (T), radial (R), and vertical (V) observations is given [from Dreger *et al.*, 2008].

Figure 29: Aerial view of surface subsidence resulting from Neolithic flint mining at Grimes Graves, Suffolk, England[17].

[17] www.english-heritage.org.uk

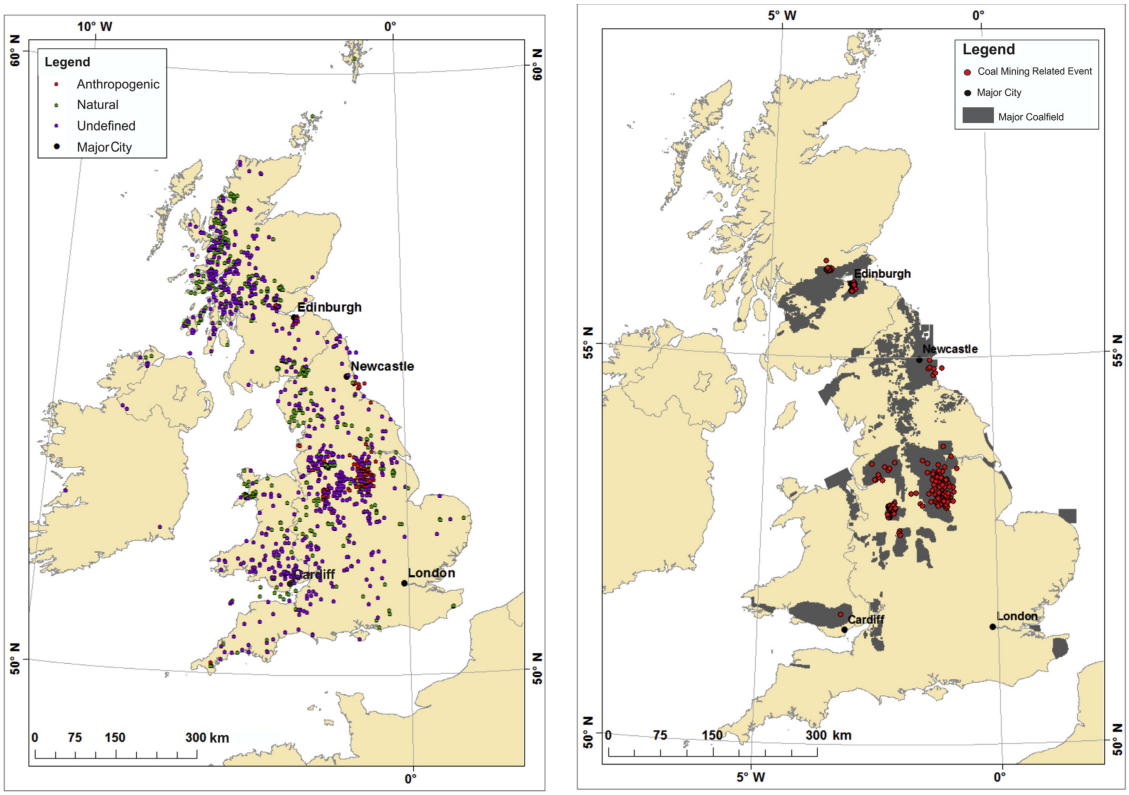

Figure 30: For earthquakes with $M_L \geq 1.5$ for the period 1970-2012, left: map of the UK showing 1769 onshore seismic events categorized as anthropogenic (red), natural (green) and undefined (purple). Right: 369 events postulated to be induced by coal mining. These correlate spatially with major coalfields (dark gray) [from Wilson *et al.*, 2015].

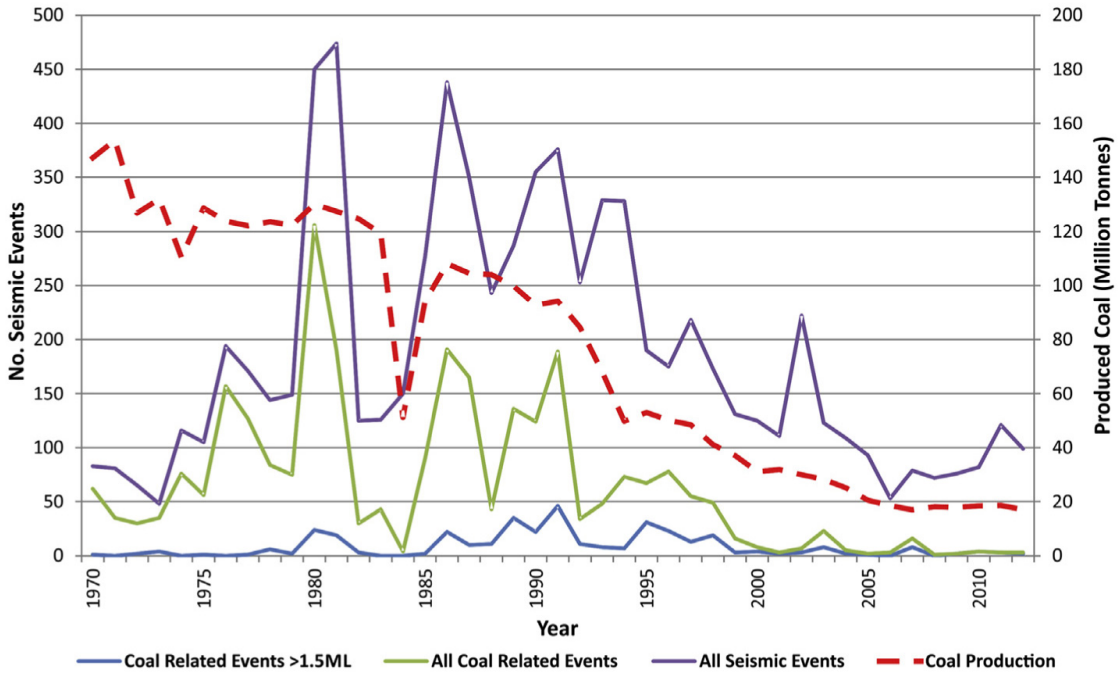

Figure 31: UK coal production (dotted red line) vs. numbers of earthquakes postulated to be induced (blue line: $M_L \geq 1.5$, green line: all located earthquakes in the British Geological Survey database) for the period 1970-2012. The effect of the miners' strike of 1984 can be seen clearly in the drop in production and seismicity [from Wilson *et al.*, 2015].

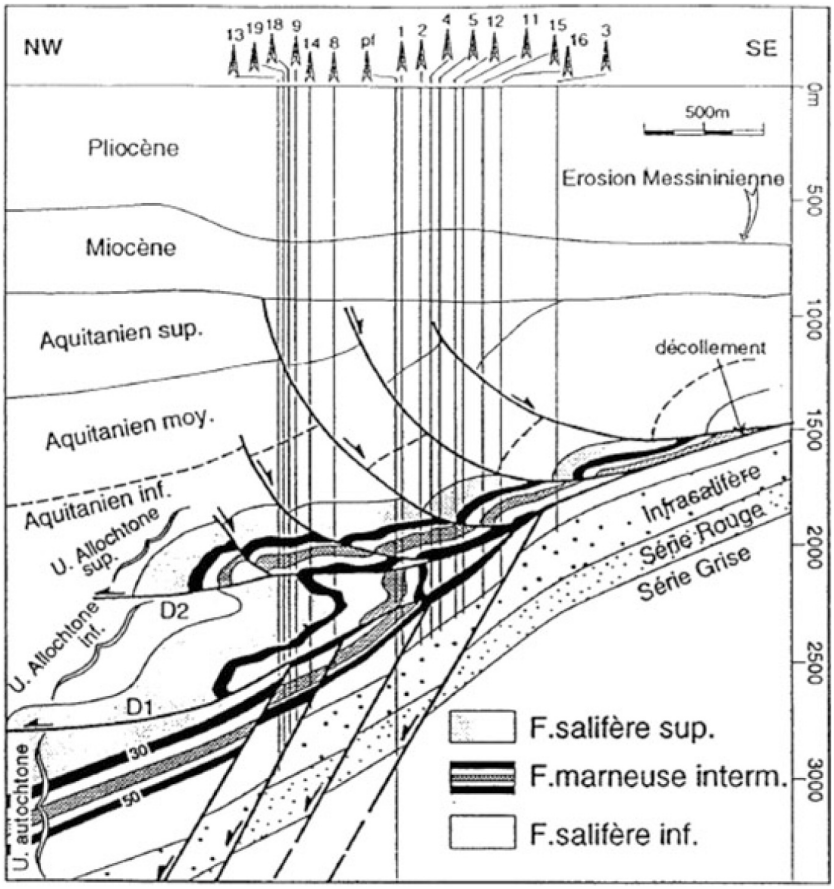

Figure 32: Geological cross-section of the Vauvert, France, solution-mined salt deposit [from Godano *et al.*, 2010].

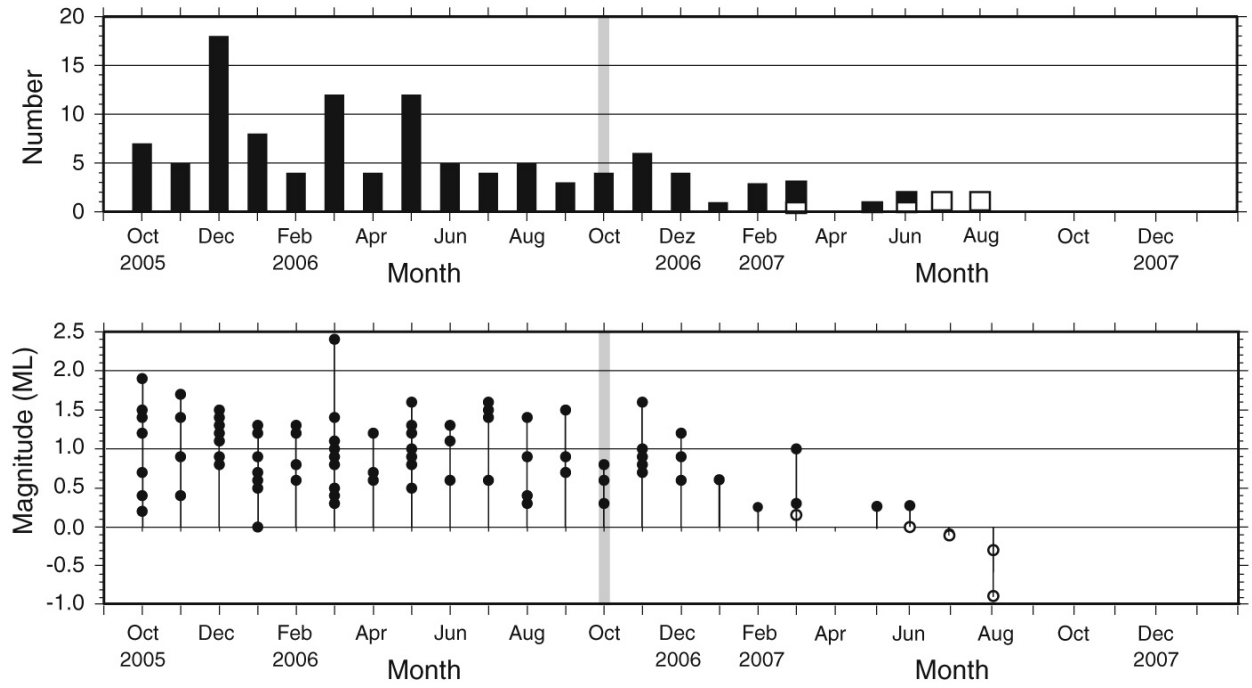

Figure 33: Temporal evolution of the seismicity observed in the vicinity of the multi-function station Faido, Switzerland, October 2005 - December 2007. Top: number of events per month. Bottom: local magnitudes. Open circles: earthquakes for which magnitude could only be computed using data from one station. Gray band marks the end of the excavation work [from Husen *et al.*, 2012].

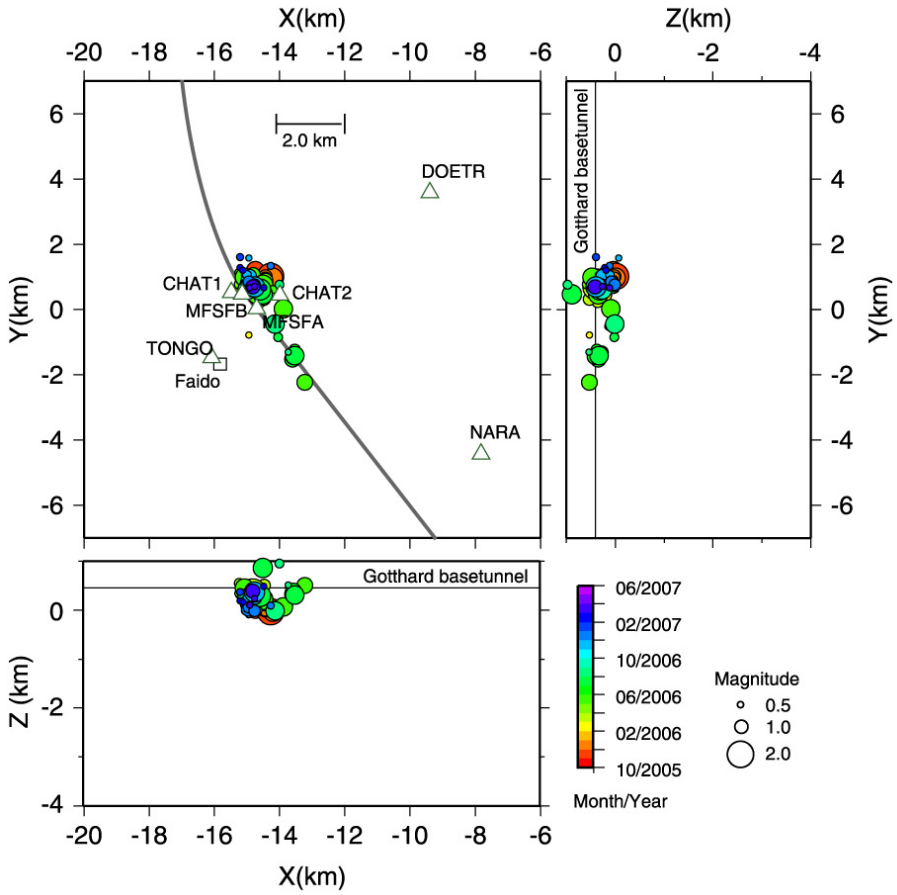

Figure 34: Hypocenter locations of earthquakes in the vicinity of the multi-function station Faido, Switzerland, October 2005 - June 2007 [from Husen *et al.*, 2012].

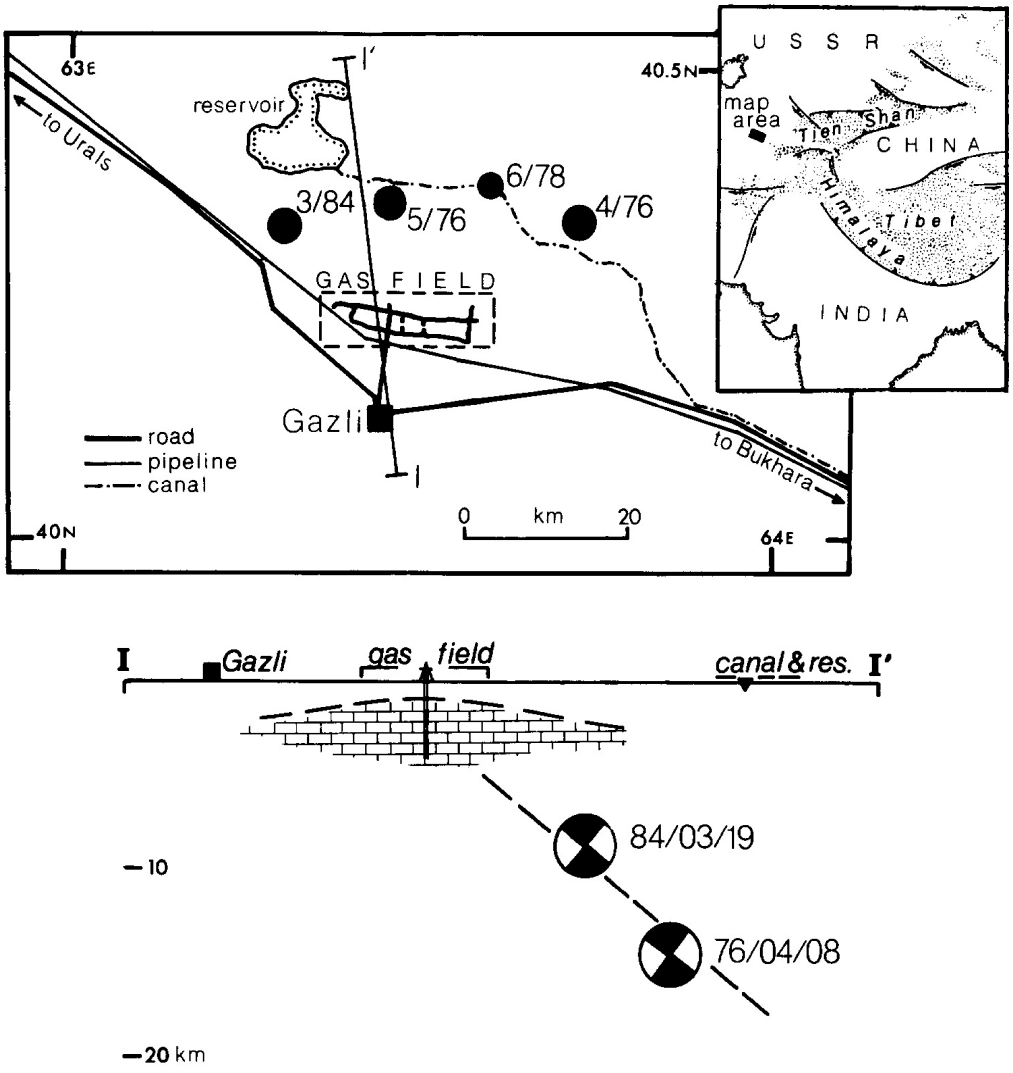

Figure 35: Top: Map of the Gazli, Uzbekistan, area showing epicenters of the three M ~7 earthquakes in 1976 and 1984, and the M 5.7 earthquake in 1978. Bottom: Cross-section with hypocenters projected at their distance from the town of Gazli, with focal mechanisms of the M_S 7.0 events of 8 April 1976 and 19 March 1984. The fault plane (dashed line) is deduced from geodetic data [from Simpson & Leith, 1985].

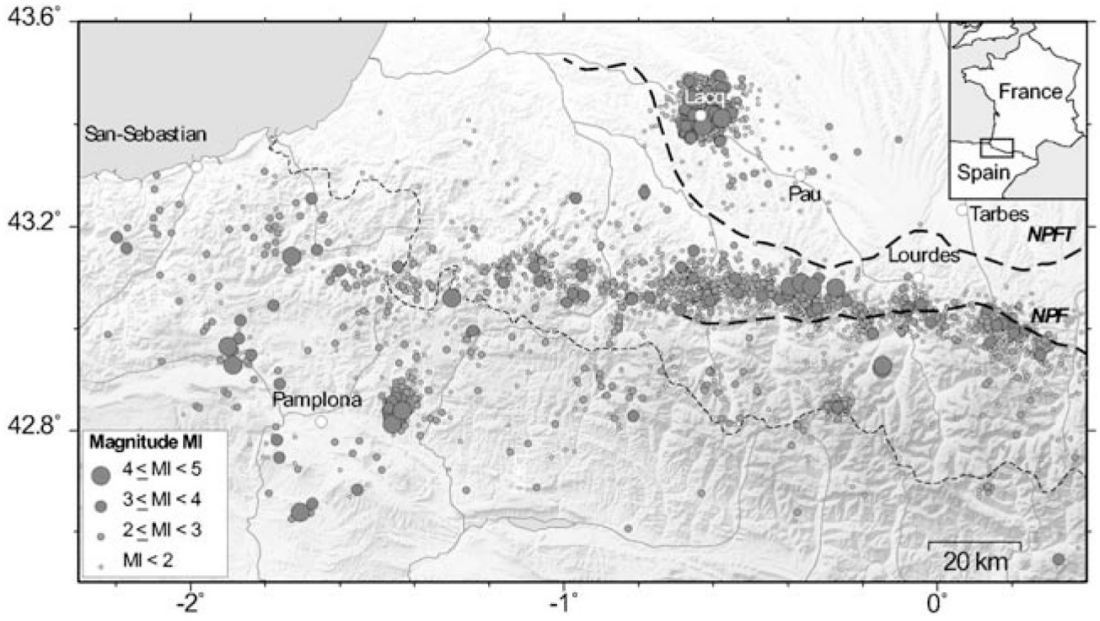

Figure 36: Seismicity of southwest France for 1997–2005[18], along with locally recorded earthquakes in the Lacq, France, area. NPF: North Pyrenean Fault. NPFT: North Pyrenean Frontal Thrust [from Bardainne *et al.*, 2008].

[18] http://www.omp.obs-mip.fr/rssp/sismicite˙pyrenees/bulletin/bulletin.html

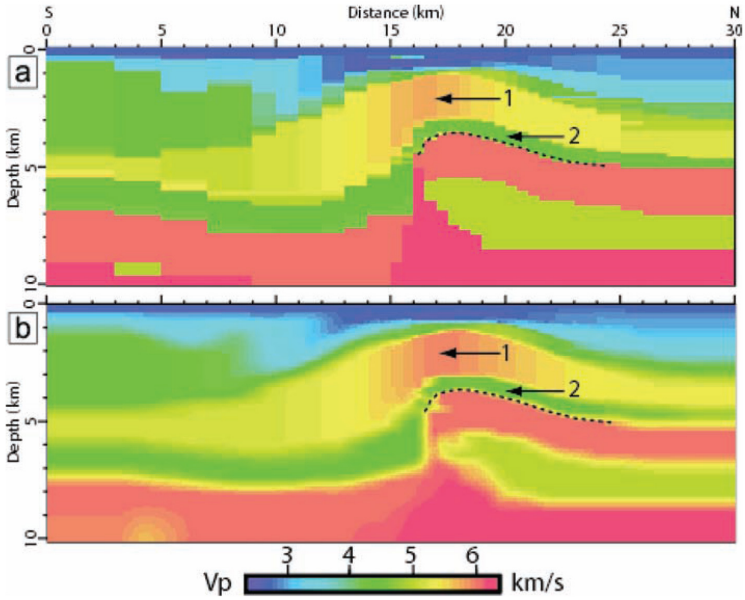

Figure 37: N-S vertical cross-section of the three-dimensional *P*-wave velocity model for the Lacq, France, area from surface seismic and well data. Dotted line: top of gas reservoir; 1: upper-Cretaceous reef; 2: ductile Cretaceous marls [from Bardainne *et al.*, 2008].

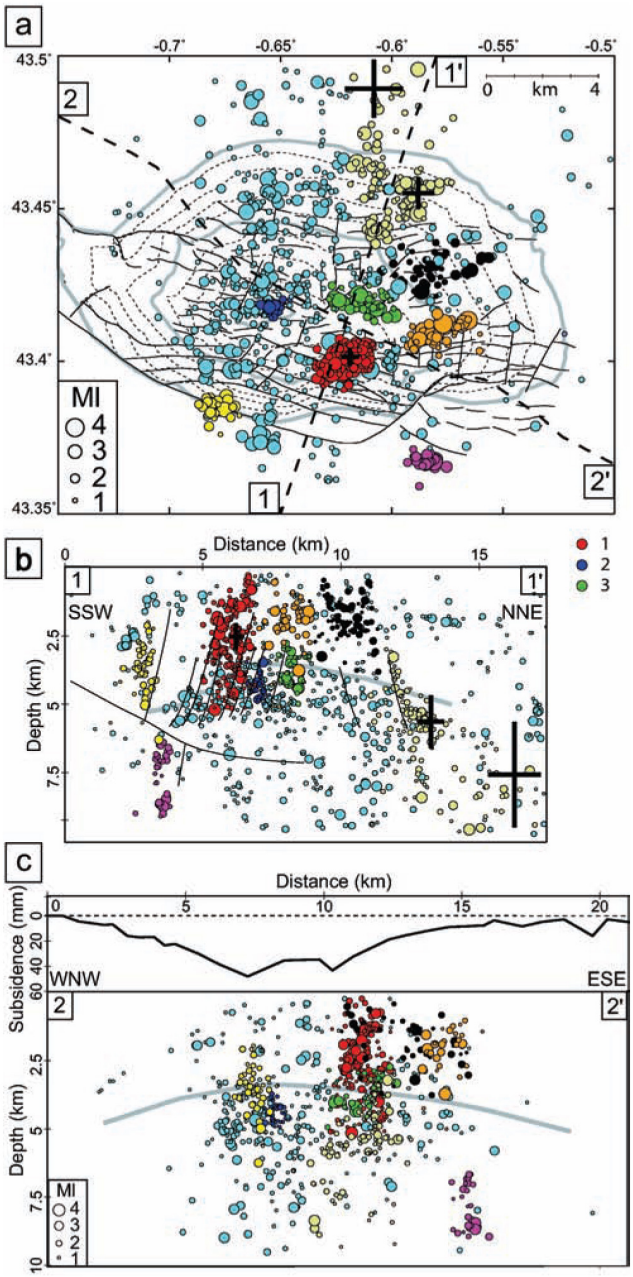

Figure 38: Seismicity in the Lacq Gasfield, France. (a) Map view and location of cross-sections. (b) SSW-NNE cross-section and (c) WNW-ESE cross section. Colors: different earthquake clusters; dashed and solid gray lines: isobaths of the gasfield; black lines: faults; crosses: location uncertainties for three swarms [from Bardainne *et al.*, 2008].

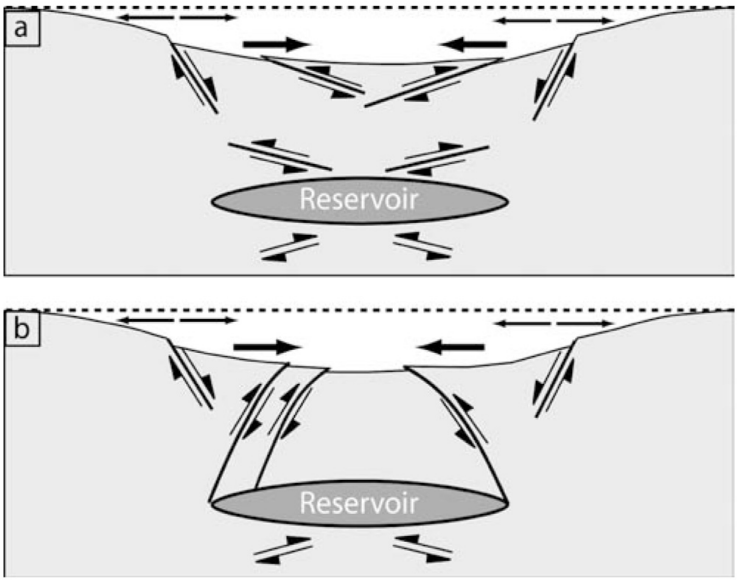

Figure 39: Deformation models of (a) Segall [1989], and (b) Odonne *et al.* [1999] for a depleting subsurface reservoir. Both models predict extensional deformation on the flanks and compressional deformation centrally in the field [from Bardainne *et al.*, 2008].

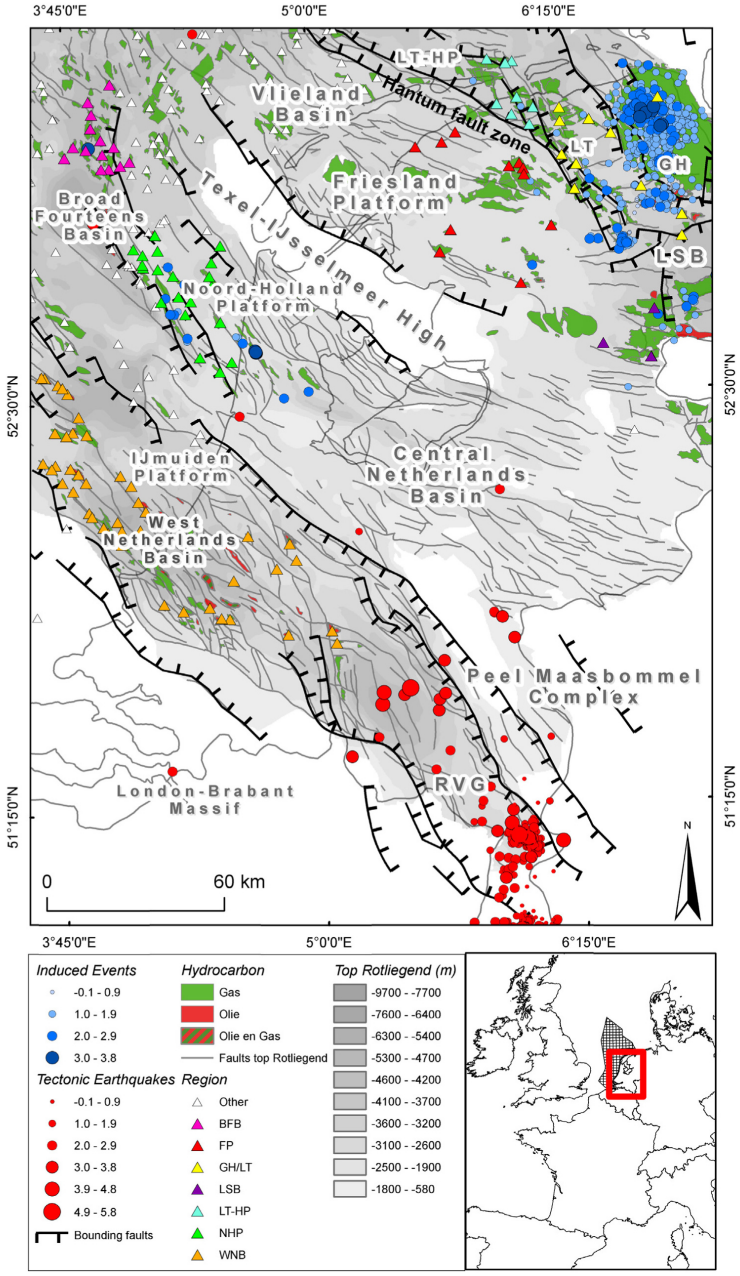

Figure 40: Tectonic map, seismicity, and hydrocarbon reservoirs in the Netherlands. Red circles: natural seismicity; blue circles: induced seismicity; green: gas reservoirs; red: oil reservoirs; solid lines: major fault zones; triangles: where leak-off tests have been performed. BFB=Broad Fourteen Basin, FP=Friesland Platform, GH/LT=Groningen High/Lauwerszee Trough, LSB=Lower Saxony Basin, LT-HP=Lauwerszee trough-Hantum Platform, NHP=Noord Holland Platform, WNB=West Netherlands Basin, RVG=Roer Valley Graben, PB=Peelrand Block, EL=Ems Low [from Van Wees *et al.*, 2014].

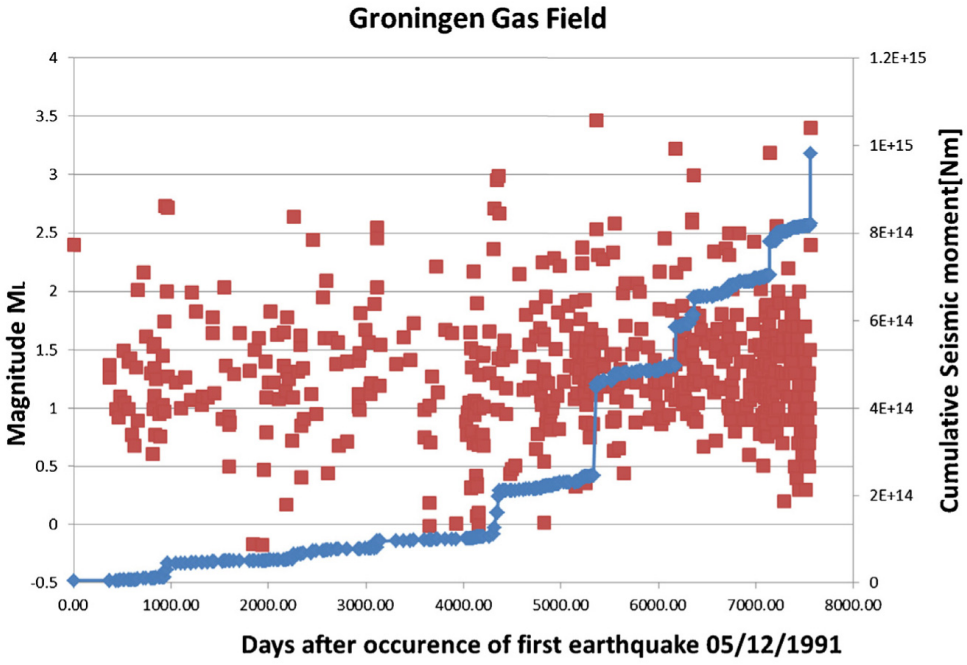

Figure 41: Magnitude of induced events in the Groningen Gasfield, Netherlands, 5 December, 1991 - 16 August, 2012, and cumulative seismic moment in Nm [from Van Wees *et al.*, 2014].

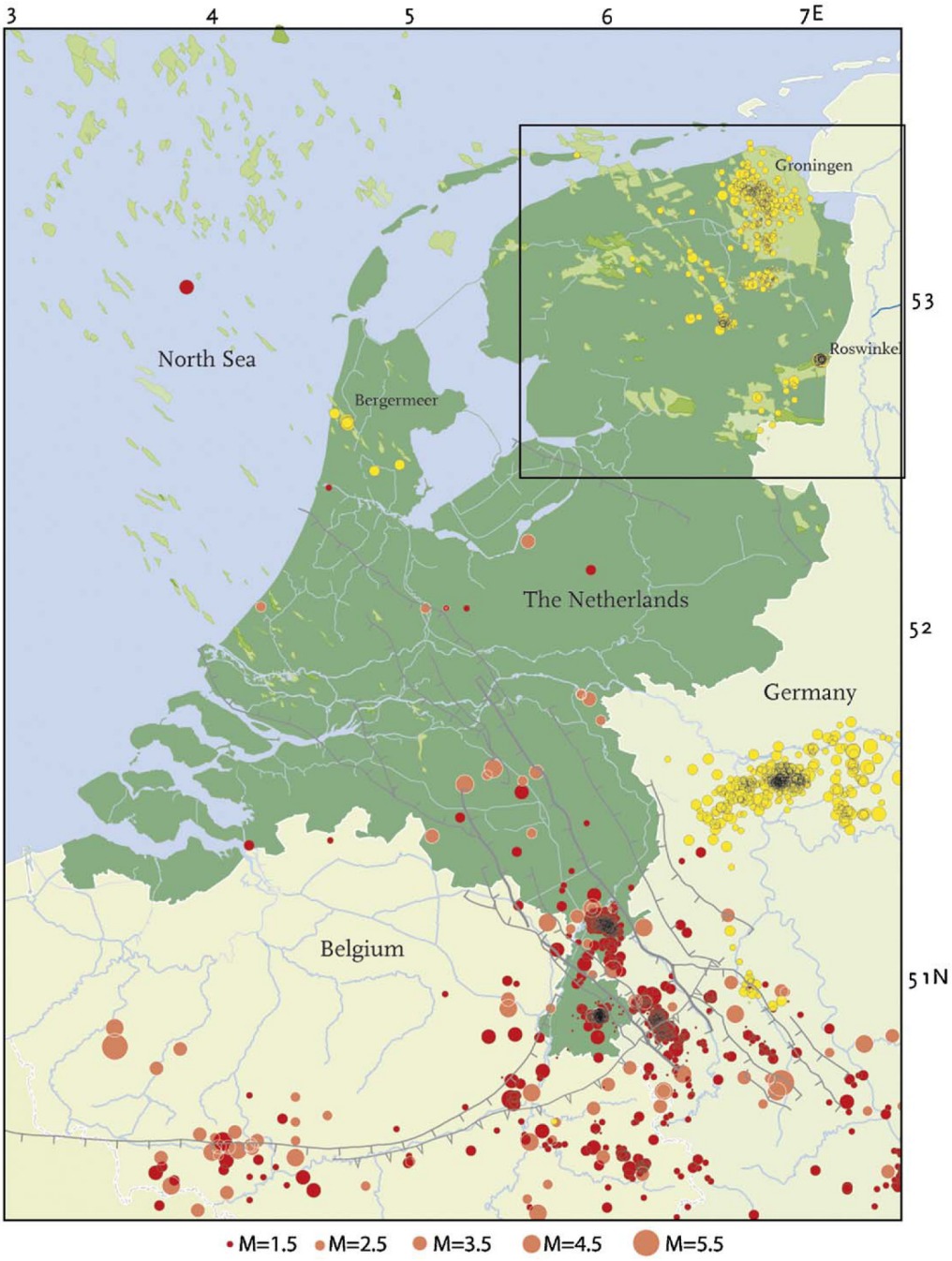

Figure 42: Seismicity in the Netherlands and surrounding region since 1900. Red circles: natural tectonic earthquakes; yellow circles: suspected induced earthquakes (usually mining or gas exploitation); gray solid lines: mapped faults in the upper-North-Sea formation; light green: approximate contours of gasfield. Detail of boxed region shown in Figure 43 [from van Eck *et al.*, 2006].

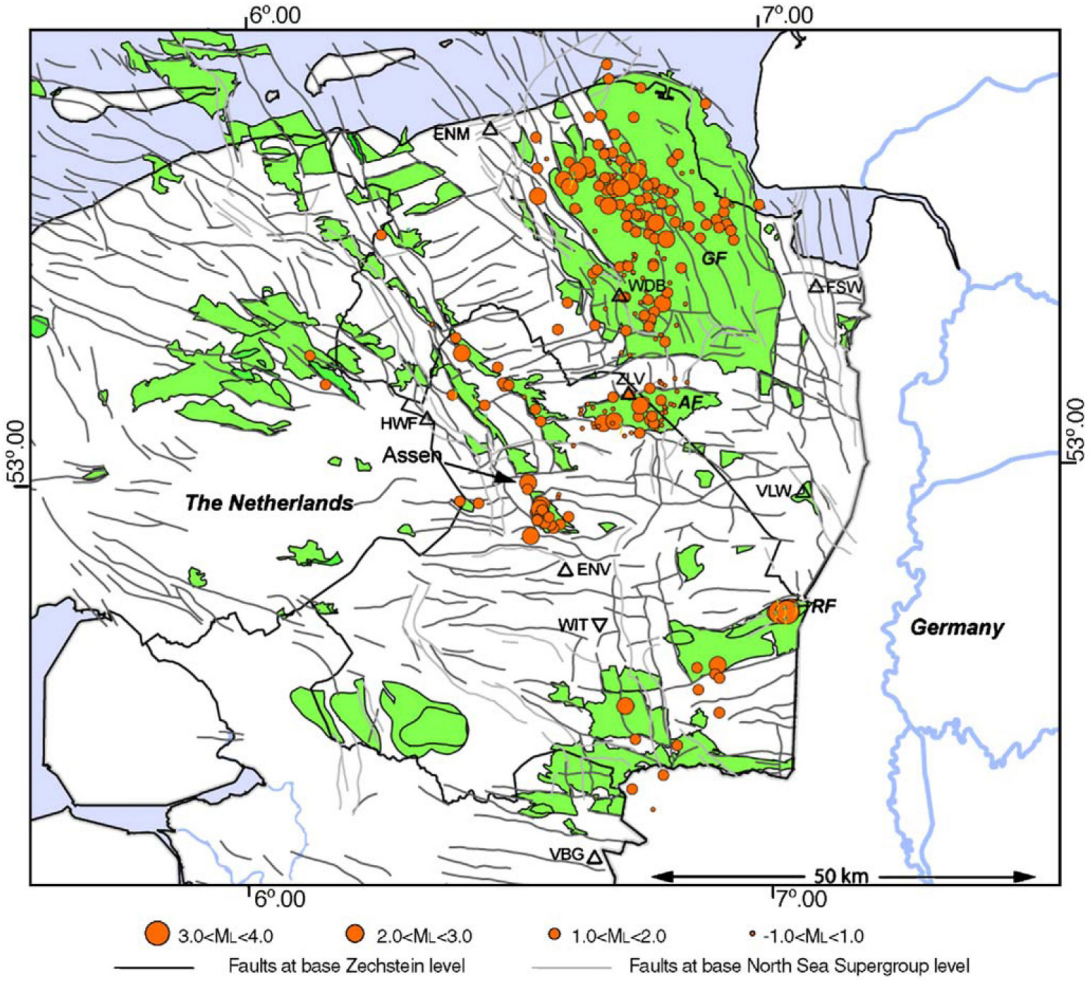

Figure 43: Map showing produced gasfields (green), major fault structures and seismicity (orange dots) in the northeast Netherlands (boxed region of Figure 42). RF: Roswinkel Field; GF: Groningen Field; EF: Eleveld Field; AF: Annerveen Field [from van Eck *et al.*, 2006].

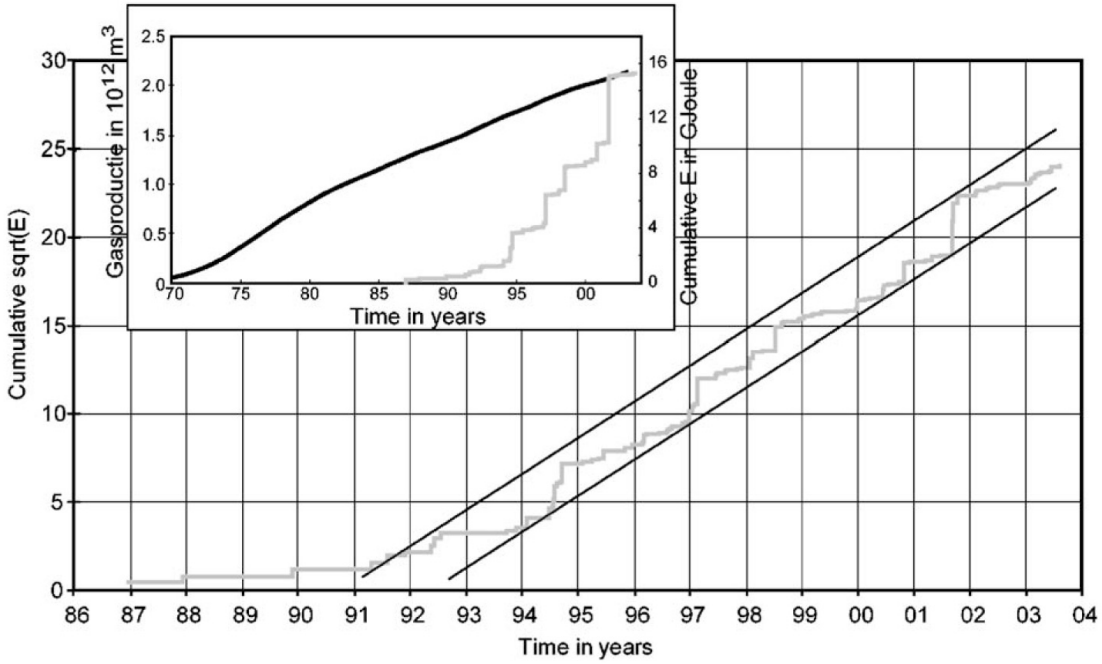

Figure 44: For the Groningen Gasfield, Netherlands, cumulative square root of the seismic energy (E) in GJ (light gray curve) of all earthquakes with M ≥ 1.5 vs. time. Inset shows cumulative seismic energy release (light gray) and cumulative gas production on land (black) [from van Eck *et al.*, 2006].

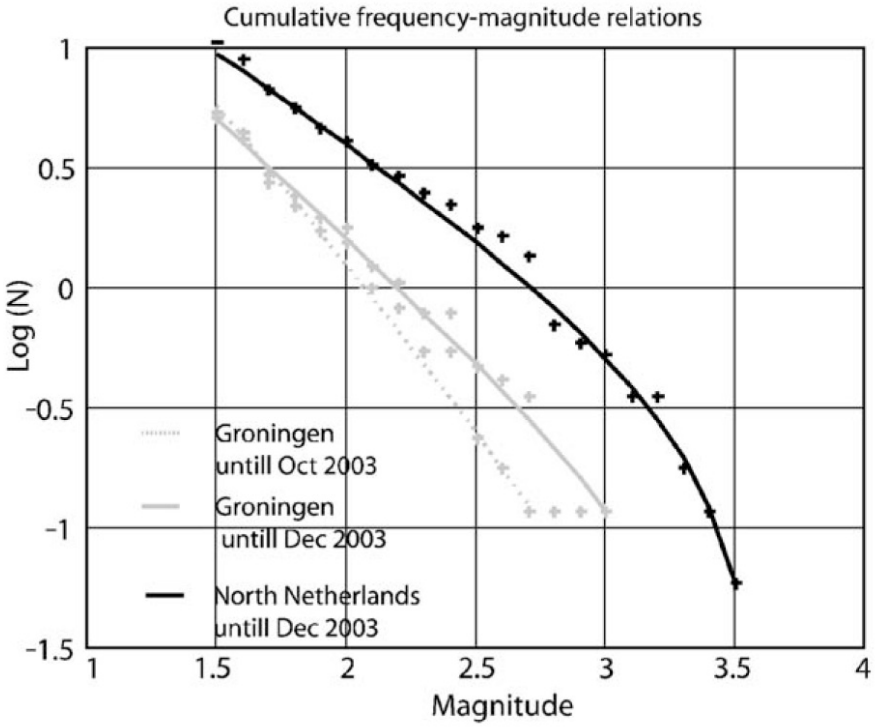

Figure 45: Cumulative annual frequency-magnitude relation for all seismicity thought to be induced in the north Netherlands for the period 1986–2003 (black curve). The same frequency-magnitude relation for all earthquakes in the Groningen Gasfield (gray curves). Gray dashed curve excludes three events with $2.7 < M < 3.0$ that occurred October–November 2003. Gray solid curve includes these events [from van Eck *et al.*, 2006].

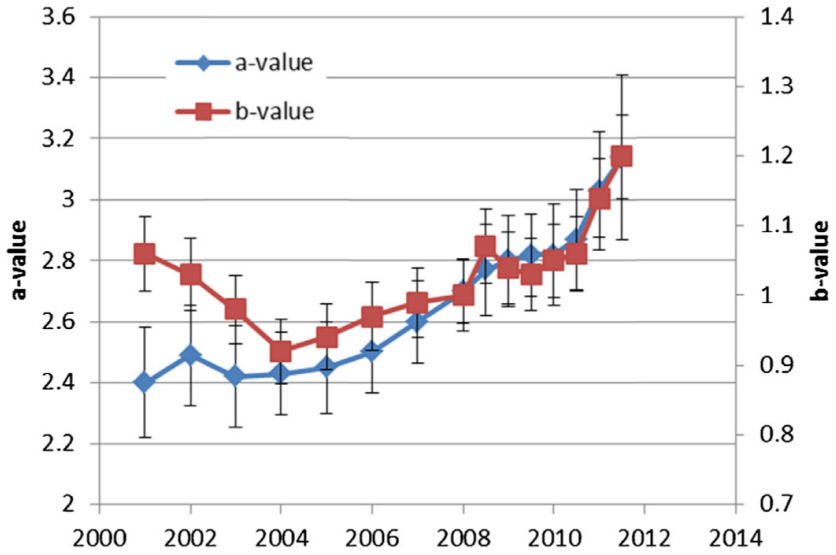

Figure 46: *a* and *b*-values of the Gutenberg-Richter relationship for seismicity in the Groningen Gasfield, Netherlands, determined using a sliding time-window of three to five years, to ensure sufficient events (> 50) in each data bin [from Van Wees *et al.*, 2014].

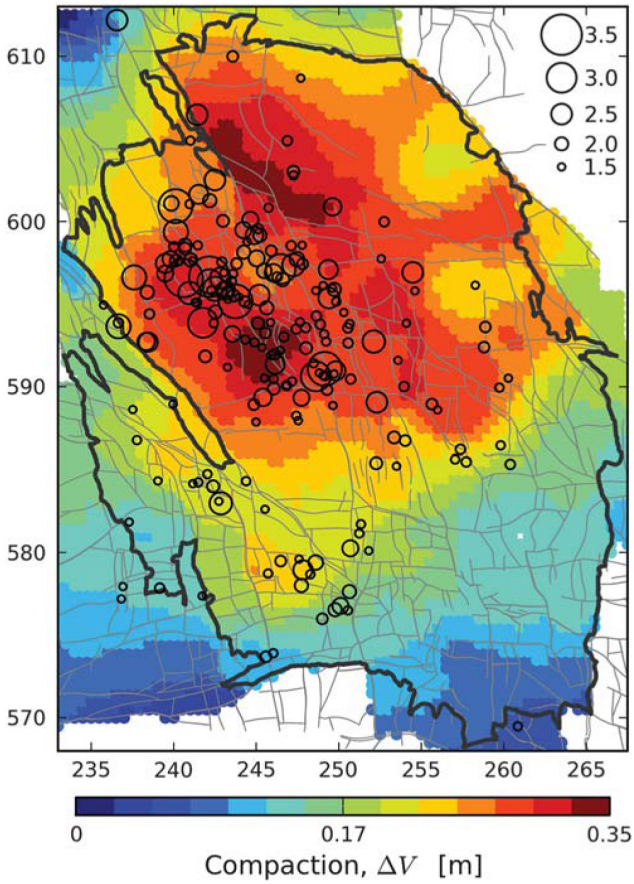

Figure 47: Earthquake epicenters for events with M ≥ 1.5 for the period 1995-2012, superimposed on a model of reservoir compaction for 1960-2012. Black line: perimeter of the Groningen Gasfield; thin gray lines: faults close to the reservoir level. Map coordinates are kilometers in the Dutch national triangulation coordinate system (Rijksdriehoek) [from Bourne *et al.*, 2015].

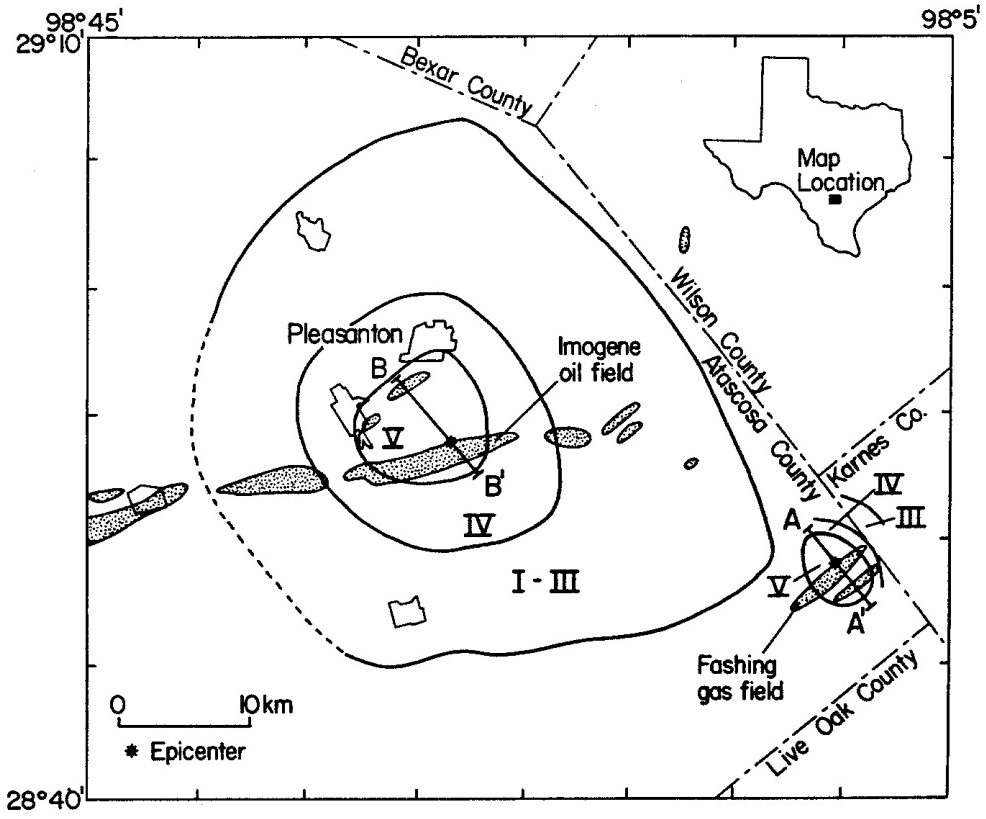

Figure 48: Oilfields and gasfields in the Imogene/Fashing area, south Texas, where earthquakes are postulated to have been induced. Shaded regions are more prominent fields. Isoseismals for the largest events on the Modified Mercalli intensity scale are shown [from Pennington *et al.*, 1986].

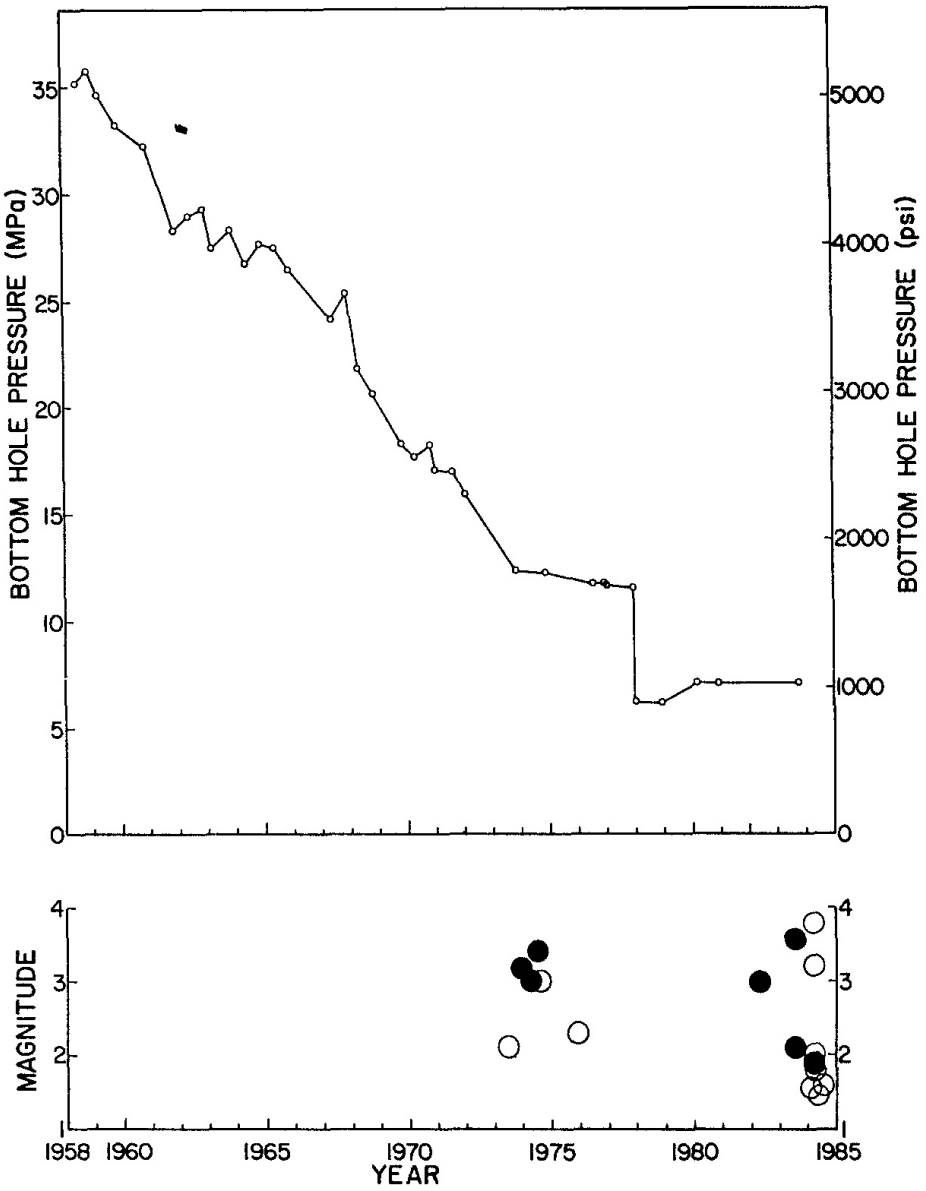

Figure 49: Pressure history of a well near the fault in the Fashing Gasfield along with known earthquakes in the Fashing-Pleasanton area. Black dots: earthquakes from the Fashing area; open circles: earthquakes from the Pleasanton (Imogene) area [from Pennington *et al.*, 1986].

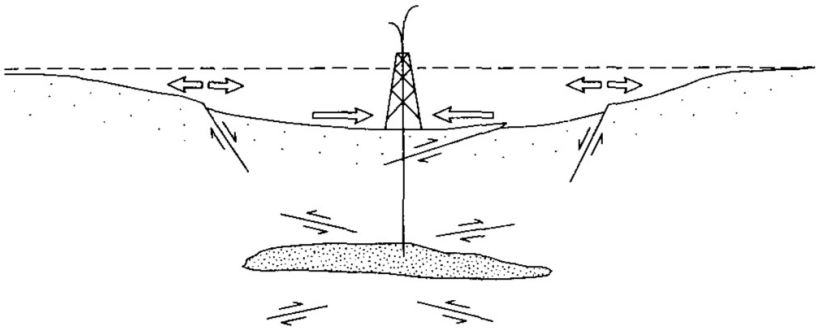

Figure 50: Schematic cross section summarizing surface deformation and faulting associated with fluid withdrawal. Normal faults develop on the flanks of the field, as observed at the Goose Creek, Texas, Oilfield. Reverse faults develop above reservoirs as observed at Wilmington, Buena Vista Hills, the Pau Basin and beneath the Strachan Field [from Segall, 1989].

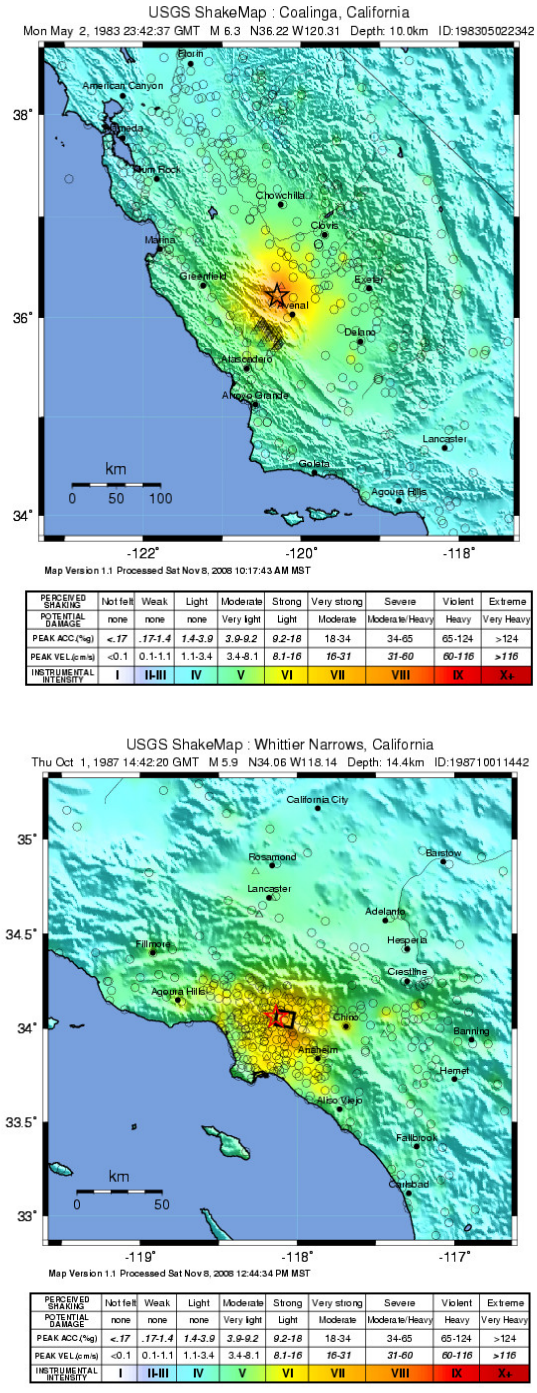

Figure 51: U.S. Geological Survey shake maps[19]. Top: 1983 M_W 6.2 Coalinga, California earthquake, which injured 94 people and was felt throughout half the state. Bottom: 1987 M_L 5.9 Whittier Narrows, California earthquake, which killed six people.

[19] http://earthquake.usgs.gov/earthquakes/shakemap/

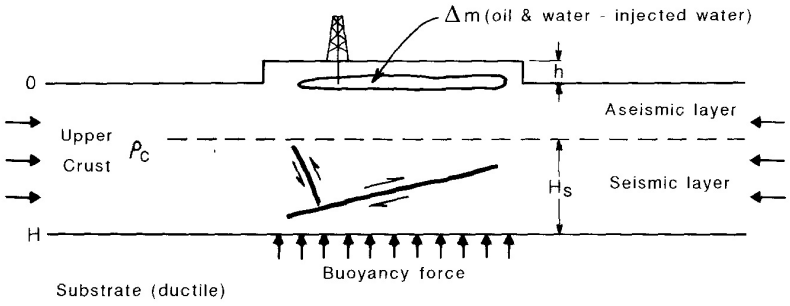

Figure 52: Schematic cross section showing proposed crustal response mechanism to oil production. Mass removal results in a vertical force imbalance causing seismic deformation in the seismogenic layer. This deformation, together with aseismic deformation in the shallow crust, restores isostatic balance [from McGarr, 1991].

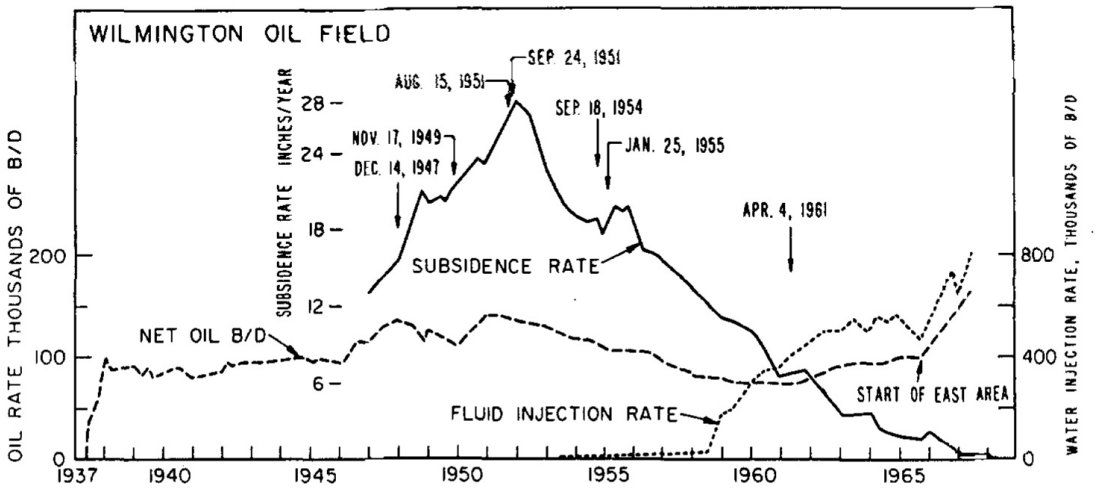

Figure 53: For the Wilmington Oilfield, California, subsidence rate in the center of the field, oil production and water injection rates. Arrows show dates of major damaging earthquakes [from Kovach, 1974].

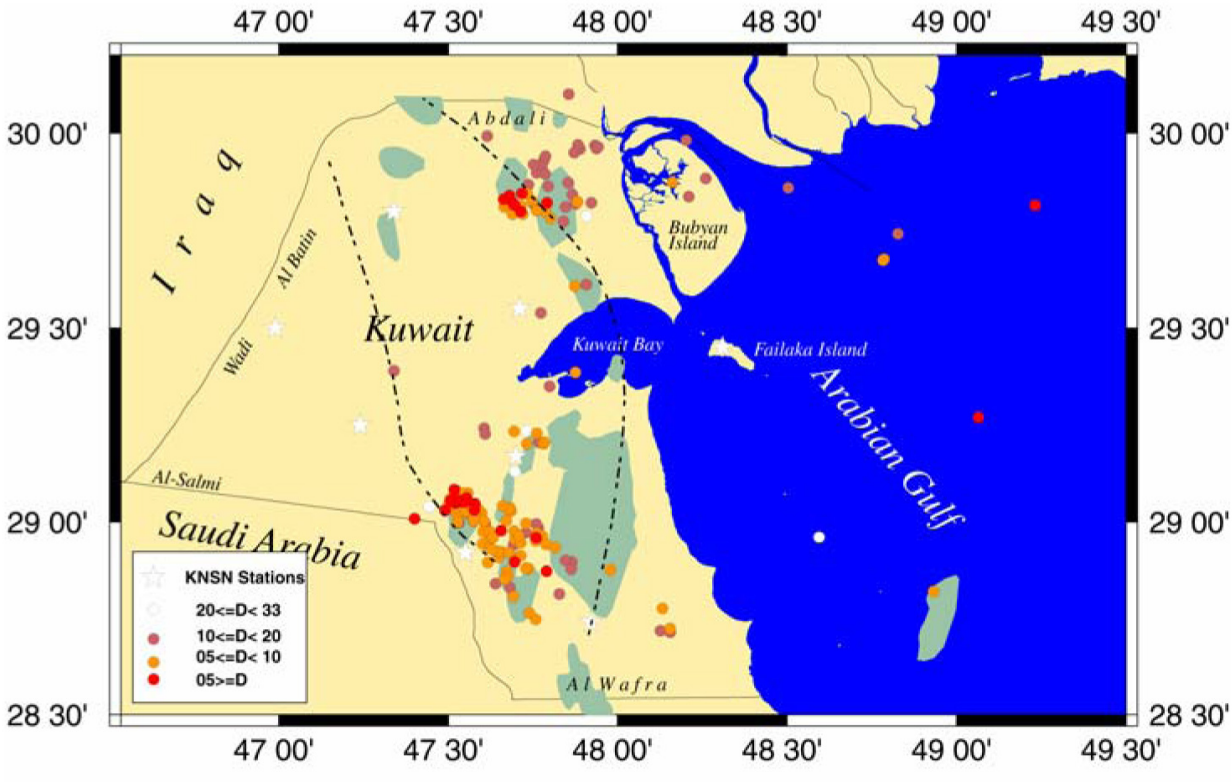

Figure 54: Seismicity of Kuwait for the period March 1997 - October 2007 [from Al-Enezi *et al.*, 2008].

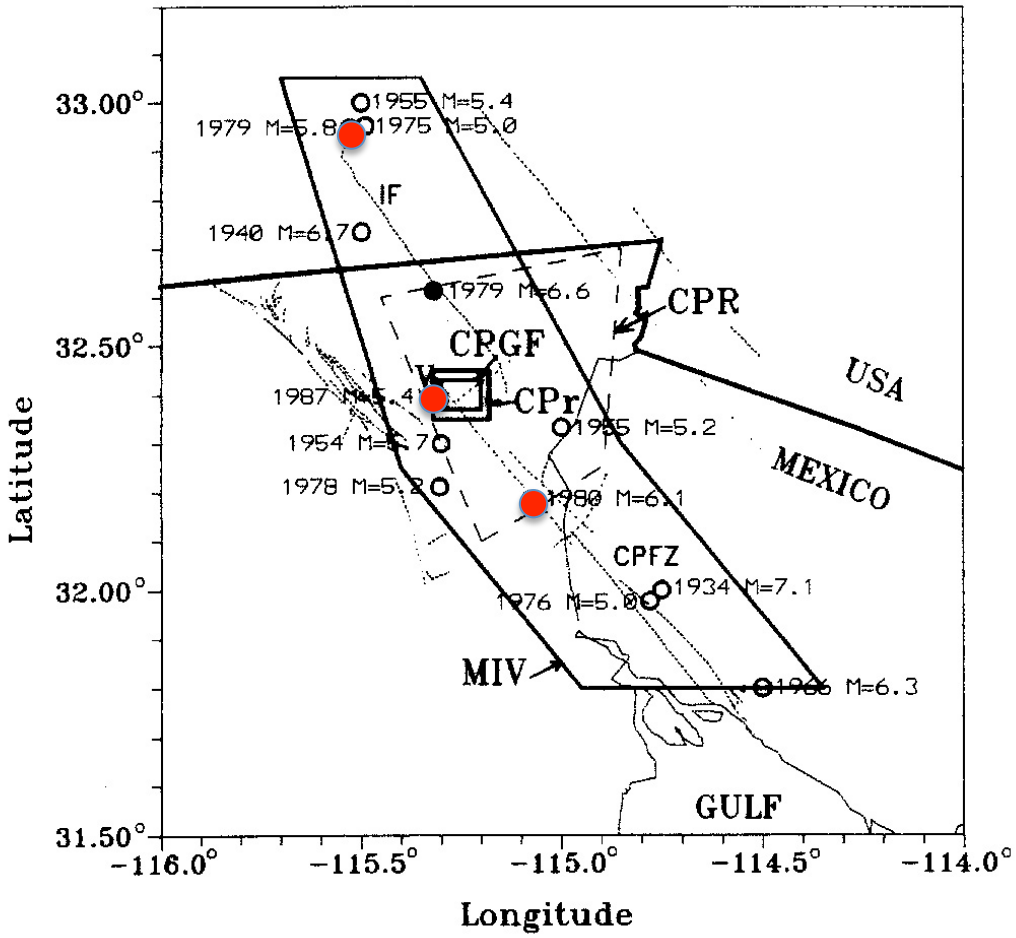

Figure 55: Map showing the Cerro Prieto geothermal field. Circles: earthquakes with M ≥ 5; red dots: earthquakes with M > 6; dotted lines: faults; IF: the Imperial fault; CPFZ: Cerro Prieto fault zone; V: the Cerro Prieto volcano [from Glowacka & Nava, 1996].

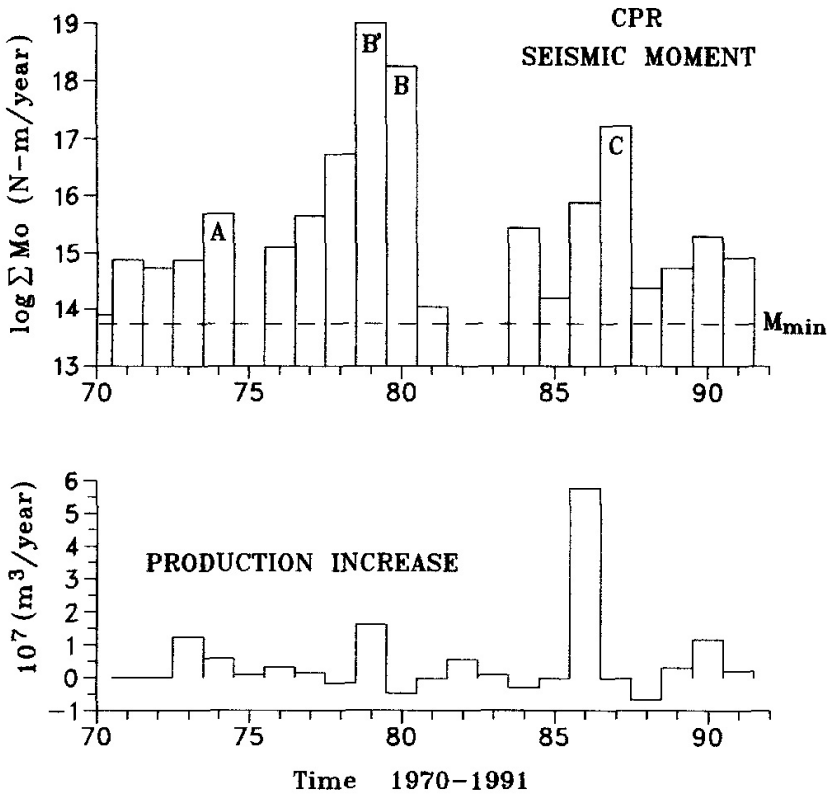

Figure 56: For the Cerro Prieto geothermal field, Mexico, top: annual seismic moment release; bottom: production rate [from Glowacka & Nava, 1996].

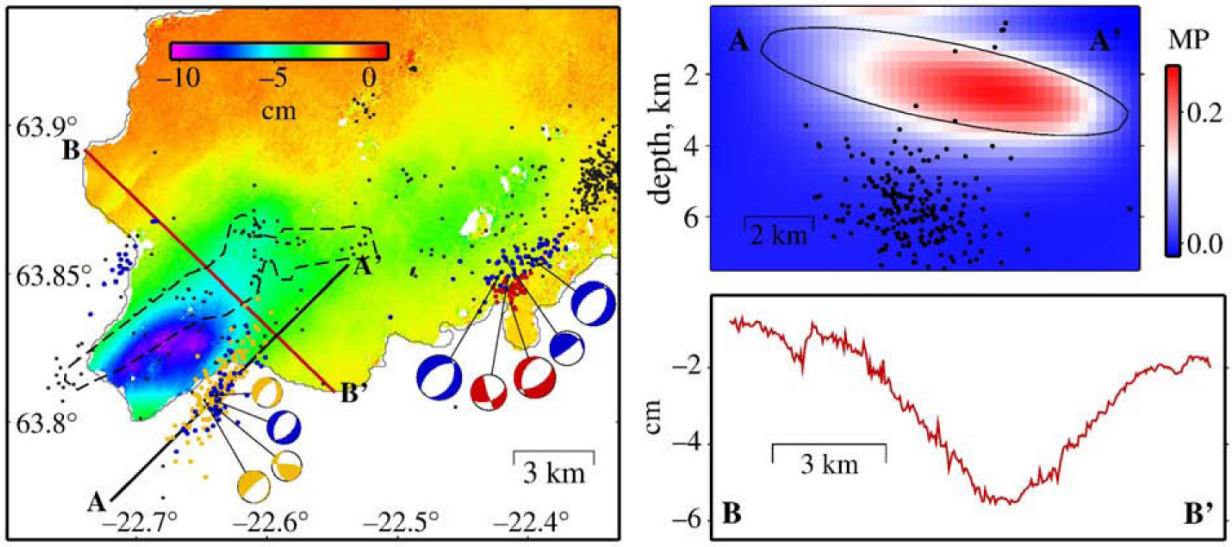

Figure 57: For the Reykjanes and Svartsengi geothermal fields, southwest Iceland, left: the near-vertical radar displacement field June 2005 - May 2008, earthquake locations and focal mechanisms. Black dots: background events. Distinct swarm events are shown for 2006 (orange), 2007 (red) and 2008 (blue). Stippled outline: location of the 1972 swarm activity from Klein *et al.* [1977]. Top right: profile AA′ shows the predicted change in Coulomb failure stress for normal slip on NE-SW-trending fault planes, computed using an elastic half-space ellipsoidal source model for subsidence around the Reykjanes geothermal field. Bottom right: profile BB′ shows the observed near-vertical radar displacement across the Reykjanes subsidence bowl [from Keiding *et al.*, 2010].

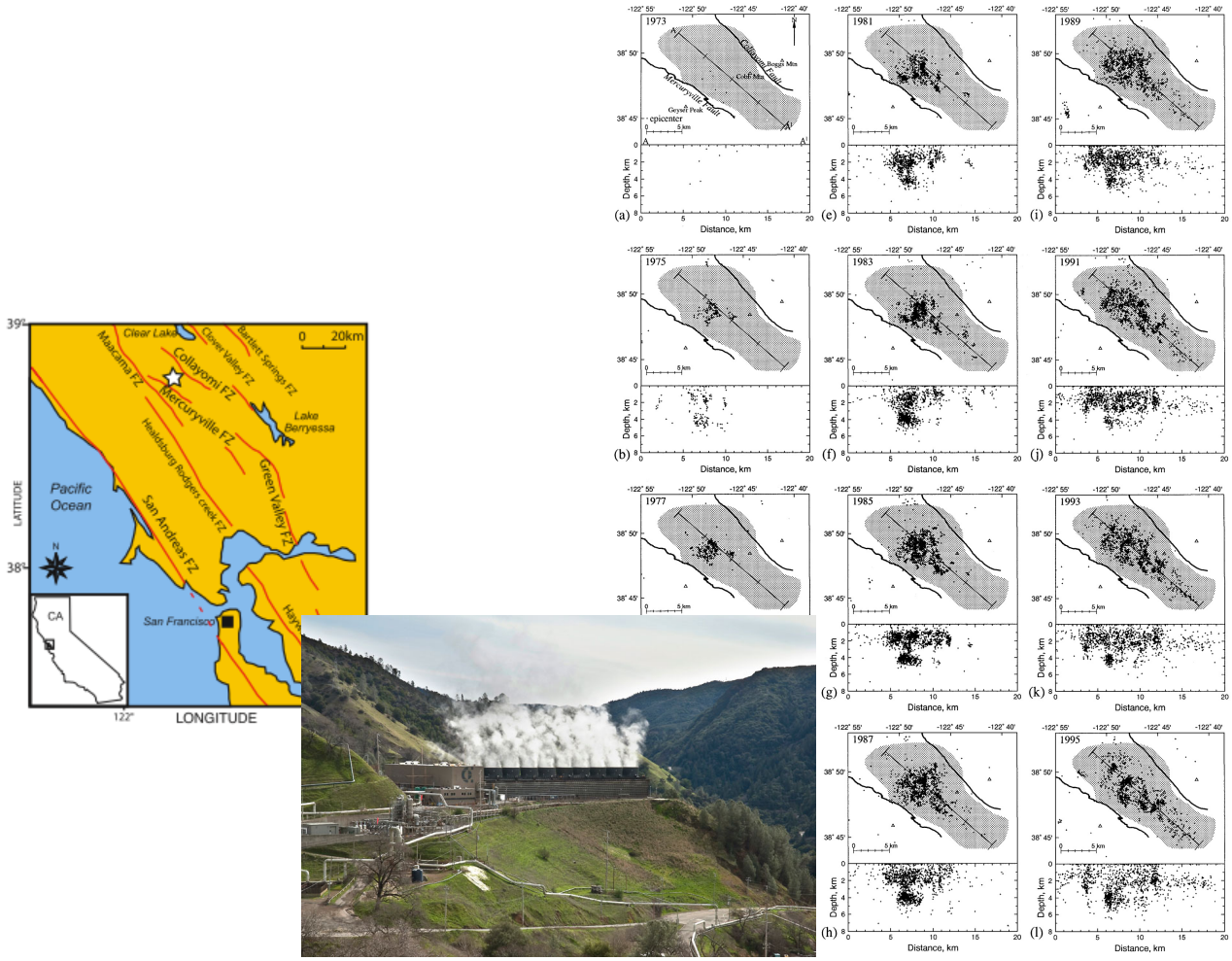

Figure 58: The Geysers geothermal field, California. Left: regional map showing location of the field. Middle: McCabe Units 5 and 6 at The Geysers[20]. Right: maps of seismicity at The Geysers at biannual intervals from 1973 to 1995. Locations are from the Northern California Seismic Network catalogue for earthquakes with M > 1.2. Gray area: steam field. Line shows line-of-section for depth sections below each map [from Ross *et al.*, 1999].

[20] http://www.energy.ca.gov/tour/geysers/

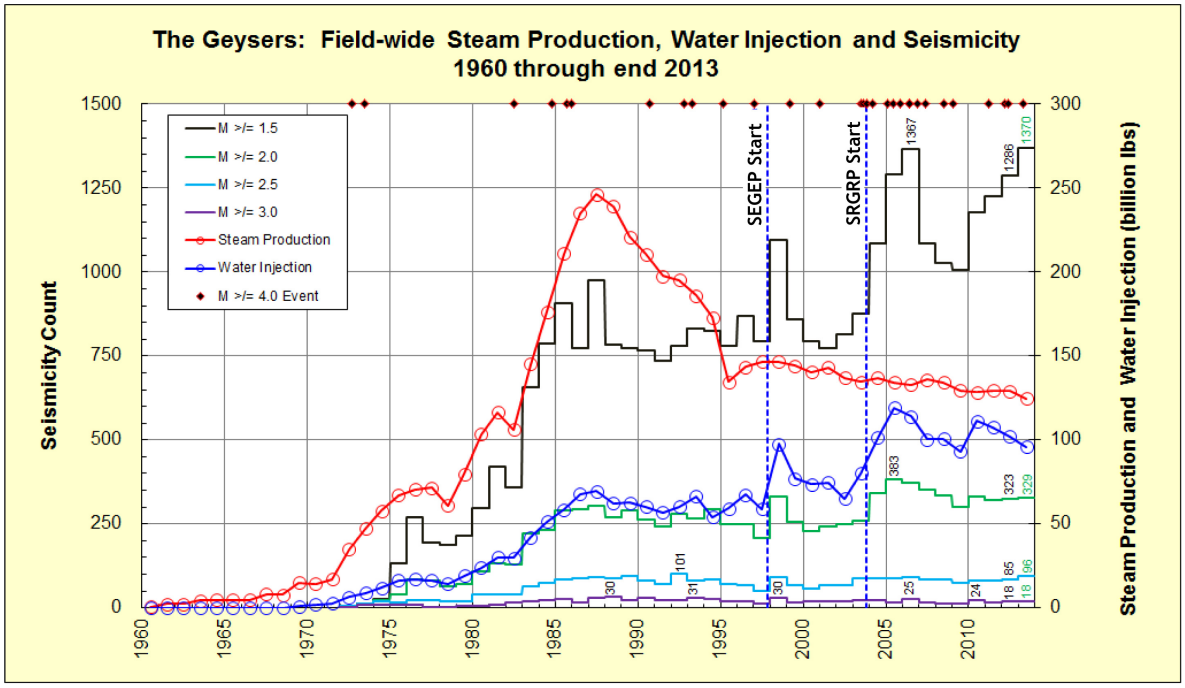

Figure 59: Yearly field-wide steam production, water injection and seismicity 1960-2013. Earthquakes with M ≥ 4 are indicated as red diamonds along the top boundary of the graph [from Hartline, 2014].

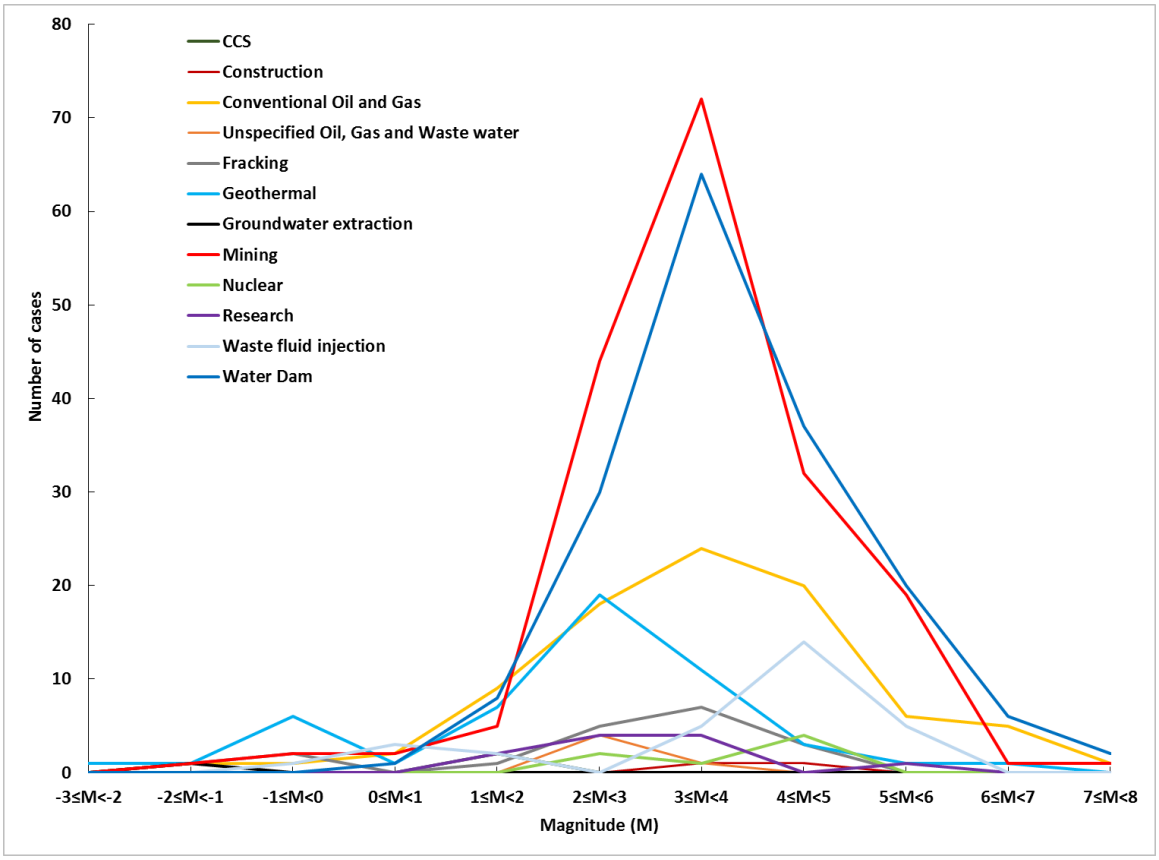

Figure 60: Number of cases reported for projects of various types vs. M_{MAX} for the 562 cases for which data are available.

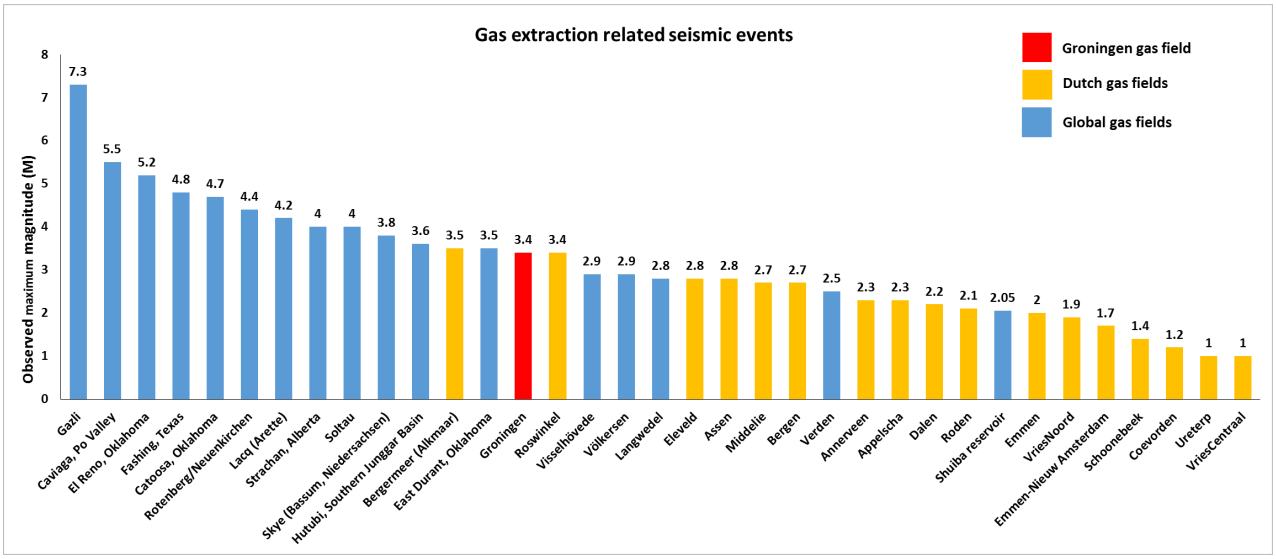

Figure 61: M_{MAX} for seismicity postulated to be induced by the extraction of natural gas at the 35 fields where this parameter is reported. The Hutubi, northwest China case is associated with both extraction and storage [Tang *et al.*, 2015].

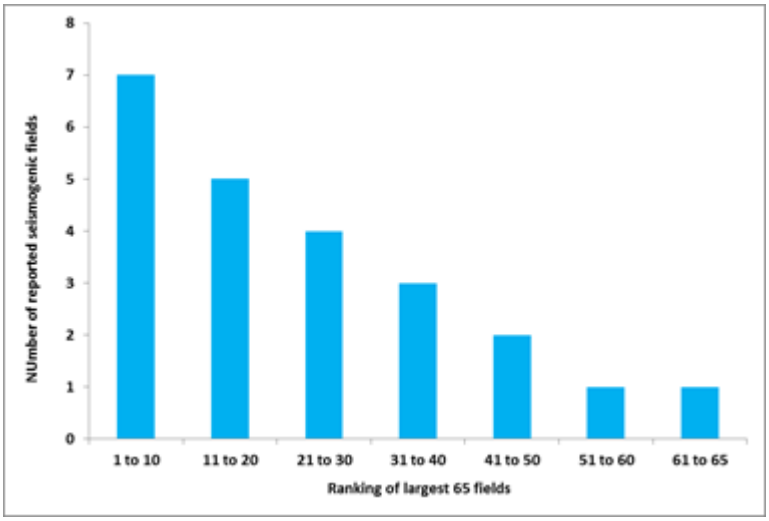

Figure 62: Number of reports of induced seismicity vs. size of field for the 65 largest global power-producing geothermal fields in groups of 10.

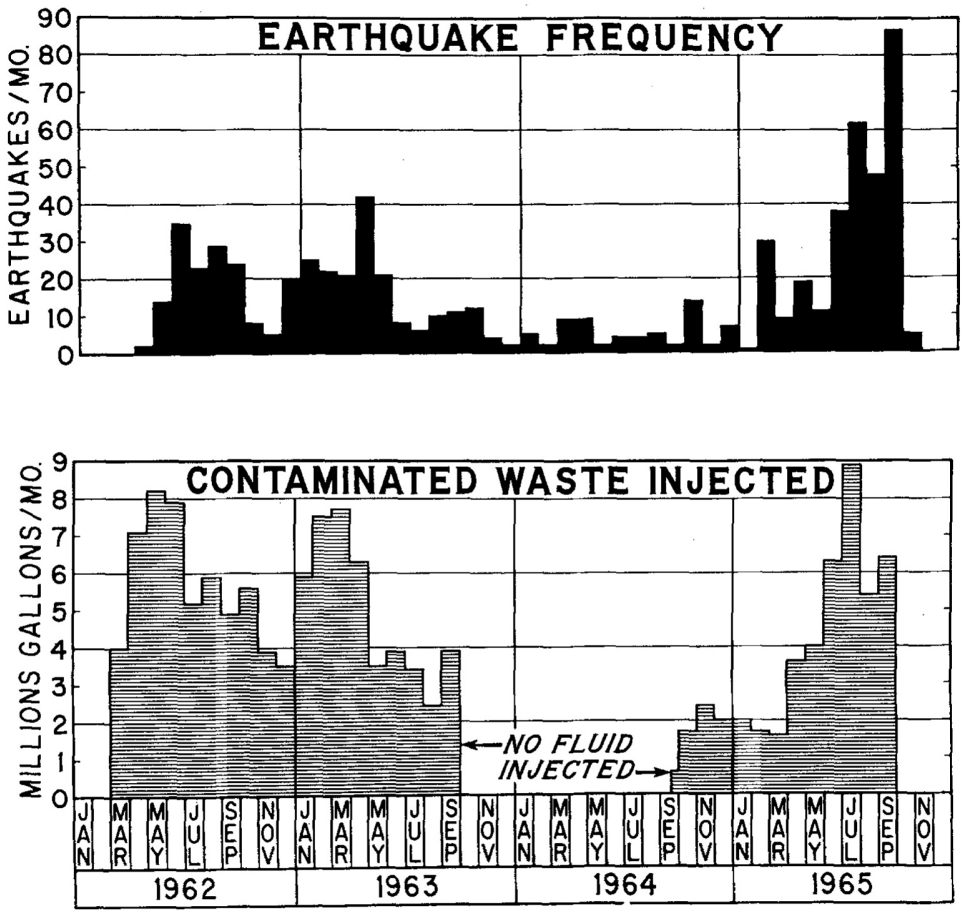

Figure 63: Top: Earthquake frequency. Bottom: injection rate at the Rocky Mountain Arsenal well, Colorado [Healy *et al.*, 1968].

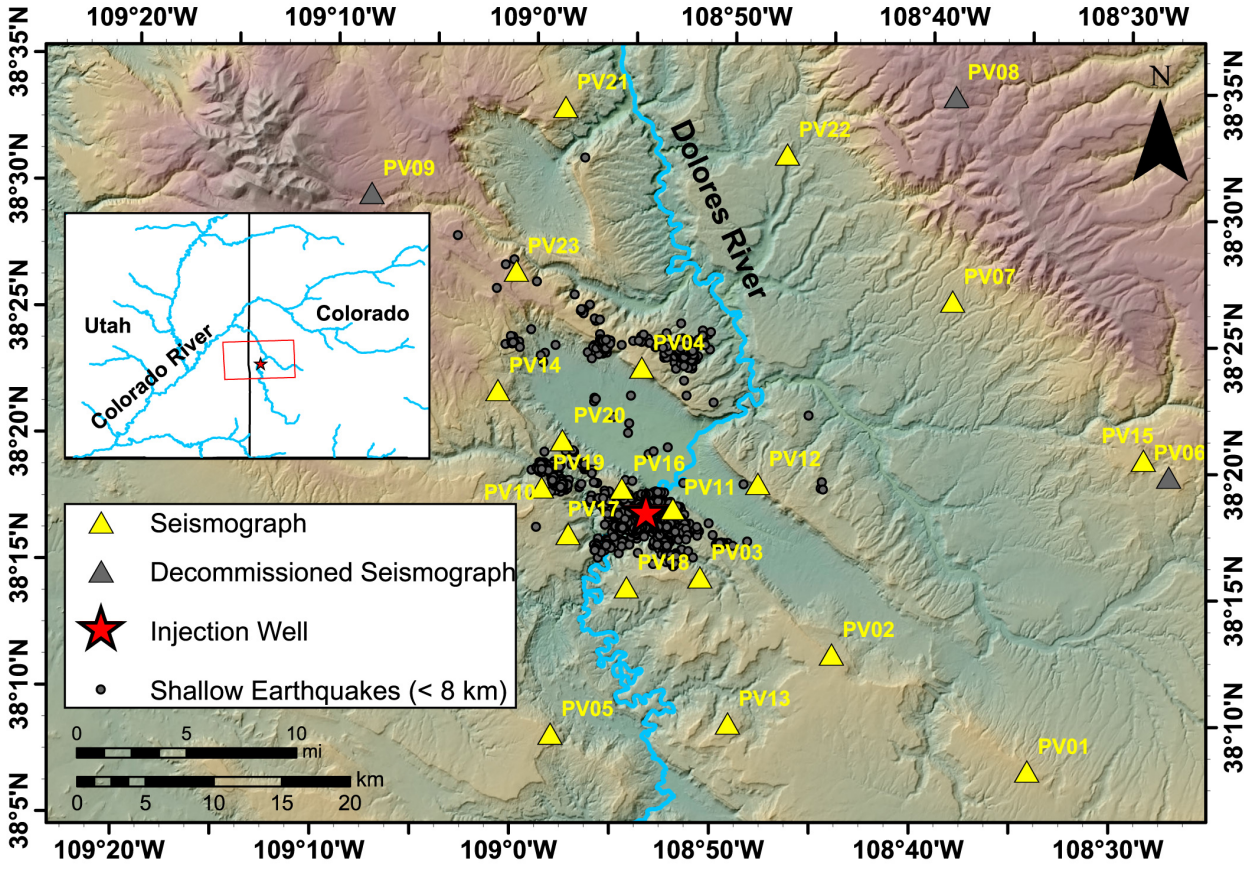

Figure 64: The region around Paradox Valley, Colorado (the northwest-oriented depression). Yellow triangles: seismic stations; gray circles: earthquakes thought to be induced by brine injections [from Yeck *et al.*, 2015].

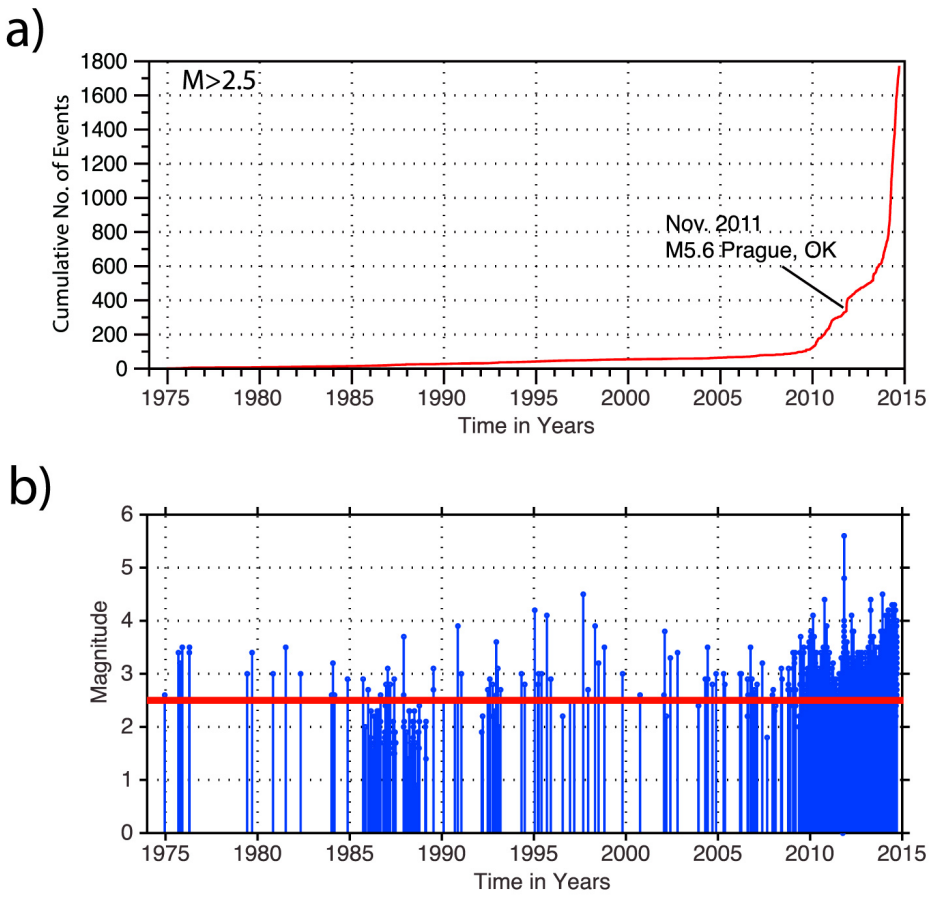

Figure 65: Earthquakes recorded on the National Earthquake Information Center (NEIC)[21] system for the period 1975 through 2014. a) Cumulative seismicity in Oklahoma with M > 2.5. b) Earthquake magnitudes [from McNamara *et al.*, 2015].

[21] http://earthquake.usgs.gov/contactus/golden/neic.php

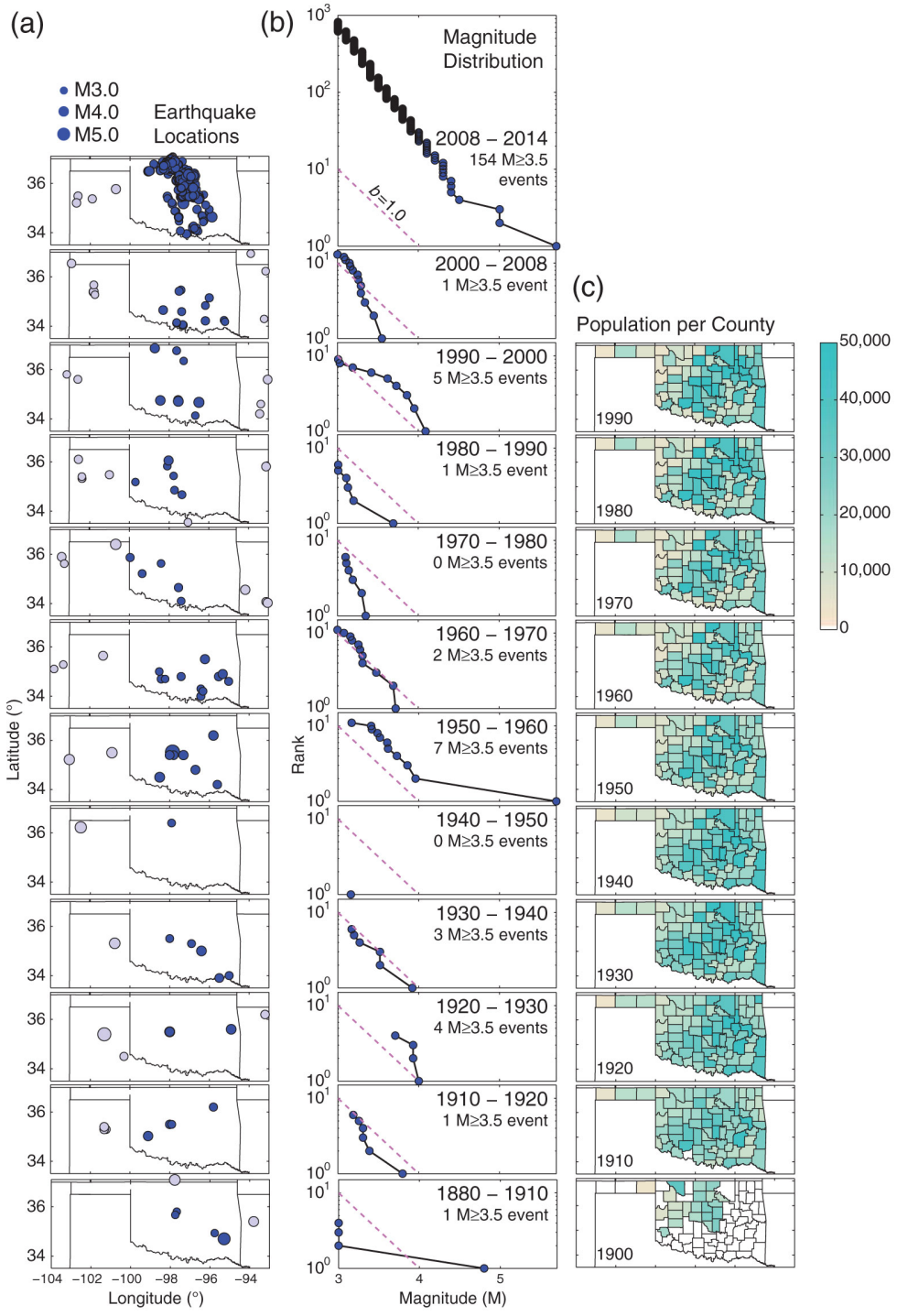

Figure 66: Oklahoma seismicity. Left panels: Earthquake locations: blue–Oklahoma, gray–neighboring states. Centre panels: magnitudes plotted cumulatively 1880 - 2014. Right panels: human population by county [from Hough & Page, 2015].

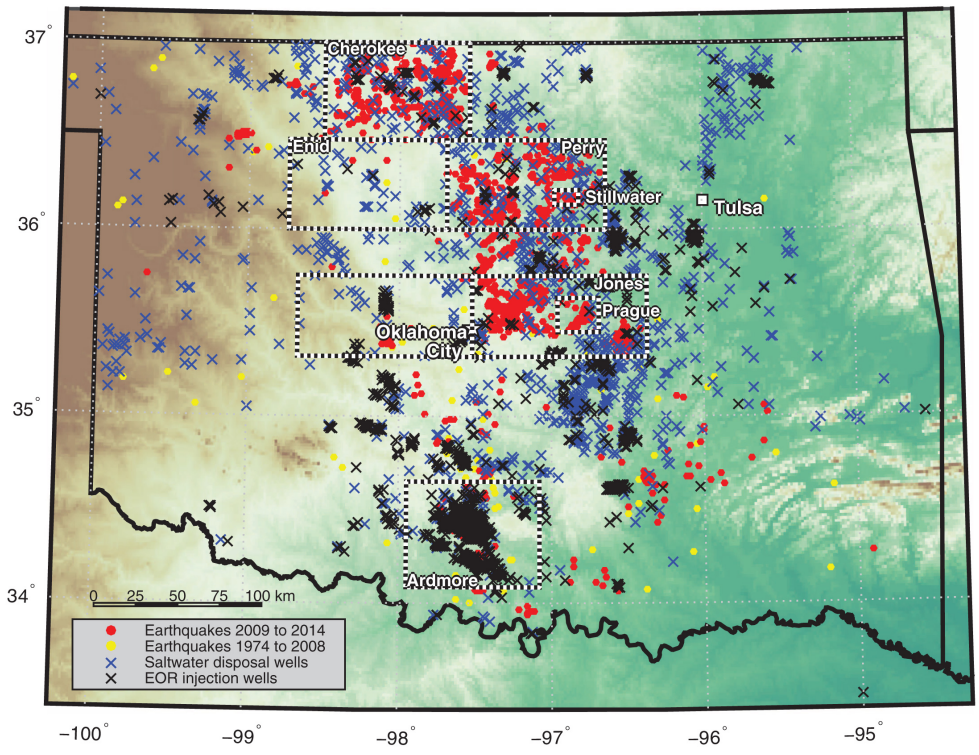

Figure 67: Earthquakes and injection wells in Oklahoma. Red dots: locations of earthquakes 2009–2014; yellow dots: historical earthquakes 1974–2008; black crosses: enhanced oil recovery wells; blue crosses: salt water disposal wells that injected more than 30,000 barrels (~4800 m^3) in any month in the most recent three years of data; boxes: areas of detailed study [from Walsh & Zoback, 2015].

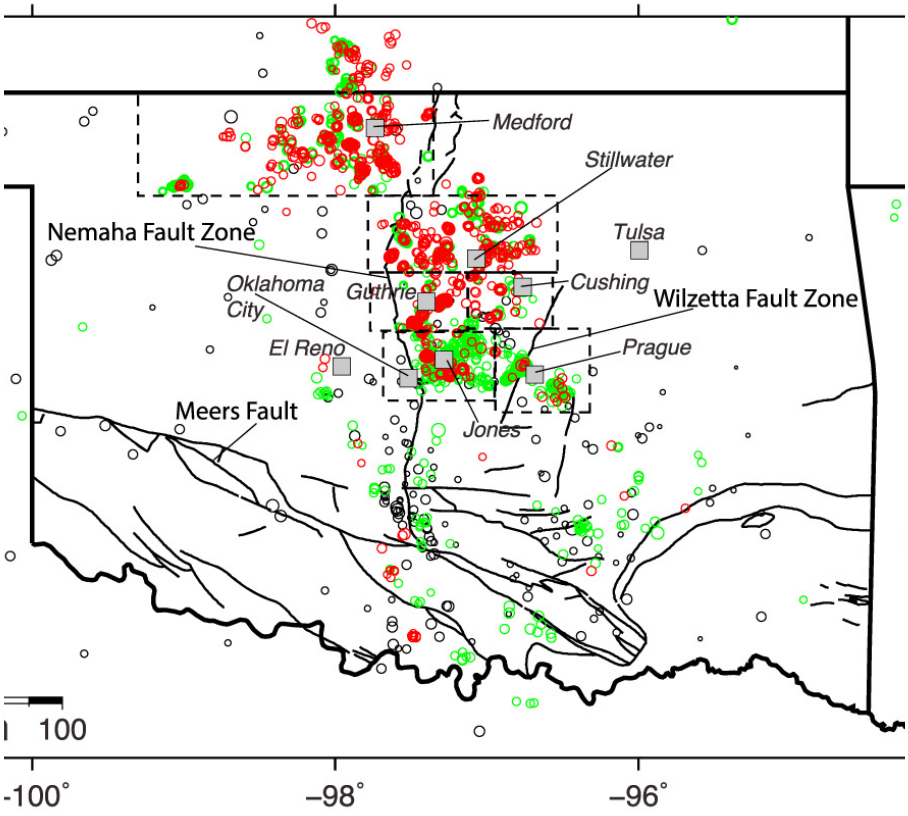

Figure 68: U.S. Geological Survey earthquake epicenters from the National Earthquake Information Center (NEIC) database[22], 1974 - 2014. Black lines: subsurface and surface faults; dashed black lines: detailed study regions; Meers fault: the only known active fault in Oklahoma prior to the recent increase in seismicity [from McNamara *et al.*, 2015].

[22] http://earthquake.usgs.gov/contactus/golden/neic.php

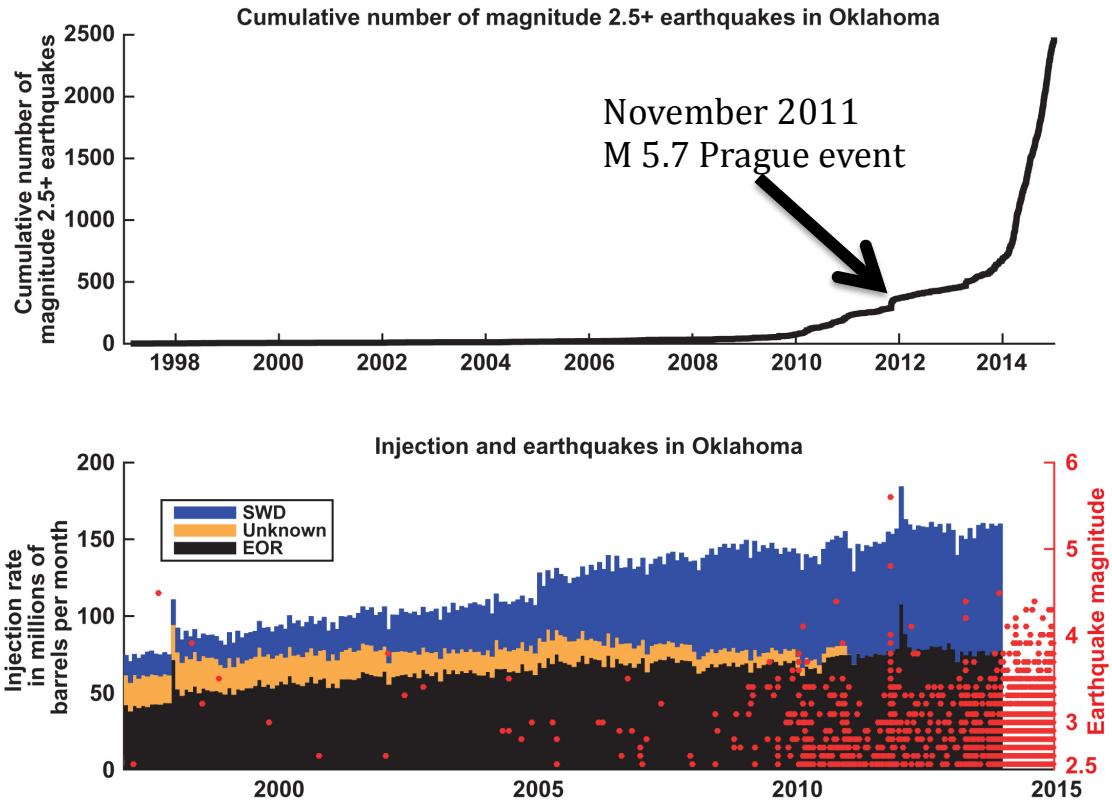

Figure 69: Fluid injection and earthquakes in Oklahoma. Top: Cumulative number of M $\geq$ 2.5 earthquakes for the period 1997-2014. Bottom: left axis shows total combined injection rate of all underground injection control wells in Oklahoma, right axis shows all earthquakes in Oklahoma by magnitude [from Walsh & Zoback, 2015].

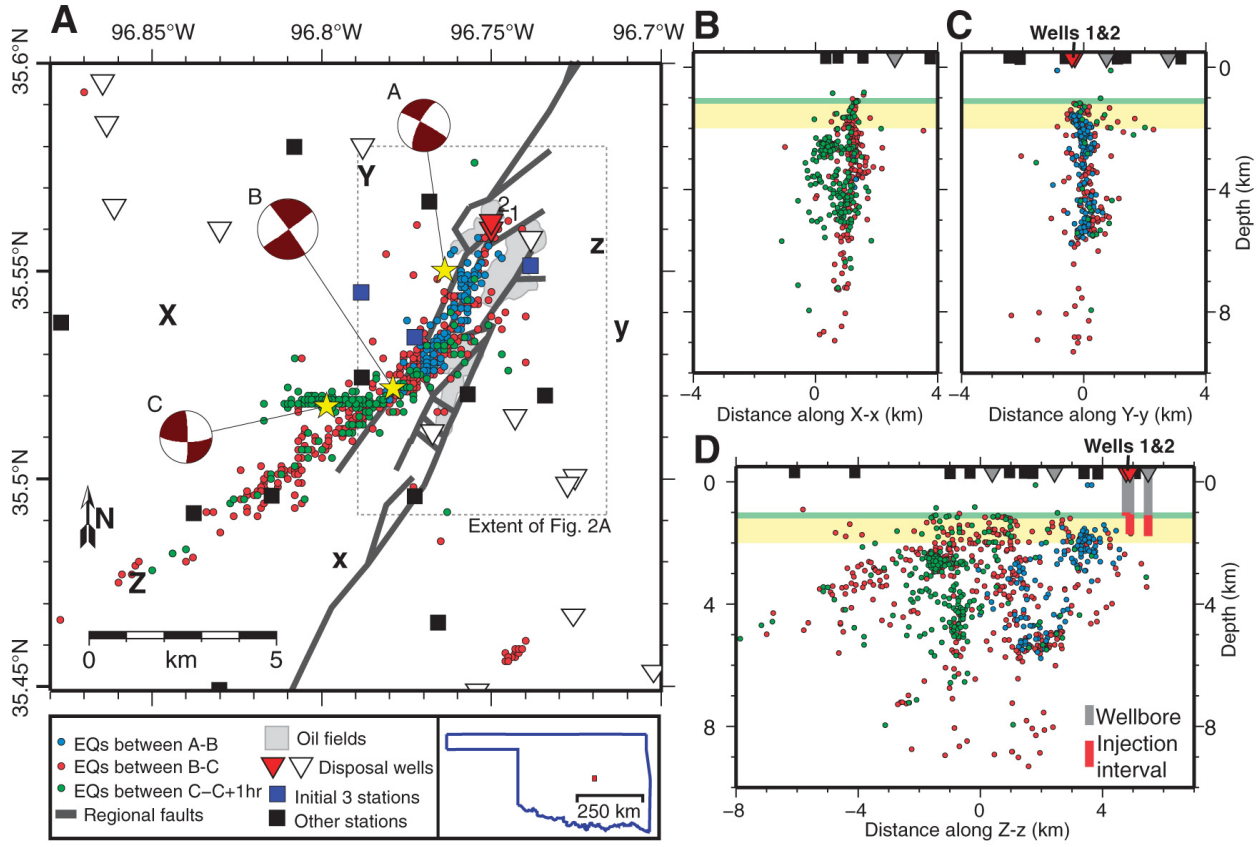

Figure 70: Seismicity, focal mechanisms, seismic stations, active disposal wells, and oilfields in the neighborhood of the 2011 Prague, Oklahoma, seismic sequence. Stars: major earthquakes in the sequence. B–D: Cross sections showing seismicity projected from up to 4 km out of plane. Vertical lines: wellbores, red where perforated or open; green bands: the Hunton and Simpson Groups; yellow bands: Arbuckle Group which overlies basement. Inset: Oklahoma and location of map area [from Keranen *et al.*, 2013].

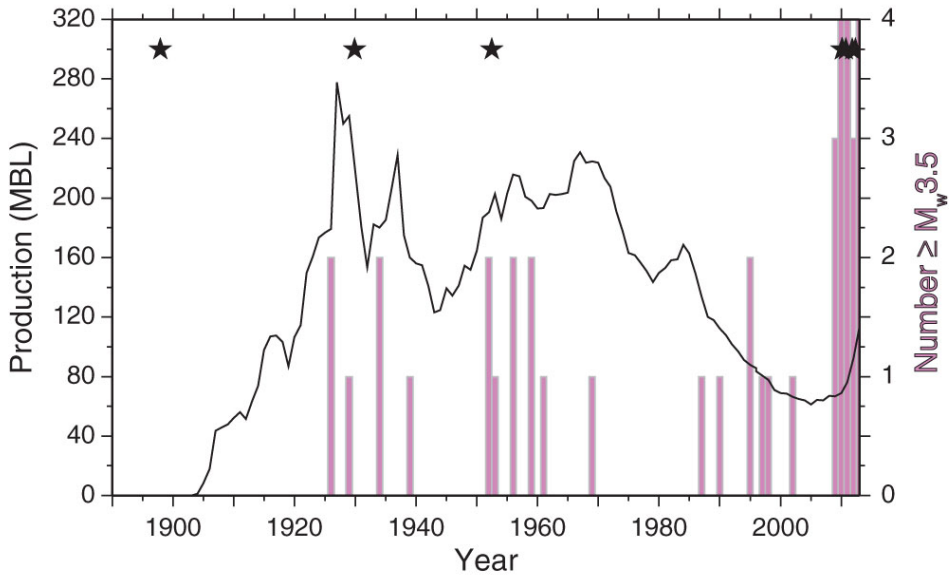

Figure 71: Oklahoma seismicity rates compared with oil production in millions of barrels (multiply by 0.159 to convert to m^3). Bars: number of earthquakes with $M \geq 3.5$ in a given year; black stars: $M \geq 4$ events [from Hough & Page, 2015].

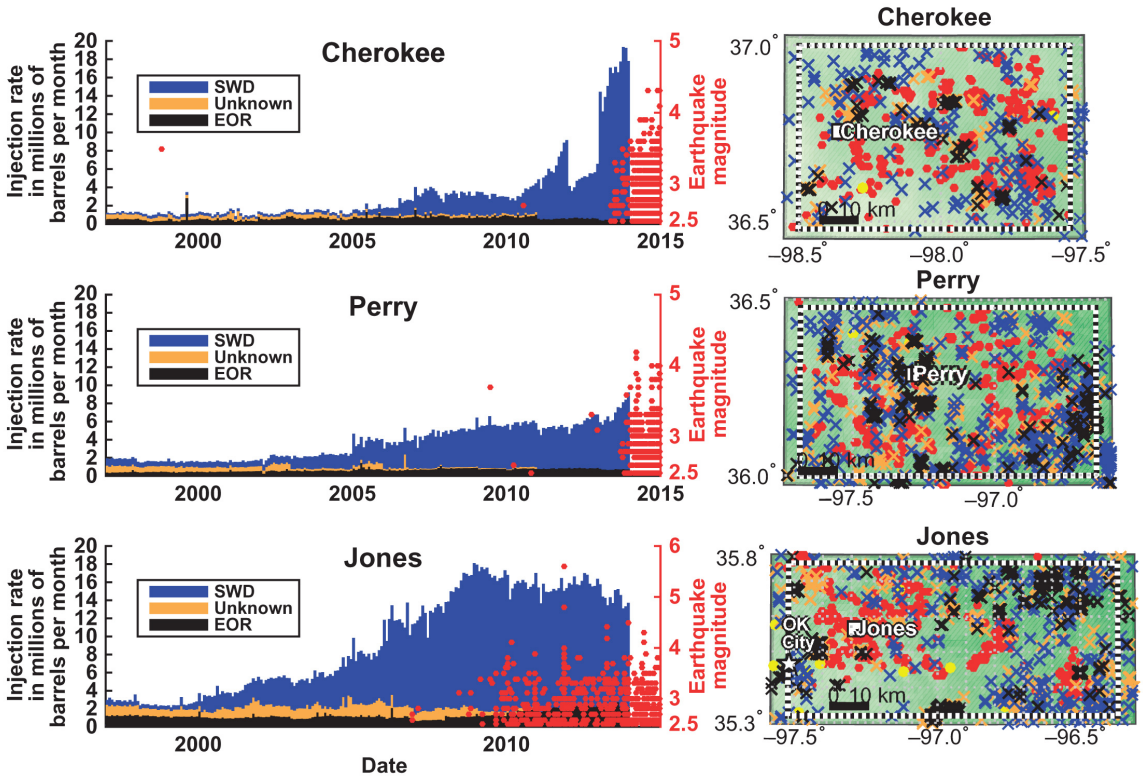

Figure 72: Injection from enhanced oil recovery, brine disposal, and unknown wells, and earthquakes in the Cherokee, Perry, and Jones study areas (boxes in Figure 67). Symbols are the same as in Figure 67. Each study area is 5000 km^2 in size [from Walsh & Zoback, 2015].

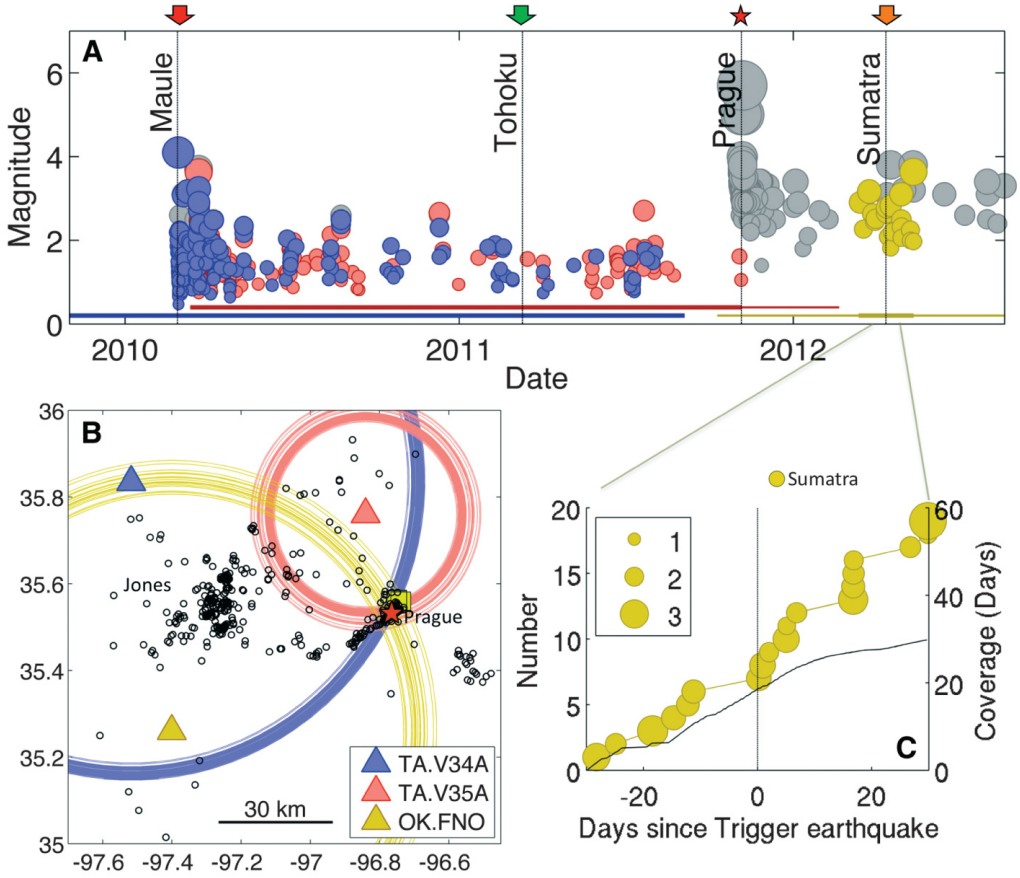

Figure 73: Earthquakes in the Prague, Oklahoma, area. (A) Detected events, showing triggering by the 2010 Maule, Chile earthquake. Red star: the 6 November 2011 M_W 5.7 mainshock. (B) Distances to detected events. (C) Cumulative number of events in the time period surrounding the 11 April 2012 M_W 8.6 and 8.2 Sumatra earthquakes [from van der Elst *et al.*, 2013].

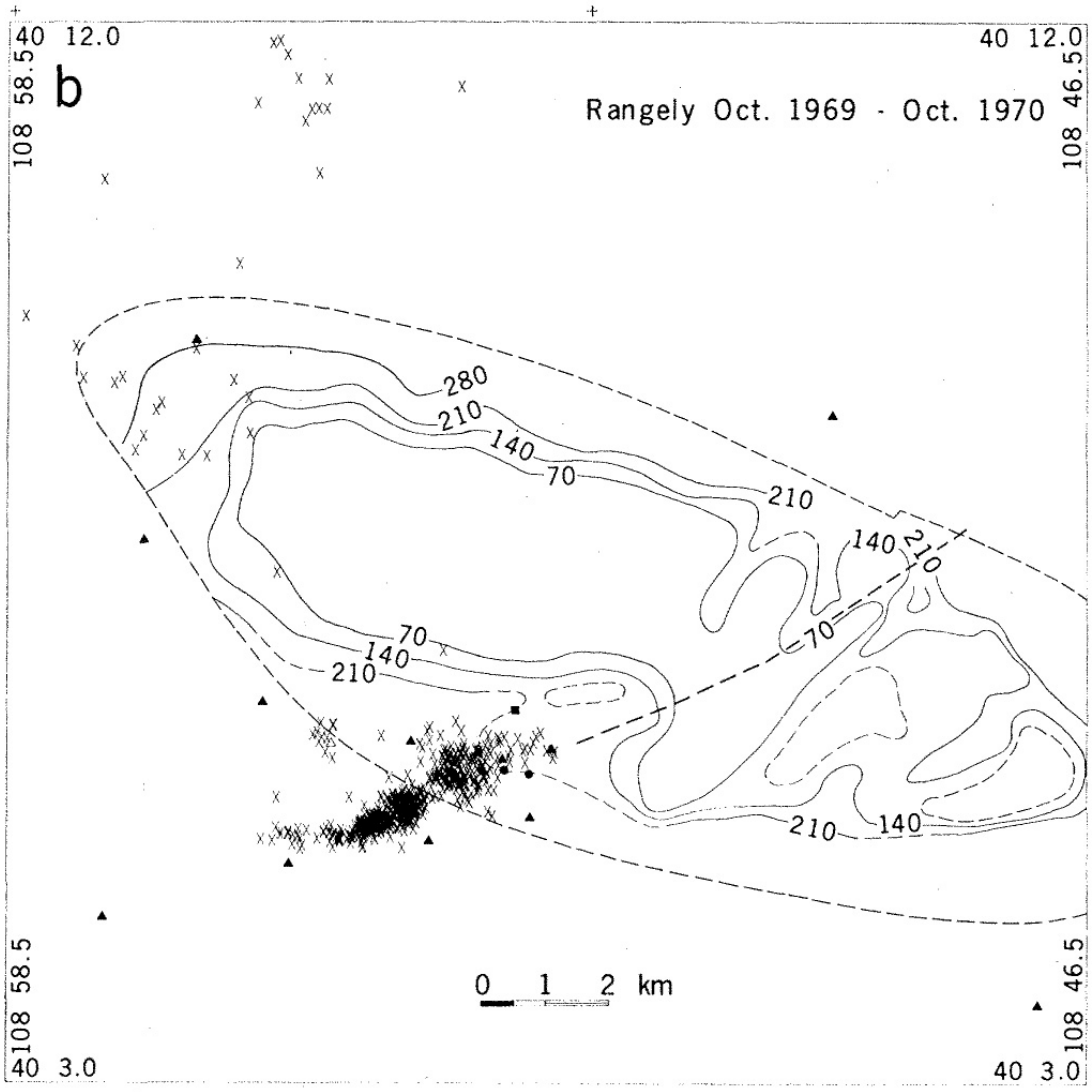

Figure 74: Earthquakes located at Rangely October 1969 - November 1970. The contours are bottom-hole, 3-day shut-in pressures as of September 1969. The interval is 7 MPa. Triangles: seismic stations; stars: experimental wells; heavy, dashed line: the fault mapped in the subsurface [from Raleigh *et al.*, 1976].

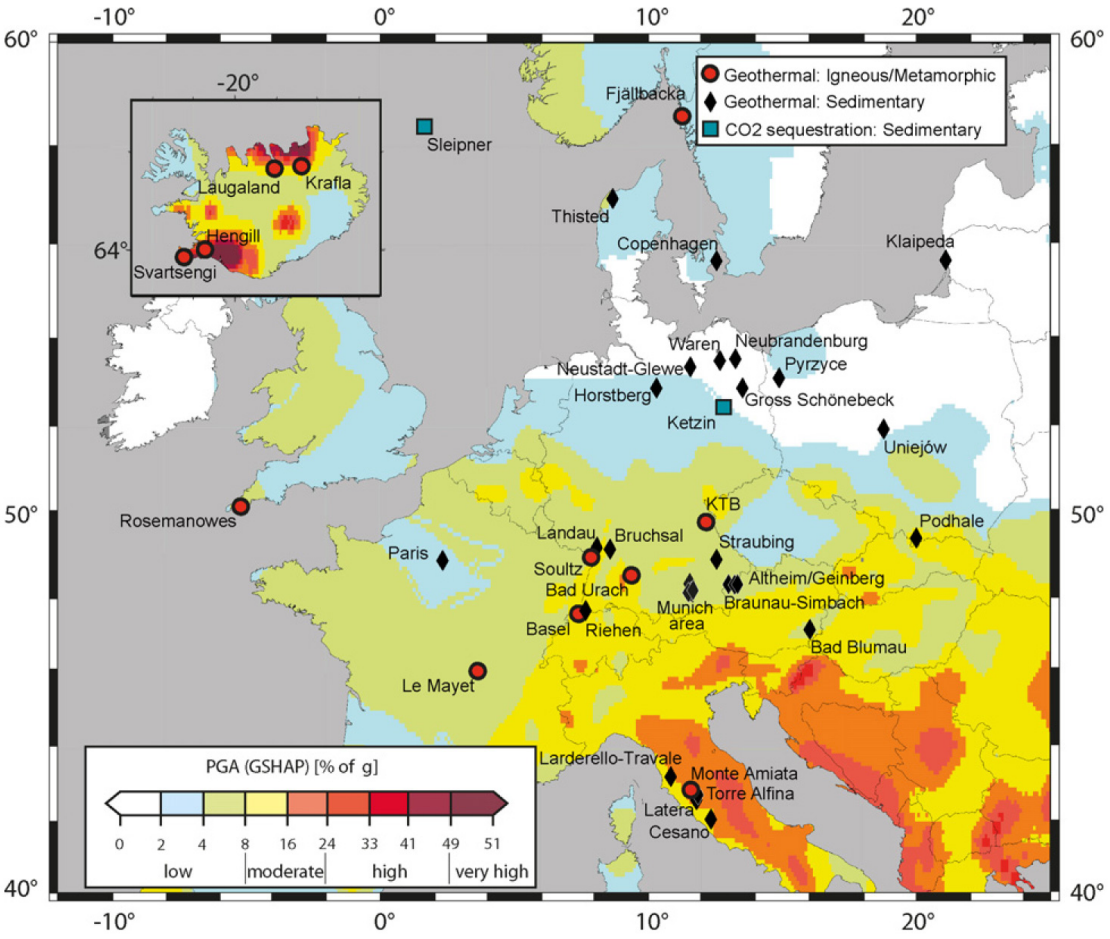

Figure 75: Location of geothermal and CO_2 injection sites in Europe, superimposed on a seismic hazard map from the Global Seismic Hazard Assessment Program (GSHAP[23]). Color scale denotes GSHAP index of local seismic hazard from natural earthquakes defined as peak ground acceleration in percent of the acceleration due to gravity (*g*) on stiff soil that has a 10% probability of being exceeded in 50 years [equivalent to a recurrence period of 475 years; from Evans *et al.*, 2012].

[23] http://www.seismo.ethz.ch/static/GSHAP

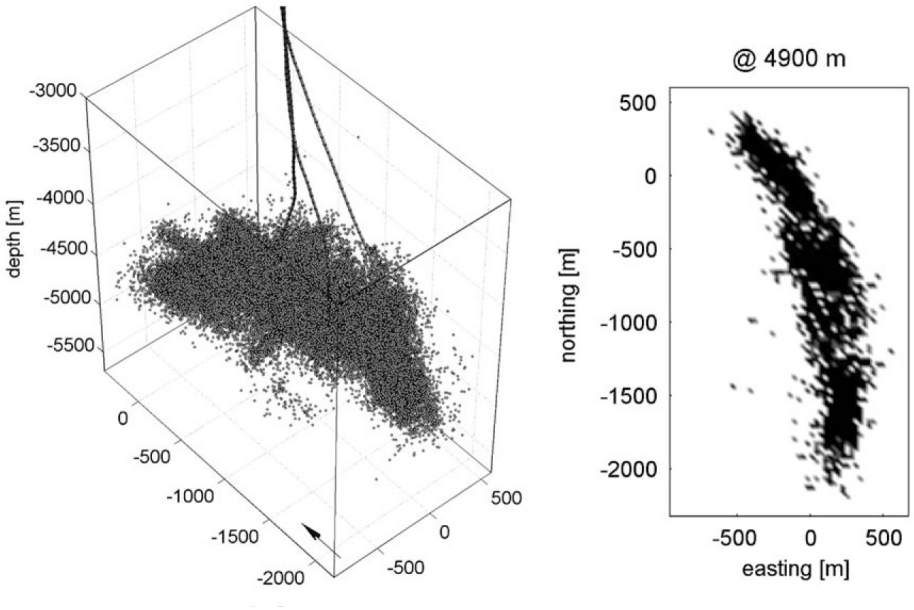

Figure 76: Top left: Distribution of earthquake hypocenters at the Soultz-sous-Forêts EGS project in perspective view. Solid lines: wells GPK2, GPK3 and GPK4. Top right: Depth slice of the hypocenter density distribution at 4900 m depth. Dark shading: regions of high density [from Baisch *et al.*, 2010].

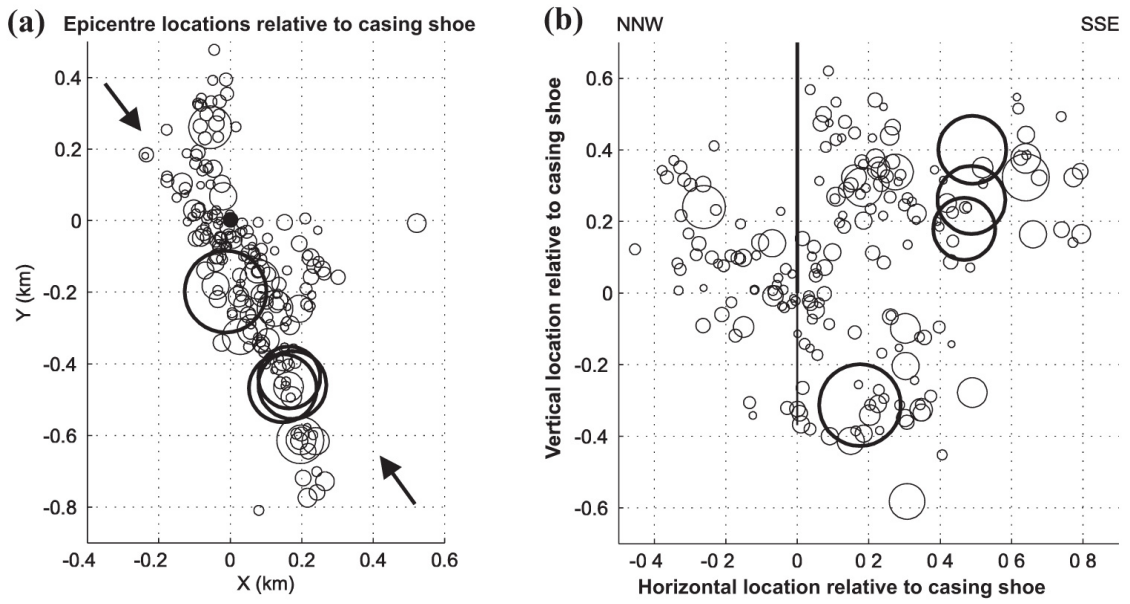

Figure 77: (a) Epicenters, and (b) cross-section showing 195 earthquakes with M 0.7–3.4, that occurred December 2, 2006 - November 30, 2007 following EGS stimulation at Basel [after Deichmann & Giardini, 2009]. The borehole is indicated by a black dot/vertical line. The size of each circle is proportional to the seismic moment of the event. The four events with $M_L > 3.0$ are shown as bold circles. The M_L 3.4 event that occurred just after shut-in on December 8 is close to the bottom of the well. The other three $M_L > 3$ events occurred 1–2 months after the well had been vented and wellhead pressures had returned to near-hydrostatic levels. The arrows in (a) indicate the mean orientation of the maximum horizontal compressive stress in the granite basement [from Evans *et al.*, 2012].

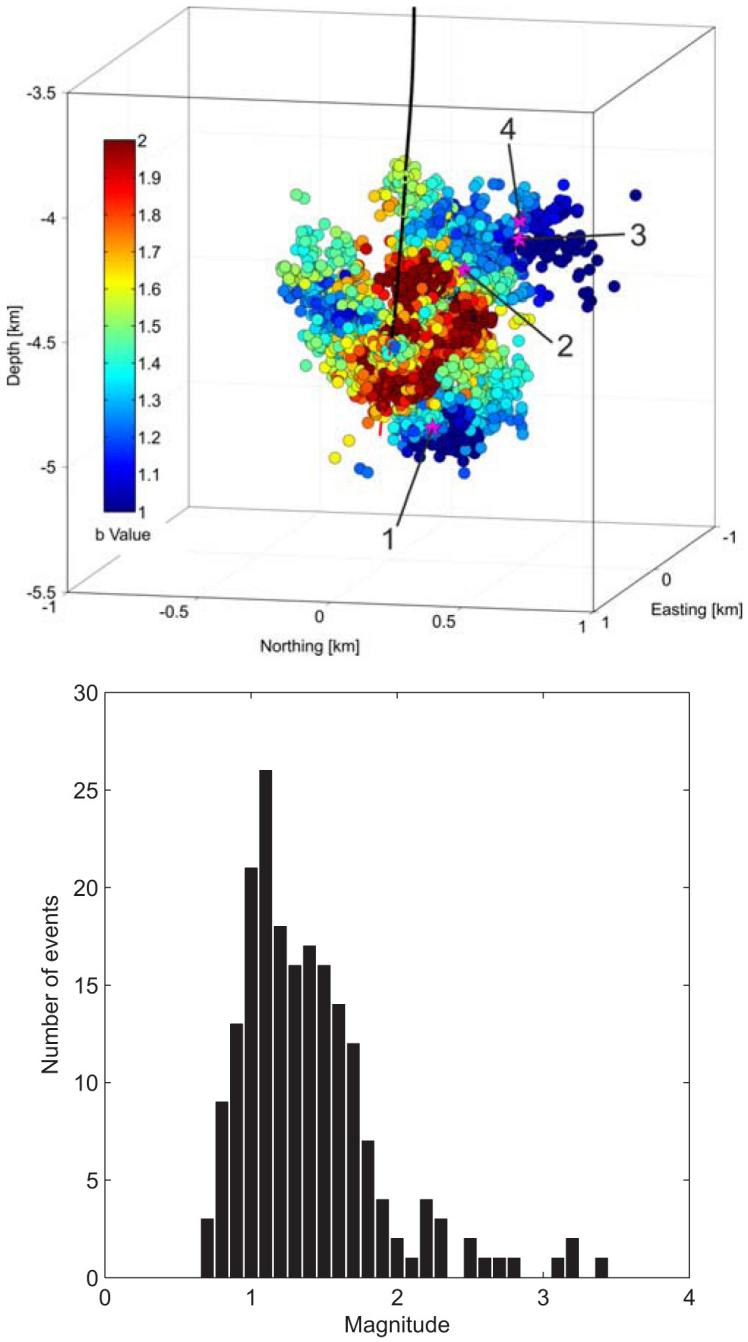

Figure 78: Top: Earthquakes induced by hydraulic stimulation of the Basel, Switzerland, EGS injection well in 2006 and 2007. Hypocenters are color coded according to *b*-values calculated for the volume in which they occurred. Stars: large earthquakes [from Zang *et al.*, 2014b]. Bottom: Magnitude histogram of the induced seismicity recorded by the Swiss Seismological Service 3 December, 2006 - 30 November, 2007 [from Deichmann & Ernst, 2009].

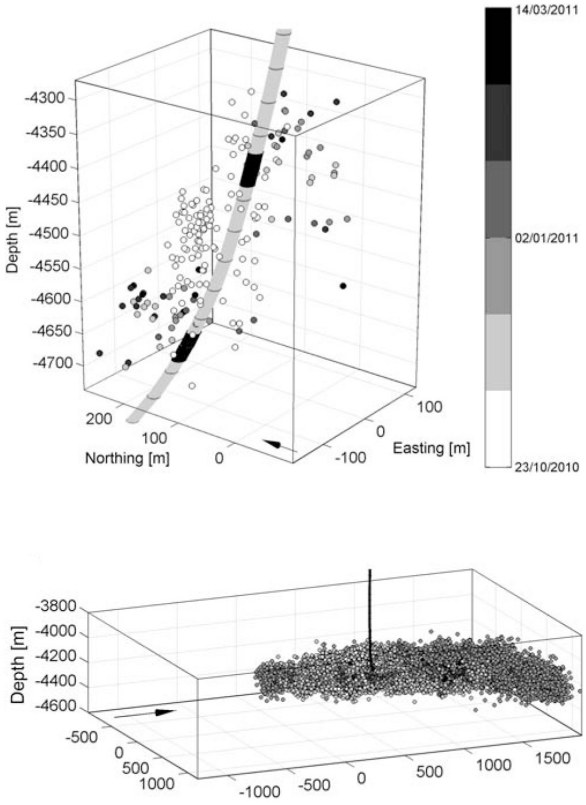

Figure 79: EGS-induced earthquakes at Cooper Basin, Australia. Top: the Jolokia Field– hypocenters of earthquakes induced by hydraulic stimulation of well 1 in in 2010. Known fracture intersections with the wellbore are shown in black. Bottom: the Habanero field– hypocetnres of earthquakes induced by stimulation of well 4 (vertical line) in 2012 [from Baisch *et al.*, 2015].

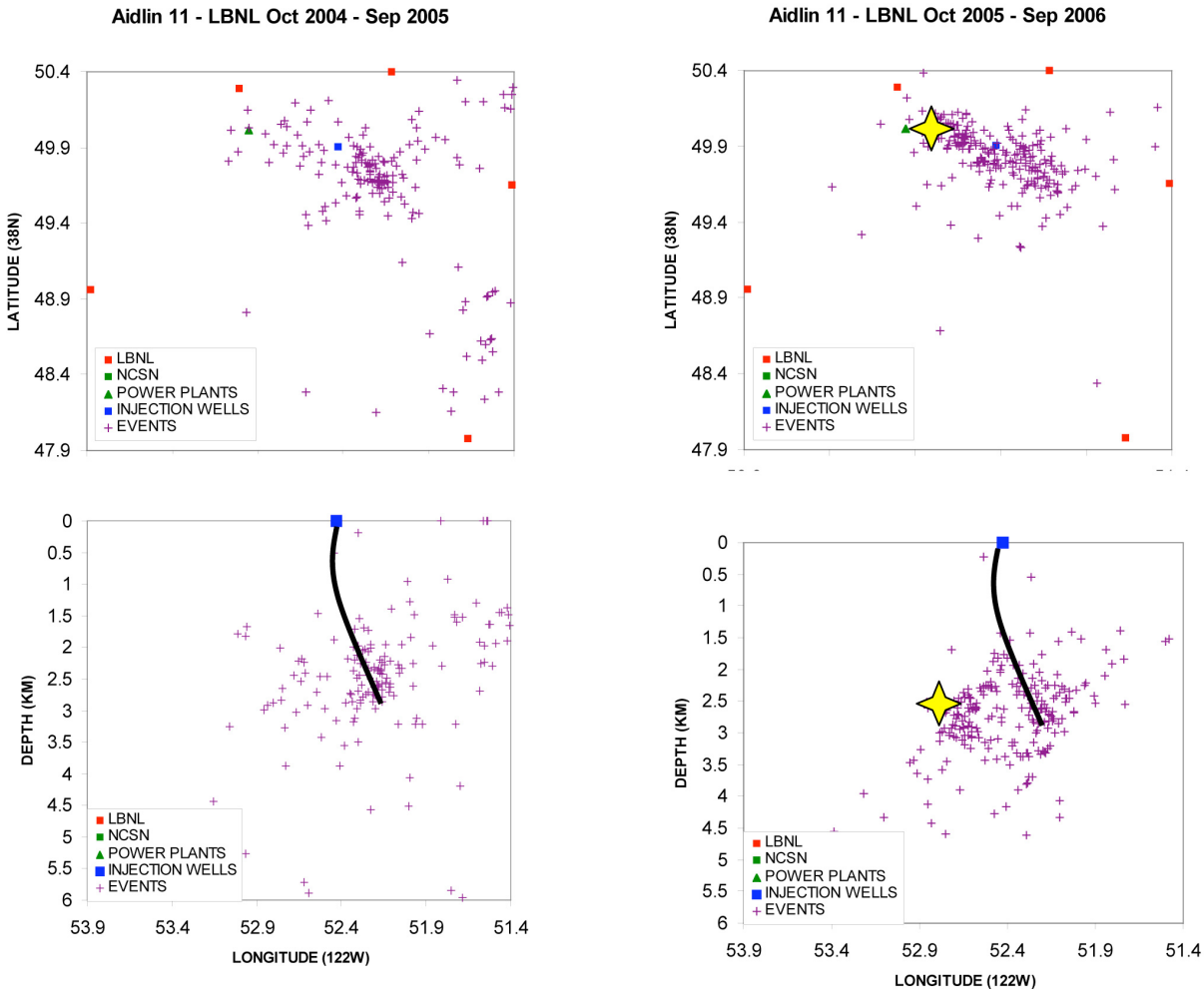

Figure 80: Earthquakes surmised to be injection-related at the northwest Geysers geothermal area. Maps and east-west cross sections show earthquakes in the Aidlin area. Blue square and black line: Injection well; yellow star: a M 4 event that occurred October 2005 [from Majer & Peterson, 2007].

Figure 81: States of the USA where shale-gas hydrofracturing is currently ongoing.

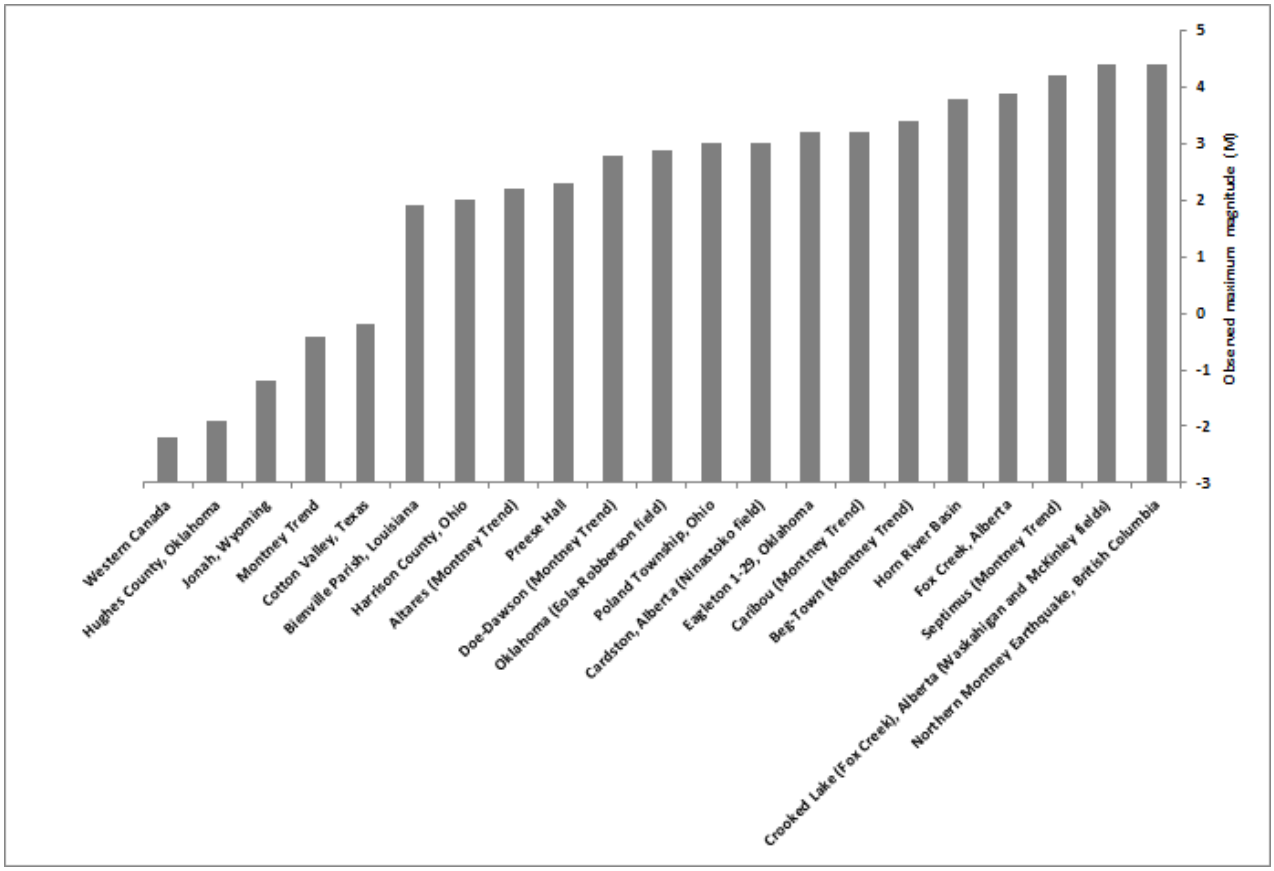

Figure 82: Histogram showing M_{MAX} for the 21 cases of shale-gas hydrofracturing-induced earthquakes in the database.

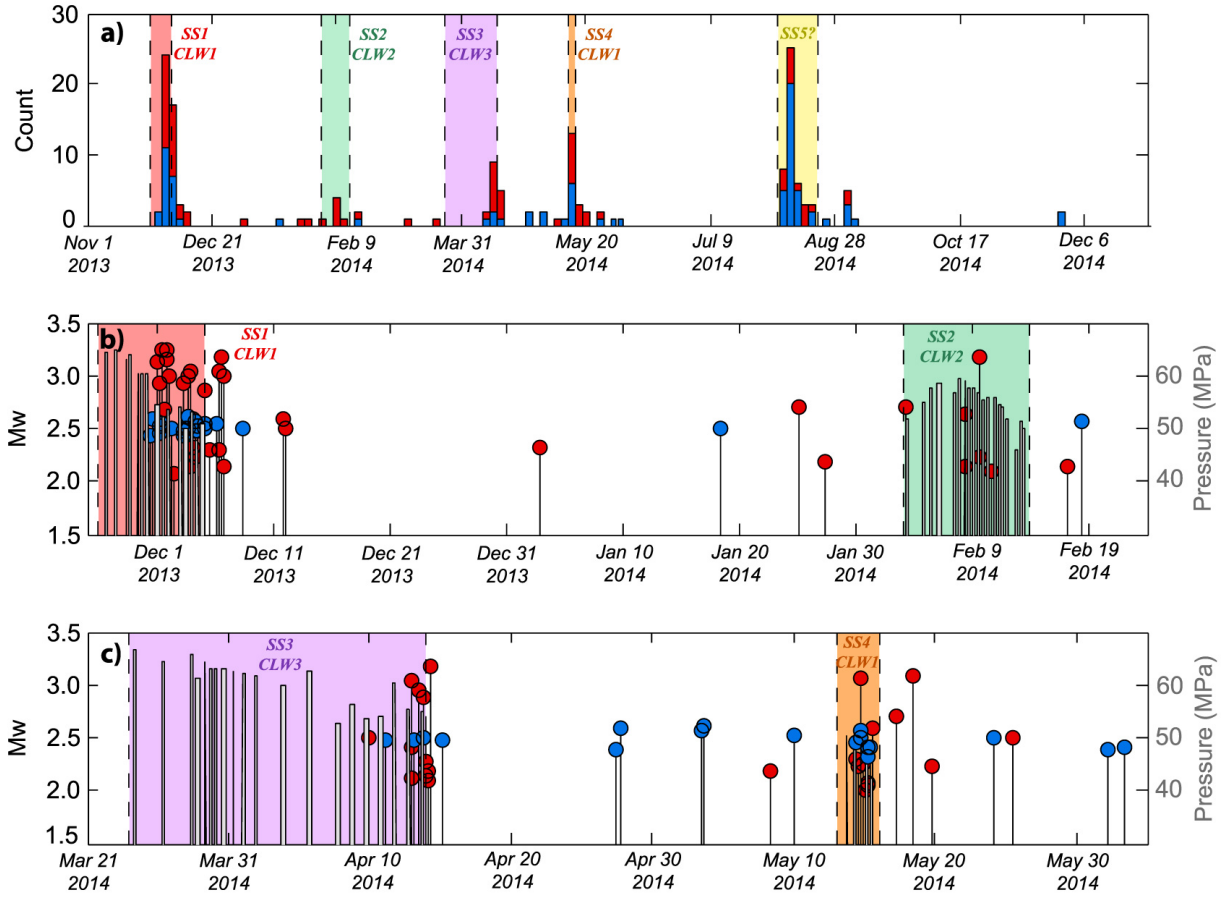

Figure 83: Comparison of earthquakes and hydraulic fracturing completions at Crooked Lake, Alberta, Canada. (a) Histogram of located seismicity (red bars), with number of earthquakes increased using waveform cross correlation (blue bars). Hydrofracture schedules are bounded by colored boxes and labeled with respective sub-sequence and borehole. (b) Magnitudes of located (red circles), detected (blue circles) earthquakes and average injection pressure during hydrofracture stages (gray bars). (c) Same as (b) for later borehole completions [from Schultz *et al.*, 2015].

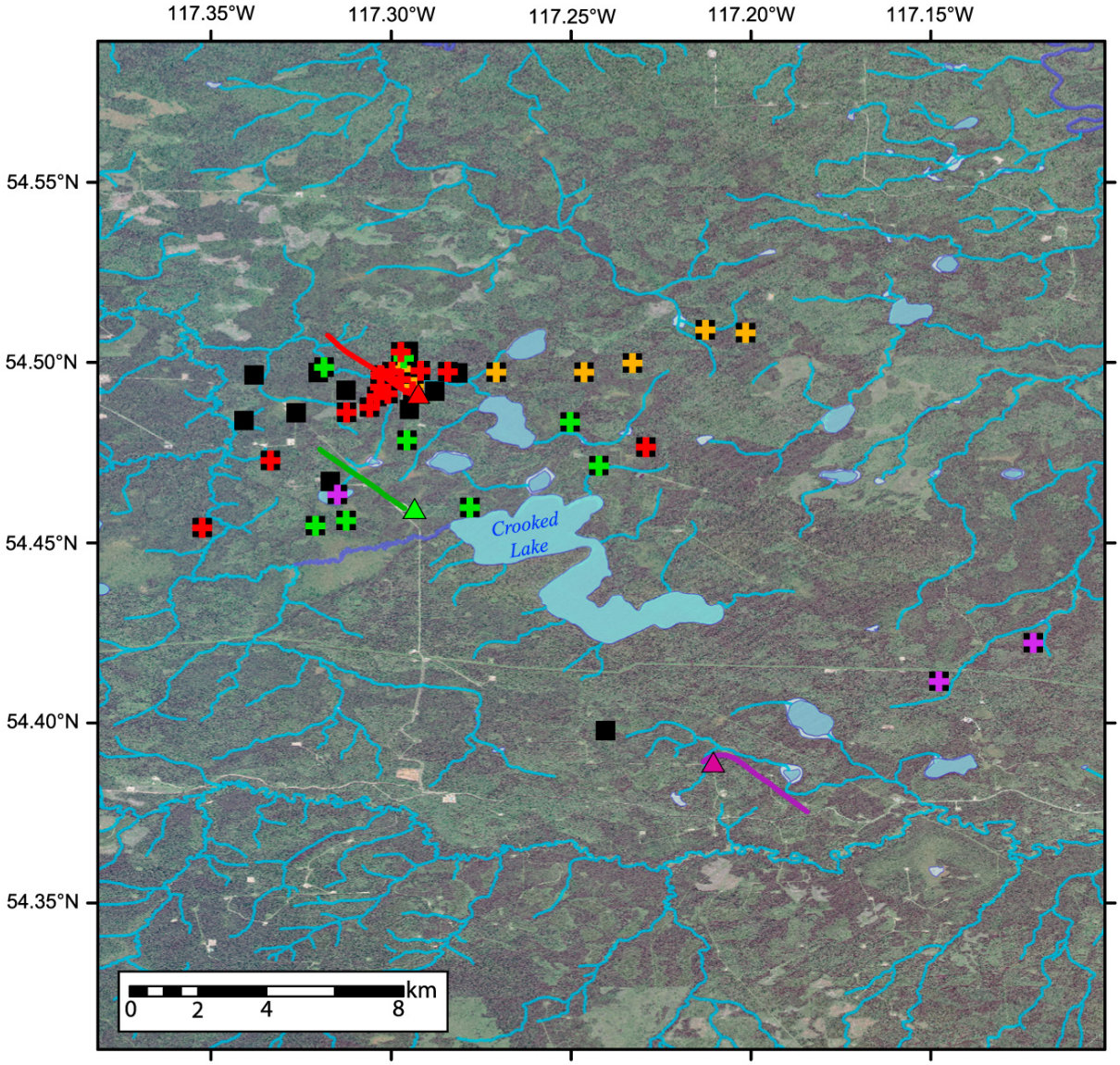

Figure 84: Epicenters (black squares) of earthquakes near Crooked Lake, Alberta, Canada, thought to be induced by hydrofracturing. Epicenters are binned according to timing of well stimulations SS1 (red crosses), SS2 (green crosses), SS3 (purple crosses), and SS4 (orange crosses). Events without crosses occurred during shut-in periods. Triangles: surface locations of wells; lines: horizontal well trajectories. Wells are color-coded with their associated seismic sequences [from Schultz *et al.*, 2015].

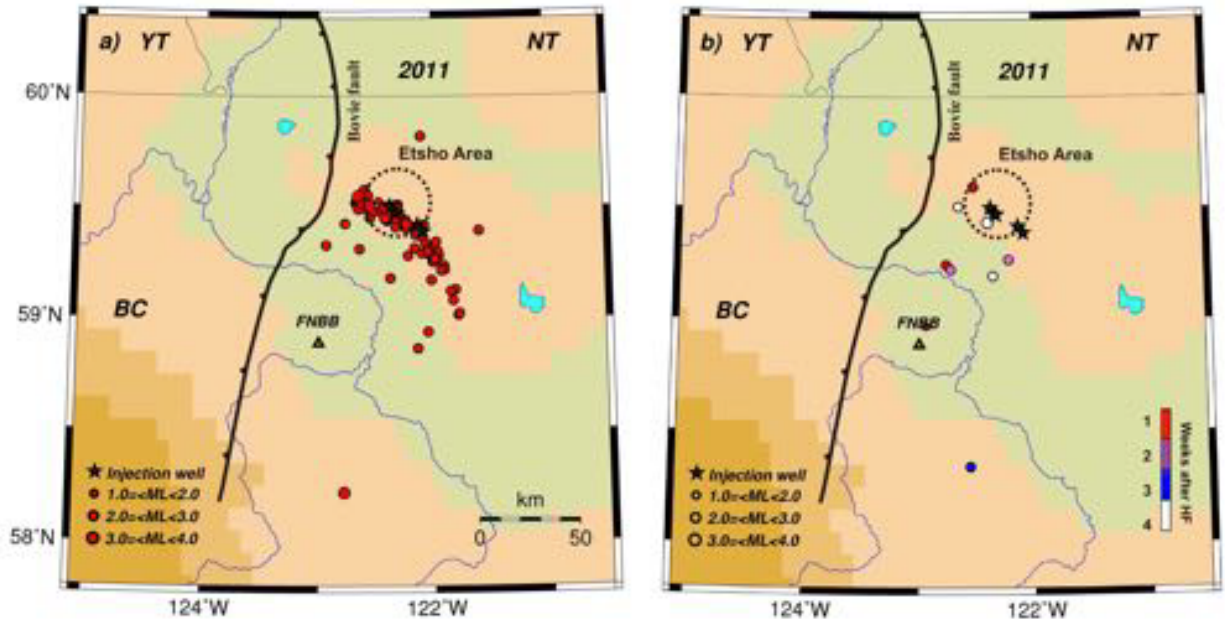

Figure 85: Map of the Horn River Basin, British Columbia, Canada. Left: seismicity on days when hydrofracturing took place. Right: days when it did not occur [from Farahbod *et al.*, 2015].

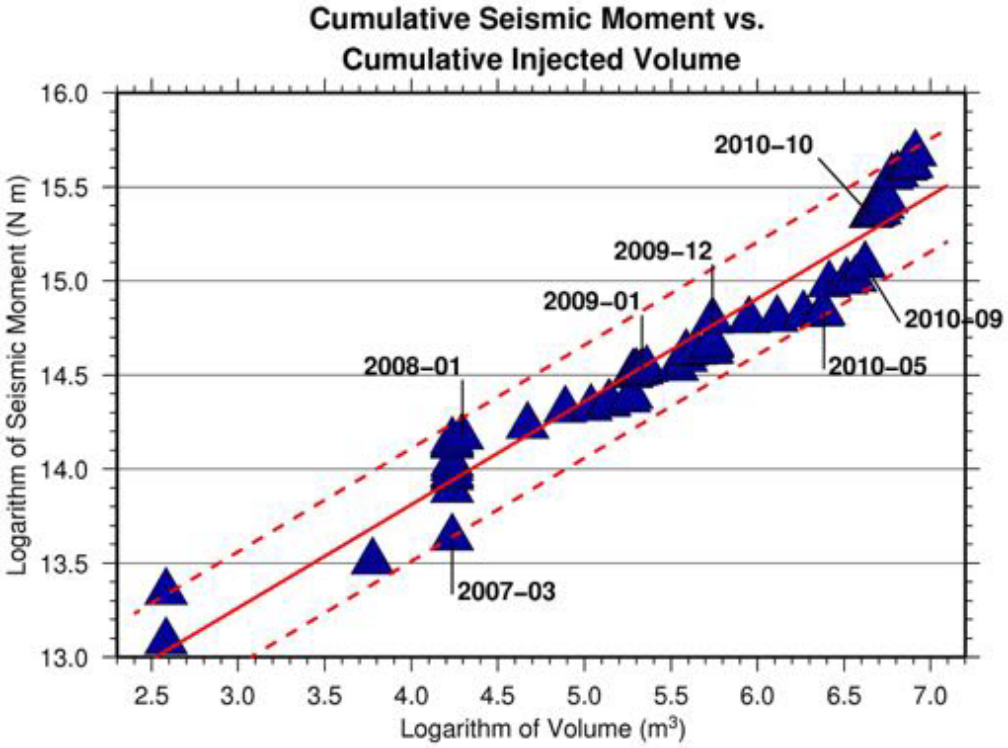

Figure 86: Logarithm of seismic moment vs. logarithm of volume injected in shale gas hydrofracturing operations in the Etsho area, Horn River Basin, British Columbia, Canada [from Farahbod *et al.*, 2015].

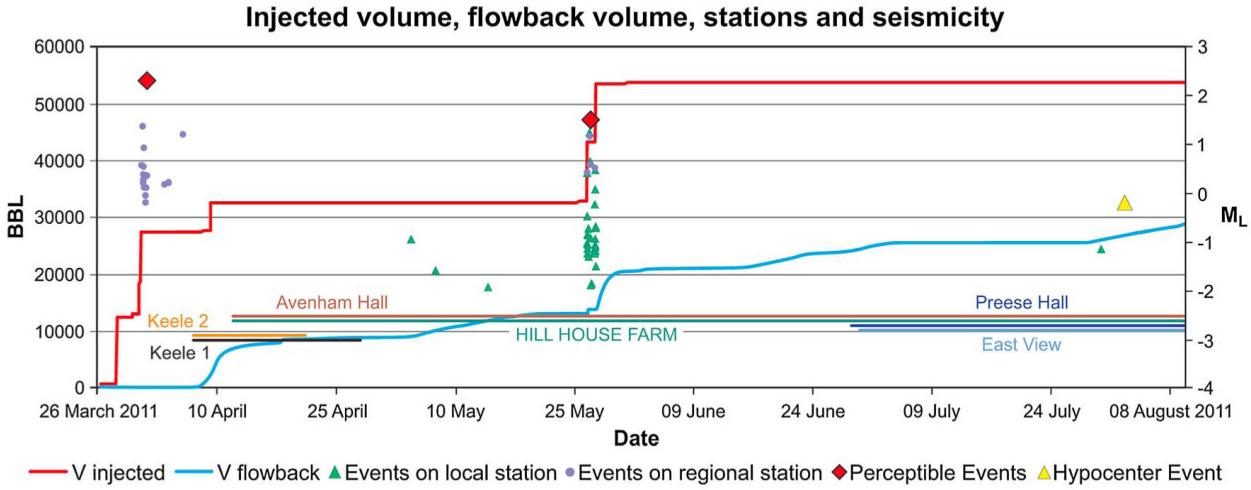

Figure 87: Injection activity and seismicity associated with shale-gas hydrofracturing at Preese Hall, Lancashire, UK. Red line: injected volume; blue line: flow-back volume from the well-head in US barrels (0.159 m^3); violet dots: earthquakes detected on seismic stations at distances of > 80 km; green triangles: earthquakes detected on two local stations; yellow triangle: event for which source mechanism and reliable hypocenter were obtained [from Clarke *et al.*, 2014b].

Figure 88: Site of the former Cacoosing Valley, Pennsylvania, quarry. Red oval: approximate boundary of the old quarry. Satellite image from Google Maps.

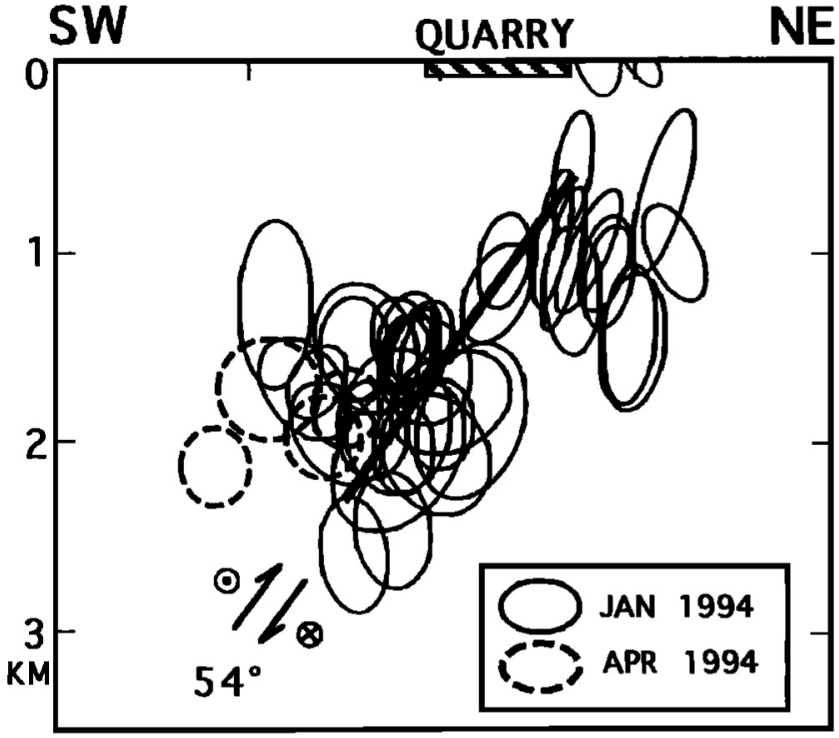

Figure 89: Section perpendicular to the inferred rupture of the 1994 Cacoosing Valley, Pennsylvania, earthquake sequence showing hypocenter confidence ellipses, the plane on which the main rupture is inferred to have occurred from focal mechanisms studies, and the location of the quarry at the surface above the hanging wall block [from Seeber *et al.*, 1998].

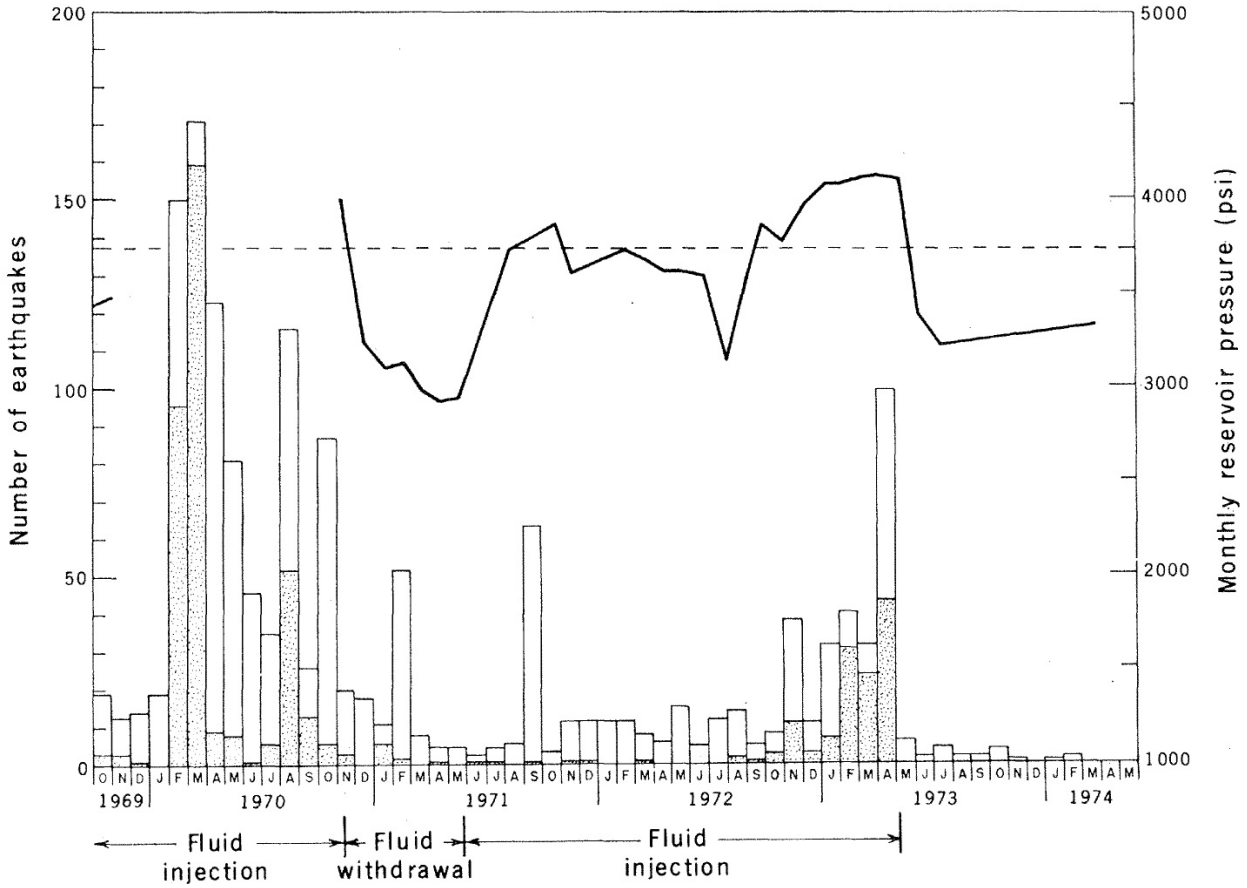

Figure 90: Frequency of earthquakes at the Rangely Oilfield, Colorado, and reservoir pressures during fluid injection and fluid withdrawal. Stippled bars: earthquakes within 1 km of injection wells; black line: pressure history in injection well Fee 69; dashed line: predicted critical reservoir pressure [from Raleigh *et al.*, 1976].

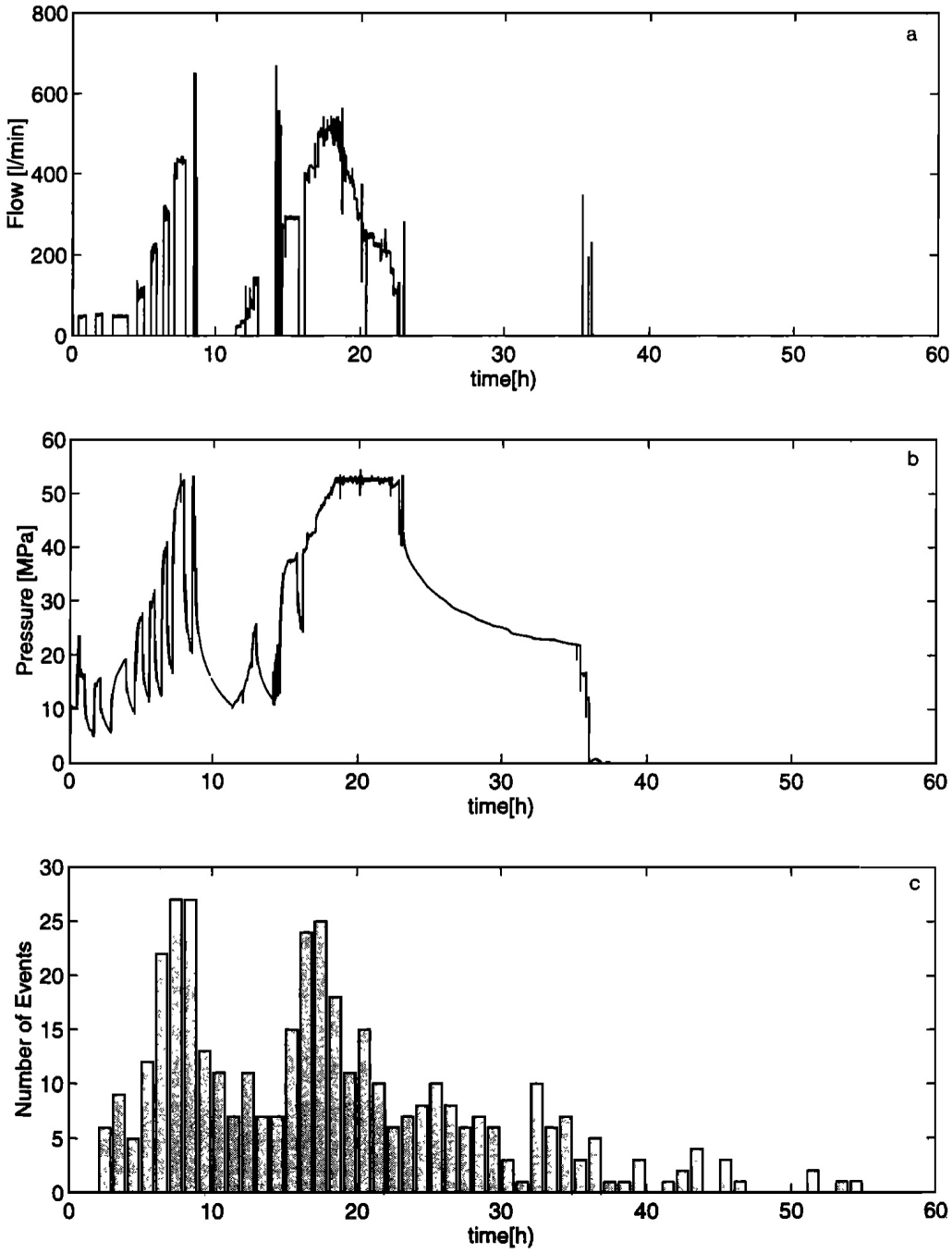

Figure 91: Flow rates, pressure and number of earthquakes induced by brine injection into the Kontinentales Tiefbohrprogramm der Bundesrepublik Deutschland (KTB–the German Continental Deep Drilling Program) borehole during a 60-hour period [from Zoback & Harjes, 1997].

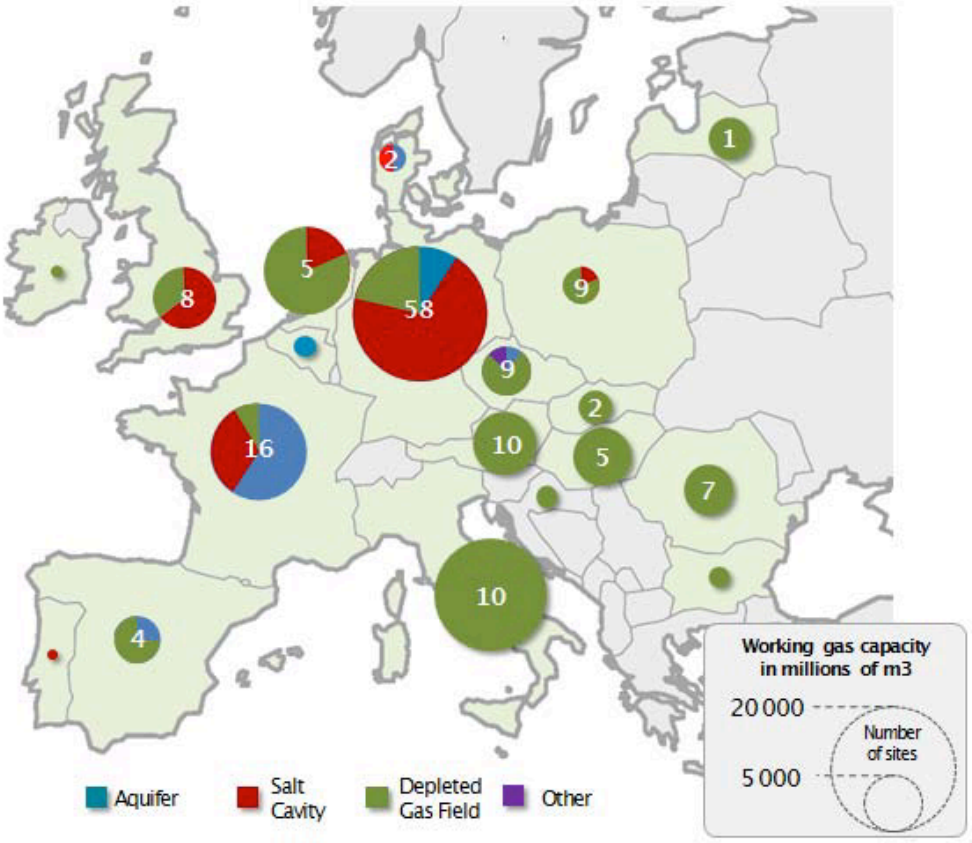

Figure 92: Working gas capacities of underground storage sites in Europe[24].

[24] http://www.gasinfocus.com/en/ ; http://www.gie.eu/index.php/maps-data/gse-storage-map

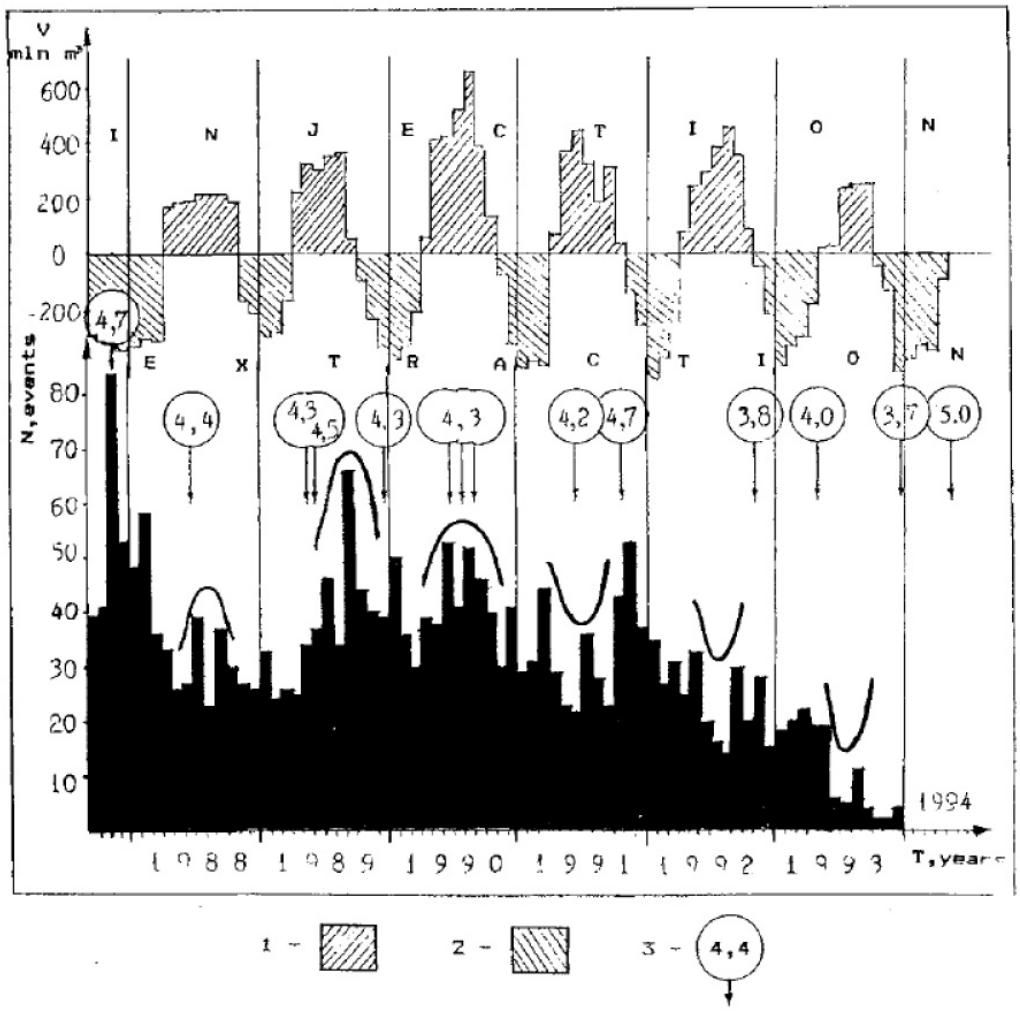

Figure 93: Seismicity in the Gazli region, Uzbekistan, during underground gas storage activities. 1: 6-monthly injection; 2: 6-monthly production. Numbers in circles indicate earthquake magnitudes [from Plotnikova *et al.*, 1996].

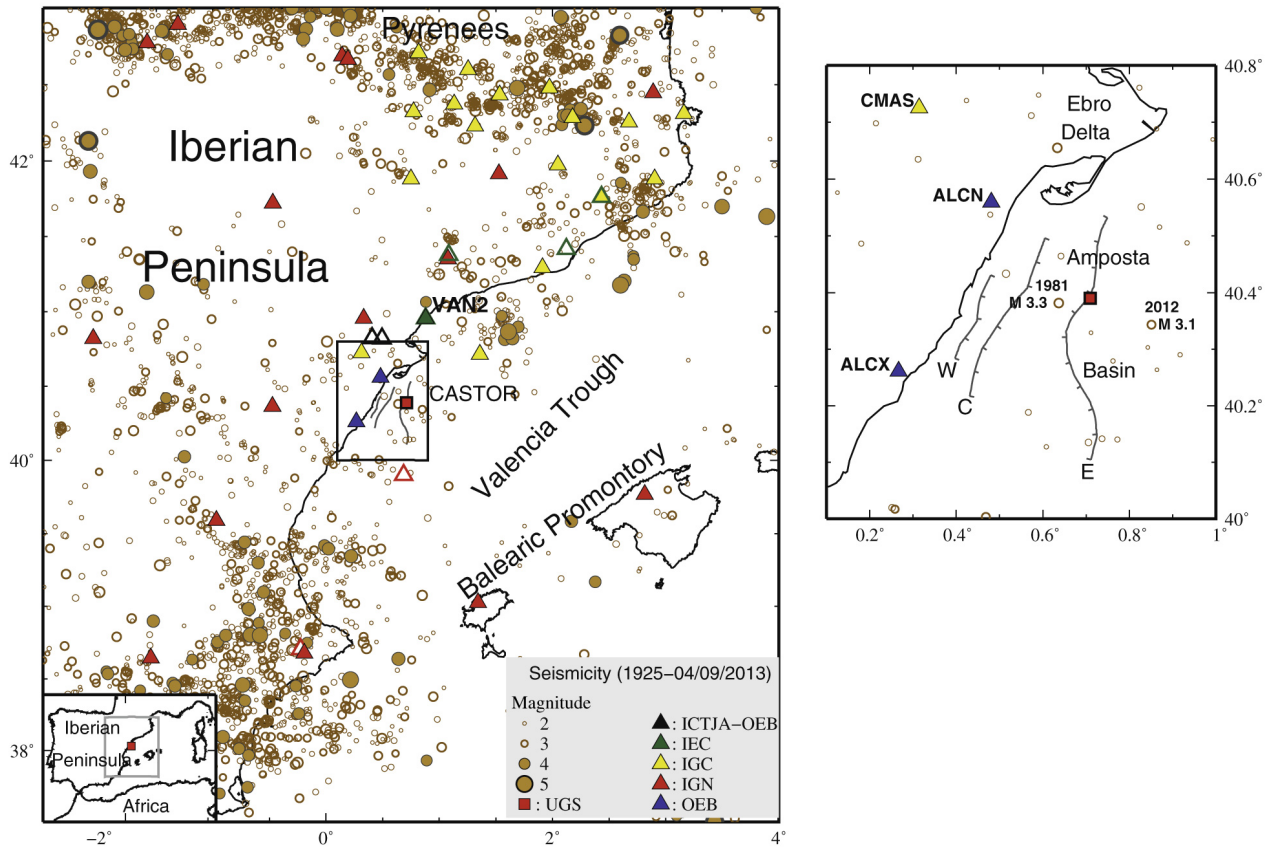

Figure 94: Seismicity of the eastern Iberian Peninsula, Spain. Triangles: seismic stations; red square: location of the Castor underground gas storage reservoir. W, C and E denote the Western, Central and Eastern Amposta faults [from Gaite *et al.*, 2016].

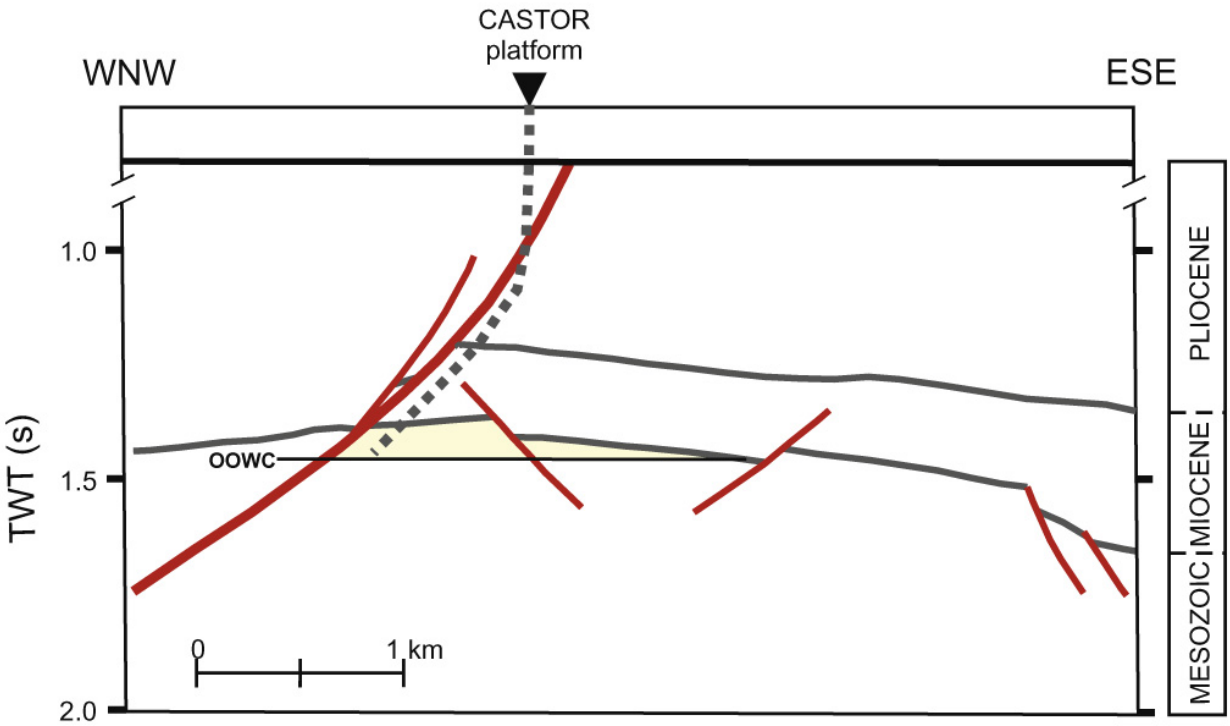

Figure 95: Schematic diagram of the old Amposta Oilfield, Spain, in WNW-ESE section. TWT: two-way traveltime; dashed line: approximate location of the Castor injection well: OOWC: original oil-water contact at 1940 m depth; yellow area: approximate location of the gas reservoir [from Gaite *et al.*, 2016].

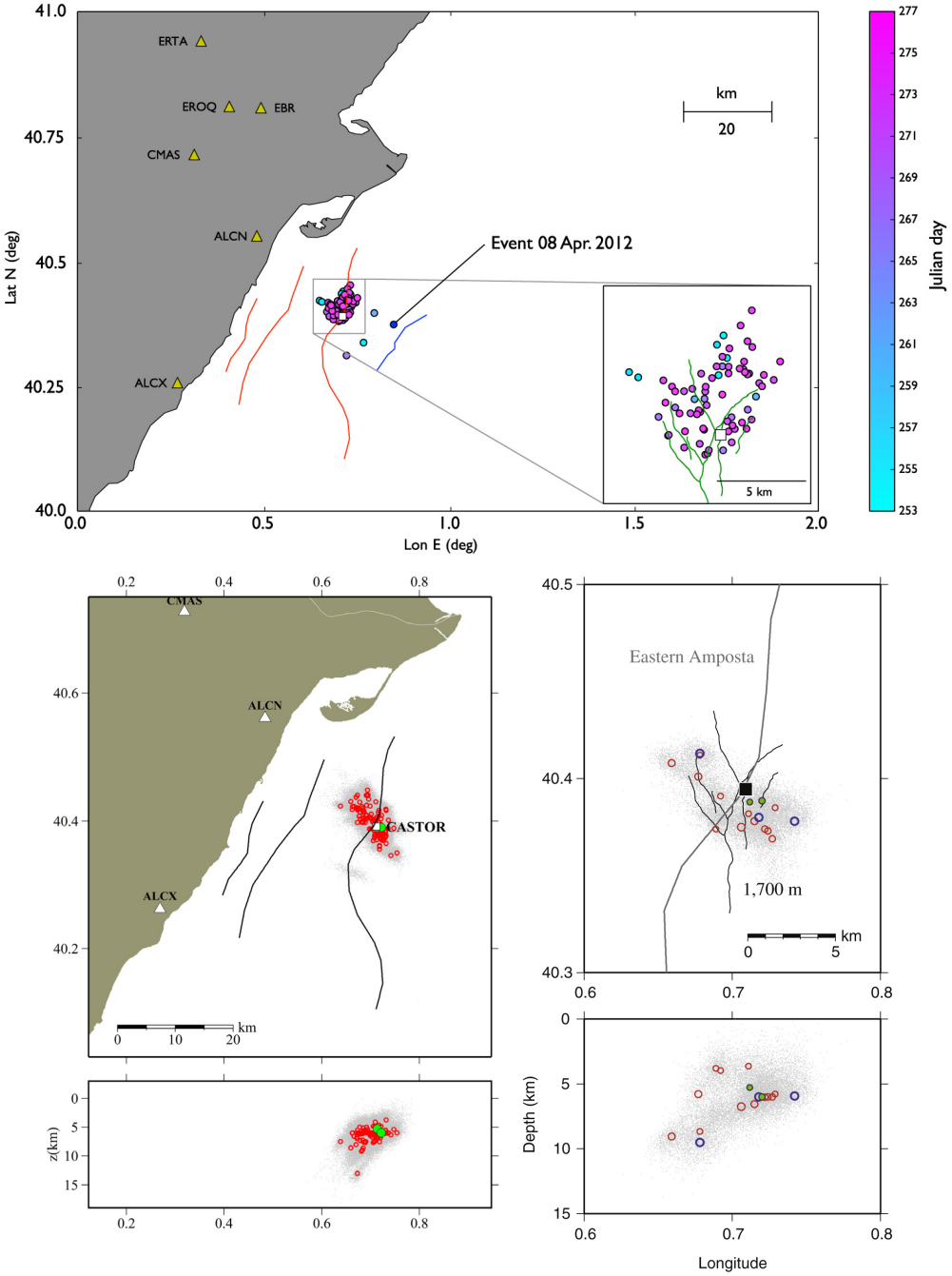

Figure 96: Top: Faults and epicenters for the largest events in the 2013 earthquake sequence in the "old Amposta Field". White square: Castor platform; colored lines: faults near the injection site; red lines: the Amposta faults; blue and green lines: additional faults [from Cesca *et al.*, 2014]. Bottom left: map and cross-section showing 116 earthquakes associated as a multiplet; triangles: seismic stations; white square: injection well; green dots: two events with M 3.0 and 3.2. Bottom right: map and cross-section of earthquakes with M > 3; black square: injection well [from Gaite *et al.*, 2016].

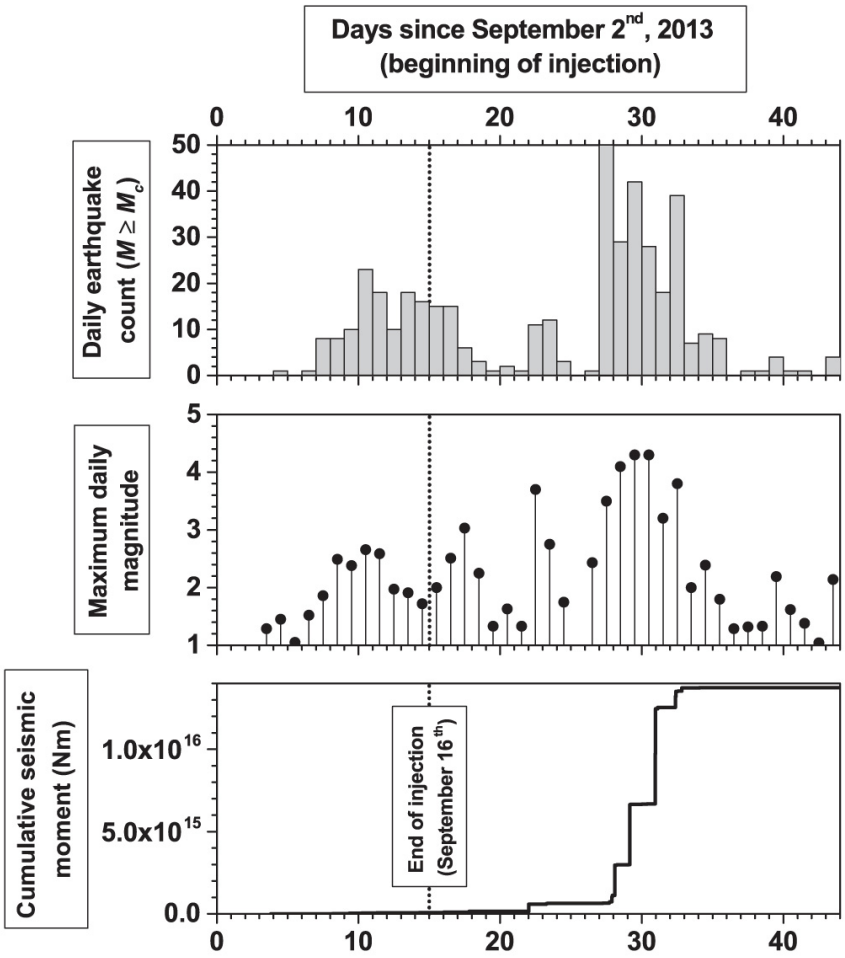

Figure 97: Temporal evolution of seismicity with M > 2 associated with the Castor project, Spain, for 44 days from the beginning of gas injection, 2 September, 2013. Top: daily number of events. Centre: maximum daily magnitude. Bottom: cumulative seismic moment [from Cesca *et al.*, 2014].

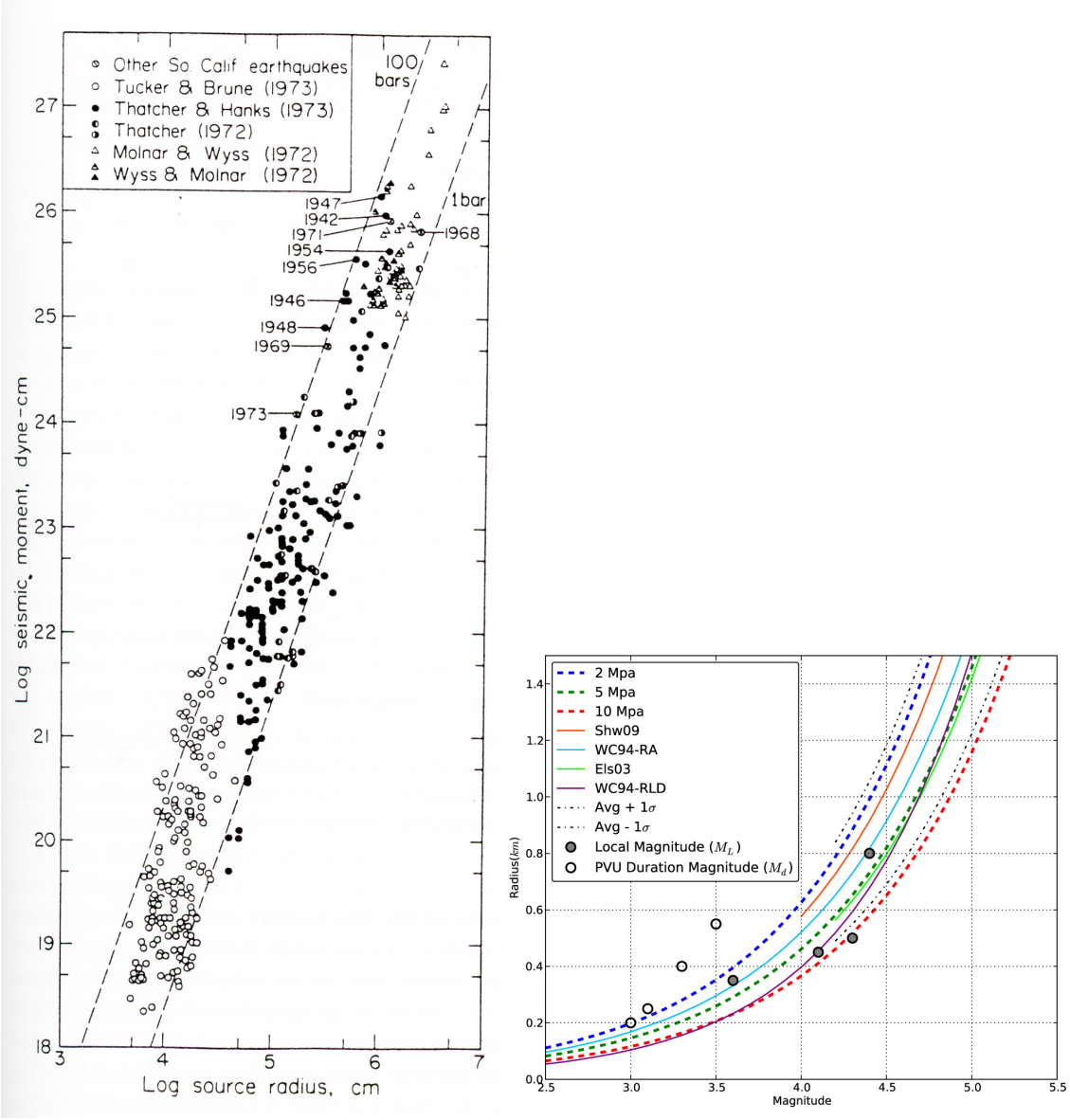

Figure 98: Left: Set of data for small earthquakes showing the relationship between seismic moment and source radius. Dashed lines are of constant stress drop [Hanks, 1977]. Right: Rupture radius vs. duration earthquake magnitude for several models. Black dotted lines: average of these relationships ±1σ; blue, green and red dashed lines: relationships derived from the moment-magnitude relation of Hanks and Kanamori [1979] for stress drops of 2, 5 and 10 MPa respectively, and estimated fault radius using half the rupture-length-at-depth parameter; gray and white circles: values for individual earthquakes induced at Paradox Valley, Colorado [from Yeck *et al.*, 2015].

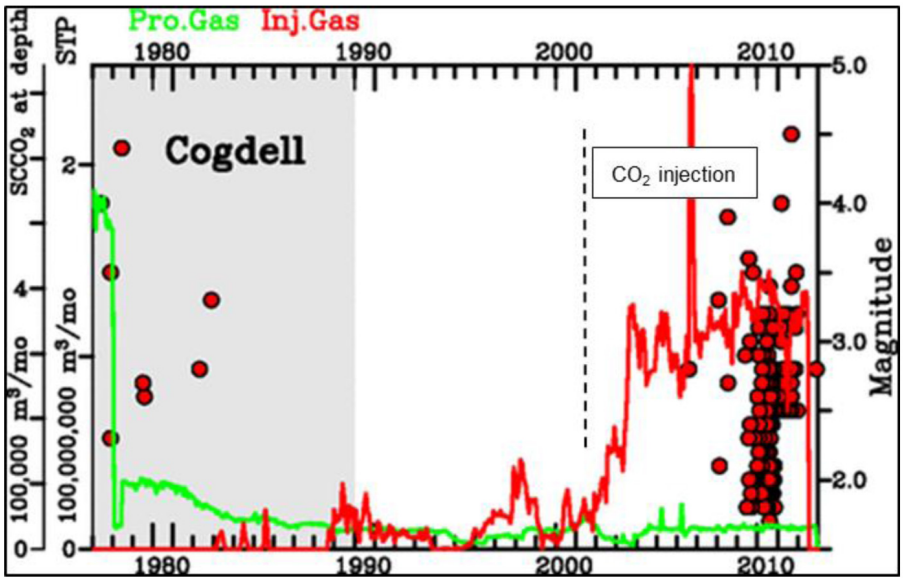

Figure 99: Operations and seismicity at the Cogdell Oilfield, Texas. Green: monthly volumes of natural gas produced; red: gas injected; red dots: earthquakes detected 1977-2012. There was a clear increase in seismic activity from 2006, five years after the start of CO_2 injection [from Gan & Frohlich, 2013].

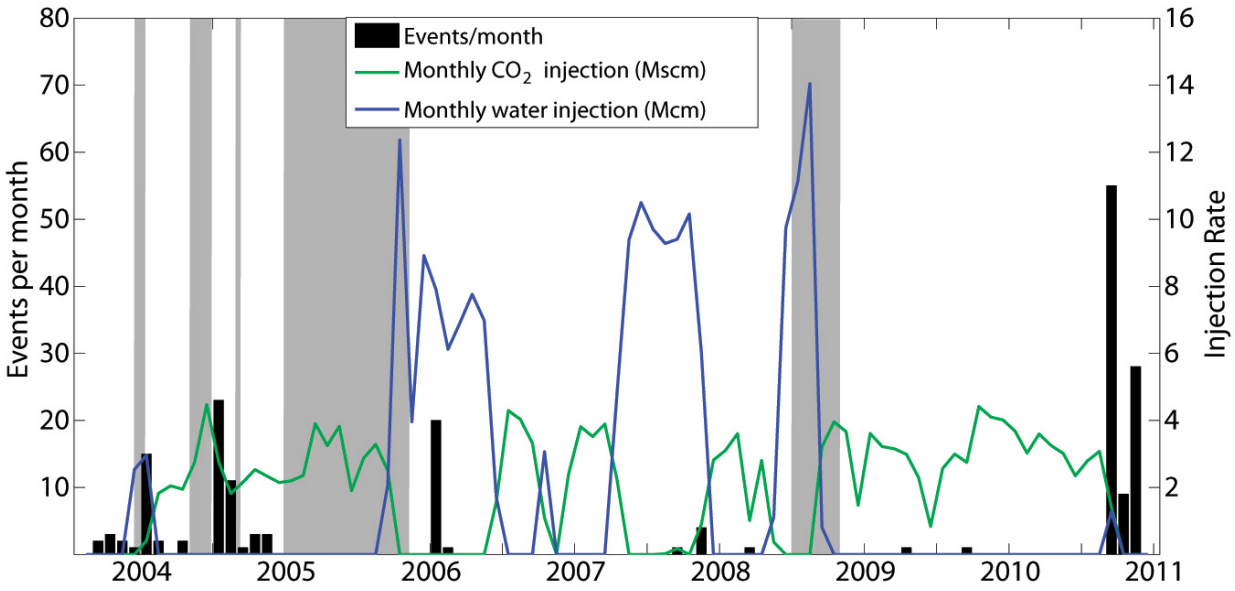

Figure 100: CO_2, water injection, and associated earthquakes at the Weyburn Oilfield, Saskatchewan, Canada. Shaded periods: monitoring array was inoperative [from Verdon *et al.*, 2013].

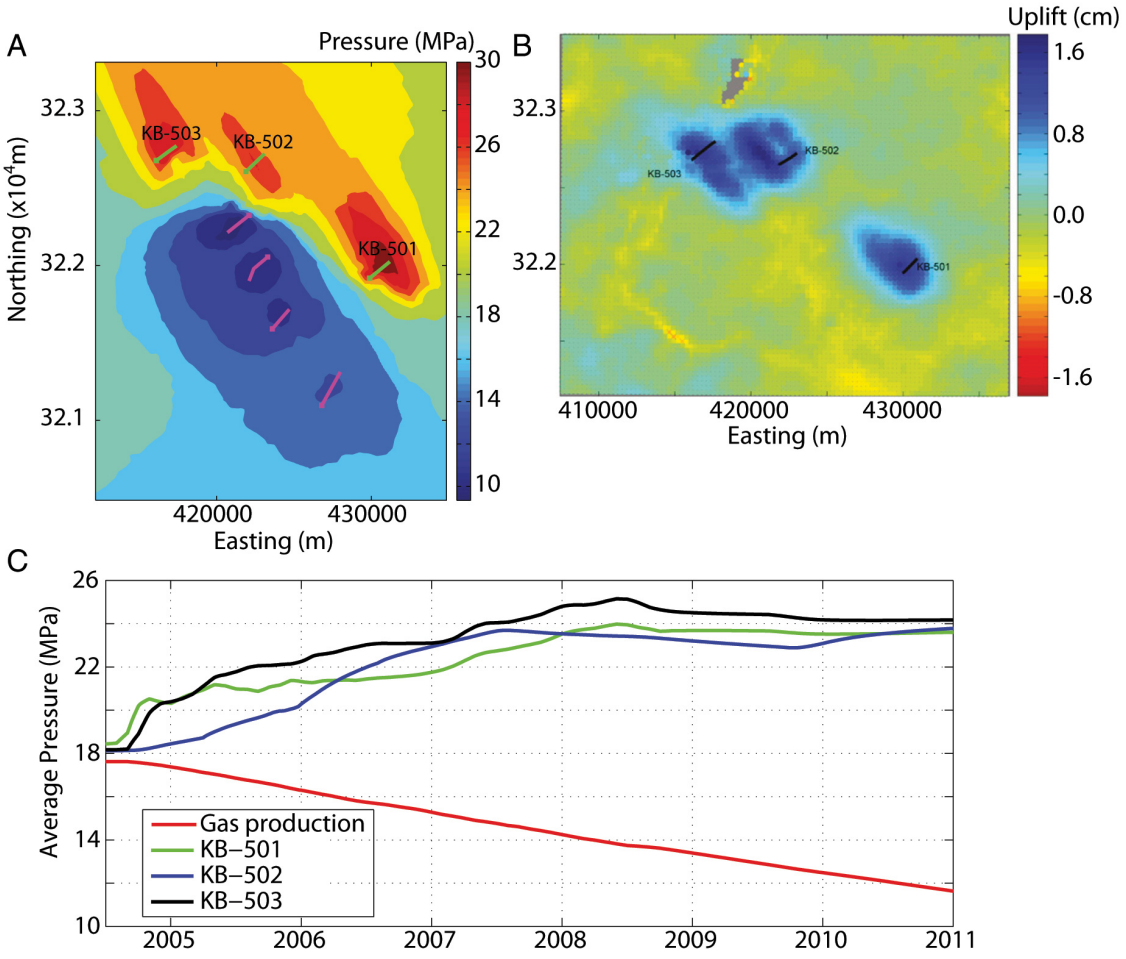

Figure 101: Modelled pore pressure and geomechanical deformation at In Salah, Algeria. A: Map of pore pressure after three years of injection. B: Surface uplift measured by InSAR. C: Modelled pressure at the three injection wells and in the producing part of the reservoir [from Verdon *et al.*, 2013].

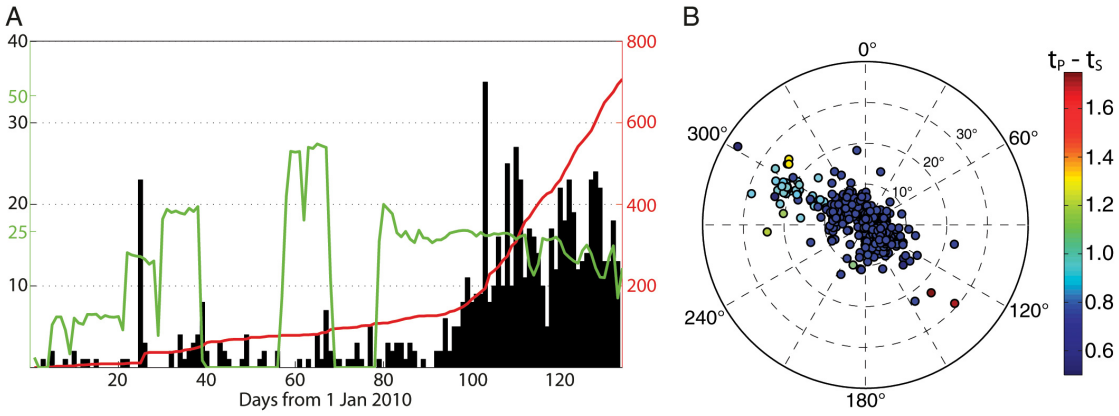

Figure 102: Microseismicity at In Salah, Algeria. A: Black: daily seismicity rate; red: cumulative number of events January-April 2010; green: CO_2 injection rate in millions of standard cubic feet per day[25]. B. Event arrival angles in polar projection, colored by differential *S*- and *P*-wave arrival times [from Verdon *et al.*, 2013].

[25] 1 million standard cubic feet of gas per day at 15˚C = 28,252.14 m^3/day

Figure 103: Aerial photograph of the Nevada test site, USA, looking southeast [26].

[26] https://en.wikipedia.org/wiki/Nevada_Test_Site

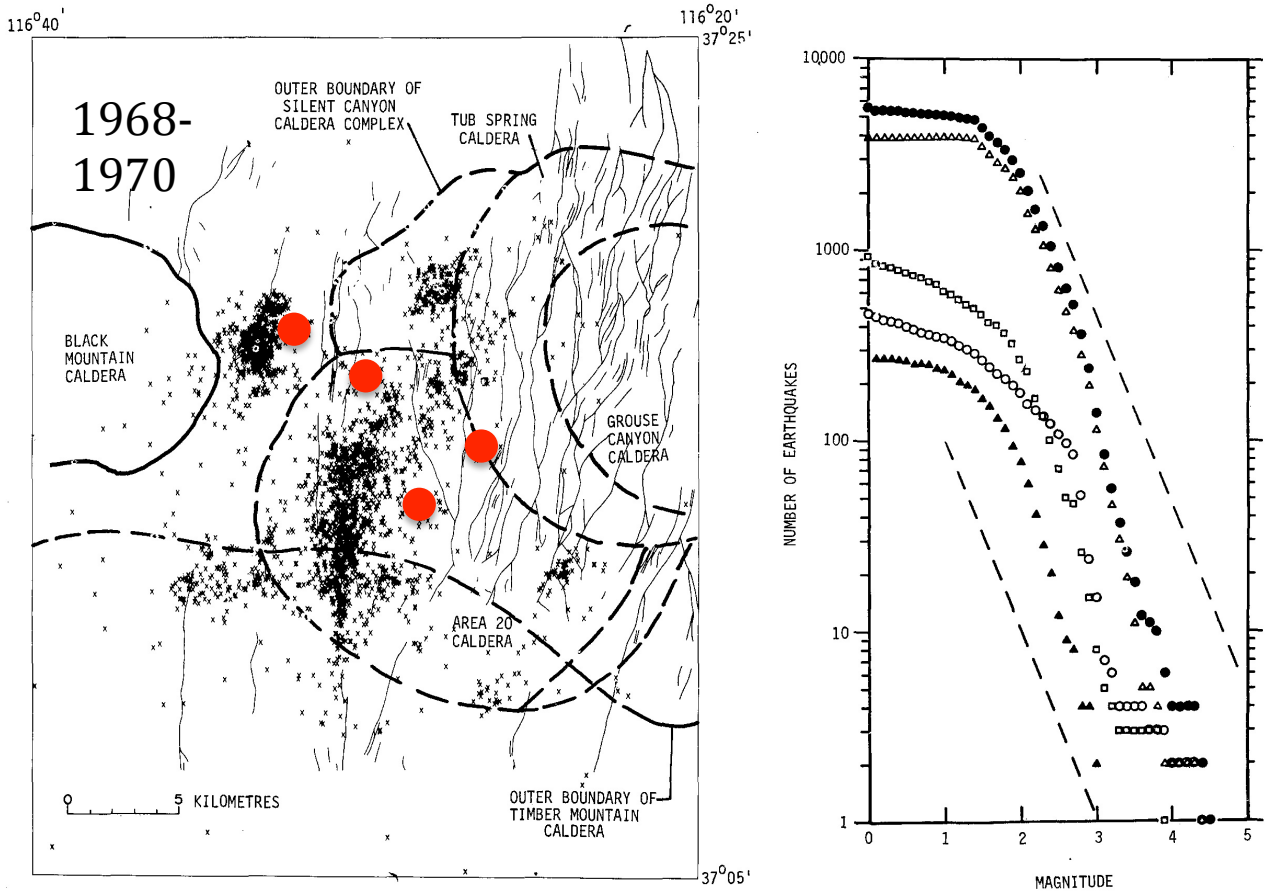

Figure 104: Left: Epicenters of aftershocks of the Benham (1968), Jorum (1969), Purse (1969), and Handley (1970) nuclear explosions at the Nevada Test Site. Heavy lines: caldera boundaries; light lines: basin-range faults; red dots: locations of nuclear explosions. Right: Frequency-magnitude distribution for aftershocks in Pahute Mesa [from Hamilton *et al.*, 1972]. Dots: entire recording period; open triangles: the period Benham to Purse; solid triangles: Purse to Jorum; circles: Jorum to Handley; squares: Handley to the end. Dashed lines have a slope of -1; the data above M 2 define "*b*-slopes" of about -1.4 [from McKeown, 1975].

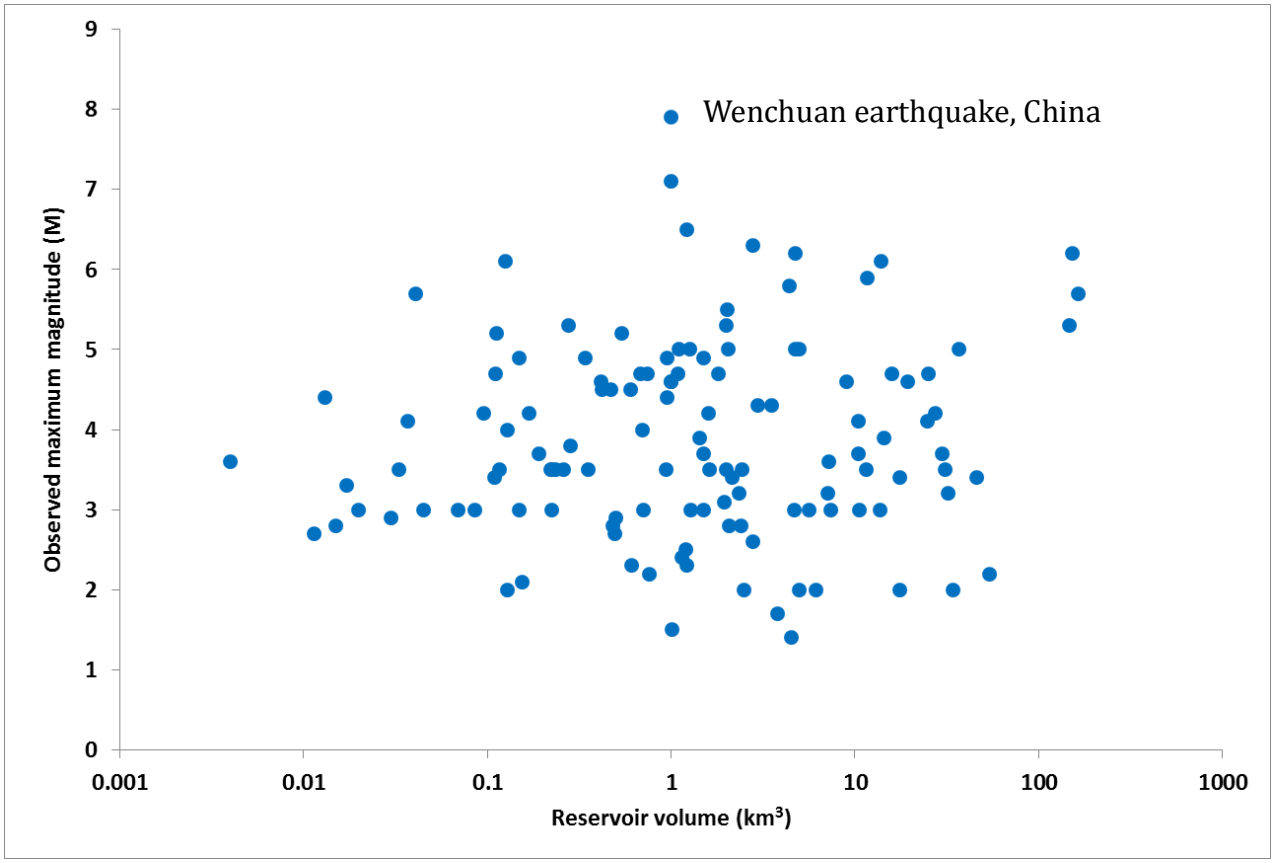

Figure 105: Plot of M_{MAX} vs. water reservoir volume for the 126 cases for which data are available.

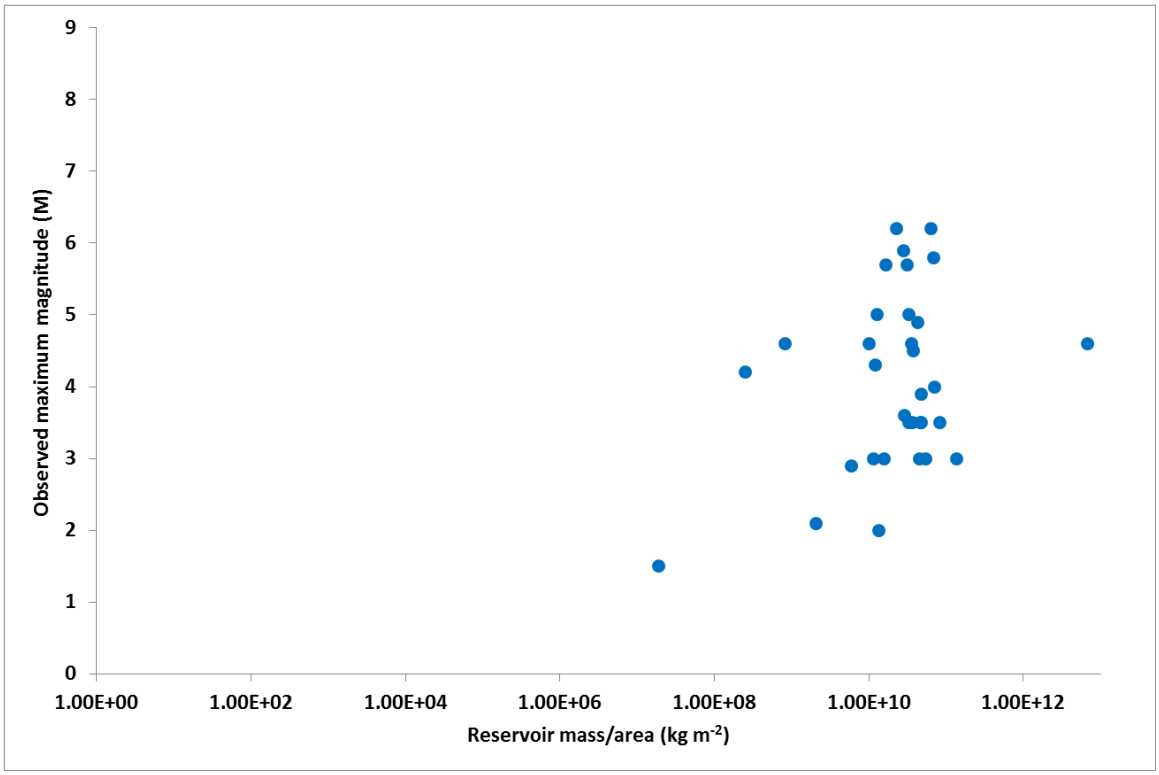

Figure 106: Plot of M_{MAX} vs. water reservoir mass per unit area for the 33 cases for which data are available.

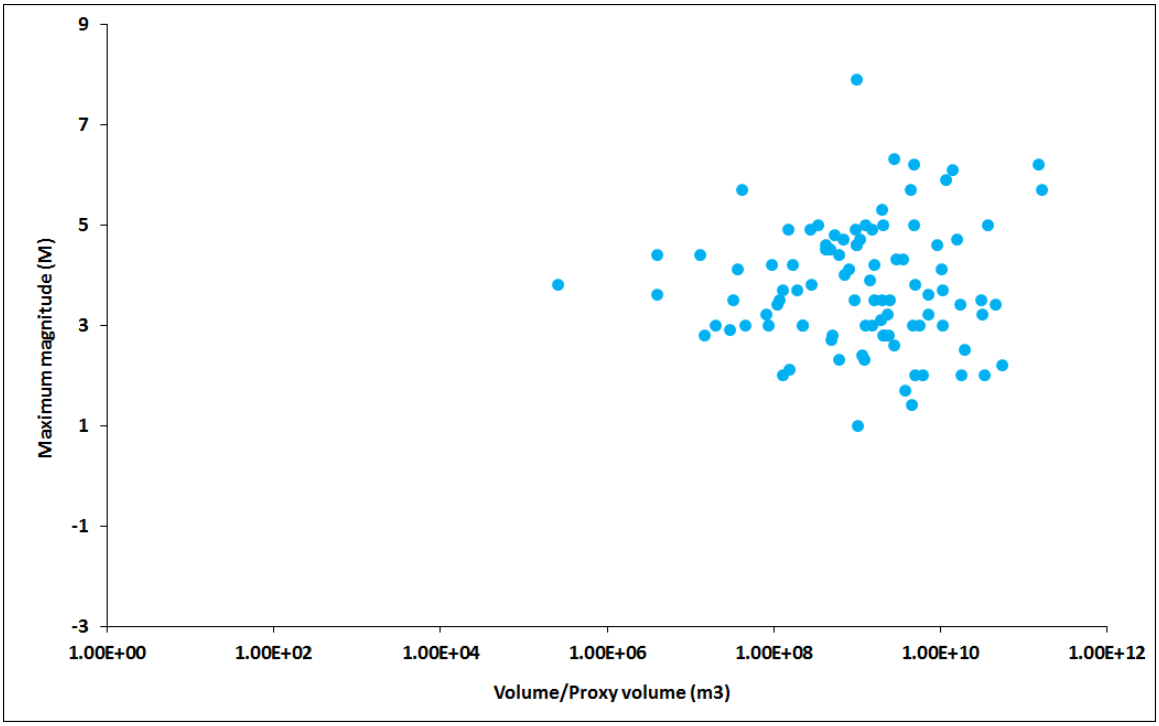

Figure 107: Plot of M_{MAX} vs. volume added or removed by surface operations.

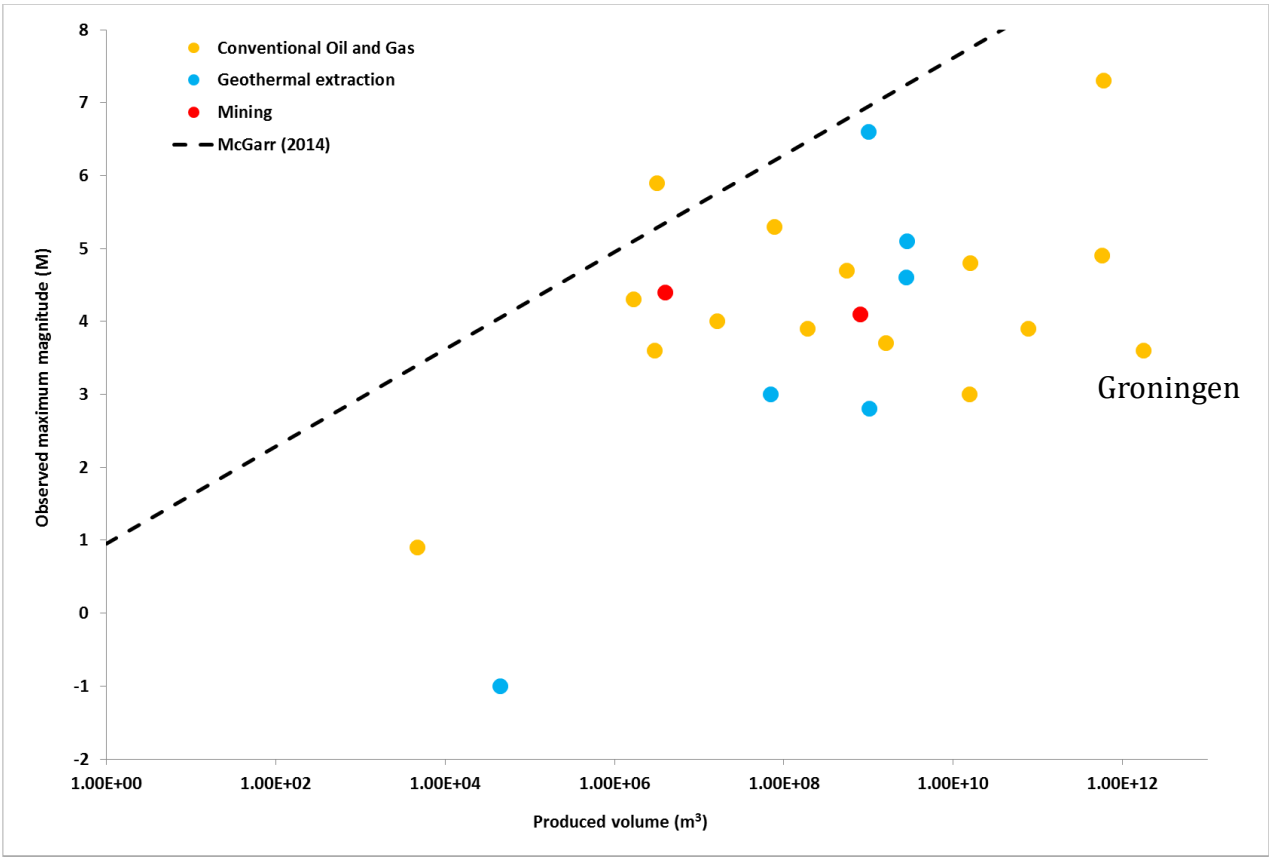

Figure 108: M_{MAX} vs. produced volume (m^3) for 23 projects that involved extraction of mass from the subsurface. Some of these projects also involved injection, so their association with projection is not certain. The upper limit to M_{MAX} proposed by McGarr [2014] on the basis of theoretical considerations is also plotted.

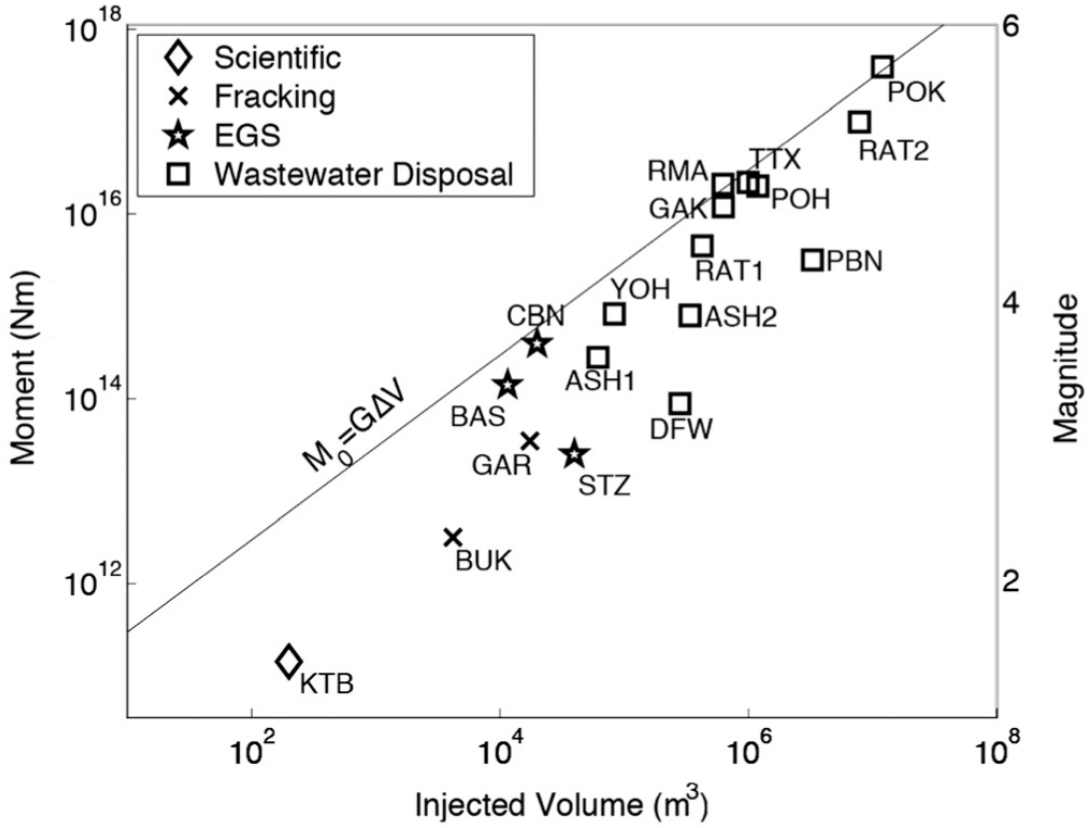

Figure 109: Maximum seismic moment and magnitude vs. total volume of injected fluid from the start of injection until the time of the largest induced earthquake. The line relates the theoretical upper bound seismic moment to the product of the modulus of rigidity and the total volume of injected fluid, and fits the data well [from McGarr, 2014].

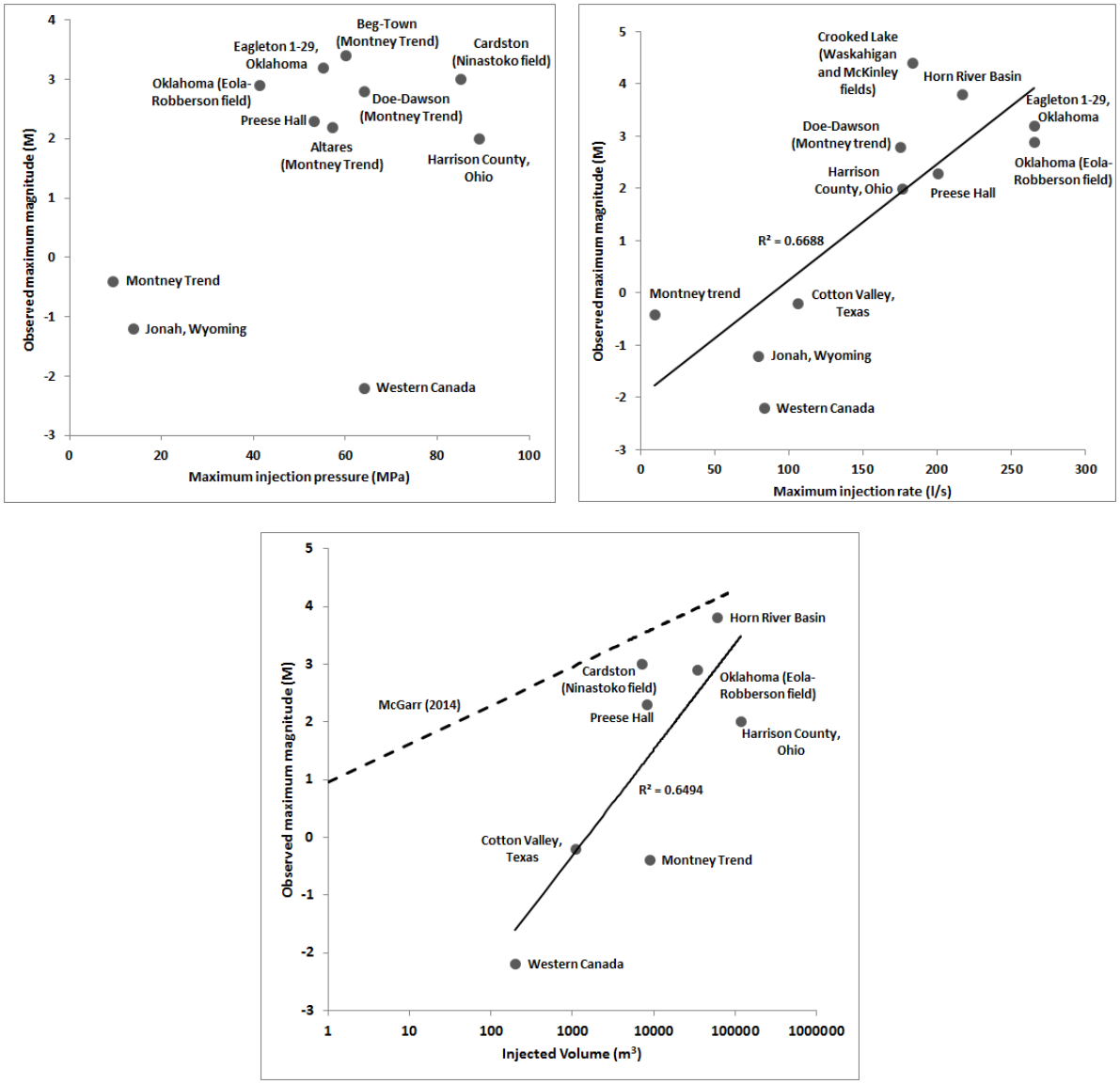

Figure 110: For all cases of shale-gas hydrofracturing-induced earthquakes in our database where data are available, top left: M_{MAX} vs. maximum injection pressure, top right: M_{MAX} vs. maximum injection rate, and bottom: M_{MAX} vs. injected volume.

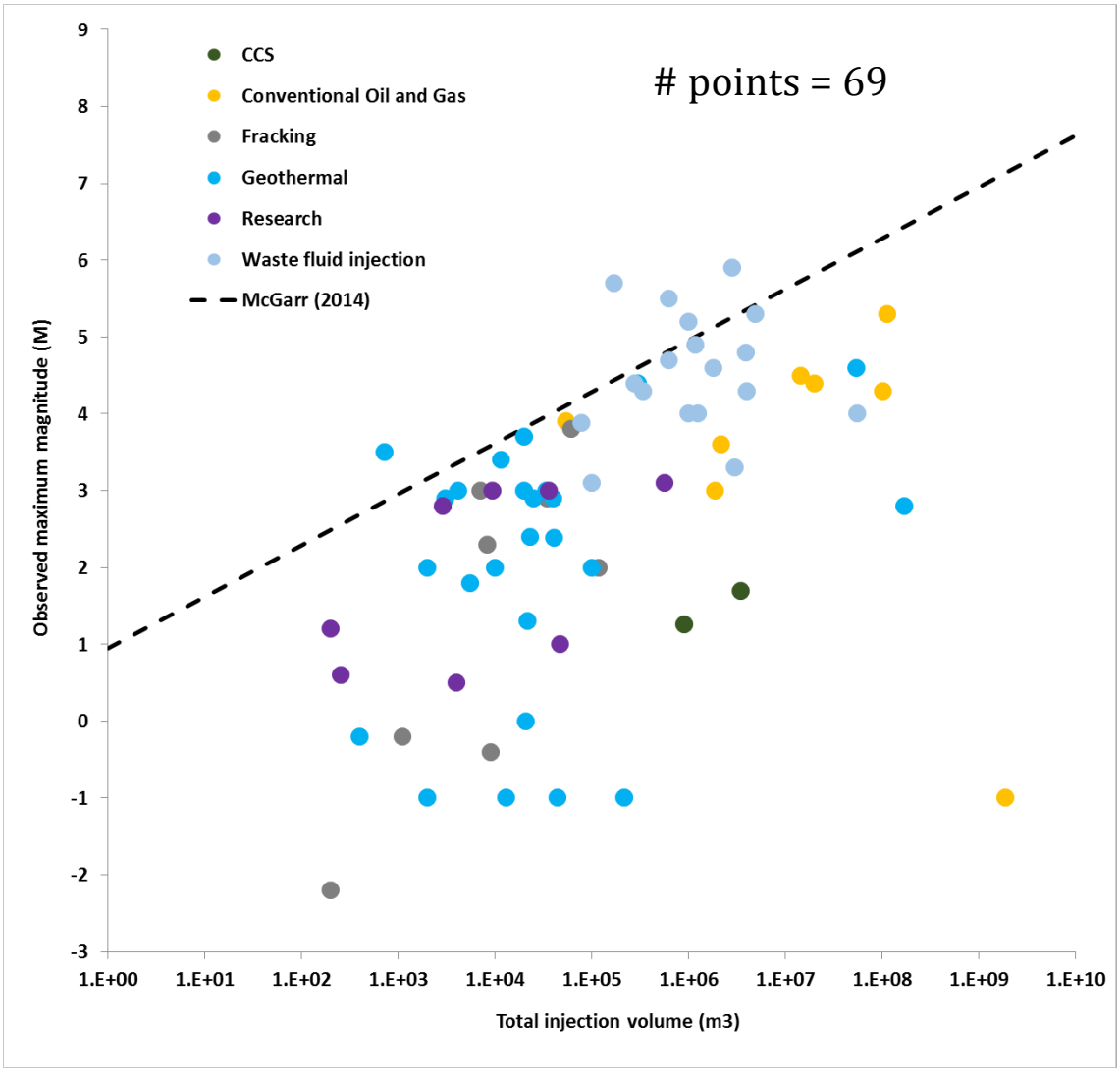

Figure 111: M_{MAX} vs. total injected volume for the 69 cases of induced seismicity for which data are available. The upper-bound magnitude limit proposed by McGarr [2014] on the basis of theoretical considerations is also plotted.

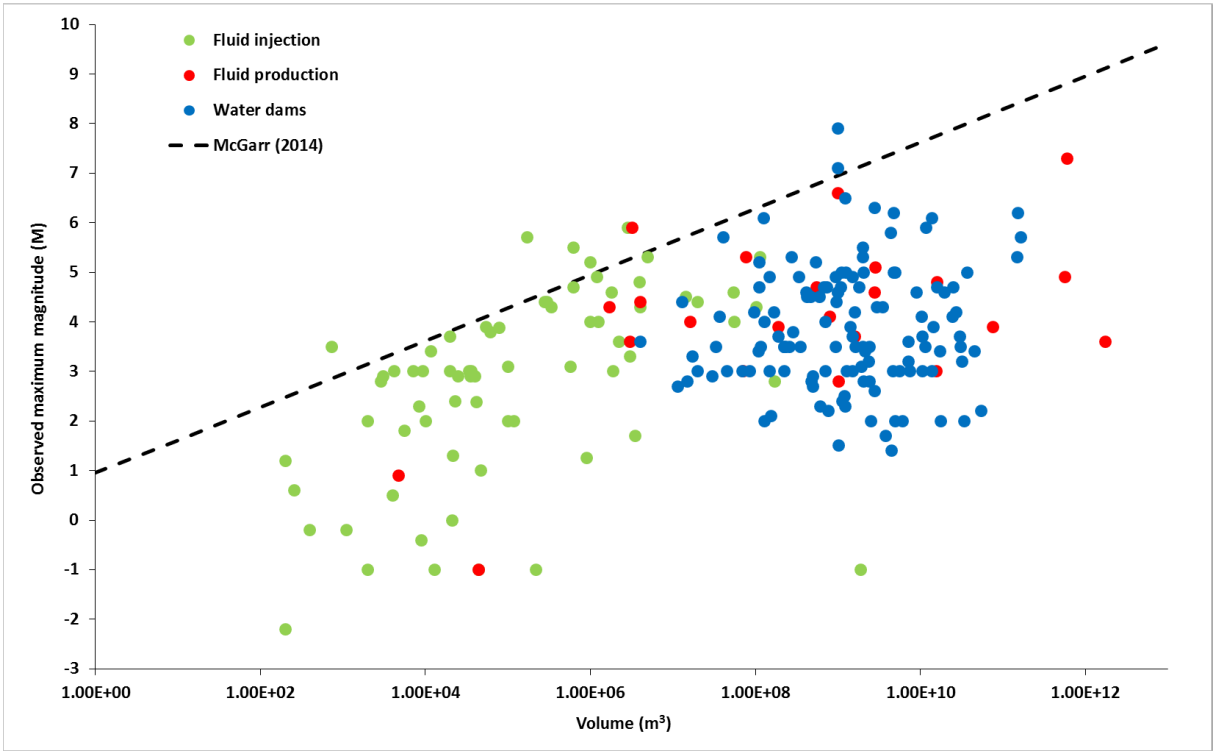

Figure 112: M_{MAX} vs volume or proxy volume of material removed or added for the 218 cases for which data are available, along with the relationship proposed by McGarr [2014] on the basis of theoretical considerations. Volumes and proxy volumes were estimated as follows: Water dams–the volume of the impounded reservoir; fluid injection or extraction–fluid volume injected into or extracted from the subsurface; mining–mass of material excavated, converted to volume using an appropriate density; construction–relevant mass converted to volume using an appropriate density for the building materials; CCS–mass of injected CO_2 converted to volume using a density of liquid CO_2 of 1100 kg/m^3.

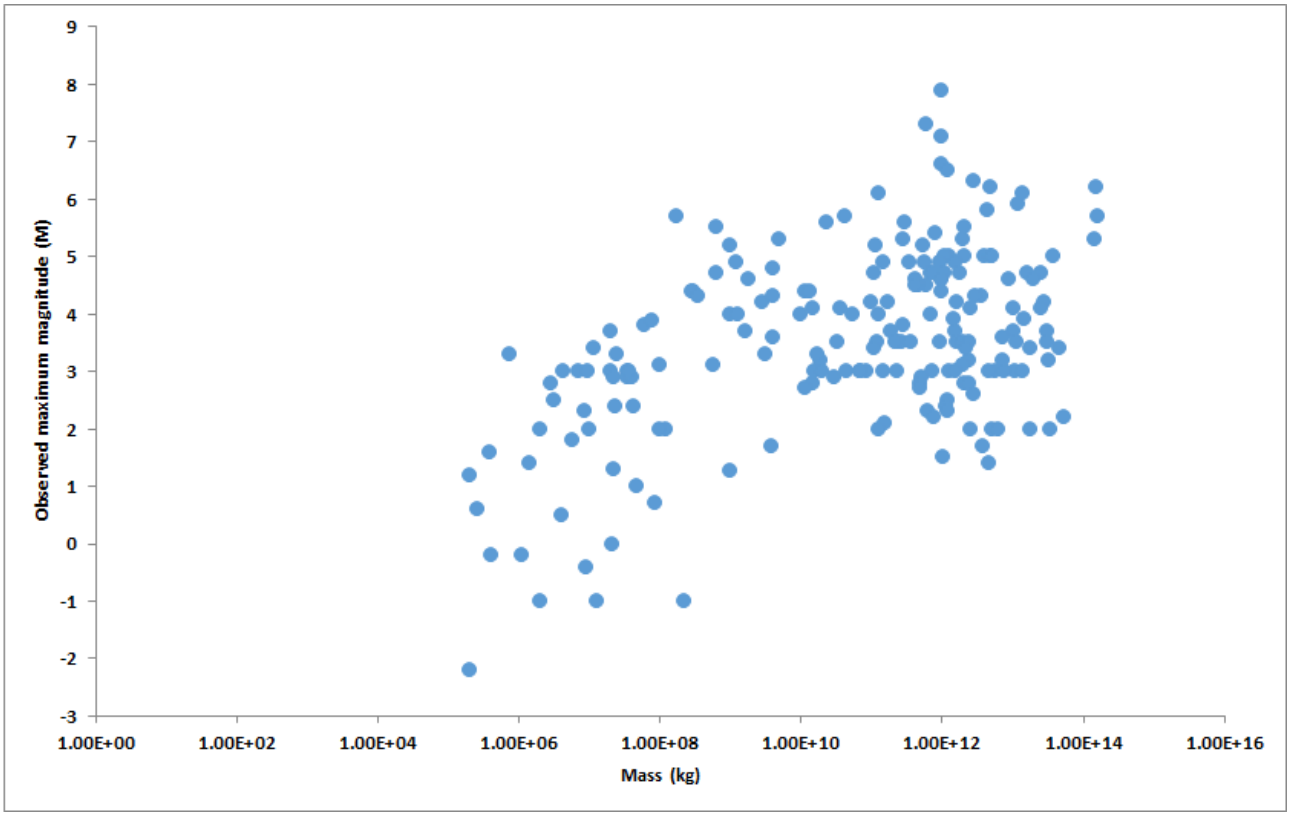

Figure 113: M_{MAX} vs. mass of material removed or added for the 203 cases where data are available. Water volumes were converted to mass using a density 1000 kg/m^3. Oil and gas are not included in this plot except where quantity was reported in units of mass. Project types plotted include CCS, construction, conventional oil and gas, shale-gas hydrofracturing, geothermal, mining, research experiments, waste fluid injection and water reservoirs.

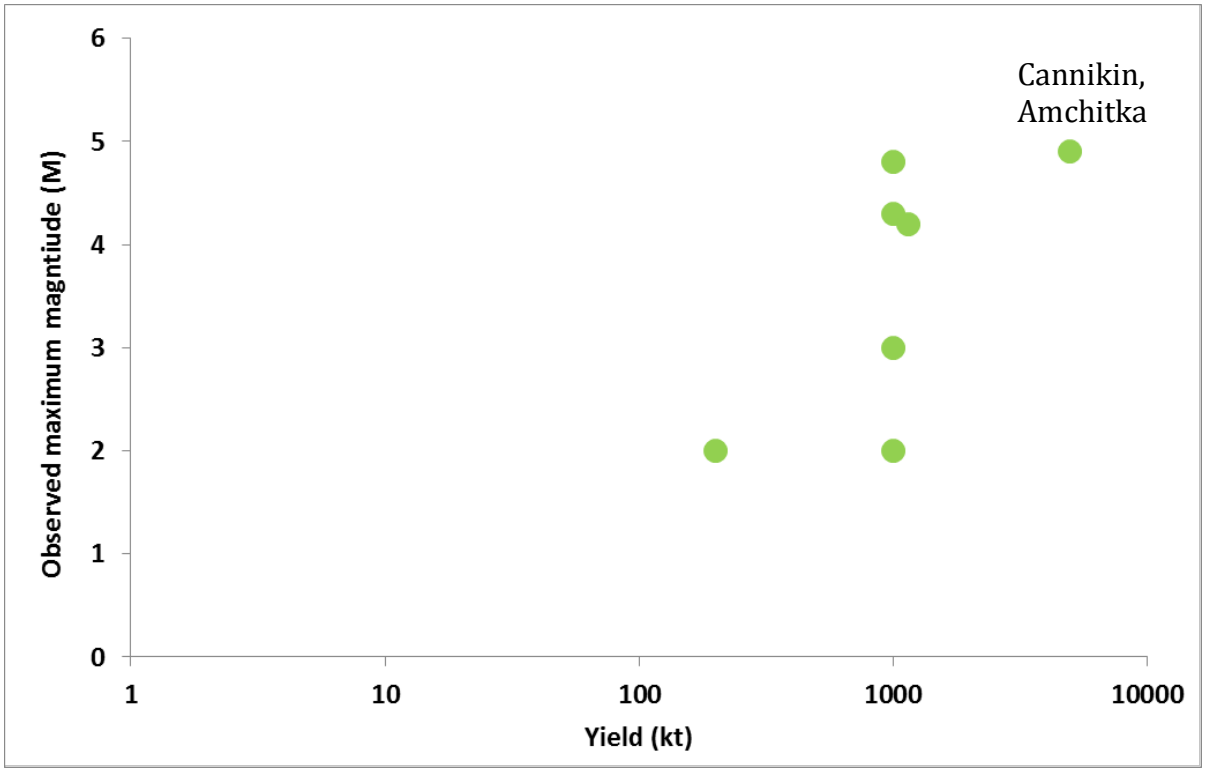

Figure 114: M_{MAX} vs. yield in kilotonnes for nuclear tests that activated faults for the seven cases reported. Only one of these (Benham) is in common with the dataset of McKeown and Dickey [1969] (Figure 115).

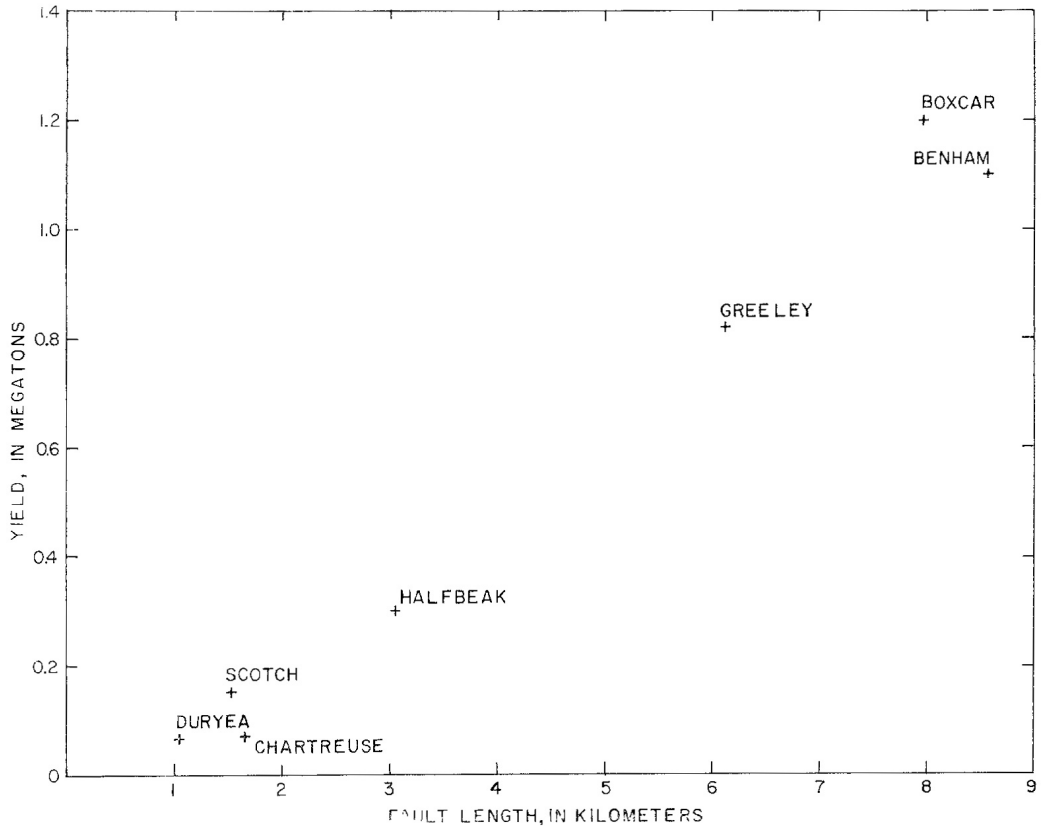

Figure 115: Fault length vs. yield for nuclear explosions that activated faults in Pahute Mesa, Nevada Test Site [from McKeown & Dickey, 1969].

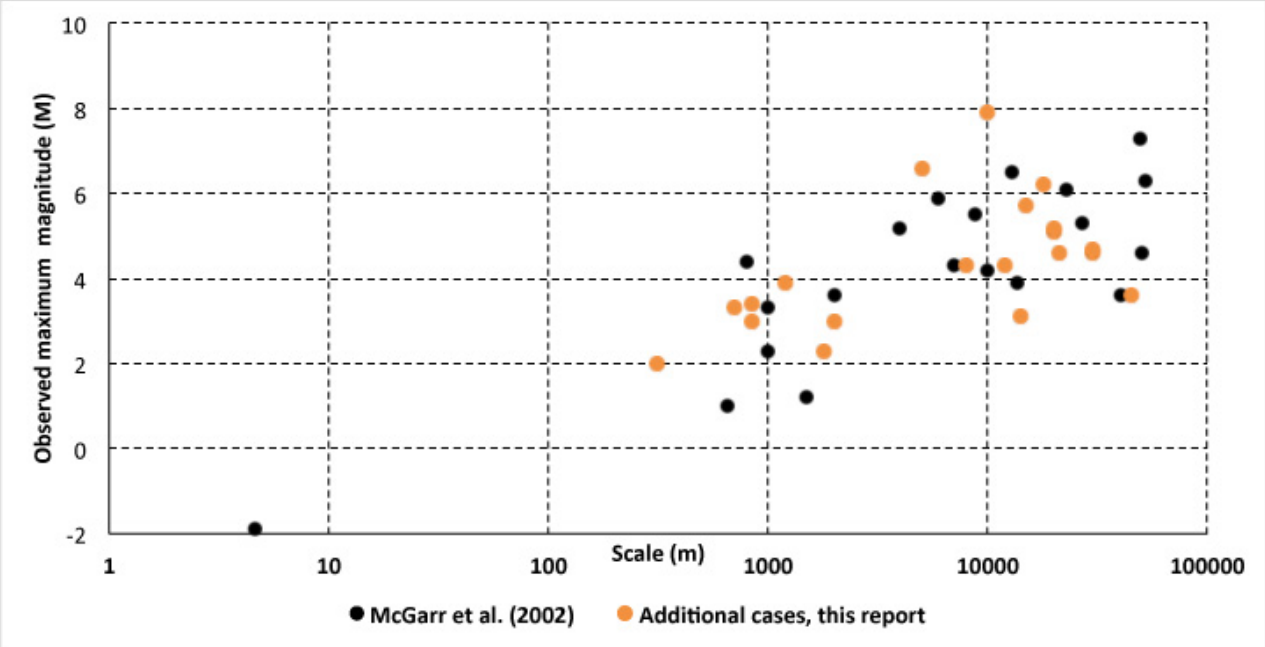

Figure 116: M_{MAX} vs. project scale in meters. Black dots: cases studied by McGarr *et al.* [2002]; orange dots: 20 additional cases from our database. Project scale was estimated using the longest dimension of the project, *e.g.*, the length of a water reservoir.

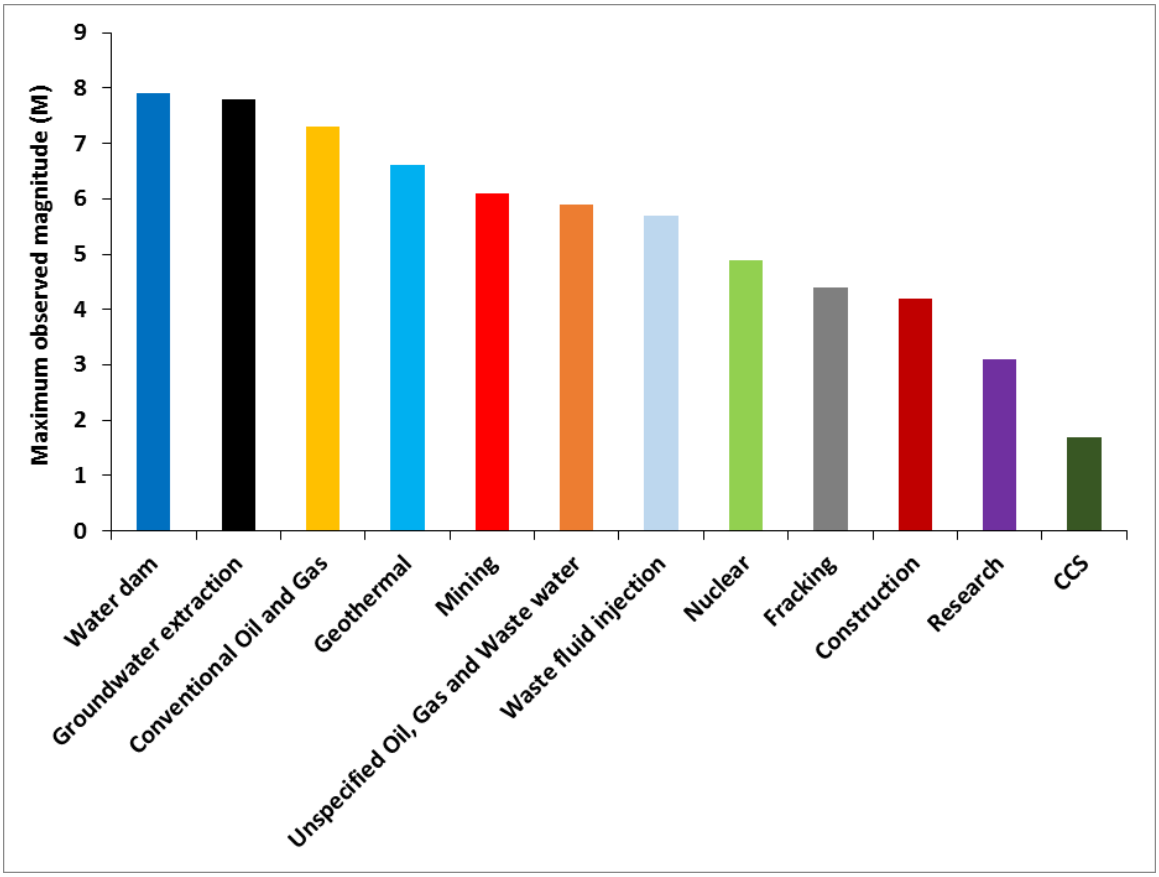

Figure 117: Histogram of M_{MAX} for different categories of project.

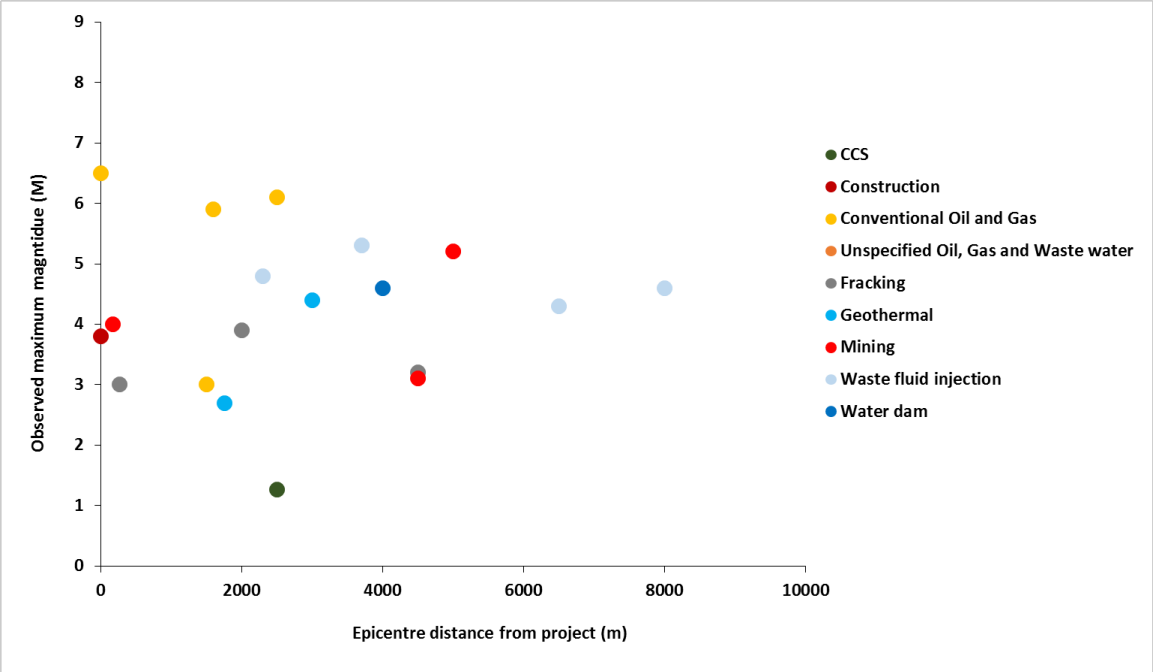

Figure 118: M_{MAX} vs. distance from project for postulated induced earthquakes up to 10 km away for the 19 cases where data are available.

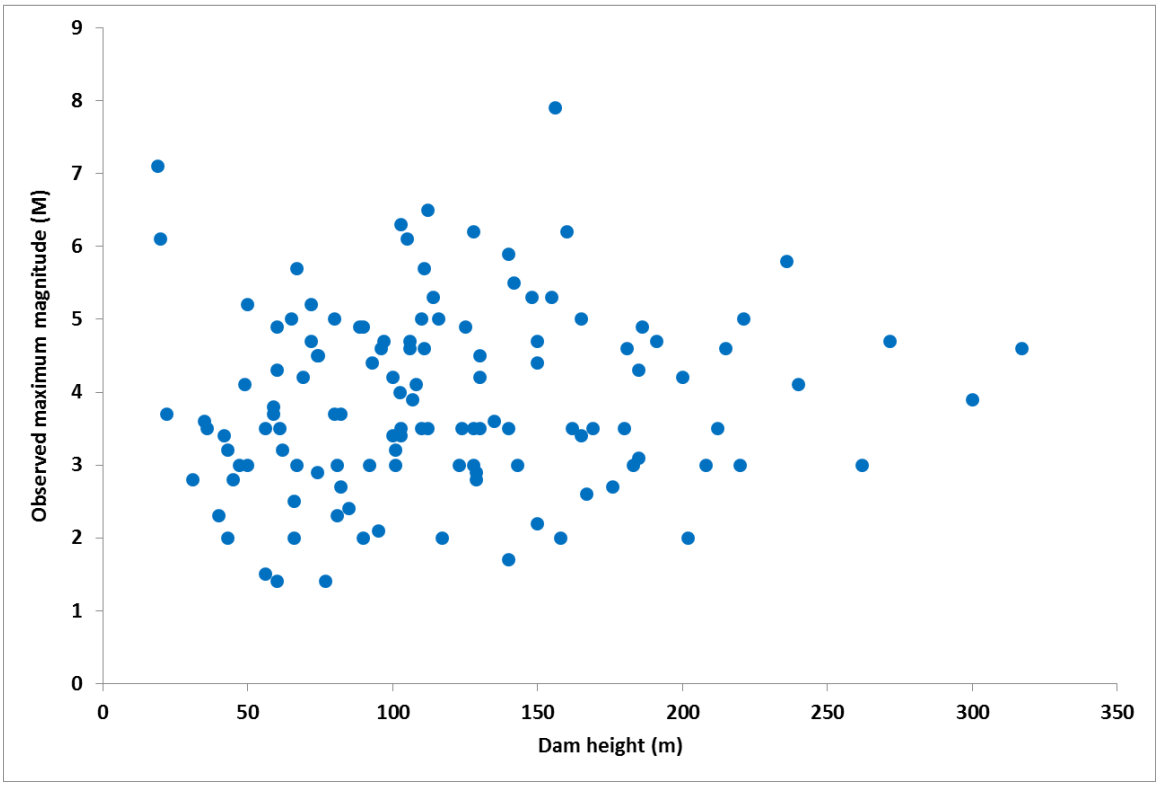

Figure 119: Plot of M_{MAX} vs. dam height for the 159 cases of seismogenic water reservoirs for which data are available.

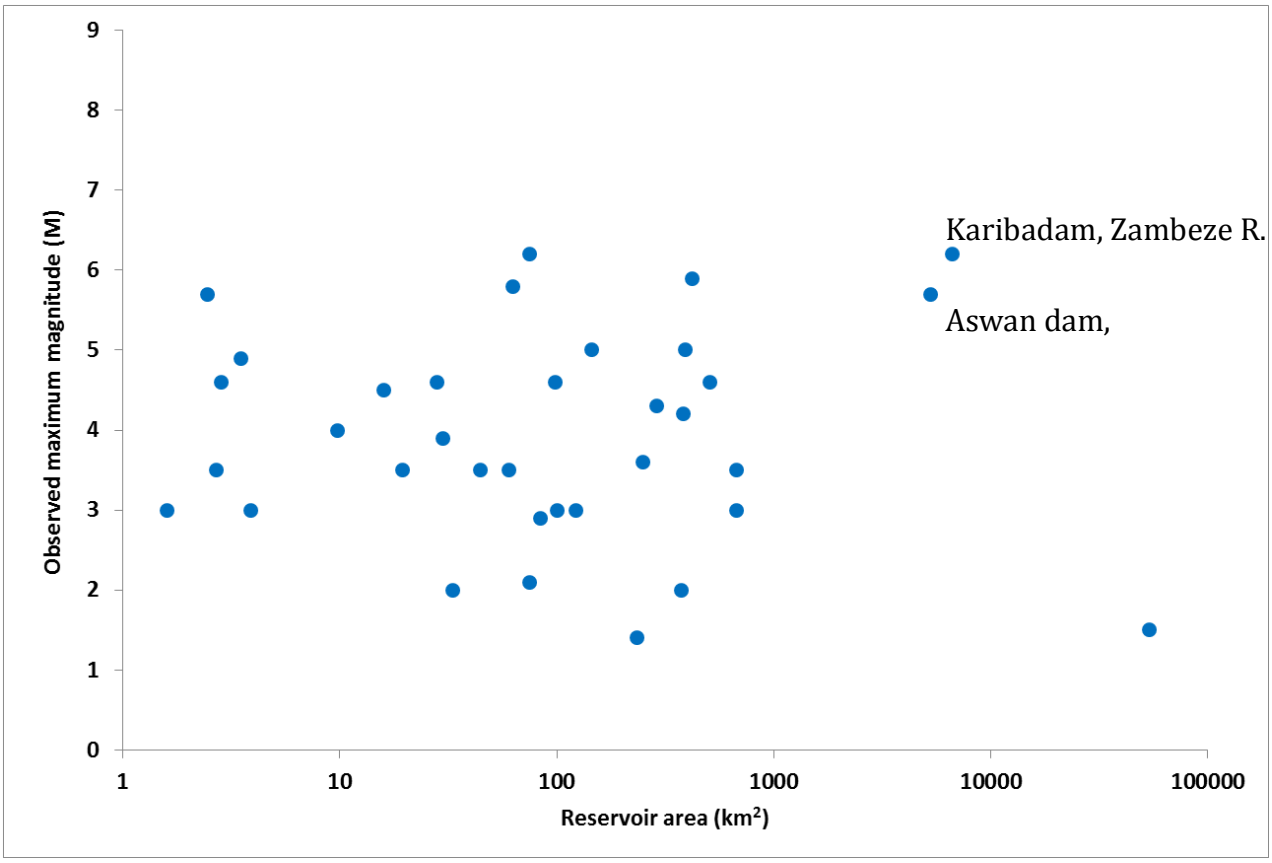

Figure 120: Plot of M_{MAX} vs. water reservoir area for the 35 cases for which data are available.

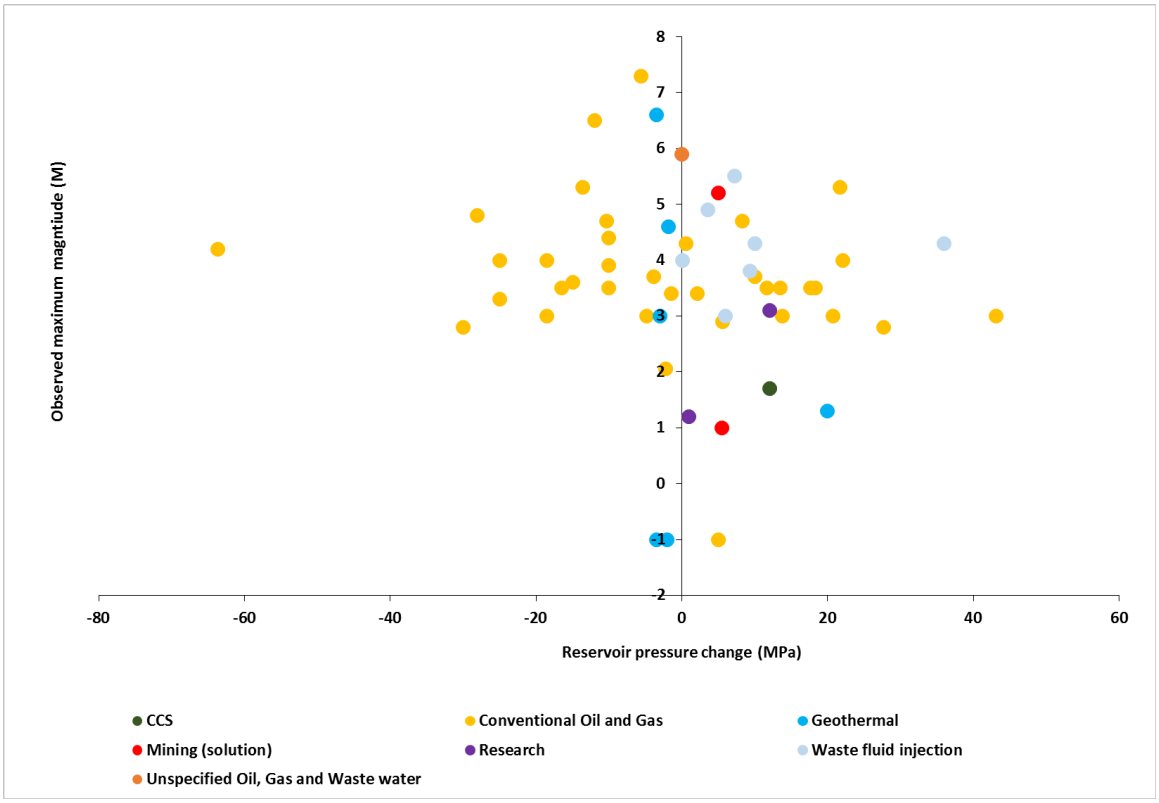

Figure 121: M_{MAX} vs. change in reservoir fluid pressure resulting from production/injection for the 55 cases where data are available. We include 9 cases of conventional oil and gas where the pressure change results from both injection and production.

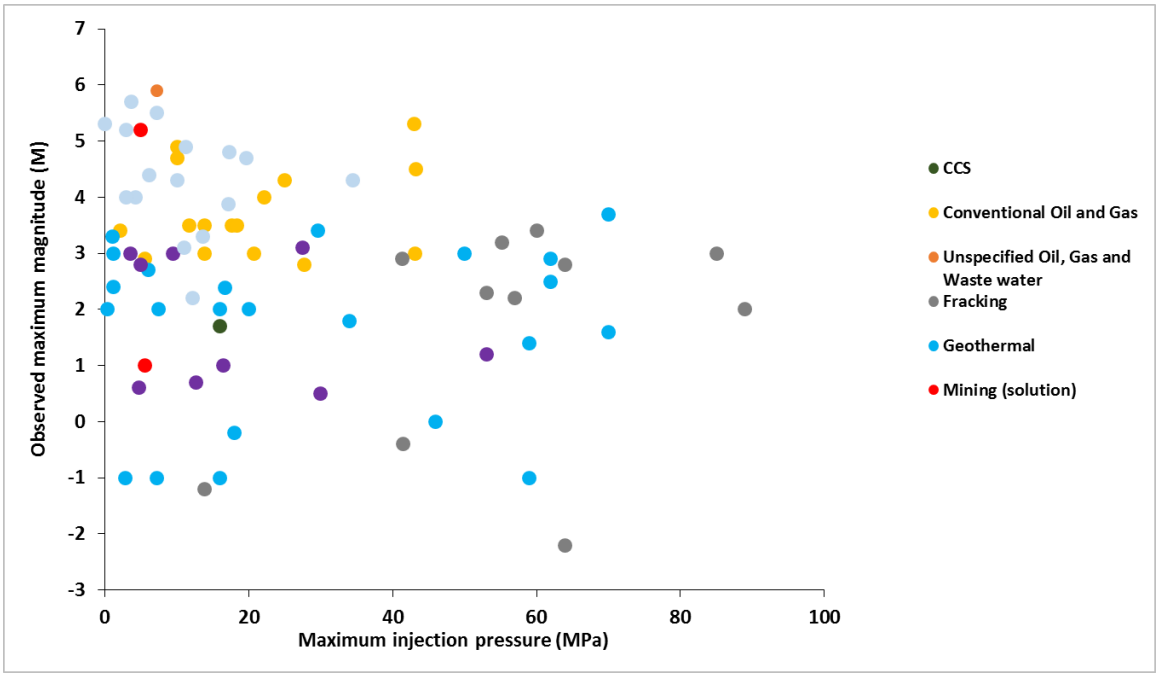

Figure 122: M_{MAX} vs. maximum wellhead injection pressure for the 79 cases where data are reported.

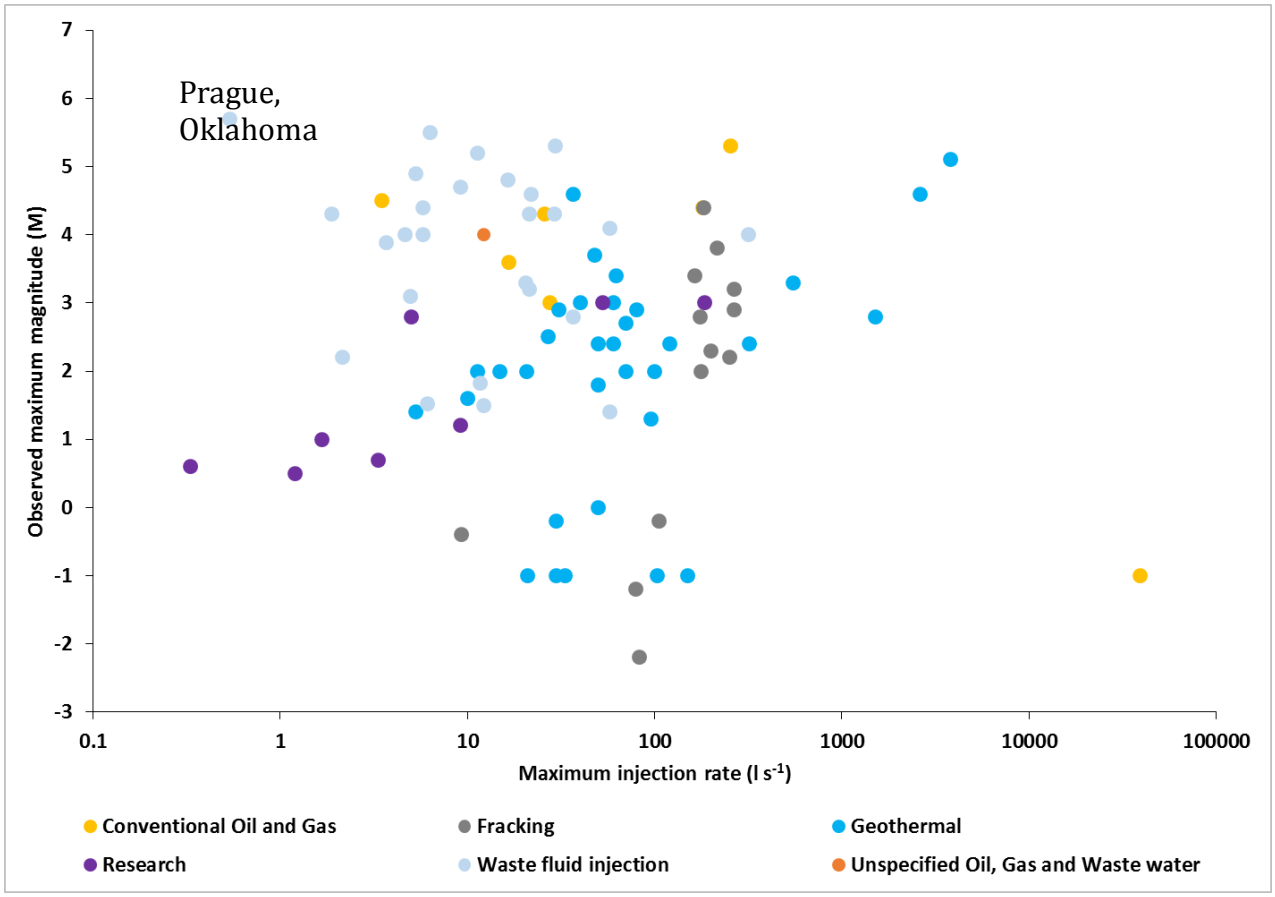

Figure 123: M_{MAX} vs. maximum injection rate for the 88 cases for which data are reported. Rates of injection varied from 0.33 to ~ 40,000 l/s. At rates greater than ~1000 l s^{-1}, values apply to entire fields rather than individual wells.

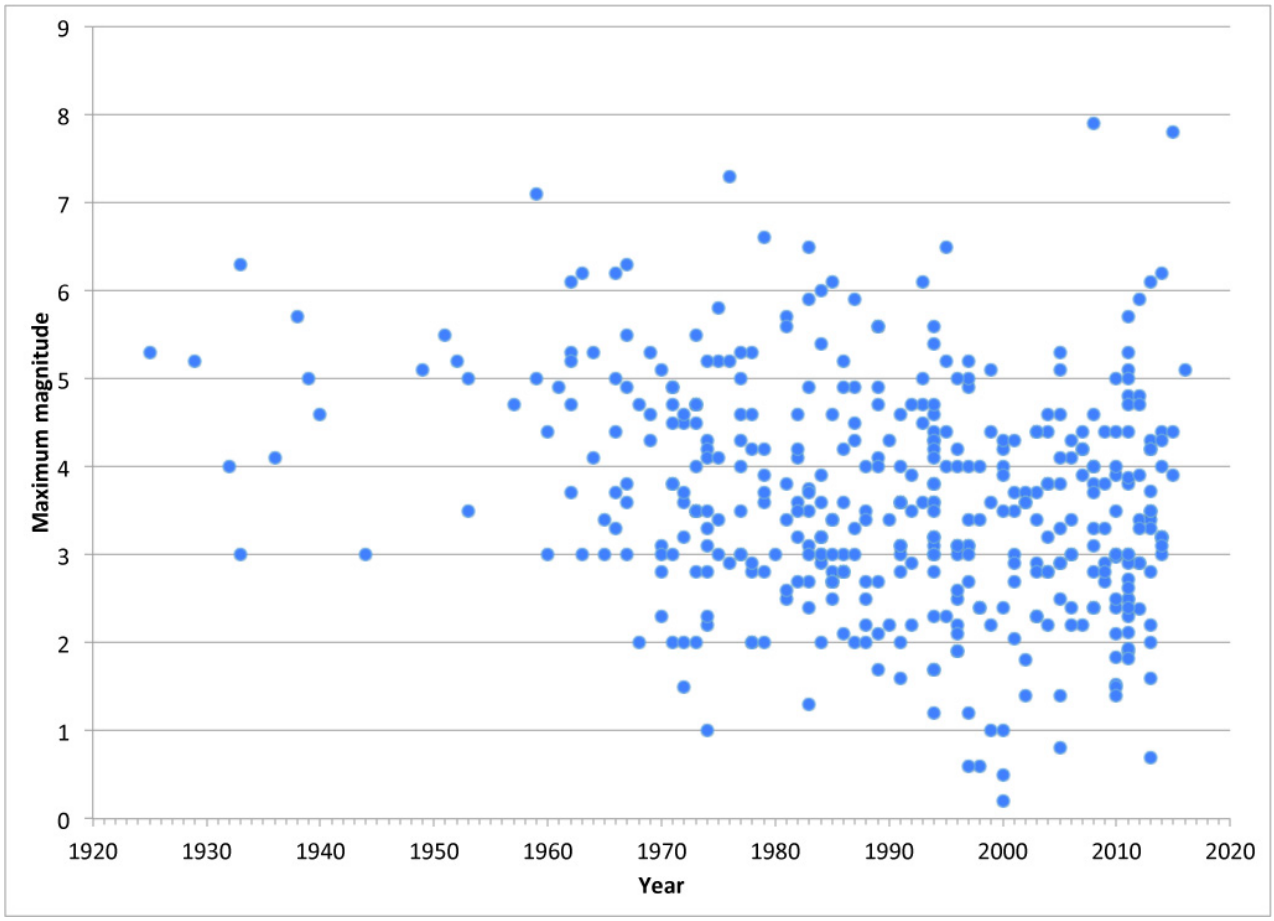

Figure 124: M_{MAX} vs. year for the 419 cases where data are available.

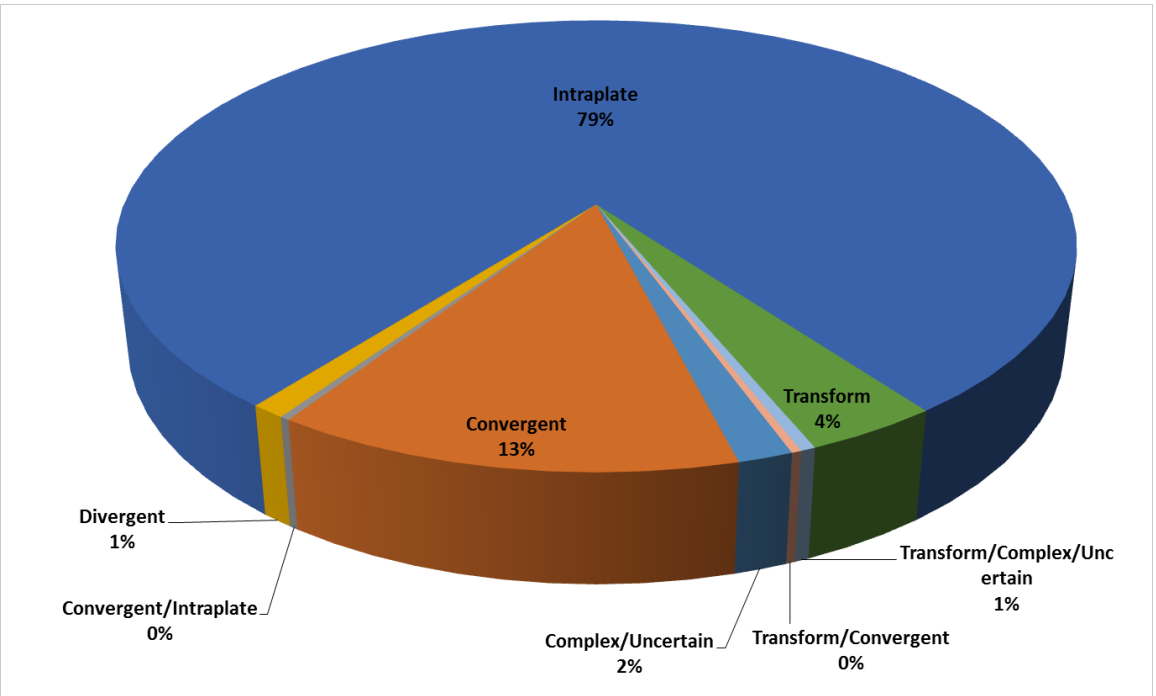

Figure 125: Tectonic settings of cases of human-induced earthquake activity.

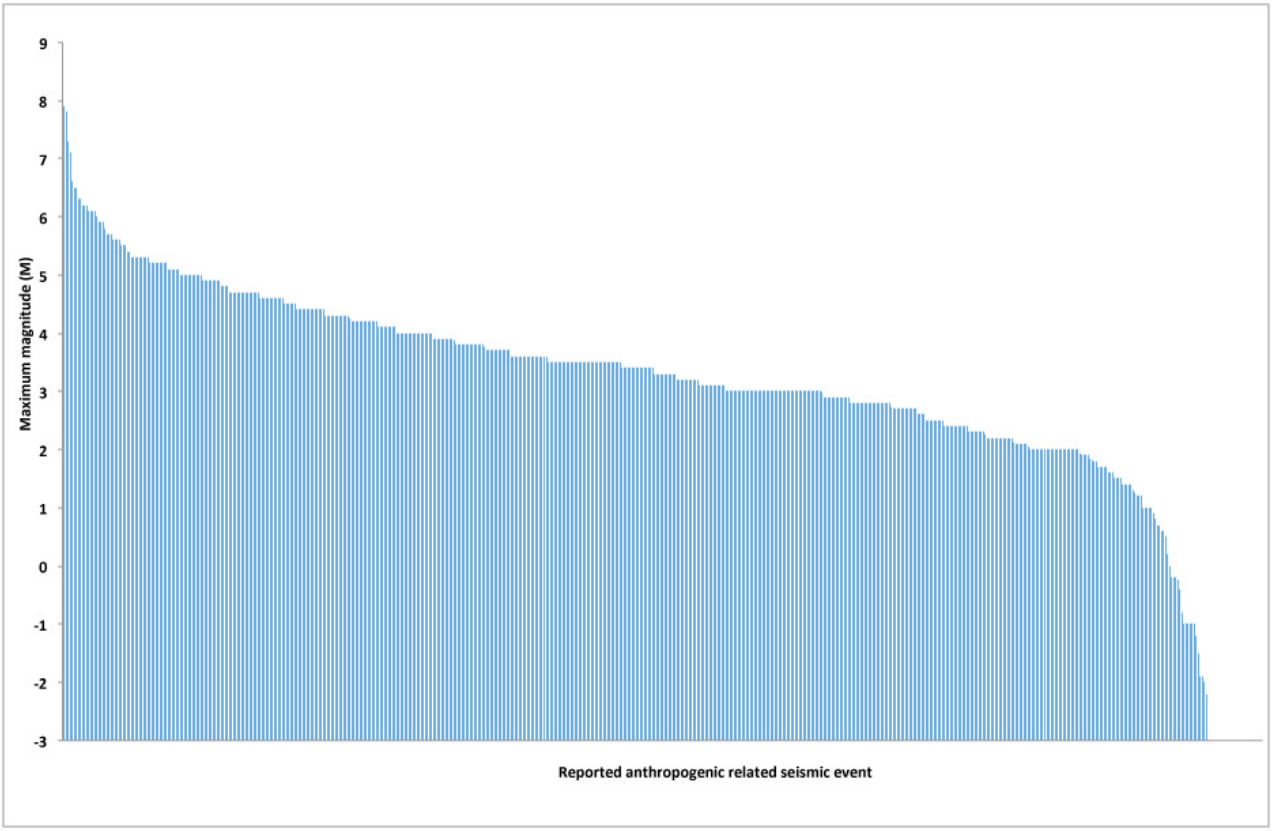

Figure 126: Histogram showing M_{MAX} for the 562 seismogenic projects where this parameter is recorded. No magnitudes are reported for 143 cases.

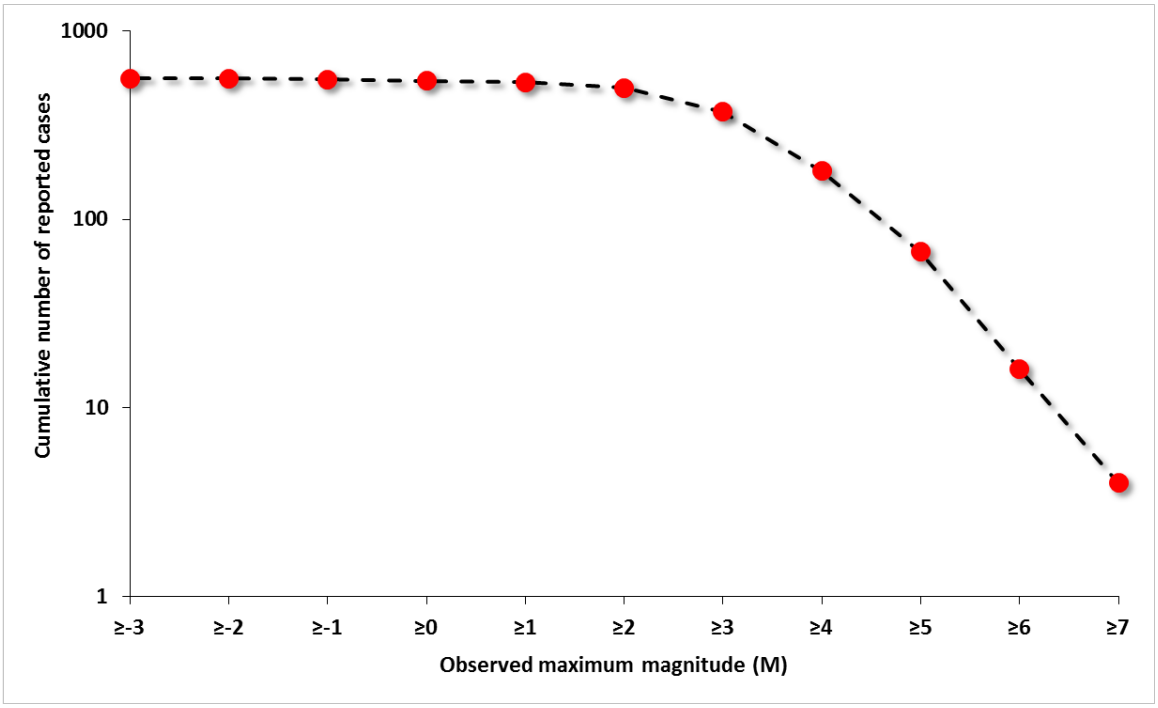

Figure 127: Cumulative number of reported cases of induced seismicity vs. M_{MAX} for the 562 cases for which data are available.

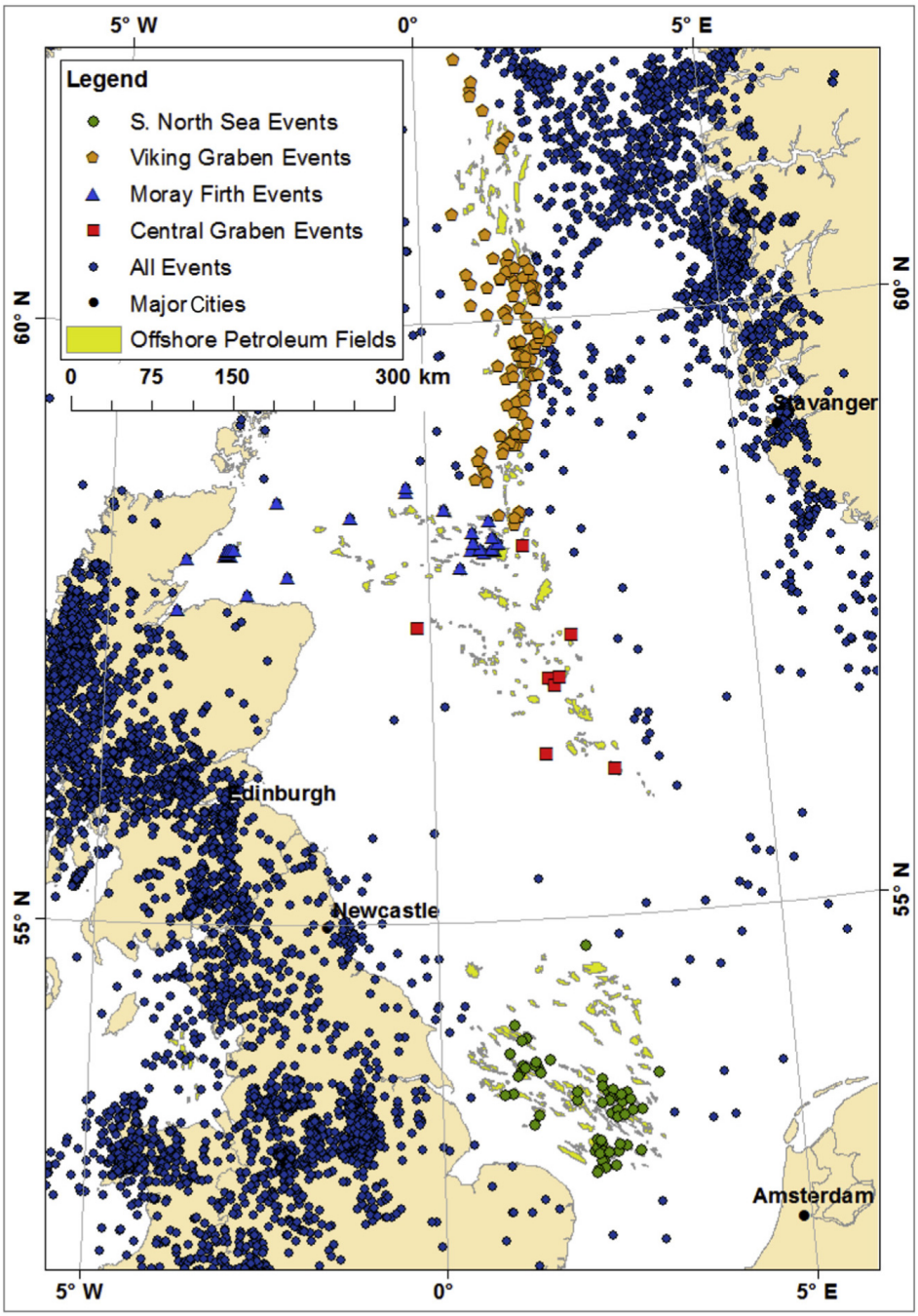

Figure 128: Epicenters from the UK earthquake catalog of the British Geological Survey. Orange circles: Viking Graben events; blue triangles: Moray Firth events; red squares: Central Graben events; green circles Southern North Sea Gas Province events; yellow shading: offshore hydrocarbon fields [from Wilson *et al.*, 2015].

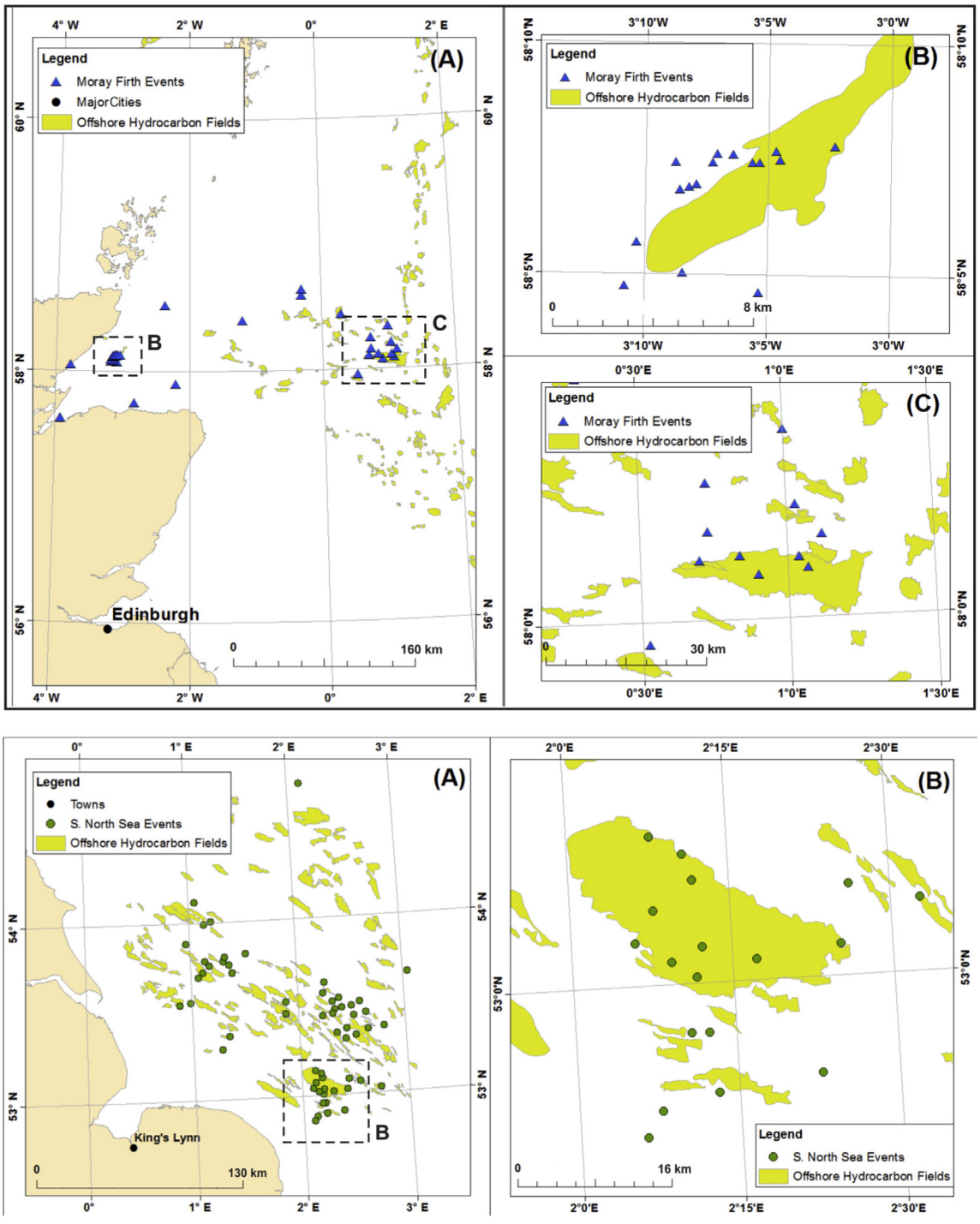

Figure 129: Expanded view of some parts of Figure 128. Top row: A–the Moray Firth. Yellow: hydrocarbon fields; blue triangles: earthquakes. B–the Beatrice Oilfield. C–the Britannia Gasfield. Bottom row: A–the Southern North Sea Gas Province. Green dots: earthquakes. Bottom row: B–the Leman Gasfield [from Wilson *et al.*, 2015].

Figure 130: Damage done to the cathedral in Canterbury, New Zealand, by the 2010 M 7.1 earthquake[27].

[27] http://www.npr.org/sections/parallels/2015/04/05/397093510/will-new-zealand-rebuild-the-cathedral-my-forefather-erected

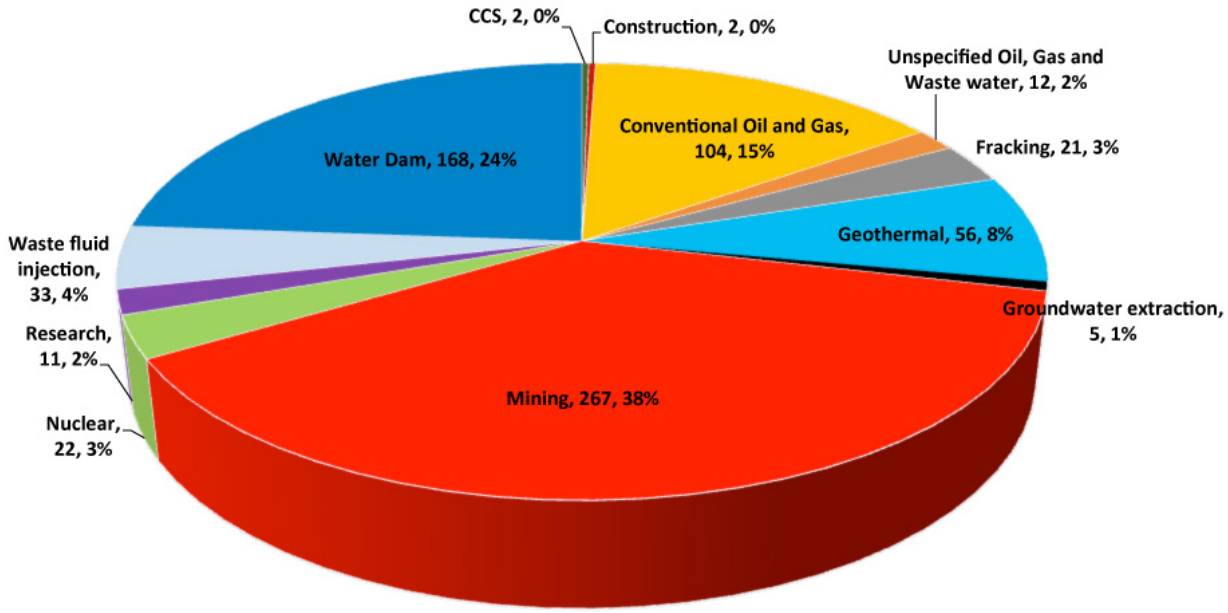

Figure 131: Percentage of total cases for each project category in the database.

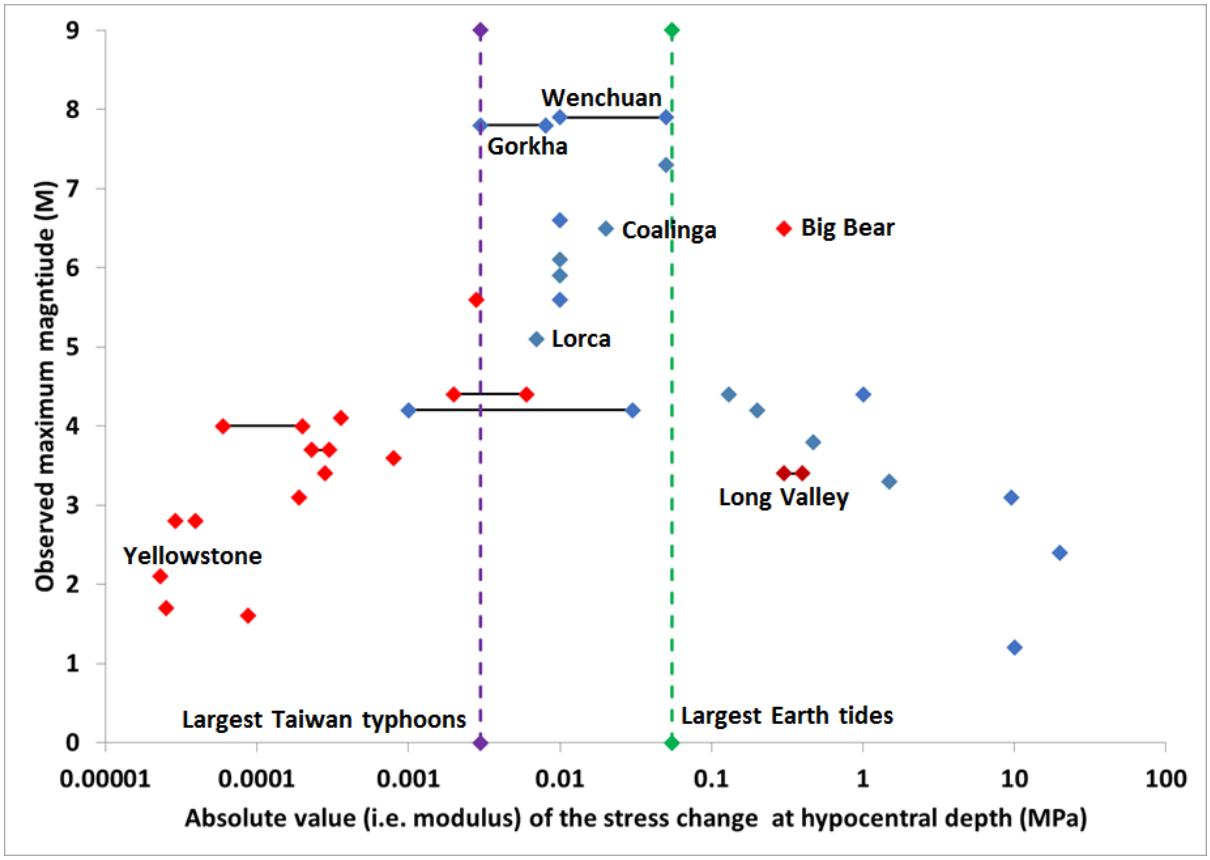

Figure 132: M_{MAX} vs. absolute value of stress changes calculated by various authors to have occurred at hypocentral depths and possibly induced earthquakes. Vertical dashed green line: largest Earth tides; vertical dashed purple line: largest Taiwan typhoons. Blue diamonds: human-induced earthquakes, diamonds connected by solid black lines: ranges of stress changes calculated. Some example earthquakes are labeled.

Red diamonds: natural earthquakes that followed the 28th June 1992 M_W 7.3 Landers, California, earthquake [data from Hill *et al.*, 1993]. These earthquakes are plotted against the calculated static stress changes except for the case of remote triggering at Long Valley where Hill *et al.* [1993] give dynamic stresses. Where the static stress changes are much smaller than Earth tides and seismogenic typhoons, they are likely to have been induced by the much-larger dynamic stresses from the passage of the shear and surface waves.

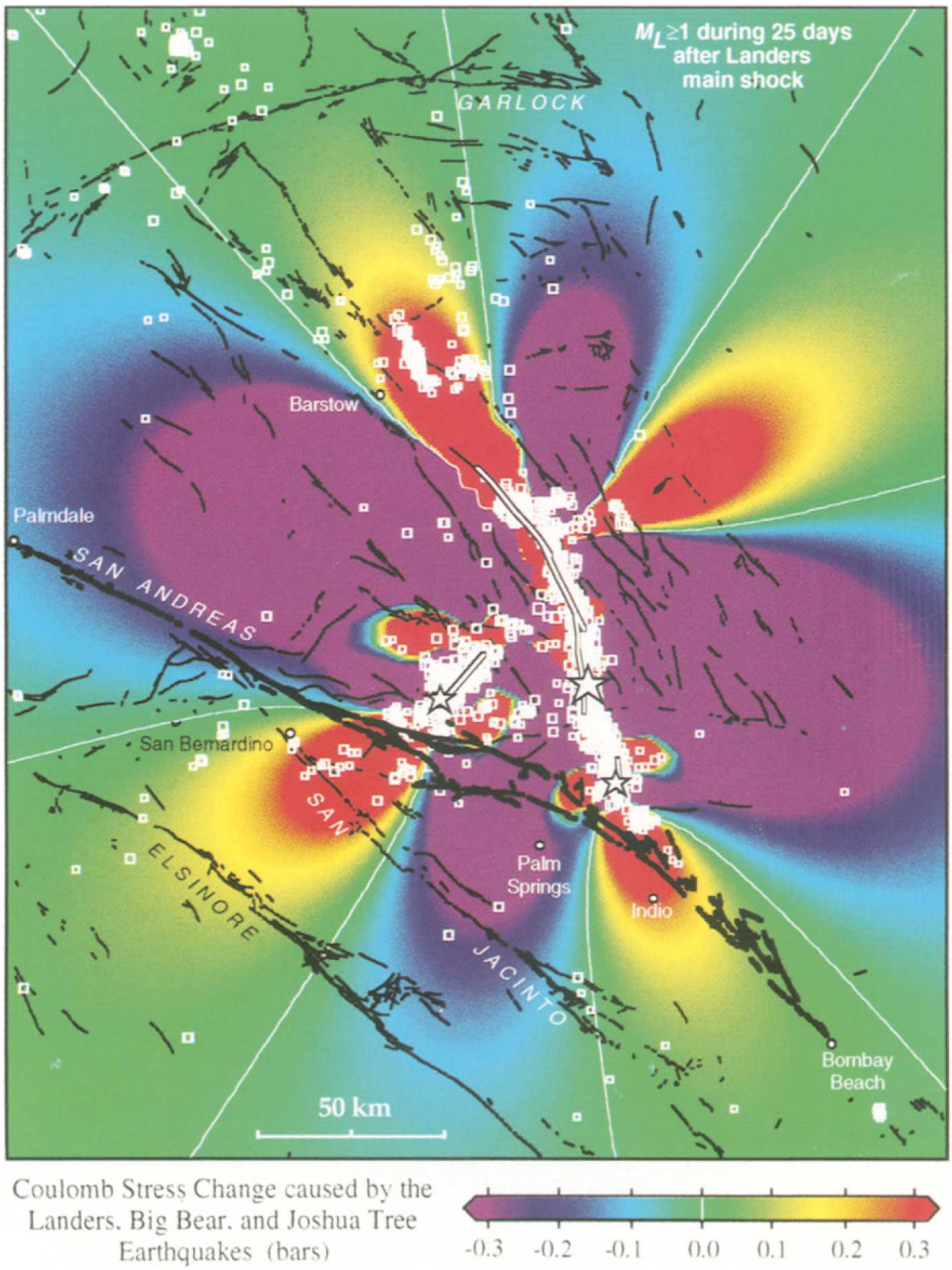

Figure 133: Coulomb stress changes at a depth of 6.25 km caused by the M_W 7.3 Landers, California, earthquake and large aftershocks [from King *et al.*, 1994].

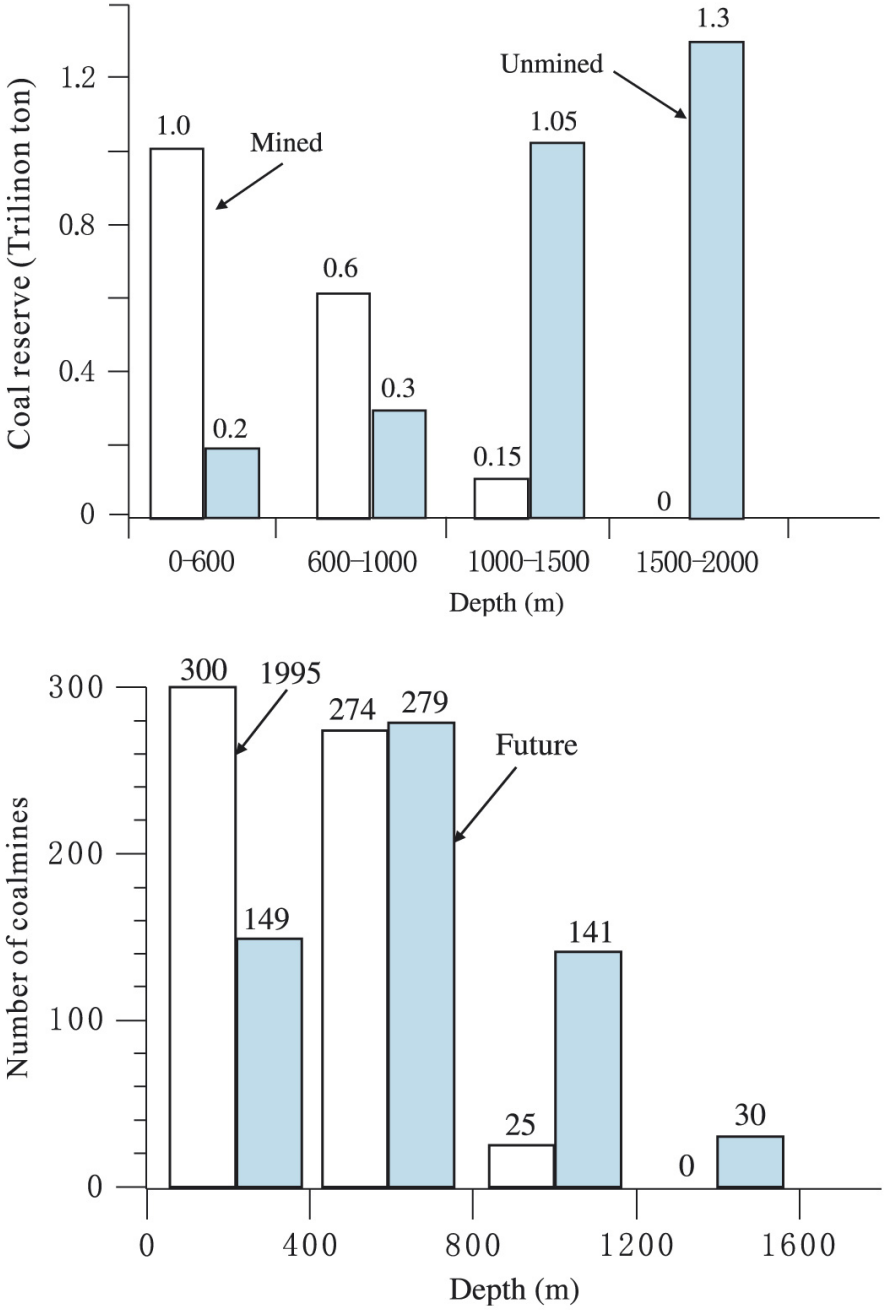

Figure 134: Top: Depth distribution of Chinese coal reserves (1995 statistics). Bottom: Depth distribution of 599 state-owned Chinese coal mines [from Li *et al.*, 2007].

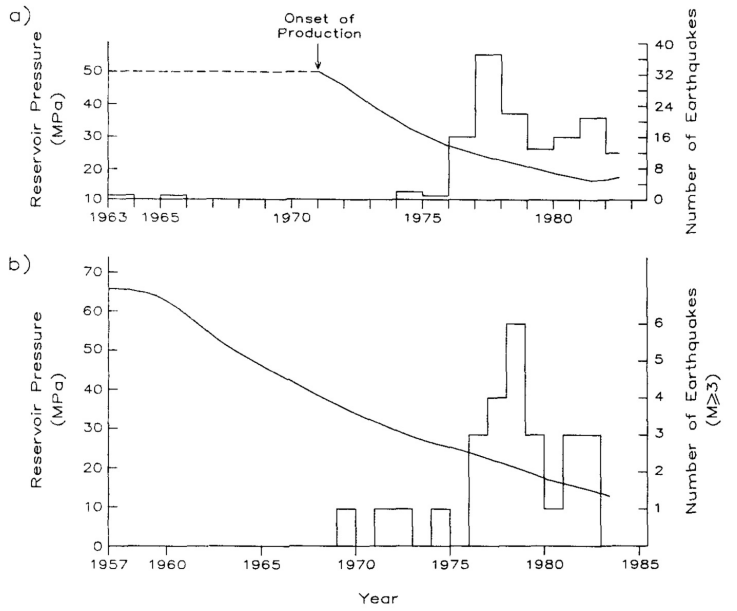

Figure 135: Number of earthquakes per year and decline in average reservoir pressure for a) the Strachan Field, Alberta, Canada, and b) the Pau basin, France [from Segall, 1989].

Appendix 1: Method used to construct the database.

In performing the literature review on which our database is founded, we proceeded as follows:

1. A single-sheet Excel spreadsheet was constructed and the raw database of Davies *et al.* [2013] was imported. Additional columns were added for new types of data, *e.g.*, Earthquake Cause (main class) and Earthquake Cause (subclass);

2. The entries were checked and updated where necessary. References were added where lacking;

3. New cases were searched for using Google Scholar. Where possible (most cases) PDFs were downloaded, digitally filed, and entered into EndNote. Where a PDF of an entire paper or report was unobtainable, information from the abstract was used;

4. Where data are not available, *e.g.*, maximum magnitude, the relevant spreadsheet cell is left blank;

5. Entries in the database were double-checked;

6. Where conflicting information is published, *e.g.*, different magnitudes, we report moment magnitude (M_W). If M_W is not available we report the largest magnitude from those available.

Description of the database

We have assembled 705 cases of industrial projects postulated to have induced earthquakes. These cases include a wide range of project types. For a large majority of industrial projects in all categories, there are no reports of seismogenesis. However, it is clear that there is large-scale under-reporting.

For the purpose of plotting figures, we divided the projects into the following categories:

Carbon Capture and Storage (CCS)

The implementation of CCS to combat climate change is still largely in the demonstration stage. To date there have been 75 CCS projects with eight of these on a commercial scale [Huaman & Jun, 2014]. Storage requires the injection of CO_2 into a subsurface formation. Two CCS projects are reported to have induced earthquakes–In Salah, Algeria and Decatur, Illinois, USA.

Construction

Projects where humans have built a structure or created artificial topography are classed as construction, with the exception of water dams which are categorized separately. Two such projects are reported to be linked to earthquakes, the erection of the Taipei 101, Taiwan, building and artificial accumulation of shingle deposits at Folkestone, UK. We searched for reports of earthquakes associated with the construction of nearby Samphire Hoe. This is a

coastal park created using ~10^{10} kg of chalk excavated on the English side of the Channel Tunnel, an order of magnitude greater than accumulated at Folkestone. However, we found none.

Conventional oil and gas (including unspecified oil, gas and waste-water projects)

There are approximately 67,000 oil- and gasfields globally. Our database contains 112 seismogenic projects in this category. The largest earthquake postulated to be related to such projects is the 1976 M_S 7.3 earthquake near the Gazli Gasfield, Uzbekistan.

Shale-gas hydrofracturing

Hydraulic fracturing to increase oil and gas production has been practiced for several decades but its recent use to extract gas from shale has attracted media attention. Every successful hydrofracture job induces seismicity because the objective is to fracture rock. Despite the fact that ~ 2.5 million such jobs have been completed, our database contains only 21 cases of induced earthquakes. Of these cases, the largest earthquake reported was M_W 4.4 and occurred in Canada in 2015.

Geothermal exploitation

There are 65 geothermal fields worldwide that produce >100 GW electric per year. Our database contains 51 cases that have been linked to earthquakes. The largest earthquake postulated to have been induced is the 1979 M_L 6.6 earthquake near the Cerro Prieto Field, California.

Groundwater extraction

Our database contains five cases where earthquakes are postulated to be linked to large-scale groundwater extraction. The largest of these case is the 2015 M_W 7.8 Gorkha, Nepal, earthquake, which resulted in ~8000 deaths and ~$10 billion of economic loss, ~50% of the Gross Domestic Product of Nepal.

Mining

Mining-related seismicity (gallery collapses, stope contractions, “rock bursts”, “coal bumps”, faulting) accounts for 38% (267 cases) of the cases in our database, the largest category. The U.S. Geological Survey estimates there are currently 13,262 active mines worldwide, in addition to inactive and historic mines. There is likely under-reporting of mining seismicity. The largest earthquake proposed to be induced by mining is the 2013 M_L 6.1 earthquake, suggested to be linked to the Bachatsky open-cast coal mine, Russia. Other countries with $M \geq 5$ earthquakes postulated to be induced by mining include Australia, Canada, Germany, Poland, South Africa and the US.

Underground nuclear explosions

We exclude the initial explosions from our database but recognize two types of related induced seismicity:

a) earthquakes associated with the collapse of the underground cavity created by the explosion, and

b) earthquakes induced on local faults.

The largest recorded seismic event of type a) was m_b 4.9 (the 5 Mt Cannikin test, Amchitka, Alaska, 1971). The largest reported event of type b) had m_b 4.8 (the 27th October 1973 Novaya Zemlya test). Of 1,352 underground nuclear tests, 22 have been associated with earthquakes [Pavlovski, 1998].

Research

The database contains 13 projects classified as research. These involve injecting water into the subsurface or flooding abandoned mines. One of the earliest of these was that at the Rangely Oilfield, Colorado, where the largest induced earthquake in this category occurred, the 1970 M_L 3.1 event. Another notable project was the Kontinentales Tiefbohrprogramm der Bundesrepublik Deutschland (KTB), the German Continental Deep Drilling Program, in which small volumes of fluid were injected as deep as ~9 km, the deepest reported fluid injection to date.

Waste fluid injection

Seismicity induced by waste-fluid injection is increasing. Of the > 151,000 Class II waste-fluid injection wells in the USA, estimates for the rate of seismogenesis range from nine cases to > 18,000. Our database contains 33 cases in this category predominantly from the US and Canada. The largest earthquake postulated to be induced by this process is the 2011 M_W 5.7 Prague, Oklahoma, earthquake.

Water dams

The database contains 168 cases of earthquakes possibly induced by impounding water behind dams. Approximately 2.5% of reservoirs with volumes > 0.1 km^3 are reported to be seismogenic. The largest postulated reservoir-related earthquake is the great 2008 M_W ~8 Wenchuan, earthquake, China (Zipingpu dam) which caused ~ 90,000 fatalities.

Appendix 2: Explanations of database column headings.

Column Heading	Description
Country	Country where the project is/was geographically located
Eq cause (main class)	Overall project type, *e.g.*, geothermal, proposed to have caused the earthquake
Eq cause (subclass)	Type of project within the main class, *e.g.*, geothermal (injection), proposed to have caused the earthquake
Name	Project name
Latitude (˚N)	Project latitude
Longitude (˚W)	Project longitude
Start date of project	Start of project or main phase relevant to earthquakes
End date of project	End of project or main phase relevant to earthquakes
Start date of earthquakes or monitoring	Date of onset of seismicity (monitoring already in place) or the date monitoring commenced
End date of earthquakes or monitoring	Date seismicity ceased or the date monitoring equipment was removed
Delay time	Time between the start of the project and the onset of seismicity
No. eqs	Number of earthquakes recorded
Max magnitude (M_{MAX})	Observed maximum magnitude reported
Mag type	Type of magnitude reported for the maximum magnitude earthquake. Moment magnitude is reported if available. If moment magnitude was not reported, the largest magnitude of any type was recorded
Depth of largest eq (m)	Hypocentral depth of largest earthquake
Date of largest eq	Date of the largest earthquake
Year of largest eq	Year of the largest earthquake
Distance of M_{MAX} to project (m)	Horizontal distance of maximum magnitude earthquake from inducing project

Max distance to project (m)	Horizontal distance between the furthest observed earthquake (not necessarily the largest) and the inducing project
Lithology/resource	Reservoir lithology, *e.g.*, sandstone, or mining resource, *e.g.*, coal
Depth of most eq activity (m)	Depth at which most earthquake activity is observed
Depth of project (m)	Depth of the inducing activity, *e.g.*, the injection
Tectonic setting	Tectonic setting of project based on simple plate boundary model
Previous seismic activity	Notes on any seismicity prior to the start of the project
Dam height (m)	Height of the dam impounding the water reservoir
Injection/extraction rate (max unless stated, units in next column)	Rate of injection or extraction of material from the subsurface
Rate units	Units for rate of injection or extraction
Total volume or mass of material injected/extracted (units in next column	Total volume or mass of material injected into or extracted from the subsurface. For dams: the volume of the water reservoir
Volume or mass units	Units for volume or mass of material
Pressure (MPa) (max unless stated)	Maximum (unless stated) well head injection pressure during the project
Change in reservoir pressure (MPa)	Change in pressure of fluid in the subsurface reservoir
Stress change (MPa)	Change in stress postulated to have induced the earthquake
Area ($x10^6$ m^2)	Area of the project, *e.g.*, surface area of water reservoir
BHT (°C)	Bottom-hole temperature of borehole
Notes	Additional information about project or data
Reference(s)	Source of information on project
Reference(s) from Davies *et al.* [2013]	Source(s) used by Davies *et al.* (2013) for project

Appendix 3: List of the 705 entries in the database.

Country	Eq cause (main class)	Eq cause (subclass)	Name	Max mag (Mmax)	Mag type	Date of largest eq
Algeria	CCS	CO2 injection	In Salah	1.7	MW	
USA	CCS	CO2 injection	Decatur, Illinois, demonstration site	1.26	MW	
UK	Construction	Coastal engineering (geoengineering)	Folkestone	4.2	ML	2007/04/28
Taiwan	Construction	Construction	Taipei 101	3.8	ML	2004/10/23
Uzbekistan	Conventional Oil and Gas	Gas extraction and storage	Gazli	7.3	MS	1976/04/08
Canada	Conventional Oil and Gas	Secondary recovery (water injection)	Snipe Lake, Alberta	5.1	ML	1970/03/08
USA	Conventional Oil and Gas	Oil extraction	Long Beach (Wilmington and Huntington Beach oilfields), California	6.3	ML	1933
Iran	Conventional Oil and Gas	Oil extraction	Cheshmeh Khosh	6.2		2014/08/18
Canada	Conventional Oil and Gas	Oil extraction and Secondary recovery (water injection)	Eagle/Eagle West	4.3		1994/05/22
Canada	Conventional Oil and Gas	Secondary recovery	Gobles, Ontario	3.4		
Canada	Conventional Oil and Gas	Secondary recovery and Waste disposal	Cold Lake, Alberta	2	ML	
Italy	Conventional Oil and Gas	Gas extraction	Caviaga, Po Valley	5.5	ML	1951/05/15
Canada	Conventional Oil and Gas	EOR (CO2 injection/part CCS project)	Weyburn, Saskatchewan	-1		
USA	Conventional Oil and Gas	Gas extraction	El Reno, Oklahoma	5.2	ML	1952
USA	Conventional Oil and Gas	Oil extraction	Wilmington, California	5.1	ML	1949
China	Conventional Oil and Gas	Secondary recovery (water injection)	Renqiu	4.5	ML	1987/06/02
USA	Conventional Oil and Gas	Oil extraction	Richland County, Illinois	4.9	ML	1987
China	Conventional Oil and Gas	Secondary recovery (water injection)	Shengli, Shandong Province			
USA	Conventional Oil and Gas	Gas extraction	Fashing, Texas	4.8	MW	2011/10/20
Denmark	Conventional Oil and Gas	Oil and Gas extraction and Secondary recovery (water injection)	Dan			
Russia	Conventional Oil and Gas	Oil extraction	Starogroznenskoe	4.7	ML	1971/03/26
Kuwait	Conventional Oil and Gas	Oil extraction and Burning	Minagish/Umm Gudair oil fields (for	4.7		1993/06/02

			largest eq)			
USA	Conventional Oil and Gas	Gas extraction	Catoosa, Oklahoma	4.7	ML	
Norway	Conventional Oil and Gas	Secondary recovery (unintentional water injection into overburden)	Ekofisk	3	ML	2001/05/07
Russia	Conventional Oil and Gas	Oil and gas extraction	Gudermes	4.5		
Germany	Conventional Oil and Gas	Gas extraction	Rotenberg /Neuenkirchen	4.4	MW	2004/10/20
Norway	Conventional Oil and Gas		Vishund			
Romania	Conventional Oil and Gas	Secondary recovery (water injection)	Tazlau	-1.5	MW	
Spain	Conventional Oil and Gas	Gas storage	Castor	4.3	MW	2013/10/01
Saudi Arabia	Conventional Oil and Gas	Oil and gas extraction	Ghawar	4.24	ML	
France	Conventional Oil and Gas	Gas extraction	Lacq (Arette)	4.2	ML	1978
USA	Conventional Oil and Gas	Oil extraction	Wortham-Mexia, Texas	4		1932/04/09
Canada	Conventional Oil and Gas	Gas extraction	Strachan, Alberta	4	ML	
Russia	Conventional Oil and Gas	Oil extraction and Secondary recovery (water injection)	Romashkinskoye (Romashkino field), Volga-Ural	4	ML	1991/10/28
Russia	Conventional Oil and Gas	Oil extraction and Secondary recovery?	Grozny, Chechen Republic	3.3	ML	
Germany	Conventional Oil and Gas	Gas extraction	Soltau	4	ML	1977/06/02
Russia	Conventional Oil and Gas	Oil extraction and Secondary recovery (water injection)	Novo-Elkhovskoye, Volga-Ural			
USA	Conventional Oil and Gas	Oil and Gas extraction	Alice (Stratton field), Texas	3.9	mbLG	2010/04/25
Germany	Conventional Oil and Gas	Gas extraction	Skye (Bassum, Niedersachsen)	3.8	ML	2005/07/15
Turkmenistan	Conventional Oil and Gas	Oil extraction and Secondary recovery (water injection)	Barsa-Gelmes-Vishka	6		1984
USA	Conventional Oil and Gas	Oil extraction and Secondary recovery (water injection)	Coalinga, California	6.5	ML	1983
China	Conventional Oil and Gas	Gas extraction and storage	Hutubi, Southern Junggar Basin	3.6	ML	
USA	Conventional Oil and Gas	Oil extraction and Secondary recovery (water injection)	Kettleman North Dome, California	6.1	MW	1985
USA	Conventional Oil and Gas	Oil extraction and Secondary recovery (water injection)	Montebello (Whittier Narrows), California	5.9	ML	1987
Netherlands	Conventional Oil and Gas	Gas extraction	Bergermeer (Alkmaar)	3.5	MW	2001/09/09
USA	Conventional Oil and Gas	Gas extraction	East Durant, Oklahoma	3.5	ML	
USA	Conventional	Secondary recovery	Cogdell Field,	5.3	ML	1978/06

	Oil and Gas	(water injection)	Texas			/16
Netherlands	Conventional Oil and Gas	Gas extraction	Groningen	3.4	ML	2012/08 /06
USA	Conventional Oil and Gas	Oil extraction and Secondary recovery (water injection)	Brewton (Big Escambia Creek, Little Rock, and Sizemore Creek fields), Alabama	4.9	MW	1997/10 /24
USA	Conventional Oil and Gas	Oil extraction and Stimulation	Orcutt, California	3.5	ML	
USA	Conventional Oil and Gas	Oil extraction and Secondary recovery (water injection)	East Texas (Gladewater), Texas	4.7		1957/03 /19
Netherlands	Conventional Oil and Gas	Gas extraction	Roswinkel	3.4	ML	1997/02 /19
USA	Conventional Oil and Gas	EOR (CO2 injection)	Cogdell Field, Texas	4.4	MW	2011/09 /11
USA	Conventional Oil and Gas	Secondary recovery	Kermit, Texas	4	ML	
USA	Conventional Oil and Gas	Oil and Gas extraction and Secondary recovery (water injection)	Imogene (Pleasanton), Texas	3.9	ML	1984/03 /03
USA	Conventional Oil and Gas	Oil and gas extraction	War-Wink, Texas	3	ML	1975
USA	Conventional Oil and Gas	Production and Secondary recovery	Inglewood, California	3.7	ML	1962
USA	Conventional Oil and Gas	Oil extraction and Secondary recovery (water injection)	Falls City, Texas	3.6	mbLg	1991/07 /20
USA	Conventional Oil and Gas	Gas/Brine extraction and Wastewater (injection)	Azle/Reno,Texas	3.6		
USA	Conventional Oil and Gas	Secondary recovery	Hunt, Alabama /Mississippi	3.6	ML	
Germany	Conventional Oil and Gas	Gas extraction	Visselhövede	2.9	ML	2012/02 /13
Germany	Conventional Oil and Gas	Gas extraction	Völkersen	2.9	ML	2012/11 /22
USA	Conventional Oil and Gas	Secondary recovery	Dollarhide, Texas/New Mexico	3.5	ML	
Germany	Conventional Oil and Gas	Gas extraction	Langwedel	2.8	ML	2008/04 /03
Netherlands	Conventional Oil and Gas	Gas extraction	Eleveld	2.8	ML	1986/12 /26
Netherlands	Conventional Oil and Gas	Gas extraction	Assen	2.8	ML	1986
USA	Conventional Oil and Gas	Secondary recovery	Keystone I&II, Texas	3.5	ML	
Netherlands	Conventional Oil and Gas	Gas extraction	Middelie	2.7	ML	1989/12 /01
Netherlands	Conventional Oil and Gas	Gas extraction	Bergen	2.7	ML	2001/10 /10
Germany	Conventional Oil and Gas	Gas extraction	Verden	2.5	ML	2011/05 /02
Netherlands	Conventional Oil and Gas	Gas extraction	Annerveen	2.3	ML	1994/08 /16

Netherlands	Conventional Oil and Gas	Gas extraction	Appelscha	2.3	ML	2003/06/16
Netherlands	Conventional Oil and Gas	Gas extraction	Dalen	2.2	ML	1996/11/17
Netherlands	Conventional Oil and Gas	Gas extraction	Roden	2.1	ML	1996/09/02
France	Conventional Oil and Gas	Well collapse/Water injection	Lacq (Arette)	1.9	ML	1996/09/18
Oman	Conventional Oil and Gas	Gas extraction	Shuiba reservoir	2.05	ML	2001/03/04
Netherlands	Conventional Oil and Gas	Gas extraction	Emmen	2	ML	1991/02/15
USA	Conventional Oil and Gas	Secondary recovery	Ward-Estes, Texas	3.5	ML	
USA	Conventional Oil and Gas	Secondary recovery	North Panhandle (Lambert), Texas	3.4	ML	
Netherlands	Conventional Oil and Gas	Gas extraction	VriesNoord	1.9		1996 (Dec.)
USA	Conventional Oil and Gas	Secondary recovery	Ward-South, Texas	3	ML	
Netherlands	Conventional Oil and Gas	Gas extraction	Emmen-Nieuw Amsterdam	1.7		1994 (Sep.)
Czech Republic	Conventional Oil and Gas	Gas storage	Příbram (Háje)	1.5	ML	
Netherlands	Conventional Oil and Gas	Gas extraction	Schoonebeek	1.4		2002 (Dec.)
Netherlands	Conventional Oil and Gas	Gas extraction	Coevorden	1.2		1997 (Feb.)
Netherlands	Conventional Oil and Gas	Gas extraction	Ureterp	1		1999 (Apr.)
Netherlands	Conventional Oil and Gas	Gas extraction	VriesCentraal	1		2000 (July)
USA	Conventional Oil and Gas	Oil extraction	Seventy Six oil field, Clinton County, Kentucky	0.9	MW	
Netherlands	Conventional Oil and Gas	Gas storage	Bergermeer	0.7		2013 (Oct.)
USA	Conventional Oil and Gas	Secondary recovery	Dora Roberts, Texas	3	ML	
USA	Conventional Oil and Gas	Secondary recovery	Monahans, Texas	3	ML	
Norway	Conventional Oil and Gas	Oil extraction	Valhall			
USA	Conventional Oil and Gas	Secondary recovery	Sleepy Hollow, Nebraska	2.9	ML	
USA	Conventional Oil and Gas	Secondary recovery and Stimulation	Love County, Oklahoma	2.8	ML	
USA	Conventional Oil and Gas	Oil and Gas extraction and Secondary recovery	Apollo-Hendrick, Texas	2	MD	
USA	Conventional Oil and Gas	Oil and gas extraction	South Houston, Texas			
USA	Conventional Oil and Gas	Oil and gas extraction	Clinton, Texas			
USA	Conventional Oil and Gas	Oil and gas extraction	MyKawa, Texas			
USA	Conventional	Oil and gas	Blue Ridge, Texas			

	Oil and Gas	extraction				
USA	Conventional Oil and Gas	Oil and gas extraction	Webster, Texas			
USA	Conventional Oil and Gas	Oil and gas extraction	Goose Creek, Texas			
Venezuela	Conventional Oil and Gas	Oil and gas extraction	Costa Oriental, Lake Maracaibo			
USA	Conventional Oil and Gas	Oil extraction and Secondary recovery (water injection)	New Harmony, Indiana	1.8	MW	
USA	Conventional Oil and Gas	Secondary recovery (water injection)	South Eugene Island, Louisianna			
France	Conventional Oil and Gas	Gas extraction	Meillon			
Netherlands	Conventional Oil and Gas	Gas Storage	Norg			
Netherlands	Conventional Oil and Gas	Gas Storage	Grijpskerk			
USA	Conventional Oil and Gas	Stimulation	Austin Chalk, Giddings Field, Texas			
Canada	Fracking	Fracking (injection)	Northern Montney Earthquake, British Columbia	4.4	MW	2014/08/04
Canada	Fracking	Fracking (injection)	Crooked Lake (Fox Creek), Alberta (Waskahigan and McKinley fields)	4.4	ML	2015/01/23
Canada	Fracking	Fracking (injection)	Septimus (Montney Trend)	4.2	ML	2013/05/27
Canada	Fracking	Fracking (injection)	Fox Creek, Alberta	3.9	MW	2015/06/13
Canada	Fracking	Fracking (injection)	Horn River Basin	3.8	ML	2011/05/19
Canada	Fracking	Fracking (injection)	Beg-Town (Montney Trend)	3.4	ML	2013/08/21
Canada	Fracking	Fracking (injection)	Caribou (Montney Trend)	3.2	ML	2014/03/02
Canada	Fracking	Fracking (injection)	Cardston, Alberta (Ninastoko field)	3	ML	2011/12/04
Canada	Fracking	Fracking (injection)	Doe-Dawson (Montney Trend)	2.8	ML	2013/10/23
Canada	Fracking	Fracking (injection)	Altares (Montney Trend)	2.2	ML	2013/11/05
Canada	Fracking	Fracking (injection)	Montney Trend	-0.4	MW	
Canada	Fracking	Fracking (injection)	Western Canada	-2.2	MW	2006
UK	Fracking	Fracking (injection)	Preese Hall	2.3	ML	2011/04/01
USA	Fracking	Fracking (injection)	Eagleton 1-29, Oklahoma	3.2	ML	2014/07/07
USA	Fracking	Fracking (injection)	Poland Township, Ohio	3	ML	2014/03/10
USA	Fracking	Fracking (injection)	Oklahoma (Eola-Robberson field)	2.9	ML	2011/01/18
USA	Fracking	Fracking (injection)	Harrison County, Ohio	2	MW	2013/10/02

USA	Fracking	Fracking (injection+production ?)	Bienville Parish, Louisiana	1.9	ML	2011/10 /15
USA	Fracking	Fracking (injection)	Cotton Valley, Texas	-0.2	MW	1997/05 /14
USA	Fracking	Fracking (injection)	Jonah, Wyoming	-1.2		
USA	Fracking	Fracking (injection)	Hughes County, Oklahoma	-1.9		2007
Mexico	Geothermal	Geothermal (extraction)	Cerro Prieto (Imperial Valley)	6.6	ML	1979/10 /15
USA	Geothermal	EGS (circulation)	Salton Sea, California	5.1		2005
USA	Geothermal	EGS (circulation)	The Geysers	4.6		1982
Mexico	Geothermal	EGS (circulation)	Los Humeros	4.6	Md	1994/11 /25
El Salvador	Geothermal	EGS (injection)	Berlín	4.4	ML	2003/09 /16
Australia	Geothermal	EGS (injection)	Cooper Basin (Habanero 1)	3.7	MW	2003/11 /14
Italy	Geothermal	EGS (circulation)	Monte Amiata	3.5	ML	1983
Switzerland	Geothermal	EGS (injection)	Basel	3.4	ML	2006/12 /08
Switzerland	Geothermal	EGS (injection)	St. Gallen	3.3	MW	2013/07 /20
New Zealand	Geothermal	Geothermal (reinjection)	Rotokawa	3.3		2012 (Feb.)
Italy	Geothermal	EGS (circulation)	Larderello-Travale	3.2	ML	1982
New Zealand	Geothermal	Geothermal (reinjection)	Mokai	3.2		
Italy	Geothermal	EGS (injection)	Torre Alfina	3	ML	1977
El Salvador	Geothermal	EGS (injection)	Ahuachapan	3	ML	1991
Iceland	Geothermal	Geothermal (extraction)	Reykjanes	3	ML	2006
Australia	Geothermal	EGS (injection)	Cooper Basin (Habanero 4)	3	ML	
Italy	Geothermal	EGS (injection)	Latera	2.9	ML	1984/12 /09
France	Geothermal	EGS (injection)	Soultz (GPK-3)	2.9	ML	2003/06 /10
Australia	Geothermal	EGS (injection)	Cooper Basin (Habanero 1 restimulation)	2.9	ML	2005
USA	Geothermal	EGS (stimulation)	Coso	2.8		2004 (Aug.)
Germany	Geothermal	EGS (circulation)	Landau	2.7	ML	2009/08 /15
New Zealand	Geothermal	Geothermal (reinjection)	Ngatamariki	2.7		
Australia	Geothermal	EGS (injection)	Paralana 2	2.5	MW	2011/11 /13
Kenya	Geothermal	Geothermal (extraction)	Olkaria	2.5	Md	1996
Philippines	Geothermal	Geothermal (reinjection)	Puhagan	2.4	ML	1983 (Feb.)
France	Geothermal	EGS (injection)	Soultz (GPK-2)	2.4	MW	2000/07

						/16
Germany	Geothermal	EGS (circulation)	Unterhaching	2.4	ML	2008 (July)
Germany	Geothermal	EGS (injection)	Insheim	2.4	ML	2010 (Apr.)
Iceland	Geothermal	EGS (injection)	Hellisheidi	2.4	ML	
USA	Geothermal	EGS (injection)	Newberry	2.39	MW	2012/07 /12
Italy	Geothermal	EGS (injection)	Cesano	2	ML	1978
UK	Geothermal	EGS (circulation)	Rosemanowes	2	ML	1987/07 /12
Iceland	Geothermal	EGS (circulation)	Krafla	2	ML	
Japan	Geothermal	EGS (injection)	Ogachi (OGC-1)	2	MW	
Indonesia	Geothermal	EGS (circulation)	Lahendong	2		
Mexico	Geothermal	EGS (injection)	Los Azufres	1.9	Md	
Germany	Geothermal	EGS (injection)	Bad Urach	1.8	MW	2002
USA	Geothermal	EGS (injection)	Desert Peak, Nevada	1.7	ML	
France	Geothermal	EGS (injection)	Rittersshoffen, Alsace	1.6	Mlv	2013/07 /02
Australia	Geothermal	EGS (injection)	Cooper Basin (Jolokia 1)	1.6	ML	
Australia	Geothermal	EGS (injection)	Paralana 2 DFIT	1.4	ML	
USA	Geothermal	EGS (injection)	Fenton Hill, New Mexico	1.3		1983
Germany	Geothermal	EGS (injection)	GeneSys, Hannover	0	ML	
Sweden	Geothermal	EGS (injection)	Fjällbacka	-0.2	ML	
Japan	Geothermal	EGS (injection)	Hijiori (SKG-2 injection/stimulation)	-1		1988
Germany	Geothermal	EGS (injection)	Groß-Schönebeck	-1	MW	2007
Iceland	Geothermal	EGS (circulation)	Laugaland	-1	ML	
Iceland	Geothermal	EGS (injection)	Svartsengi	-1	ML	
Japan	Geothermal	EGS (circulation)	Hijiori (SkG-2 circulation)	-1		
USA	Geothermal	EGS (injection)	Baca, New Mexico	-2		1982 (May)
Mexico	Geothermal	Drilling, Stimulation and Production tests	Tres Virgenes, LV-06			
Turkey	Geothermal	EGS (circulation)	Salavatli, Aydin			
USA	Geothermal	EGS (circulation)	Brady, Nevada			
Indonesia	Geothermal	EGS (injection)	Darajat			
Indonesia	Geothermal	EGS (injection)	Wayang Windu			
USA	Geothermal	EGS (circulation)	Raft River, Idaho			
Nepal		Groundwater (extraction)	Gorkha earthquake, Indo-Gangetic plains	7.8	MW	2015/04 /25
Spain		Groundwater (extraction)	Lorca	5.1	MW	2011/05 /11
Spain		Groundwater extraction/Water dam	Jaen (Giribaile reservoir)	3.72	MW	2013/05 /02
Brazil		Groundwater	Bebedouro, Paraná	2.9		2005

		(extraction)	Basin			(Mar.)
USA		Groundwater extraction	San Joaquin Valley			
Russia	Mining	Mining	Bachatsky, Kuzbass	6.1	ML	2013/06/18
Germany	Mining	Mining (collapse/fluid-induced rockburst)	Volkershausen (Ernst Thaelmann/Merkers mine)	5.6	ML	1989/03/13
Australia	Mining	Mining and Groundwater extraction	Newcastle	5.6	ML	1989/12/27
South Africa	Mining	Mining	President Brand Mine, Welkom	5.6	mb	1994/10/30
Australia	Mining	Mining	Ellalong	5.4	ML	1994/08/06
Australia	Mining	Mining	Maitland	5.3	ML	18/06/1868
Australia	Mining	Mining	Boolaroo	5.3	ML	1925/12/18
South Africa	Mining	Mining	Klerksdorp (DRDGold's North West Operations)	5.3	ML	2005/03/09
USA	Mining	Mining (solution)	Attica, New York	5.2	ML	1929/08/12
Germany	Mining	Mining	Sunna (Suenna)	5.2	ML	1975/06/23
South Africa	Mining	Mining	Welkom	5.2	ML	1976/12/08
USA	Mining	Mining (collapse)	Solvay mine, Wyoming	5.2	mb	1995/02/03
Russia	Mining	Mining (rock burst)	Umbozero Mine	5.1	ML	1999/08/17
Germany	Mining	Mining	Heringen	5	ML	
Poland	Mining	Mining	Lubin mine	5	ML	1977/03/24
South Africa	Mining	Mining	Hartebeesfontein	5	ML	1997/08/21
Australia	Mining	Mining	Kalgoorlie Super Pit	5	ML	2010/04/20
Canada	Mining	Mining (rockburst)	Wright-Hargreaves mine, Ontario	5		1905/05/17
South Africa	Mining	Mining	Free State Goldfield	4.7	ML	1989/01/25
South Africa	Mining	Mining	Carletonville	4.7	ML	1992/03/07
Russia	Mining	Mining (collapse)	Solikamsk, Upper Kama	4.7		1994/01/05
Germany	Mining	Mining (collapse)	Saale (Halle) (Teutschental mine)	4.6	MW	42/5/1940
China	Mining	Mining (solution)	Salt mine, Zigong, Sichuan	4.6	ML	1985/03/29
Germany	Mining	Mining	Ibbenbüren	4.6	ML	1991/05/16
USA	Mining	Mining	Moss No. 2, Virginia	4.5	ML	1972/05/20

USA	Mining	Mining (extraction and abandonment)	Cacoosing Valley (Sinking Springs), Pennsylvania	4.4	ML	1994/01/16
Russia	Mining	Mining (rock burst)	SKRU-2, Ural Mountains	4.4		1995/01/05
Australia	Mining	Mining	Appin, Tower and West Cliff Collieries	4.4		1999/03/17
Belarus	Mining	Mining	Soligorsk (Starobin deposit)	4.4		2003/12/18
South Africa	Mining	Mining	Savuka, Carletonville	4.4	ML	2007
China	Mining	Mining	Taiji mine, Beipiao, Liaoning	4.3	ML	1977/04/28
China	Mining	Mining	Chayuan mine, Shizhu, Sichuan	4.3	ML	1987/07/02
Russia	Mining	Mining (rock burst)	Kurgazakskaya Mine	4.3	ML	1990/05/28
China	Mining	Mining	Louguanshan #4 well, South Bureau, Sichuan	4.3	ML	1994/04/15
China	Mining	Mining	Weixi mine, Leshan, Sichuan	4.2	ML	1979/08/15
China	Mining	Mining	Mentougou mine, Beijing, Beijing	4.2	ML	1994/05/19
USA	Mining	Mining	Willow Creek, Utah	4.2	ML	2000/03/07
Poland	Mining	Mining	Rudna mine	4.2	ML	2013/03/19
Germany	Mining	Mining	Ruhr area	4.1	MW	1936/11/03
China	Mining	Mining	Huachu mine, Liuzhi, Guizhou	4.1	ML	1982/03/20
Russia	Mining	Mining (rock burst)	Kirovsky Mine, Khibiny Massif (Kola Peninsula)	4.1	ML	1989/04/16
Russia	Mining	Mining (rock burst)	Blinovo-Kamensky Mine	4.1	ML	1994/07/29
Canada	Mining	Mining	Creighton, Ontario	4.1	MN	2006/11/29
France	Mining	Mining	Lorraine	4	MW	1973/04/20
USA	Mining	Mining	Buchanan No. 1, Virginia	4	ML	1988/04/14
USA	Mining	Mining	Lynch mine, Kentucky	4		1995/03/11
South Africa	Mining	Mining	Western Deep Levels East	4	ML	1996/05/05
Germany	Mining	Mining	Saar (Primsmulde), Saarland	4	ML	2008/02/23
South Africa	Mining	Mining	Kloof	4	ML	
Italy	Mining	Mining (tunneling) and hydrologic changes	Gran Sasso	3.9		1992/08/25
South Africa	Mining	Mining	Deelkraal	3.9	ML	
South Africa	Mining	Mining	East Driefontain	3.9	ML	

Germany	Mining	Mining	Peissenberg	3.8	MW	1967/09/16
China	Mining	Mining	Wacang/Shimacao/ Chenjiapo mines, Yichang, Hubei	3.8	ML	1971/06/17
USA	Mining	Mining (collapse)	King #4, Utah	3.8	ML	1981/05/14
USA	Mining	Mining	Lynch No. 37, Kentucky	3.8	ML	1994/08/03
China	Mining	Mining	Wulong mine, Fuxin, Liaoning	3.8	ML	2004/06/16
Canada	Mining	Mining	Copper Cliff North, Ontario	3.8	MN	2008/09/11
Canada	Mining	Mining	Kidd Creek, Ontario	3.8	MN	2009/01/06
South Africa	Mining	Mining	Elandsrand	3.8	ML	
Czech Republic	Mining	Mining	CSA Mine, Ostrava-Karvina Coal Basin	3.75		1983/04/27
China	Mining	Mining	Nanshan mine, Hegang, Heilongjiang	3.7	ML	2001/02/01
China	Mining	Mining	Laohutai mine, Fushun, Liaoning	3.7	ML	2002/01/26
Germany	Mining	Mining	Saar/Lorraine	3.7	MW	2008/02/23
South Africa	Mining	Mining	Mponeng	3.7	ML	
South Africa	Mining	Mining	Leeudoorn	3.7	ML	
China	Mining	Mining	Huaibaoshi mine, Zigui, Yichang, Hubei	3.6	ML	1972/03/13
Poland	Mining	Mining	Belchatow	3.6	ML	1979/08/17
China	Mining	Mining	Taozhuang mine, Zaozhuang, Shandong	3.6	ML	1982/01/07
USA	Mining	Mining (collapse and rockburst)	Jim Walter Resources, Inc., No. 4, Alabama	3.6	ML	1986/05/07
China	Mining	Mining	Liu zhi mine, Yingpan, Liuzhi, Guizhou	3.6	ML	1991/07/09
China	Mining	Mining	Bingshuijing mine, Yingpan, Liuzhi, Guizhou	3.6	ML	1991/07/09
USA	Mining	Mining	Soldier Creek, Utah	3.6	ML	1993/01/21
USA	Mining	Mining (collapse)	Retsof, New York	3.6		1994/03/12
USA	Mining	Mining (collapse)	Genesseo, New York	3.6		1994
Russia	Mining	Mining (rock burst)	Tashtagol Mine	3.6	ML	1999/10/24
China	Mining	Mining (collapse)	Shunyuan mine, Zaozhuang, Shandong	3.6	ML	2002/05/20
Russia	Mining	Mining (rock burst)	Karnasurt Mine	3.6	ML	2002/12

						/17
USA	Mining	Mining (collapse)	Cottonwood, Utah	3.5	ML	1992/07 /05
Germany	Mining	Mining	Saar (Dilsburg Ost), Saarland	3.5	ML	2000 (Nov.)
Russia	Mining	Mining	Mine 15-15bis	3.5	ML	2010/02 /13
Australia	Mining	Mining	Olympia Dam	3.5		2013/05 /01
USA	Mining	Mining	Lucky Friday Mine, Idaho	3.5		
USA	Mining	Mining	Olga, West Virginia	3.4	ML	1965/04 /26
UK	Mining	Mining (extraction and collapse)	North Staffordshire (Stoke on Trent)	3.4	mb	1975/07 /15
USA	Mining	Mining (collapse)	Sunnyside #3, Utah	3.4	ML	1981/09 /21
China	Mining	Mining	Xujiadong 711 mine, Chenzhou, Hunan	3.4	ML	1998/03 /12
China	Mining	Mining	San he jian mine, Xuzhou, Jiangsu	3.4	ML	2003/05 /08
China	Mining	Mining	Chengzi mine, Beijing, Beijing	3.4	ML	
USA	Mining	Mining	Wappingers Falls, New York	3.3	mbn	1974/06 /07
USA	Mining	Mining	Trail Mountain, Utah	3.3	ML	1987/12 /16
Germany	Mining	Mining (tunneling)	Saar (Primsmulde), Saarland (Roadway construction)	3.3	ML	2005 (May)
Canada	Mining	Mining	Garson, Ontario	3.3	MN	2008/12 /05
China	Mining	Mining	Huating mine, Pingliang, Gansu	3.3	ML	
Canada	Mining	Mining (rockburst)	Campbell mine, Ontario	3.3	MN	
UK	Mining	Mining	Nottinghamshire	3.2	ML	1984/03 /22
China	Mining	Mining	Niumasi mine, Shaoyang, Hunan	3.2	ML	1994/09 /04
Russia	Mining	Mining (rock burst)	Mine 14-14bis	3.2	ML	2004/03 /25
Sweden	Mining	Mining (rock burst)	Grängesberg ore mine	3.1	ML	1974/08 /30
Germany	Mining	Mining	S-Harz	3.1	MW	1983/07 /02
China	Mining	Mining	Xifeng Nan shan mine, Lindong, Guizhou	3.1	ML	1991/04 /06
USA	Mining	Mining (collapse)	Star Point #2, Utah	3.1	ML	1991/02 /06
Bulgaria	Mining	Mining (solution)	Provadia	3.1	MD	1994/06 /20
China	Mining	Mining	Qixingjiezhen mine, Lianyuan, Hunan	3.1	ML	1996/03 /28

China	Mining	Mining	Shanjiaocun mine, Panjiang, Guizhou	3.1	ML	1997/12/05
China	Mining	Mining	Yueliangtian mine, Panjiang, Guizhou	3.1	ML	1997/12/05
Canada	Mining	Mining	Macassa, Ontario	3.1	MN	2008/07/12
India	Mining	Mining (abandonment)	Champion Reef, Kolar Gold field	3.09	ML	
Canada	Mining	Mining	Cory Mine, Saskatchewan	3	mb	1980/02/29
USA	Mining	Mining (collapse)	Deer Creek, Utah	3	ML	1984/03/21
USA	Mining	Mining (collapse)	Castle Gate #3, Utah	3	ML	1986/10/30
USA	Mining	Mining	VP No. 3, Virginia	3	ML	1987/03/04
China	Mining	Mining	Xindong mine, Shaoyang, Hunan	3	ML	1994/11/20
USA	Mining	Mining	Skyline #3, Utah	3	ML	1996/06/02
China	Mining	Mining	Fangshan mine, Beijing, Beijing	3	ML	1997/02/18
USA	Mining	Mining (solution)	Cleveland, Ohio	3	ML	
USA	Mining	Mining (abandonment and flooding)	Mineville, New York	3	Mc	
USA	Mining	Mining	Galena mine, Idaho	3	ML	
Canada	Mining	Mining (rockburst)	Quirke mine, Ontario	3		
Poland	Mining	Mining	Polkowice mine	3	MW	
China	Mining	Mining	En kou mine, Lowde, Hunan	2.9	ML	1976/01/08
USA	Mining	Mining	Dillsburg, Pennsylvania	2.9	ML	2009/04/24
China	Mining	Mining	Huayazi mine, Zigui, Yichang, Hubei	2.8	ML	1973 (Mar.)
China	Mining	Mining	Sheng li mine, Fushun, Liaoning	2.8	ML	1978/09/21
China	Mining	Mining	Da he bian mine, Shiucheng, Guizhou	2.8	ML	1985/07/09
UK	Mining	Mining	Midlothian	2.8	ML	1986/10/09
China	Mining	Mining	Mei tan ba mine, Xifenglun, Hunan	2.8	ML	1991/04/23
China	Mining	Mining	Niwan mine, Xiangtan, Hunan	2.8	ML	2003/01/17
China	Mining	Mining	Benxi Caitun mine, Shenyang, Liaoning	2.8	ML	2004/04/13
China	Mining	Mining	Baidong mine, Datong, Shanxi	2.7	ML	1983 (Sep.)
China	Mining	Mining	Sijiaotian mine, Yingpan, Liuzhi, Guizhou	2.7	ML	1985/01/21

China	Mining	Mining	Dizong mine, Yingpan, Liuzhi, Guizhou	2.7	ML	1985/01/21
China	Mining	Mining	Dayong mine, Yingpan, Liuzhi, Guizhou	2.7	ML	1985/01/21
Canada	Mining	Mining	Strathcona, Ontario	2.7	mN	1988/06/19
China	Mining	Mining	Dahuatang mine, Shaoyang, Hunan	2.7	ML	1997/12/04
China	Mining	Mining	Qingshan mine, Lianyuan, Hunan	2.6	ML	1996/07/01
Sweden	Mining	Mining	Zingruvan	2.6	MW	
China	Mining	Mining	Longfeng mine, Fushun, Liaoning	2.5	ML	1981/02/16
China	Mining	Mining	Doulishan mine, Lowde, Hunan	2.5	ML	1985/03/04
China	Mining	Mining	Yan guan mine, Zigui, Yichang, Hubei	2.5	ML	1988/05/14
France	Mining	Mining (abandonment and flooding)	Gardanne	2.5		2005 (Nov.)
Spain	Mining	Mining (collapse)	Lo Tacón (Torre Pacheco)	2.4	MW	1998/05/02
Switzerland	Mining	Mining (tunneling)	MFS Faido (Gotthard basetunnel)	2.4	ML	2006/03/25
Canada	Mining	Mining	Fraser, Ontario	2.4	MN	2008/10/16
Korea	Mining	Mining	Dogye	2.4	ML	
USA	Mining	Mining	Lompoc diatomite mine, California	2.3	MD	1995/04/05
USA	Mining	Mining	Florida, New York	2.3		2003
China	Mining	Mining	Gangdong mine, Shuangyashan, Heilongjiang	2.3	ML	
Sweden	Mining	Mining	Dannemora	2.27	MD	
China	Mining	Mining	Qiao tou he mine, Lowde, Hunan	2.2	ML	1974/05/31
UK	Mining	Mining	Rotherham (Yorkshire)	2.2	ML	1988/10/14
China	Mining	Mining	Kaiyang mine, Jinzhong, Kaiyang, Guizhou	2.2	ML	1990/10/23
UK	Mining	Mining	Bargoed Mid Glamorgan (South Wales)	2.2	ML	1992/08/17
South Africa	Mining	Mining	TauTona, Carletonville	2.2		2004/12/12
Canada	Mining	Mining	Craig, Ontario	2.2	MN	2007/06/22
Poland	Mining	Mining	Wujek mine	2.2	MW	
Poland	Mining	Mining	Ziemowit mine	2.2	MW	
Japan	Mining	Mining (hydraulic extraction rockburst)	Sunagawa mine	2.1	ML	1986/01/29

UK	Mining	Mining	Buxton (Derbyshire)	2.1	ML	1989/09/04
China	Mining	Mining	Jinhuagong mine, Datong, Shanxi	2.1	ML	
UK	Mining	Mining	Sunderland (Durham and Northumberland)	2	ML	1988/05/05
China	Mining	Mining	Shuikoushan mine, Hengnan, Hunan	2	ML	
Czech Republic	Mining	Mining	Mayrau mine	2	ML	
UK	Mining	Mining	Bolton (Lancashire)	1.7	ML	1989/03/11
China	Mining	Mining	Shi xia jiang mine, Shaoyang, Hunan	1.6	ML	1991 (Dec.)
Finland	Mining	Mining	Pyhäsalmi	1.2	MW	
USA	Mining	Mining	Beatrice, Virginia	1	ML	1974/05/15
USA	Mining	Mining (solution)	Dale, New York	1	ML	
Australia	Mining	Mining (rock fracture)	Moonee Colliery	0.6	MW	1998
USA	Mining	Mining (collapse)	Springfield Pike Quarry, Pennsylvania	0.2	MW	2000/02/21
China	Mining	Mining	Dagandsham Hydropower Station	-0.2	MW	
France	Mining	Mining (solution)	Arkema-Vauvert	-0.24	MW	
Canada	Mining	Shaft excavation	Underground Research Laboratory, Manitoba	-1.9	MW	
South Africa	Mining	Mining (collapse)	Ophirton			1908
USA	Mining	Mining (collapse)	Wilkes-Barre, Pennsylvania			1954 (Feb.)
China	Mining	Mining (tunneling rock burst)	Dongguashan (Shizishan copper mine), Tongling, Hunan (Roadway construction)			1999 (Mar.)
China	Mining	Mining (tunneling rock burst)	Tianshengqiao II Hydropower Station (Head race tunnel construction)			1990/12/11
Chile	Mining	Mining	El Teniente			1992 (Mar.)
India	Mining	Mining	Chinakuri Colliery			
Russia	Mining	Mining	Gluboky Mine, Streltsovsk			
Australia	Mining	Mining	Mount Charlotte Mine			
Russia	Mining	Mining (collapse)	Berezniki-1 Mine			
Kazakhstan	Mining	Mining	Zhezkazgan Mine			
Australia	Mining	Mining	Southern Colliery, German Creek			
Japan	Mining	Mining	Horonai			
Norway	Mining	Mining (tunneling rock burst)	Road tunnel			

Sweden	Mining	Mining (tunneling rock burst)	Head race tunnel
Iraq	Mining	Mining (solution)	Mishraq
Sweden	Mining	Mining	Malmberget
Switzerland/Italy	Mining	Mining (tunneling rock burst)	Simplon Tunnel
Japan	Mining	Mining (tunneling rock burst)	Shimizu Tunnel
Japan	Mining	Mining (tunneling rock burst)	Kanetsu (Kan-Etsu) Tunnel
Sweden	Mining	Mining (tunneling rock burst)	Forsmark Nuclear Plant (Hydraulic tunnels construction)
Sweden	Mining	Mining (tunneling rock burst)	Ritsem Traffic Tunnel
China	Mining	Mining (tunneling rock burst)	Yuzixi I Hydropower Station (Head race tunnel construction)
China	Mining	Mining (tunneling rock burst)	Erlangshan Tunnel (Sichuan-Tibet Highway)
China	Mining	Mining (tunneling rock burst)	Qinling Railway Tunnel
China	Mining	Mining (tunneling rock burst)	Cangling Tunnel (Taizhou-Jiyun Highway)
China	Mining	Mining (tunneling rock burst)	Pubugou Hydropower Station
China	Mining	Mining (tunneling rock burst)	Jinping II Hydropower Station (Auxiliary tunnel)
China	Mining	Mining	Fuli mine, Hegang, Heilongjiang
China	Mining	Mining	Zhenxing mine, Hegang, Heilongjiang
China	Mining	Mining	Didao mine, Jixi, Heilongjiang
China	Mining	Mining	Yingcheng mine, Shulang, Jilin
China	Mining	Mining	Xian mine, Liaoyuan, Jilin
China	Mining	Mining	Tai xin mine, Liaoyuan, Jilin
China	Mining	Mining	Tiechang mine, Tonghua, Jilin
China	Mining	Mining	Hongtoushan mine, Fushun, Liaoning
China	Mining	Mining	Gaode mine, Fuxin, Liaoning
China	Mining	Mining	Dongliang mine, Fuxin, Liaoning
China	Mining	Mining	Guanshan mine, Beipiao, Liaoning
China	Mining	Mining	Benxi Niu xin tai mine, Shenyang, Liaoning

China	Mining	Mining	Binggou mine, Jianchang county, Liaoning
China	Mining	Mining	Chang/Zhang gou yu mine, Beijing, Beijing
China	Mining	Mining	Datai mine, Beijing, Beijing
China	Mining	Mining	Muchengjian mine, Beijing, Beijing
China	Mining	Mining	Tang shan mine, Kailuan, Hebei
China	Mining	Mining	Guan tai mine, Cixian, Hebei
China	Mining	Mining	Tongjialiang mine, Datong, Shanxi
China	Mining	Mining	Xin zhou yao mine, Datong, Shanxi
China	Mining	Mining	Meiyukou mine, Datong, Shanxi
China	Mining	Mining	Yongdingzhuang mine, Datong, Shanxi
China	Mining	Mining	Bayi mine, Zaozhuang, Shandong
China	Mining	Mining	Chaili mine, Zaozhuang, Shandong
China	Mining	Mining	Huafeng mine, Xinwen, Shandong
China	Mining	Mining	Sun cun mine, Xinwen, Shandong
China	Mining	Mining	Zhangzhuan mine, Xinwen, Shandong
China	Mining	Mining	Pan xi mine, Xinwen, Shandong
China	Mining	Mining	Dong tan mine, Yankuang, Shandong
China	Mining	Mining	Bao dian mine, Yankuang, Shandong
China	Mining	Mining	#2 mine, Weishanhu, Shandong
China	Mining	Mining	Qianqiu mine, Yima, Henan
China	Mining	Mining	Wumei mine, Hebi, Henan
China	Mining	Mining	Shier (Shi'er kuang?) mine, Pingdingshan, Henan
China	Mining	Mining	Quantai mine, Xuzhou, Jiangsu
China	Mining	Mining	Qishan mine, Xuzhou, Jiangsu
China	Mining	Mining	Zhangxiaolou mine, Xuzhou, Jiangsu

China	Mining	Mining	Zhangji mine, Xuzhou, Jiangsu
China	Mining	Mining	Yaoqiao mine, Datun, Jiangsu
China	Mining	Mining	Kong zhuang mine, Datun, Jiangsu
China	Mining	Mining	Leigu mine, Mianyang Beichuan, Sichuan
China	Mining	Mining	Wuyi mine, Shanxi
China	Mining	Mining	Tianchi mine, Mianzhu, Sichuan
China	Mining	Mining	Yanshitai mine, Wansheng district, Nantong, Chongqing
China	Mining	Mining	Nantong mine, Nantong, Chongqing
China	Mining	Mining	Hua gu shan mine, Xinyu, Jiangxi
China	Mining	Mining	Bajing mine, Gaoan, Jiangxi
China	Mining	Mining	Tungsten ore mine, Jiangxi
China	Mining	Mining	Manganese mine, Zunyi, Guizhou
China	Mining	Mining	Dongguashan (Shizishan copper mine), Tongling, Hunan
China	Mining	Mining	South manganese mine, Huayuan, Hunan
China	Mining	Mining	Manganese mine, Taojiang, Hunan
China	Mining	Mining	Phosphorus mine, Yichang, Hubei
China	Mining	Mining	Fengdouyan, Jiupanshan, Qishuping and Beitou mines, Jiupanshan, Yichang, Hubei
China	Mining	Mining	Yangmuxi mine, Changyang, Yichang, Hubei
China	Mining	Mining	Songyi mine, Yichang, Hubei
China	Mining	Mining	Gaofeng mine, Dachangjingtian, Guangxi
China	Mining	Mining	Tongkeng mine, Dachangjingtian, Guangxi
China	Mining	Mining	Manganese mine, Dounan, Yunnan
China	Mining	Mining	Manganese mine, Heqing, Yunnan

China	Mining	Mining (tunneling rock burst)	Lujialiang Tunnel (Chongqing-Yichang Highway)		
Australia	Mining	Mining	Cadia		
Australia	Mining	Mining	Queenstown, Tasmania		
Canada	Mining	Mining (rockburst)	Brunswick No. 12 mine		
Canada	Mining	Mining (rockburst)	Denison mine, Ontario		
Poland	Mining	Mining	Pstrowski mine		
Japan	Mining	Mining (rock burst)	Miike mine		
USA	Nuclear	Seismicity/faulting following nuclear detonation	Cannikin	4.9	mb
Russia	Nuclear	Seismicity/faulting following nuclear detonation	Novaya Zemlya site	4.8	mb
USA	Nuclear	Seismicity/faulting following nuclear detonation	Milrow	4.3	mb
USA	Nuclear	Seismicity/faulting following nuclear detonation	Benham, Nevada	4.2	ML
USA	Nuclear	Seismicity/faulting following nuclear detonation	Jorum, Nevada	3	ML
USA	Nuclear	Seismicity/faulting following nuclear detonation	Purse, Nevada	2	ML
USA	Nuclear	Seismicity/faulting following nuclear detonation	Handley, Nevada	2	ML
USA	Nuclear	Seismicity/faulting following nuclear detonation	Faultless		
USA	Nuclear	Seismicity/faulting following nuclear detonation	Hard Hat, Nevada		
USA	Nuclear	Seismicity/faulting following nuclear detonation	Rex, Nevada		
USA	Nuclear	Seismicity/faulting following nuclear detonation	Halfbeak, Nevada		
USA	Nuclear	Seismicity/faulting following nuclear detonation	Greeley, Nevada		
USA	Nuclear	Seismicity/faulting following nuclear detonation	Bourbon, Nevada		
USA	Nuclear	Seismicity/faulting following nuclear detonation	Buff, Nevada		
USA	Nuclear	Seismicity/faulting following nuclear detonation	Charcoal, Nevada		
USA	Nuclear	Seismicity/faulting following nuclear	Chartreuse		

		detonation				
USA	Nuclear	Seismicity/faulting following nuclear detonation	Nash, Nevada			
USA	Nuclear	Seismicity/faulting following nuclear detonation	Dumont, Nevada			
USA	Nuclear	Seismicity/faulting following nuclear detonation	Tan, Nevada			
USA	Nuclear	Seismicity/faulting following nuclear detonation	Boxcar, Nevada			
USA	Nuclear	Seismicity/faulting following nuclear detonation	Duryea, Nevada			
USA	Nuclear	Seismicity/faulting following nuclear detonation	Scotch, Nevada			
USA	Oil and Gas	Oil and Water extraction	Fashing Region (D Cluster)	3		2010/12/21
USA	Oil and Gas	Oil and Water extraction	Dimmit County (K Cluster), Texas	2.98		2010/03/08
USA	Oil and Gas	Oil and Water extraction	Dimmit County (M Cluster), Texas	2.72		2011/06/26
USA	Oil and Gas	Oil and Water extraction	Fashing Region (H Cluster)	2.62		2011/05/22
USA	Oil and Gas	Oil and Water extraction	Fashing Region (G Cluster)	2.4		2011/04/09
USA	Oil and Gas	Oil and Water extraction	Fashing Region (C Cluster)	2.12		2011/07/05
USA	Oil and Gas	Oil and Water extraction	Fashing Region (Event B)	1.94		2011/01/15
USA	Oil and Gas	Oil and Water extraction	Dimmit County (L Cluster), Texas	1.83		2010/04/26
Italy	Oil and Gas/Waste fluid injection	Oil and Gas/Wastewater injection	Cavone and San Giacomo fields, Mirandola License (Emilia sequence)	5.9	ML	2012/05/20
USA	Oil and Gas/Waste fluid injection	Oil and Gas/Wastewater injection	Fashing Region (F Cluster), Texas	3		2010/03/08
USA	Oil and Gas/Waste fluid injection	Oil and Gas/Wastewater injection	Bakken, North Dakota	2.5		2010/03/21
USA	Oil and Gas/Waste fluid injection	Oil and Gas/Wastewater injection	Cedar Creek Anticline, Montana	2.1		2010/04/27
USA	Research	Research and Secondary recovery (water injection)	Rangely, Colorado	3.1	ML	1970/04/21
New Zealand	Research	Water injection	Wairakei	3		1984 (June)
Philippines	Research	Research (injection)	Tongonan Geothermal field	3	mc	
Japan	Research	Water injection	Matsushiro	2.8		1970/01/25
Germany	Research	Brine (KBr, KCl)	KTB	1.2	ML	1994

		injection				
China	Research	Research (injection)	WFSD-3P	1		
Germany	Research	Fluid injection	KTB	0.7	ML	
Japan	Research	Research (injection)	Nojima	0.6		1997
Germany	Research	Water injection	KTB	0.5	ML	2000
France	Research	Research (solution mining)	Cerville-Buissoncourt	-0.8	MW	
France	Research	Research (injection)	Laboratoire Souterrain à Bas Bruit			
Germany	Research	Mine flooding	Hope mine			
USA	Research	Waste disposal	Frio Formation, Beaumont, near Jasper County, Texas			
USA	Waste fluid injection	Wastewater (injection)	Prague, Oklahoma	5.7	MW	2011/11/06
USA	Waste fluid injection	Waste disposal	Rocky Mountain Arsenal (Denver), Colorado	5.5	ML	1967
USA	Waste fluid injection	Wastewater (injection)	Raton Basin, Colorado and New Mexico	5.3	MW	2011/08/23
China	Waste fluid injection	Wastewater (injection)	Rongchang gas field	5.2	ML	1997/08/13
USA	Waste fluid injection	Wastewater (injection)	Oklahoma	5.1		2016/02/13
USA	Waste fluid injection	Wastewater (injection)	Painesville (Perry), Ohio	4.9	MW	1986/01/31
USA	Waste fluid injection	Wastewater (injection)	Timpson, East Texas	4.8	MWrmt	2012/05/17
USA	Waste fluid injection	Wastewater (injection)	Arkansas	4.7		2011/02/27
USA	Waste fluid injection	Wastewater (injection)	Central Valley (WWF), California	4.6	MW	2005/09/22
China	Waste fluid injection	Wastewater (injection)	Huangjiachang gas field	4.4	ML	2009/02/16
USA	Waste fluid injection	Brine injection	Paradox Valley, Colorado	4.3		2000/05/27
USA	Waste fluid injection	Waste disposal	Ashtabula, Ohio	4.3	Mblg	2001/01/26
USA	Waste fluid injection	Wastewater injection	Cushing, Oklahoma	4.3	MW	2014 (Oct.)
USA	Waste fluid injection	Wastewater (injection)	Dagger Draw, New Mexico	4.1	MW	2005 (Dec.)
Canada	Waste fluid injection	Wastewater (injection)	Cordel (Brazeau Cluster)	4	ML	1997/03/31
Canada	Waste fluid injection	Wastewater (injection)	Graham (Montney Trend)	4	ML	2010
USA	Waste fluid injection	Wastewater injection	Marcotte oil field (Palco), Kansas	4		1989
USA	Waste fluid injection	Wastewater injection	Guthrie, Oklahoma	4		2014
USA	Waste fluid injection	Wastewater (injection)	Jones, Oklahoma	4		2008?
USA	Waste fluid	Wastewater	Youngstown, Ohio	3.88	MW	2011/12

	injection	(injection)				/31
USA	Waste fluid injection	Waste disposal	Lake Charles, Louisiana	3.8	ML	
USA	Waste fluid injection	Wastewater (injection)	Dallas-Fort Worth, Texas	3.3	mb	2009/05/16
USA	Waste fluid injection	Wastewater (injection)	Greeley, Colorado	3.2		2014/06/01
Canada	Waste fluid injection	Wastewater (injection)	Pintail (Montney Trend)	3.1	ML	2014
USA	Waste fluid injection	Waste disposal	El Dorado, Arkansas	3	ML	1983
USA	Waste fluid injection	Wastewater (injection)	Lillian (J-A cluster), Barnett Shale, Texas	3		2011/07/17
USA	Waste fluid injection	Deep fluid injection	Avoca, New York	2.9	Mblg	2001
USA	Waste fluid injection	Wastewater (injection)	Cleburne, Texas	2.8	MbLg	2009/06/09
Italy	Waste fluid injection	Wastewater injection	Val d'Agri oil field (CM2 well)	2.2	ML	2006
USA	Waste fluid injection	Wastewater injection	Fashing Region (A Cluster), Texas	1.82		2011/08/26
USA	Waste fluid injection	Wastewater injection	Dimmit County (Event J), Texas	1.52		2010/11/29
USA	Waste fluid injection	Wastewater injection	Center, Texas	1.5	ML	2010/12/01
USA	Waste fluid injection	Wastewater injection	Cedar Creek Anticline, North Dakota	1.4		2010/06/14
China	Water dam	Water dam	Zipingpu (Wenchuan earthquake)	7.9	MW	2008/05/12
USA	Water dam	Water dam	Lake Hebgen, Montana	7.1	MS	1959/08/17
Greece	Water dam	Water dam	Polyphyto	6.5	MS	1995/05/13
India	Water dam	Water dam	Koyna	6.3	MS	1967/12/10
Zambia–Zimbabwe	Water dam	Water dam	Kariba	6.2		1963/09/23
Greece	Water dam	Water dam	Kremasta	6.2		1966/02/05
China	Water dam	Water dam	Hsinfengkiang (Hsingfengchiang, Xinfengjiang)	6.1	MS	1962/03/18
India	Water dam	Water dam	Killari	6.1	MW	1993/09/30
Thailand	Water dam	Water dam	Srinagarind	5.9	ML	1983
USA	Water dam	Water dam	Oroville, California	5.8	ML	1975/08/01
Greece	Water dam	Water dam	Marathon	5.7		1938/07/20
Egypt	Water dam	Water dam	Aswan	5.7	ML	1981/11/14
Greece	Water dam	Water dam	Pournari	5.6	ML	1981/03/10

Australia	Water dam	Water dam	Warragamba (Varragamba)	5.5		1973/03/09
Greece	Water dam	Water dam	Asomata	5.4	MS	1984/10/25
France	Water dam	Water dam	Monteynard	5.3	ML	1962
Ghana	Water dam	Water dam	Akosombo	5.3		1964 (Nov.)
India	Water dam	Water dam	Kinnersani	5.3		1969/04/13
Uzbekistan	Water dam	Water dam	Charvak	5.3	ML	1977/03/15
USA	Water dam	Water dam	Coyote Valley (Leroy Anderson?), California	5.2		1962/06/06
China	Water dam	Water dam	Shenwo/Shenwu	5.2	ML	1974/12/02
Greece	Water dam	Water dam	Sfikia	5.2	MS	1986/02/18
USA	Water dam	Water dam	Hoover (Lake Mead), Nevada/Arizona	5	ML	1939
Australia	Water dam	Water dam	Eucumbene	5		1959/05/18
New Zealand	Water dam	Water dam	Benmore	5	ML	1966/07/07
India	Water dam	Water dam	Warna (Warana)	5		1993
Australia	Water dam	Water dam	Thomson	5	ML	1996
Zambia	Water dam	Water dam	Itezhi-Tezhi	5		2011/07/21
Japan	Water dam	Water dam	Kurobe	4.9	MS	1961/08/19
Serbia	Water dam	Water dam	Bajina Basta	4.9	ML	1967/07/03
USA	Water dam	Water dam	Kerr, Montana	4.9		1971/07/28
India	Water dam	Water dam	Bhatsa	4.9	ML	1983/09/15
Vietnam	Water dam	Water dam	Hoa Binh	4.9		1989
Russia	Water dam	Water dam	Lake Baikal	4.8		
Spain	Water dam	Water dam	Canelles	4.7		1962/06/09
Iran	Water dam	Water dam	Sefia Rud	4.7		1968/08/02
Canada	Water dam	Water dam	McNaughton (Mica)	4.7	ML	1973
China	Water dam	Water dam	Danjiangkou	4.7	ML	1973/11/29
USA	Water dam	Water dam	Anderson, Idaho	4.7	ML	1973
Vietnam	Water dam	Water dam	Song Tranh 2	4.7		2012/11/15
Georgia	Water dam	Water dam	Enguri (Inguri)	4.7		
Greece	Water dam	Water dam	Kastraki	4.6	ML	1969
Tadjikistan	Water dam	Water dam	Nurek	4.6	MS	1972/11/27
Kyrgyzstan	Water dam	Water dam	Toktogul	4.6	ML	1977

New Zealand	Water dam	Water dam	Lake Pukaki	4.6	ML	1978/12/17
Spain	Water dam	Water dam	Itoiz	4.6	mbLg	2004/09/18
China	Water dam	Water dam	Three Gorges	4.6	ML	2008/11/22
France	Water dam	Water dam	Vouglans	4.5	MW	1971/06/21
China	Water dam	Water dam	Foziling	4.5		1973/08/11
China	Water dam	Water dam	Dahua	4.5		1993
Italy	Water dam	Water dam	Pieve de Cadore	4.4		1960/01/13
Italy	Water dam	Water dam	Piastra	4.4		1966/04/07
China	Water dam	Water dam	Dongjing/Dongqing	4.4		2010/01/17
USA	Water dam	Water dam	Clark Hill, South Carolina/Georgia	4.3	ML	1974/08/02
Iran	Water dam	Water dam	Karun III	4.3	ML	2006/05/12
Brazil	Water dam	Water dam	P. Colombia/Volta Grande	4.2		1974/02/24
Armenia	Water dam	Water dam	Tolors	4.2		1982
Albania	Water dam	Water dam	Komani	4.2	ML	1986
Russia	Water dam	Water dam	Bratsk	4.2		1996
China	Water dam	Water dam	Longtan	4.2	ML	2007/07/17
Spain	Water dam	Water dam	Camarillas	4.1		1964/04/15
Canada	Water dam	Water dam	Mica	4.1		1974/01/05
Canada	Water dam	Water dam	Manic-3, Quebec	4.1	mbLg	1975/10/23
Brazil	Water dam	Water dam	Nova Ponte	4	mb	1998 (May)
Spain	Water dam	Water dam	Tous New	4	mb	2000/10/08
USA	Water dam	Water dam	Jocassee, South Carolina	3.9	ML	1979/08/25
Paraguay	Water dam	Water dam	Yacyreta	3.9	mR	2000/04/28
Algeria	Water dam	Leakage from pumping between reservoirs (unintentional injection)	Beni Haroun dam/reservoir and the Oued Athmania reservoir	3.9	Md	2007/12/18
China	Water dam	Water dam	Xiaowan	3.9	ML	2012/09/16
USA	Water dam	Water dam	Keowee, South Carolina	3.8		1971/07/13
India	Water dam	Water dam	Dhamni	3.8	ML	1994
USA	Water dam	Water dam	Palisades, Idaho	3.7		1966/06/10

Brazil	Water dam	Water dam	Carmo do Cajuru	3.7		1972/01/23
Brazil	Water dam	Water dam	Capivara	3.7		27/3/1979, 07/01/1989
Canada	Water dam	Water dam	LG 3, Quebec	3.7	ML	1983
Pakistan	Water dam	Water dam	Mangla	3.6	ML	1967/05/28
China	Water dam	Water dam	Shengjiaxia (Shenjia Xiashuiku)	3.6		1984
Switzerland	Water dam	Water dam	Lac de Salanfe	3.5	MW	1953/10/17
Australia	Water dam	Water dam	Blowering	3.5		1973/01/06
Australia	Water dam	Water dam	Talbingo	3.5		1973/01/06
Turkey	Water dam	Water dam	Keban	3.5		1973
Switzerland	Water dam	Water dam	Emosson	3.5	ML	1974
India	Water dam	Water dam	Idukki	3.5		1977/07/02
India	Water dam	Water dam	Gandipet (Osman Sagar)	3.5	ML	1982
Italy	Water dam	Water dam	Ridracoli	3.5		1988
China	Water dam	Water dam	Yantan	3.5		1994
Poland	Water dam	Water dam	Czorsztyn Lake	3.5		2013/03/01
France	Water dam	Water dam	Eguzon	3.5		
India	Water dam	Water dam	Nagarjuna Sagar	3.5		
Japan	Water dam	Water dam	Hitotsuse	3.5		
Japan	Water dam	Water dam	Arimine	3.5		
Japan	Water dam	Water dam	Kuzuryu	3.5		
Japan	Water dam	Water dam	Midono	3.5		
Japan	Water dam	Water dam	Makio	3.5		
Japan	Water dam	Water dam	Miomote	3.5		
Japan	Water dam	Water dam	Nagawado	3.5		
Japan	Water dam	Water dam	Narugo	3.5		
Japan	Water dam	Water dam	Ohkura	3.5		
Japan	Water dam	Water dam	Tohri (Tori)	3.5		
Japan	Water dam	Water dam	Uchikawa	3.5		
Japan	Water dam	Water dam	Yuda	3.5		
Brazil	Water dam	Water dam	Tucurui	3.4		1985
China	Water dam	Water dam	Wujiangdu	3.4	ML	1985
China	Water dam	Water dam	Lubuge	3.4		1988
Brazil	Water dam	Water dam	Balbina	3.4	mb	1990/03/25
France	Water dam	Water dam	Serre-Poncen	3.3		1966/08/23
China	Water dam	Water dam	Zhelin	3.2	ML	1972/10/14
India	Water dam	Water dam	Sriramsagar	3.2		1984/07

						/21
China	Water dam	Water dam	Shuikou	3.2		1994
Lesotho	Water dam	Water dam	Katse	3.1		1996
Algeria	Water dam	Water dam	Oued Fodda	3		1933 (May)
USA	Water dam	Water dam	Shasta, California	3		1944
Italy	Water dam	Water dam	Vajont	3	ML	1960
India	Water dam	Water dam	Mangalam	3		1963
Switzerland	Water dam	Water dam	Contra	3		1965 (Oct.)
Bosnia and Herzegovina	Water dam	Water dam	Grancarevo	3		1967
Japan	Water dam	Water dam	Kamafusa	3		1970
China	Water dam	Water dam	Qianjin	3		1971/10 /20
Brazil	Water dam	Water dam	Paraibuna– Paraitinga	3		1977
Brazil	Water dam	Water dam	Jaguari	3	mb	1985/12 /17
Cyprus	Water dam	Water dam	Kouris	3		1994-1995
Brazil	Water dam	Water dam	Irapé	3	ML	2006/05 /14
India	Water dam	Water dam	Rihand	3		
India	Water dam	Water dam	Parambikulam	3		
India	Water dam	Water dam	Ukai	3		
Pakistan	Water dam	Water dam	Tarbela	3		
Thailand	Water dam	Water dam	Tsengwen (Zengwen)	3		
USA	Water dam	Water dam	Monticello (Fairfield), California	2.9		1978 (Oct.)
China	Water dam	Water dam	Tongjiezi	2.9		1992
China	Water dam	Water dam	Nanchong	2.8		1974/07 /25
China	Water dam	Water dam	Hunanzhen	2.8		1979
Brazil	Water dam	Water dam	Açu	2.8		1994
Romania	Water dam	Water dam	Vidra Lotru	2.8		
Romania	Water dam	Water dam	Vidraru-Arges	2.8		
Japan	Water dam	Water dam	Takase	2.7		1982
USA	Water dam	Water dam	Heron, New Mexico	2.7	ML	
Albania	Water dam	Water dam	Fierza	2.6		1981
India	Water dam	Water dam	Kadana	2.5		
Brazil	Water dam	Water dam	Miranda	2.4	mb	1998/04 /07
China	Water dam	Water dam	Nanshui	2.3		1970
China	Water dam	Water dam	Huangshi	2.3		1974/09 /21
Brazil	Water dam	Water dam	Serra da Mesa	2.2	mb	1999/06 /13
France	Water dam	Water dam	Sainte-Croix	2.2		

Italy	Water dam	Water dam	Pertusillio	2.1	ML	
USA	Water dam	Water dam	Cabin Creek, Colorado	2		1968
South Africa	Water dam	Water dam	Hendrik Verwoerd (Gariep)	2		1971
Spain	Water dam	Water dam	Almendra	2		1972 (Jan.)
Austria	Water dam	Water dam	Schlegeis	2		1973 (Apr.)
Brazil	Water dam	Water dam	Marimbondo	2	ML	1978/07/25
Brazil	Water dam	Water dam	Sobradinho	2		1979
Brazil	Water dam	Water dam	Emborcacao	2		1984
India	Water dam	Water dam	Sholayar	2		
India	Water dam	Water dam	Sharavathi (Sharavati)	2		
Romania	Water dam	Water dam	Ievorul Muntelui-Bicaz	2		
Brazil	Water dam	Water dam	Xingó	1.7	mb	1994/07/20
India	Water dam	Water dam	Mula	1.5		1972
Canada	Water dam	Water dam	Toulnustouc	1.4	mN	2005/02/26
Brazil	Water dam	Water dam	Castanhão	1.4	mb	
Canada	Water dam	Hydroelectric tunnel	Toulnustouc	0.8	mN	2005/04/09
France	Water dam	Water dam	Grandval			1963/08/05
Spain	Water dam	Water dam	El Cenajo			1973
Australia	Water dam	Water dam	Gordon River Power Development Storage			
Indonesia	Water dam	Water dam	Saguling-Cirata			
Spain	Water dam	Water dam	El Grado			
Spain	Water dam	Water dam	La Cohilla			1975
USA	Water dam	Water dam	Rocky Reach, Washington			
USA	Water dam	Water dam	San Luis, California			
USA	Water dam	Water dam	Sanford, Michigan			

Appendix 4: Electronic copy of the database.

Appendix 5: Electronic copy of the EndNote library of publications relating to induced earthquakes.

Appendix 6: Bibliography.

Adams, R. D. (1969), Seismic effects at Mangla Dam, Pakistan, Nature, 222, 1153-1155.

Adushkin, V. V., V. Rodionov, N, S. Turuntaev, and A. E. Yudin (2000), Seismicity in the oil field.

Adushkin, V. V., and A. Spivak (2015), Underground explosions, DTIC Document.

Ake, J., K. Mahrer, D. O'Connell, and L. Block (2005), Deep-injection and closely monitored induced seismicity at Paradox Valley, Colorado, Bulletin of the Seismological Society of America, 95, 664-683.

Albaric, J., V. Oye, N. Langet, M. Hasting, I. Lecomte, K. Iranpour, M. Messeiller, and P. Reid (2014), Monitoring of induced seismicity during the first geothermal reservoir stimulation at Paralana, Australia, Geothermics, 52, 120-131.

Alcott, J. M., P. K. Kaiser, and B. P. Simser (1998), Use of microseismic source parameters for rockburst hazard assessment, in Seismicity caused by mines, fluid injections, reservoirs, and oil extraction, pp. 41-65, Springer.

Al-Enezi, A., L. Petrat, R. Abdel-Fattah, and G. D. M. Technologie (2008), Induced seismicity and surface deformation within Kuwait's oil fields, paper presented at Proc. Int. Conf. Geol. Seismol.

Allis, R. G., S. A. Currie, J. D. Leaver, and S. Sherburn (1985), Results of injection testing at Wairakei geothermal field, New Zealand, Trans. GRC, 289-294.

Alvarez-Garcia, I. N., F. L. Ramos-Lopez, C. Gonzalez-Nicieza, M. I. Alvarez-Fernandez, and A. E. Alvarez-Vigil (2013), The mine collapse at Lo Tacón (Murcia, Spain), possible cause of the Torre Pacheco earthquake (2nd May 1998, se Spain), Engineering Failure Analysis, 28, 115-133.

Amidzic, D., S. K. Murphy, and G. Van Aswegen (1999), Case study of a large seismic event at a South African gold mine, paper presented at 9th ISRM Congress, International Society for Rock Mechanics.

Amos, C. B., P. Audet, W. C. Hammond, R. Bürgmann, I. A. Johanson, and G. Blewitt (2014), Uplift and seismicity driven by groundwater depletion in central California, Nature, 509, 483-486.

Arabasz, W. J., J. Ake, M. K. McCarter, and A. McGarr (2002), Mining-induced seismicity near Joes Valley dam: Summary of ground-motion studies and assessment of probable maximum magnitude, Technical Report, University of Utah Seismograph Stations, Salt Lake City, Utah, 35 pp. Accessible online at www/seis. utah. edu/Reports/sitla2002b.

Arabasz, W. J., S. J. Nava, M. K. McCarter, K. L. Pankow, J. C. Pechmann, J. Ake, and A. McGarr (2005), Coal-mining seismicity and ground-shaking hazard: A case study in the Trail Mountain area, Emery County, Utah, Bulletin of the Seismological Society of America, 95, 18-30.

Arkhipova, E. V., A. D. Zhigalin, L. I. Morozova, and A. V. Nikolaev (2012), The Van earthquake on October 23, 2011: Natural and technogenic causes, paper presented at Doklady Earth Sciences, Springer.

Armbruster, J. G., D. W. Steeples, and L. Seeber (1989), The 1989 earthquake sequence near Palco, Kansas: A possible example of induced seismicity (abstract), Seismological Research Letters, 60, 141.

Asanuma, H., N. Soma, H. Kaieda, Y. Kumano, T. Izumi, K. Tezuka, H. Niitsuma, and D. Wyborn (2005), Microseismic monitoring of hydraulic stimulation at the Australian HDR project in Cooper Basin, paper presented at Proceedings World Geothermal Congress.

Assumpção, M., V. Marza, L. Barros, C. Chimpliganond, J. E. Soares, J. Carvalho, D. Caixeta, A. Amorim, and E. Cabral (2002), Reservoir-induced seismicity in Brazil, in The mechanism of induced seismicity, pp. 597-617, Springer.

Assumpção, M., T. H. Yamabe, J. R. Barbosa, V. Hamza, A. E. V. Lopes, L. Balancin, and M. B. Bianchi (2010), Seismic activity triggered by water wells in the Paraná Basin, Brazil, Water Resources Research, 46.

Avouac, J.-P. (2012), Earthquakes: Human-induced shaking, Nature Geoscience, 5, 763-764.

Awad, M., and M. Mizoue (1995), Earthquake activity in the Aswan region, Egypt, in Induced seismicity, pp. 69-86, Springer.

Baecher, G. B., and R. L. Keeney (1982), Statistical examination of reservoir-induced seismicity, Bulletin of the Seismological Society of America, 72, 553-569.

Baisch, S., E. Rothert, H. Stang, R. Vörös, C. Koch, and A. McMahon (2015), Continued geothermal reservoir stimulation experiments in the Cooper Basin (Australia), Bulletin of the Seismological Society of America.

Baisch, S., and R. Vörös (2011), Geomechanical study of Blackpool seismicity.

Baisch, S., R. Vörös, R. Weidler, and D. Wyborn (2009), Investigation of fault mechanisms during geothermal reservoir stimulation experiments in the Cooper Basin, Australia, Bulletin of the Seismological Society of America, 99, 148-158.

Baisch, S., R. Weidler, R. Vörös, D. Wyborn, and L. de Graaf (2006), Induced seismicity during the stimulation of a geothermal HFR reservoir in the Cooper Basin, Australia, Bulletin of the Seismological Society of America, 96, 2242-2256.

Baker, K., D. Hollett, and A. Coy (2014, February), Geothermal technologies office 2013 peer review report.

Balassanian, S. Y. (2005), Earthquakes induced by deep penetrating bombing?, Acta Seismologica Sinica, 18, 741-745.

Balfour, N., E. Borleis, C. Bugden, V. Dent, D. H. Glanville, D. Hardy, D. Love, M. Salmon, M. Sambridge, and A. Wallace (2014), Australian seismological report 2013.

Bardainne, T., N. Dubos-Sallée, G. Sénéchal, P. Gaillot, and H. Perroud (2008), Analysis of the induced seismicity of the Lacq gas field (southwestern France) and model of deformation, Geophysical Journal International, 172, 1151-1162.

Bardainne, T., P. Gaillot, N. Dubos-Sallée, J. Blanco, and G. Sénéchal (2006), Characterization of seismic waveforms and classification of seismic events using chirplet atomic decomposition. Example from the Lacq gas field (western Pyrenees, France), Geophysical Journal International, 166, 699-718.

Basham, P. W. (1969), Canadian magnitudes of earthquakes and nuclear explosions in south-western North America, Geophysical Journal International, 17, 1-13.

Bella, F., P. F. Biagi, M. Caputo, E. Cozzi, G. Della Monica, A. Ermini, W. Plastino, and V. Sgrigna (1998), Aquifer-induced seismicity in the central Apennines (Italy), Pure and applied geophysics, 153, 179-194.

Bennett, T. J., M. E. Marshall, K. L. Mclaughlin, B. W. Barker, and J. R. Murphy (1995), Seismic characteristics and mechanisms of rockbursts, DTIC Document.

Bennett, T. J., K. L. McLaughlin, M. E. Marshall, B. W. Barker, and J. R. Murphy (1995), Investigations of the seismic characteristics of rockbursts, DTIC Document.

Benz, H. M., N. D. McMahon, R. C. Aster, D. E. McNamara, and D. B. Harris (2015), Hundreds of earthquakes per day: The 2014 Guthrie, Oklahoma, earthquake sequence, Seismological Research Letters, 86, 1318-1325.

Bertani, R. (2012), Geothermal power generation in the world 2005–2010 update report, Geothermics, 41, 1-29.

Bertini, G., M. Casini, G. Gianelli, and E. Pandeli (2006), Geological structure of a long-living geothermal system, Larderello, Italy, Terra Nova, 18, 163-169.

Białoń, W., E. Zarzycka, and S. Lasocki (2015), Seismicity of Czorsztyn Lake region: A case of reservoir triggered seismic process?, Acta Geophysica, 63, 1080-1089.

Bischoff, M., A. Cete, R. Fritschen, and T. Meier (2010), Coal mining induced seismicity in the Ruhr area, Germany, Pure and applied geophysics, 167, 63-75.

Bommer, J. J., S. Oates, J. M. Cepeda, C. Lindholm, J. Bird, R. Torres, G. Marroquín, and J. Rivas (2006), Control of hazard due to seismicity induced by a hot fractured rock geothermal project, Engineering Geology, 83, 287-306.

Boucher, G., A. Ryall, and A. E. Jones (1969), Earthquakes associated with underground nuclear explosions, Journal of Geophysical Research, 74, 3808-3820.

Bou-Rabee, F. (1994), Earthquake recurrence in Kuwait induced by oil and gas extraction, Journal of Petroleum Geology, 17, 473-480.

Bou-Rabee, F., and A. Nur (2002), The 1993 M4.7 Kuwait earthquake: Induced by the burning of the oil fields, Kuwait J. Sci. Eng, 29, 155-163.

Bourne, S. J., and S. J. Oates (2014), An activity rate model of induced seismicity within the Groningen field.

Bowers, D. (1997), The October 30, 1994, seismic disturbance in South Africa: Earthquake or large rock burst?, Journal of Geophysical Research: Solid Earth, 102, 9843-9857.

Breede, K., K. Dzebisashvili, X. Liu, and G. Falcone (2013), A systematic review of enhanced (or engineered) geothermal systems: Past, present and future, Geothermal Energy, 1, 1-27.

British Columbia Oil and Gas Commission (BCOGC) (2012), Investigation of observed seismicity in the Horn River Basin.

British Columbia Oil and Gas Commission (BCOGC) (2014), Investigation of observed seismicity in the Montney trend.

Brodsky, E. E., and L. J. Lajoie (2013), Anthropogenic seismicity rates and operational parameters at the Salton Sea geothermal field, Science, 341, 543-546.

Bromley, C. J., C. F. Pearson, and D. M. Rigor (1987), Microearthquakes at the Puhagan geothermal field, Philippines—a case of induced seismicity, Journal of volcanology and geothermal research, 31, 293-311.

Brune, J. N., and P. W. Pomeroy (1963), Surface wave radiation patterns for underground nuclear explosions and small‐magnitude earthquakes, Journal of Geophysical Research, 68, 5005-5028.

Bukchin, B. G., A. Z. Mostinsky, A. A. Egorkin, A. L. Levshin, and M. H. Ritzwoller (2001), Isotropic and nonisotropic components of earthquakes and nuclear explosions on the Lop Nor test site, China, in Monitoring the comprehensive nuclear-test-ban treaty: Surface waves, pp. 1497-1515, Springer.

Calò, M., C. Dorbath, and M. Frogneux (2014), Injection tests at the EGS reservoir of Soultz-Sous-Forêts. Seismic response of the GPK4 stimulations, Geothermics, 52, 50-58.

Caloi, P., M. De Panfilis, D. Di Filippo, L. Marcelli, and M. C. Spadea (1956), Terremoti della Val Padana del 15-16 Maggio 1951, Annals of Geophysics, 9, 63-105.

Carder, D. S. (1945), Seismic investigations in the Boulder dam area, 1940-1944, and the influence of reservoir loading on local earthquake activity, Bulletin of the Seismological Society of America, 35, 175-192.

Carpenter, P. J., and I. W. El-Hussain, Reservoir induced seismicity near Heron and El Vado reservoirs, northern New Mexico, and implications for fluid injection within the San Juan Basin, paper presented at AAPG Annual Convention and Exhibition.

Cesca, S., F. Grigoli, S. Heimann, Á. González, E. Buforn, S. Maghsoudi, E. Blanch, and T. Dahm (2014), The 2013 September–October seismic sequence offshore Spain: A case of seismicity triggered by gas injection?, Geophysical Journal International, 198, 941-953.

Chadha, R. K. (1995), Role of dykes in induced seismicity at Bhatsa reservoir, Maharashtra, India, in Induced seismicity, pp. 155-165, Springer.

Chen, L., and P. Talwani (1998), Reservoir-induced seismicity in China, Pure and applied geophysics, 153, 133-149.

Chouhan, R. K. S. (1986), Induced seismicity of Indian coal mines, Physics of the earth and planetary interiors, 44, 82-86.

Chouhan, R. K. S. (1992), Combating the rockburst problem - a seismological approach, in Induced seismicity, edited by P. Knoll, Balkema, Rotterdam.

Číž, R., and B. Růžek (1997), Periodicity of mining and induced seismicity in the Mayrau mine, Czech Republic, Studia Geophysica et Geodaetica, 41, 29-44.

Cladouhos, T. T., S. Petty, Y. Nordin, M. Moore, K. Grasso, M. Uddenberg, M. Swyer, B. Julian, and G. Foulger (2013), Microseismic monitoring of Newberry volcano EGS demonstration, paper presented at Proceedings of the 38th Workshop on Geothermal Reservoir Engineering, Stanford, CA.

Clark, D. (2009), Potential geologic sources of seismic hazard in the Sydney Basin, Proceedings volume of a one day workshop. Geoscience Australia Record 2009/11. 115pp.

Clarke, H., L. Eisner, P. Styles, and P. Turner (2014), Felt seismicity associated with shale gas hydraulic fracturing: The first documented example in Europe, Geophysical Research Letters, 41, 8308-8314.

Dahm, T., S. Cesca, S. Hainzl, T. Braun, and F. Krüger (2015), Discrimination between induced, triggered, and natural earthquakes close to hydrocarbon reservoirs: A probabilistic approach based on the modeling of depletion‐induced stress changes and seismological source parameters, Journal of Geophysical Research: Solid Earth, 120, 2491-2509.

Dahm, T., F. Krüger, K. Stammler, K. Klinge, R. Kind, K. Wylegalla, and J.-R. Grasso (2007), The 2004 Mw 4.4 Rotenburg, northern Germany, earthquake and its possible relationship with gas recovery, Bulletin of the Seismological Society of America, 97, 691-704.

Darold, A., A. A. Holland, C. Chen, and A. Youngblood (2014), Preliminary analysis of seismicity near Eagleton 1‐29, Carter County, July 2014.

Davies, R., G. Foulger, A. Bindley, and P. Styles (2013), Induced seismicity and hydraulic fracturing for the recovery of hydrocarbons, Marine and Petroleum Geology, 45, 171-185.

Davis, S. D., and C. Frohlich (1993), Did (or will) fluid injection cause earthquakes?-criteria for a rational assessment, Seismological Research Letters, 64, 207-224.

Davis, S. D., P. A. Nyffenegger, and C. Frohlich (1995), The 9 April 1993 earthquake in south-central Texas: Was it induced by fluid withdrawal?, Bulletin of the Seismological Society of America, 85, 1888-1895.

Davis, S. D., and W. D. Pennington (1989), Induced seismic deformation in the Cogdell oil field of west Texas, Bulletin of the Seismological Society of America, 79, 1477-1495.

De Pater, C. J., and S. Baisch (2011), Geomechanical study of Bowland Shale seismicity, Synthesis Report, 57.

Deichmann, N., and J. Ernst (2009), Earthquake focal mechanisms of the induced seismicity in 2006 and 2007 below Basel (Switzerland), Swiss Journal of Geosciences, 102, 457-466.

Diaz, A. R., E. Kaya, and S. J. Zarrouk (2016), Reinjection in geothermal fields‐ a worldwide review update, Renewable and Sustainable Energy Reviews, 53, 105-162.

Doblas, M., N. Youbi, J. De Las Doblas, and A. J. Galindo (2014), The 2012/2014 swarmquakes of Jaen, Spain: A working hypothesis involving hydroseismicity associated with the hydrologic cycle and anthropogenic activity, Natural hazards, 74, 1223-1261.

Doornenbal, H., and A. Stevenson (2010), Petroleum geological atlas of the southern Permian Basin area, EAGE.

Doser, D. I., M. R. Baker, M. Luo, P. Marroquin, L. Ballesteros, J. Kingwell, H. L. Diaz, and G. Kaip (1992), The not so simple relationship between seismicity and oil production in the Permian Basin, west Texas, Pure and applied geophysics, 139, 481-506.

Dost, B., and J. Spetzler (2015), Probabilistic seismic hazard analysis for induced earthquakes in Groningen; update 2015.

Downing, J. A., Y. T. Prairie, J. J. Cole, C. M. Duarte, L. J. Tranvik, R. G. Striegl, W. H. McDowell, P. Kortelainen, N. F. Caraco, and J. M. Melack (2006), The global abundance and size distribution of lakes, ponds, and impoundments, Limnology and Oceanography, 51, 2388-2397.

Dreger, D. S., S. R. Ford, and W. R. Walter (2008), Source analysis of the Crandall Canyon, Utah, mine collapse, Science, 321, 217-217.

Durrheim, R. J. (2010), Mitigating the risk of rockbursts in the deep hard rock mines of South Africa: 100 years of research, in Extracting the science: A century of mining research, Brune, J. (eds), Society for Mining, Metallurgy, and Exploration, Inc, pp. 156-171.

Durrheim, R. J., R. L. Anderson, A. Cichowicz, R. Ebrahim-Trolloped, G. Hubert, A. Kijko, A. McGarr, W. Ortlepp, and N. van der Merwe (2006), The risks to miners, mines, and the public posed by large seismic events in the gold mining districts of South Africa, paper presented at Proceedings of the Third International Seminar on Deep and High Stress Mining, 2-4 October 2006, Quebec City, Canada.

Durrheim, R. J., R. L. Anderson, A. Cichowicz, R. Ebrahim-Trolloped, G. Hubert, A. Kijko, A. McGarr, W. D. Ortlepp, and N. van der Merwe (2006), Investigation into the risks to miners, mines, and the public associated with large seismic events in gold mining districts, Department of Minerals and Energy.

Eagar, K. C., G. L. Pavlis, and M. W. Hamburger (2006), Evidence of possible induced seismicity in the Wabash Valley seismic zone from improved microearthquake locations, Bulletin of the Seismological Society of America, 96, 1718-1728.

El-Hussain, I. W., and P. J. Carpenter (1990), Reservoir induced seismicity near Heron and El Vado reservoirs, northern New Mexico, Bulletin of the Association of Engineering Geologists, 27, 51-59.

Ellsworth, W. L. (2013), Injection-induced earthquakes, Science, 341, 1225942.

Emanov, A. F., A. A. Emanov, A. V. Fateev, E. V. Leskova, E. V. Shevkunova, and V. G. Podkorytova (2014), Mining-induced seismicity at open pit mines in Kuzbass (Bachatsky earthquake on June 18, 2013), Journal of Mining Science, 50, 224-228.

Engdahl, E. R. (1972), Seismic effects of the Milrow and Cannikin nuclear explosions, Bulletin of the Seismological Society of America, 62, 1411-1423.

Eremenko, V. A., A. A. Eremenko, S. V. Rasheva, and S. B. Turuntaev (2009), Blasting and the man-made seismicity in the Tashtagol mining area, Journal of mining science, 45, 468-474.

Evans, K. F., A. Zappone, T. Kraft, N. Deichmann, and F. Moia (2012), A survey of the induced seismic responses to fluid injection in geothermal and CO2 reservoirs in Europe, Geothermics, 41, 30-54.

Fabriol, H., and A. Beauce (1997), Temporal and spatial distribution of local seismicity in the Chipilapa-Ahuachapán geothermal area, El Salvador, Geothermics, 26, 681-699.

Fajklewicz, Z., and K. Jakiel (1989), Induced gravity anomalies and seismic energy as a basis for prediction of mining tremors, in Seismicity in mines, pp. 535-552, Springer.

Farahbod, A. M., H. Kao, D. M. Walker, J. F. Cassidy, and A. Calvert (2015), Investigation of regional seismicity before and after hydraulic fracturing in the Horn River Basin, northeast British Columbia, Canadian Journal of Earth Sciences, 52, 112-122.

Feng, Q., and J. M. Lees (1998), Microseismicity, stress, and fracture in the Coso geothermal field, California, Tectonophysics, 289, 221-238.

Ferguson, G. (2015), Deep injection of waste water in the Western Canada Sedimentary Basin, Groundwater, 53, 187-194.

Ferreira, J. M., G. S. França, C. S. Vilar, A. F. do Nascimento, F. H. R. Bezerra, and M. Assumpção (2008), Induced seismicity in the Castanhão reservoir, ne Brazil—preliminary results, Tectonophysics, 456, 103-110.

Fletcher, J. B., and L. R. Sykes (1977), Earthquakes related to hydraulic mining and natural seismic activity in western New York state, Journal of Geophysical Research, 82, 3767-3780.

Folger, P. F., and M. Tiemann (2014), Human-induced earthquakes from deep-well injection: A brief overview, Congressional Research Service.

Ford, S. R., D. S. Dreger, and W. R. Walter (2008), Source characterization of the 6 August 2007 Crandall Canyon mine seismic event in central Utah, Seismological Research Letters, 79, 637-644.

Friberg, P. A., G. M. Besana‐Ostman, and I. Dricker (2014), Characterization of an earthquake sequence triggered by hydraulic fracturing in Harrison County, Ohio, Seismological Research Letters.

Fritschen, R. (2010), Mining-induced seismicity in the Saarland, Germany, Pure and applied geophysics, 167, 77-89.

Frohlich, C. (2012), Two-year survey comparing earthquake activity and injection-well locations in the Barnett Shale, Texas, Proceedings of the National Academy of Sciences, 109, 13934-13938.

Frohlich, C., and M. Brunt (2013), Two-year survey of earthquakes and injection/production wells in the Eagle Ford Shale, Texas, prior to the Mw4.8 20 October 2011 earthquake, Earth and Planetary Science Letters, 379, 56-63.

Frohlich, C., and S. D. Davis (2002), Texas earthquakes, University of Texas Press.

Frohlich, C., W. Ellsworth, W. A. Brown, M. Brunt, J. Luetgert, T. MacDonald, and S. Walter (2014), The 17 May 2012 M4.8 earthquake near Timpson, east Texas: An event possibly triggered by fluid injection, Journal of Geophysical Research: Solid Earth, 119, 581-593.

Frohlich, C., J. Glidewell, and M. Brunt (2012), Location and felt reports for the 25 April 2010 mbLg 3.9 earthquake near Alice, Texas: Was it induced by petroleum production?, Bulletin of the Seismological Society of America, 102, 457-466.

Frohlich, C., C. Hayward, B. Stump, and E. Potter (2011), The Dallas–Fort Worth earthquake sequence: October 2008 through May 2009, Bulletin of the Seismological Society of America, 101, 327-340.

Frohlich, C., and E. Potter (2013), What further research could teach us about “close encounters of the third kind”: Intraplate earthquakes associated with fluid injection.

Frohlich, C., J. I. Walter, and J. F. W. Gale (2015), Analysis of transportable array (USarray) data shows earthquakes are scarce near injection wells in the Williston Basin, 2008–2011, Seismological Research Letters.

Gahalaut, K., V. K. Gahalaut, and M. R. Pandey (2007), A new case of reservoir triggered seismicity: Govind Ballav Pant reservoir (Rihand dam), central India, Tectonophysics, 439, 171-178.

Gaite, B., A. Ugalde, A. Villaseñor, and E. Blanch (2016), Improving the location of induced earthquakes associated with an underground gas storage in the Gulf of Valencia (Spain), Physics of the Earth and Planetary Interiors, 254, 46-59.

Galybin, A. N., S. S. Grigoryan, and S. A. Mukhamediev (1998), Model of induced seismicity caused by water injection, paper presented at SPE/ISRM Rock Mechanics in Petroleum Engineering, Society of Petroleum Engineers.

Gan, W., and C. Frohlich (2013), Gas injection may have triggered earthquakes in the Cogdell oil field, Texas, Proceedings of the National Academy of Sciences, 110, 18786-18791.

Gasparini, P., P. Styles, S. Lasocki, P. Scandone, E. Huenges, F. Terlizzese, and S. Esposito (2015), The ICHESE report on the relationship between hydrocarbon exploration and the May 2012 earthquakes in the Emilia region (Italy) and their consequences.

Gaucher, E., M. Schoenball, O. Heidbach, A. Zang, P. A. Fokker, J.-D. van Wees, and T. Kohl (2015), Induced seismicity in geothermal reservoirs: A review of forecasting approaches, Renewable and Sustainable Energy Reviews, 52, 1473-1490.

Ge, S., M. Liu, N. Lu, J. W. Godt, and G. Luo (2009), Did the Zipingpu reservoir trigger the 2008 Wenchuan earthquake?, Geophysical Research Letters, 36.

Gendzwill, D. J., R. B. Horner, and H. S. Hasegawa (1982), Induced earthquakes at a potash mine near Saskatoon, Canada, Canadian Journal of Earth Sciences, 19, 466-475.

Genmo, Z., C. Huaran, M. Shuqin, and Z. Deyuan (1995), Research on earthquakes induced by water injection in China, in Induced seismicity, pp. 59-68, Springer.

German, V. I. (2014), Rock failure prediction in mines by seismic monitoring data, Journal of Mining Science, 50, 288-297.

Gestermann, N., T. Plenefisch, U. Schwaderer, and M. Joswig (2015), Induced seismicity at the natural gas fields in northern Germany, in Schatzalp Induced Seismicity Workshop, 10-13 March 2015, Davos, Switzerland.

Gibowicz, S. J. (1998), Partial stress drop and frictional overshoot mechanism of seismic events induced by mining, in Seismicity caused by mines, fluid injections, reservoirs, and oil extraction, pp. 5-20, Springer.

Gibowicz, S. J., A. Bober, A. Cichowicz, Z. Droste, Z. Dychtowicz, J. Hordejuk, M. Kazimierczyk, and A. Kijko (1979), Source study of the Lubin, Poland, tremor of 24 March 1977, Acta Geophys. Pol, 27, 3-38.

Gibowicz, S. J., Z. Droste, B. Guterch, and J. Hordejuk (1981), The Belchatow, Poland, earthquakes of 1979 and 1980 induced by surface mining, Engineering Geology, 17, 257-271.

Gibowicz, S. J., R. P. Young, S. Talebi, and D. J. Rawlence (1991), Source parameters of seismic events at the Underground Research Laboratory in Manitoba, Canada: Scaling relations for events with moment magnitude smaller than −2, Bulletin of the Seismological Society of America, 81, 1157-1182.

Gibson, G., and M. Sandiford (2013), Seismicity and induced earthquakes, Office of the New South Wales Chief Scientist and Engineer.

Gilyarov, V. L., E. E. Damaskinskaya, A. G. Kadomtsev, and I. Y. Rasskazov (2014), Analysis of statistic parameters of geoacoustic monitoring data for the Antey Uranium Deposit, Journal of Mining Science, 50, 443-447.

Glowacka, E., and F. A. Nava (1996), Major earthquakes in Mexicali valley, Mexico, and fluid extraction at Cerro Prieto geothermal field, Bulletin of the Seismological Society of America, 86, 93-105.

Göbel, T. (2015), A comparison of seismicity rates and fluid-injection operations in Oklahoma and California: Implications for crustal stresses, The Leading Edge, 34, 640-648.

Godano, M., E. Gaucher, T. Bardainne, M. Regnier, A. Deschamps, and M. Valette (2010), Assessment of focal mechanisms of microseismic events computed from two three‐component receivers: Application to the Arkema‐Vauvert field (France), Geophysical prospecting, 58, 775-790.

Goebel, T. H. W., S. M. Hosseini, F. Cappa, E. Hauksson, J. P. Ampuero, F. Aminzadeh, and J. B. Saleeby (2016), Wastewater disposal and earthquake swarm activity at the southern end of the Central Valley, California, Geophysical Research Letters.

Goldbach, O. D. (2009), Flooding-induced seismicity in mines, paper presented at 11th SAGA Biennial Technical Meeting and Exhibition.

Gomberg, J., and L. Wolf (1999), Possible cause for an improbable earthquake: The 1997 Mw 4.9 southern Alabama earthquake and hydrocarbon recovery, Geology, 27, 367-370.

González, P. J., K. F. Tiampo, M. Palano, F. Cannavó, and J. Fernández (2012), The 2011 Lorca earthquake slip distribution controlled by groundwater crustal unloading, Nature Geoscience, 5, 821-825.

Gough, D. I., and W. I. Gough (1970), Load-induced earthquakes at Lake Kariba—II, Geophysical Journal International, 21, 79-101.

Grasso, J.-R. (1992), Mechanics of seismic instabilities induced by the recovery of hydrocarbons, Pure and applied geophysics, 139, 507-534.

Green, C. A., P. Styles, and B. J. Baptie (2012), Preese Hall shale gas fracturing review & recommendations for induced seismic mitigation: UK department of energy and climate change.

Groos, J., J. Zeiß, M. Grund, and J. Ritter (2013), Microseismicity at two geothermal power plants at Landau and Insheim in the Upper Rhine Graben, Germany, paper presented at EGU General Assembly Conference Abstracts.

Ground Water Research & Education Foundation (GWREF) (2013), White paper II summarizing a special session on induced seismicity.

Grünthal, G. (2014), Induced seismicity related to geothermal projects versus natural tectonic earthquakes and other types of induced seismic events in central Europe, Geothermics, 52, 22-35.

Guglielmi, Y., F. Cappa, J.-P. Avouac, P. Henry, and D. Elsworth (2015), Seismicity triggered by fluid injection–induced aseismic slip, Science, 348, 1224-1226.

Guha, S. K., and D. N. Patil (1990), Large water-reservoir-related induced seismicity, Gerlands Beitr Geophys, 99, 265-288.

Gupta, H. K. (2002), A review of recent studies of triggered earthquakes by artificial water reservoirs with special emphasis on earthquakes in Koyna, India, Earth-Science Reviews, 58, 279-310.

Gupta, H. K. (2011), Artificial water reservoir triggered earthquakes, Encyclopedia of Solid Earth Geophysics, 15-24.

Hamilton, R. M., B. E. Smith, F. G. Fischer, and P. J. Papanek (1972), Earthquakes caused by underground nuclear explosions on Pahute Mesa, Nevada test site, Bulletin of the Seismological Society of America, 62, 1319-1341.

Haney, F., J. Kummerow, C. Langenbruch, C. Dinske, S. A. Shapiro, and F. Scherbaum (2011), Magnitude estimation for microseismicity induced during the KTB 2004/2005 injection experiment, Geophysics, 76, WC47-WC53.

Hasegawa, H. S., R. J. Wetmiller, and D. J. Gendzwill (1989), Induced seismicity in mines in Canada—an overview, Pure and applied geophysics, 129, 423-453.

Hauksson, E., T. Göbel, J.-P. Ampuero, and E. Cochran (2015), A century of oil-field operations and earthquakes in the Greater Los Angeles Basin, southern California, The Leading Edge, 34, 650-656.

Heck, N. H., and R. R. Bodle (1931), United States earthquakes 1929, US Coast and Geodetic Survey, Serial.

Hedley, D. G. F., and J. E. Udd (1989), The Canada-Ontario-industry rockburst project, in Seismicity in mines, pp. 661-672, Springer.

Heesakkers, V., S. K. Murphy, G. van Aswegen, R. Domoney, S. Addams, T. Dewers, M. Zechmeister, and Z. Reches (2005), The rupture zone of the M= 2.2 earthquake that reactivated the ancient Pretorius fault in Tautona mine, South Africa, paper presented at AGU Fall Meeting Abstracts.

Heick, C., and D. Flach (1989), Microseismicity in a flooded potash mine, the Hope mine, Federal Republic of Germany, in Seismicity in mines, pp. 475-496, Springer.

Herrmann, R. B. (1978), A seismological study of two Attica, New York earthquakes, Bulletin of the Seismological Society of America, 68, 641-651.

Hill, D. P., P. A. Reasenberg, A. Michael, W. J. Arabaz, G. Beroza, D. Brumbaugh, J. N. Brune, R. Castro, S. Davis, and W. L. Ellsworth (1993), Seismicity remotely triggered by the magnitude 7.3 Landers, California, earthquake, Science, 260, 1617-1623.

Holland, A. (2011), Examination of possibly induced seismicity from hydraulic fracturing in the Eola field, Garvin County, Oklahoma.

Holland, A. A. (2013), Earthquakes triggered by hydraulic fracturing in south-central Oklahoma, Bulletin of the Seismological Society of America, 103, 1784-1792.

Holmgren, J. (2015), Induced seismicity in the Dannemora mine, Sweden, Uppsala Universitet.

Holschneider, M., G. Zöller, and S. Hainzl (2011), Estimation of the maximum possible magnitude in the framework of a doubly truncated Gutenberg–Richter model, Bulletin of the Seismological Society of America, 101, 1649-1659.

Holub, K., J. Holečko, J. Rušajová, and A. Dombkova (2012), Long-term development of seismic monitoring networks in the Ostrava-Karviná coal mine district, Acta Geodynamica et Geomaterialia, 9, 115-132.

Hong, T. K., C. E. Baag, H. Choi, and D. H. Sheen (2008), Regional seismic observations of the 9 October 2006 underground nuclear explosion in North Korea and the influence of crustal structure on regional phases, Journal of Geophysical Research: Solid Earth, 113.

Hornbach, M. J., H. R. DeShon, W. L. Ellsworth, B. W. Stump, C. Hayward, C. Frohlich, H. R. Oldham, J. E. Olson, M. B. Magnani, and C. Brokaw (2015), Causal factors for seismicity near Azle, Texas, Nature communications, 6.

Horner, R. B., J. E. Barclay, and J. M. MacRae (1994), Earthquakes and hydrocarbon production in the Fort St. John area of northeastern British Columbia, Canadian Journal of Exploration Geophysics, 30, 39-50.

Horton, S. (2012), Disposal of hydrofracking waste fluid by injection into subsurface aquifers triggers earthquake swarm in central Arkansas with potential for damaging earthquake, Seismological Research Letters, 83, 250-260.

Hough, S. E., and M. Page (2015), A century of induced earthquakes in Oklahoma?, Bulletin of the Seismological Society of America, 105, 2863-2870.

Hsieh, P. A., and J. D. Bredehoeft (1981), A reservoir analysis of the Denver earthquakes: A case of induced seismicity, Journal of Geophysical Research: Solid Earth, 86, 903-920.

Hsiung, S. M., W. Blake, A. H. Chowdhury, and T. J. Williams (1992), Effects of mining-induced seismic events on a deep underground mine, Pure and applied geophysics, 139, 741-762.

Hua, W., Z. Chen, S. Zheng, and C. Yan (2013), Reservoir-induced seismicity in the Longtan reservoir, southwestern China, Journal of seismology, 17, 667-681.

Hua, W., H. Fu, Z. Chen, S. Zheng, and C. Yan (2015), Reservoir-induced seismicity in high seismicity region—a case study of the Xiaowan reservoir in Yunnan province, China, Journal of Seismology, 19, 567-584.

Hua, W., S. Zheng, C. Yan, and Z. Chen (2013), Attenuation, site effects, and source parameters in the Three Gorges reservoir area, China, Bulletin of the Seismological Society of America, 103, 371-382.

Huaman, R. N. E., and T. X. Jun (2014), Energy related CO2 emissions and the progress on CCS projects: A review, Renewable and Sustainable Energy Reviews, 31, 368-385.

Husen, S., E. Kissling, and A. von Deschwanden (2012), Induced seismicity during the construction of the Gotthard Base Tunnel, Switzerland: Hypocenter locations and source dimensions, Journal of seismology, 16, 195-213.

Iannacchione, A. T., and J. C. Zelanko (1995), Occurrence and remediation of coal mine bumps: A historical review, Paper in Proceedings: Mechanics and Mitigation of Violent Failure in Coal and Hard-Rock Mines. US Bureau of Mines Spec. Publ, 01-95.

Improta, L., L. Valoroso, D. Piccinini, C. Chiarabba, and M. Buttinelli (2015), A detailed analysis of initial seismicity induced by wastewater injection in the Val d'Agri oil field (Italy), in Schatzalp Induced Seismicity Workshop, 10-13 March 2015, Davos, Switzerland.

Jaku, E. P., A. Z. Toper, and A. J. Jager (2001), Updating and maintaining the accident database, Safety in Mines Research Advisory Committee.

Jiménez, A., K. F. Tiampo, A. M. Posadas, F. Luzón, and R. Donner (2009), Analysis of complex networks associated to seismic clusters near the Itoiz reservoir dam, The European Physical Journal Special Topics, 174, 181-195.

Julià, J., A. A. Nyblade, R. Durrheim, L. Linzer, R. Gök, P. Dirks, and W. Walter (2009), Source mechanisms of mine-related seismicity, Savuka mine, South Africa, Bulletin of the Seismological Society of America, 99, 2801-2814.

Julian, B. R., G. R. Foulger, and F. C. Monastero (2009), Seismic monitoring of EGS stimulation tests at the Coso geothermal field, California, using microearthquake locations and moment tensors, paper presented at Thirty-Fourth Workshop on Geothermal Reservoir Engineering, Stanford University, Stanford, California, February.

Julian, B. R., A. Ross, G. R. Foulger, and J. R. Evans (1996), Three-dimensional seismic image of a geothermal reservoir: The Geysers, California, Geophysical Research Letters, 23, 685-688.

Jupe, A. J., A. S. P. Green, and T. Wallroth (1992), Induced microseismicity and reservoir growth at the Fjällbacka hot dry rocks project, Sweden, International journal of rock mechanics and mining sciences & geomechanics abstracts, 29, 343-354.

Justinic, A. H., B. Stump, C. Hayward, and C. Frohlich (2013), Analysis of the Cleburne, Texas, earthquake sequence from June 2009 to June 2010, Bulletin of the Seismological Society of America, 103, 3083-3093.

Kaieda, H., H. Ito, K. Kiho, K. Suzuki, H. Suenaga, and K. Shin (2005), Review of the Ogachi HDR project in Japan, paper presented at World Geothermal Congress.

Kaieda, H., S. Sasaki, and D. Wyborn (2010), Comparison of characteristics of micro-earthquakes observed during hydraulic stimulation operations in Ogachi, Hijiori and Cooper Basin HDR projects, paper presented at World Geothermal Congress.

Kalkan, E. (2016), An automatic P-phase arrival-time picker, Bulletin of the Seismological Society of America.

Kalkan, E., C. Gurbuz, and E. Zor (2014), The usage of correlation method for micro-earthquake analysis at Salavatli geothermal area, Aydin, Turkey, paper presented at AGU Fall Meeting Abstracts.

Kaneko, K., K. Sugawara, and Y. Obara (1989), Microseismic monitoring for coal burst prediction in the Miike coal mine, Gerlands Beitrage zur Geophysik, 98, 447-460.

Kangi, A., and N. Heidari (2008), Reservoir-induced seismicity in Karun III dam (southwestern Iran), Journal of Seismology, 12, 519-527.

Kao, H., A. M. Farahbod, J. F. Cassidy, M. Lamontagne, D. Snyder, and D. Lavoie (2015), Natural resources Canada's induced seismicity research, in Schatzalp Induced Seismicity Workshop, 10-13 March 2015, Davos, Switzerland.

Kaven, J. O., S. H. Hickman, A. F. McGarr, and W. L. Ellsworth (2015), Surface monitoring of microseismicity at the Decatur, Illinois, CO2 sequestration demonstration site, Seismological Research Letters, 86, 1096-1101.

Keck, R. G., and R. J. Withers (1994), A field demonstration of hydraulic fracturing for solids waste injection with real-time passive seismic monitoring, paper presented at SPE Annual Technical Conference and Exhibition, Society of Petroleum Engineers.

Keiding, M., T. Árnadóttir, S. Jonsson, J. Decriem, and A. Hooper (2010), Plate boundary deformation and man-made subsidence around geothermal fields on the Reykjanes Peninsula, Iceland, Journal of Volcanology and Geothermal Research, 194, 139-149.

Keranen, K. M., C. Hogan, H. M. Savage, G. A. Abers, and N. van der Elst (2013), Variable seismic response to fluid injection in central Oklahoma, paper presented at AGU Fall Meeting Abstracts.

Keranen, K. M., H. M. Savage, G. A. Abers, and E. S. Cochran (2013), Potentially induced earthquakes in Oklahoma, USA: Links between wastewater injection and the 2011 Mw 5.7 earthquake sequence, Geology, 41, 699-702.

Keranen, K. M., M. Weingarten, G. A. Abers, B. A. Bekins, and S. Ge (2014), Sharp increase in central Oklahoma seismicity since 2008 induced by massive wastewater injection, Science, 345, 448-451.

Kerr, R. A. (2009), After the quake, in search of the science--or even a good prediction, Science, 324, 322-322.

Kerr, R. A., and R. Stone (2009), A human trigger for the great quake of Sichuan?, Science, 323, 322-322.

Kertapati, E. K. (1987), Saguling-Cirata water reservoirs along Citarum river west Java, Indonesia as reservoir induced seismicity, YY1-YY9.

Kim, W. Y. (2013), Induced seismicity associated with fluid injection into a deep well in Youngstown, Ohio, Journal of Geophysical Research: Solid Earth, 118, 3506-3518.

Kim, W.-Y., M. Gold, C. Schamberger, J. Jones, and H. Delano (2009), The 2008-2009 earthquake swarm near Dillsburg, Pennsylvania.

King, G. C. P., R. S. Stein, and J. Lin (1994), Static stress changes and the triggering of earthquakes, Bulletin of the Seismological Society of America, 84, 935-953.

King, G. E. (2012), Hydraulic fracturing 101: What every representative, environmentalist, regulator, reporter, investor, university researcher, neighbor and engineer should know about estimating frac risk and improving frac performance in unconventional gas and oil wells, paper presented at SPE Hydraulic Fracturing Technology Conference, Society of Petroleum Engineers.

Kinscher, J., P. Bernard, I. Contrucci, A. Mangeney, J. P. Piguet, and P. Bigarre (2015), Location of microseismic swarms induced by salt solution mining, Geophysical Journal International, 200, 337-362.

Király, E., V. Gischig, D. Karvounis, and S. Wiemer (2014), Validating models to forecasting induced seismicity related to deep geothermal energy projects, paper presented at Proceedings, 39th Workshop on Geothermal Reservoir Engineering.

Kitano, K., Y. Hori, and H. Kaieda (2000), Outline of the Ogachi HDR project and character of the reservoirs, paper presented at World Geothermal Congress, Kyushu-Tohoku, Japan, May 28-June 10

Klose, C. D. (2007), Coastal land loss and gain as potential earthquake trigger mechanism in SCRs, paper presented at AGU Fall Meeting Abstracts.

Klose, C. D. (2007), Geomechanical modeling of the nucleation process of Australia's 1989 M5.6 Newcastle earthquake, Earth and Planetary Science Letters, 256, 547-553.

Klose, C. D. (2007), Mine water discharge and flooding: A cause of severe earthquakes, Mine Water and the Environment, 26, 172-180.

Klose, C. D. (2010), Human-triggered earthquakes and their impacts on human security, Achieving Environmental Security: Ecosystem Services and Human Welfare, 13-19.

Klose, C. D. (2012), Evidence for anthropogenic surface loading as trigger mechanism of the 2008 Wenchuan earthquake, Environmental Earth Sciences, 66, 1439-1447.

Klose, C. D. (2013), Mechanical and statistical evidence of the causality of human-made mass shifts on the Earth's upper crust and the occurrence of earthquakes, Journal of Seismology, 17, 109-135.

Klose, C. D., and L. Seeber (2007), Shallow seismicity in stable continental regions, Seismological Research Letters, 78, 554-562.

Knoll, P., G. Kowalle, K. Rother, B. Schreiber, and I. Paskaleva (1996), Analysis of microtremors within the Provadia region near a salt leaching mine, in Induced seismic events, pp. 389-407, Springer.

Kouznetsov, O., V. Sidorov, S. Katz, and G. Chilingarian (1995), Interrelationships among seismic and short-term tectonic activity, oil and gas production, and gas migration to the surface, Journal of Petroleum Science and Engineering, 13, 57-63.

Kovach, R. L. (1974), Source mechanisms for Wilmington oil field, California, subsidence earthquakes, Bulletin of the Seismological Society of America, 64, 699-711.

Kraaijpoel, D., D. Nieuwland, B. Wassing, and B. Dost (2012), Induced seismicity at an underground gas storage facility in the Netherlands, paper presented at EGU General Assembly Conference Abstracts.

Kreitler, C. W. (1976), Faulting and land subsidence from ground-water and hydrocarbon production, Houston-Galveston, Texas, paper presented at Proceedings of the Anaheim Symposium.

Kremenetskaya, E. O., and V. M. Trjapitsin (1995), Induced seismicity in the Khibiny Massif (Kola Peninsula), in Induced seismicity, pp. 29-37, Springer.

Kundu, B., N. K. Vissa, and V. K. Gahalaut (2015), Influence of anthropogenic groundwater unloading in Indo-Gangetic Plains on the 25 April 2015 Mw 7.8 Gorkha, Nepal earthquake, Geophysical Research Letters, 42.

Kwee, J. (2012), Micro-seismicity in the Bergermeer gas storage field, University of Utrecht, The Netherlands.

Kwiatek, G., M. Bohnhoff, G. Dresen, A. Schulze, T. Schulte, G. Zimmermann, and E. Huenges (2010), Microseismicity induced during fluid-injection: A case study from the geothermal site at Groß Schönebeck, North German Basin, Acta Geophysica, 58, 995-1020.

Lamontagne, M., Y. Hammamji, and V. Peci (2008), Reservoir-triggered seismicity at the Toulnustouc hydroelectric project, Quebec north shore, Canada, Bulletin of the Seismological Society of America, 98, 2543-2552.

Leblanc, G., and F. Anglin (1978), Induced seismicity at the Manic 3 reservoir, Quebec, Bulletin of the Seismological Society of America, 68, 1469-1485.

Lee, M. F., P. Mikula, and E. Kinnersly (2006), In situ rock stress measurements and stress change monitoring at Mt Charlotte gold mine, western Australia, paper presented at In-Situ Rock Stress: International Symposium on In-Situ Rock Stress, Trondheim, Norway, 19-21 June 2006, CRC Press.

Lehner, B., C. R. Liermann, C. Revenga, C. Vörösmarty, B. Fekete, P. Crouzet, P. Döll, M. Endejan, K. Frenken, and J. Magome (2011), High-resolution mapping of the world's reservoirs and dams for sustainable river-flow management, Frontiers in Ecology and the Environment, 9, 494-502.

Lei, X., S. Ma, W. Chen, C. Pang, J. Zeng, and B. Jiang (2013), A detailed view of the injection-induced seismicity in a natural gas reservoir in Zigong, southwestern Sichuan Basin, China, Journal of Geophysical Research: Solid Earth, 118, 4296-4311.

Lei, X., G. Yu, S. Ma, X. Wen, and Q. Wang (2008), Earthquakes induced by water injection at ~3 km depth within the Rongchang gas field, Chongqing, China, Journal of Geophysical Research: Solid Earth, 113.

Li, T., M. F. Cai, and M. Cai (2007), A review of mining-induced seismicity in China, International Journal of Rock Mechanics and Mining Sciences, 44, 1149-1171.

Lin, C. H. (2005), Seismicity increase after the construction of the world's tallest building: An active blind fault beneath the Taipei 101, Geophysical Research Letters, 32.

Lizurek, G., Ł. Rudziński, and B. Plesiewicz (2015), Mining induced seismic event on an inactive fault, Acta Geophysica, 63, 176-200.

Llenos, A. L., and A. J. Michael (2013), Modeling earthquake rate changes in Oklahoma and Arkansas: Possible signatures of induced seismicity, Bulletin of the Seismological Society of America, 103, 2850-2861.

Lockridge, J. S., M. J. Fouch, and J. R. Arrowsmith (2012), Seismicity within Arizona during the deployment of the Earthscope USarray transportable array, Bulletin of the Seismological Society of America, 102, 1850-1863.

Long, L. T., and C. W. Copeland (1989), The Alabama, USA, seismic event and strata collapse of May 7, 1986, Pure and applied geophysics, 129, 415-421.

Lorenz, J. C. (2001), The stimulation of hydrocarbon reservoirs with subsurface nuclear explosions, Oil-Industry History, 2, 56-63.

Lovchikov, A. V. (2013), Review of the strongest rockbursts and mining-induced earthquakes in Russia, Journal of Mining Science, 49, 572-575.

Ma, T. H., C. A. Tang, L. X. Tang, W. D. Zhang, and L. Wang (2015), Rockburst characteristics and microseismic monitoring of deep-buried tunnels for Jinping II hydropower station, Tunnelling and Underground Space Technology, 49, 345-368.

Ma, W. (2012), Analysis on the disaster mechanism of rock collapse of M4.4 reservoir-induced earthquake on January 17, 2010, at Dongjing reservoir in Guizhou Province, China, Natural hazards, 62, 141-148.

Maggi, A., J. A. Jackson, D. Mckenzie, and K. Priestley (2000), Earthquake focal depths, effective elastic thickness, and the strength of the continental lithosphere, Geology, 28, 495-498.

Mahdi, S. K. (1988), Tarbela reservoir a question of induced seismicity, in International Conference on Case Histories in Geotechnical Engineering.

Majer, E. L. (2011), Workshop on induced seismicity due to fluid injection/production from energy-related applications, Lawrence Berkeley National Laboratory.

Majer, E. L., R. Baria, M. Stark, S. Oates, J. Bommer, B. Smith, and H. Asanuma (2007), Induced seismicity associated with enhanced geothermal systems, Geothermics, 36, 185-222.

Majer, E. L., and J. E. Peterson (2008), The impact of injection on seismicity at The Geysers, California geothermal field, International Journal of Rock Mechanics and Mining Sciences, 44, 1079-1090.

Malovichko, D., R. Dyagilev, D. Y. Shulakov, P. Butyrin, and S. V. Glebov (2009), Seismic monitoring of large-scale karst processes in a potash mine, Controlling seismic hazard and sustainable development of deep mines, 2, 989-1002.

Matrullo, E., I. Contrucci, P. Dominique, M. Bennani, H. Aochi, J. Kinsher, P. Bernard, and P. Bigarré (2015), Analysis and interpretation of induced micro-seismicity by flooding of the Gardanne Coal Basin (Provence–southern France), paper presented at 77th EAGE Conference and Exhibition-Workshops.

Maurer, V., N. Cuenot, E. Gaucher, M. Grunberg, J. Vergne, H. Wodling, M. Lehujeur, and J. Schmittbuhl (2015), Seismic monitoring of the Rittershoffen EGS project (Alsace, France), paper presented at World Geothermal Congress.

Maxwell, S. C., D. Cho, T. L. Pope, M. Jones, C. L. Cipolla, M. G. Mack, F. Henery, M. Norton, and J. A. Leonard (2011), Enhanced reservoir characterization using hydraulic fracture microseismicity, paper presented at SPE Hydraulic Fracturing Technology Conference, Society of Petroleum Engineers.

Maxwell, S. C., and H. Fabriol (2004), Passive seismic imaging of CO2 sequestration at Weyburn.

Maxwell, S. C., U. Zimmer, R. W. Gusek, and D. J. Quirk (2009), Evidence of a horizontal hydraulic fracture from stress rotations across a thrust fault, SPE Production & Operations, 24, 312-319.

Mazzoldi, A., A. Borgia, M. Ripepe, E. Marchetti, G. Ulivieri, M. della Schiava, and C. Allocca (2015), Faults strengthening and seismicity induced by geothermal exploitation on a spreading volcano, Mt. Amiata, Italia, Journal of Volcanology and Geothermal Research, 301, 159-168.

McClure, M. W., and R. N. Horne (2014), Correlations between formation properties and induced seismicity during high pressure injection into granitic rock, Engineering Geology, 175, 74-80.

McGarr, A. (1991), On a possible connection between three major earthquakes in California and oil production, Bulletin of the Seismological Society of America, 81, 948-970.

McGarr, A. (2014), Maximum magnitude earthquakes induced by fluid injection, Journal of Geophysical Research: Solid Earth, 119, 1008-1019.

McGarr, A., B. Bekins, N. Burkardt, J. Dewey, P. Earle, W. Ellsworth, S. Ge, S. Hickman, A. Holland, and E. Majer (2015), Coping with earthquakes induced by fluid injection, Science, 347, 830-831.

McGarr, A., and D. Simpson (1997), A broad look at induced and triggered seismicity, Rockbursts and Seismicity in Mines, 385-396.

McGarr, A., D. Simpson, and L. Seeber (2002), Case histories of induced and triggered seismicity, in International geophysics series, international handbook of earthquake and engineering seismology, pp. 647-664.

McKavanagh, B., B. Boreham, K. McCue, G. Gibson, J. Hafner, and G. Klenowski (1995), The CQU regional seismic network and applications to underground mining in Central Queensland, Australia, Pure and applied geophysics, 145, 39-57.

McKeown, F. A. (1975), Relation of geological structure to seismicity at Pahute Mesa, Nevada test site, Bulletin of the Seismological Society of America, 65, 747-764.

McKeown, F. A., and D. D. Dickey (1969), Fault displacements and motion related to nuclear explosions, Bulletin of the Seismological Society of America, 59, 2253-2269.

McNamara, D. E., H. M. Benz, R. B. Herrmann, E. A. Bergman, P. Earle, A. Holland, R. Baldwin, and A. Gassner (2015), Earthquake hypocenters and focal mechanisms in central Oklahoma reveal a complex system of reactivated subsurface strike-slip faulting, Geophysical Research Letters, 42, 2742-2749.

McNamara, D. E., G. P. Hayes, H. M. Benz, R. A. Williams, N. D. McMahon, R. C. Aster, A. Holland, T. Sickbert, R. Herrmann, and R. Briggs (2015), Reactivated faulting near Cushing, Oklahoma: Increased potential for a triggered earthquake in an area of United States strategic infrastructure, Geophysical Research Letters, 42, 8328-8332.

Mercerat, E. D., L. Driad-Lebeau, and P. Bernard (2010), Induced seismicity monitoring of an underground salt cavern prone to collapse, Pure and applied geophysics, 167, 5-25.

Mereu, R. F., J. Brunet, K. Morrissey, B. Price, and A. Yapp (1986), A study of the microearthquakes of the Gobles oil field area of southwestern Ontario, Bulletin of the Seismological Society of America, 76, 1215-1223.

Milev, A. M., and S. M. Spottiswoode (2002), Effect of the rock properties on mining-induced seismicity around the Ventersdorp Contact Reef, Witwatersrand Basin, South Africa, in The mechanism of induced seismicity, pp. 165-177, Springer.

Milne, W. G., and M. J. Berry (1976), Induced seismicity in Canada, Engineering Geology, 10, 219-226.

Mirzoev, K. M., A. V. Nikolaev, A. A. Lukk, and S. L. Yunga (2009), Induced seismicity and the possibilities of controlled relaxation of tectonic stresses in the Earth's crust, Izvestiya, Physics of the Solid Earth, 45, 885-904.

Moeck, I., T. Bloch, R. Graf, S. Heuberger, P. Kuhn, H. Naef, M. Sonderegger, S. Uhlig, and M. Wolfgramm (2015), The St. Gallen project: Development of fault controlled geothermal systems in urban areas, paper presented at World Geothermal Congress.

Mogren, S., and M. Mukhopadhyay (2013), Study of seismogenic crust in the eastern province of Saudi Arabia and its relation to the seismicity of the Ghawar fields, paper presented at AGU Fall Meeting Abstracts.

Morrison, D. M. (1989), Rockburst research at Falconbridge's Strathcona mine, Sudbury, Canada, Pure and applied geophysics, 129, 619-645.

Mossop, A., and P. Segall (1999), Volume strain within The Geysers geothermal field, Journal of Geophysical Research: Solid Earth, 104, 29113-29131.

Mulargia, F., and A. Bizzarri (2014), Anthropogenic triggering of large earthquakes, Scientific Reports, 4.

Mulyadi (2010), Case study: Hydraulic fracturing experiment in the Wayang Windu geothermal field, paper presented at World Geothermal Congress, Bali, Indonesia, 25-29 April 2010.

National Research Council (NRC) (2013), Induced seismicity potential in energy technologies, National Academies Press, Committee on Induced Seismicity Potential in Energy Technologies.

Neuhaus, C. W., and J. L. Miskimins (2012), Analysis of surface and downhole microseismic monitoring coupled with hydraulic fracture modeling in the Woodford Shale, paper presented at SPE Europec/EAGE Annual Conference, Society of Petroleum Engineers.

Nicholson, C., E. Roeloffs, and R. L. Wesson (1988), The northeastern Ohio earthquake of 31 January 1986: Was it induced?, Bulletin of the Seismological Society of America, 78, 188-217.

Nicholson, C., and R. L. Wesson (1992), Triggered earthquakes and deep well activities, Pure and applied geophysics, 139, 561-578.

Nicholson, C. J. (1992), Earthquakes associated with deep well activities-comments and case histories, paper presented at The 33th US Symposium on Rock Mechanics (USRMS), American Rock Mechanics Association.

Nicol, A., R. Carne, M. Gerstenberger, and A. Christophersen (2011), Induced seismicity and its implications for CO2 storage risk, Energy Procedia, 4, 3699-3706.

Nuannin, P., O. Kulhanek, L. Persson, and T. Askemur (2005), Inverse correlation between induced seismicity and b-value, observed in the Zingruvan mine, Sweden, Acta Geodynamica et Geomaterialia, 2, 5.

Ohtake, M. (1974), Seismic activity induced by water injection at Matsushiro, Japan, Journal of Physics of the Earth, 22, 163-176.

Orlic, B., B. B. T. Wassing, and C. R. Geel (2013), Field scale geomechanical modeling for prediction of fault stability during underground gas storage operations in a depleted gas field in the Netherlands, paper presented at 47th US Rock Mechanics/Geomechanics Symposium, American Rock Mechanics Association.

Orzol, J., R. Jung, R. Jatho, T. Tischner, and P. Kehrer (2005), The Genesys-Project: Extraction of geothermal heat from tight sediments, paper presented at World Geothermal Congress.

Ottemöller, L., H. H. Nielsen, K. Atakan, J. Braunmiller, and J. Havskov (2005), The 7 May 2001 induced seismic event in the Ekofisk oil field, North Sea, Journal of Geophysical Research: Solid Earth, 110.

Oye, V., E. Aker, T. M. Daley, D. Kühn, B. Bohloli, and V. Korneev (2013), Microseismic monitoring and interpretation of injection data from the In Salah CO2 storage site (Krechba), Algeria, Energy Procedia, 37, 4191-4198.

Oye, V., and M. Roth (2005), Source parameters of microearthquakes from the 1.5 km deep Pyhäsalmi ore mine, Finland, paper presented at Proceedings, Thirtieth Workshop on Geothermal Reservoir Engineering, Stanford University, Stanford, California, January.

Paskaleva, I., A. G. Aronov, R. R. Seroglazov, and T. I. Aronova (2006), Characteristic features of induced seismic processes in mining regions exemplified by the potassium salt deposits in Belarus and Bulgaria, Acta Geodaetica et Geophysica Hungarica, 41, 293-303.

Pavlou, K., G. Drakatos, V. Kouskouna, K. Makropoulos, and H. Kranis (2016), Seismicity study in Pournari reservoir area (w. Greece) 1981–2010, Journal of Seismology, 20, 701-710.

Pavlou, K., G. Kaviris, K. Chousianitis, G. Drakatos, V. Kouskouna, and K. Makropoulos (2013), Seismic hazard assessment in Polyphyto dam area (nw Greece) and its relation with the "unexpected" earthquake of 13 May 1995 (Ms= 6.5, nw Greece), Nat. Hazards Earth Sys. Sci, 13, 141-149.

Pavlovski, O. A. (1998), Radiological consequences of nuclear testing for the population of the former USSR (input information, models, dose, and risk estimates), in Atmospheric nuclear tests, pp. 219-260, Springer.

Pechmann, J. C., W. J. Arabasz, K. L. Pankow, R. Burlacu, and M. K. McCarter (2008), Seismological report on the 6 August 2007 Crandall Canyon mine collapse in Utah, Seismological Research Letters, 79, 620-636.

Pennington, W. D., S. D. Davis, S. M. Carlson, J. DuPree, and T. E. Ewing (1986), The evolution of seismic barriers and asperities caused by the depressuring of fault planes in oil and gas fields of south Texas, Bulletin of the Seismological Society of America, 76, 939-948.

Petersen, M. D., C. S. Mueller, M. P. Moschetti, S. M. Hoover, A. L. Llenos, W. L. Ellsworth, A. J. Michael, J. L. Rubinstein, A. F. McGarr, and K. S. Rukstales (2016), One-year seismic hazard forecast for the central and eastern United States from induced and natural earthquakes, US Geological Survey.

Petersen, M. D., C. S. Mueller, M. P. Moschetti, S. M. Hoover, J. L. Rubinstein, A. L. Llenos, A. J. Michael, W. L. Ellsworth, A. McGarr, and A. A. Holland (2015), Incorporating induced seismicity in the 2014 United States national seismic hazard model: Results of 2014 workshop and sensitivity studies, US Department of the Interior, US Geological Survey.

Phillips, W. S., T. D. Fairbanks, J. T. Rutledge, and D. W. Anderson (1998), Induced microearthquake patterns and oil-producing fracture systems in the Austin Chalk, Tectonophysics, 289, 153-169.

Phillips, W. S., J. T. Rutledge, L. S. House, and M. C. Fehler (2002), Induced microearthquake patterns in hydrocarbon and geothermal reservoirs: Six case studies, in The mechanism of induced seismicity, pp. 345-369, Springer.

Piccinelli, F. G., M. Mucciarelli, P. Federici, and D. Albarello (1995), The microseismic network of the Ridracoli dam, north Italy: Data and interpretations, Pure and applied geophysics, 145, 97-108.

Plotnikova, L. M., B. S. Nurtaev, J. R. Grasso, L. M. Matasova, and R. Bossu (1996), The character and extent of seismic deformation in the focal zone of Gazli earthquakes of 1976 and 1984, M> 7.0, in Induced seismic events, pp. 377-387, Springer.

Pomeroy, P. W., D. W. Simpson, and M. L. Sbar (1976), Earthquakes triggered by surface quarrying-the Wappingers falls, New York sequence of June, 1974, Bulletin of the Seismological Society of America, 66, 685-700.

Pramono, B., and D. Colombo (2005), Microearthquake characteristics in Darajat geothermal field, Indonesia, paper presented at World Geothermal Congress 2005, Antalya, Turkey, 24–29 April, 2005.

Prioul, R., F. H. Cornet, C. Dorbath, I. Dorbath, M. Ogena, and E. Ramos (2000), An induced seismicity experiment across a creeping segment of the Philippine fault, Journal of geophysical research, 105, 13,595-513,612.

Rajendran, K. (1995), Sensitivity of a seismically active reservoir to low-amplitude fluctuations: Observations from Lake Jocassee, South Carolina, Pure and applied geophysics, 145, 87-95.

Raleigh, C. B., J. H. Healy, and J. D. Bredehoeft (1976), An experiment in earthquake control at Rangely, Colorado, Science, 191, 1230-1237.

Rastogi, B. K., C. V. R. K. Rao, R. K. Chadha, and H. K. Gupta (1986), Microearthquakes near Osmansagar reservoir, Hyderabad, India, Physics of the earth and planetary interiors, 44, 134-141.

Redmayne, D. W. (1988), Mining induced seismicity in UK coalfields identified on the BGS national seismograph network, Geological Society, London, Engineering Geology Special Publications, 5, 405-413.

Reyners, M. (1988), Reservoir-induced seismicity at Lake Pukaki, New Zealand, Geophysical Journal International, 93, 127-135.

Ringdal, F., P. D. Marshall, and R. W. Alewine (1992), Seismic yield determination of Soviet underground nuclear explosions at the Shagan River test site, Geophysical Journal International, 109, 65-77.

Rojas, E., P. Cavieres, R. Dunlop, and S. Gaete (2000), Control of induced seismicity at El Teniente mine Codelco-Chile, Proceeding, Massmin 2000, 777-781.

Ross, A., G. R. Foulger, and B. R. Julian (1999), Source processes of industrially-induced earthquakes at The Geysers geothermal area, California, Geophysics, 64, 1877-1889.

Rubinstein, J. L., W. L. Ellsworth, and A. McGarr (2012), The 2001-present triggered seismicity sequence in the Raton Basin of southern Colorado/northern New Mexico, paper presented at AGU Fall Meeting Abstracts.

Rubinstein, J. L., W. L. Ellsworth, A. McGarr, and H. M. Benz (2014), The 2001–present induced earthquake sequence in the Raton Basin of northern New Mexico and southern Colorado, Bulletin of the Seismological Society of America.

Rubinstein, J. L., and A. B. Mahani (2015), Myths and facts on wastewater injection, hydraulic fracturing, enhanced oil recovery, and induced seismicity, Seismological Research Letters, 86, 1060-1067.

Rutledge, J. T., W. S. Phillips, and B. K. Schuessler (1998), Reservoir characterization using oil-production-induced microseismicity, Clinton County, Kentucky, Tectonophysics, 289, 129-152.

Sanford, A. R., T. M. Mayeau, J. W. Schlue, R. C. Aster, and L. H. Jaksha (2006), Earthquake catalogs for New Mexico and bordering areas II: 1999–2004, New Mexico Geology, 28.

Sargsyan, L. S. (2009), Reservoir-triggered seismicity in Armenian large dams, Journal of Seismology and Earthquake Engineering, 11, 153.

Sasaki, S. (1998), Characteristics of microseismic events induced during hydraulic fracturing experiments at the Hijiori hot dry rock geothermal energy site, Yamagata, Japan, Tectonophysics, 289, 171-188.

Sato, K., and Y. Fujii (1988), Induced seismicity associated with longwall coal mining, paper presented at International Journal of Rock Mechanics and Mining Sciences & Geomechanics Abstracts, Elsevier.

Sato, K., and Y. Fujii (1989), Source mechanism of a large scale gas outburst at Sunagawa coal mine in Japan, Pure and applied geophysics, 129, 325-343.

Sato, K., T. Isobe, N. Mori, and T. Goto (1986), 9. Microseismic activity associated with hydraulic mining, paper presented at International Journal of Rock Mechanics and Mining Sciences & Geomechanics Abstracts, Elsevier.

Schlutz, R., V. Stern, and Y. J. Gu (2014), An investigation of seismicity clustered near the Cordel field, west central Alberta, and its relation to a nearby disposal well, Journal of Geophysical Research: Solid Earth, 119, 3410-3423, doi:10.1002/2013JB010836.

Schultz, R., S. Mei, D. Pană, V. Stern, Y. J. Gu, A. Kim, and D. Eaton (2015), The Cardston earthquake swarm and hydraulic fracturing of the Exshaw Formation (Alberta Bakken Play), Bulletin of the Seismological Society of America.

Schultz, R., V. Stern, M. Novakovic, G. Atkinson, and Y. J. Gu (2015), Hydraulic fracturing and the Crooked Lake sequences: Insights gleaned from regional seismic networks, Geophysical Research Letters, 42, 2750-2758.

Seeber, L., J. G. Armbruster, and W.-Y. Kim (2004), A fluid-injection-triggered earthquake sequence in Ashtabula, Ohio: Implications for seismogenesis in stable continental regions, Bulletin of the Seismological Society of America, 94, 76-87.

Seeber, L., J. G. Armbruster, W. Y. Kim, N. Barstow, and C. Scharnberger (1998), The 1994 Cacoosing Valley earthquakes near Reading, Pennsylvania: A shallow rupture triggered by quarry unloading, Journal of Geophysical Research: Solid Earth, 103, 24505-24521.

Segall, P. (1985), Stress and subsidence resulting from subsurface fluid withdrawal in the epicentral region of the 1983 Coalinga earthquake, Journal of Geophysical Research: Solid Earth, 90, 6801-6816.

Segall, P. (1989), Earthquakes triggered by fluid extraction, Geology, 17, 942-946.

Semmane, F., I. Abacha, A. K. Yelles-Chaouche, A. Haned, H. Beldjoudi, and A. Amrani (2012), The earthquake swarm of December 2007 in the Mila region of northeastern Algeria, Natural hazards, 64, 1855-1871.

Shapiro, S. A., C. Dinske, C. Langenbruch, and F. Wenzel (2010), Seismogenic index and magnitude probability of earthquakes induced during reservoir fluid stimulations, The Leading Edge, 29, 304-309.

Shapiro, S. A., J. Kummerow, C. Dinske, G. Asch, E. Rothert, J. Erzinger, H. J. Kümpel, and R. Kind (2006), Fluid induced seismicity guided by a continental fault: Injection experiment of 2004/2005 at the German deep drilling site (KTB), Geophysical Research Letters, 33.

Sherburn, S., S. Bourguignon, S. Bannister, S. Sewell, B. Cumming, C. Bardsley, J. Quinao, and I. Wallis (2013), Microseismicity at Rotokawa geothermal field, 2008 to 2012, paper presented at Proceedings of the 35th New Zealand geothermal workshop. Rotorua, New Zealand.

Sherburn, S., C. Bromley, S. Bannister, S. Sewell, and S. Bourguignon (2015), New Zealand geothermal induced seismicity: An overview.

Shirley, J. E. (1980), Tasmanian seismicity—natural and reservoir-induced, Bulletin of the Seismological Society of America, 70, 2203-2220.

Shivakumar, K., M. V. M. S. Rao, C. Srinivasan, and K. Kusunose (1996), Multifractal analysis of the spatial distribution of area rockbursts at Kolar gold mines, paper presented at International journal of rock mechanics and mining sciences & geomechanics abstracts, Elsevier.

Silitonga, T. H., E. E. Siahaan, and Suroso (2005), A Poisson's ratio distribution from Wadati diagram as indicator of fracturing of Lahendong geothermal field, north Sulawesi, Indonesia, paper presented at World Geothermal Congress 2005, Antalya, Turkey, 24–29 April, 2005.

Simiyu, S. M., and G. R. Keller (2000), Seismic monitoring of the Olkaria geothermal area, Kenya Rift Valley, Journal of volcanology and geothermal research, 95, 197-208.

Simpson, D. W., and W. Leith (1985), The 1976 and 1984 Gazli, USSR, earthquakes—were they induced?, Bulletin of the Seismological Society of America, 75, 1465-1468.

Simpson, D. W., and S. K. Negmatullaev (1981), Induced seismicity at Nurek reservoir, Tadjikistan, USSR, Bulletin of the Seismological Society of America, 71, 1561-1586.

Skoumal, R. J., M. R. Brudzinski, and B. S. Currie (2015), Earthquakes induced by hydraulic fracturing in Poland Township, Ohio, Bulletin of the Seismological Society of America, 105, 189-197.

Son, M. (2015), Microevent detection based on waveform cross-correlation in the Dogye mining area, Korea, paper presented at 2015 AGU Fall Meeting.

Stein, S., M. Liu, T. Camelbeeck, M. Merino, A. Landgraf, E. Hintersberger, and S. Kuebler (2015), Challenges in assessing seismic hazard in intraplate Europe, Geological Society, London, Special Publications, 432, SP432. 437.

Stork, A. L., J. P. Verdon, and J.-M. Kendall (2015), The microseismic response at the In Salah carbon capture and storage (CCS) site, International Journal of Greenhouse Gas Control, 32, 159-171.

Styles, P., P. Gasparini, E. Huenges, P. Scandone, S. Lasocki, and F. Terlizzese (2014), Report on the hydrocarbon exploration and seismicity in Emilia region, 1-213.

Suckale, J. (2009), Induced seismicity in hydrocarbon fields, Advances in geophysics, 51, 55-106.

Sumy, D. F., E. S. Cochran, K. M. Keranen, M. Wei, and G. A. Abers (2014), Observations of static coulomb stress triggering of the November 2011 M5.7 Oklahoma earthquake sequence, Journal of Geophysical Research: Solid Earth, 119, 1904-1923.

Sun, X., and S. Hartzell (2014), Finite-fault slip model of the 2011 Mw 5.6 Prague, Oklahoma earthquake from regional waveforms, Geophysical Research Letters, 41, 4207-4213.

Swanson, P. L. (1992), Mining-induced seismicity in faulted geologic structures: An analysis of seismicity-induced slip potential, Pure and applied geophysics, 139, 657-676.

Sylvester, A. G., and J. Heinemann (1996), Preseismic tilt and triggered reverse faulting due to unloading in a diatomite quarry near Lompoc, California, Seismological Research Letters, 67, 11-18.

Sze, E. K.-M. (2005), Induced seismicity analysis for reservoir characterization at a petroleum field in Oman, Massachusetts Institute of Technology.

Tadokoro, K., M. Ando, and K. y. Nishigami (2000), Induced earthquakes accompanying the water injection experiment at the Nojima fault zone, Japan: Seismicity and its migration, Journal of Geophysical Research: Solid Earth, 105, 6089-6104.

Talwani, P. (1995), Speculation on the causes of continuing seismicity near Koyna reservoir, India, Pure and applied geophysics, 145, 167-174.

Tang, C., T. Ma, and X. Ding (2009), On stress-forecasting strategy of earthquakes from stress buildup, stress shadow and stress transfer (SSS) based on numerical approach, Earthquake Science, 22, 53-62.

Tang, C. a., J. Wang, and J. Zhang (2010), Preliminary engineering application of microseismic monitoring technique to rockburst prediction in tunneling of Jinping II project, Journal of Rock Mechanics and Geotechnical Engineering, 2, 193-208.

Taylor, O.-D. S., T. A. Lee III, and A. P. Lester (2015), Hazard and risk potential of unconventional hydrocarbon development-induced seismicity within the central United States, Natural Hazards Review, 16, 04015008.

Taylor, O.-D. S., A. P. Lester, and T. A. Lee III (2015), Unconventional hydrocarbon development hazards within the central United States. Report 1: Overview and potential risk to infrastructure, DTIC Document.

Telesca, L., T. Matcharasvili, T. Chelidze, and N. Zhukova (2012), Relationship between seismicity and water level in the Enguri high dam area (Georgia) using the singular spectrum analysis, Natural Hazards and Earth System Science, 12, 2479-2485.

Terakawa, T., S. A. Miller, and N. Deichmann (2012), High fluid pressure and triggered earthquakes in the enhanced geothermal system in Basel, Switzerland, Journal of Geophysical Research: Solid Earth, 117.

Terashima, T. (1981), Survey on induced seismicity at Mishraq area in Iraq, Journal of Physics of the Earth, 29, 371-375.

Teyssoneyre, V., B. Feignier, J. Šilény, and O. Coutant (2002), Moment tensor inversion of regional phases: Application to a mine collapse, in The mechanism of induced seismicity, pp. 111-130, Springer.

Tiira, T. (1996), Discrimination of nuclear explosions and earthquakes from teleseismic distances with a local network of short period seismic stations using artificial neural networks, Physics of the Earth and Planetary Interiors, 97, 247-268.

TNO (2014), Literature review on injection-related induced seismicity and its relevance to nitrogen injection.

Torcal, F., I. Serrano, J. Havskov, J. L. Utrillas, and J. Valero (2005), Induced seismicity around the Tous New dam (Spain), Geophysical Journal International, 160, 144-160.

Townend, J., and M. D. Zoback (2000), How faulting keeps the crust strong, Geology, 28, 399-402.

Trifu, C.-I., T. I. Urbancic, and R. P. Young (1995), Source parameters of mining-induced seismic events: An evaluation of homogeneous and inhomogeneous faulting models for assessing damage potential, Pure and applied geophysics, 145, 3-27.

Trippi, M. H., H. E. Belkin, S. Dai, S. J. Tewalt, and C.-J. Chou (2014), USGS compilation of geographic information system (GIS) data representing coal mines and coal-bearing areas in China, US Geological Survey.

Turbitt, T. (1988), Bulletin of British earthquakes. British Geological Survey technical report wl/88/11.

Turuntaev, S. B. (1994), Temporal and spatial structures of triggered seismicity in Romashkinskoye oil-field, paper presented at Rock Mechanics in Petroleum Engineering, Society of Petroleum Engineers.

Urban, E., and J. F. Lermo (2012), Relationship of local seismic activity, injection wells and active faults in the geothermal fields of Mexico, paper presented at Proceedings of Thirty-Seventh Workshop on Geothermal Reservoir Engineering, Stanford University, Stanford, CA, SGP-TR-194.

Urban, E., and J. F. Lermo (2013), Local seismicity in the exploitation of Los Humeros geothermal field, Mexico, paper presented at Proceedings of the Thirty-Eighth Workshop on Geothermal Reservoir Engineering.

Urbancic, T. I. J., V. J. Shumila, J. T. J. Rutledge, and R. J. J. Zinno (1999), Determining hydraulic fracture behavior using microseismicity, paper presented at Vail Rocks 1999, The 37th US Symposium on Rock Mechanics (USRMS), American Rock Mechanics Association.

Vallejos, J. A., and S. D. McKinnon (2011), Correlations between mining and seismicity for re-entry protocol development, International Journal of Rock Mechanics and Mining Sciences, 48, 616-625.

Valoroso, L., L. Improta, L. Chiaraluce, R. Di Stefano, L. Ferranti, A. Govoni, and C. Chiarabba (2009), Active faults and induced seismicity in the Val d'Agri area (southern Apennines, Italy), Geophysical Journal International, 178, 488-502.

van der Elst, N. J., H. M. Savage, K. M. Keranen, and G. A. Abers (2013), Enhanced remote earthquake triggering at fluid-injection sites in the midwestern United States, Science, 341, 164-167.

van der Voort, N., and F. Vanclay (2015), Social impacts of earthquakes caused by gas extraction in the province of Groningen, the Netherlands, Environmental Impact Assessment Review, 50, 1-15.

Van Eck, T., F. Goutbeek, H. Haak, and B. Dost (2006), Seismic hazard due to small-magnitude, shallow-source, induced earthquakes in the Netherlands, Engineering Geology, 87, 105-121.

Van Eijs, R. M. H. E., F. M. M. Mulders, M. Nepveu, C. J. Kenter, and B. C. Scheffers (2006), Correlation between hydrocarbon reservoir properties and induced seismicity in the Netherlands, Engineering Geology, 84, 99-111.

Van Wees, J. D., L. Buijze, K. Van Thienen-Visser, M. Nepveu, B. B. T. Wassing, B. Orlic, and P. A. Fokker (2014), Geomechanics response and induced seismicity during gas field depletion in the Netherlands, Geothermics, 52, 206-219.

Verdon, J. P. (2014), Significance for secure CO2 storage of earthquakes induced by fluid injection, Environmental Research Letters, 9, 064022.

Verdon, J. P., J.-M. Kendall, A. L. Stork, R. A. Chadwick, D. J. White, and R. C. Bissell (2013), Comparison of geomechanical deformation induced by megatonne-scale CO2 storage at Sleipner, Weyburn, and In Salah, Proceedings of the National Academy of Sciences, 110, E2762-E2771.

Walsh, F. R., and M. D. Zoback (2015), Oklahoma's recent earthquakes and saltwater disposal, Science advances, 1, e1500195.

Walter, J. I., P. J. Dotray, C. Frohlich, and J. F. W. Gale (2016), Earthquakes in northwest Louisiana and the Texas–Louisiana border possibly induced by energy resource activities within the Haynesville Shale Play, Seismological Research Letters, 87, 285-294.

Wang, P., M. J. Small, W. Harbert, and M. Pozzi (2016), A Bayesian approach for assessing seismic transitions associated with wastewater injections, Bulletin of the Seismological Society of America.

Wang, R., Y. J. Gu, R. Schultz, A. Kim, and G. Atkinson (2016), Source analysis of a potential hydraulic fracturing induced earthquake near Fox Creek, Alberta, Geophysical Research Letters.

Wang, W., X. Meng, Z. Peng, Q. F. Chen, and N. Liu (2015), Increasing background seismicity and dynamic triggering behaviors with nearby mining activities around Fangshan pluton in Beijing, china, Journal of Geophysical Research: Solid Earth, 120, 5624-5638.

Wang, Z., C. N. Tang, T. H. Ma, L. C. Li, and Y. F. Yang (2012), Research on the surrounding rock damage of deep hard rock tunnels caused by bottom excavation, paper presented at Applied Mechanics and Materials, Trans Tech Publ.

Weingarten, M., S. Ge, J. W. Godt, B. A. Bekins, and J. L. Rubinstein (2015), High-rate injection is associated with the increase in US mid-continent seismicity, Science, 348, 1336-1340.

Weiser, D. A. (2016), Maximum magnitude and probabilities of induced earthquakes in California geothermal fields: Applications for a science-based decision framework, University of California.

Westbrook, G. K., N. J. Kusznir, C. W. A. Browitt, and B. K. Holdsworth (1980), Seismicity induced by coal mining in Stoke-on-Trent (UK), Engineering Geology, 16, 225-241.

Wettainen, T., and J. Martinsson (2014), Estimation of future ground vibration levels in Malmberget town due to mining-induced seismic activity, Journal of the Southern African Institute of Mining and Metallurgy, 114, 835-843.

Wheeler, R. L. (2009), Sizes of the largest possible earthquakes in the central and eastern United States-summary of a workshop, September 8-9, 2008, Golden, Colorado, US Geological Survey.

Wilson, M. P., R. J. Davies, G. R. Foulger, B. R. Julian, P. Styles, J. G. Gluyas, and S. Almond (2015), Anthropogenic earthquakes in the UK: A national baseline prior to shale exploitation, Marine and Petroleum Geology, 30, e17.

Windsor, C. R., P. Caviares, E. Villaescusa, and J. Pereira (2006), Reconciliation of strain, structure and stress in the El Teniente mine region, Chile, paper presented at Proceedings of International Symposium on In Situ Rock Stress, Trondheim, Norway.

Wiszniowski, J., N. Van Giang, B. Plesiewicz, G. Lizurek, D. Q. Van, L. Q. Khoi, and S. Lasocki (2015), Preliminary results of anthropogenic seismicity monitoring in the region of Song Tranh 2 reservoir, central Vietnam, Acta Geophysica, 63, 843-862.

Wolhart, S. L., T. A. Harting, J. E. Dahlem, T. Young, M. J. Mayerhofer, and E. P. Lolon (2006), Hydraulic fracture diagnostics used to optimize development in the Jonah field, paper presented at SPE Annual Technical Conference and Exhibition, Society of Petroleum Engineers.

Xie, L., K.-B. Min, and Y. Song (2015), Observations of hydraulic stimulations in seven enhanced geothermal system projects, Renewable Energy, 79, 56-65.

Xiumin, M. A., L. I. Zhen, P. E. N. G. Hua, J. I. A. N. G. Jingjie, Z. H. A. O. Fang, H. A. N. Chaopu, Y. U. A. N. Pengxiang, L. U. Shengzhou, and P. E. N. G. Liguo (2015), Fluid-injection-induced seismicity experiment of the WFSD-3P borehole, Acta Geologica Sinica (English Edition), 89, 1057-1058.

Xu, N.-w., C.-a. Tang, H. Li, F. Dai, K. Ma, J.-d. Shao, and J.-c. Wu (2012), Excavation-induced microseismicity: Microseismic monitoring and numerical simulation, Journal of Zhejiang University SCIENCE A, 13, 445-460.

Yeck, W. L., A. F. Sheehan, M. Weingarten, J. Nakai, and S. Ge (2014), The 2014 Greeley, Colorado earthquakes: Science, industry, regulation, and media, paper presented at AGU Fall Meeting Abstracts.

Younger, P. L., J. G. Gluyas, and W. E. Stephens (2012), Development of deep geothermal energy resources in the UK, Proceedings of the Institution of Civil Engineers-Energy, 165, 19-32.

Yu, Q., C.-A. Tang, L. Li, G. Cheng, and L.-X. Tang (2015), Study on rockburst nucleation process of deep-buried tunnels based on microseismic monitoring, Shock and Vibration, 501, 685437.

Zaliapin, I., and Y. Ben-Zion (2016), Discriminating characteristics of tectonic and human-induced seismicity, Bulletin of the Seismological Society of America.

Zang, A., V. Oye, P. Jousset, N. Deichmann, R. Gritto, A. McGarr, E. Majer, and D. Bruhn (2014), Analysis of induced seismicity in geothermal reservoirs–an overview, Geothermics, 52, 6-21.

Zedník, J., and J. Pazdírková (2014), Seismic activity in the Czech Republic in 2012, Studia Geophysica et Geodaetica, 58, 342.

Zedník, J., J. Pospíšil, B. Růžek, J. Horálek, A. Boušková, P. Jedlička, Z. Skácelová, V. Nehybka, K. Holub, and J. Rušajová (2001), Earthquakes in the Czech Republic and surrounding regions in 1995–1999, Studia Geophysica et Geodaetica, 45, 267-282.

Zhang, W.-d., and T.-h. Ma (2013), Research on characteristic of rockburst and rules of microseismic monitoring at headrace tunnels in Jinping II hydropower station, paper presented at Digital Manufacturing and Automation (ICDMA), 2013 Fourth International Conference on, IEEE.

Zhang, Y., W. Feng, L. Xu, C. Zhou, and Y. Chen (2009), Spatio-temporal rupture process of the 2008 great Wenchuan earthquake, Science in China Series D: Earth Sciences, 52, 145-154.

Zhang, Y., M. Person, J. Rupp, K. Ellett, M. A. Celia, C. W. Gable, B. Bowen, J. Evans, K. Bandilla, and P. Mozley (2013), Hydrogeologic controls on induced seismicity in crystalline basement rocks due to fluid injection into basal reservoirs, Groundwater, 51, 525-538.

Zoback, M. D., and S. M. Gorelick (2012), Earthquake triggering and large-scale geologic storage of carbon dioxide, Proceedings of the National Academy of Sciences, 109, 10164-10168.

Zoback, M. D., and H. P. Harjes (1997), Injection-induced earthquakes and crustal stress at 9 km depth at the KTB deep drilling site, Germany, Journal of Geophysical Research: Solid Earth, 102, 18477-18491.

Zoback, M. D., and J. C. Zinke (2002), Production-induced normal faulting in the Valhall and Ekofisk oil fields, in The mechanism of induced seismicity, pp. 403-420, Springer.

Appendix 7: Maps of the cases in the database for the world and a selection of smaller regions.

The following maps are given:

1. Symbols used on the maps. Colors indicate different categories of seismogenic activity, circle sizes indicate the magnitudes of the largest reported induced earthquakes in each category, and inverted triangles indicate cases for which this magnitude was not reported.

2. Cases of induced seismicity world-wide. (Mollweide projection, centered on the Greenwich meridian.)

3. Cases of induced seismicity world-wide. Red boxes show the locations of the regional maps. (Mollweide projection, centered on the Greenwich meridian.)

4. Cases of induced seismicity world-wide. (Mollweide projection, centered on longitude 180°.)

5. Cases of induced seismicity world-wide. Red boxes show the locations of the regional maps. (Mollweide projection, centered on longitude 180°.)

6. Regional map: Europe

7. Regional map: the Middle East

8. Regional map: central Asia

9. Regional map: east Asia

10. Regional map: India and vicinity

11. Regional map: southern Africa

12. Regional map: North America

13. Regional map: The USA and southern Canada

14. Regional map: South America

15. Regional map: central America

16. Regional map: New Zealand

17. Regional map: Australia.

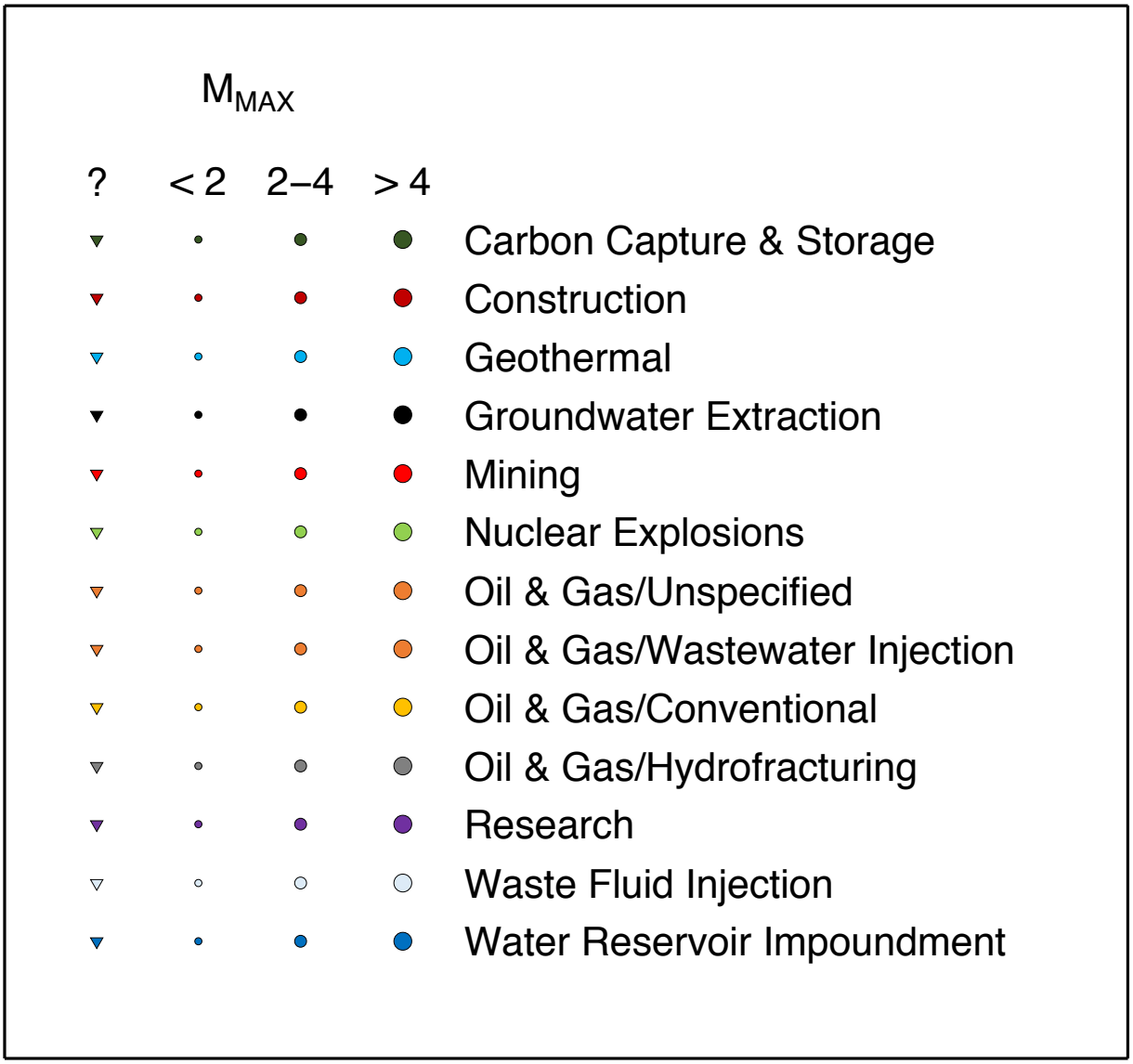
M_{MAX}
?
< 2
2–4
> 4
Carbon Capture & Storage
Construction
Geothermal
Groundwater Extraction
Mining
Nuclear Explosions
Oil & Gas/Unspecified
Oil & Gas/Wastewater Injection
Oil & Gas/Conventional
Oil & Gas/Hydrofracturing
Research
Waste Fluid Injection
Water Reservoir Impoundment

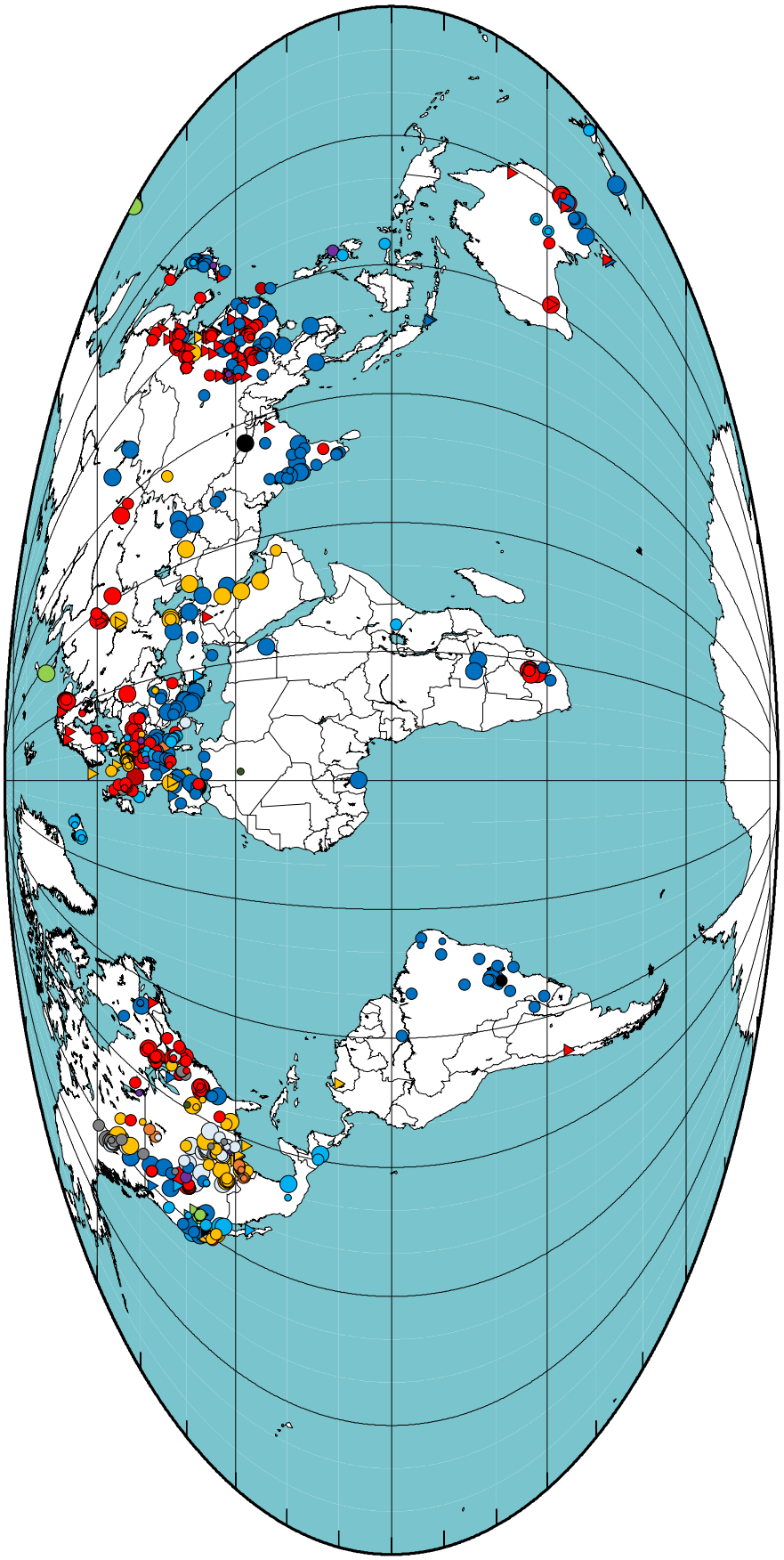

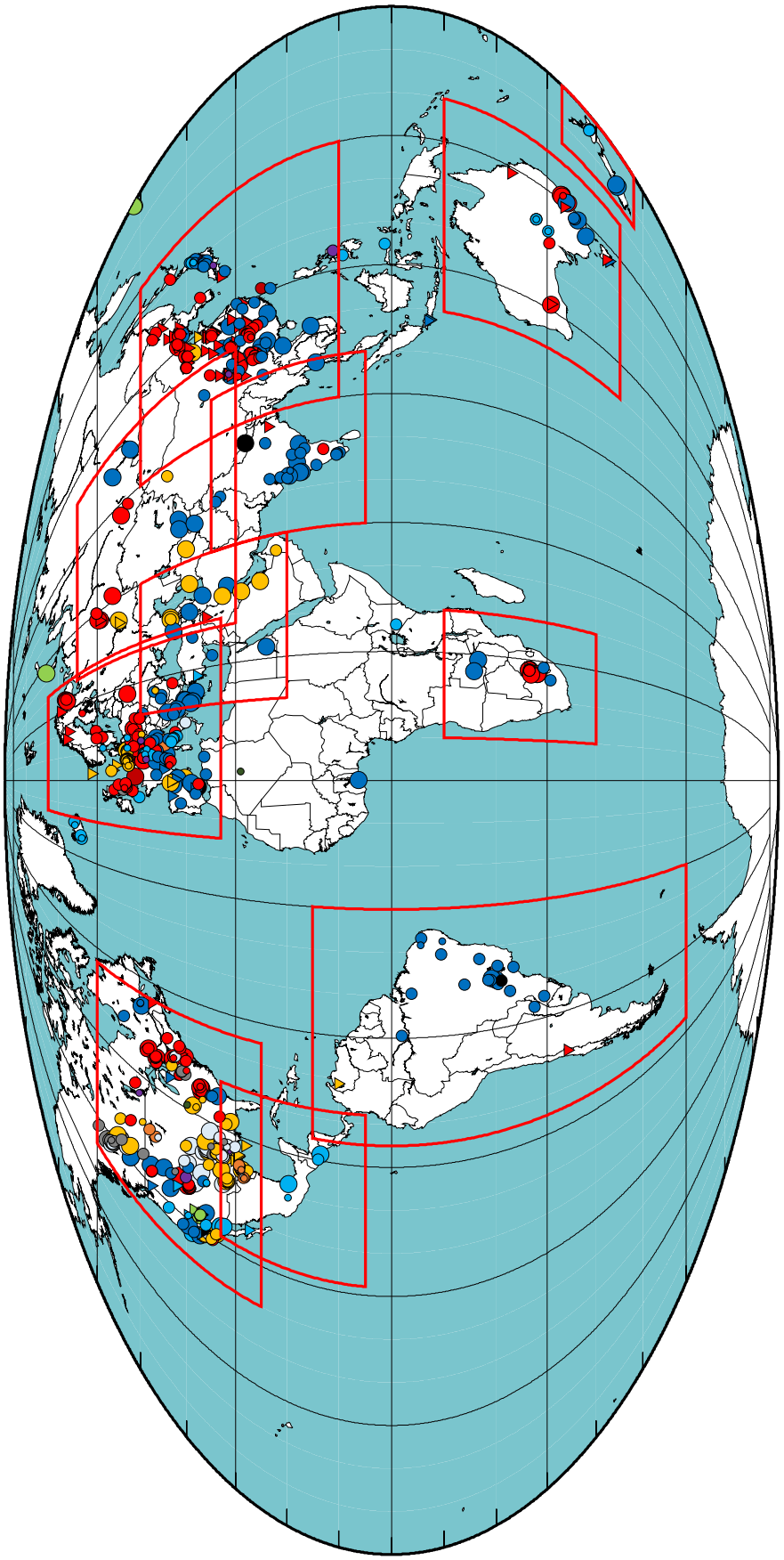

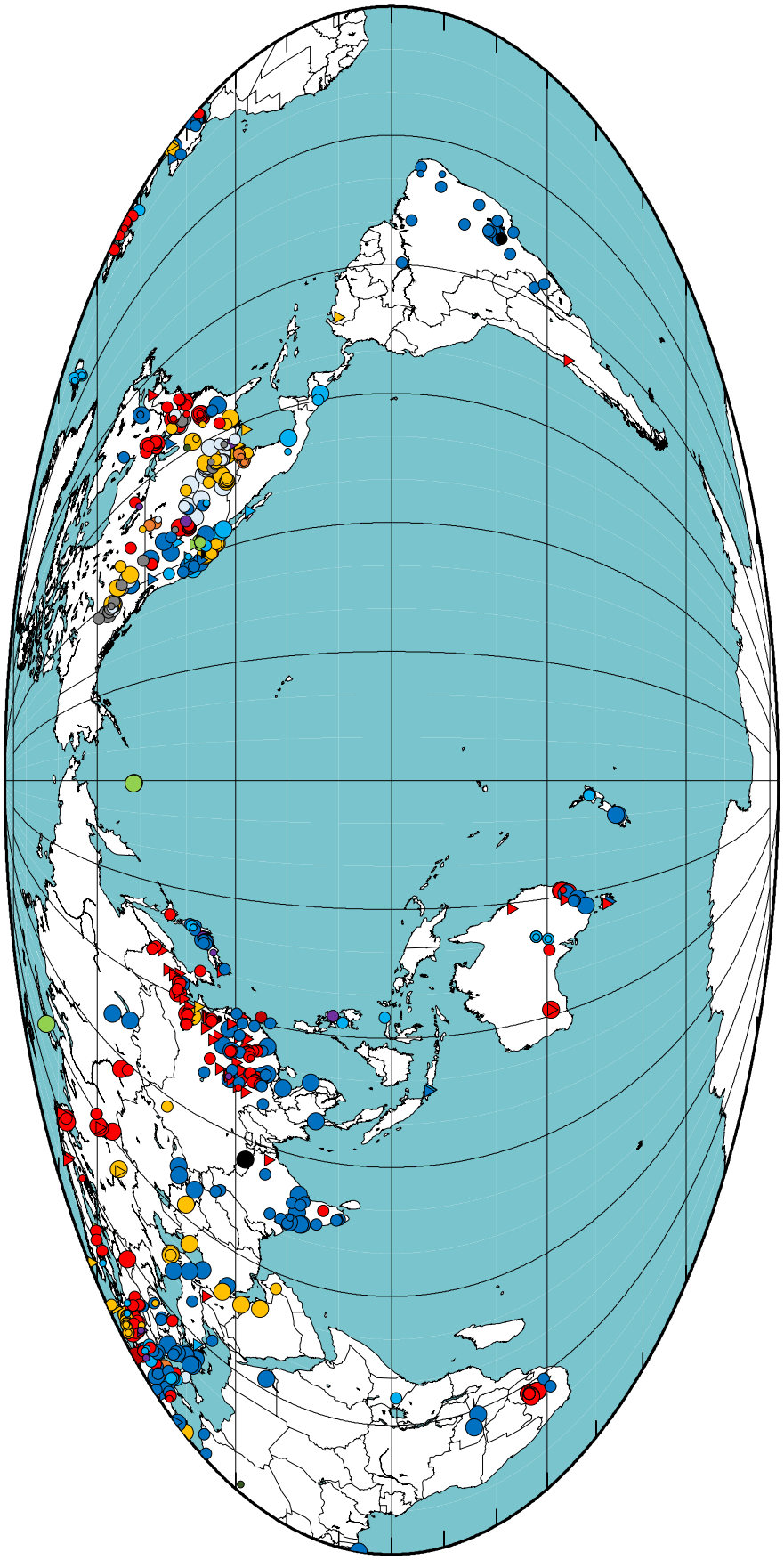

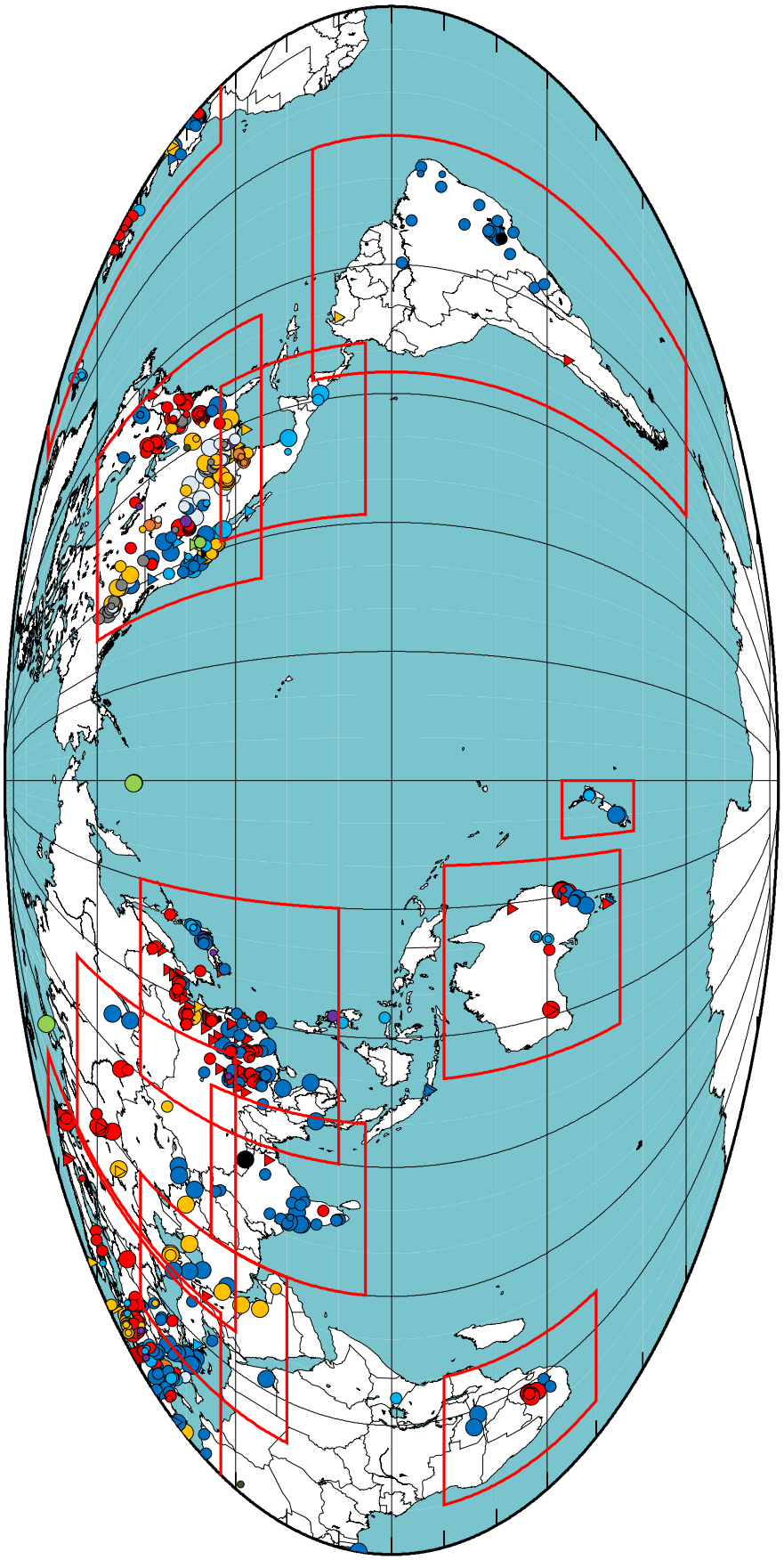

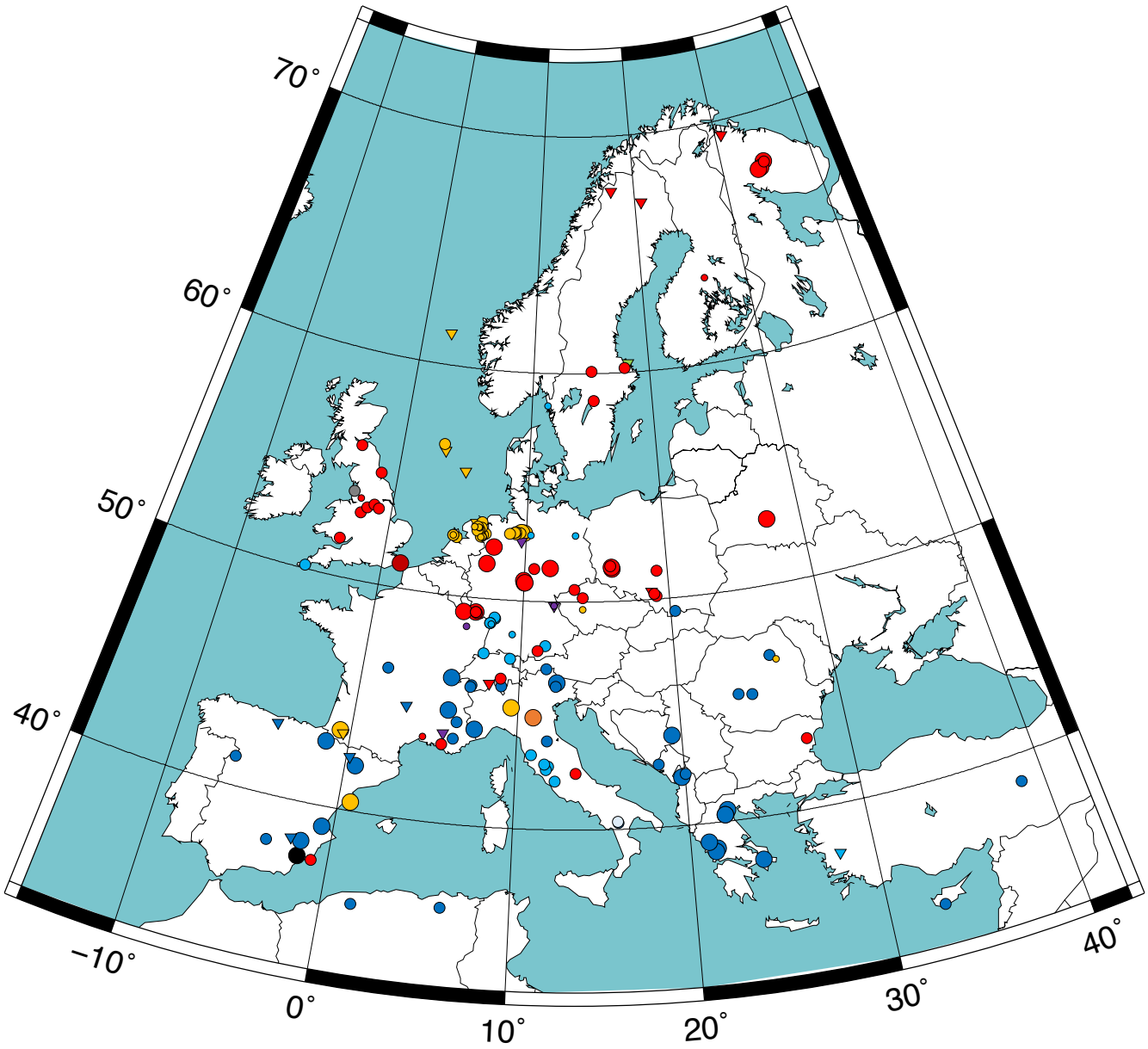
70°
60°
50°
40°
−10°
0°
10°
20°
30°
40°

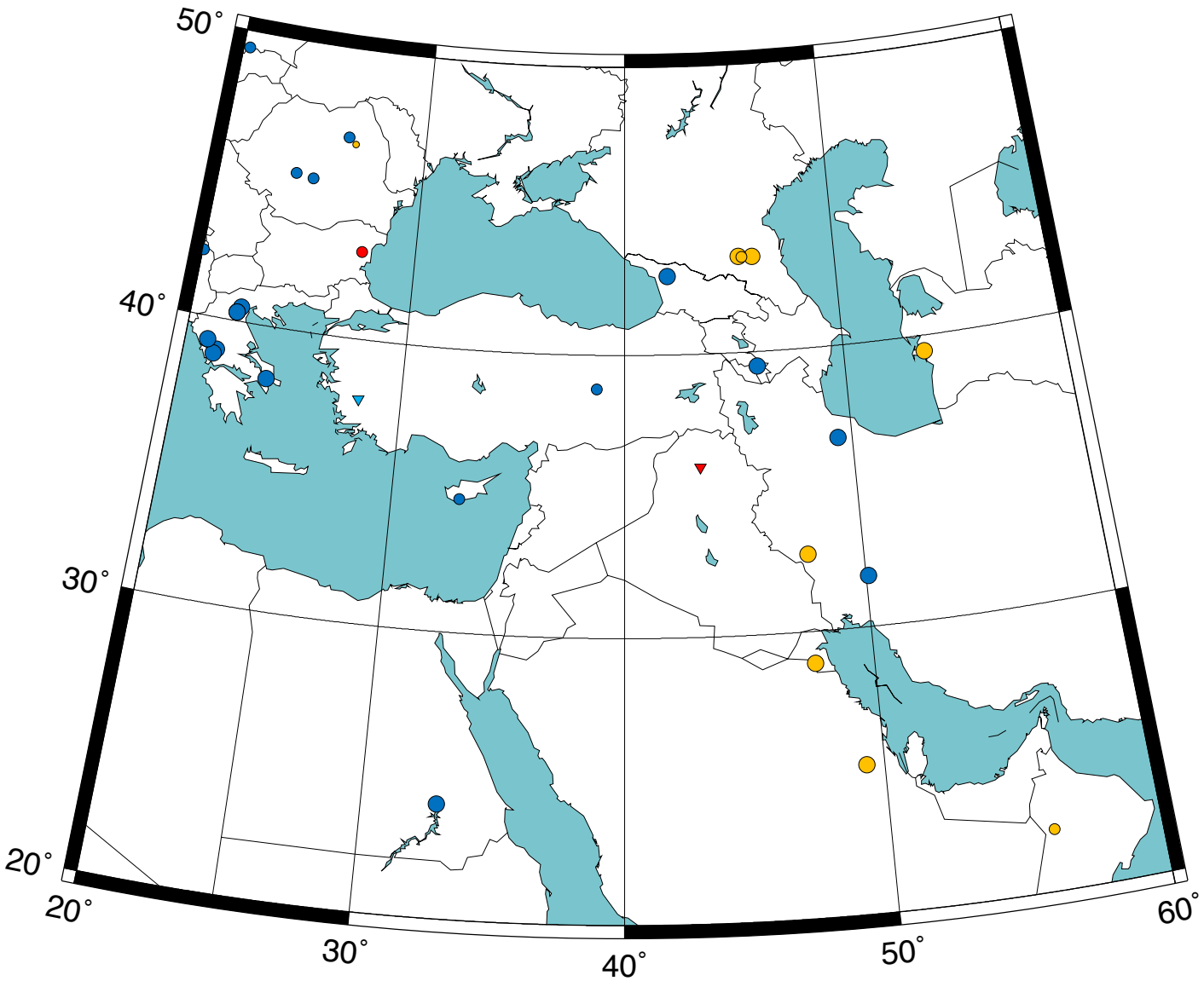
50°
40°
30°
20°
20°
30°
40°
50°
60°

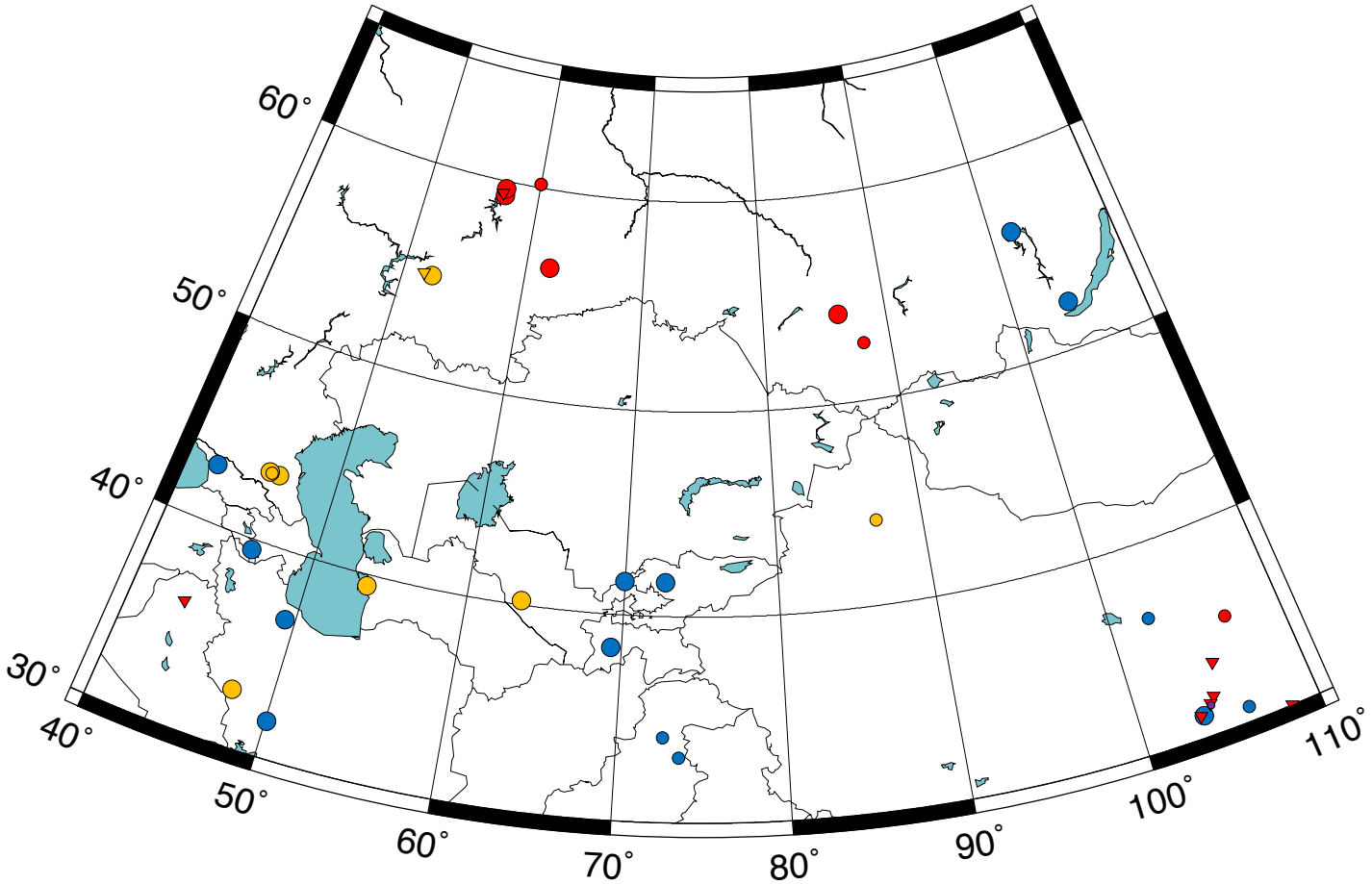
60°
50°
40°
30°
40°
50°
60°
70°
80°
90°
100°
110°

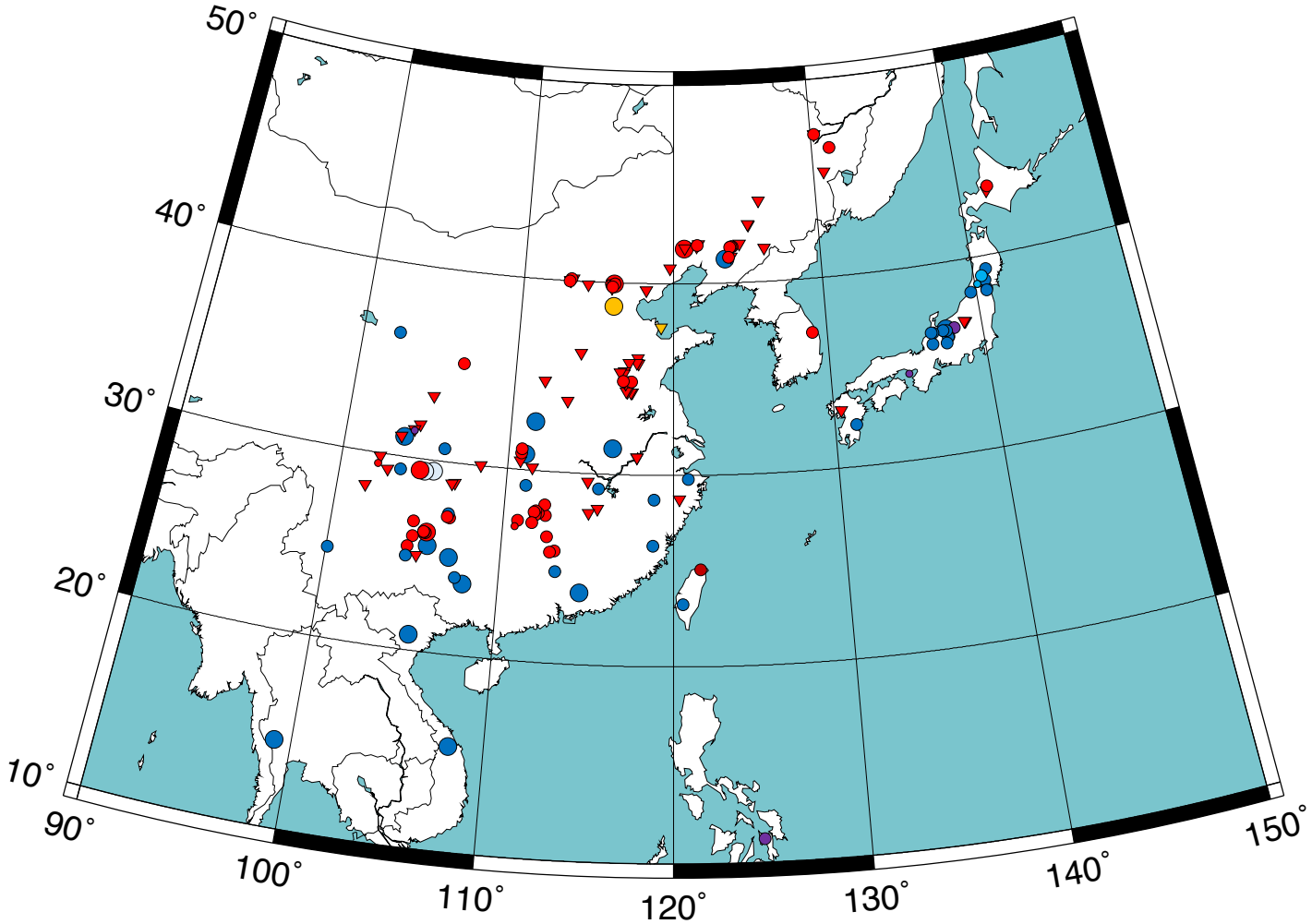
50°
40°
30°
20°
10°
90°
100°
110°
120°
130°
140°
150°

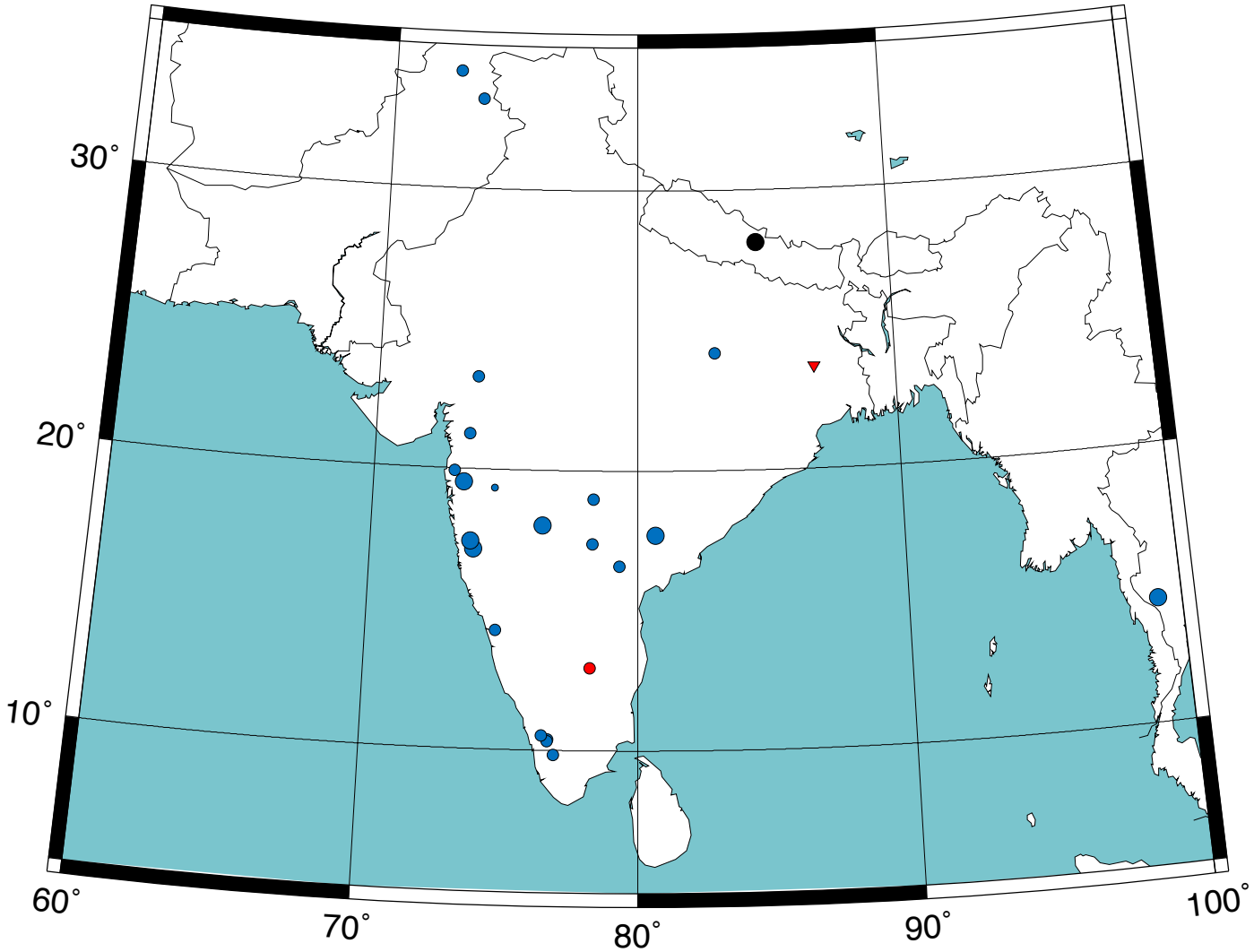
30°
20°
10°
60°
70°
80°
90°
100°

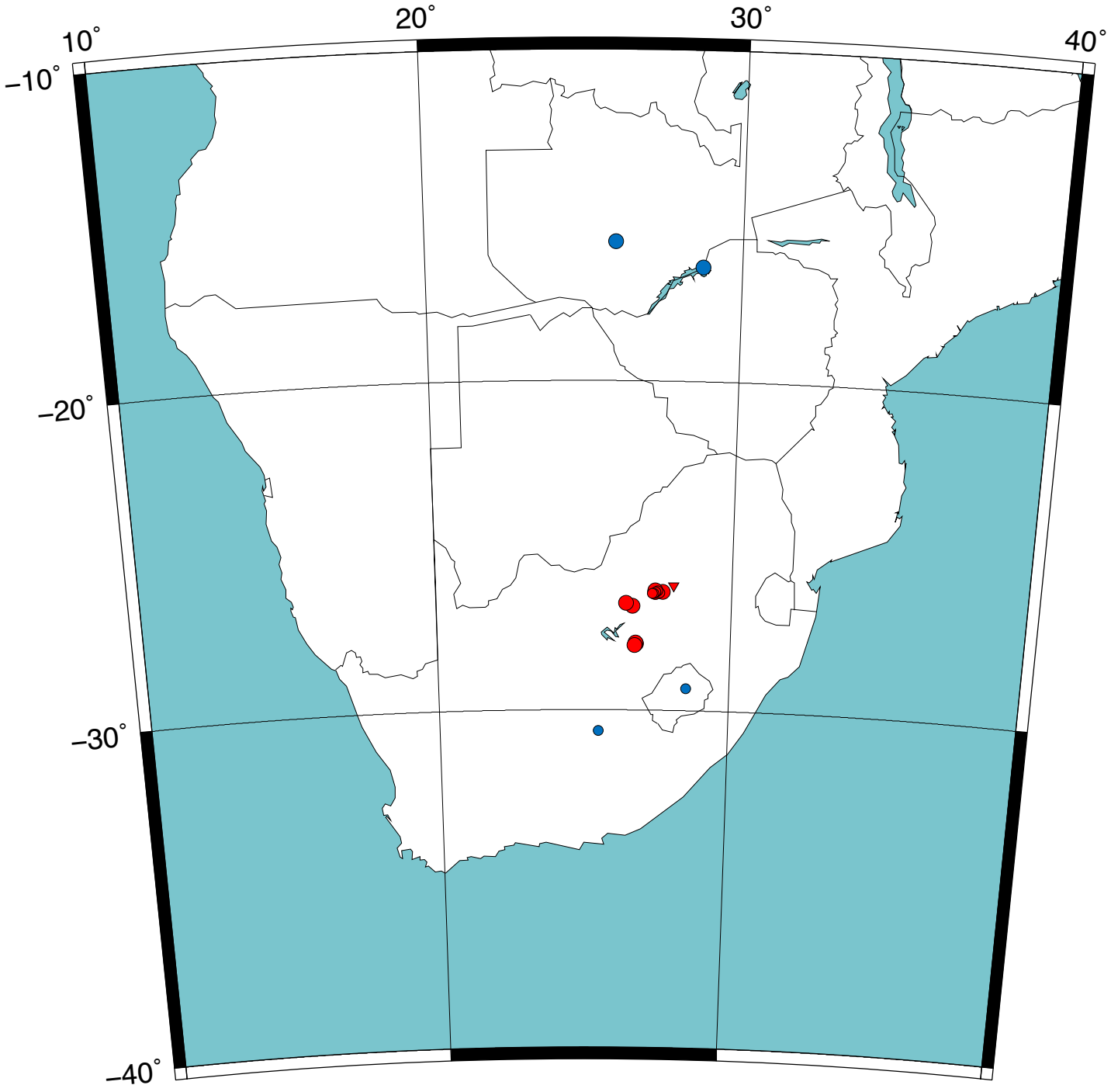
10°
20°
30°
40°
−10°
−20°
−30°
−40°

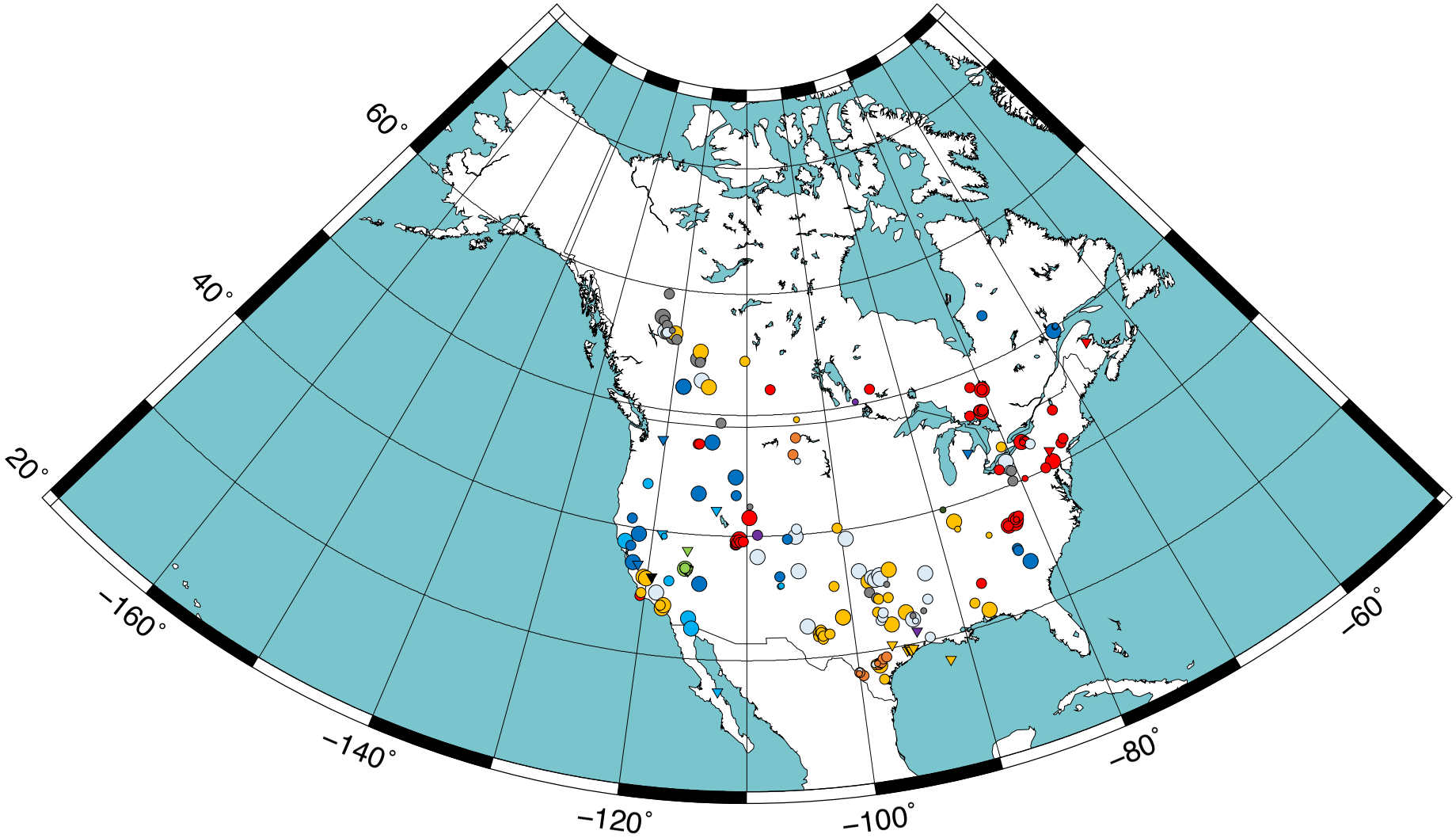
60°
40°
20°
−160°
−140°
−120°
−100°
−80°
−60°

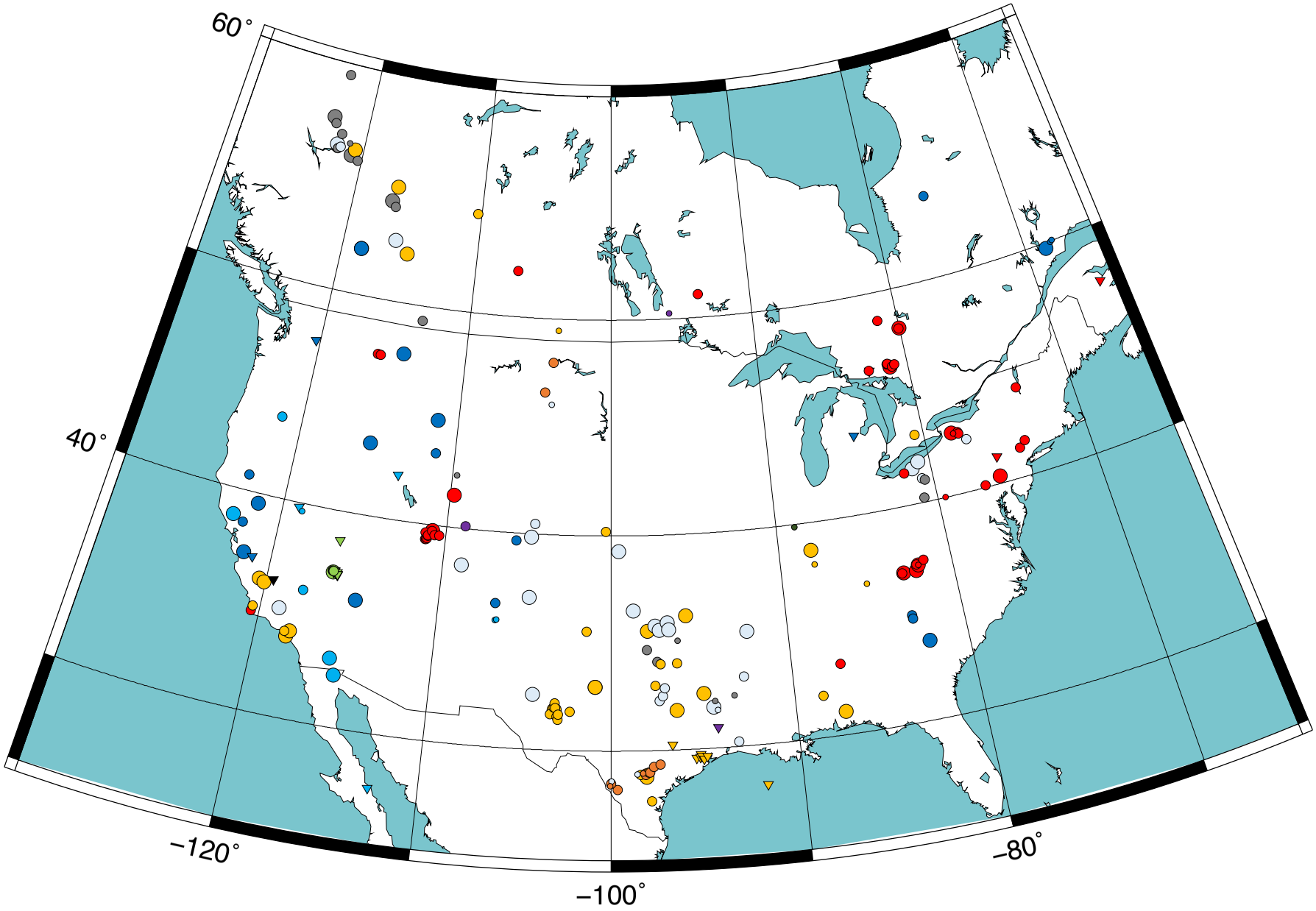
60°
40°
−120°
−100°
−80°

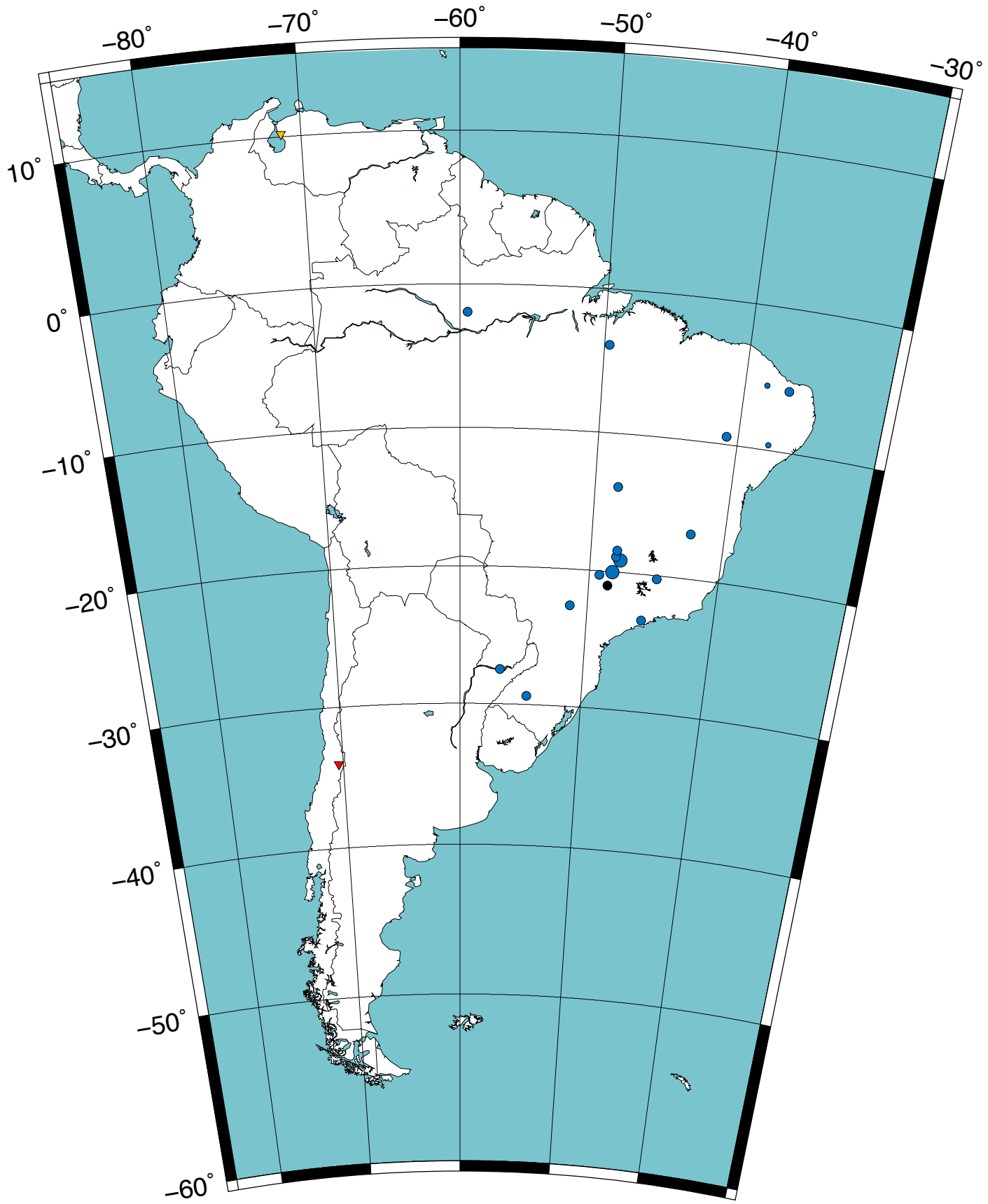
−80°
−70°
−60°
−50°
−40°
−30°
10°
0°
−10°
−20°
−30°
−40°
−50°
−60°

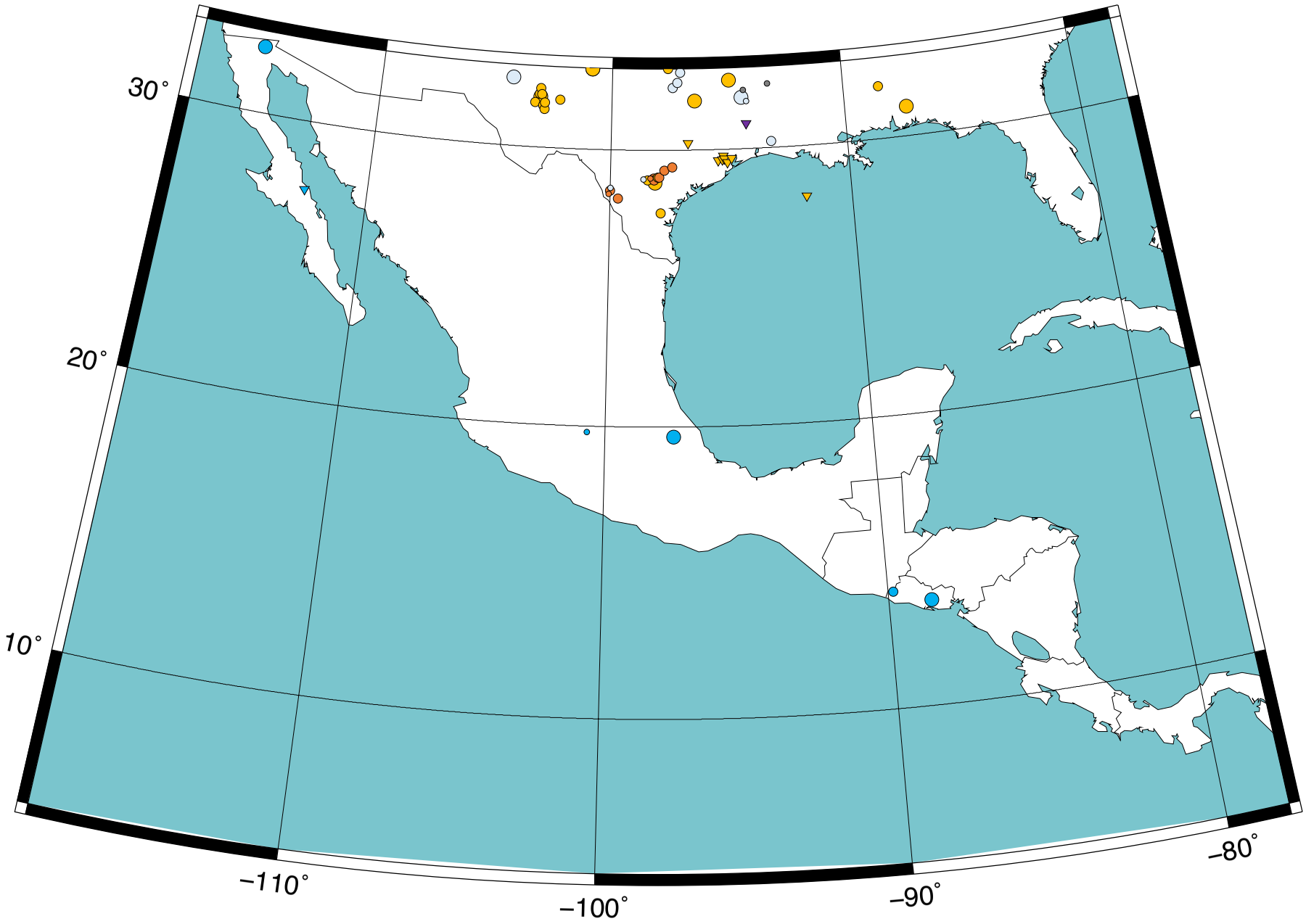
30°
20°
10°
−110°
−100°
−90°
−80°

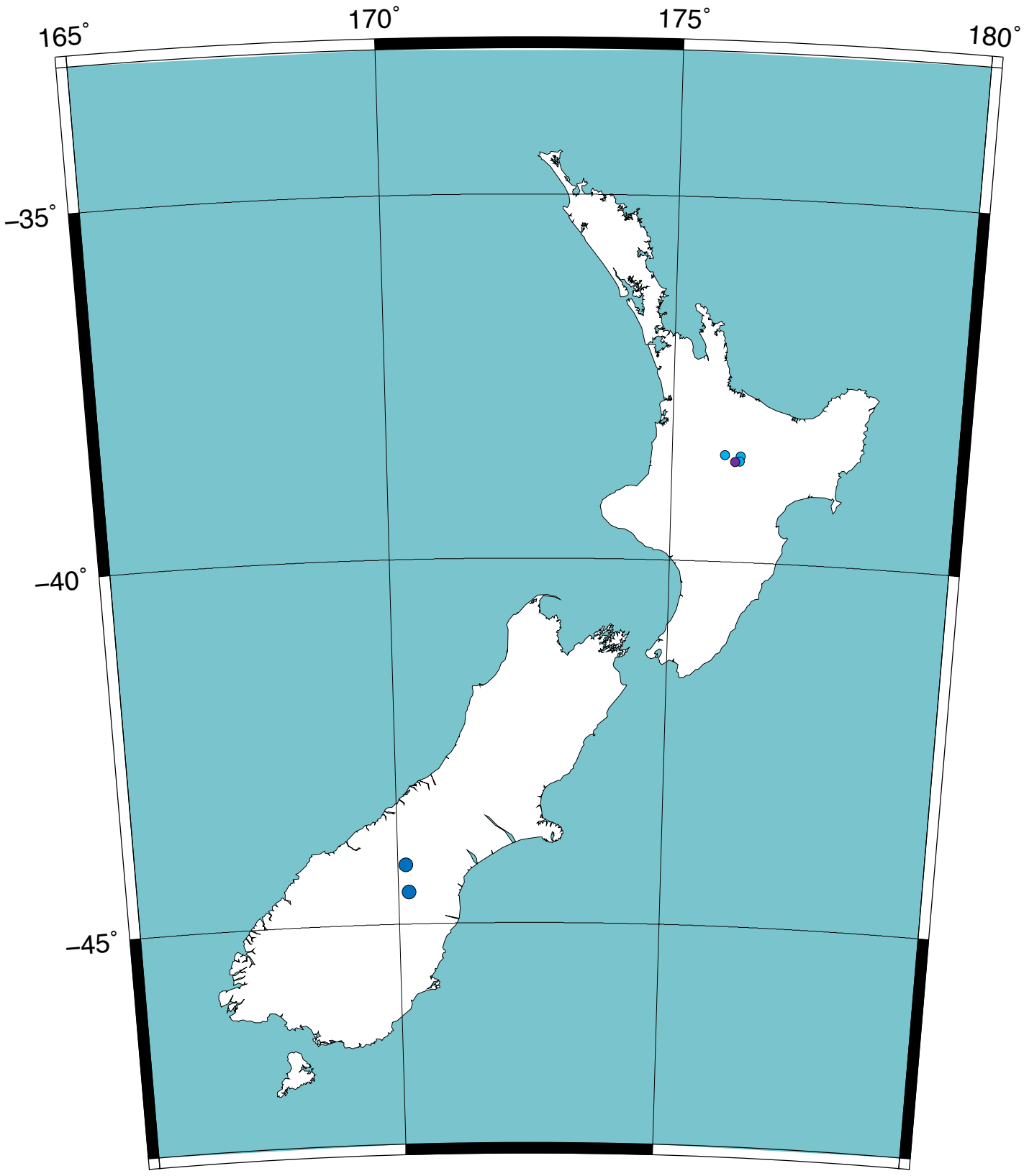
165°
170°
175°
180°
–35°
–40°
–45°

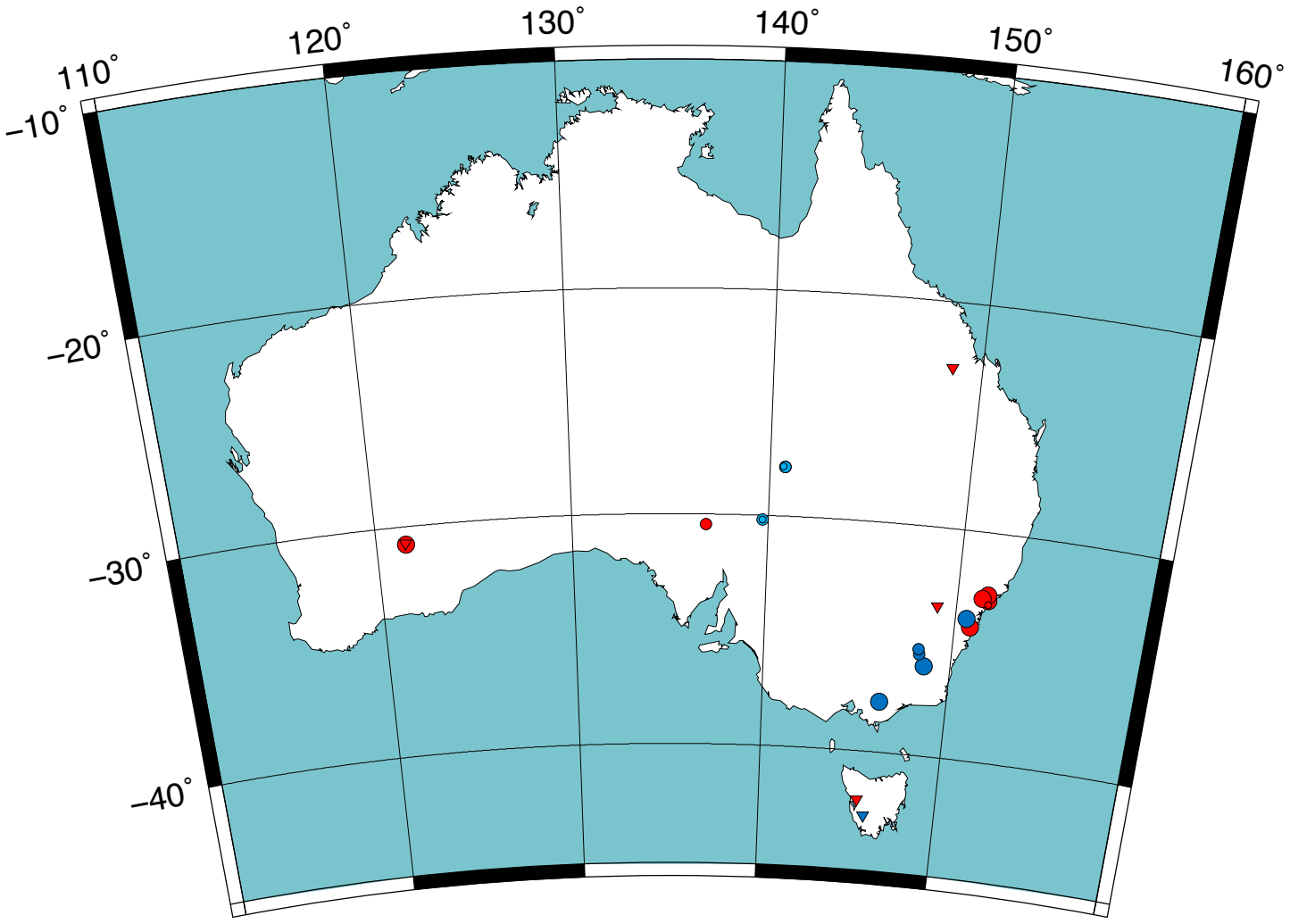
110°
120°
130°
140°
150°
160°
−10°
−20°
−30°
−40°